SOLAR REFRIGERATION

A thesis

submitted in fulfilment

of the requirements for the Degree

of

Doctor of Philosophy

in

Chemical and Process Engineering

in the

University of Canterbury

Christchurch

New Zealand

by

Tadipatri Srinivasa Prasad

1986

DEDICATED

TO

MY PARENTS AND WIFE

ACKNOWLEDGEMENTS

I wish to thank my supervisor Professor A.G.Williamson for his valuable guidance, encouragement and financial support during the last stages of this project. My thanks are due to my co-supervisor Dr.A.S.Tucker for his assistance and willingness to discuss problems at a short notice.

I wish to thank Mr.N.Foot for his technical assistance and valuable suggestions in building the apparatus. Also thanks are due to other technical staff especially Messrs R.G.Gordon and I.J.Murray, whose help is much appreciated. I wish to thank Mr.T.R.Berry for the photographs.

I wish to acknowledge the receipt of the Commonwealth Scholarship and I wish to thank the U.G.C. and in particular Miss K.L.Anderson and Mrs.K.Wills.

I wish to thank the other staff members especially Dr.J.Abrahamson for their encouragement. Thanks are due to fellow postgraduates for their help and useful suggestions.

I am greatful to all my friends who helped me in several ways, without whom it would have been very difficult to finish this work. My sincere thanks are due to Khris and Abanti Mahanty for their care and guidance during our stay in NZ. Many thanks are due to Raj and Rekha Gupta for their care and help, especially while writing the thesis. I wish to thank Vimal for helping me in typing, Pat and Huub for their assistance with the computers.

I am very greatful to my parents, parents-in-law, other members of the family, relatives and friends, who are many miles away but never failed to show their moral support and encouragement. Last but not the least my special thanks are due to my wife Ambika for her understanding, support and encouragement and to my little daughter Karunya for cheering me up.

CONTENTS

ABSTRACT

Solar refrigeration is a natural application of solar energy as the demand and supply match very well. Electrolux refrigerators have considerable appeal as solar driven devices because they do not require any electrical connections or mechanical drivers. The aim of the present investigation was to develop a solar refrigeration system based on an Electrolux refrigerator.

Because of the lack of adequate information two Electrolux refrigerators were tested and their perforamances evaluated. The optimum generator temperature and the optimum generator energy input were 175°C and 100 W respectively.

The temperatures required by an Electrolux refrigerator are beyond the range of most flat plate collectors. A novel hybrid nontracking collector was developed in which the desirable characteristics of a flat plate heat pipe solar collector are used in conjunction with a semi-cylindrical reflector and a special glazing arrangement to achieve a collector which works in the range suitable for the Electrolux system.

A detailed computer model of the collector was developed to predict the performance curve of several versions of the basic collector design. Two collectors were fabricated, the second one incorporating several improvements over the first one. The second panel attained a stagnation temperature of 215°C as against the model prediction of 222°C, at an insolation of 946 $W.m^{-2}$ and an ambient of 26°C. With the heat transfer oil circulating, the collector attained a thermal efficiency of 21% at an average oil temperature of 147°C.

In order to link the collector with the refrigerator, the latter had to be modified. A jacket with internal fins was fitted to the generator tube and the performance of the refrigerator operating on hot oil was evaluated. At a generator temperature of 144°C and an ambient of 14°C it attained a real COP of 0.47 with the freezer operating at -9°C and cabinet at 2.5°C.

The collector was then linked to the refrigerator and the heat losses from various parts of the system were evaluated. Only 16% of the total energy input to the system was utilized by the refrigerator, while the rest was lost to the surroundings via the secondary circuits used in the measurements. Recommendations are made to reduce the heat losses and to link the collector to the refrigerator in different ways.

CHAPTER 1

INTRODUCTION

The first section of this chapter describes briefly the importance of energy in a modern society, the classification of energy resources, the energy crisis and a logical way of solving it and finally, the amounts of renewable sources of energy available and predicted contributions. Section two describes solar energy, its merits and demerits, especially over its main contender - nuclear energy. The third section deals with the different methods of harnessing solar energy and in particular the currently popular ones - solar heating and solar cooling. In the final section the research objective is defined, giving the reasons for choosing the particular topic, its scope and how it was achieved.

1.1 Energy Picture

Every step of human life is associated with some form or other of energy. The need for energy in a modern society can hardly be over-emphasized. It is the fundamental input required to sustain economy and provide the basic amenities of life to the entire population of a country. The use of energy has become so much interlinked with our lives that the per capita energy consumption of a country has become a yard stick of its development.

Energy resources can be classified in a number of ways, depending on the characteristics one is interested in. However, for our purposes, various sources can be conveniently classified as shown in Fig. 1.1 (Hickok, 1975). Non-renewable sources are limited by their available amounts, while the renewable sources are limited by their flux density.

The engine of industrial civilization is at present run by fossil fuels which fulfil about 90% (Ion, 1975) of the total world energy demands (excluding firewood). The use of such large amounts of fossil fuels (equivalent to about 3×10^{20} Joules per annum; WEC, 1978) has resulted in numerous pollution problems. The global annual average energy growth rate measured at the point of

FIGURE 1.1 Classification of Energy Sources (Hickok, 1975)

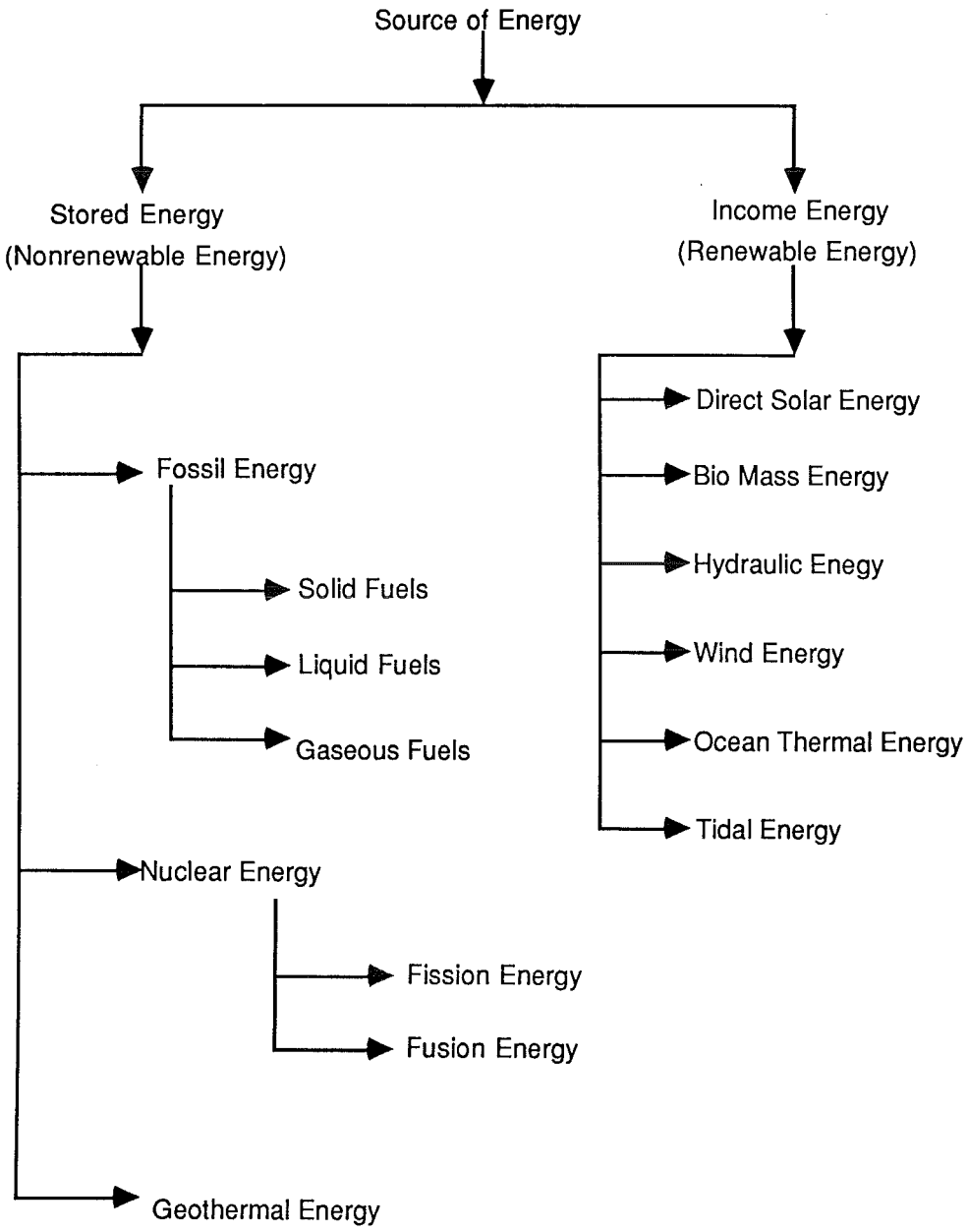

TABLE 1.1 Renewable Energy Sources (WEC, 1978)

Energy Source and Application	Global Abundance in TW (a)	Theoretically Recoverable in TW (b)	Range of Contribution by year 2020 in TW (c,d)
Solar Energy	178,000	50-100	
Heating & Cooling			0.5-2.0
Electricity			0.1-0.3
Fuel			
Wind Energy	350		
Electricity			< 0.01
Mechanical Work			< 0.2
Ocean Thermal Energy	150		very small
Biomass Energy	50	10	very small
Wave Energy	3	0.1-1.0	
Electricity			< 0.01
Fuel			
Tidal Energy	3	0.06	
Electricity			<0.01
Hydralic Energy			
Electricity		2.2	1.8

Notes: (a) Crude estimate

(b) Assuming appropriate technology can be developed economically

(c) Assuming current projections for near future technological sucesses are true

(d) Current global annual average rate of energy use is about 10^{13} W and is expected to increase to $3\text{-}4\times10^{14}$ W by the year 2020

(e) 1 TW = 10^{12} W

end use is about 3 to 5% (King, 1973). Also the trend of change is from an illiterate, simple, farming pattern of life to a literate, industrial and more sophisticated urban pattern of life, which implies a large per capita demand for energy. Even at present consumption rates oil may not last more than 30 to 50 years (Cook, 1976). In any case fossil fuels are being consumed at rates far greater than the rates of formation and hence are bound to run out some time in the near future. Moreover petroleum, which is an important source for as many as 2500 chemicals, is being used merely as a fuel.

Among the different ways of tackling the energy crisis, switching over from non-renewable to renewable sources seems to be a logical and permanent solution (Ruedisili & Firebaugh, 1975). Various renewable energy sources, their total quantities available in the entire world, theoretically recoverable amounts and predicted contributions by the year 2020 are shown in Table 1.1 (WEC, 1978).It can be clearly seen from the table that solar energy has tremendous potential for development and it is one of the most promising alternatives to the current sources.

1.2 Solar Energy

The amount of solar radiation reaching the earth's surface is about 1.2×10^{17} W, which is equivalent to the thermal energy inputs to 40 million 1000 MW power plants (King, 1974). Although the total energy arriving from the sun is immense, the flux density is very small by present day engineering standards. At the top of the atmosphere, the maximum value of the flux density is about 1300 $W.m^{-2}$ (Brinkworth, 1974), but a variety of scattering and absorbing processes reduce this, to about 900 $W.m^{-2}$ at the surface. Except for a few drawbacks such as availability in diffused state, diurnal and seasonal variation, solar energy possesses several advantages (Patton, 1975). It is "inexhaustable", completely pollution free and not localised like other renewable sources of energy. The raw material cost is nil, cost of conversion is stable and easy to predict and the operating cost is very small. It can be adapted to any level of technology, starting from simple solar cookers, through to complicated power plants. Other benefits such as decentralization, rural development, reduction of monopolies and savings in foreign exchange can be achieved.

The main competitor of solar energy, as a future energy source, is nuclear energy. However nuclear energy has certain serious disadvantages such as radioactive and thermal pollution, waste disposal problems and dependence on sophisticated technology. In addition to the technological problems of nuclear energy there are sociopolitical considerations such as the issue of non-proliferation of nuclear weapons and terrorism.

The relative merits and demerits of the different sources, and their technologies, are to be judged not only on the amount of energy they might produce, and the corresponding economies, but also on the environmental and sociological effects. Hence the issue is not one of "good or bad" but one of balancing the beneficial aspects of energy use against its undesirable environmental and sociological effects, so as to maximise the public good. Keeping these points in view, solar energy undoubtedly is superior to all its rivals.

1.3 Methods of Harnessing Solar Energy

Green plants have been known for centuries to tap solar energy and store the greater part of the catch in the form of diverse chemicals. Indeed the so called fossil fuels are legacies left by green vegetation that covered the planet during a distant geological era. There are three main processes by which solar energy can be put to use:

(1) heliochemical, which nature has used in the production of plants and oxygen, by photosynthesis, since the earliest days of this planet,

(2) helioelectrical or photovoltaic, which is the newest and the only entirely man-made method of using solar energy and

(3) heliothermal, which is both ancient in its natural manifestations and modern in its technological applications.

Various solar energy conversion technologies and applications can be summarized under two main categories (Hickok, 1975).

(1) Direct conversion of solar energy : Heliothermal processes come under this category. Depending upon the temperature range they can be further divided into three groups:

(a) low range (< 120°C), such as water and space heating, solar
drying and evaporation,

(b) intermediate range (120°C to 500°C) such as solar cooling and refrigeration, solar pumps;

(c) high range (> 500°C) such as solar furnaces and power plants.

(2) Indirect conversion of solar energy : Heliochemical and helioelectrical processes come under this category and depending on the final manifestations of solar energy they can be divided into three groups:

(a) solar energy as light such as photochemical and photoelectrical processes,

(b) wind energy and

(c) ocean thermal energy.

Of the various methods of harnessing solar energy, solar scientists are generally more involved, in either direct conversion techniques, or photovoltaics, which tend to have greater scope for development and application. Among the different direct conversion processes solar heating and solar cooling/refrigeration are the two most promising and most widely applied ones. Although they are presently handicapped by higher investment costs as compared to conventional systems, they are bound to become economically competitive as the availability of traditional fuels decreases. Certain parts of the world need almost year round cooling, while the other parts of the world need cooling for only part of the year, and hence, year round employment of solar collection systems, for both heating and cooling, contributes to making these solar applications economically even more attractive.

Solar cooling is a natural application of solar energy, since the sun is used to overcome its own discomforting effect. In contrast with other applications of solar energy such as solar heating, solar cooling is needed most when the solar radiation is at its peak, making its use for this purpose particularly attractive.

Thus solar energy is in principle better suited to space cooling and refrigeration, than to space heating, but until recently this application of solar energy has received little attention. However, energy for air conditioning has been one of the fastest growing segments of energy consumption, in several developed countries. For example the United States is currently

using about 3% of its total electricity consumption for air conditioning only (Dunkerley, 1978). On the other hand several developing countries are urgently in need of small solar driven refrigeration units for preservation of food and medicines in remote rural areas where electricity is not readily available and there is need for research and development in this field.

1.4 Research Objective

As described in the next chapter several solar cooling and refrigeration systems have been developed and one of the most popular ones is the solar absorption refrigeration system. Amongst these systems water-lithium bromide systems are used for air conditioning applications, while ammonia-water systems are used for refrigeration applications. A number of researchers have worked on ammonia-water systems utilizing pumps for the circulation of ammonia solution. (Farber et al., 1975, 1976; Dao et al., 1977; Geoola et al., 1980; Johnston and O'Sullivan, 1981).

However, very few have worked on ammonia-water systems, without utilizing pumps, like Electrolux or Servel type of refrigerators (Chari, 1958). One of the main reasons for this is the high temperature requirement of such systems (generator temperature of about 150°C, as shall be seen in later chapters), which forces one to go in for more expensive tracking concentrators or evacuated tubular collectors. Chari (1958) used a parabolic concentrator in his solar refrigeration system. Another reason for not working with Electrolux systems is that their popularity decreased drastically after the introduction of vapour compression refrigeration systems, and also, the Electrolux systems are not very well understood because of the inadequate knowledge regarding the internal workings and interrelationship amongst the various parameters of the system.

Our research objective was to develop a solar refrigeration system based on the Electrolux refrigerator.

The first hurdle in achieving this objective was to understand the Electrolux systems thoroughly, in order to find the optimum generator temperature and optimum power input to the generator, so that an appropriate solar collector system could be chosen or designed. A thorough knowledge of the Electrolux refrigerator is also important for the modification of the system, in order to run it with solar heated fluid. Hence, experiments

were conducted to study two refrigerators in detail, at the end of which the better one was modified for solar application.

Then the major hurdle was to develop a simple and inexpensive solar collector, capable of attaining temperatures high enough to run an Electrolux refrigerator. A nontracking hybrid solar collector (with a "heat sheet absorber" HSA, based on the heat pipe principle and a "semi-circular cylindrical reflector" SCCR), which was under development in the Department of Chemical and Process Engineering (University of Canterbury, Christchurch) was selected for this purpose. Webb (1979) predicted, with the help of a simple computer model, that the HSA-SCCR collector with several refinements should be capable of attaining stagnation temperatures as high as 265°C. One such collector was designed and built, but it failed to reach the predicted temperatures. The design was analysed in this project using a more detailed, more versatile and more accurate computer model. The model was used to design an improved collector whose predicted stagnation temperature was less than that of Webb's model. A collector was built to this design and good agreement was obtained between the predicted and observed performance.

Finally the refrigerator was linked to the solar collector system, via a storage or buffer tank, and the performance of the combined system was evaluated. A detailed analysis was done to find out the heat losses from various parts of the system in order to know the total energy requirements of the system.

Although the present system is not a totally solar operated one, suggestions have been made for future work to eliminate the auxiliary source of energy.

FIGURE 2.1 Classification of Solar Cooling/Refrigeration Systems

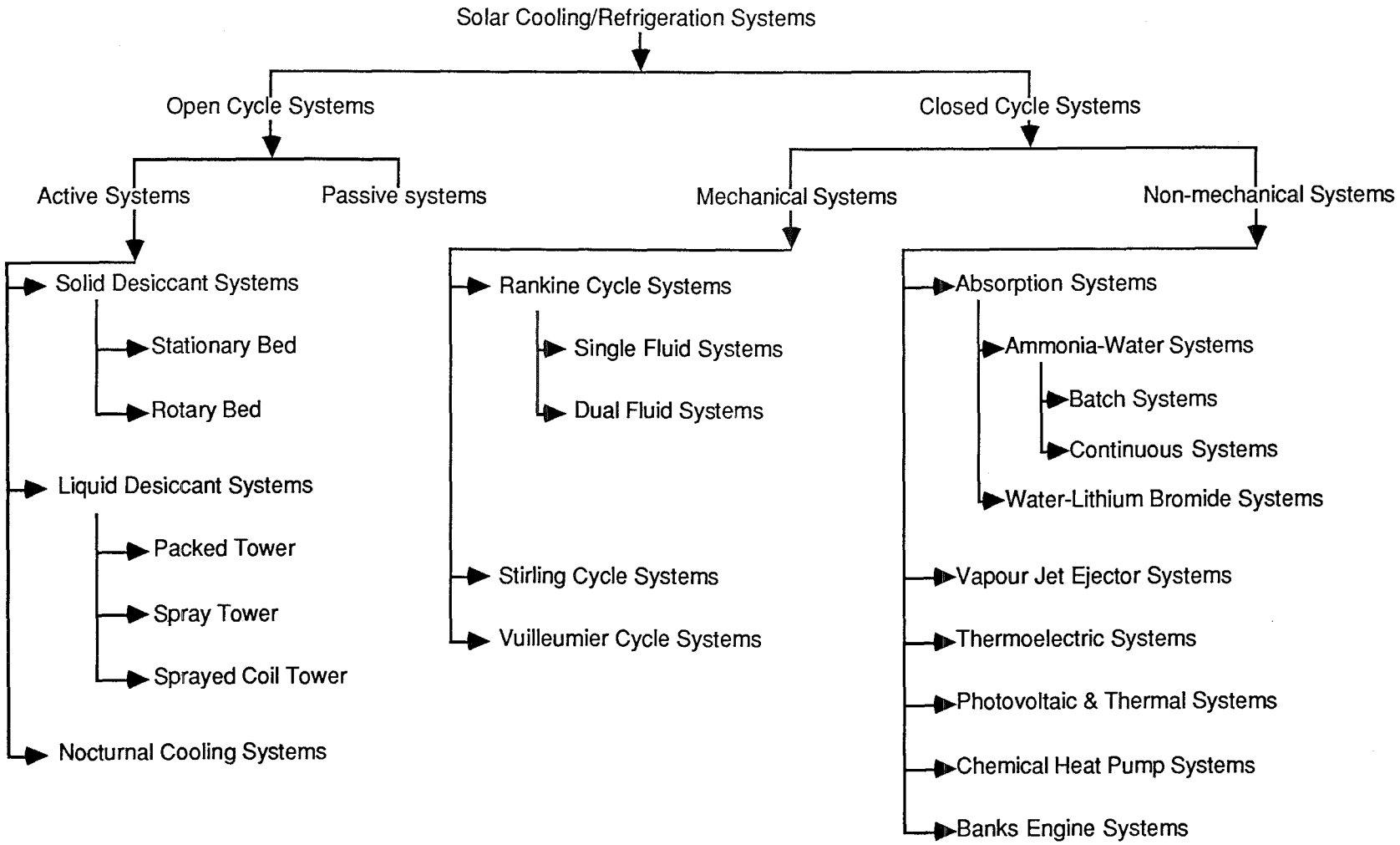

CHAPTER 2

SOLAR COOLING/REFRIGERATION SYSTEMS

Although solar cooling represents a potentially significant application of solar energy, it is not as advanced as solar heating technology. Several viable solar cooling/refrigeration schemes are described in this chapter, along with their merits and demerits, which may be used as general guidelines in selecting a particular system. Finally the reasons for selecting an absorption refrigeration system, and in particular the Electrolux system, are given.

The various types of solar cooling/refrigeration systems can be broadly classified into two categories as shown in Fig. 2.1 (Prasad and Williamson, 1982): open cycle systems, which depend for their operation on water vapour exchange with the atmosphere; and closed cycle systems, in which the working fluids are totally enclosed and heat only exchanged with the surroundings. In open cycle systems the temperature is lowered by adiabatic vaporization of moisture into the air, while in closed cycle systems the lowering of the air temperature is achieved by actual cooling of the air.

2.1 Open Cycle Systems

The cooling in these systems is achieved by controlled dehumidification and evaporation and hence these systems are also known as humidification/dehumidification (HDH) systems or evaporative cooling systems. The water is used as an expendable refrigerant, which is not recovered and in this sense the system is said to be open.

The advantages of open cycle systems over closed cycle systems are: (a) both the humidity and the temperature can be controlled, (b) the working fluid being air water mixture, small leaks are of no importance, (c) since the system operates close to atmospheric pressure, heavy construction is not required, (d) the "stuffiness" frequently encountered in usual air conditioning systems is totally eliminated as large quantities of fresh air can be introduced and (e) they can be run continuously under part load

FIGURE 2.2 Principle of Desiccant Cooling Systems

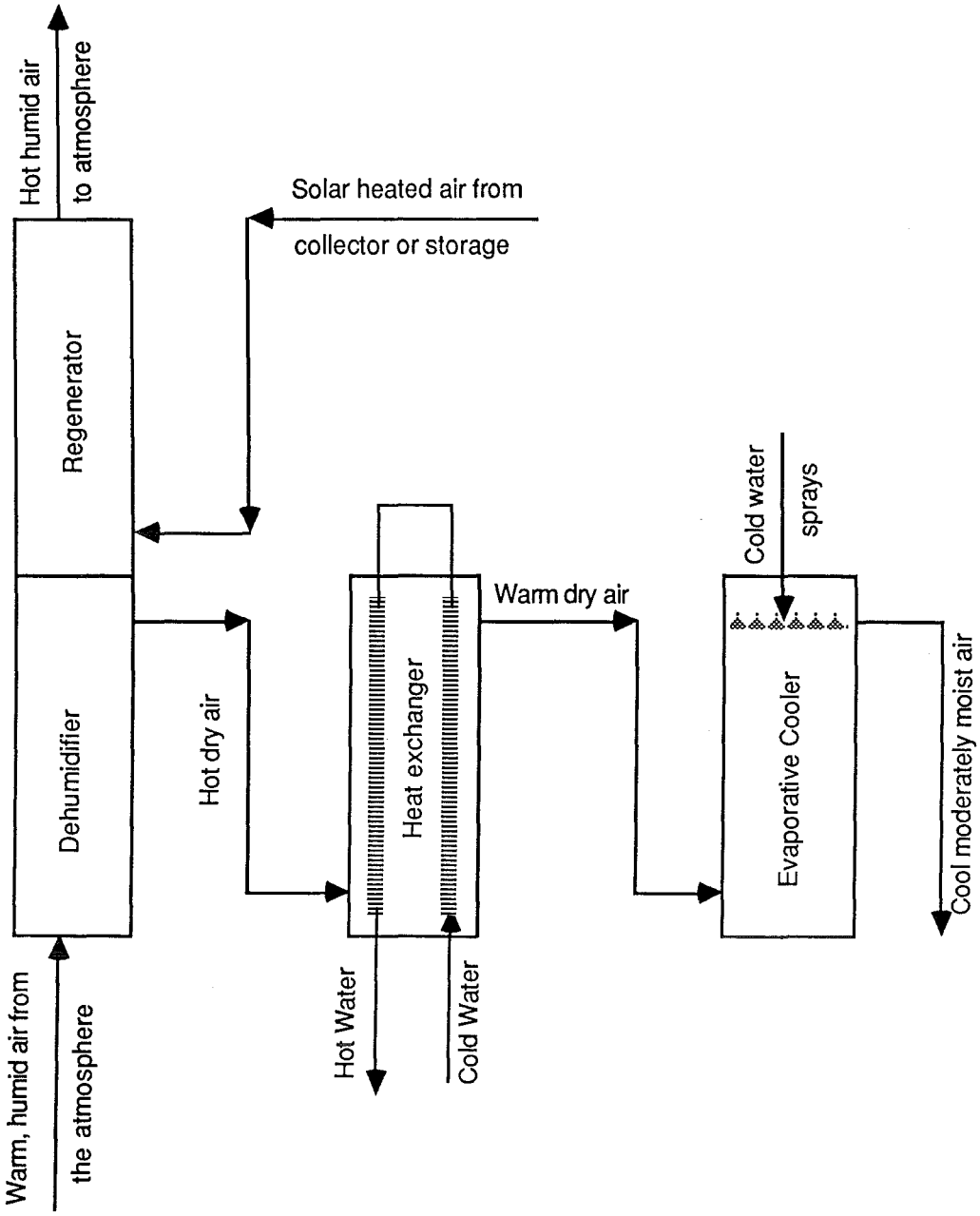

conditions using multi-speed motors for circulating fans and thus the power requirements can be reduced considerably.

The open cycle systems can be further subdivided into two categories, active systems and passive systems. The active systems are characterised by energy transport in fluid loops, active control systems that divert flows of fluids to various subsystems and solar collectors in which forced convection is the mode of heat transfer. The passive systems are identified as those in which the heat transfer is by free convection and radiation, in which no pumps or blowers are required, and in which solar collection and storage subsystems are combined into one component.

2.1.1 Active systems

The active systems can be further divided into three groups as shown in Fig. 2.1. They are solid and liquid desiccant systems and nocturnal systems.

2.1.1.1 Solid desiccant systems

The principle of desiccant cooling system is shown in Fig. 2.2. The warm, humid air passes through the dehumidifier, where the moisture is removed. The hot dry air is then cooled in a heat exchanger and then in an evaporative cooler. The solar heated air is used to regenerate the desiccant.

The solid desiccants can be either absorbents such as chlorides of lithium, calcium and strontium, or adsorbents like silica gel, activated alumina, alumina gel and molecular sieves (Schmidt and Neilson, 1978). From amongst the solid desiccants silica gel and molecular sieves appear to be favoured in the current research and development effort, (Satcunanathan and O'Brien, 1977).

The general advantages of solid desiccant systems are: (a) cheapness, (b) low corrosion, (c) no problems of leaks, (d) no crystallization hazards, (e) little maintenance and (f) no losses due to evaporation.

Solid desiccant dehumidifiers are essentially of two types: stationary bed type, which are used for batch operation and rotary bed type, which are used for continuous operation. Dunkle's system (1965) consisted of a rotating dehumidifier with silica gel as the adsorbing medium. Shelpuk (1979) and Mei et al. (1979) have reported on different aspects of solid desiccant systems.

The coefficient of performance of solid desiccant systems (which is the ratio of the energy extracted from the room air to the energy supplied to the regenerator), excluding the collector efficiency, is generally in the range of 0.52 to 0.62 (Grossman & Johannsen, 1981). In general, solid desiccant systems appear to be more suitable for residential applications due to their greater reliability and low maintenance as compared to liquid desiccant systems. However, they are also well suited for medium and large scale applications.

2.1.1.2 Liquid desiccant systems

The operating principle of liquid desiccant systems is the same as that of solid desiccant systems, except for the fact that the dehumidifier and the regenerator are two different chambers. Liquid desiccants include aqueous solutions of lithium chloride, lithium bromide, and calcium chloride and the glycols of the ethylene glycol group. A comparison of various liquid desiccants is given by Grossman and Johannsen (1981). The two liquid desiccants which have reasonably good potential for solar systems are triethylene glycol and lithium chloride.

In general, the advantages of liquid desiccant systems include: (a) low air pressure drop, (b) ease of isothermal dehumidification, (c) ease of heat recovery, (d) storage capability and (e) the possibility of removing micro-organisms using bacteriostatic desiccants like triethylene glycol and lithium chloride.

Liquid desiccant dehumidifiers can be divided into three categories: packed tower, spray chamber and sprayed coil. Lof's (1955) system consisted of a sprayed coil dehumidifier and triethylene glycol desiccant (Johannsen, 1979), while Baum and Kakabayev (1978) have reported a combined collector and regenerator with lithium chloride as desiccant. The coefficient of performance of liquid desiccant systems (excluding the collector efficiency) is generally in the range of 0.52 to 0.62. Liquid desiccant systems are generally preferred for commercial applications in medium and large scale.

2.1.1.3 Nocturnal systems

In many parts of the world, normal summer temperatures show wide day-night differences, even up to 20°C (Lof, 1955). If a

FIGURE 2.3 Trombe Wall Principle

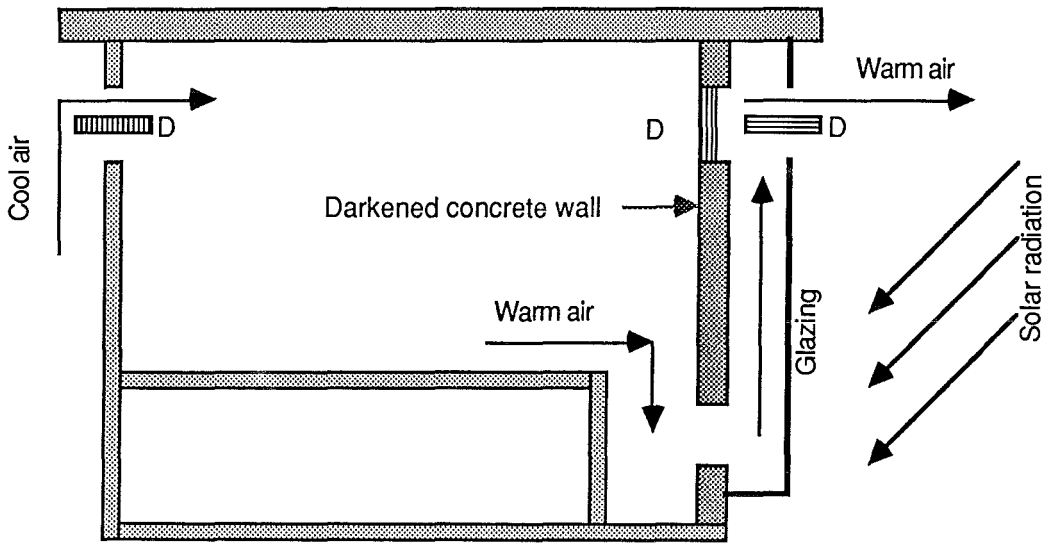

D = Damper

solar heat storage unit is cooled at night, by transferring heat from the storage to the atmosphere, this stored cold material can be used during the following hot day, as a source of cool air, or water, for circulation through the house. Under clear sky conditions, there is considerable thermal radiation from exposed surfaces to the night sky, and hence, a further cooling can be achieved using suitable radiating surfaces. Close (1965) suggested a rock bed regenerator (RBR) through which cool night air is drawn to cool the rock pile. To further cool the air, water can be sprayed on to the rock bed (Karaki and Armstrong, 1978).

2.1.2 Passive systems

Almost all the passive cooling systems are based on the same principle namely chimney-effect cooling. Solar heat absorbed in a glazed concrete wall facing the equator warms the air in front of it, which escapes through vents at the top, drawing cooler air into the rooms through vents in the wall facing the pole. Instead of a conventional fan, solar energy provides all the power needed to move this air. Based on this principle, Hay and Yellott (1970) and Buckley (1976) have reported modifications to improve the cooling capacity. The Trombe wall (Trombe et al., 1977) shown in Fig. 2.3 is based on the same principle. Dampers are employed to control the flow of air and the concrete wall is blackened to make it a good absorber of radiator.

Passive systems, though difficult to incorporate into existing buildings, must be kept in mind during the construction of new buildings in order to greatly reduce the cooling loads. They have to be designed for the particular climate in each region, and, are not as universal as the active systems. However, they have a large potential for energy conservation.

2.2 Closed Cycle Systems

Closed cycle systems are well established mainly because of the vast amount of experience and knowledge accumulated with them in conventional refrigeration. The advantages of closed cycle systems over open cycle systems are: (a) temperatures below zero can be obtained, (b) they can be used for comfort cooling, refrigeration and cold storage, (c) they are more compact, (d) they can be built in any size, (e) they are easy to adapt existing units for solar applications, (f) lower initial investments

FIGURE 2.4 Schematic Diagram of a Single Fluid, Solar Powered, Rankine Cycle Vapour Compression Refrigeration System

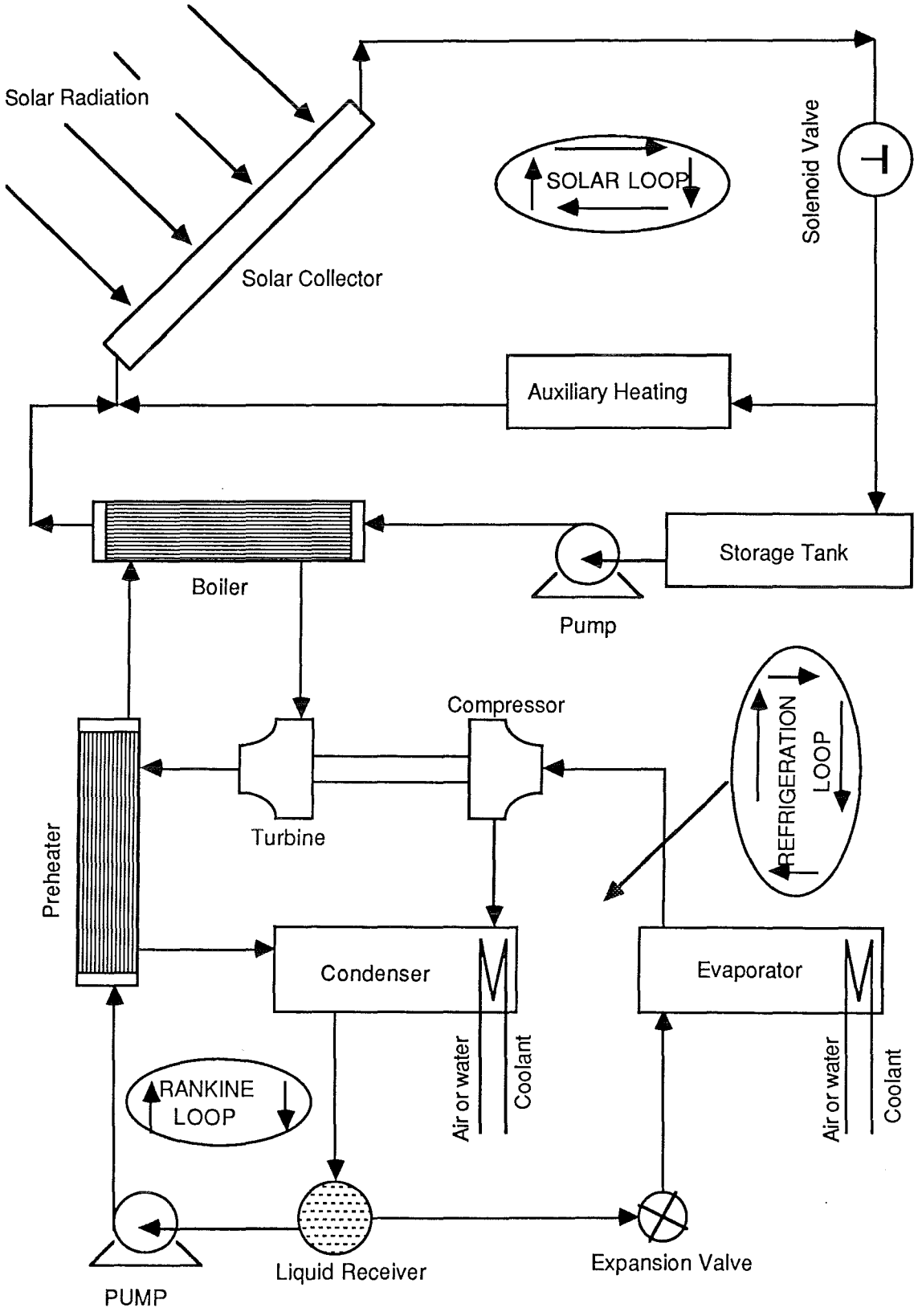

especially in small capacities and (h) they can be used under any entering air conditions.

These systems can be further divided into two main groups, mechanical systems and non-mechnical systems. Mechanical systems are characterised by the fact that the solar energy is first converted to mechanical energy, which in turn is used to run a refrigeration system. In the case of non-mechanical systems solar energy is used in different ways in different systems.

2.2.1 Mechanical systems

There are a number of mechanical systems suitable for solar energy application, but Rankine cycle cooling is most widely used and is the main contender against the absorption refrigeration cycle. Mechanical systems can be further divided into three categories as shown in Fig. 2.1, namely Rankine,Vuilleumier and Stirling systems.

2.2.1.1 Rankine cycle systems

Rankine cycle cooling has attracted the attention of many solar scientists, as it simply couples the conventional vapour compression refrigeration system to the solar operated Rankine heat engine system. The main advantages of Rankine cycle systems, over absorption systems, are their significantly higher COP values (1.08 to 1.63 times as given by Ward, 1979) at lower condensing temperatures and the fact that by proper choice of the working fluid, they can be operated over a wider temperature range. Rankine cooling systems can be further sub-divided into two categories single fluid systems and dual fluid systems.

The schematic diagram of a single-fluid, solar powered vapour compression refrigeration system is shown in Fig. 2.4. Single fluid systems use the same fluid in both the Rankine loop and the refrigeration loop and also share a single condenser between the two loops. These systems have long life and need minimum maintenance compared to dual fluid systems (Teagen and Sargent, 1975). A number of fluids have been tried depending on the temperature range. Barber (1979) has given a comparison of various working fluids.

Dual fluid systems employ different fluids in the power loop and the refrigeration loop and they have higher COP values than single fluid systems (Prigmore and Barber, 1975). The overall COP

FIGURE 2.5 Vuilleumier Machine

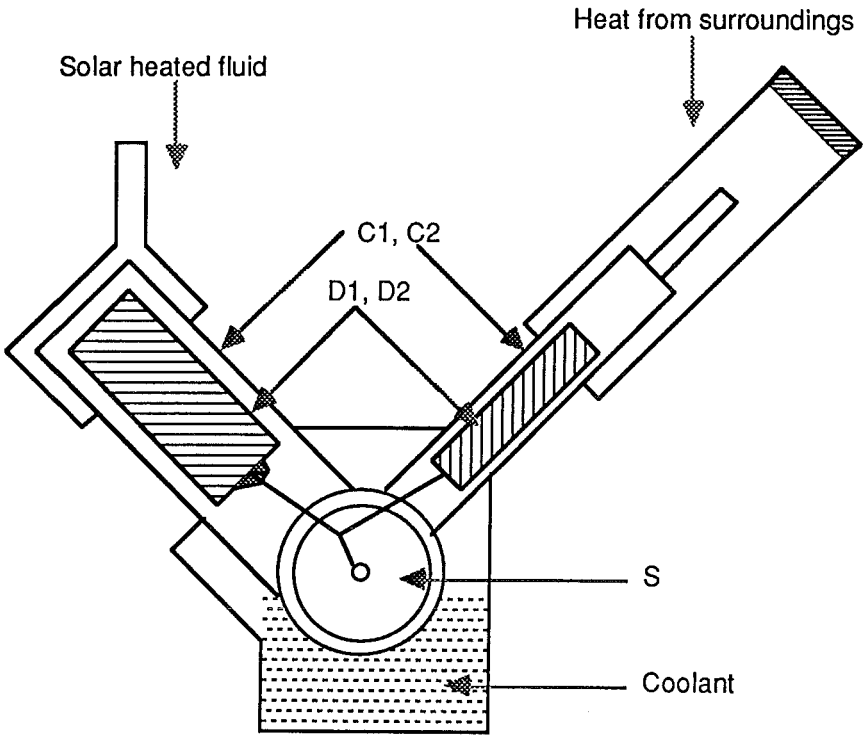

Notes: C1, C2 = Cylinders

D1, D2 = Displacers

S = Crank case

of the Rankine cooling system is a function of both the power cycle COP and cooling cycle COP and varies from 0.5 to 1.5 compared to the absorption system COP which varies from 0.4 to 1.1 (Eckard and Bond, 1976; Koai et al., 1984).

2.2.1.2. Vuilleumier cycle systems

The schematic diagram of a Vuilleumier engine is shown in Fig. 2.5. It consists of two cylinders (C1, C2), one larger than the other, mounted on a common crank case (S). Each cylinder contains a displacer (D1 or D2), and the two are coupled to a common crankshaft, so that the displacers move simultaneously but operate out of phase. External work is supplied to the crank case to move the displacers. It is important to recognise that the necessary power is very small, since only the fluid-friction and mechanical friction need to be over come. External work is not required to compress or expand the working fluid, but is needed merely to displace it from one space to another.

Shelpuk (1974) conducted experimments on two solar operated Vuilleumier cycle refrigerators: one requiring no mechanical input and the other with mechanical displacer activation. He achieved an actual COP of 1 to 1.2. The advantages of the Vuillemier system are high reliability and no bearing problems, due to the absence of pistons.

2.2.1.3 Stirling cycle systems

The ideal Stirling cycle consists of two isothernal processes, one compression and one expansion, and two processes of heat transfer at constant volume. The principal advantage of the Stirling cycle over the Carnot cycle lies in the replacement of two isentropic processes by two constant volume processes, which greatly increases the area of the P-V diagram and thus reduces the necessity to resort to high pressures and swept volumes (Walker, 1973).

The Stirling engine can be used in two ways for solar-cooling. Firstly, the mechanical power produced from the Stirling engine can be used to run a cooling system. Secondly, the Stirling engine can be used as an integral part of the solar cooling system. The first approach offers more flexibility in the design and allows for a broader selection of cooling systems. The integral system design uses a single drive mechanism for both the

engine and cooling units, thereby reducing total mechanical friction and possibly offering a better efficiency. The integral design is self-contained and uses the same working fluid for cooling as in the engine. At high input temperatures, the Stirling engine is more efficient than the Rankine cycle engine (Pedroso, 1976). The practical COP of these systems is about 0.4 (Didion et al., 1979).

2.2.2 Non-mechanical systems

The non-mechanical systems can be further divided into six categories (Fig. 2.1): absorption, vapour jet ejector, thermoelectric, photovoltaic/thermal, chemical heat pump and Banks engine systems. Of the various non-mechanical system investigated so far, the absorption refrigeration systems are most commonly used for solar cooling applications.

2.2.2.1 Absorption refrigeration systems

Absorption refrigeration is currently given most serious attention, in solar cooling applications. It appears more logical to use the solar heat directly in a cooling system, rather than converting it to mechanical or electrical energy, which in turn is used to run a refrigeration system. A principle advantage of this method is the small amount of mechanical work required. Although an absorption cycle requires a heat input many times greater than the work input of a mechanical vapour compression cycle, it can be attractive economically if the heat available is sufficiently cheap as is the case with solar energy.

The advantages of absorption systems over their main contender Rankine cycle systems are: (a) they can be operated at reduced evaporating temperatures or pressure with little decrease in refrigerating capacity, (b) liquid carry-over from the evaporator does not cause difficulties, (c) they can be operated at low temperatures such as are obtainable even from a flat plate collector (Satcunanathan and Kochchar, 1975), (d) at reduced load they are as efficient as at full load, (e) they are simpler and more compact for high capacities, (f) lower capital costs, (g) lower maintenance, (h) less noise and less wear and tear due to the presence of very few moving parts and (i) their capability to use low quality energy such as thermal energy directly, instead of high quality energy such as electricity.

FIGURE 2.6 Schematic Diagram of a Solar Powered Absorption Refrigeration System

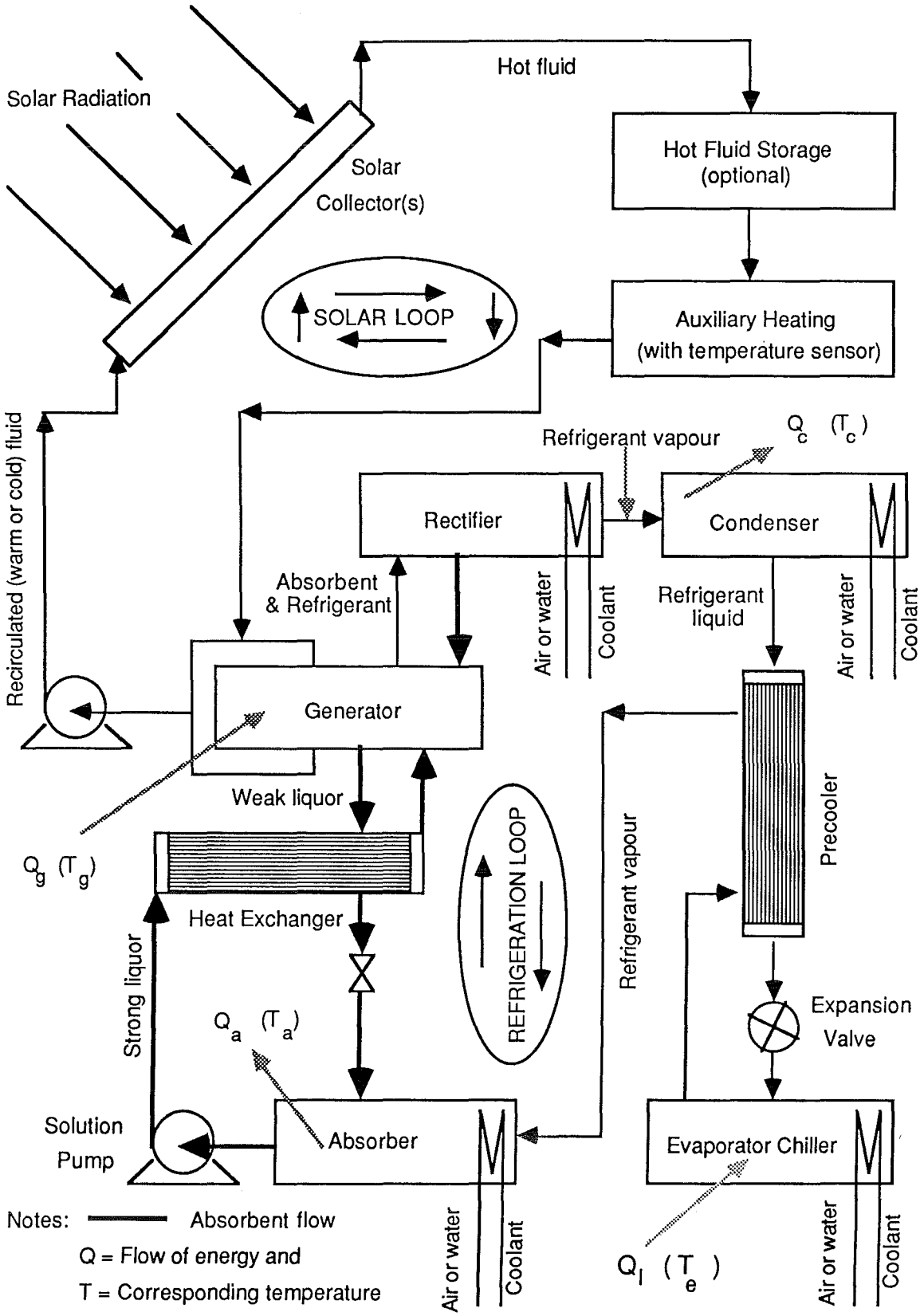

Feasibility studies of solar absorption cooling have been carried out by several authors including Wilber and Mitchell (1975), Macriss (1976) and Alefeld (1980).

2.2.2.1.1 Working principle

The schematic diagram of a solar powered absorption refrigeration system is shown in Fig. 2.6. The system consists of two loops, the solar loop and the refrigeration loop. The solar loop supplies the necessary heat Q_g at the high temperature T_g to the generator of the refrigeration loop. The solar loop may include an auxiliary heater and a hot storage unit.

The refrigeration loop consists of a generator, a condenser, an absorber, an expansion valve and an evaporator. There are two working fluids in this loop: a refrigerant and an absorbent. Liquid refrigerant evaporates at low temperature T_e in the evaporator, while removing Q_l amount of heat from the cooled medium. The vapour goes into the absorber, where it is absorbed by the weak liquor, with a low concentration of the refrigerant. The liquor must be cooled during the process, to remove Q_a amount of heat (which is nearly equal to the heat of dilution) and keep its temperature low, close to the ambient temperature. This is necessary for maintaining a low vapour pressure which allows for efficient absorption. The effect of this process on the refrigerant vapour is equivalent to the compressor suction in the vapour compression cycle.

The strong liquor leaves the absorber and is pumped via the heat exchanger into the generator. It is heated to the high temperature, supplied by the solar loop, and its vapour pressure increases to the point where it can no longer contain the amount of refrigerant it had. The latter is released at a high pressure and flows into the condenser. The result produced by this process is similar to that of the compressor discharge in vapour compression. The refrigerant entering the condenser (in a superheated state) condenses, releasing heat to the air or water coolant. The liquid refrigerant, passes through the expansion valve to further cool, before entering the evaporator chiller. The weak liquor having released the refrigerant leaves the generator and returns to the absorber.

Since the absorbent solution must be heated in the generator and cooled in the absorber, a recuperative heat exchanger is

FIGURE 2.7 Thermodynamic Representation of an Absorption Refrigeration Cycle

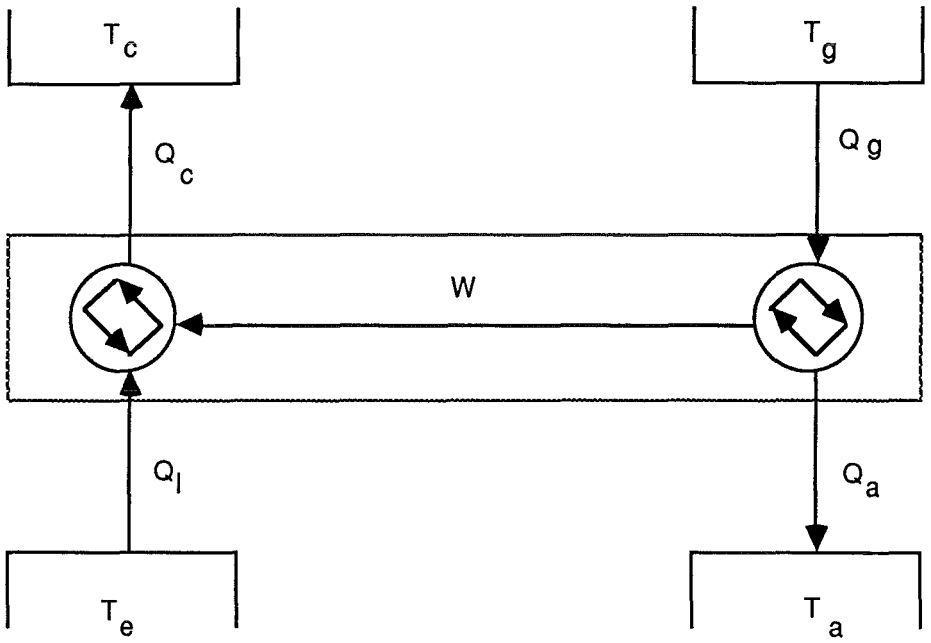

Notes:
- T_c = Condenser temperature
- T_g = Generator temperature
- T_e = Evaporator temperature
- T_a = Absorber temperature
- Q_a = Heat rejected at the absorber
- Q_c = Heat rejected at the condenser
- Q_g = Heat supplied at the generator
- Q_l = Heat absorbed at the evaporator
- W = Work supplied by the heat engine cycle to the refrigeration cycle

provided between the two streams to recover heat from the weak liquor and preheat the strong liquor. A circulation pump is also needed to transfer the solution from the low pressure absorber to the high pressure generator. In some designs (like Electrolux or Servel) the pump is replaced by a thermosyphon system. Another recuperative heat exchanger is also generally employed to cool the liquid refrigerant coming from the condenser, by the refrigerant vapour leaving the evaporator. With certain refrigerant-absorbent combinations such as ammonia-water a rectifier or a reflux condenser is provided on the top of the generator to avoid carryover of absorbent into the condenser. It can be a separate heat exchanger cooled by air or water in bigger systems or a simple pipe, slightly slanted (to allow the condensed absorbent to flow back into the generator) as in small Electrolux systems.

2.2.2.1.2 Analysis of the cycle

The absorption refrigeration cycle can be described in basic thermodynamic concepts as a combination of two cyclic devices operating together, one as a heat engine and the other as a refrigerator. Hence the maximum attainable COP of an absorption refrigeration system (COP_{max}) is equal to the COP of a Carnot refrigerating cycle (β_r) working between the evaporator temperature (T_e) and the condenser temperature (T_c), multiplied by the efficiency of a Carnot engine (η_{carnot}) working between the generator temperature (T_g) and the absorber temperature (T_a), as shown in Fig. 2.7. "W" represents the work input to the pump to transfer the solution from the low pressure absorber to the high pressure generator.

The Carnot efficiency of the heat engine (η_{carnot}) and the COP of the refrigerator (β_r) are given by

$$\eta_{carnot} = W/Q_g = 1 - (T_a/T_g) \qquad (2.1)$$

$$\beta_r = Q_l/W = T_e / (T_c - T_e) \qquad (2.2)$$

Hence, the Carnot COP of the absorption refrigerating system, defined as the ratio of the heat absorbed by the evaporator (Q_l) to the heat delivered to the generator (Q_g) is given by (Whitlow, 1976).

$$COP_{max} = Q_l/Q_g = \frac{T_e\ (T_g - T_a)}{T_g\ (T_c - T_e)} \qquad (2.3)$$

FIGURE 2.8 Pressure-Temperature-Concentration Diagram for Ideal Ammonia-Water Absorption Refrigeration Cycle

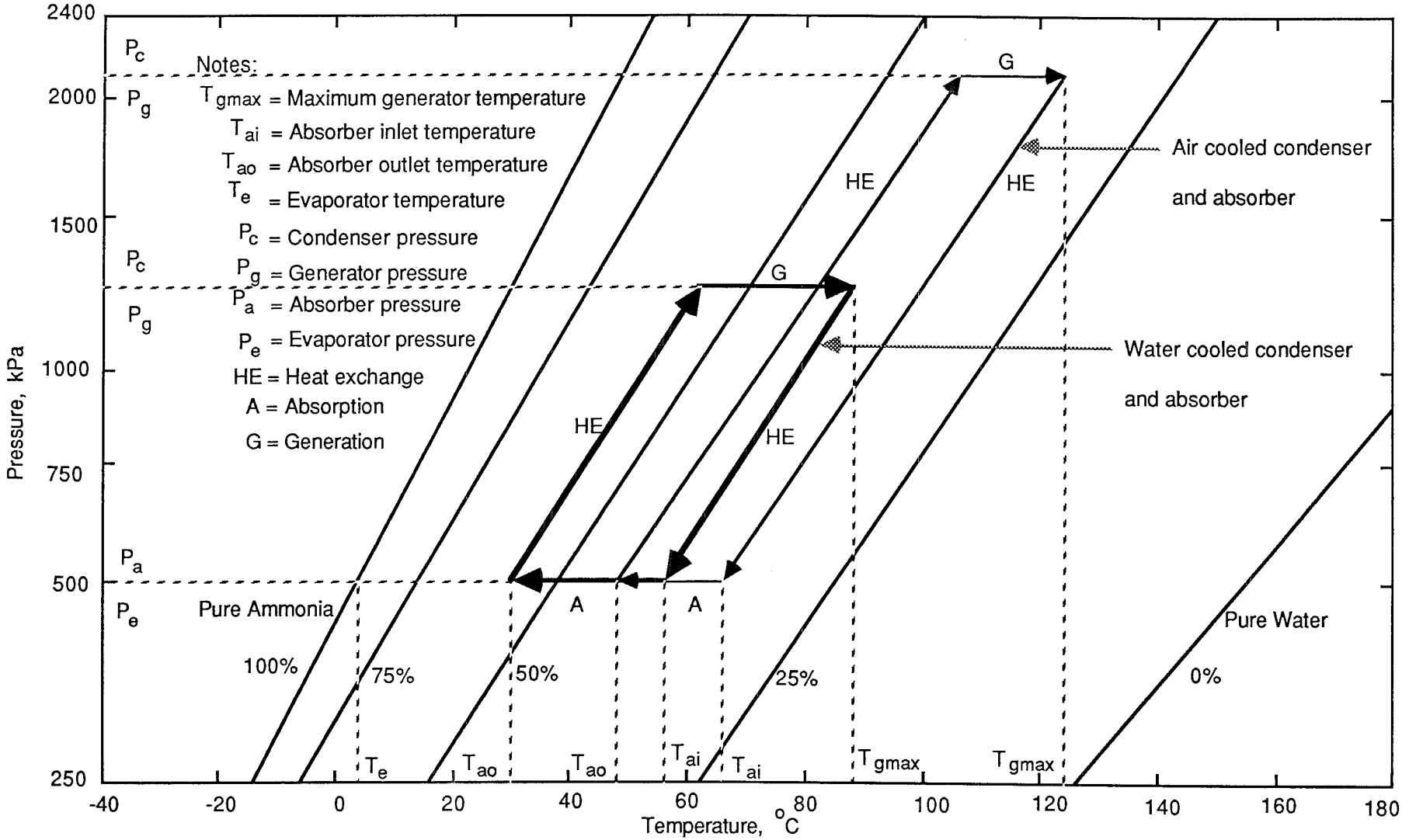

The solar COP or the actual COP is defined as the ratio of the cooling obtainable to the amount of solar energy absorbed by the collector plate.

2.2.2.1.3 Refrigerant-absorbent combinations

The starting point in the design of a solar absorption refrigeration system is the selection of a suitable refrigerant-absorbent combination. The desirable properties of a suitable combination are given by ASHRAE (1977). Hainsworth (1944) listed nearly 175 theoretically feasible combinations. Several combinations have been investigated for solar absorption systems, but the most extensively used systems are ammonia-water and water-lithium bromide systems.

2.2.2.1.4 Ammonia-water systems

The working principle of an ammonia-water system is the same as that shown in Fig. 2.6. The ideal steps in the solution cycle are shown on pressure-temperature-concentration diagram in Fig. 2.8. The pressure, in the condenser and generator, is fixed largely by the condenser fluid coolant temperature, and the temperature drops across the heat transfer surfaces in the generator, the rectifier and the condenser. The pressure in the evaporator and the absorber, is fixed by the temperature of the cooling medium to the absorber, and the temperature drop across the heat transfer surfaces in the evaporator and absorber (Duffie and Beckman, 1976).

2.2.2.1.5 System variations

The condenser and absorber can be either air cooled or water cooled, but the former requires much higher generator temperatures (Fig. 2.8). The generator temperatures for air cooling are in the range of 125° to 170°C and for water cooling they range from 95° to 120°C (Phillips, 1976).

The operation of the system can be either intermittent or continuous, depending on whether the regeneration and the cooling take place at different times or simultaneously. The intermittent systems have the interesting feature of built in storage which is useful in solar applications, but at the same time, the inventory of refrigerant and absorbent makes them very costly. Intermittent systems have been investigated by several authors including

FIGURE 2.9 Single Stage Absorption System Performance (Wilber and Mitchell, 1975)

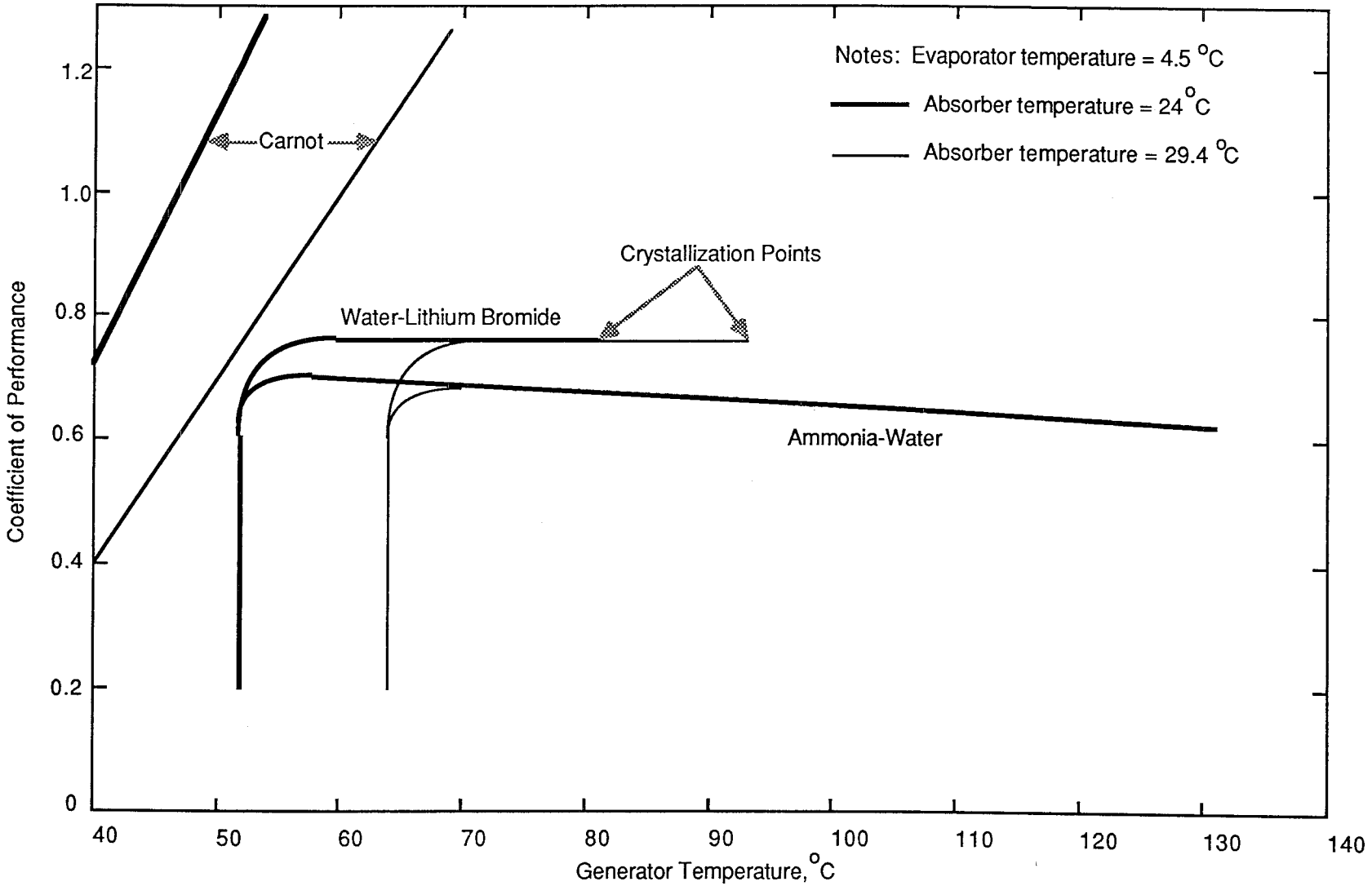

Swaminathan and Swartman (1970) and Farber et al. (1978) and continuous systems by and Dao et al. (1977) and Johnston and O'Sullivan (1981).

The system can be either a single stage or multistage. Chinnappa (1974) and Johnston (1980) investigated multistage systems. The solar loop and refrigeration loop can be either separate or combined into a single loop, in which the solar collector was also used as the generator (Farber, 1970).

2.2.2.1.6 Water-lithium bromide systems

The working principle is the same as that shown in Fig. 2.6, except that the rectifying section is eliminated, as the volatility of the absorbent (lithium bromide) is very low. The ideal steps in the solution cycle are similar to ammonia-water cycle, except for the fact that the pressures and temperatures are lower in this case. Different aspects of this system have been discussed by Sheridan (1972), Newton (1976), Picking (1979) and Grossman et al. (1979).The comparisons of water-lithium bromide and ammonia-water systems are given in Table 2.1, and in Fig. 2.9 (Anderson, 1976; Wilber and Manicini, 1976).

2.2.2.2 Vapour jet ejector systems

In the ejector cooling systems, as shown in Fig. 2.10, the solar heated fluid expands through a nozzle, providing a high momentum motive jet which entrains low pressure vapour from the flash evaporator, chilling the water in it. Although, steam is the most commonly used motive fluid, several other fluids have also been tried. The system has the advantages of simplicity, absence of moving parts, low wear and little maintenance requirements. The main drawback is low efficiency, resulting from the highly irreversible nature of the ejector. Anderson (1975) analysed a solar powered butane vapour jet ejector. Zaren et al. (1978) studied a system involving a freon jet pump and obtained COP values of about 0.2.

2.2.2.3 Thermoelectric systems

The thermoelectric refrigerator consists of two parts, (Fig. 2.11) a generator heated by solar energy, and a refrigerator to cool the space. Each in turn has a number of thermocouples. The best materials to use for the thermocouples are alloys based on

TABLE 2.1 Comparison of Ammonia-Water and Water-Lithium Bromide Systems

Ammonia-Water System	Water-Lithium Bromide System
(1) Temperatures below zero can be obtained and hence it can be used for refrigeration purposes also.	(1) Because water is used as the refrigerant, temperatures below zero can not be obtained and hence restricted to air conditioning applications only.
(2) The COP is generally lower for single stage systems (up to 0.7),though for multistage systems it can be higher.	(2) The COP is generally higher (up to 0.9).
(3) Generally air cooled and hence requires no cooling tower.	(3) Generally water cooled and hence requires a cooling tower.
(4) Rectifier is needed to avoid the carry over of the absorbent, which is water.	(4) No carry over problems as lithium bromide is a solid at the room temperature.
(5) Higher operating pressures need heavier equipment.	(5) Operating pressures are generally lower.
(6) Generator temperatures are usually higher (95° to 120°C).	(6) Generator temperatures are usually lower (75° to 95°C).
(7) As the pressure difference between the absorber and the generator is high mechanical pumps may be required, except in Electrolux systems.	(7) As the pressure difference is low vapour lift pumps may be employed.
(8) There are no problems of crystallization.	(8) Problems of crystallization can be encountered, especially at high temperatures.
(9) Ammonia can be irritant.	(9) Lithium bromide is non toxic.

FIGURE 2.10 Schematic Diagram of a Vapour Jet Ejector Cooling System

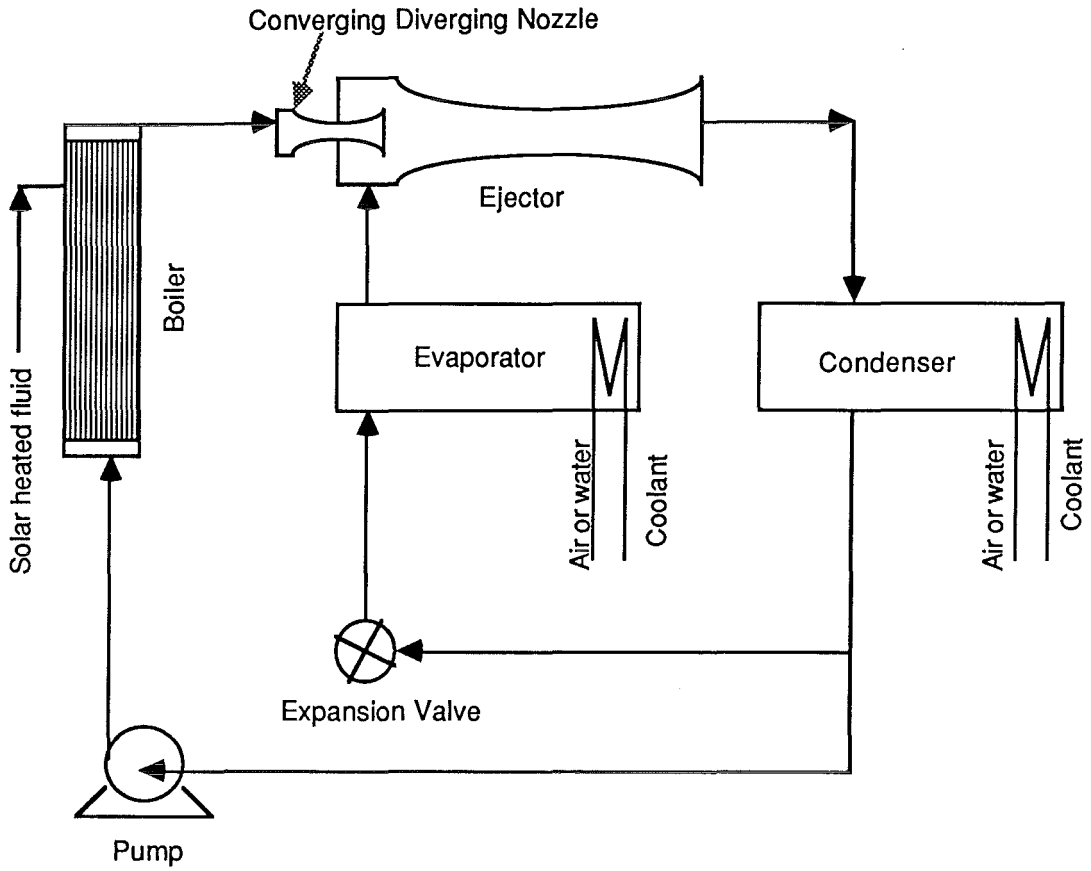

FIGURE 2.11 Schematic Diagram of a Solar Thermoelectric Refrigerator

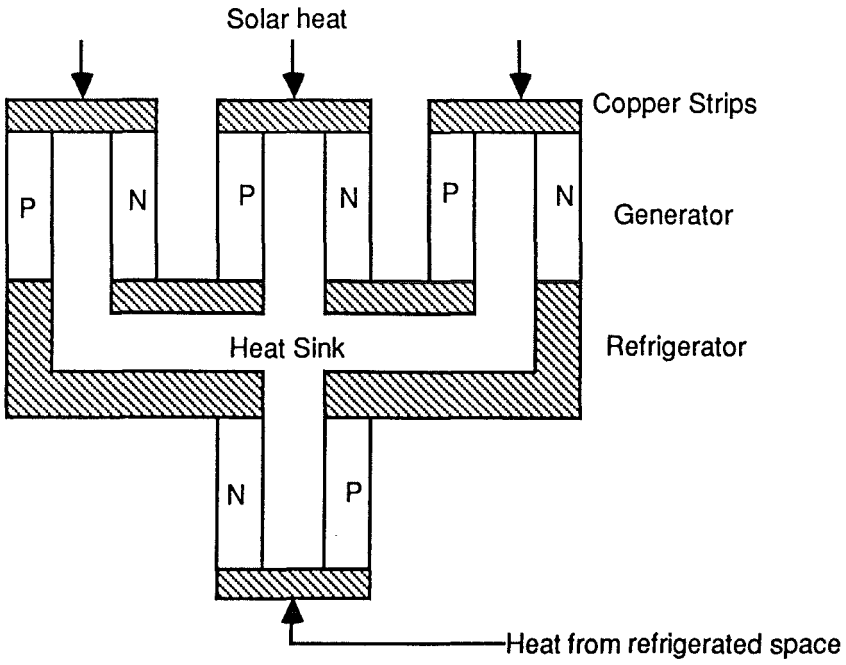

FIGURE 2.12 Solar Chemical Heat Pump System

(a) Regeneration Step

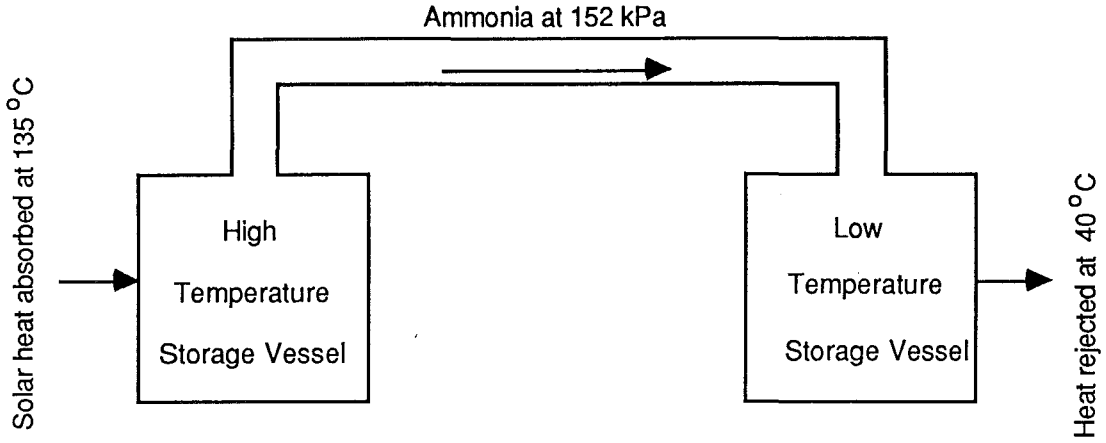

(2.4) $FeCl_2.6NH_3(s) + 52.3\ kJ/Mole\ NH_3 \xrightarrow[135\,^{o}C\ and\ 152\ kPa]{Ammonia\ at} FeCl_2.2NH_3(s) + 4NH_3(g)$

(2.5) $CaCl_2.4NH_3(s) + 4\,NH_3(g) \xrightarrow[40\,^{o}C\ and\ 152\ kPa]{Ammonia\ at} CaCl_2.8NH_3(s) + 41\ kJ/Mole\ NH_3$

(b) Cooling (or Heat Pump) Step

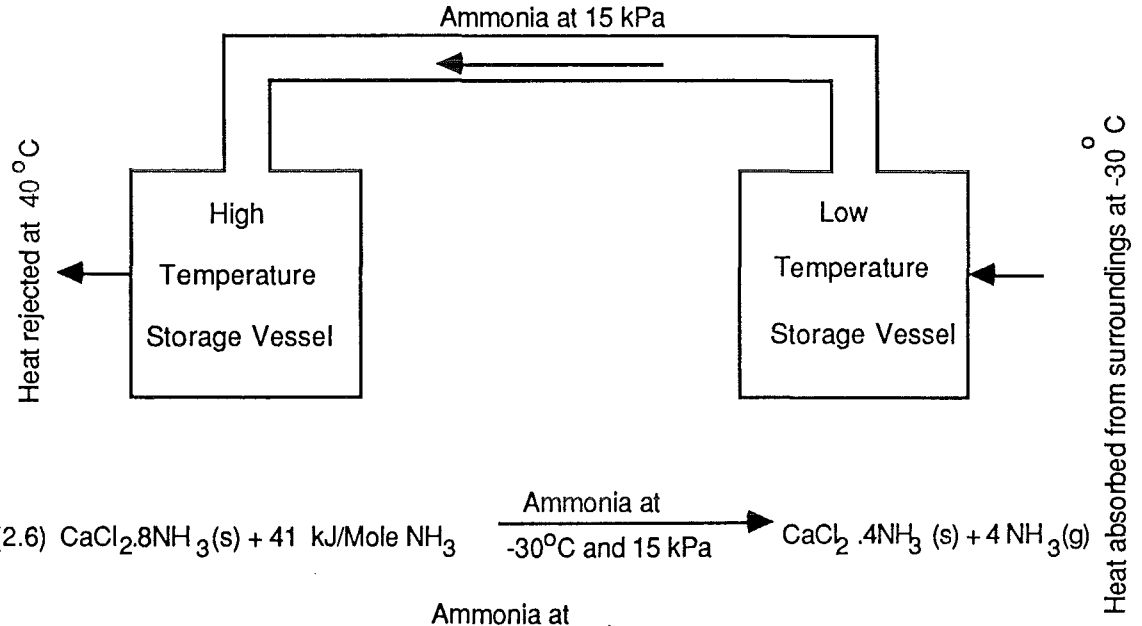

(2.6) $CaCl_2.8NH_3(s) + 41\ kJ/Mole\ NH_3 \xrightarrow[-30\,^{o}C\ and\ 15\ kPa]{Ammonia\ at} CaCl_2.4NH_3(s) + 4\,NH_3(g)$

(2.7) $FeCl_2.2NH_3(s) + 4NH_3(g) \xrightarrow[40\,^{o}C\ and\ 15\ kPa]{Ammonia\ at} FeCl_2.6NH_3(s) + 52.3\ kJ/Mole\ NH_3$

the compound bismuth telluride. Vella et al. (1976) have found that the thermocouple ratio between generator and absorber is 2-4:1.

The advantages of such systems are the absence of moving parts and refrigerant, and can operate under zero gravity. But they have very low COP values (practical COP of about 0.055 to obtain temperatures below 0°C for a temperature difference across the generator of about 40 K (Newton, 1965).

2.2.2.4 Photovoltaic/thermal systems

Solar cells convert only a fraction of the absorbed radiation to electrical energy, hence they can be used as the energy absorbing surface in flat plate collectors, so that the rest of the thermal energy can also be effectively tapped. The advantages are: the collector works as protective and mounting system for solar cells, it is less costly and requires less space than the equivalent separate collector and solar cell systems (M.I.T., 1979). The drawback is that the performance of solar cells diminishes as their temperature increases, and permanent damage can be caused at high temperatures. Hence these systems are limited to low temperature operation only. Solar cells are made from several materials, but silicon and cadmium sulphide are most commonly used and they have conversion efficiences of 15% and 6% respectively (Meinel and Meinel, 1977). Boer (1973) experimented with cadmium sulphide cells and limited the temperature of the collector to 70°C.

2.2.2.5 Chemical heat pump systems

Chemical heat pumps are distinguished from the general class of heat pumps as those which rely on chemical equilibria rather than mechanical compressors for their operation. A chemical heat pump, in principle, consists of two different reversible chemical reactions, each running at different temperatures as shown in Fig. 2.12. The reaction that runs at the higher temperature (represented by Eqs. 2.4 and 2.5) absorbs solar energy, while the reaction that runs at lower temperature (given by Eqs. 2.6 and 2.7) can be used to store and subsequently to pump out heat. The advantages of chemical heat pumps are: (a) simplicity, (b) ease of regulation, (c) lower thermal losses, (d) minimal leak problems and (e) the absence of moving parts. Hall and Howerton (1976) and

Offenhartz (1976, 1979) described such systems and an overall COP of 1.8 was claimed. Fuji et al. (1977) gave a totally different concept and showed that a chemical heat pump should consist of a three step cycle and not a two step cycle. Hydride heat pumps constitute a very important group of chemical heat pumps. Cottingham (1977) and Gruen et al. (1977, 1978) have worked on solar assisted hydride heat pumps.

2.2.2.6 Banks engine systems

This is a heat engine which exploits the crystalline transformations of a homogenous nickel titanium alloy called "Nitinol". It has two crystalline forms and at the threshold temperature it switches between these two phases. It can work at low temperatures (as low as -150°C) with small temperature differences (25° to 40°C). Banks (1974) and Hermandez (1974) report full details of the system.

2.3 Selection of the Refrigeration System

The various solar cooling and refrigeration systems discussed so far have their own advantages and disadvantages and it is difficult to say which system is the best one. A particular system has to be chosen depending on the requirements of the specific application, the overall system performance, the availability of the materials and the equipment, and finally the cost. The advantages of various systems described in previous sections may be taken as general guidelines.

Closed cycle systems are more highly developed and have several advantages over the open cycle systems (Section 2.2). Amongst the closed cycle systems the most popular ones in solar applications include absorption systems and Rankine cycle systems. The advantages of absorption systems over Rankine systems are given in Section 2.2.2.1 and absorption systems appear to be better suited for solar refigeration. Rankine systems generally need much higher temperatures as compared to absorption systems for the same cooling load. Tabor (1977) has analysed this aspect thermodynamically and concluded that, with the existing equipment the absorption systems need a heat source temperature of about 100°C, whereas the Rankine systems need about 240°C for the same overall COP. For any solar collector the efficiency decreases with increase in operating temperature. Also, high temperature

collectors are generally more expensive. We therefore decided to use an absorption refrigeration system in this investigation.

Of the various absorption systems the two most commonly employed ones are ammonia-water and water-lithium bromide systems, the comparison of which has been given in Section 2.2.2.1.7. Curran (1975), Chinnappa & Martin (1976), Mansoori & Patel (1979), Alizadeh et al. (1979) and Solar Energy Research Group (1982) have done extensive comparative studies of the two systems and found that the ammonia-water system was superior to the water-lithium bromide system in several aspects. Because solar refrigeration was the aim of the project and not solar air conditioning, the ammonia-water system was chosen.

As the development and building of a suitable absorption system for solar applications was not within the scope of the present investigation, it was decided to choose a suitable one from the several ammonia-water systems available on the market and to modify this to run it with the hot fluid from the solar collectors. A small domestic refrigerator of the "Electrolux" type was chosen, which is based on an air cooled ammonia-water absorption refrigeration cycle (air cooling was preferred as water cooling needs a continuous supply of cold water) was chosen. It uses a vapour lift pump, which does not require external power to run it; thus the only energy input to the system is the thermal energy at the generator. As the ultimate aim of the project is to use the whole unit in remote and interior areas where neither electricity nor petroleum based fuels are easily accessable, the Electrolux unit appeared best suited.

FIGURE 3.1 Working Principle of a Basic Electrolux Refrigeration System

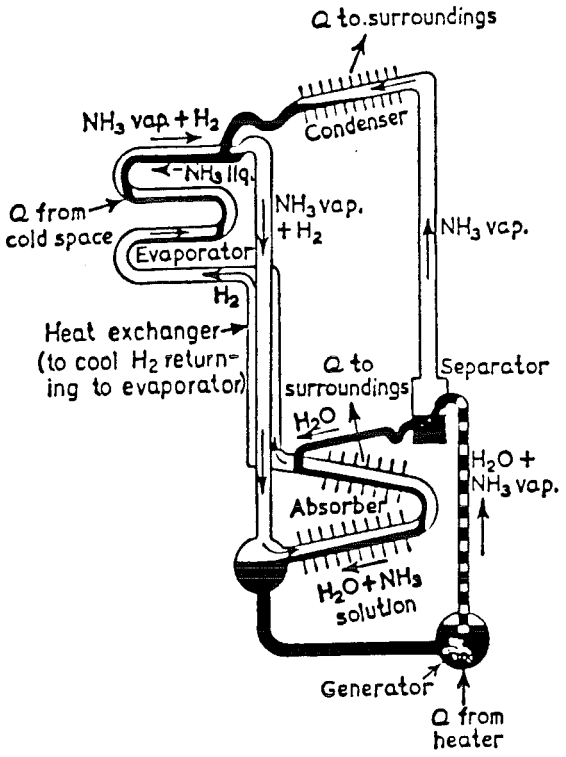

Note: Q is heat flow

CHAPTER 3

ELECTROLUX REFRIGERATION SYSTEM

Although the absorption refrigeration mechanism utilizing ammonia as refrigerant was originated in 1824 by Faraday, no commercial units without the use of pumps were built till 1925, when Carl Munters and Baltzar Von Platen invented the "Miracle" refrigerators at the Royal Institute of Technology in Stockholm. American rights were acquired from the Swedish Electrolux company by Servel, Inc. The basic system has been modified and refined since then.

This chapter describes the construction, workings and background theory of an Electrolux refrigerator, and experiments conducted with two such units, ER1 and ER2, to evaluate their performance characteristics. The modifications of the Electrolux system to operate with hot oil from the solar collector and performance evaluation of the same under normal operating conditions are described in latter sections of this chapter.

3.1 Working Principle

The working principle of a simple Electrolux refrigerator is shown in Fig. 3.1. It basically consists of the same parts as in an absorption refrigeration system described in Section 2.2.2.1.1, except that the solution pump is replaced by a thermosyphon system and a third working fluid (hydrogen) is introduced into the system. In the generator ammonia is distilled from the strong liquor which rises to the separator along with the weak liquor and then it is condensed in the condenser. The resulting liquid ammonia passes to the evaporator where it absorbs heat from the surrounding space and vaporizes in presence of hydrogen. Then the ammonia vapour and hydrogen enter the absorber from bottom, counter current to the weak liquor flowing downwards from the separator into the absorber. The resulting strong liquor flows back to the generator to complete the cycle.

FIGURE 3.2 Schematic Diagram of a Refined Electrolux Refrigerator

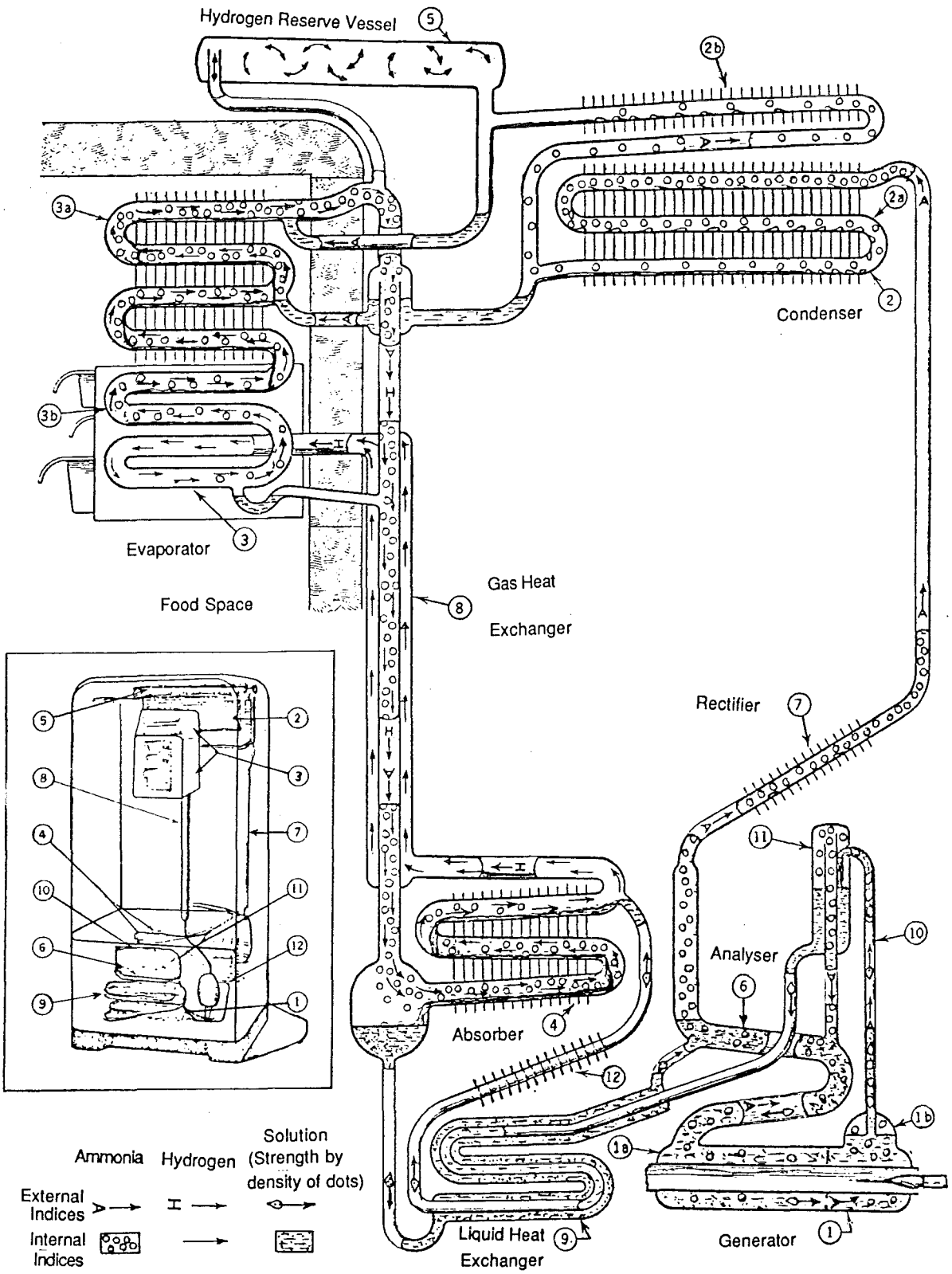

3.2 Description of the System

The schematic diagram of a refined Electrolux refrigerator is shown in Fig. 3.2 (SERVEL Inc., 1946). It is made up of a number of steel vessels and pipes welded together to form a hermetically sealed system. All the spaces of the system are in open and unrestricted communication so that all parts are at the same total pressure.

The charge includes an aqua-ammonia solution of a strength of about 30% concentration (ammonia by weight) and hydrogen gas. For a unit of sufficient capacity, for a 0.14 m^3 (140 litres) cabinet, the approximate charge is 0.5 kg of ammonia, 1.2 kg of water and 0.01 kg of hydrogen. Small amounts of dichromate are added to avoid rusting and sodium hydroxide to reduce acidity. The liquid is charged into the unit as solution and then the hydrogen gas is introduced into the system at about 1620 kPa. Hydrogen gas causes the flow of ammonia, by varying the partial pressures of ammonia in different parts of the system, but at the same time maintaining the same pressure throughout the system, which facilitates the flow of various fluids under gravity. Liquid ammonia evaporates in the presence of air or other gases, the lighter the gas, the faster the evaporation. Since hydrogen is the lightest gas and is also non-corrosive and insoluble in water, it is best suited for this purpose.

There are three distinct fluid circuits in the system (Fig. 3.3) such as: an ammonia circuit including the generator (1) condenser (2), evaporator (3) and absorber (4); a hydrogen circuit including the evaporator and absorber; and a solution circuit including the generator and absorber.

In the generator heat is applied to expel ammonia from solution. The ammonia vapour thus generated along with some water vapour flows to the condenser via analyser (6) and rectifier (7) to eliminate the water. In the analyser ammonia passes through the strong solution which is on its way from the absorber to the generator. This reduces the temperature of the vapour somewhat to condense water vapour without condensing ammonia and the resulting heating of the strong solution expels some ammonia vapour without additional heat input. The ammonia vapour then passes through the rectifier where the residual small amount of water vapour is condensed by atmospheric cooling and drains to the generator by way of the analyzer. The ammonia vapour which is still warm,

FIGURE 3.3 Fluid Circuites in an Electrolux Refrigerator

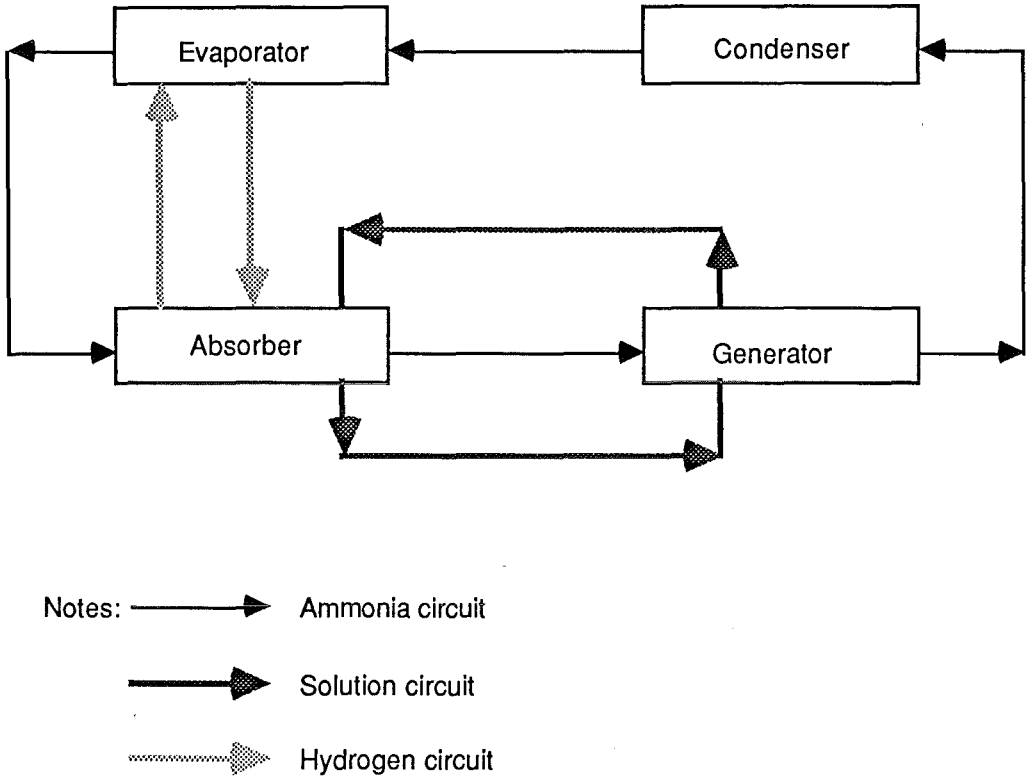

passes on to the lower section (2a) of the ammonia condenser (2), where it is liquified by air cooling. The condenser is provided with fins for this purpose. The liquified ammonia flows into the upper evaporator section (3a) via a liquid trap to avoid hydrogen. The section (3a) is provided with fins and directly cools the food space. The ammonia vapour which does not condense in the lower section 2a passes to the upper section (2b) of the condenser and is liquified and flows through another trap into the lower ice freezing evaporator section (3b).

Hydrogen gas enters the lower evaporator section (3b) and, after passing through a precooling pipe part, flows upwards, in counter flow to the downwardly flowing liquid ammonia. The effect of placing a hydrogen atmosphere above the liquid ammonia in the evaporator is to reduce the partial pressure of ammonia vapour in accordance with Dalton's law of partial pressures. Consequently the total pressure in the condenser almost equals the vapour pressure of ammonia as it contains substantially pure ammonia. Similarly, in the evaporator the partial pressure of ammonia is (substantially) less than the total pressure by the value of partial pressure of the hydrogen and this results in the evaporation of the ammonia with consequent absorption of heat from the surrounding space, which is well insulated to lessen the heat losses.

The cool heavy gas mixture of hydrogen and ammonia leaves the top of the evaporator and passes downwardly through the centre of the gas heat exchanger (8) to the absorber. In the absorber ammonia is absorbed by water, and the hydrogen, which is practically insoluble, passes upwards from the top of the absorber through the external chamber of the gas heat exchanger (8) into the evaporator. Perfect separation of gases is not possible and so it is more accurate to call the gas flowing from the evaporator to the absorber strong gas (hydrogen in strong ammonia) and call the gas flowing from the absorber to the evaporator weak gas (hydrogen in weak ammonia). Since the molecular weight of ammonia is 17 and that of hydrogren is 2, strong gas is heavier. This difference in specific weights is alone sufficient to initiate and maintain circulation between the evaporator and the absorber.

Since the absorber is below the evaporator, it is possible to have upward gas flow in the evaporator. The gas heat exchanger transfers heat from the weak gas to the strong gas. This saves

some cooling in the evaporator by precooling the entering gas. A liquid drain at the bottom of the evaporator is connected to the down flow space of the gas heat exchanger.

Counter-current flow in the evaporator permits the location of the box cooling section of the evaporator in the most effective position, at the very top of the food space. Also, the gas leaving the lower temperature evaporator section (3b) can pick up more ammonia at the higher temperature prevailing in the box cooling evaporator section (3a), thereby increasing capacity and efficiency. There is still another advantage in that liquid ammonia flowing to the lower temperature evaporator section is pre-cooled in the upper evaporator section. The dual liquid connection between the condenser and the evaporator is advantageous in applying the unit to the cabinet. It permits extending the condenser below the top of the evaporator to provide more surface while having gravity flow of the liquid ammonia to the evaporator. The two temperature evaporator partially segregates the ice freezing function from the box cooling function. This provides a better humidity condition in the food space because, due to the higher temperature of the box cooling section (though adequately low for proper preservation) and due to the reduced surface of the low temperature section permitted by the partial segregation of function, less moisture is extracted to form frost.

In the absorber, weak liquor (containing about 2% ammonia) comes in direct contact with the strong gas, flowing counter-current. The weak liquor is thus enriched while the strong gas in weakened. From the absorber, the strong solution flows through the liquid heat exchanger (9) to the analyser (6) and then to the strong liquor chamber (1a) of the generator (1). Heat applied to this chamber causes vapour to pass upwards through analyser (6) and to the condenser. The solution passes through an aperture in the generator partition into the weak liquid chambers (1b). Heat applied to this chamber causes vapour and liquid to pass upwardly through the small diameter pipe (10), as in an air or vapour lift to the separation vessel (11). This vapour lift operates on the same principle that lifts coffee to the top of a coffee percolator. Liberated ammonia passes to the condenser via the analyser, and the weak solution flows through the liquid heat exchanger (9) to the absorber. The liquid heat exchanger precools

the liquid entering the absorber and preheats the liquid entering the generator. Further precooling of the weak solution is obtained in the finned air cooled loop (12) between the liquid heat exchanger and the absorber. The heat which is liberated by absorption of ammonia in the absorber is removed by absorber fins. Some designs have a coil (containing a small quantity of volatile fluid) around the absorber with a secondary condenser (having fins) at the top, which enables advantageous positioning of the air cooled coil.

The hydrogen reserve vessel (5) which is connected between the condenser outlet and the hydrogen circuit may be described as a reservoir for hydrogen gas while the refrigerator is operating under normal room temperature conditions. Under these conditions an appreciable part of the hydrogen in the system is stored in the reserve vessel. The remainder is located in the evaporator-absorber circuit and serves to balance the condenser pressure. This pressure must be adequate to liquify the ammonia vapour in the condenser. If the pressure is increased, the efficiency under normal conditions will be impaired, and yet it is necessary to have a higher pressure in the system to ensure condensation of the ammonia under high room temperature conditions. The reserve vessel works as an automatic pressure variant to take care of variable room temperatures. When the room temperature rises and ammonia vapour fails to condense in adequate quantity, some vapour flows to the hydrogen reserve vessel, displacing the hydrogen out into the active part of the system. The ammonia vapour now in the reserve vessel corresponds to a quantity of ammonia (by weight) which was previously in solution and therefore occupied only a fraction of the space it now occupies in the reserve vessel. This displacement of hydrogen by ammonia and the redistribution of hydrogen has a double effect. The pressure in the system is increased due to the additional ammonia gas present. This results in an adequate condensing pressure at the higher room temperature. At the same time the additional hydrogen in the evaporator serves to balance the increased condenser pressure without increasing the partial pressure of ammonia in the evaporator, which otherwise would have increased the evaporator temperature. When the room temperature decreases again, the more effective condensation in the condenser causes the ammonia gas to return from the reserve vessel to the ammonia condenser and hydrogen (weak gas) flows from

the evaporator, absorber circuit into the reserve vessel. In some designs the hydrogren reserve vessel is located near the absorber with the top end connected to the condenser outlet and bottom end to the absorber.

The performance is further improved by automatic control of ammonia solution strength. In order to have higher efficiency it is desirable to have the strongest solution consistent with good operation under normal room temperature. Yet it is desirable to reduce this concentration if efficient absorption is to be obtained at high room temperatures. To accomplish this, ammonia is automatically removed from the solution and stored in the hydrogren reserve vessel as liquid ammonia. When the extreme conditions are experienced, some of the ammonia which passes into the hydrogen vessel condenses on the inner walls of the vessel and drains to the bottom. It collects at this point and is effectively removed from the active part of the system, thereby reducing the concentration of ammonia in the solution. As soon as normal conditions return, hydrogen flows into the reserve vessel and the liquid ammonia stored in the bottom of the vessel evaporates and is returned to the solution in the absorber by diffusion.

3.3 Experiments on Electrolux Refrigerator ER1

Although Electrolux refrigerators have been on the market for several decades, there is little technical information available regarding these systems. Because of the introduction of mechanical vapour compression systems the demand for Electrolux systems drastically decreased. There is substantial information available in the literature correlating the various parameter to the COP of absorption refrigeration systems utilizing pumps, but there are no equations or graphs available relating the four important temperatures (generator, absorber, condenser and evaporator temperatures), with COP of an Electrolux system. In order to modify the Electrolux refrigerator for solar operation, it is necessary to study and understand the system and the effect of the four temperatures on COP. It is also required to find out certain important operating parameters such as the optimum generator temperature and the optimum generator energy input to run the system as its maximum efficiency or maximum COP. These parameters are characteristic of each type of refrigerator and in fact they do vary substantially from one size to other even in a similar

FIGURE 3.4 Simple Aqua Ammonia Absorption Refrigeration Cycle

(Stoecker and Reed, 1971)

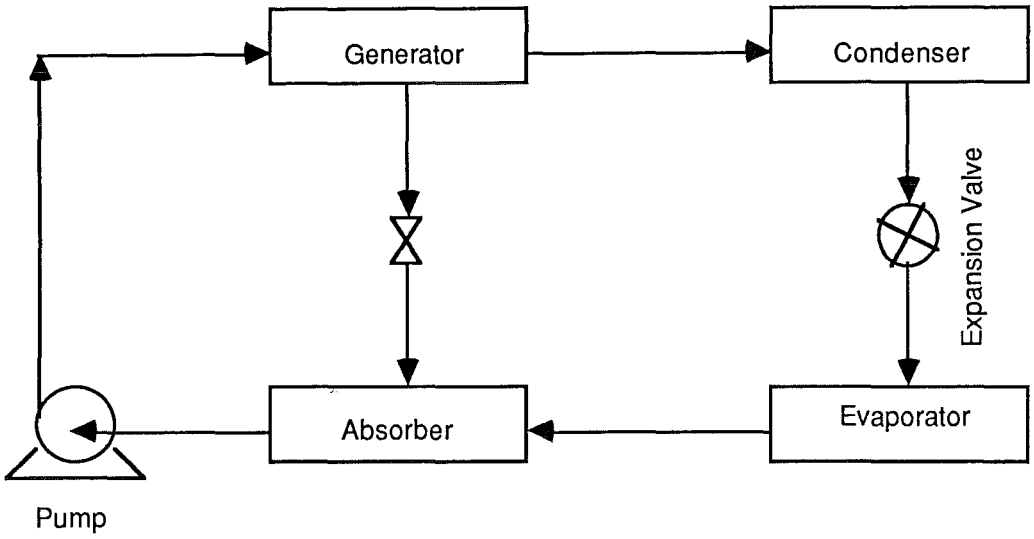

FIGURE 3.5 Refined Aqua Ammonia Absorption Refgrigeration Cycle,With Inclusion of Generator-Absorber Heat Exchanger & Rectifier

(Stoecker and Reed, 1971)

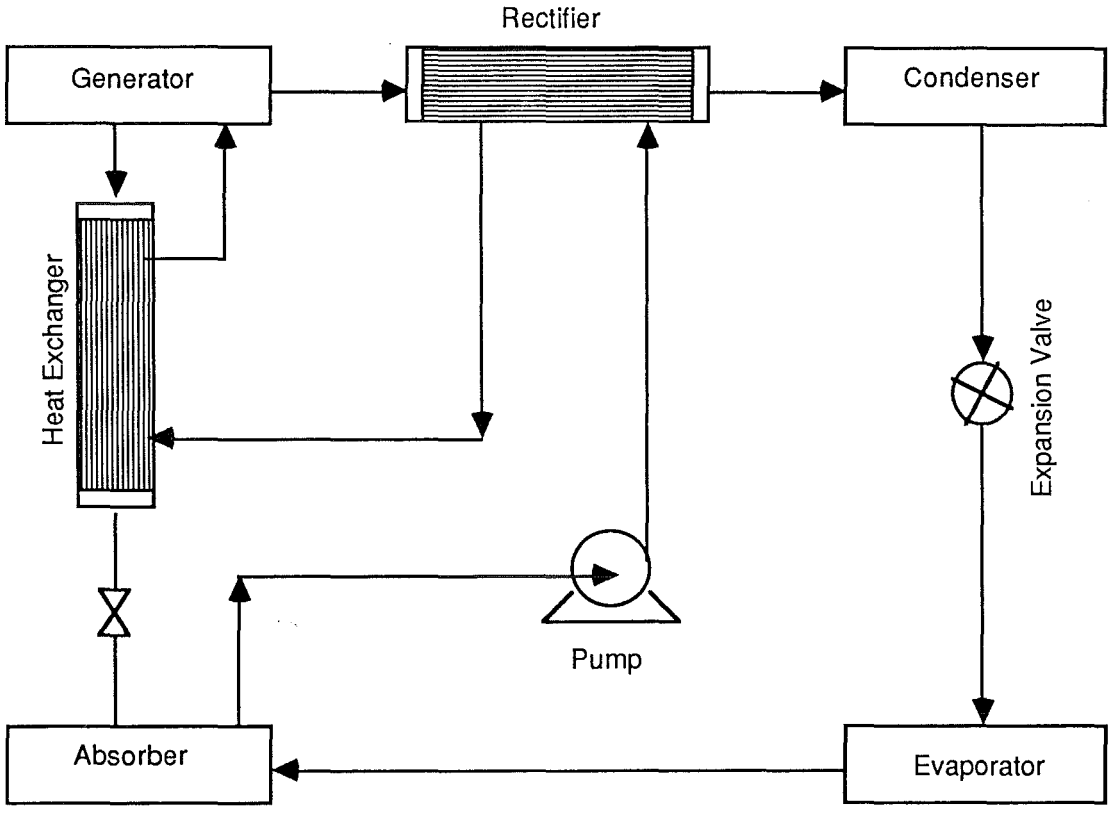

type. These variations are more prominent in the case of the Electrolux refrigerators because the performance is very closely linked with not only the design conditions, (such as ammonia concentration and hydrogen pressure) but also the construction details including the intricate piping network, positioning of components and the sizes of different parts of the system.

Before going into the details of the experiments, it would be helpful to understand the effect of various operating parameters on the COP of pumped systems and minimum generator temperature requirements of an absorption refrigeration system.

3.3.1 Effect of operating parameters on COP

The effect of operating parameters on COP of an ammonia-water system has been investigated theoretically by Stocker and Reed (1971), Satcunanathan and Kochhar (1975) and Geoola et al. (1980). The important operating variables are, the four temperatures and the solution circulation rate. The effect of solution circulation rate on COP, has been discussed by Jacob et al. (1969) and Whitlow (1971 & 1976), but is not given here because it cannot be directly controlled in "Electrolux" systems, because of the absence of the pump.

The effect of operating temperatures on COP (Figs. 3.6 to 3.10) is calculated for three different cycles. (1) Carnot cycle: the COP of which is calculated from Eq. (2.3). (2) Basic cycle (Fig. 3.4), which has very basic components. (3) Refined cycle (Fig. 3.5), which has liquid heat exchanger and a rectifier. In case of basic and refined cycles the COP is calculated from ammonia-water solution properties (IGT-AGA Tables, 1964). The base temperatures taken for these caluclations are - for generator 121°C, for absorber 46°C, for condenser 49°C and for evaporator 7°C.

The evaporator outlet temperature is assumed to be 5.5°C higher than the inlet value. This rise in temperature in the evaporator, even though the pressure is constant is due to the presence of water in the ammonia. In the refined cycle, the heat exchanger is assumed to be of fixed size, with the product of the overall heat transfer coefficient and the area as 10 $W.K^{-1}$ for a pump flow rate of 7.5×10^{-3} $kg.s^{-1}$. The base temperature of the rectifier is taken as 80°C. The effects of generator, evaporator inlet, condenser, absorber and rectifier exit temperatures on COP

FIGURE 3.6 Effect of Generator Temperature on COP
(Stoecker and Reed, 1971)

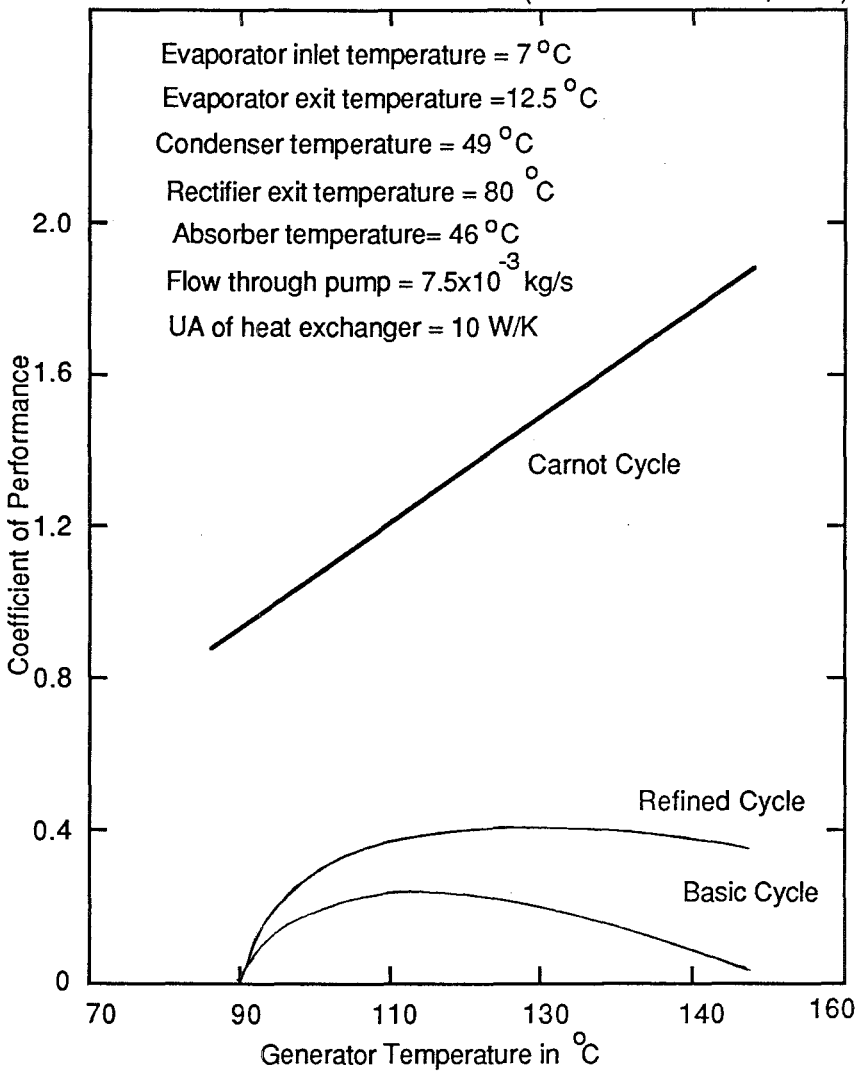

FIGURE 3.7 Effect of Evaporator Temperature on COP
(Stoecker and Reed, 1971)

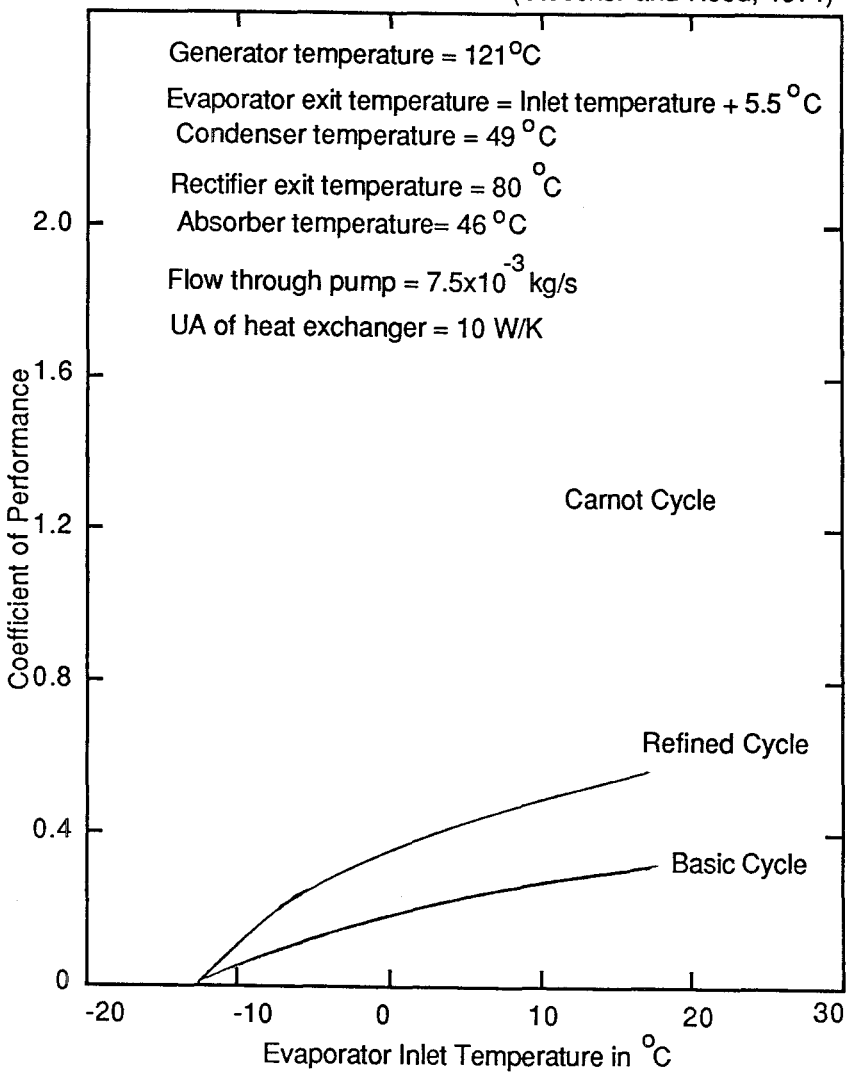

of all three cycles (except for the rectifier temperature) are shown in Figs. 3.6 to 3.10 respectively (Stoecker and Reed, 1971).

3.3.1.1 Effect of generator temperature (T_g)

In the ideal cycle the increase in T_g causes an almost linear increase in COP (Fig. 3.6). In the basic cycle, COP reaches a peak value at about 110°C. At a low T_g value the vapour that leaves the generator is rich in ammonia and this requires an elevated high side pressure. This combination of low temperature and high pressure in the generator results in ammonia rich liquid leaving the generator for the absorber. In fact, at about 90°C the liquid from the absorber has the same ammonia concentration as the liquid leaving the generator, which permits no vapour to leave the generator, thus COP drops to zero. On the right side of the peak as T_g increases the water content in the vapour leaving the generator increases, thus reducing COP. Once again as T_g approaches 140°C, the ammonia concentration in the vapour becomes 65%, burdening the evaporator with water and decreasing the low side pressure, which finally results in zero COP. In the refined cycle the same minimum exists, but COP rises more rapidly as T_g increases, because the rectifier removes water from the vapour leaving the generator and the COP is not subjected to the pronounced drop off at high T_g.

3.3.1.2 Effect of evaporator temperature (T_e)

The Carnot cycle COP increases, as T_e increases because the load on the generator decreases (Fig. 3.7) in the same way as the vapour compression cycle. The same trend can be observed with basic and refined cycles. As the T_e decreases the low side pressure also drops, the solution leaving the absorber becomes progressively more lean in ammonia such that its concentration approaches that of the liquid returning from the generator. When these two liquid concentrations equal one another, as occurs at $T_e = -12°C$, no vapour can leave the generator and the refrigeration ceases.

3.3.1.3 Effect of condenser temperature (T_c)

The Carnot cycle COP decreases as T_c increases because the sink temperature increases (Fig. 3.8). The trend is the same in the basic cycle for T_c values higher than about 45°C, but the COP

FIGURE 3.8 Effect of Condenser Temperature on COP
(Stoecker and Reed, 1971)

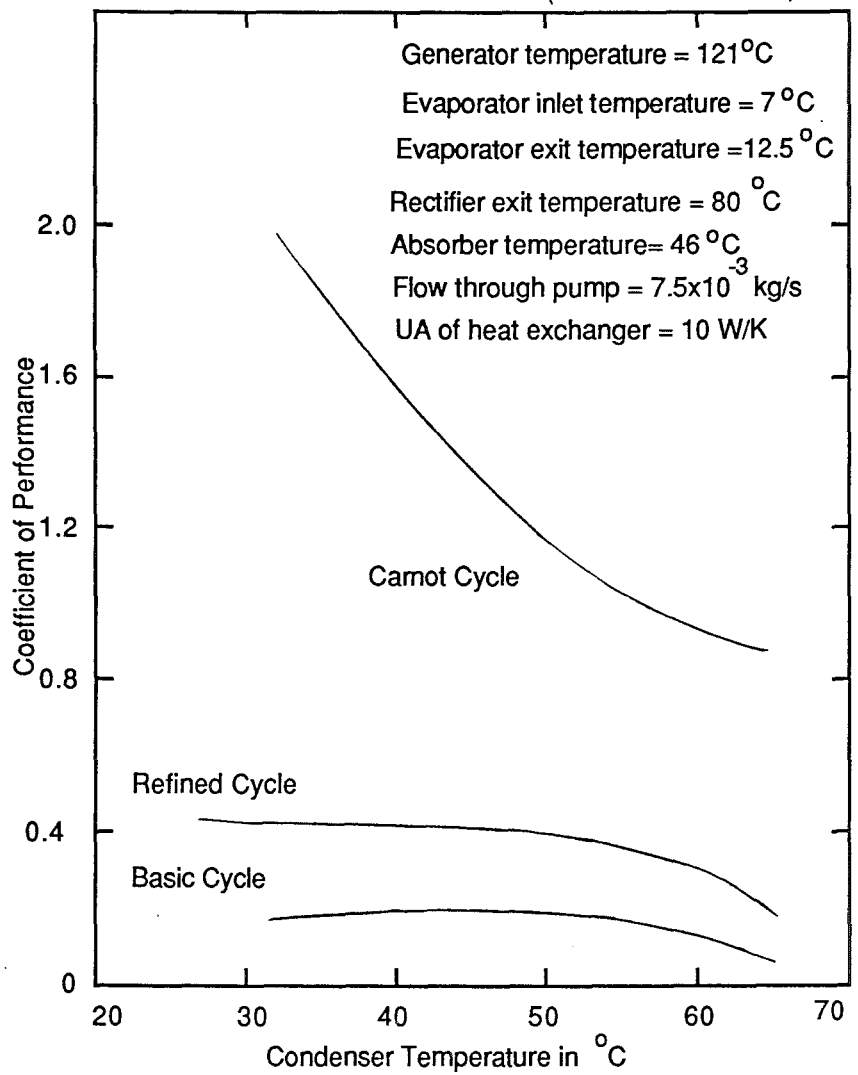

FIGURE 3.9 Effect of Absorber Temperature on COP
(Stoecker and Reed, 1971)

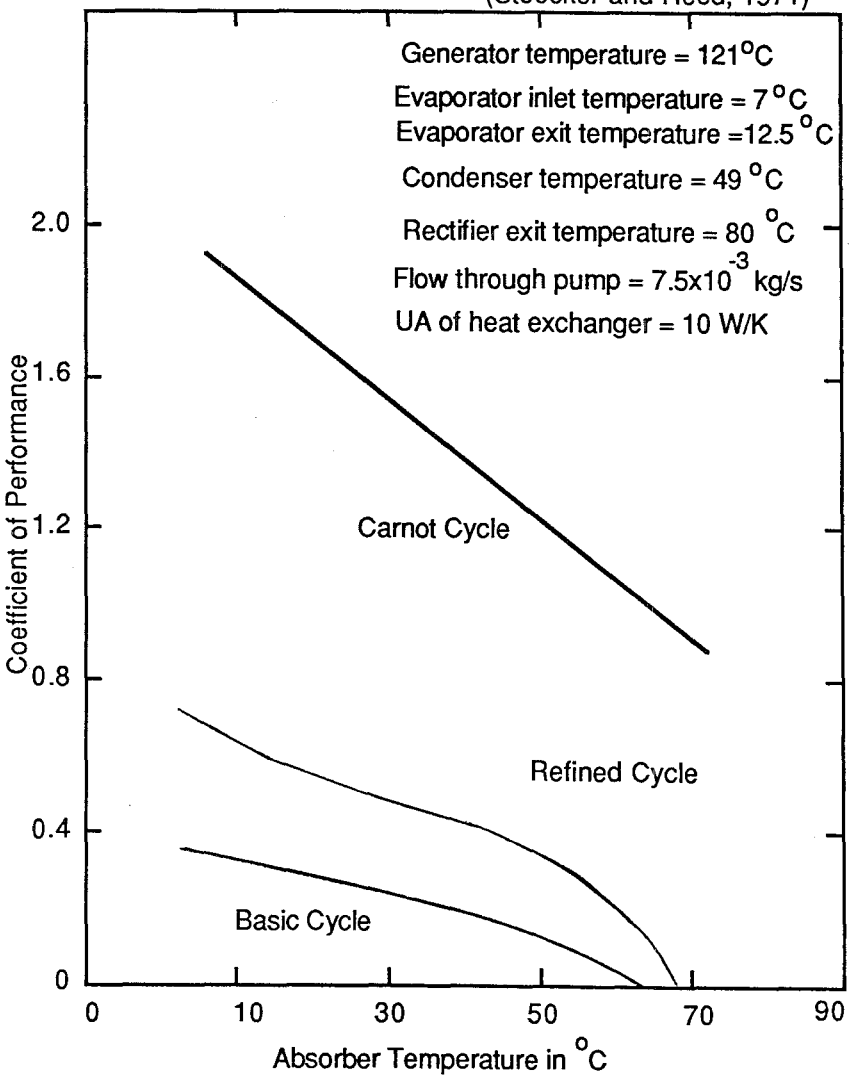

decreases slowly for T_c values lower than 45°C. The explanation for the discrepancy at low T_c is that the high side pressure drops, which, for a given T_g results in vapour leaving the generator with a high water content. The penalty for high water content is paid in the evaporator by a reduction in capacity. The drop off of COP at high T_c manifests itself in the cycle performance as elevated high pressures, which result in liquid of high ammonia concentration leaving the generator. Thus the difference in liquid concentrations entering and leaving the absorber shrinks, permitting less vapour to flow to the condenser and evaporator. In the refined cycle the reaction to the increase in T_c is fairly insensitive until T_c rises more than 55°C.

3.3.1.4 Effect of absorber temperature (T_a)

The Carnot cycle COP decreases linearly as T_a increases because the sink temperature increases(Fig. 3.9). The trends are the same in the basic refined cycles. When T_a becomes nearly 65°C, the COP drops to zero. At this condition, the ammonia concentration of the liquid leaving the absorber, equals, that entering the absorber, and the absorber is no longer capable of absorbing vapour from the evaporator. It can also be noticed from Figs. 3.8 and 3.9 that the COP is much more sensitive to T_a than to T_c. That is why the cooling water from cooling towers in large absorption refrigeration systems is directed first to the absorber, in case of a series connection.

3.3.1.5 Effect of rectifier temperature (T_r)

As T_r increases the rectifier becomes less effective in removing the water from the vapour leaving the generator (Fig. 3.10). At T_r of 121°C, there is no rectification, as it equals T_g and the increase in COP (of 0.25) over the basic cycle is solely due to the heat exchangers.

From the above discussion it is clear that in case of the refined cycle the shift in COP is more towards that of the Carnot cycle not only in magnitude, but also in the shape of the curve. The reason for discussing the performance of the basic as well as the refined cycle is that the Electrolux system lies somewhere in between the two and for a clear understanding of the system it is helpful to know both the limits.

FIGURE 3.10 Effect of Rectifier Exit Temperature on COP

(Stoecker and Reed, 1971)

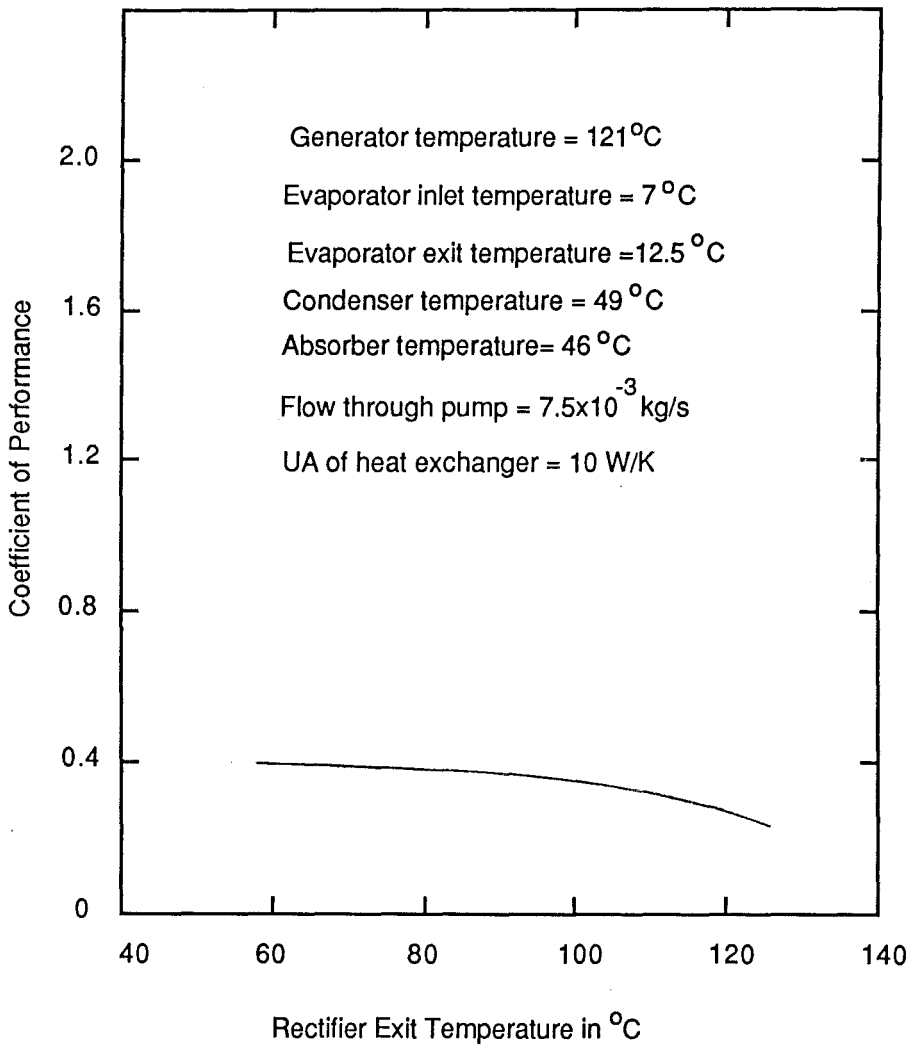

FIGURE 3.11 Minimum Generator Temperature Requirement for Ammonia-Water Absorption Refrigeration System

(Richter, 1962)

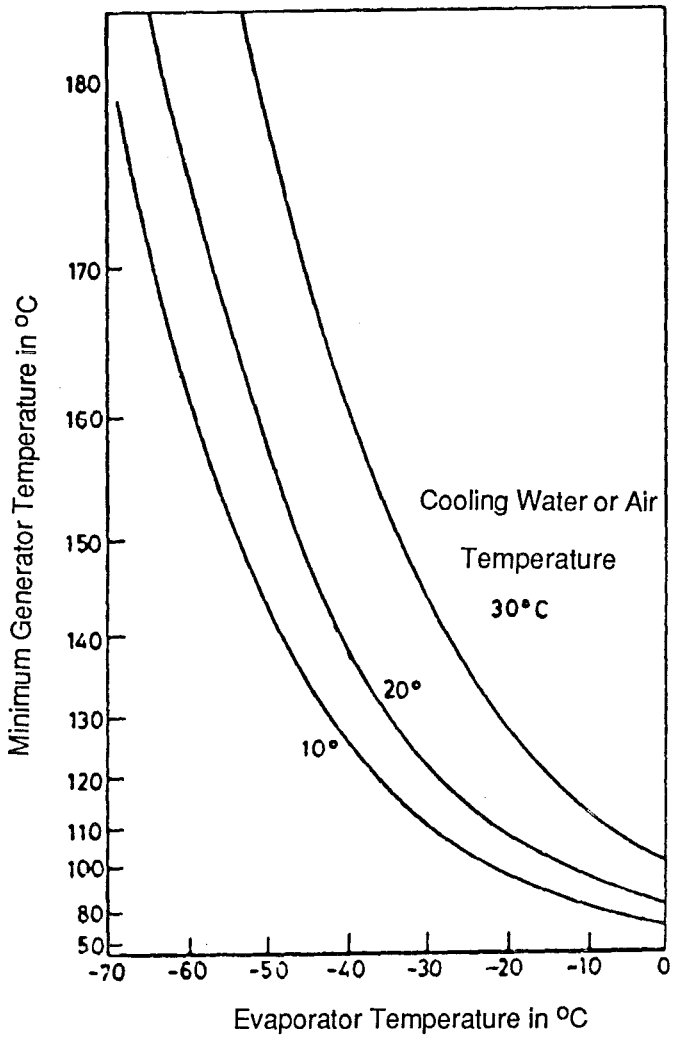

3.3.2 Minimum generator temperature requirements

It is evident from Figs. 2.9 and 3.6 that a minimum generator temperature exists for any absorption refrigeration system, below which the system ceases to operate. This minimum exists because the temperature drop from the generator temperature to the condenser temperature must be at least of the same order of magnitude as the temperature rises from the evaporator to the absorber in order for a feasible heat pumping cycle to exist. As the generator temperature goes down the ammonia vapours leaving the generator decreases, resulting in an increase in ammonia concentration of the liquor leaving the generator. At the minimum generator temperature, weak and strong liquor have almost the same ammonia concentration, thus bringing the operation to a standstill. However, this minimum generator temperature (Fig. 3.11) is a function of the evaporator temperature and the ambient temperature in air-cooled units, or the cooling water temperature in water-cooled units. The minimum generator temperature increases with either increase in ambient temperature or decrease in evaporator temperature (Fig. 3.11).

3.3.3 Description of the refrigerator

ER1 was a small portable Electrolux refrigerator obtained from COLT New Zealand Ltd. The refrigerator had external dimensions of 360 x 400 x 500 mm and internal dimensions of 280 x 320 x 420 mm with a capacity of 37.6 litres. It had 40 mm thick insulation of expanded polyurethene foam.

The schematic diagram of the refrigerator is shown in Fig. 3.12. The working principle is same as described earlier (Fig. 3.2) except that it was not as much refined. The rectification of the vapours leaving the generator and heat recuperation between different streams was very poor, as it was a small portable unit. The generator tube was attached to three tubes of the same diameter (15 mm) so that it could be heated by gas, or 230 V A.C. supply, or 12 V D.C. supply. In the present case 230 V electric supply was used. All these tubes were wrapped in 40 mm thick glass wool to reduce the heat losses.

3.3.4 Description of the experimental set up

The COP in an Electrolux system mainly depends on the four temperatures such as generator, absorber, condenser and evaporator

FIGURE 3.12 Schematic Diagram of the Electrolux Refrigerator ER1

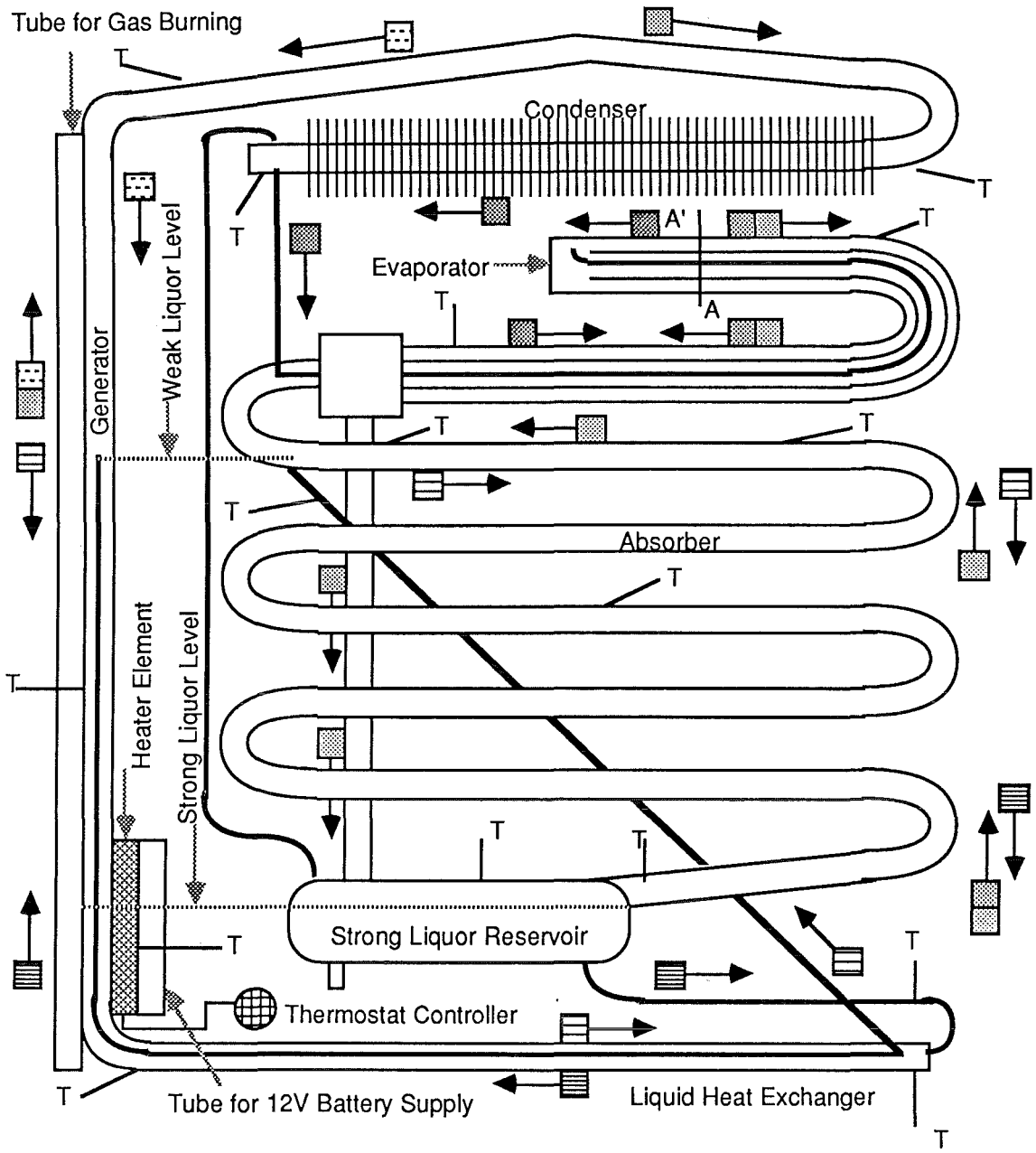

Notes:

- Strong ammonia liquor
- Weak ammonia liquor
- Liquid ammonia
- Ammonia gas
- Hydrogen gas
- Water

T = Thermocouple point

Cross Section AA'

- Hydrogen and ammonia gas
- Hydrogen gas
- Ammonia liquid
- Hydrogen gas
- Hydrogen and ammonia gas

FIGURE 3.13 Schematic Diagram of the Experimental Setup to Evaluate the Performace of the Electrolux Refrigerator ER1

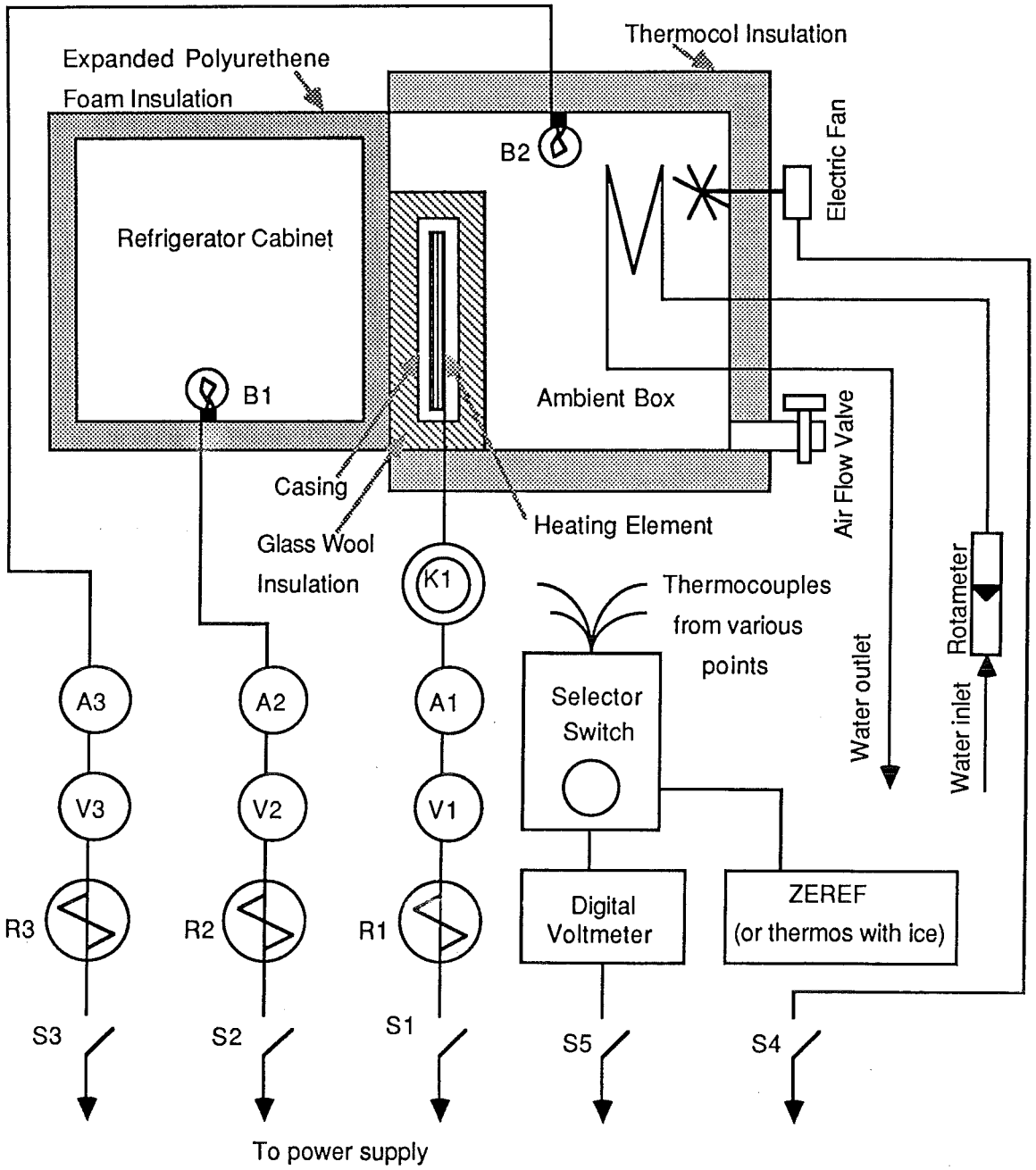

Notes: A1 to A3 = Ammeters
B1 and B2 = Electric bulbs
K1 = Kilowatt-hour meter
R1 to R3 = Rheostats
S1 to S5 = Switches
V1 to V3 = Voltmeters

temperatures. The generator temperature can be controlled directly, by the power input to the heating element. The absorber and condenser are air cooled, and so their temperatures can be indirectly controlled by the ambient box temperature only. Thus the two practical variables are the generator temperature (or more correctly generator energy input) and the ambient temperature. Hence experiments were performed changing one of these two variables each time, keeping the other constant, which would give the optimum generator temperature and the optimum generator energy input. These experiments would also throw light on the inter-relationships between the COP and the four system temperatures ann ambient temperature.

The schematic diagram of the experimental set up is shown in Fig. 3.13. The generator heating element was connected to the power supply via the switch S1, the variac R1 (to control the power input into the element), kilowatt-hour meter K1 (to measure the long term power consumption by the refrigerator), voltmeter V1 and ammeter A1 (to cross check the kWhr meter). A 15 W electric bulb B1 was located inside the refrigerator cabinet and could be used to change the inside temperature of the cabinet. The bulb was connected via the switch S2, the variac R2 (to adjust the input power), ammeter A2 and voltmeter V2 to measure the power consumed by the bulb. In order to control the ambient temperature, a galvanised iron sheet box was built at the back enclosing various parts of the refrigerator: this box will be referred to from now onwards as the ambient box. A 50 mm thick expanded polystyrene foam insulation was provided surrounding the box to reduce the heat losses. A small electric fan was provided at the top of the box for proper circulation of air inside the box.

A 25 mm diameter outlet pipe with a valve was provided at the bottom of the box through which air could flow in and out easily. Two copper tube (of 8 mm outside diameter) coils were provided, one at the top and one at the bottom of the ambient box for the removal of heat. It was found that the total length of copper tubing required was about 13 m to absorb about 100 W, this figure of 100 W being chosen because, the power consumption at 230 V supply voltage as specified by the manufacturer was 85 W and it was intended to study the system at higher voltages. The heat transfer area for the cooling coil was calculated based on the minimum temperature difference of about 6°C (between the cooling

water and the ambient box) and minimum overall heat transfer coefficient of 55 $W.m^{-2}.K^{-1}$ (Perry and Green, 1985). For effective heat transfer, a coil with 10 m long tubing was placed at the top, in front of the fan. For further temperature control, in the ambient box, an electric bulb (15 W) B2 was provided via the switch S3, the variac R3 (to control the power input), an ammeter A3 and voltmeter V3 (to measure the input power).

Several copper-constantan thermocouples were used (after calibration, as described in Appendix A1) at different locations as shown in Fig. 3.12. They were attached to various surfaces with "Araldite" at cold to moderate temperatures and silicone based glue at high temperatures. Convection and radiation losses are minimized by insulating the points (with glasswool) where the thermocouples are connected to different surfaces. Teflon coated thermocouples were used at high temperatures. All the thermocouples were connected to a selector switch. For the zero reference point a thermos flask with ice was used at first and then it was replaced with electronically controlled zero reference point instrument "Zeref" (made by Mectron Frigistor, Buck. U.K.). A digital voltmeter was used to measure the thermocouple voltages.

Later on it was decided to find out the effect of scaling down the whole room into a small ambient box. The ambient box with insulation, cooling coils, small electric fan were removed and the refrigerator with all the measuring instruments was shifted to a temperature controlled room which would be referred to as ambient room from now onwards. The ambient temperature was controlled inside the room with the help of an on-off electronic controller (or toluene-mercury contact thermometer) along with a radiative heater, fan heater, radiative cooler and a large circulating fan.

3.3.5 Experimental procedure

In order to study the effect of generator energy input and the ambient temperature, experiments were performed changing one of these two variables, while the other was maintained constant. Each time a change was made the system was allowed to come to a quasi-steady state, by maintaining the same conditions for at least sixteen hours. After the steady state was reached the thermocouple readings, the ammeter, the voltmeter, the kilowatt-hour meter, and the rotameter readings were noted down. Three mercury in glass thermometers were used (one in the refrigerator

cabinet, one in the ambient box and one in the outside environment) to cross check the thermocouple readings. The time taken for a fixed numer of revolutions, was taken for a quick check of the Kilowatt-hour meter reading. The water flow rate via the rotameter was checked, by a measuring cylinder and stop watch. The surface temperatures of the different surfaces of the refrigerator and ambient box were measured with the help of a surface thermometer probe. Silicone heat transfer grease was used to improve the contact between the surface and the probe. As the surfaces were not isothermal, several (up to 20) measurements were taken for each surface. The data were collected hourly from 9 a.m. to 5 p.m. (to even out the fluctuations), and the average value for the day was used in calculations for each variable.

In order to find the effect of generator power input, the ambient box temperature was maintained at about 30°C and the input voltage to the generator was decreased with variac R1 from 260 V to 170 V (at which voltage the refrigerator stopped working) at an intervals of 10 V. For each voltage setting several sets of readings were taken during the whole day and at the end of the day the voltage setting was changed to the next one, so that by the next day when another set of readings were taken the system would have reached steady state (or at least quasi-steady state). These runs were repeated with an ambient of 25°C.

To find the effect of ambient temperature, the supply voltage to the generator was kept constant at 230 V and the ambient temperature was varied from 25°C to 40°C at an interval of 5°C. Once again several sets of readings were taken for each ambient temperature and the average was calculated.

In order to find out the effect of scaling down the whole room into a small ambient box, the whole set of experiments (carried out with the ambient box) were repeated, after the removal of the ambient box, inside an ambient controlled room.

Several experiments were repeated to check the repeatability of the experiments. During all the experiments the thermostat attached to the refrigerator was set at such a position as to attain maximum cooling and to avoid it switching off the power supply automatically.

FIGURE 3.14 Effect of Generator Temperature on COP

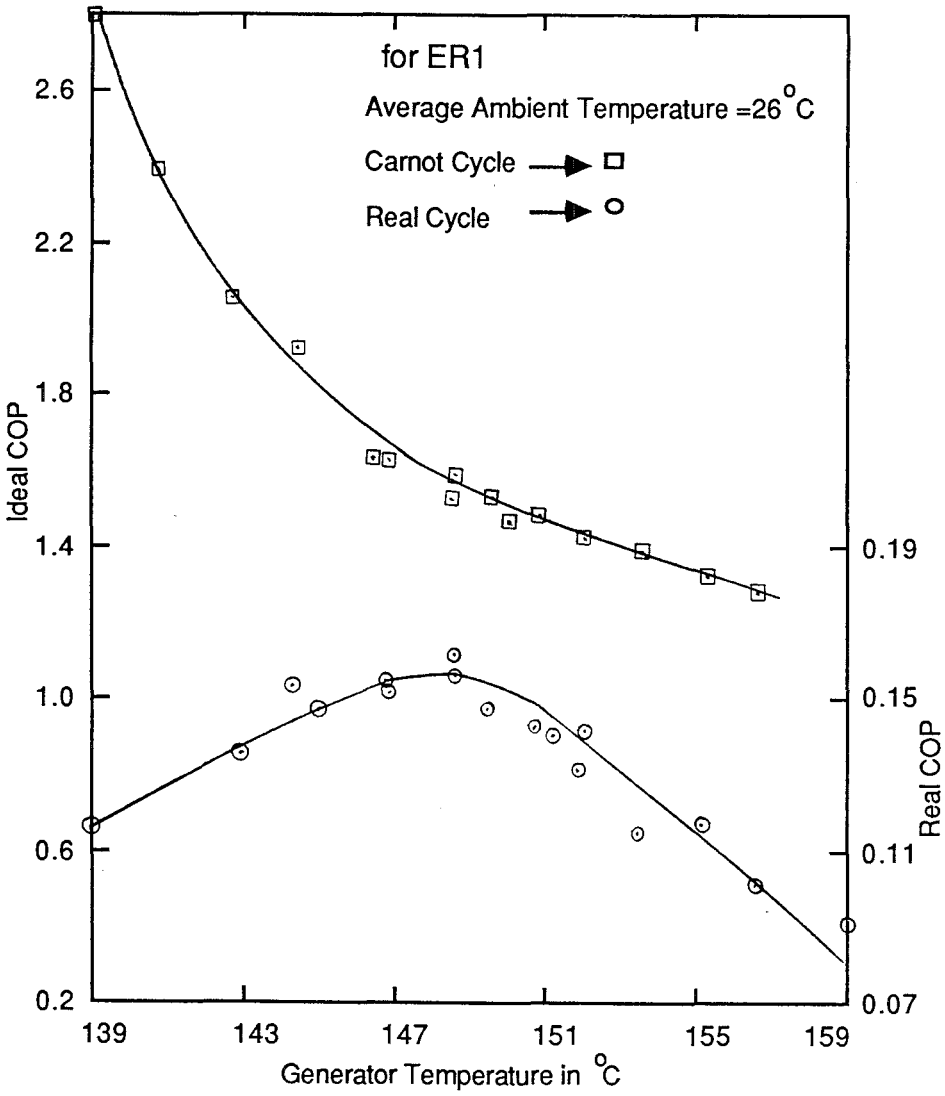

FIGURE 3.15 Effect of Generator Temperature on Cold Space and Evaporator Temperatures

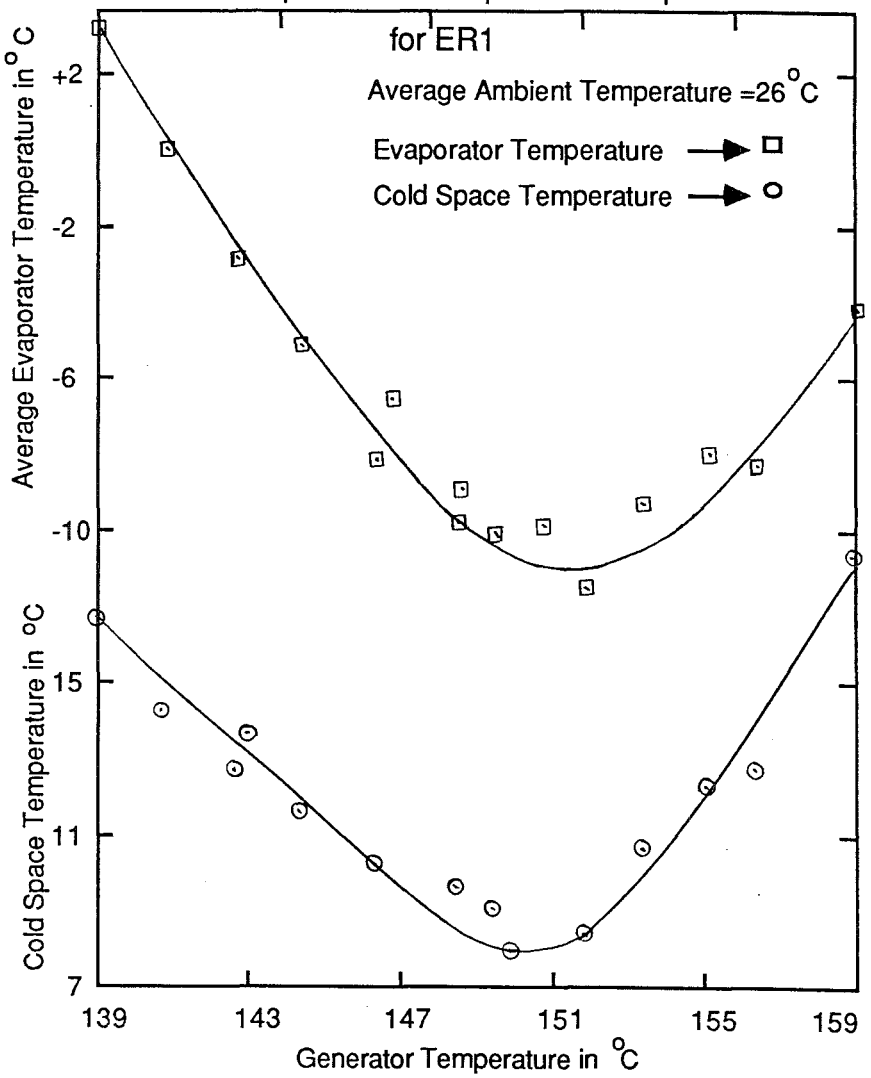

3.3.6 Calculations and results

The calculations and summary of results are given in Appendix A2. The Carnot COP was evaluated from Eq. (2.3), by substituting the appropriate measured temperature values. The real COP, defined as the ratio of energy leak Q_l into the cabinet to the total energy supplied to the generator Q_g, was evaluated from different expressions (Appendix A2.1). The experimental evaluation of U_o (necessary to evaluate the heat leak Q_l) is also given in the same appendix. The summary of results (Appendix A2.2) includes average temperatures of various parts of the system, the power input to the refrigerator, the heat leak into the cabinet, ideal and real COP values for the experiments conducted with the ambient box (at an external ambient of 30°C and 25°C) and the ambient room. These are plotted in various figures as described in the following section.

3.3.7 Discussions and conclusions

The inter-relationships between various important parameters are illustrated in Figs. 3.14 to 3.23. The results can be discussed under three headings: (1) the effect of generator temperature and generator power input, (2) the effect of various other refrigeration system temperatures and (3) the effect of ambient temperature. Before going into the details of these effects one should bear in mind the draw backs of the present experimental set up and the Electrolux system. In order to find out the individual effects of various refrigeration system temperatures on the COP, all the variables except the one under study should be maintained constant. These effects can be easily evaluated theoretically over a wide range as described in Section 3.3.1, but are difficult to find out experimentally in case of the Electrolux systems, because a change in one variable affects all other variables. One would need very elaborate arrangements to precisely control each of the system temperatures individually and this was not within the scope of the present research project.

As the Electrolux system was air cooled it posed a further problem in temperature control. Also it was difficult to place the thermocouples accurately at proper positions because, the whole system was a continuous one and there was no exact point of beginning or end of a particular part of the system (such as evaporator or condenser). It is necessary to alter the variable

FIGURE 3.16 Effect of Generator Temperature on Absorber and Condenser Temperatures

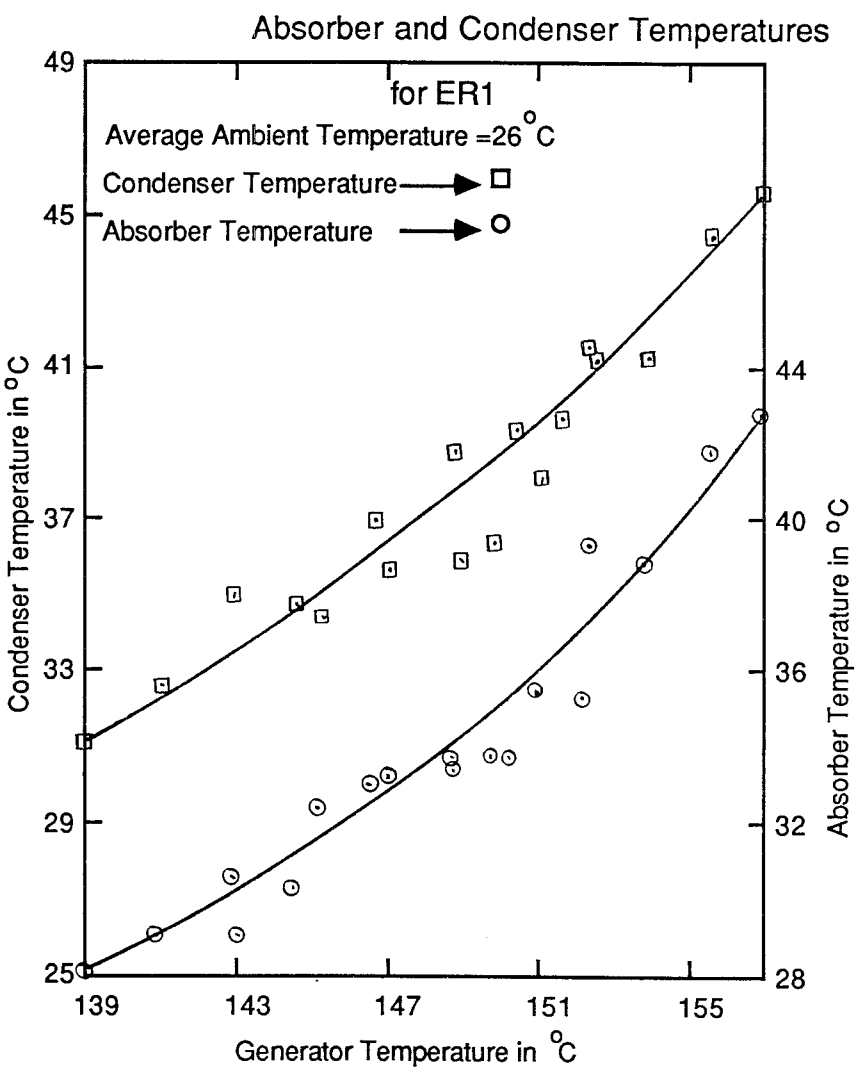

FIGURE 3.17 Effect of Generator Power Input on COP

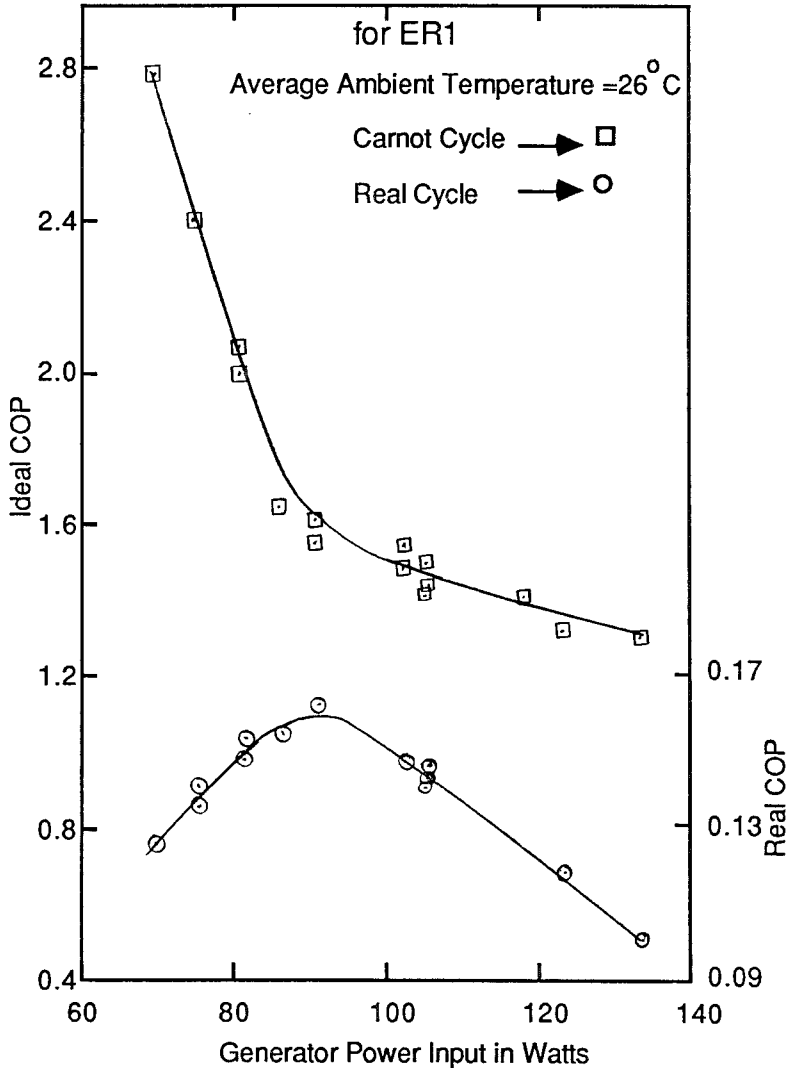

under study over a wide range (keeping others constant) in order to find any appreciable effect on other variables. However, this is not possible with the Electrolux system, for example, ER1 stopped working at generator temperatures below 139°C and above 159°C, restricting the operating range to 20°C only, whereas in the reported literature the working range is at least 70°C (Fig. 3.6).

3.3.7.1 Effects of generator temperature T_g and generator energy input P_g

These are the most important variables in the design of a solar refrigeration system. The design and performance of the solar collation system is entirely dependent on the generator temperature. The generator energy input is required in the design of the solar collection system and in linking the same with the refrigeration system. The effect of the generator temperature on the COP of the system is shown in Fig. 3.14. The Carnot COP decreases with increase in generator temperature (T_g). This trend is not in agreement with the expected trend shown in Fig. 3.6. The reason for this discrepancy appears to be increase in the condenser and the absorber temperatures with T_g (Fig. 3.16), resulting in decrease of the Carnot COP (Figs. 3.19 and 3.20).

However real COP is of main concern to us and it behaves the same way as the basic cycle (Fig. 3.6). ER1 does not have a rectifier and it is not a refined cycle and so this trend can be expected (Webb, Prasad and Williamson, 1984). Our aim was to operate the refrigeration system at its maximum real COP and it can be seen from the Fig. 3.14 that it occurs at about 150°C. So the base design temperature for the solar refrigeration system can be taken as 150°C. This fact is reinforced from Fig. 3.15 which shows the effect of generator temperature on the cold space (or cabinet) temperature and average evaporator temperature. The evaporator and the cold space temperatures attain minimum values at a generator temperature of 150°C.

The effects of generator temperature on the condenser and absorber temperatures are shown in Fig. 3.16. with increase in T_g more ammonia vapours are evolved, thus increasing the load on the condenser and absorber which in turn pushes the two temperatures upwards. At T_g value of 150°C, the absorber and condenser temperatures lie between 30° and 40°C which is not very high and

FIGURE 3.18 Effect of Evaporator Inlet Temperature on COP for ER1

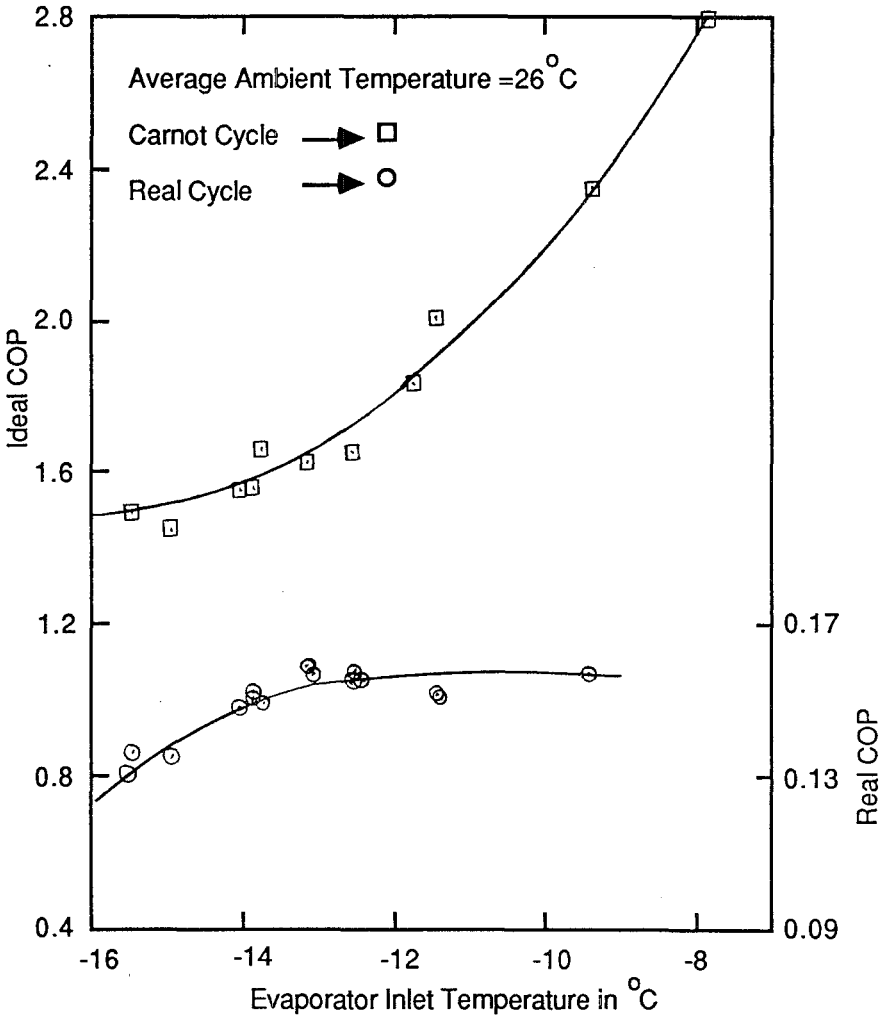

FIGURE 3.19 Effect of Condenser Temperature on COP for ER1

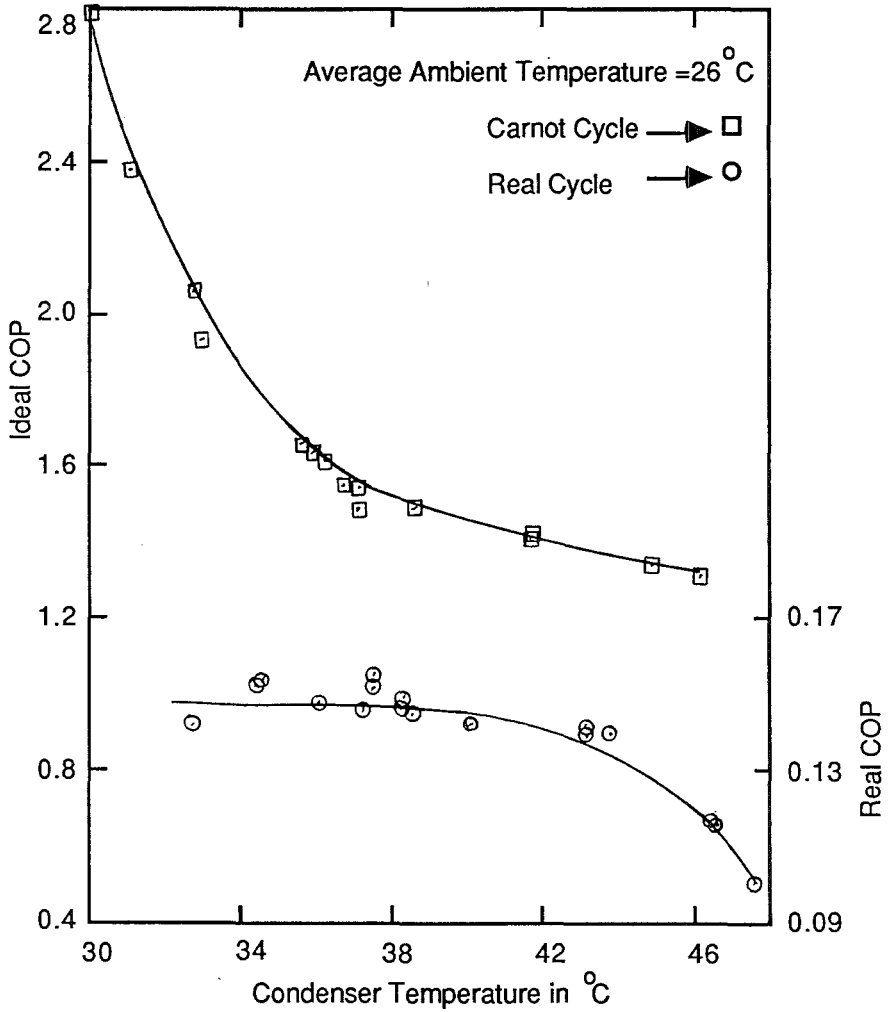

there is no need to make extra efforts to reduce these temperatures.

Fig. 3.17 depicts the trends in the ideal and real COP values with increasing generator energy input. As the generator temperature is directly linked to the energy input to the generator, the trend is the same as that shown in Fig. 3.14. The maximum real COP occurs at an energy input of about 90 W, which is quite close to the specified value (by the refrigerator manufacturers) of 85 W. This value of 90 W becomes another design parameter.

In confirmity with the theory, a minimum generator temperature of 139°C exists (Table A2.1) below which the unit stops working. This temperature corresponds to a generator energy input of 69 W and a voltage of 170 V. It can be noticed that the Carnot and real COP values in the present case are in the same range as given by Stoecker and Reed (1971) and shown in Fig. 3.6.

3.3.7.2 Effects of other refrigeration system temperatures

The effects of evaporator inlet, condenser and absorber temperatures on COP (Figs. 3.18 to 3.20) are necessary for better understanding of the refrigerator and for the design of the solar refrigeration system. These trends are as expected and can be compared with Figs. 3.7 to 3.9. The real COP and Carnot COP increase with increasing evaporator inlet temperature, but decreases with increasing condenser and absorber temperatures. Once again these figures confirm the fact that ER1 is a basic cycle refrigerator.

3.3.7.3 Effect of ambient temperature

The effect of ambient temperature on the system parameters is necessary to understand how well the refrigerator operates under different ambient conditions. As the ambient temperature increases the Carnot COP and real COP decrease (Fig. 3.21) because the absorber and condenser temperatures increase rapidly with ambient temperature. With the increase in ambient temperature all the refrigeration system temperatures increase. It can also be noticed that the gradients of these curves also increase with ambient temperature. Although the generator energy input is constant, the generator temperature increases because the losses from the

FIGURE 3.20 Effect of Absorber Temperature on COP for ER1

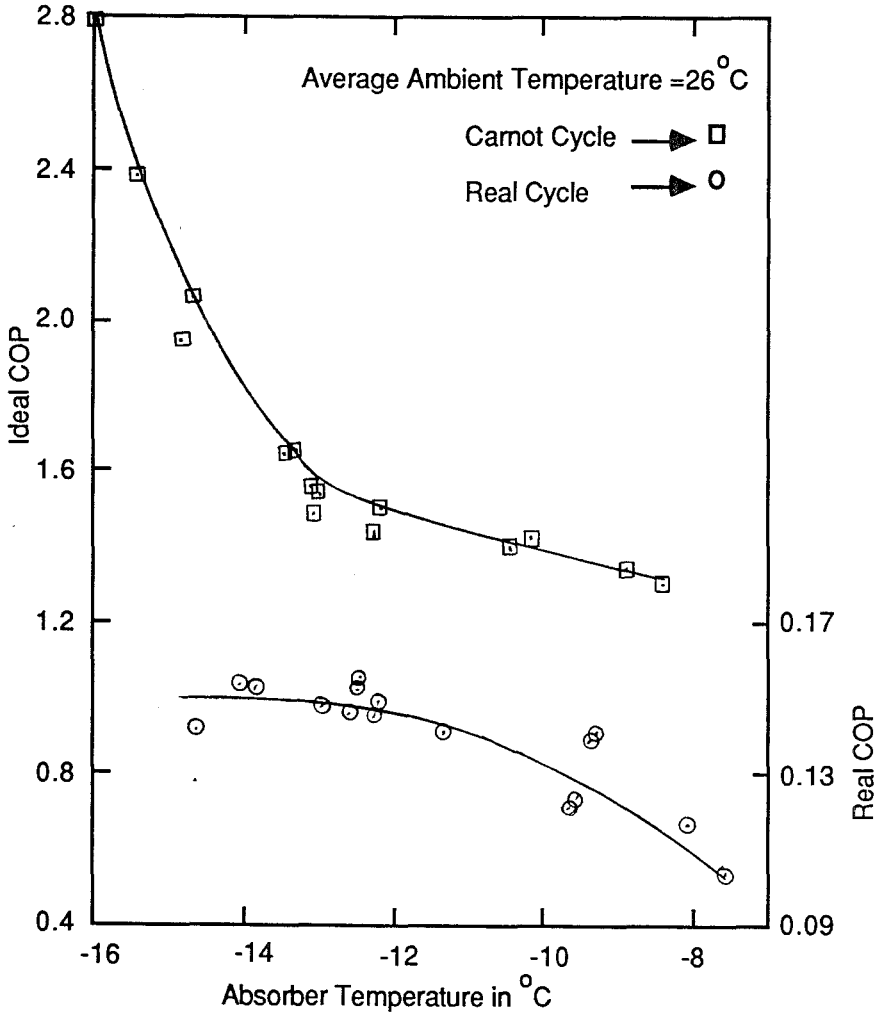

FIGURE 3.21 Effect of Ambient Temperature on COP for ER1

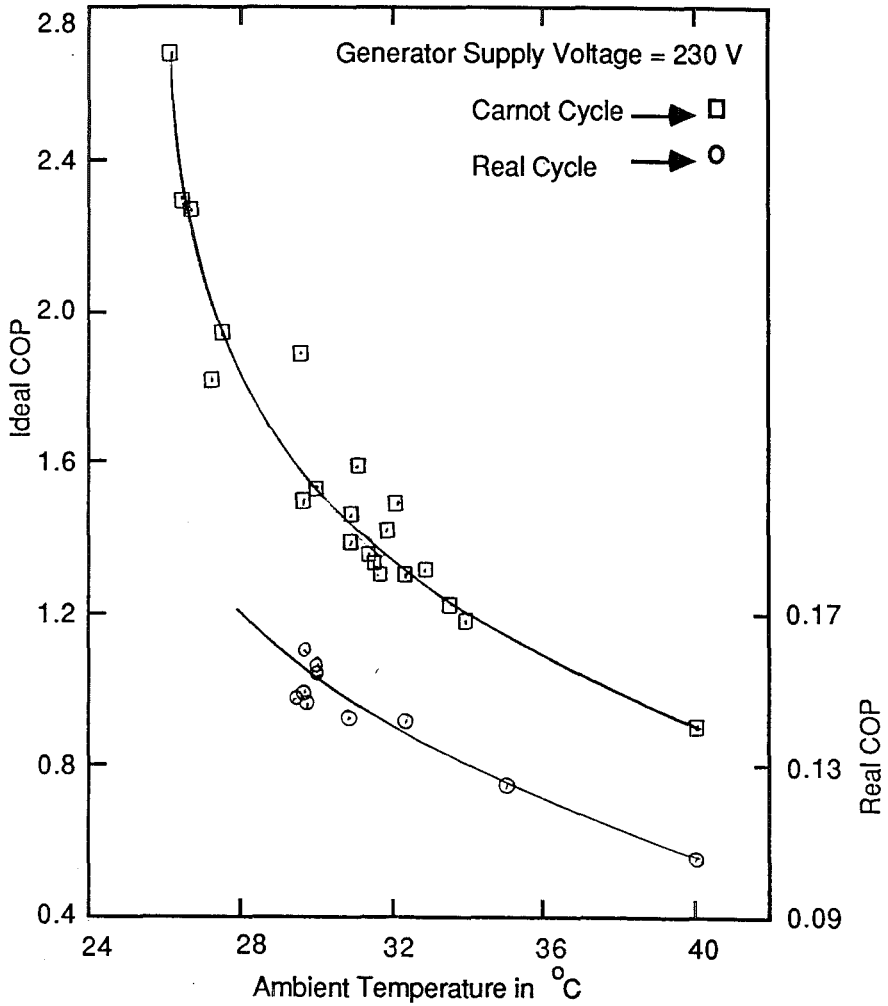

FIGURE 3.22 Effect of Ambient Temperature on Various Other Temperatures of the System for ER1

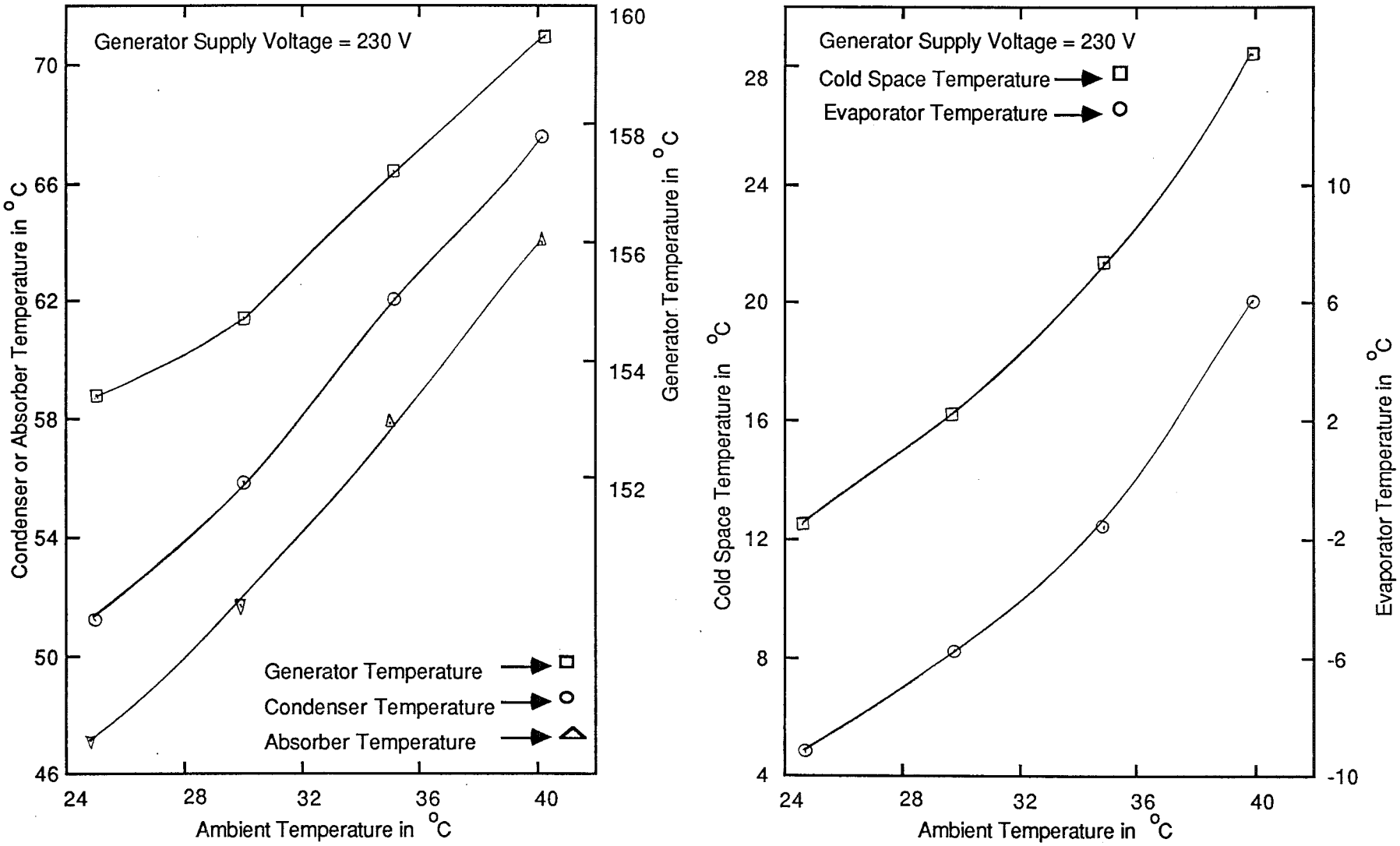

generator-heater element combination decreases with increase in ambient temperature (Fig. 3.22).

The effect of enlarging the ambient box into the ambient controlled room is illustrated in Fig. 3.23. On comparison of this figure with Figs. 3.15 and 3.16, it can be observed that the trends remain same in both cases. However it can be noticed that the condenser and absorber temperatures are substantially higher in the case of ambient controlled room. The main reason for this discrepancy arises from the fact that there was substantial radiation heat losses from the condenser and the absorber to the cooling coils, in the case of the ambient box. The ambient box was quite small and the surface area of the absorber and condenser were much less, as compared to the surface area of the cooling coil. Hence the absorber and condenser could mainly "see" the cooling coil which was at much lower temperature and this resulted in higher radiation losses from the condenser and the absorber. Also the condenser and evaporator temperatures are less in the case of the ambient box because the external ambient temperature was lower than the ambient box temperature, which resulted in lower heat leak into the refrigerator cabinet as compared to the situation where the whole system was exposed to higher temperature (as in the case with the ambient controlled room). Another reason for this discrepancy is that Fig. 3.23 represents the situation for 30°C ambient temperature while Figs. 3.15 and 3.16 are for 26°C ambient box temperature and hence the system temperatures are lower in the latter case.

It was found that the ambient box had some more disadvantages other than the radiation exchange between the absorber/condenser and the cooling coil. The box was small and, as well as the temperature control being difficult it was found that the temperature was not very uniform within the box. One of the main reasons for this was that the fan which was heated up due to continuous usage. However, it was verified with the ambient controlled room that the final predictions remained more or less the same.

3.4 Experiments with Electrolux Refrigerator ER2

The experiments with ER1 revealed the inter-relationships between various system temperatures, ambient temperature and COP. It was also observed that the optimum generator temperature was

FIGURE 3.23 Effect of Generator Temperature on Various Other Temperatures of the System in Ambient Controlled Room

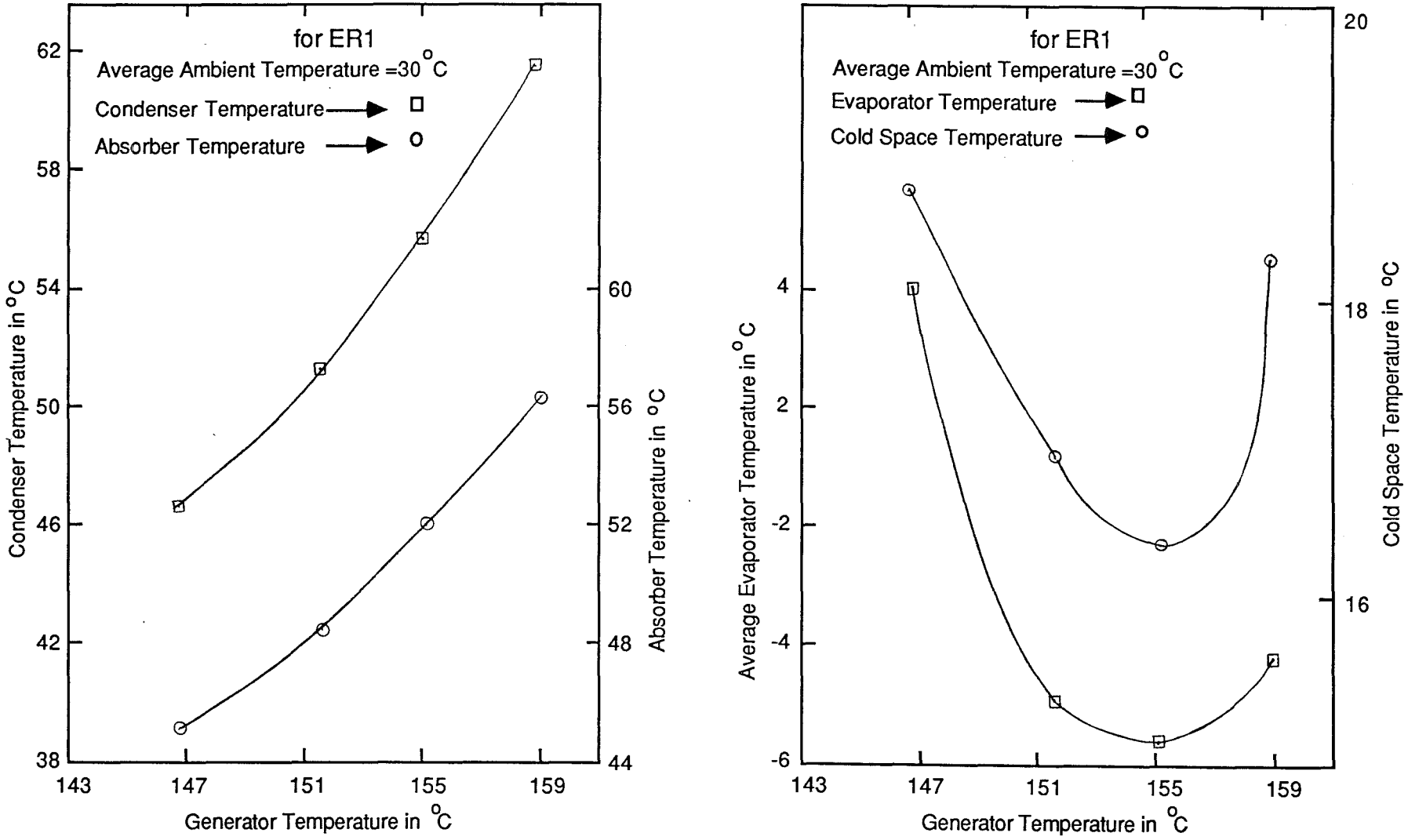

150°C (from Figs. 3.14 and 3.15) and the corresponding energy input to the heating element was 100 W (Table A2.1) for ER1. The lowest temperatures observed for the refrigerator cabinet and the evaporator were 8.4°C and -11.8°C respectively (Fig. 3.15). When the evaporator temperature was -11.8°C, the freezer temperature should be more than -11.8°C. However, no measurements of the freezer temperature could be made as there was no seperate freezer compartment in ER1. The cabinet temperature of 8.4°C is also substantially higher than the usual value of 4°C typical for a general household refrigerator.

The highest real COP obtained (Fig. 3.14) was 0.16, which was quite low. For succesful operation of the unit it would be necessary to pump in continuously 100 W of energy into the ammonia liquor in the generator tube. The area of the generator tube available for heat transfer was extremely small (only 0.005 m^2) and it was not easy to increase this area. The heating element tube external temperature was about 200°C, corresponding to the generator temperature of 150°C (Table A2.1). The temperature difference of 50°C could be easily obtained with the help of an electric heating element in ER1. However, in the solar appliances such large temperature differences were unacceptable because the collector efficiency falls with increasing operating temperature.

Hence it was necessary to search for another Electrolux refrigerator which would operate at acceptable values of freezer and cabinet temperatures (below 0° and 4°C respectively), at lower generator temperatures, lower energy input to the generator and high real COP values as compared to ER1. In order to make sure that other units do possess advantages over the existing unit, measurements were made with an unit in regular use at a house. It was observed that much lower freezer and cabinet temperatures could be obtained with more or less the same amount of energy input, even though the size of the refrigerator was nearly twice the present one. Hence another unit was purchased for further experimentation.

3.4.1 Description of the refrigerator

ER2 is similar to ER1, except that it is nearly twice as big. The external dimensions of the refrigerator are 915 x 550 x 590 mm and internal dimensions are 705 x 400 x 300 mm, with a capacity of 84.6 litres. It has glass wool as insulation material the

FIGURE 3.24 Schematic Diagram of Electrolux Refrigerator ER2

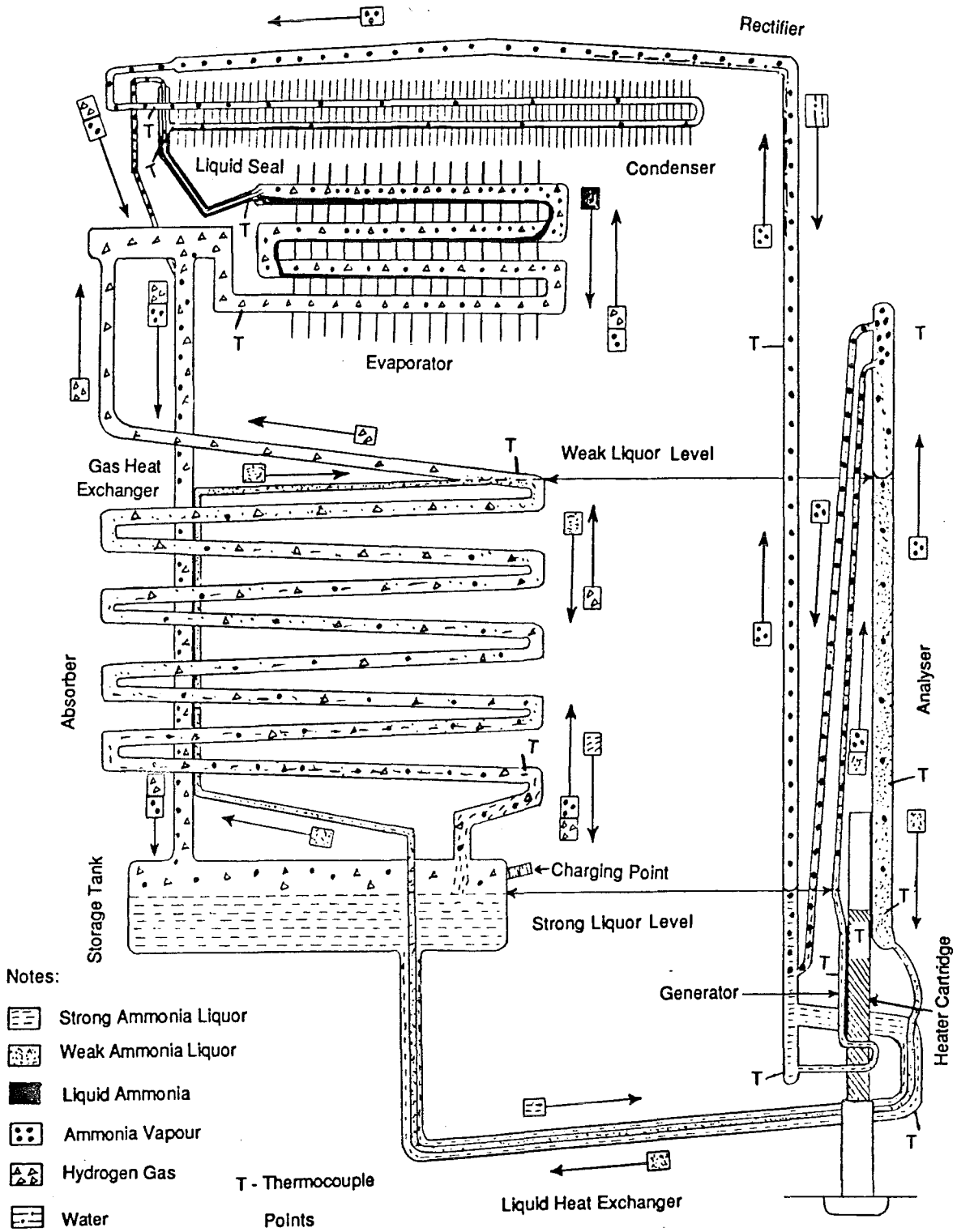

thickness of which is 75 mm on all sides except the back with 120 mm and the front door with 40 mm.

The schematic diagram of the refrigerator is shown in Fig. 3.24. On comparison with Fig. 3.12, it can be clearly noticed that ER2 is a more refined unit than ER1. The main difference is that ER2 has an analyser which should improve its performance over ER1. The working principle of ER2 is same as described in Section 3.1.

The Plate 1 shows the Electrolux refrigerator ER2. The back view of the refrigerator without any insulation (with a few thermocouples) on the generator tube assembly is shown in Plate 1a. The front view with the door open is shown in Plate 1b, which also shows the hygrothermograph, an electric bulb and a digital thermometer used with the performance evaluation of ER2.

3.4.2 Description of the experimental set up

The schematic diagram of the experimental set up is shown in Fig. 3.25, which is similar to that of ER1 (Fig. 3.13). A voltage regulator was added to the circuit to avoid voltage fluctuations. The ambient temperature inside the room was controlled with a 1 kW bar heater (as base heater), 1 or 2 kW fan heater (as controlled heater) and a temperature controller. An electric fan was used for uniformity of the ambient temperature. The freezer temperature was measured with the help of a digital thermometer. The cabinet and ambient temperatures were recorded by hygrothermographs. These temperatures were also checked by mercury-in-glass thermometers. Copper-constantan thermocouples were attached to various surfaces as shown in Fig. 3.24. The thermocouple readings were measured with a digital voltmeter.

3.4.3 Experimental procedure

The same procedure as described in section 3.3.5 (with ER1) was followed. It was found that the overall heat loss coefficient varied substantially with temperature drop. Hence, several readings were taken at different temperature drops (obtained by varying the power input to bulb B1 shown in Fig. 3.25 and maintaining constant ambient temperature) and the heat loss coefficient was calculated in each case. The other calculations were done in the same way as with ER1 and the summary of results are given in Appendix A2.2, which are shown in Figs. 3.26 to 3.29.

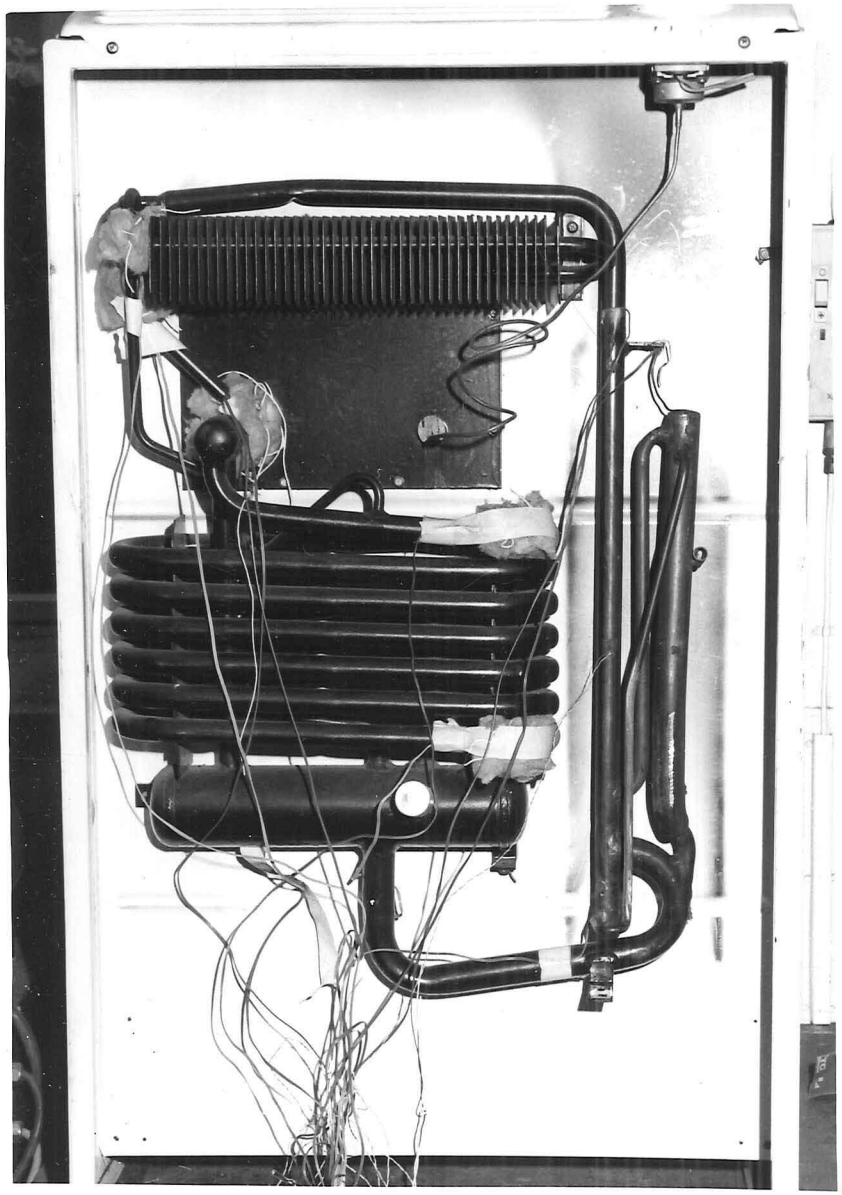

(a) Back View

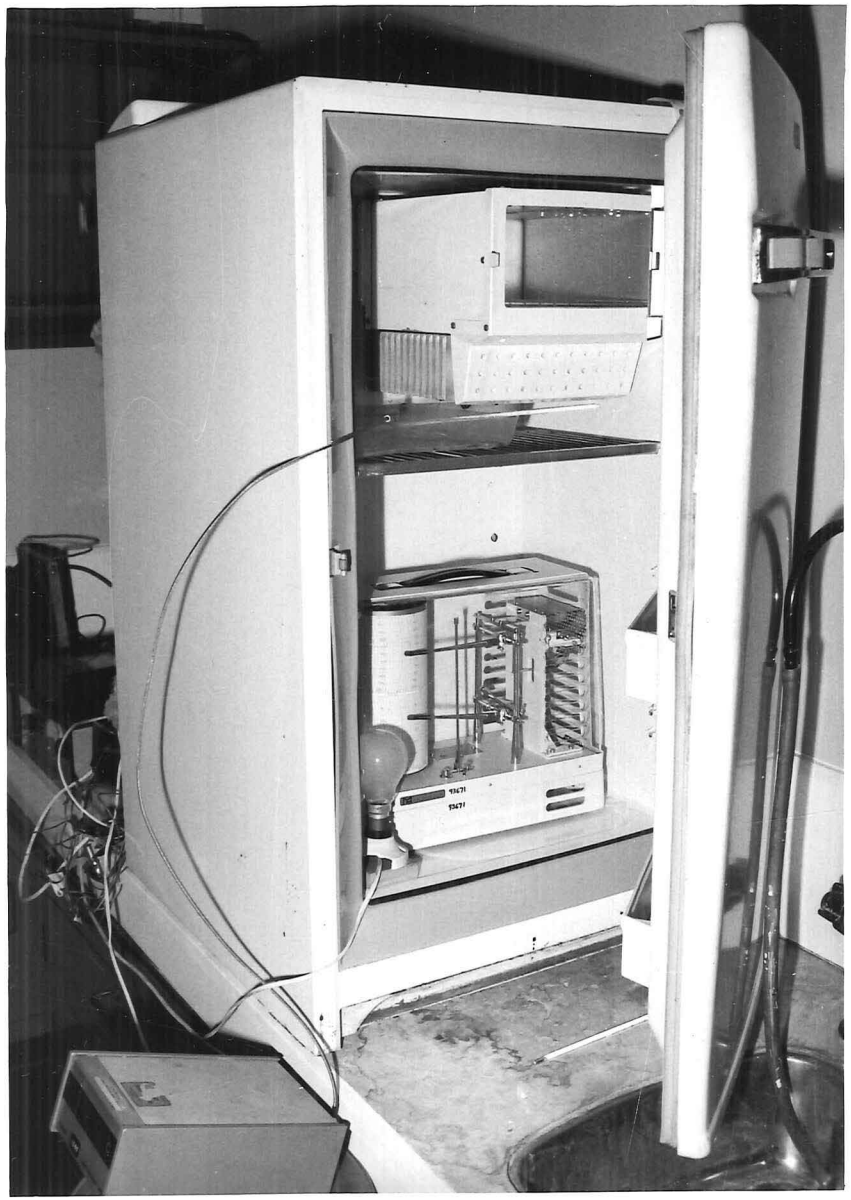

(b) Front View

PLATE 1 Electrolux Refrigerator ER2

FIGURE 3.25 Schematic Diagram of the Experimental Setup to Evaluate the Performance of the Electrolux Refrigerator ER2

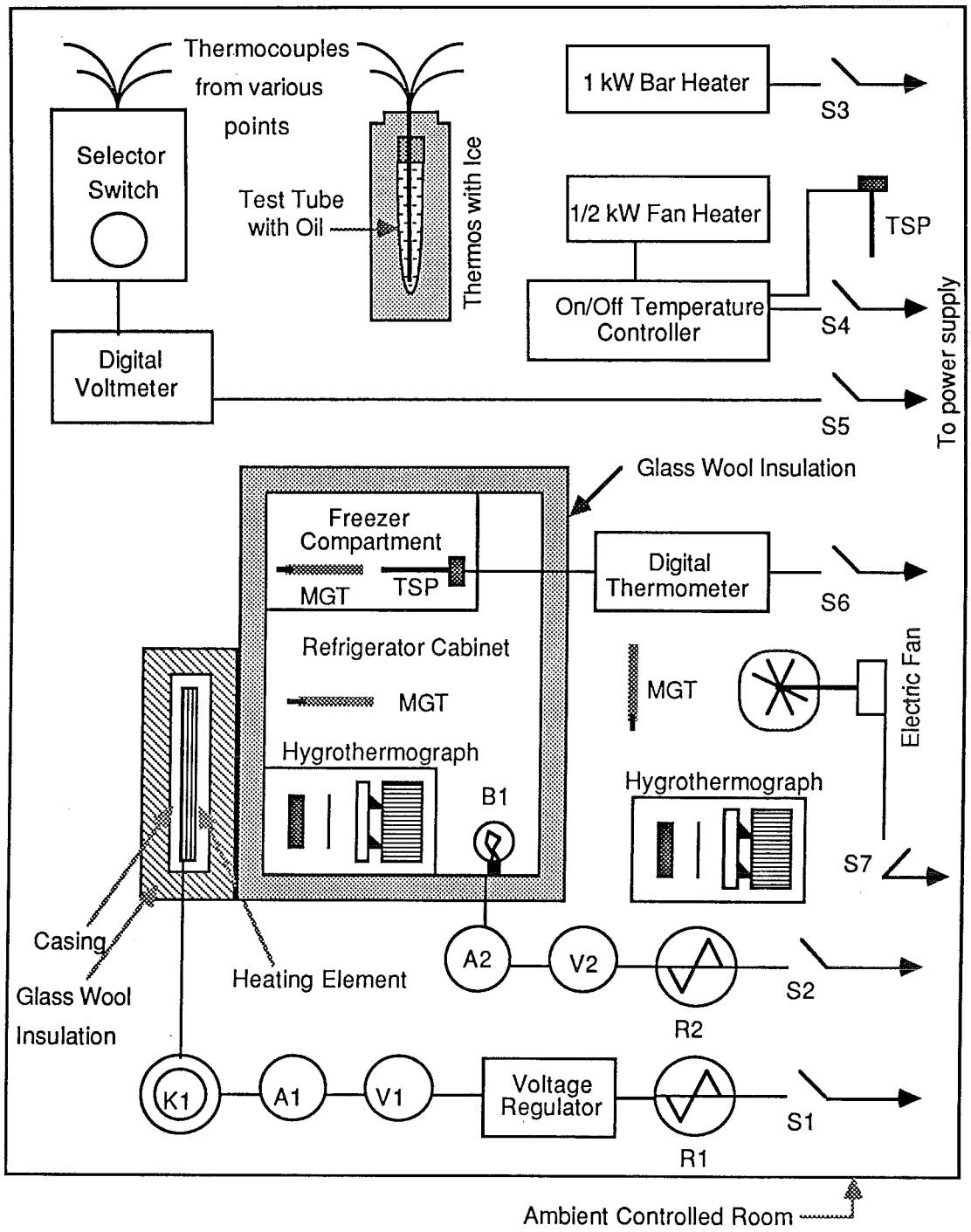

Notes: A1 & A2 = Ammeters
B1 = Electric bulb
K1 = Kilowatt-hour meter
R1 & R2 = Rheostats
S1 to S7 = Switches
V1 & V2 = Voltmeters
MGT = Mercury in glass thermometer
TSP = Temperature sensing probe

FIGURE 3.26 Effect of Generator Temperature on COP for ER2

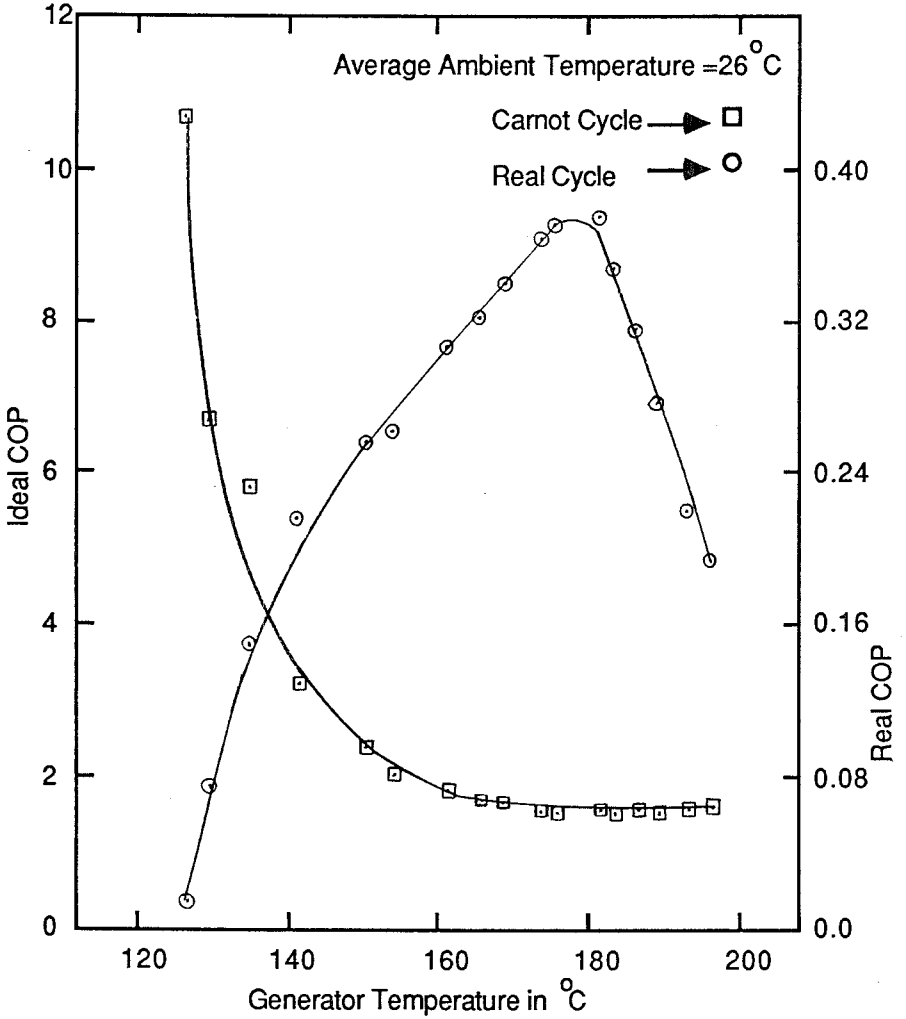

FIGURE 3.27 Effect of Generator Temperature on Freezer and Cabinet Temperatures for ER2

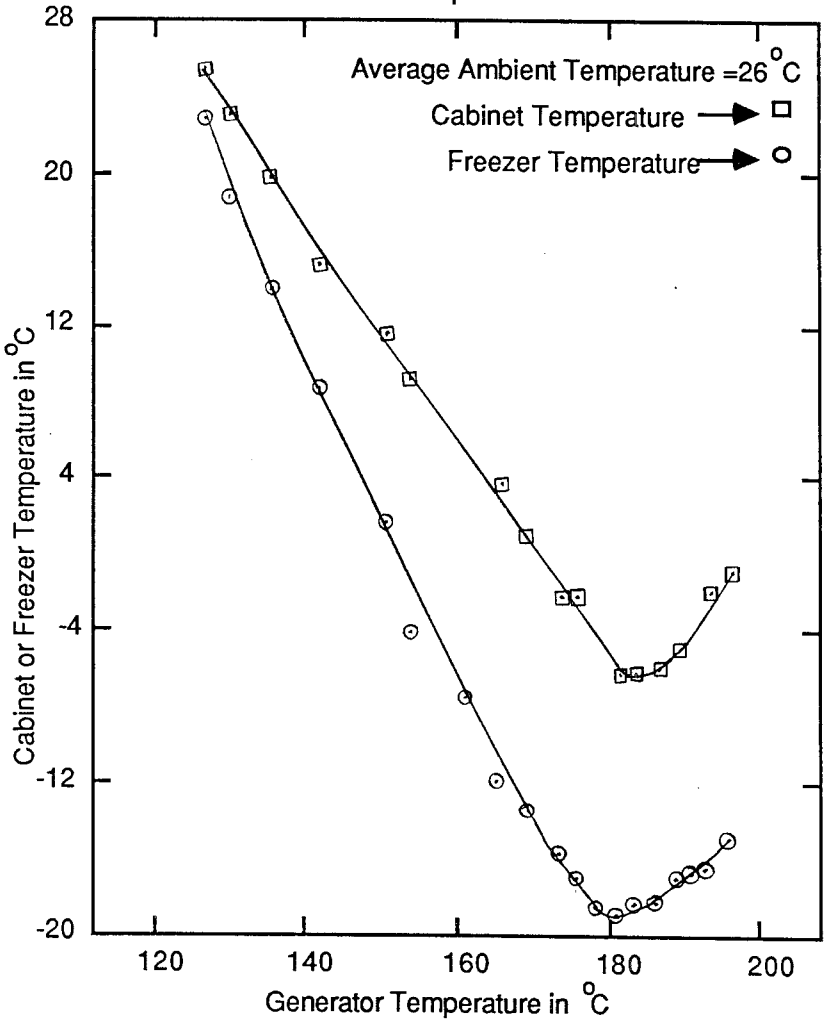

3.4.4 Discussions and conclusions

The most important variables under study in the experiments with ER2 were the generator temperature and the generator energy input. The effect of these two input variables (strictly speaking only one because with electrical heating the controlling variable is the power input to the heating element which controls the generator temperature and with oil heating it is the oil temperature, oil flow rate and heat exchanger design that control the energy input to the generator) on the three output variables of concern to us - the freezer temperature, the cabinet temperature and the COP are shown in Figs. 3.26 to 3.29. The trends shown are the same as those obtained with ER1 and hence the same explanations hold good here. However, the absolute values are significantly different. As seen from Figs. 3.26 and 3.28, the real COP reaches a maximum value of 0.37 at a generator temperature of 175°C and at a generator energy input of 100 W. From Figs. 3.27 and 3.29, it can be observed that a minimum freezer temperature of -19°C, and a minimum cabinet temperature of -7°C, occur at a generator temperature of 180°C, and a generator energy input of 120 W. These are discussed in more detail in the following comparison of the two refrigerators.

Fig. 3.30 illustrates the effect of temperature difference on overall heat loss coefficient and it increases with temperature difference. This is because the net heat flow also increases with temperature difference (as indicated by the energy input to bulb B1). In order to reduce the value of overall heat loss coefficient and its dependence on temperature difference, the quality and thickness of the insulation should be increased as it constituted the major resistance to heat flow. Heat losses dominate the scene in several solar energy applications and hence, it is necessary to have adequate resistances in the path of heat losses.

3.5 Comparison of Experiments on ER1 and ER2

The important aspects are compared, for ER1 and ER2, in Table 3.1. It is evident from this comparison that ER2 outperforms and is superior to ER1 in almost all respects. The main reasons for selecting ER2 for solar refrigeration are given below.

(1) ER2 is based on a refined cycle with analyser, rectifier and additional heat exchangers. It has a freezer compartment for

FIGURE 3.28 Effect of Generator Power Input on COP for ER2

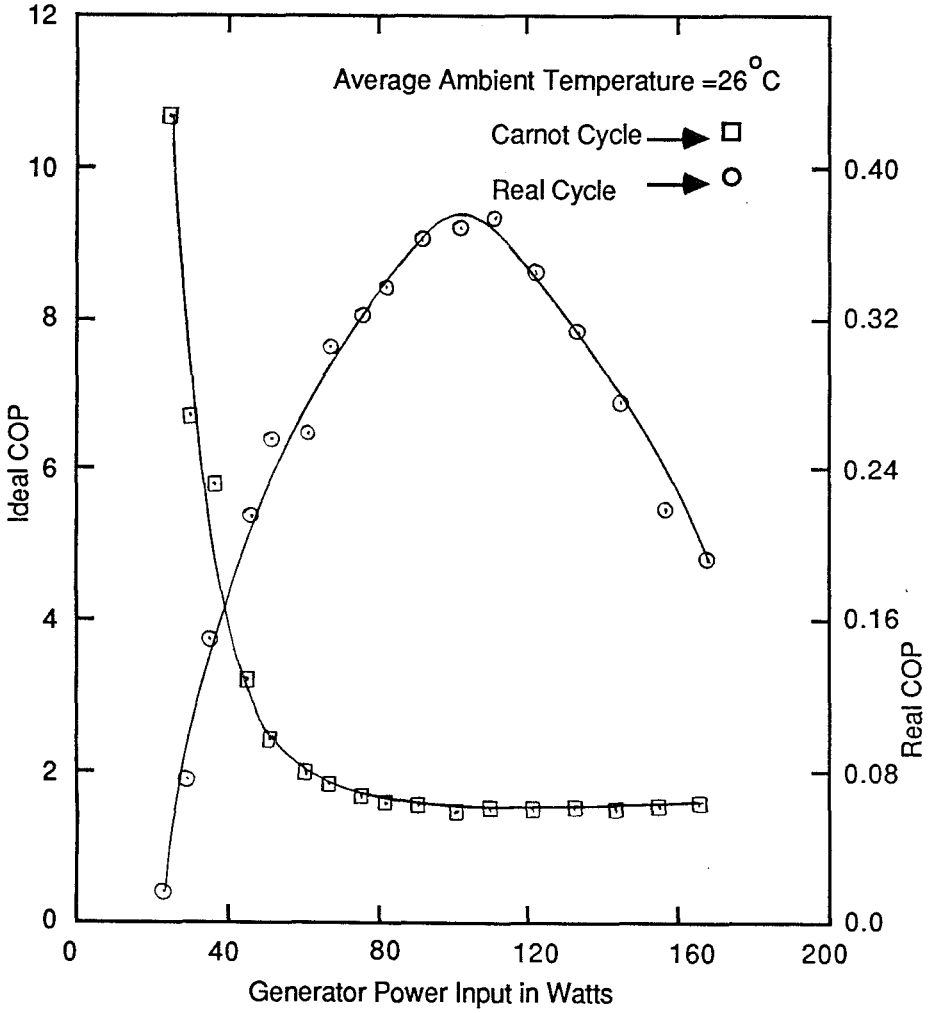

FIGURE 3.29 Effect of Generator Power Input on Freezer and Cabinet Temperatures for ER2

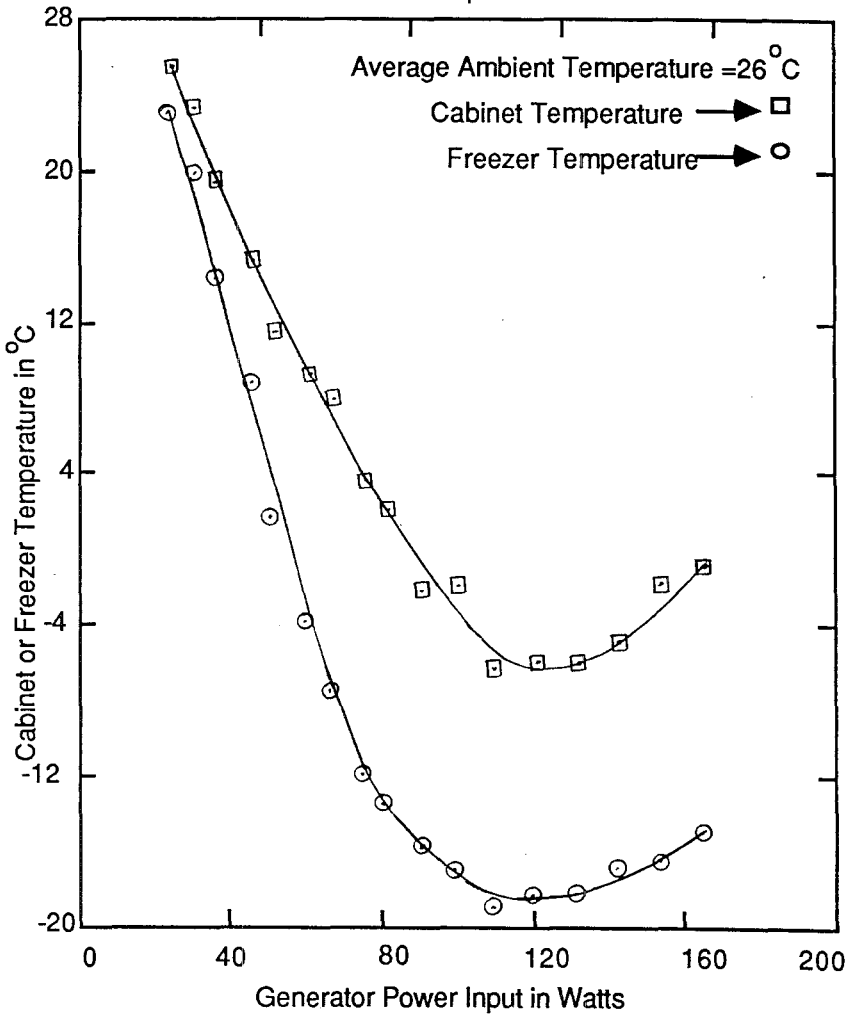

FIGURE 3.30 Calibration Chart for Finding the Overall Heat Loss Coefficient of the Electrolux Refrigerator ER2

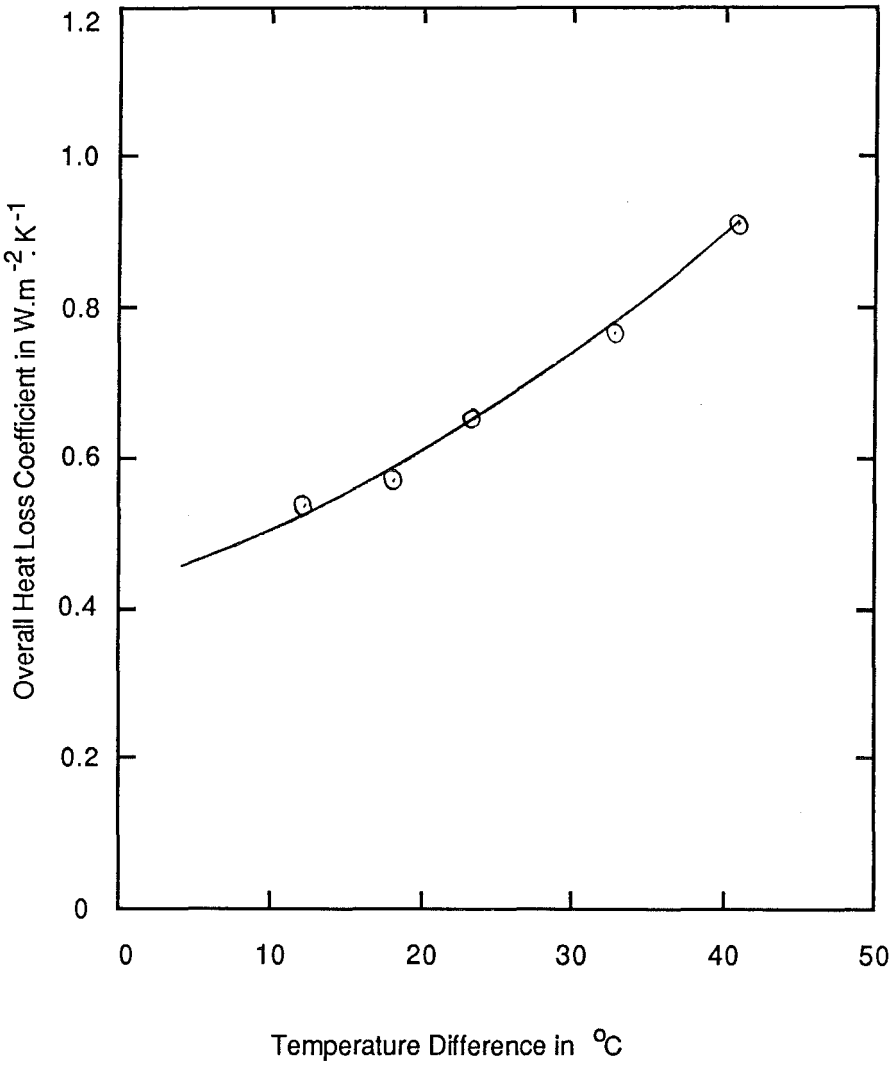

TABLE 3.1 Comparison of the Electrolux Refrigerators ER1 and ER2

Aspect For Comparison	ER1	ER2
(1) Capacity in litres	37.6	84.6
(2) Added features	no analyser no freezer	analyser freezer
(3) Optimum real COP	0.156±0.015	0.370±0.031
(4) Generator temperature T_g in oC		
(a) Working range	139 to 159	126 to 195
(b) Optimum corresponding to		
(i) optimum real COP T_{g1}	148	175
(ii) minimum freezer and cabinet temperatures T_{g2}	151	180
(5) Generator heating element energy input		
(a) Working range (i) in Watts	68 to 132	24 to 165
(ii) in Volts	170 to 260	100 to 260
(c) Optimum corresponding to		
(i) optimum real COP in Watts	90	100
(ii) minimum freezer and cabinet temperatures in Watts	104	120
(6) Heating element casing external temperature in °C		
(a) Working range	166 to 220	156 to 333
(b) Corresponding to optimum T_{g1}	190	260
(7) Freezer temperature in °C		
(a) Minimum	> -11.8	-21
(b) Corresponding to optimum T_{g1}	> -11	-19
(8) Minimum evaporator temperature in °C	-11.8	< -21
(9) Cabinet temperature in °C		
(a) Minimum	8.4	-7
(b) Corresponding to optimum T_{g1}	8	-6.4
(10) Absorber temperature in °C		
(a) Working range	28 to 64	28 to 56
(b) Corresponding to optimum T_{g1}	47	39
(11) Condenser temperature in °C		
(a) Working range	29 to 68	27 to 49
(b) Corresponding to optimum T_{g1}	51	36

making ice. As defined before our aim is to obtain temperatures below 0°C.

(2) In spite of the fact that ER2 is more than twice the size of ER1, it requires nearly the same amount of energy at optimum conditions, which are far superior in case of ER2 (-19°C and -7°C as compared to -11°C and 8°C of ER1). In fact, to achieve reasonable temperatures of a houshold refrigerator (that is cabinet temperature of less than 4°C and a freezer temperature of less than 0°C), the power required is 75 W only, which is 25% less than the optimum value. With this energy input a freezer temperature of -12°C and a cabinet temperature of about 3°C can be achieved (Table 3.1). In the case of ER1 irrespective of the energy input, it was not possible to get cabinet temperatures below 8°C.

(3) The real COP values obtainable with ER2 are nearly twice those of ER1 and this is particularly important, as it is desirable to use minimum possible energy to achieve refrigeration to a particular degree.

(4) Optimum generator temperature is an important parameter in selecting a particular refrigerator because it decides the operating temperature of the collector, which in turn determines the efficiency of the solar collector system (Webb, Prasad and Williamson, 1985). The optimum generator temperature for ER2 is 175°C as compared to 148°C for ER1. However, it was believed that the loss in collector efficiency due to higher operating temperature in case of ER2 is more than offset by the higher COP values and lower freezer and cabinet temperatures.

It can be concluded from this chapter that it is required to have a heat source capable of producing temperatures above 165°C for the operation of the Electrolux refrigerator ER2. Hence the next step towards solar refrigeration is to build a solar collection system capable of reaching such temperatures.

FIGURE 4.1 Types of Solar Collectors

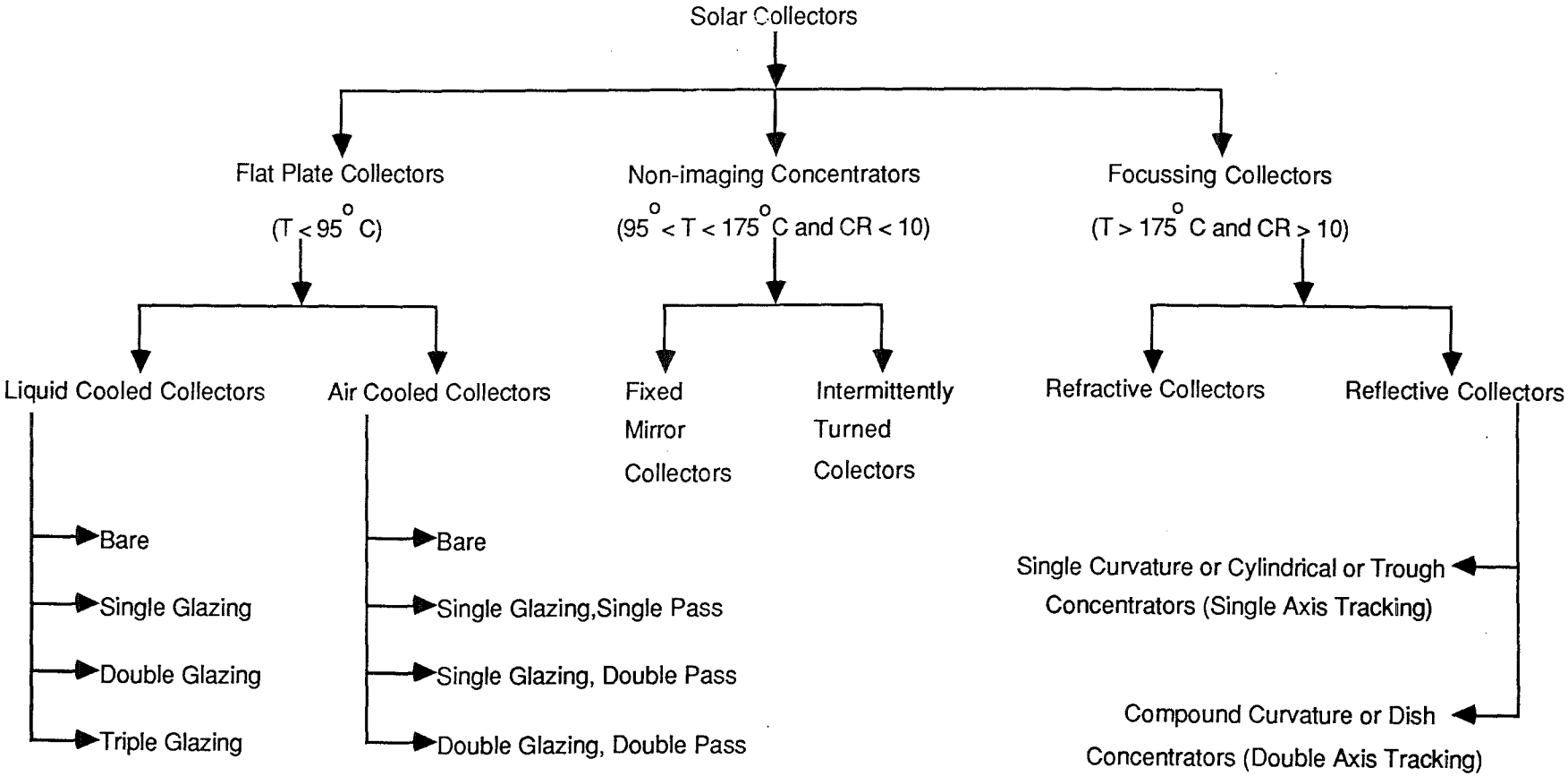

Notes: T = Working temperature and CR = Concentration ratio = $\frac{\text{Aperture area}}{\text{Absorber area}}$

CHAPTER 4

SOLAR COLLECTION SYSTEM

The following three steps are common to almost all the applications of solar energy and they are,

(1) collection of solar energy,

(2) conversion of collected energy to usable forms and

(3) storage of the energy for continuous use.

The first section of this chapter describes the types of solar collectors, the second section deals with the background theory in collector performance evaluation and the third section describes the selection of a hybrid solar collector known as HSA-SCCR (Heat Sheet Absorber-Semi Circular Cylindrical Reflector). The next four sections describe in detail the merits/demerits, computer simulation/modelling, design and fabrication of the HSA-SCCR collector. The final two sections describe the experiments conducted with two such collectors.

4.1 Types of Solar Collectors

Solar collectors are special kinds of heat exchangers that transform solar radiant energy into heat. They form the most important part of any solar energy appliance. The hundreds of types of solar collectors that have been developed and studied by various scientists in the past few decades can be broadly divided into three categories as shown in Fig 4.1

4.1.1 Flat plate collectors

The first category consists of flat plate collectors, which are the most widely used collectors, mainly because of their simplicity and low cost, as compared to the other types. The four main components of a flat plate collector are shown in Fig 4.2 (Prasad, 1980), and they are described below.

(1) Absorber plate : It is made of metals such as copper, steel and aluminium or plastics, and is coated with either black paint, or selective coating, which has high absorptivity in the visible spectrum, and low emissivity in the infrared region. Solar radiation is absorbed by the absorber plate, and is transferred to

FIGURE 4.2 Basic Components of a Flat Plate Collector

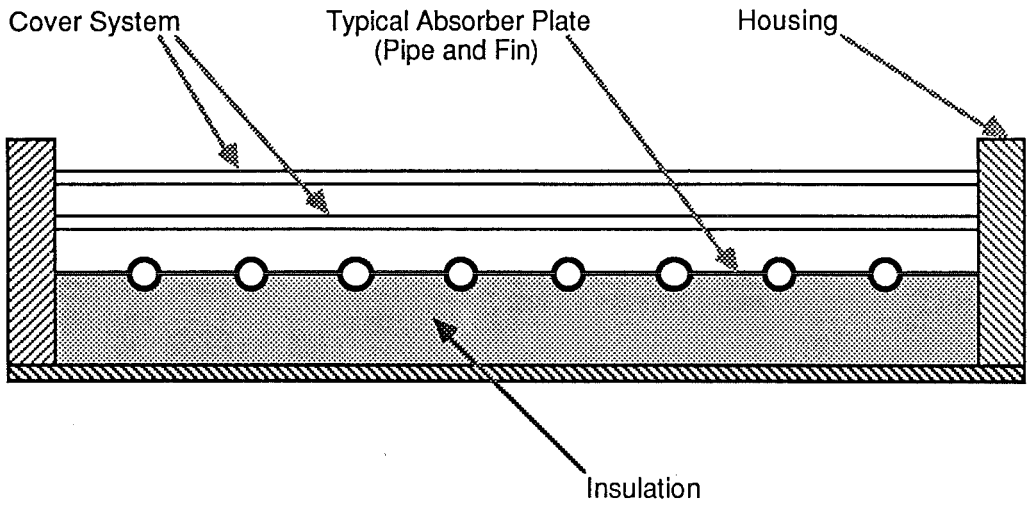

the fluid flowing through the channels, which are connected to, or integral with the absorber plate.

(2) The Cover system : This consists of one or more clear covers on the top of the absorber plate and is made of glass or durable plastic and spaced away from the plate with an air gap. The cover system allows the sun's rays to reach the flat plate, but reduces substantially the subsequent losses from the flat plate to the outside air. Glass is preferred over plastic as it gives a better "green house" effect and is not affected by ultraviolet rays. As the number of cover plates is increased, the amount of heat which is lost from the absorber to the surroundings is reduced, but at the same time it also reduces the total amount of radiation reading the absorber plate. The number of covers chosen, depends on the temperature difference between the absorber plate and the surrounding air. For almost all cooling and heating applications the optimum number of cover plates, suggested by Jordan (1967) and Lof & Tybout (1973) is two to three.

(3) Insulation : Below the absorber plate insulation is provided to reduce the heat losses from the back of the collector. The thickness of the insulation, and the proper choice of the insulating material, depends on the difference between the absorber plate temperature and the ambient temperature. Glass wool or foam plastic are generally used as insulating materials.

(4) Housing : A strong and durable housing to hold the first three components of the collector is needed. The housing material is generally coated with a weather resistant paint. Housing materials include wood, fibre reinforced plastic, galvanised steel sheet and aluminium. Various cover plate, insulating and housing materials and their thermal properties have been listed in the literature (Kreith & Kreider, 1978; Duffie & Beckman, 1980; AMETEK, 1979).

Neville, (1977) has shown that generally a fixed flat plate collector may receive, only half as much energy, as an ideal dual axis tracking flat plate, over a one year period. However, tracking mechanisms are too expensive to warrant their use with flat plate collectors. Instead the collector is usually kept with its axis matching the East-West direction, and tilted towards the equator, at an angle to the horizontal, which is approximately equal to

$(\phi - 10)$ for summer operation,

FIGURE 4.3 Heat Loss Factors in a Flat Plate Collector

(Solar Energy Handbook, 1979)

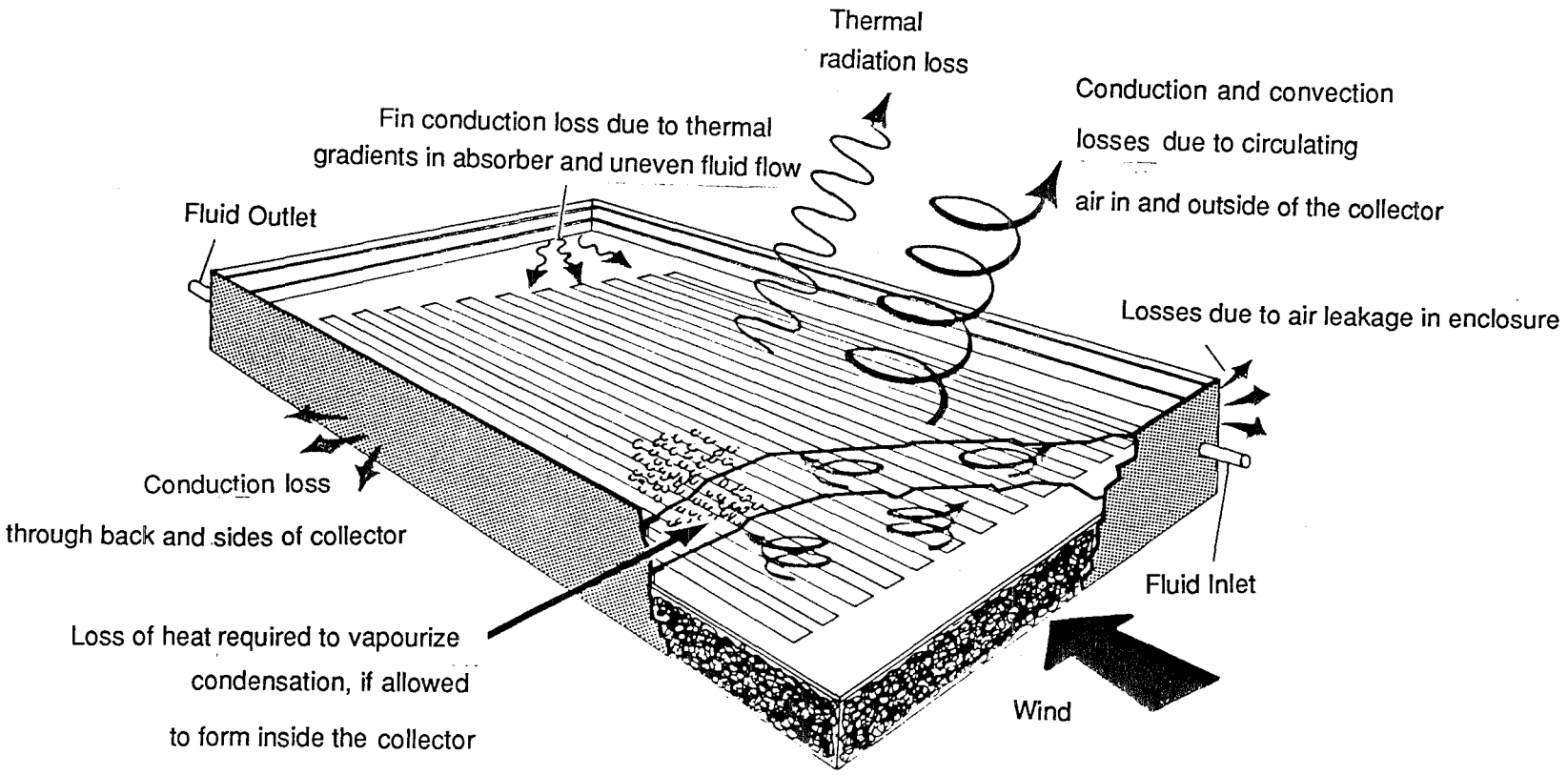

(ϕ + 10) for winter operation and

ϕ for year-round operation, where ϕ is the latitude of its location. (Duffie & Beckman, 1975).

Based on the heat removal medium flat plate collectors can be divided into two categories.

(1) Flat plate collectors utilizing liquid (generally water) as the heat removal medium.

(2) Flat plate collectors utilizing gas (generally air) as the heat removal medium.

Within each of these categories, there are several types depending on the type of absorber plate, flow channels or the way the plate and the channels are attached.

Collector performance, expressed as collection efficiency, is defined as the ratio of useful energy gained by the heat removal fluid to the incident solar energy over a given period of time. Two general methods exist for significantly improving the performance of solar collectors above the minimum flat plate collector level. The first method involves optical concentration of solar energy on to the absorbing surface as done by focussing collectors. The second method aims at reducing the heat losses from the absorber plate. Various heat losses from a flat plate collector are shown in Fig. 4.3. The major heat loss is from conduction and convection, due to circulation of air. The next biggest loss is radiation loss, from the absorber plate. These losses can be minimised by several methods, but the two important ways are given below.

(1) Application of honeycombs between absorber plate and glazing suppresses free connection heat transfer across the air gap and reduces radiation losses from the collector (Hollands 1965, Buchberg et al., 1971; Buchberg & Edwards, 1976; Gani, 19781; Simons & Cathro, 1981). Honeycombs are devices consisting of planar arrays of closely packed hexagonal, square or rectangular cells made up of glass or clear plastic. However, this is not as effective as the following method and the stagnation temperature (which is the maximum temperature, the absorber plate will reach, when no heat is recovered from it) of the collector does not increase very much.

(2) The second method involves utilization of evacuated tubular collectors, which provide means for complete elimination of convection losses by surrounding the absorber, or receiver

FIGURE 4.4 Basic Components of a Concentrator

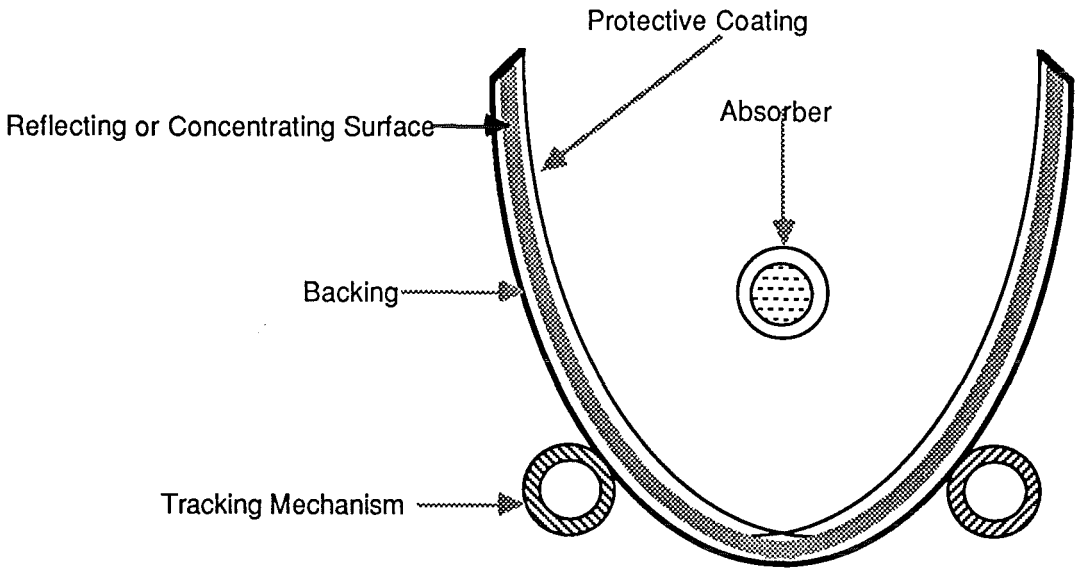

tube with a vacuum of the order of 10^{-4} mm Hg (Speyer, 1965; Beekley & Mather, 1975; Mather, 1980; Morrison, 1984). Since such a vacuum would cause a typical flat plate collector to collapse, this technique is used, in conjunction with tubular designs only. Just like flat plate collectors, evacuated tubular collectors can also collect both direct and diffuse radiation and do not require tracking. They can reach stagnation temperatures as high as 316°C, (Kreider & Kreith, 1982). However, they are much more expensive and fragile as compared to simple flat plate collectors.

4.1.2 Focussing collectors

The second and third categories shown in Fig. 4.1, are both based on the same principle of optical concentration, to increase the energy flux density on the receiver or absorber. A common term used to describe concentrating collectors is concentration ratio, denoted by CR and defined as the ratio of the net collecting aperture area (or net area of the collector that intercepts solar radiation) to the total area of the receiver or absorber receiving concentrated radiation. The second category, known as non-imaging concentrators, do not produce a well defined focal spot and are capable of achieving temperatures up to about 175°C. These systems require no tracking if their concentration ratio is below 2 and only seasonal adjustments at concentration ratios up to 10. The third category is that of concentrating collectors, which are designed to produce very high energy density and temperature at the receiver, by means of accurate focussing devices and continuous precise tracking of the sun's virtual motion. The upper limits of optical concentration, for two and three dimensional concentrators, are of the order of 200 and 40000, respectively. It is possible to achieve temperatures as high as 3000°C from the concentrators.

Though concentrators vary a lot from one another, in general a concentrator consists of the following parts as shown in Fig. 4.4.

(1) Reflecting or concentrating surface : This concentrates the solar radiation incident on the surface to a focal point, or focal line, depending on the shape and type of the surface. Mirrors, lenses, highly polished metallic surfaces and metallized plastics such as aluminized mylar sheets are used for this purpose.

(2) Protective coating : Sometimes a transparent protective coating is applied, on the top of the reflecting surface, to protect it from damage, to make it weather resistant, and to facilitate easy removal of dust. Generally a durable plastic like epoxy resin is used for the purpose.

(3) Backing : In order to give support and structural strength to the reflecting surface a strong backing is given. Generally a backing frame of the required shape is made and the reflecting surface is attached to it with an adhesive. Backing materials include fibre reinforced plastics metallic sheets and asbestos cement.

(4) Absorber : An absorber is placed at the focal point or focal line of the reflector, to absorb the reflected solar radiation. A heat transfer fluid flows through the absorber, which is generally made of copper. The absorber is often coated with black or selective coating to enhance the absorptivity, and is surrounded by a glass or plastic envelope, which is generally evacuated to minimise the convection losses.

(5) Tracking mechanism : As the concentrators can use only beam radiation, tracking mechanisms are employed, to track either the reflectors or the absorbers.

Various concentrators may be classified (Meinel and Meinel, 1977) according to,

(1) the operating temperature range (intermediate and high),

(2) the amount of tracking required, to maintain the sun, within the acceptance angle, for certain hours a day (occasional or continuous tracking) and

(3) type of tracking required (single or double axis).

4.1.3 Comparison of flat plate and focussing collectors

The relative advantages and disadvantages of flat plate and focussing collectors are given in Table 4.1 (Prasad, 1980; Bharadwaj, 1967).

It is evident from Table 4.1 that, no single type of collector can be regarded as the best for all applications. The decision, as to which collector type to be used for specific task should be made, after analysing the whole situation, which includes the output temperatures needed with reasonable collector efficiency, availability and overall costs. Before selecting a particular type of collector, it is necessary to understand the

TABLE 4.1 Comparison of Flat Plate and Focussing Collectors

Flat Plate Collector	Focussing Collector
(1) Simple, easy to build in any size and shape and high degree of precision is not very important.	(1) Sophisticated, harder to build in bigger sizes and high degree of precision is required.
(2) Quality of energy is low as the maximum attainable temperature is generally about 100°C and hence restricted to low temperature applications only.	(2) High quality energy is obtainable, because temperatures as high as 3000°C can be achieved and hence are suitable for high temparature applications also.
(3) Accept both direct and diffuse radiation and hence can be used on cloudy days.	(3) Accept only direct radiation and hence not effective on cloudy days.
(4) Fixed; orientation is not critical and need little maintenance.	(4) Daily and/or seasonal tracking is required as orientation is critical and need more maintenance.
(5) Daily and seasonal variationof output energy due to non tracking nature.	(5) More even output as the incidence angle is maintained at zero by tracking the sun.
(6) As the concentration ratio is one, absorber or receiver area is the same as the aperture area and hence thermal mass is high which results in greater transient effects.	(6) As the concentration ratio can be as high as 40000, receiver area is small, thermal mass is less and hence transient effects are less.

(Continued on the next page)

TABLE 4.1 Comparison of Flat Plate and Focussing Collectors

(continued)

Flat Plate Collector	Focussing Collector
(7) Lower thermal efficiency due to higher heat loss area.	(7) Higher thermal efficiency due to reduction in heat loss area reletive to the receiver area.
(8) More rugged and can be put conveniently on roof tops.	(8) Delicate and can not be used on roof tops as part of housing construction.
(9) Antifreeze is required in cold climates due to large absorber areas which emit radiation during night.	(9) Little antifreeze is required.
(10) Initial investments and operating costs are generally low.	(9) Needs higher capital and higher operating costs.

methods in which collectors are tested, their performance reported and the terms associated with it.

4.2 Theory on Collector Performance Evaluation

The performance of a solar system depends largely on the performance of the solar collectors. Thus, the measurement of the performance of solar collectors is an important and necessary step for an understanding of the total system function. It also enables the comparison of individual collectors which have been tested on a similar basis and the determination of the economic efficiency.

Although analytical design procedures are in reasonably good agreement with test results, it is preferable to base a system design on actual collector test data. There are two basic methods for testing collectors: the instantaneous and the calorimetric procedures. For the instantaneous method it is only necessary to measure the mass flow rate of the heat transfer fluid, its inlet and outlet temperatures, and the insolation on the absorber (Hill and Streed, 1976). The calorimetric procedure employs a closed system in which the time rate of change of temperature of a constant thermal mass and the insolation are measured (Hill et al., 1976). The instantaneous method, unlike the calorimetric procedure, is simple and does not require an expensive set up. Although it is not as accurate as the calorimetric method suggested by the National Bureau of Standards (NBS; Hill et al., 1976) or the American Society of Heating, Refrigeration, and Air Conditioning Engineers (ASHRAE, 1978), it can be easily carried out on the field site, with commercially available instrumentation (to an accuracy of about 10%; Simon, 1976), which is convenient for small groups of people testing panels occasionally.

There are a number of ways of reporting the performance of flat plate collectors (Tabor, 1955, 1978; Klein et al., 1974, 1975; Stickford, 1976; Sager et al., 1978; Ong, 1978), but they are all derived from the Hottel-Whillier-Bliss equation (Hottel and Woertz, 1942; Hottel, 1954; Hottel and Whillier, 1955; Bliss, 1959) as given below.

Useful energy = Energy absorbed - Energy lost to environment (4.1)

$$Q_u = I\ A_{ab}\ (\tau\alpha)_e - U_L\ A_{ab}\ (T_{ab} - T_{amb}) \qquad (4.2)$$

where Q_u is the useful energy delivered by the collector; I is the total insolation; A_{ab} is the effective absorber area; τ is

the solar transmittance of the glazing; α is the solar absorptance of the absorber panel; $(\tau\alpha)_e$ is the effective transmittance absorptance product; U_L is the collector overall heat loss coefficient to the environment; T_{ab} is the mean absorber temperature; T_{amb} is the ambient air temperature.

The factor $(\tau\alpha)_e$ is more than the simple product of τ and α, as it takes into account the absorptivity of the glazing (which increases its temperature and consequently reduces the heat losses), and multiple reflections between the absorber and glazing due to their individual reflectivities.

It is usually difficult to evaluate the average absorber temperature due to the temperature gradients existing in the absorber, and hence, Eq. (4.2) can be modified to (Duffie and Beckman, 1980)

$$Q_u = I\ A_{ab}\ F'(\tau\alpha)_e - U_o\ A_{ab}\ (T_{af} - T_{amb}) \qquad (4.3)$$

where, F' is the collector plate efficiency factor; U_o is the overall heat loss coefficient from the heat removal fluid to the environment; T_{af} is the average heat removal fluid temperature.

F' and T_{af} are given by

$$F' = U_o / U_L \qquad (4.4)$$

$$T_{af} = (T_{if} + T_{of}) / 2 \qquad (4.5)$$

where, T_{if} and T_{of} are the inlet and the outlet fluid temperatures, respectively.

The factor F' represents the ratio of the actual useful energy gain, to the useful energy gain that would result if the collector absorbing surface had been at the local fluid temperature.

Since a large portion of collector losses are by radiation to the sky, which the collector sees as a black body at some equivalent sky temperature (which is less than the ambient temperature), T_{amb} should be replaced by an effective ambient temperature T_{eamb} whose value is recommended by Pott and Cooper (1976) as $(T_{amb} - 3^oC)$.

The collector performance is usually expressed as its thermal efficiency η_{th}, which is defined as the ratio of the useful energy delivered to the solar radiation incident on the collector and it is given by

$$\eta_{th} = \frac{Q_u}{I\ A_{ab}} = F'(\tau\alpha)_e - \frac{U_o\ (T_{af} - T_{eamb})}{I} \qquad (4.6)$$

FIGURE 4.5 Performance Curve for a Typical Black Painted, Single Glazed Flat Plate Collector (Kreider and Kreith, 1977)

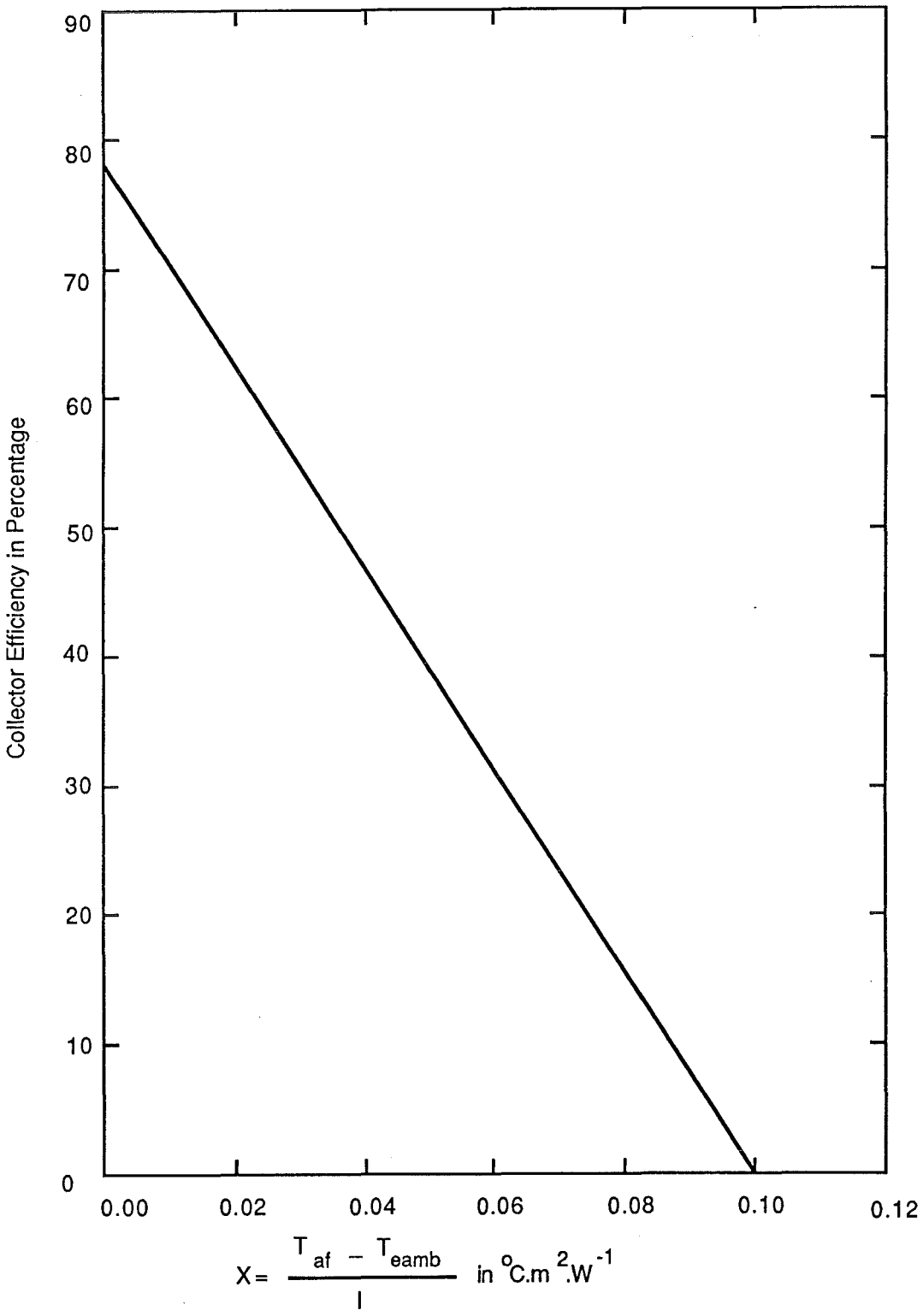

The generalised collector performance curve (known as the HWB plot, and shown in Fig. 4.5) is obtained from Eq. (4.6) by plotting the collector thermal efficiency η_{th} as a function of X, which is given by

$$X = (T_{af} - T_{eamb}) / I \qquad (4.7)$$

This curve reduces to a straight line with a slope of $-U_o$ and an intercept of $F'(\tau\alpha)_e$, provided U_o is constant. Cooper and Symons (1978) suggested the following relation (for a given wind speed) for evaluating a more accurate value of U_o

$$U_o = a + b\ (T_{af} - T_{eamb}) \qquad (4.8)$$

where 'a' and 'b' are constants for a given collector. However, in practice U_o is commonly treated as constant.

The experimental evaluation of η_{th} can be done, from the relation

$$\eta_{th} = \frac{Q_u}{I\ A_{ab}} = \frac{q_f\ c_{pf}\ \rho_f\ (T_{of} - T_{if})}{I\ A_{ab}} \qquad (4.9)$$

where q_f, c_{pf} and ρ_f are the volumetric flow rate, the specific heat capacity and the density of the fluid respectively.

The efficiency of stationary mirror systems can also be defined in a similar way (Tabor, 1958). The instantaneous collection efficiency $\eta_{inst(T)}$ at a temperature T is given by

$$\eta_{inst(T)} = (\tau\alpha)_{er} - \frac{Q_L(T)}{I_{ap}\ A_{ab}\ CR} \qquad (4.10)$$

where $Q_L(T)$ is the rate of heat loss from the absorber at temperature T; CR is the concentration ratio; I_{ap} is the intensity of solar radiation measured at the aperture of the collector; $(\tau\alpha)_{er}$ is the effective $\tau\alpha$ product for the reflector system. Rable (1976) suggested that $(\tau\alpha)_{er}$ can be expressed as,

$$(\tau\alpha)_{er} = \tau\alpha\rho_{ref}\ N \qquad (4.11)$$

where ρ_{ref} is the reflectivity of the reflector and N is the average number of reflections.

For hybrid solar collectors, with a flat plate collector and a stationary reflector, the intercept $(\tau\alpha)_e$ of the collector performance curve may be regarded as the optical efficiency of the collector η_{opt}.

From the performance curve of a solar collector shown in Fig. 4.5, one can obtain four important variables.

(1) Optical efficiency (η_{opt}) : The optical efficiency of the collector is the maximum possible efficiency, or the efficiency at which the absorber temperature is the same as the ambient temperature. As the name suggests the optical efficiency indicates how effectively the solar radiation incident on the collector is absorbed by the collector. The higher the value, the better are the optical characteristics of the collector.

(2) Collectors figure of merit (X_s) : It is the abscissa value of the HWB plot or X value at zero efficiency and it is given by

$$X_s = (T_s - T_{eamb}) / I \qquad (4.12)$$

where T_s is the absorber plate temperature, at stagnation conditions.

At stagnation conditions no useful energy is transferred to the heat transfer fluid and hence the thermal efficiency is zero. At these conditions all the energy input to the solar collector is lost to the environment. The higher the abscissa value X_s, the lower the "critical solar flux" required to produce the heat transfer fluid at a given temperature, for a given ambient conditions. (Liu and Jordon, 1963). Also the greater the figure of merit, the more the number of hours per year, the collector can collect solar energy and hence, the more the energy it may collect even if its optical efficiency is lower.

(3) Stagnation temperature (T_s) : The stagnation temperature of the absorber plate can be evaluated from Eq. (4.12), for any given set of ambient temperature and solar insolation, and it denotes the maximum attainable temperature of the absorber plate for the particular conditions. It is a very important parameter needed for the design of any solar system.

(4) Overall heat loss coefficient (U_o) : The numerical value of U_o is equal to the gradient of the HWB plot. It determines the heat loss characteristics of the collector.

Above all the performance curve of the collector is universally used for comparison with other collectors.

4.3 Selection of Solar Collector Type

As stated in the previous section, the aim in this investigation was to run an absorption refrigeration system (in particular an Electrolux system) using solar energy. This automatically restricted the temperature range, such that

FIGURE 4.6 Schematic Diagram of a Basic HSA-SCCR Collector

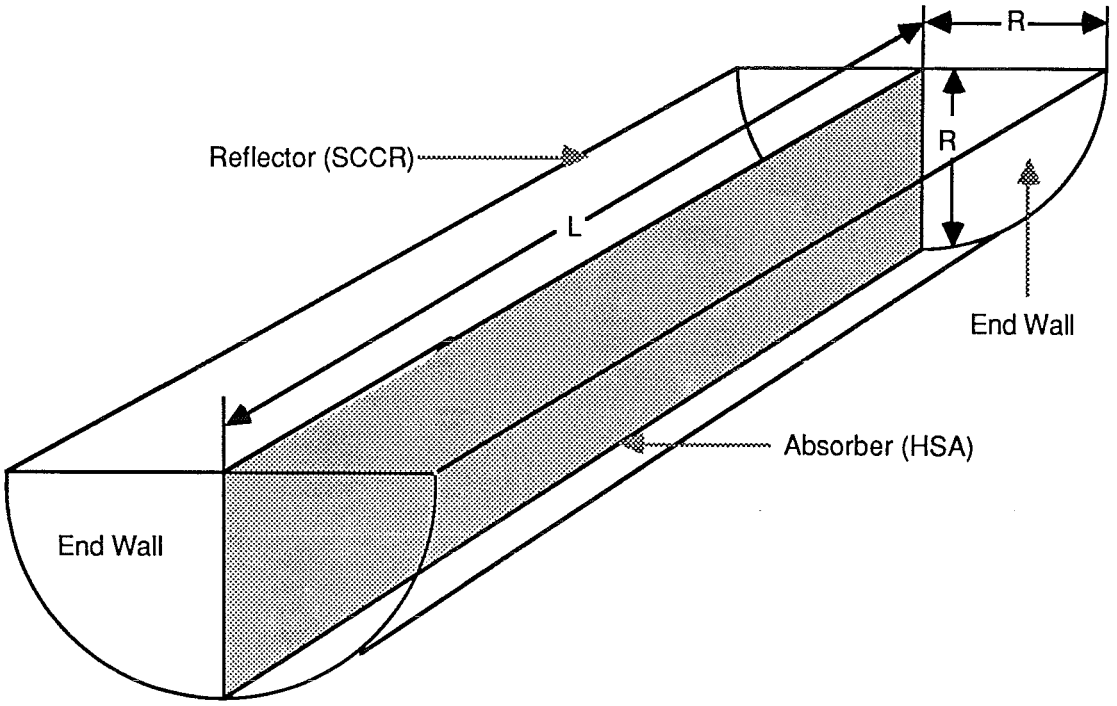

collectors operating above 150°C were sought. Hence, simple flat plate collectors are not suitable for this application.

Although focussing collectors are capable of producing these temperatures very easily, their use was considered undesirable because of the various disadvantages listed in Table 4.1, especially their complexity, necessity of tracking mechanisms and high overall cost. As mentioned in this section, the stagnation temperature of a non-tracking & non-focussing collector may be improved significantly (as high as 316°C) by utilizing evacuated tubular collectors, but, this option was also discarded because of the high cost and complexity. Finally a novel type known as HSA-SCCR (heat sheet absorber-semi circular cylindrical reflector) collector, under development in this Department was chosen.

The HSA-SCCR collector is a hybrid non-tracking solar collector, incorporating a flat plate collector based on heat pipe principle, referred to as a "heat sheet" absorber (HSA) and a non-imaging fixed mirror concentrator, described as a semi-circular cylindrical reflector (SCCR). The schematic diagram of a basic HSA-SCCR collector is shown in Fig. 4.6. The absorber of length L and width R, sits in the axial plane of a reflector of radius R. The details of this collector are given in the next section.

Webb (1979) built one such collector with a black painted HSA panel and single glazing on the aperture, in this Department. He also developed a simple computer model of the collector, and obtained reasonably good agreement with the experimental results. With the help of the computer model, he predicted the performance of the collector with various modifications such as end wall insulation, selective surface and double glazing (Table 4.2). The variables listed in the table include the optical efficiency of the collector, the stagnation temperature of the absorber panel, the collectors figure of merit and the overall heat loss coefficient; at an ambient temperature of 17°C and insolation of 850 $W.m^{-2}$.

However, Webb's model was based on several simplifying assumptions and hence, a much more detailed model was developed (which will be described in Section 4.5), whose predictions are also included in the same table. As seen from Table 4.2 this model predicted up to about 23% lower values than Webb's model. In spite of the lower predicted values, certain modifications shown in Table 4.2 have absorber panel stagnation temperatures higher than

Table 4.2 Computer Model Predictions of HSA-SCCR Collector

Modification	Webb's (1979) predictions				Predictions with present model				
	η_{opt}	T_s	X_s	U_o	η_{opt}	T_s	X_s	U_o	ΔT_s
	%	°C	$m^2.°C.W^{-1}$	$W.m^{-2}.K^{-1}$	%	°C	$m^2.°C.W^{-1}$	$W.m^{-2}.K^{-1}$	%
(1) BP, SG	63	102	0.104	6.1	63	101	0.102	6.2	1
(2) BP, SG, EWI	63	107	0.110	5.7	63	105	0.107	5.9	2
(3) BP, DG	56	136	0.144	3.9	56	129	0.141	4.0	5
(4) BP, DG, EWI	56	140	0.149	3.8	56	132	0.144	3.9	6
(5) SS, SG	67	174	0.188	3.6	67	151	0.161	4.1	13
(6) SS, SG, EWI	67	188	0.205	3.3	67	157	0.168	4.0	16
(7) SS, DG	59	260	0.289	2.0	59	198	0.217	2.7	23
(8) SS, DG, EWI	59	265	0.294	2.0	59	208	0.227	2.6	21
(9) SS, DG, ρ_s=0.86	66	282	0.310	2.1	66	225	0.248	2.7	20

Notes: η_{opt} = Collector optical efficiency; T_s = Stagnation temperature of HSA panel; ΔT_s = Deviation in T_s; X_s = Collector's figure of merit; U_o = Overall heat loss coefficient; BP = Black painted panel with short wave absorptivity = long wave emissivity = 0.95; SG = Single glazing on the aperture; EWI = End wall insulation (50 mm thick glass wool); SS = Selective surface with short wave absorptivity = 0.95 and long wave emissivity = 0.1; DG = Double glazing with one on HSA panel and one on the aperture; ρ_s = Specular reflectivity of the reflector = 0.76 (except in modification 9); Ambient temperature = 17°C; Insolation = 850 $W.m^{-2}$.

FIGURE 4.7 Performance Curves for Selected Collector Designs

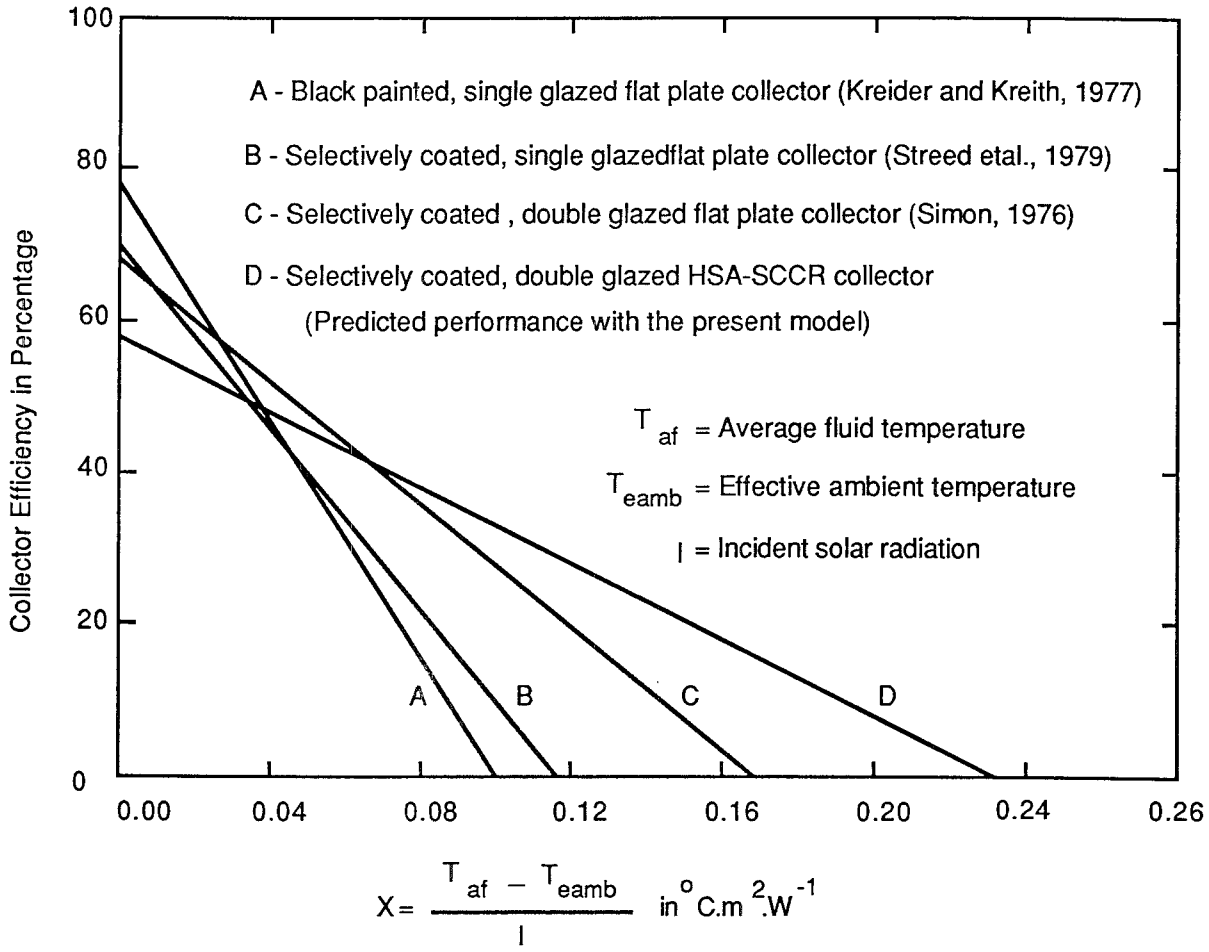

200°C, which appear to make them suitable for this investigation. Fig. 4.7 shows the superiority of the HSA-SCCR collector over three commonly used flat plate collectors. A flatter performance curve with higher abscissa value indicates the capability of this collector operating at high temperatures with reasonably good thermal efficiency.

4.4 HSA-SCCR Collector

The important characteristics of the HSA-SCCR collector are: (a) virtual flat plate, (b) negligible back losses and (c) nonuniform energy distribution, overcome by heat sheet absorber. The SCCR and HSA are discussed in detail, including their merits and demerits, in this section, after the evaluation of the colletor geometry.

4.4.1 Collector geometry evaluation

The evaluation of HSA-SCCR collector geometry is described in Appendix A3. Any ray entering the aperture of the SCCR, which is specularly reflected, must eventually reach the absorber, provided it is not absorbed by the reflector or air or the inner glazing (Appendix A3.1). In order to evaluate the performance of SCCR it is necessary to understand the sun's virtual motion (keeping the earth fixed) as described in Appendix A3.2. It is also shown in the same appendix that the SCCR has a maximum acceptance angle (±45°), as compared to any other concentrator and hence, it will accept direct radiation for atleast 8 hours and 34 minutes, every day of the year. However, the absorber tube (generally used with trough type reflectors) has been replaced with HSA panel, resulting in further increase in accepting angle. An SCCR with HSA in its axial plane has an acceptance angle of ±90° because it behaves exactly like a flat plate collector (except for uneven flux distribution), whose total area (2LR) is equal to the total aperture area.

The energy flux distribution on the absorber plate has been determined (Appendix A3.3), by following the paths of individual ray, as they enter the collector and are reflected to the absorber, which is divided into a number of segments (75 in this case). The ray trace technique has been used to develop equations, which are then solved with the help of a computer programme TPEFD, to obtain the energy flux distribution on each of 75 segments in

FIGURE 4.8 Ray Trace Pattern for the HSA-SCCR Collector Showing Energy Flux Distribution on the HSA Panel

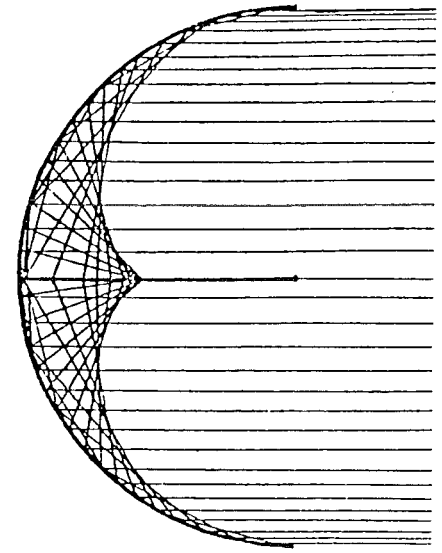

Angle of Incidence = 0 degrees

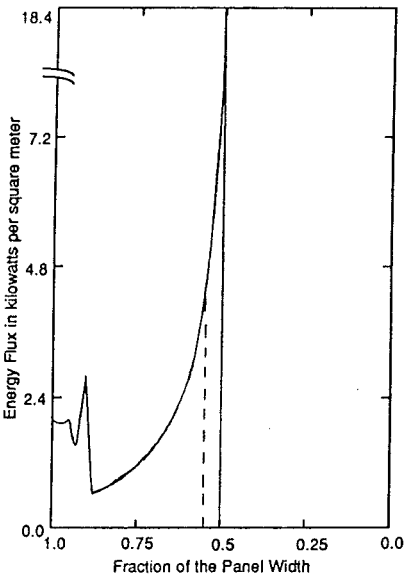

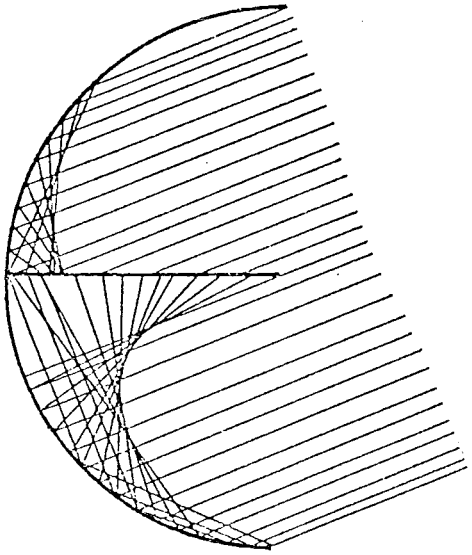

Angle of Incidence = 22.5 degrees

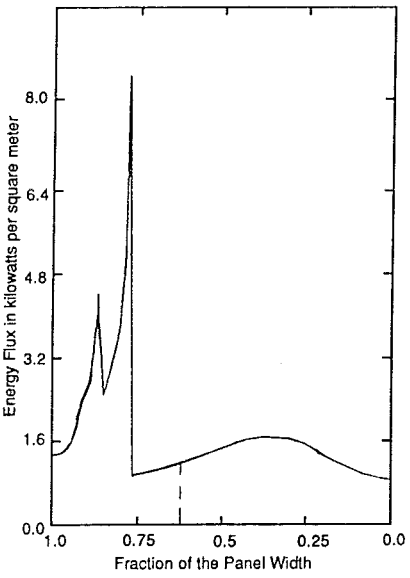

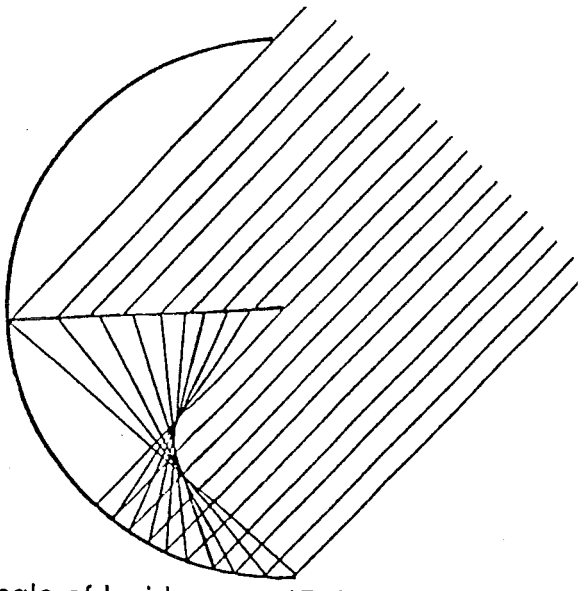

Angle of Incidence = 45 degrees

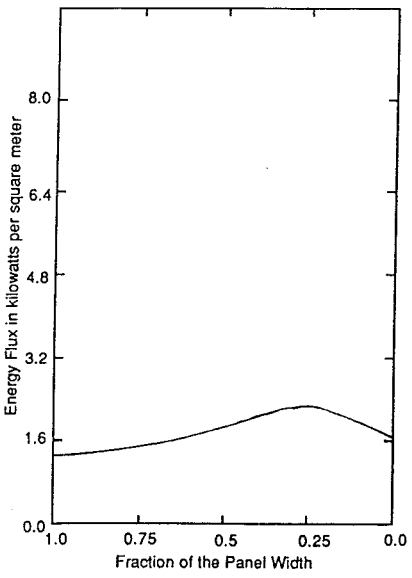

Notes: Insolation = 1000 $W.m^{-2}$

the top and bottom quadrants separately. A listing of the computer programme TPEFD, along with a sample set of results (for an angle of incidence of 10°) are given in Appendix A3.3. As the angle of incidence changes throughout the day, so does the energy flux distribution on the absorber plate as shown in Fig. 4.8.

These three values of angles of incidence (θ) include the two extremes and one intermediate value, representing about eight hours of solar energy collection on a single day. It is evident from the figure that the flux on the absorber plate becomes very nonuniform during the course of the day. At $\theta = 0°$ all radiation which is specularly reflected falls on the back half of the absorber and then the collector acts as a concentrator, with a concentration ratio of two. As the angle of incidence increases the concentration effect decreases and the flux becomes more uniform, with fairly uniform flux at $\theta = 45°$.

The Fig. 4.8 also shows three plots for the three angles of incidence, depicting the energy flux distribution on the absorber panel as a function of the fraction of the absorber width. If grafically integrated, the area under each curve would represent the total energy incident on the absorber panel. The dashed vertical line indicates the points on the absorber either side of which half the total energy is absorbed, or in other words, the area under the curve to the left of the line equals the area under the curve to the right of it.

It is also apparent from the Fig. 4.8 that the number of reflections the radiation undergoes before striking the absorber panel decreases and the amount of radiation directly incident on the panel increses as θ increases. The nonuniform flux suggests that there may be an advantage in reducing the size of the absorber panel and th ereflector and this aspect has been discussed later (Section 4.6.1).

However, because of the use of a heat sheet absorber this does not have a serious effect on the collector performance, as discussed in the following sections.

4.4.2 Semi circular cylindrical reflector (SCCR)

In any type of solar collector the absorber is usually the most expensive component and this is especially so if the absorber has extra features such as selective coating, evacuated tubes or heat pipes. By the use of a SCCR both sides of the absorber plate

FIGURE 4.9 Methods of Improving the Flat Plate Collector Efficiency or Output Temperature

(a) Mirror Boosters

(1) Single Mirror System (Tabor, 1958)

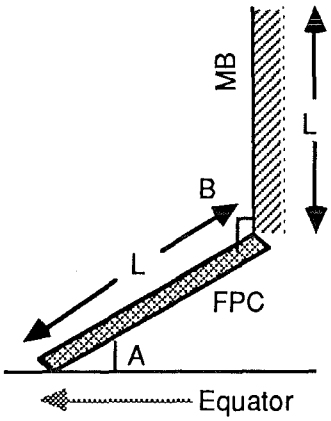

(2) Double Mirror System

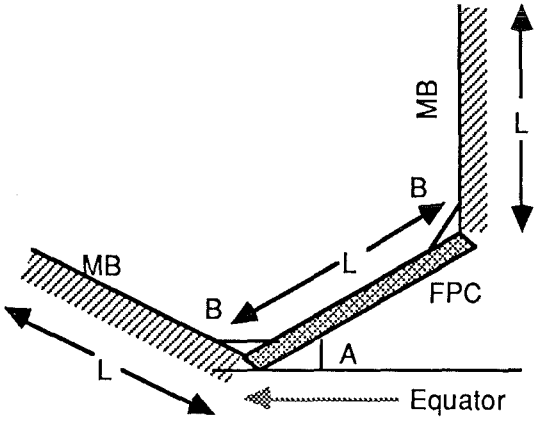

(3) Four Mirror System (Tabor, 1966)

Notes: FPC = Flat plate collector
MB = Mirror booster
A = Absorber tilt angle
= Latitude - 10° in summer
= Latitude - 23.5° in winter
B = Angle between the absorber and mirror = 90° to 120°

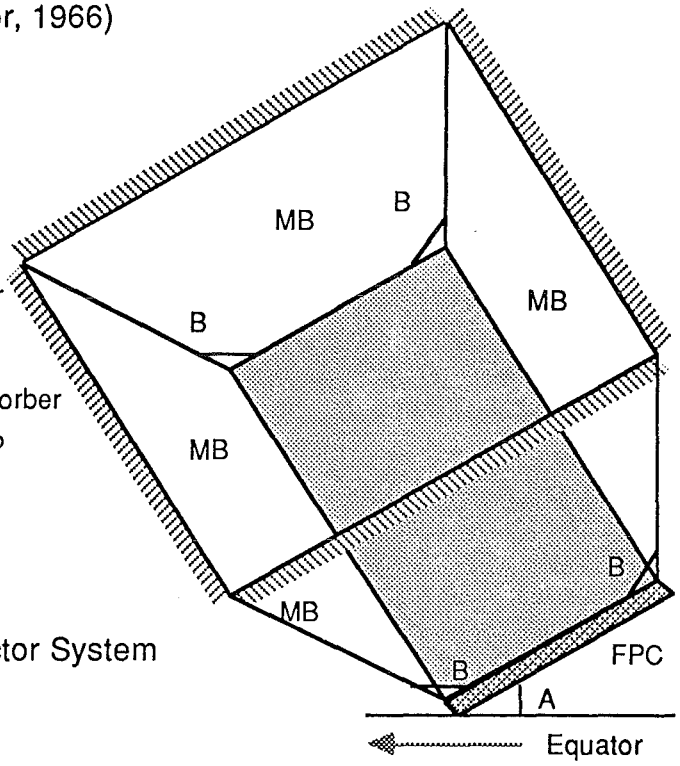

(4) Alternate Absorber-Reflector System (Delyannis, 1978)

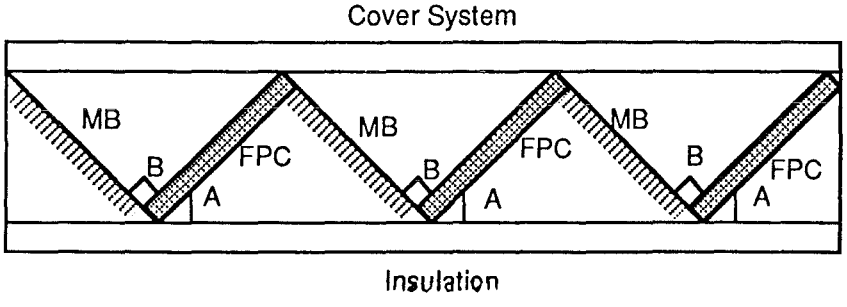

can be effectively used, thus cutting down the absorber costs by half and this was one of the initial reasons for developing the SCCR collectors. As the SCCR can be made of simple, low cost metallised plastic sheets such as aluminised mylar, it costs much less than the absorber. Although a concentration ratio of up to two is possible with SCCR due to the sun's virtual motion, in effect the overall concentration ratio becomes one, because the total absorber area (2LR) is same as that of the aperture area as shown in Fig. 4.6.

4.4.2.1 Background

Several researchers have developed different means of upgrading the quality of energy or improving the efficiency of flat plate collectors as shown in Fig. 4.9. Tabor (1958, 1966) and McDaniels et al. (1975) have reported obtaining, up to double the usual output of a flat plate collector (especially in winter) by employing flat mirror boosters (one to four, as shown in Fig. 4.9a) in the East-West direction. Seitel (1975), Espy (1978) and Delyannis (1978) have investigated the optimum orientation of mirror boosters and suggested different sizes and types of reflectors (Fig. 4.9a). However, they used only one side of the absorber.

Souka and Safwat (1966), Savery et al. (1976) and Larson & Savery (1978) developed double exposure collectors, wherein they used three flat mirrors (Fig. 4.9b) to reflect radiation on to both sides of the absorber. However, to get year-round better performance the mirror boosters need to be adjusted periodically.

Tabor and Zeimer (1962) used an inflated cylindrical plastic collector (Fig. 4.9c) with the bottom half reflecting and the top half transparent, and an absorber in an isosceles triangular profile containing three selectively coated tubes connected by fins and enclosed in another plastic envelope. They obtained temperatures as high as 150°C and a concentration ratio of three.

Kooi (1978) reported a 40% increase in annual efficiency using a partially reflecting semi circular cylindrical plastic dome, (which effectively tilts the solar energy collecting plane as shown in Fig. 4.9d) on solar ponds.

A reversed selectively coated flat plate absorber (Fig. 4.9e) with insulation on the top surface and a semi-cylinder reflecting radiation on the bottom surface has been reported to have obtained

FIGURE 4.9 Methods of Improving the Flat Plate Collector Efficiency or Output Temperature (*Continued*)

(b) Double Exposure Collector or DEC (Larson and Savery, 1978)

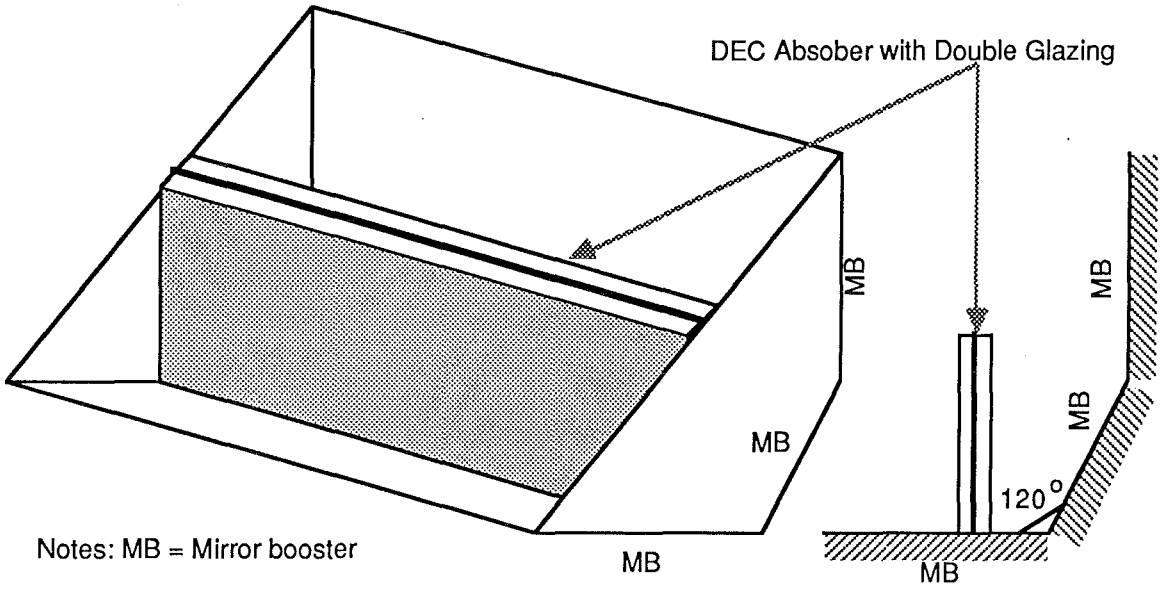

(c) Inflated Cylindrical Plastic Collector (Tabor and Zeimer, 1962)

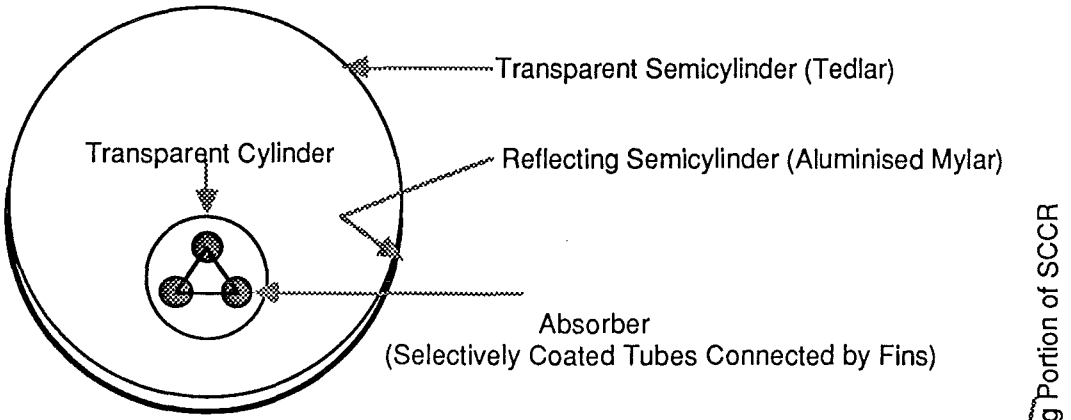

(d) Partially Reflecting SCCR (Kooi, 1978)

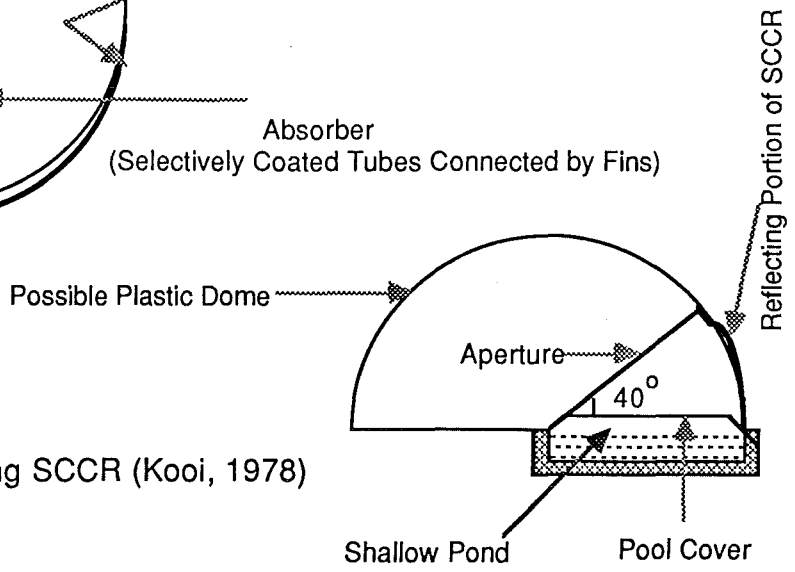

FIGURE 4.9 Methods of Improving the Flat Plate Collector Efficiency or Output Temperature (*Continued*)

(e) Reverse Flat Board Type Collector (Electrotechnical Laboratory, 1978)

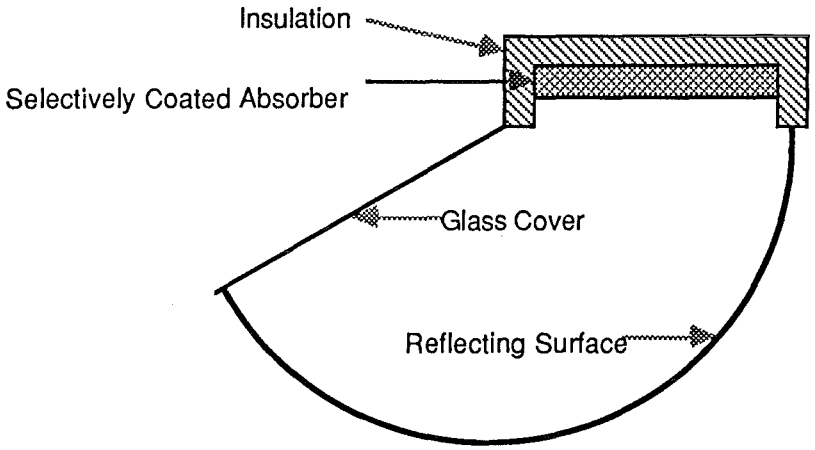

(f) Reversed Flat Plate Collector (Das and Wibulswas, 1983)

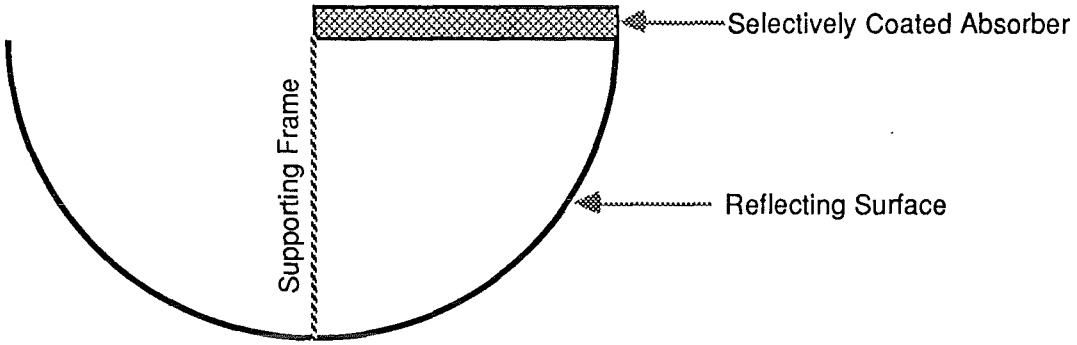

(g) SCCR with Split Plate Absorber (Robertson, 1979)

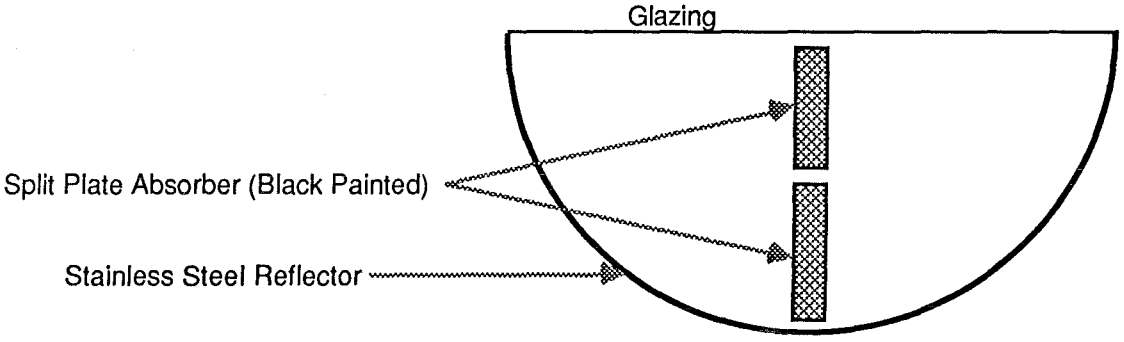

a stagnation temperature of about 180°C (Electrotechnical laboratory, 1978). Das and Wibulswas (1983) have also experimented with a reversed flat plate collector (Fig. 4.9f) but without any insulation on the top surface of the absorber, thus utilizing both sides of the absorber. None of these researchers tried to use a flat plate absorber in the axial plane of SCCR, which has several advantages.

However, Robertson (1979) suggested the use of split plate absorbers, with SCCRs as concentrating collectors (Fig. 4.9g). With SCCR, localised concentration occurs on the back absorber because for most of the time more than half of the incident radiation reaching the absorber strikes the back half (as noted from previous section). Hence, the front absorber acts as a preheater working at low temperatures and high efficiency. It feeds preheated fluid to the back absorber working at high temperatures under concentration, where losses are kept low due to its smaller surface area. The front and back absorbers are thermally isolated from each other so they can operate at different temperatures. Webb (1979) built one such unit with a stainless steel reflector and concluded that the increase in performance of 8% would not offset the extra effort needed to fabricate a split plate absorber, as compared to a single plate absorber.

4.4.2.2 Merits and demerits

There are several advantages in using the SCCR along with a flat plate absorber as compared with any other concentrator or a simple flat plate collector by itself and they are given below.

(1) Both sides of the absorber are used, so only half as much of the absorber area is needed for any particular application, thus reducing the capital costs. SCCR costs much less compared to almost any other type of concentrator because cheap materials such as aluminised mylar can be utilized for the reflector.

(2) Conduction losses through the back of the collector are minimised as the absorber, which is at the highest temperature, (in any solar collector) is not in direct contact with the insulation. The SCCR, which is in direct contact with insulation, is at a much lower temperature.

FIGURE 4.10 Working Principle of a Thermosyphon Heat Pipe

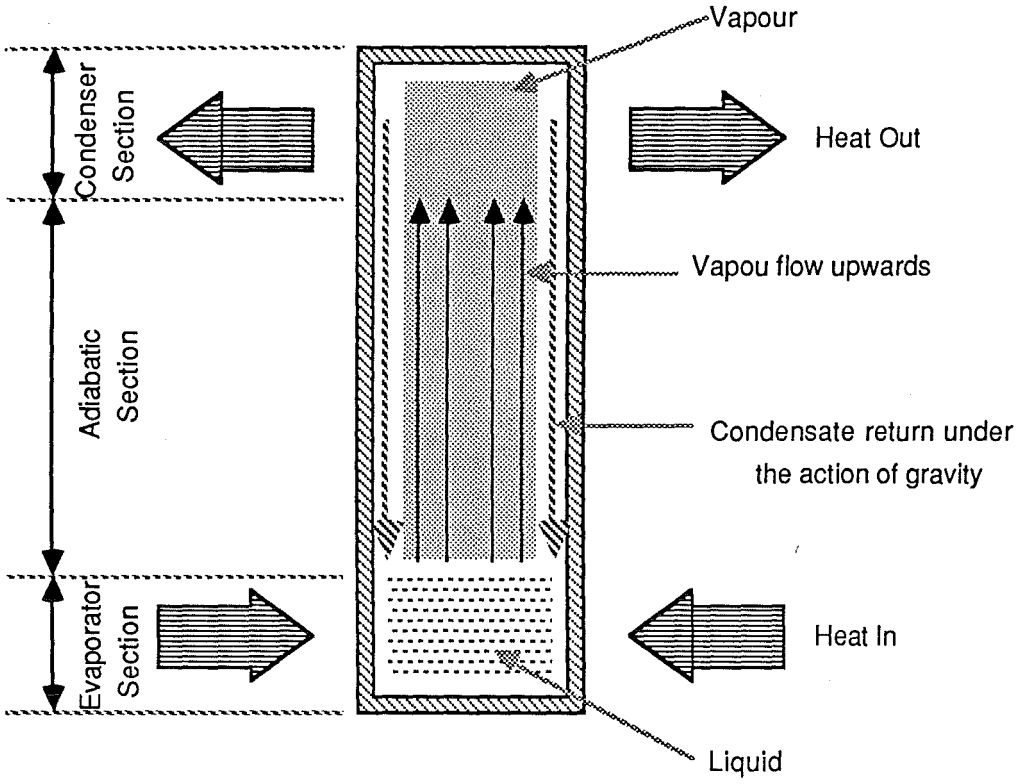

(3) Convection losses can also be reduced, by totally encapsulating the absorber in inner glazing and having an outer glazing on the aperture.

(4) The SCCR with the HSA panel has a maximum acceptance angle (±90°) as compared to other cylindrical reflectors as discussed earlier. Hence, any ray entering the aperture is redirected to the absorber plate situated in its axial plane.

(5) The SCCR collector can collect solar radiation for at least eight hours every day of the year without adjustment if it is oriented with its longitudinal axis in the East-West direction (Section 4.4.1). Thus the average yearly efficiencies are improved.

(6) Operating and maintenance costs of tracking mechanisms are eliminated completely. The SCCR does not need even seasonal adjustments.

(7) It is a very simple shape and easy to build.

The disadvantages of SCCR are given below.

(1) A larger collector box is needed and also it is harder to construct as compared with the simple rectangular box necessary for a flat plate collector.

(2) As no reflector has 100% reflectivity the amount of radiation reaching the absorber is reduced.

(3) It produces an uneven energy flux distribution on the absorber plate (as described earlier).

These disadvantages have been overcome to a large extent as described in the following sections. The collector box, although of odd shape, can be folded out of a metal sheet, or vacuum formed from plastic. There are highly reflective sheets with plastic backings (such as aluminised mylar), whose reflectivity can be more than 90%, hence the loss of radiation is not substantial. The uneven flux distribution is offset by the isothermal nature of the HSA panel.

4.4.3 Heat sheet absorber (HSA)

The heat sheet absorber is based on the principle of a thermosyphon heat pipe or a wickless heat pipe, which is illustrated in Fig. 4.10. A heat pipe consists of a closed container (usually but not necessarily a tube or pipe), which is evacuated and then charged with a small amount of volatile working

fluid. When heat is applied to the bottom section, known as the evaporator section, the liquid in the heat pipe vaporises, and the vapour travels upwards via the adiabatic section (where no heat is exchanged with the surroundings) to the condenser section, where the vapours are condensed, giving out heat to an external fluid, and the resulting condensate returns to the evaporator section by gravity. Thus a heat pipe basically employs an evaporating-condensing cycle.

The adiabatic section is optional and not necessary for the operation of a heat pipe. Many heat pipes employ a wick structure close to the walls of the heat pipe to create capillary forces and assist in the flow of the condensate. The heat pipes employing wicks can be oriented in any convenient position, unlike thermosyphon heat pipes, where it is necessary to locate the condenser section above the evaporator section. The theory, design and applications of heat pipes has been well described by Cotter (1965), Chisholm (1971) and by Dunn & Reay (1978). In particular the characteristics of thermosyphon heat pipes have been described by Grover et al. (1964), Lee & Mital (1972) and Lee & Bedrossian (1978).

4.4.3.1 Use of heat pipes as solar collectors

Though heat pipes have been used in various other applications, it is not until recently that their use in solar technology has been investigated. Bienert (1973) first reported the use of heat pipes for solar energy collectors at the first International Heat Pipe conference in 1973. In the same year Kupler & Kogles (1973) reported use of such collectors in sea water desalination, and Jordans et al. (1973) in power systems. However, all the researchers have used "heat pipes attached to flat plates" as solar collectors.

There are basically three ways in which heat pipes can be incorporated into an absorber plate as shown in Fig. 4.11 (Biernert 1974) and most commonly, the types A and B are employed.

In typical heat pipe collectors the heat pipes replace ordinary liquid carrying pipes in a pipe and fin absorber as shown in Fig. 4.12 (Bienert & Wolf, 1976). The heat pipe collectors, as shown in the figure consists of an array of heat pipe elements, cooled by a common heat exchanger, denoted as a condenser block in the diagram. The heat exchanger forms an important part of the

FIGURE 4.11 Incorporation of Heat Pipes into Absorber Plate

(a) Individual Heat Pipes Bonded to Absorber Plate in Preformed Grooves

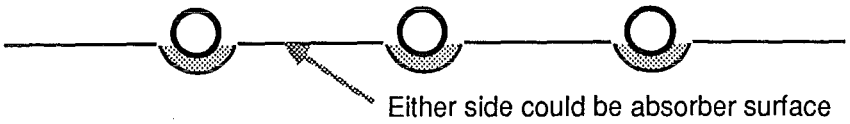

(b) Individual Heat Pipes Extruded with Integral Absorber Fins

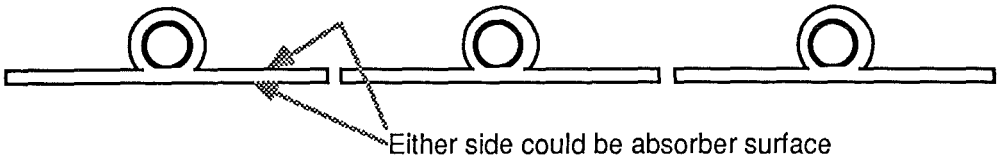

(c) Absorber Plate with Integral Heat Pipes Formed in 2-Piece Bonded Plate

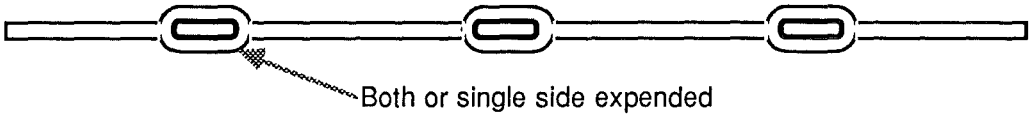

FIGURE 4.12 Roll Bond Heat Pipe Absorber

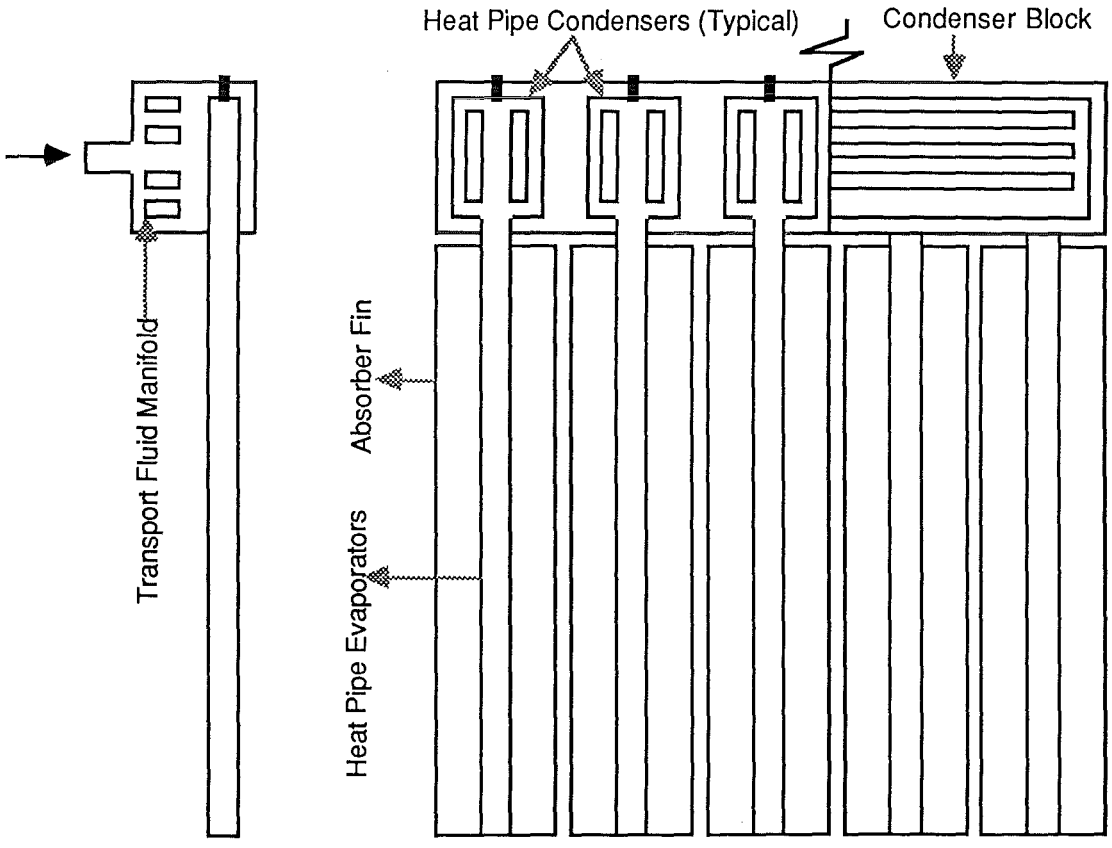

heat pipe collector as it offers the principal resistance to heat flow (resistances in a heat pipe collector are discussed later in this chapter) and hence needs careful consideration. There are several ways of attaching heat pipes to liquid or air manifolds and Fig. 4.11 shows one way of attaching a liquid manifold (Bienert and Wolf, 1975). The manifold can be made an integral part of the absorber plate or made detachable using a mounting saddle and clamp, but the resistance to heat flow is increased.

Bienert and Wolf (1975, 1976) have performed extensive work with solar collectors employing mainly roll-bond heat pipe absorbers (Fig. 4.12). They have reported detailed studies on various configurations, performance analysis, and economic analysis. The same authors have also reported using a series of stationary Fresnel lenses to concentrate solar radiation on a heat pipe absorber panel, and achieved, on the average over a whole year, 30% more useful energy at a temperature difference between fluid output and ambient of 55°C. However, these systems are more expensive, more complicated and achieve lower stagnation temperatures (about 150°C) and hence, they are not suitable for solar refrigeration. An important conclusion that can be arrived at from their work is that heat pipe absorbers have higher resistance (about 2 to 5 times), and slightly lower instantaneous efficiency (1 to 5%), but have higher annual average efficiency (of about 10%), and higher overall system efficiency, as compared with ordinary flat plate collectors.

Francken (1975, 1978) and de Vries et al. (1980) have reported a similar system employing an array of heat pipes connected by a common condenser tube, but only for low temperature applications. Rao and Rao (1976) and Sion et al. (1979) have also reported, collectors with fluid undergoing a phase change, which were employed for pumping water for irrigation purposes. Rush and Sendall (1977) used a modified heat pipe absorber in which the heat pipes have two parallel tubes, one below the other, so that only the evaporator tubes are connected to the blackened copper plate while the condenser tubes are not.

Other solar collectors employ an array of heat pipes encapsulated in evacuated chambers (to reduce heat losses) and hence, they are not attached to a flat metal sheet. They have construction which is very similar to that of evacuated tubular collectors. They employ various types of working fluids depending

FIGURE 4.13 Heat Sheet Absorber Panel

(a) Front View

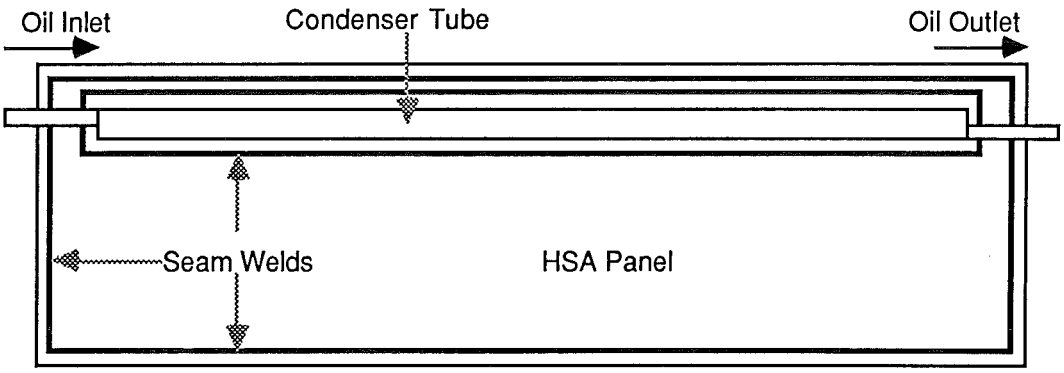

(b) Cross Section

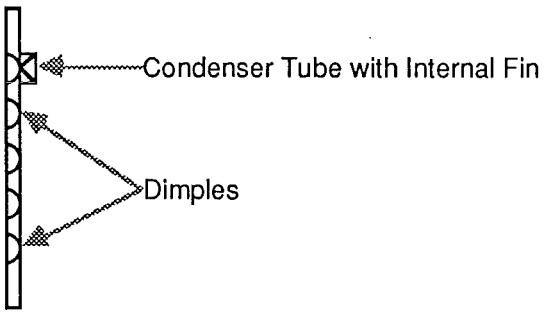

on the operating temperature range. Mahdjuri (1978), Hermann et al. (1978), Ortabassi (1976) and Russell (1978) have reported performance studies of such collectors. The commercial organisations that sell such collectors include Dornier (West Germany), Redpoint Associates Ltd. (England), Solar Research (USA), Philco Italiana (Italy) and Mann-Russell Electronics, Inc. (Western Australia). Although these collectors are more efficient and have flatter HWB plots, they are much more complicated and expensive than conventional tube and plate collectors.

To overcome some of the deficiencies of the heat pipe collectors a simple two dimensional (flat plate) thermosyphon absorber known as a "heat sheet absorber" has been developed in this Department. It is quite different to the flat plate heat pipe used extensively in electronics cooling, in which the heat is transferred between the two flat plates (Dunn and Reay, 1978).

The heat sheet absorber (HSA) as shown in Fig. 4.13 consists of two plates seam welded together around the edges to form an envelope which is evacuated and then loaded with a small amount of working fluid and hermetically sealed. One of the two sheets is punched with a dimple pattern to prevent the envelope from collapsing under reduced internal pressure. The condenser section of the HSA is formed by attaching a heat exchanger (either circular or rectangular in cross section) to the top of the panel. As shown in Fig. 4.13 a rectangular condenser tube with internal fins was used (the details of which will be described later). As the solar radiation heats up the fluid in the envelope it vaporizes and travels upwards through the tortuous path made by the dimples to the top end of the panel where it condenses giving up its latent heat to the fluid running through the condenser tube. The condensate then returns to the bottom portion of HSA being distributed over the whole surface by the dimples.

4.4.3.2 Merits and demerits

The HSA possesses almost all the merits and demerits of a thermosyphon heat pipe. It has also a few advantages over ordinary flat plate collectors.

Advantages of heat pipes and HSA

(1) A heat pipe has the ability to act on as a thermal flux transformer. That is, it can take heat from a small region and deliver it into a large region or vice versa and this feature is

very useful in solar collectors because of the very dilute nature of the solar energy.

(2) As the condensation film coefficient is very high the main resistance in the heat pipe is the conduction resistance of the wall. A heat pipe therefore carries approximately about 100 to 1000 times that conducted by a solid bar of the same metal of equal length. Hence, the disadvantage of non-uniform flux distribution of the SCCR can be offset by the isothermal nature of HSA.

This property also leads to:

(a) usage of cheaper materials with lower thermal conductivity such as steel,

(b) the limiting case of allowable tube spacing (of a pipe and fin type collector) and thus making it possible to use just one condenser tube,

(c) high rates of heat transfer,

(d) high power handing capability (Heat fluxes as high as 15 $kW.cm^{-2}$ have been measured with heat pipes by Besse et al, 1968) and

(e) transporting thermal energy with very small temperature differences.

(3) A wide range of heat pipe working fluids is available and hence a particular fluid can be selected for any working temperature range. Corrosion and freezing problems can be eliminated by proper choice of the working fluids.

(4) Thermosyphon heat pipes have no wick structure (unlike ordinary heat pipes, thus avoiding problems concerned with wicks) to accomplish condensate return and hence energy transport occurs only in upward direction. Because of the unidirectional energy transport characteristic these are also known as "thermal diodes". This thermal diode nature of heat pipe collectors offers the following advantages:

(a) The diode property prevents the panel from acting like a radiative cooler during the periods of no insolation or low insolation, as the only link between the condenser fluid and panel is through conduction from the tube to the plate. Since this is one of the major thermal resistances in the system, and since the driving force will be much smaller than in the heating mode, there will be relatively little heat transfer back to the panel. de Vries et al. (1980) evaluated the resistances in a conventional

collector and in a heat pipe collector (both of 1 m^2 area). They found that the absorber fluid resistance in the case of conventional collectors was 0.0022 $K.W^{-1}$, and remained the same, when $T_p > T_f$ and $T_p < T_f$ (where T_p and T_f are the temperatures of the panel and the condenser fluid respectively). But in a heat pipe collector, the resistance was 0.01 $K.W^{-1}$, when $T_p > T_f$ and it was 10 $K.W^{-1}$, when $T_p < T_f$. This would mean that separate temperature sensors are not required to stop the circulation of the condenser fluid, when $T_p < T_f$. On the other hand the thermal diode type of control works on individual panels in a set.

(b) This property suppresses the heat losses during the transient periods of insolation. Bienert and Wolf (1976) found that the heat losses from the heat pipe collectors are about one quarter of that of ordinary flat plate collector of similar dimensions, during transient periods. This effect automatically leads to a higher overall collector efficiency. They also found that, under certain ambient conditions and solar insolation, the diode characteristics of a heat pipe absorber panel can provide twice the energy supplied by an identical non-dioding collector.

(c) Special collector designs can be devised in which the diode feature increases the collector efficiency during periods of low insolation. These designs include stationary concentrators such as small flat reflectors located at right angles to the absorber surfaces. This results in increased efficiency during periods of oblique incidence because the illuminated portions of the surface contribute to the energy collection in accordance with the higher local incident flux, whereas the shaded portions do not contribute to heat losses. Thus diode action can be used to spread out high efficiency energy collection over large portions of the day. Biernert & Wolf (1975) reported that at a temperature difference between fluid output and ambient of 80°C, the stationary concentrator will double the annual output, per unit of collector area as compared to a flat plate collector having identical parameters. Thus the combination of HSA with SCCR can be advantageous and fully justified.

(5) The heat capacity of a heat pipe collector is lower than that of a simple flat plate collector mainly because of the small amount of fluid contained by the former collector. It has been shown in Appendix A5, that the heat capacity of a conventional flat plate collector with similar parameters is about 2.6 times

that of HSA. This property causes the HSA to have a faster warm up in the mornings and react more quickly on cloudy days when the energy source is intermittant.

(6) The adiabatic section of the heat pipe can be increased and the energy transported longer distances without a pump (and through smaller lines) to any required parts of the system. Thus the circulating pump and subsequent costs can be eliminated and a very efficient passive system can result. The has potential application of this in solar refrigeration discussed in Chapter 6.

Apart from these advantages, the HSA has the following merits as compared to other heat pipe collectors.

(1) It is simpler to build and costs less

(2) The condenser tube can be easily attached with much less resistance, resulting in better heat transfer between the condenser fluid and heat pipe fluid.

(3) The area of contact between the condenser tube and the heat pipe is more and it is easy to increase even further.

(4) The whole area of HSA is available for solar energy collection and is equally effective, unlike other heat pipe collectors, where the major portion is the fin area through which heat needs to be transferred first by conduction; thus introducing an extra major resistance in the path of heat flow.

(5) The HSA is a single heat pipe unlike other heat pipe collectors which have several heat pipes each of which must be evacuated and charged separately, consequently increasing the manufacturing costs.

Potential disadvantages of HSA

(1) The working fluid needs to be selected very carefully as the operating pressure inside the panel should never exceed one atmosphere (as otherwise it may rupture the panel) at maximum stagnation temperature. At the same time a reasonably high vapour pressure is required at the working temperature.

By proper selection of the working fluid, experimentally evaluating the vapour pressure (if data is not available in the literature) and by careful observation of the operating pressure of the panel, with the help of a pressure gauge, this problem can be eliminated.

(2) Since the HSA has two sheets seam welded together, the integrity of the seam weld is critical to the length of service given by a panel.

However, HSA panels have been tested in this Department and no problems have been experienced with seamwelds, during the past eight years.

It is advantageous to analyse and understand the significance of different components of the HSA-SCCR collector, before building the physical model. Hence, the simulation and modelling of the collector has been described in the next section along with the sensitivity test, before going into the details of the collector design.

4.5 Modelling of HSA-SCCR Collector

Computer modelling is a very important tool as it enables one to examine possible modifications and study their effects, without having to physically perform the changes and this saves enormous amounts of money, effort and time. Modelling is especially useful in solar energy applications because it enables one to make comparisons at identical conditions, which is difficult to achieve with actual equipment.

As mentioned in Section 4.3, Webb (1979) developed a simple model of a SCCR-HSA collector. Based on the predictions of Webb's model the first solar collector of this investigation was built, and when it failed to reach the predicted stagnation temperature (which was about 21% higher than the actual value, as shown in Table 4.2), the model was examined thoroughly, and several simplifying assumptions were found. Hence, that model was discarded completely, and a model incorporating all possible details was developed.

This model is useful in several ways. It can estimate several temperatures, heat flows and resistances, at stagnation conditions. which are difficult, cumbersome and expensive to measure. Thus, it providing a means of understanding how far each component plays a role in the overall working of the collector. It can be used as an important design tool as one can find out the effects of various possible changes such as using different reflectors, glazings, selective coatings, insulating materials, box construction materials and dimensions, HSA panel length and width in order to choose the best possible combination for the

FIGURE 4.14 The Solar Spectrum

(Solar Energy Handbook, 1979)

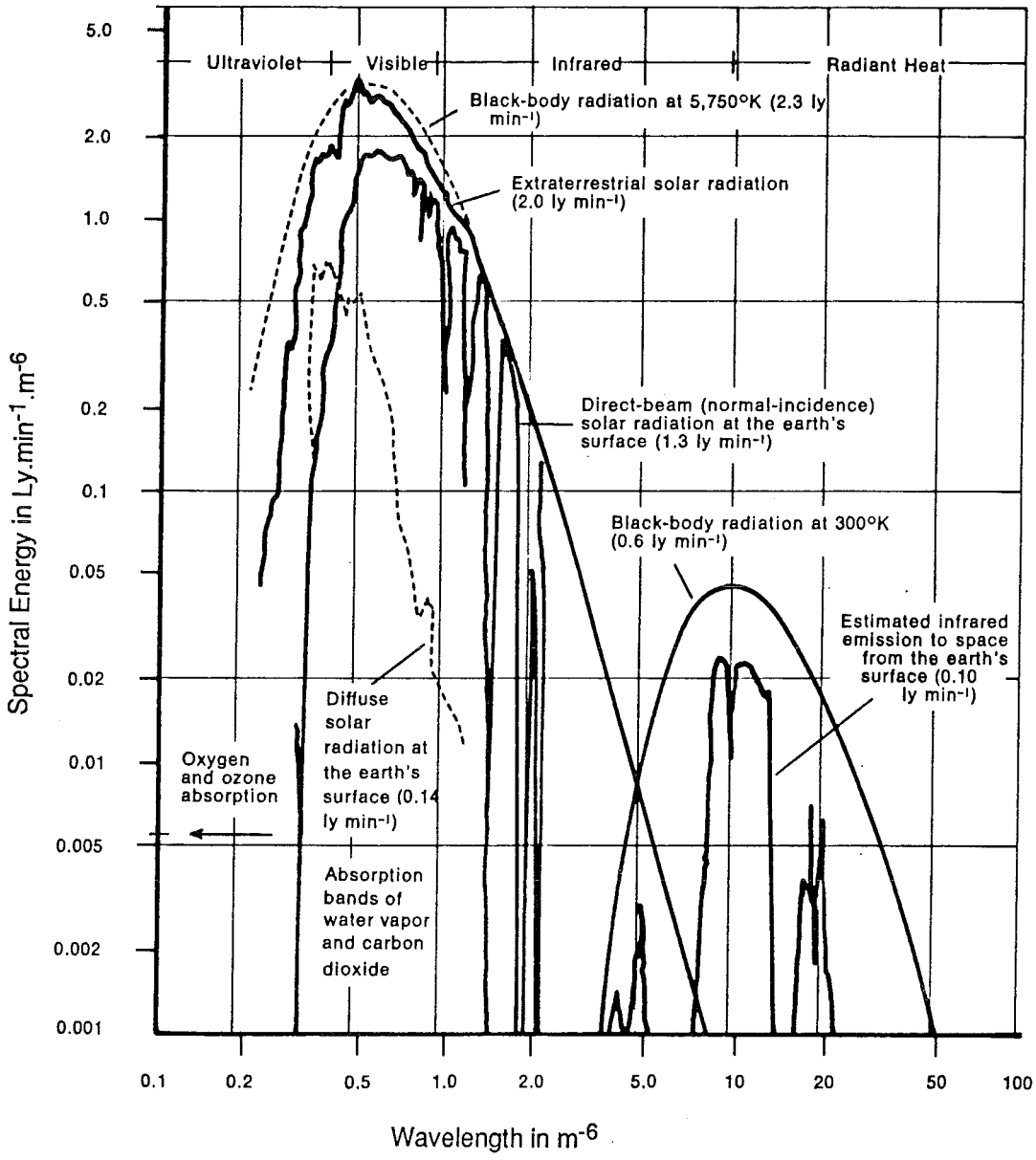

Notes: Ly = Langley

$Ly.min^{-1} = 697.3\ W.m^{-2}$

specific application (Prasad, Webb and Williamson, 1984). One can find the components which have major effects on the performance of the collector and concentrate attention on those particular parts. Also it is possible to couple this with cost data to do a complete optimisation.

The model can predict the optical efficiency and the stagnation temperature of the absorber panel and hence the HWB plot for a collector. This plot can be used for various purposes as mentioned in Section 4.2. One can use this information to find the area of collectors needed for a specific application (using the f-chart method as described by Duffie and Beckman, 1977), thus facilitating the design of the entire system. The model can also evaluate the performance under various ambient conditions, insolations, wind speeds and latitudes, which would be helpful in predicting the performance of the collector in different seasons of the year and different parts of the world.

It should be mentioned here that the simulation is a static one, as dynamic simulation of two phase closed thermosyphon system is very complicated, and beyond the scope of present investigation. Mathematical description of these systems (and not of HSA panels used in solar collection) has been reported by Ali (1977), Lee & Mital (1972), Lee & Bedrossian (1978), Bezrodnyi & Alekseenko (1977) and Streltsov (1975). However, static simulation is sufficient to yield large amounts of information about the collector and its performance as mentioned earlier.

When dealing with solar collectors, one encounters two types of radiation, the first being called the solar or short wave radiation and the second the thermal or long wave radiation. These terms can be best understood from the solar spectrum shown in Fig. 4.14. Almost all the solar radiation incident on the collector has a wave length between 0.2 to 2 microns (assuming the sun is approximated as a black body at 5750 K), with a peak value at about 0.5 microns, while virtually all the radiant heat or thermal radiation emitted by a body at 300 K has a wave length greater than 3 microns.

Thus, there is little overlap between the two types of radiations and they can be treated separately. Short wave or solar radiation is the input to the collector, which raises the temperature of various components of the collector that it encounters in its path. Once the temperature is raised above the

ambient, the collector starts losing heat and this is the output energy emitted in the long wave region. The material properties such as reflectance, transmittance, absorptance and emittance are sometimes strong functions of wave length and hence not the same for solar and thermal radiation. For this reason short wave and long wave are analysed separately.

In many solar energy applications it is necessary to determine the position of the sun in order to find out the angle of incidence of the sun's rays, because the performance of a solar collector does depend on the angle of incidence. Hence, the first step in modelling a solar collector is to find out the position of the sun.

Thus the collector model consists of three main parts:

(1) determination of the sun's position,

(2) analysis of short wave radiation or optical behaviour, and

(3) analysis of long wave radiation or thermal behaviour.

4.5.1 Determination of the sun's position

The American Ephemeris and Nautical Almanac contains tables (Newcomb, 1898) for determining the position of the sun, but these tables are not of much use for computer modelling. Furthermore, the algorithm for generating the tabular values (HMSO, 1961) is very complicated because the values are calculated to an angular resolution of 0.1 second of an arc. To achieve this kind of accuracy, detailed perturbations of the earth's orbit by the moon and planets, and other small effects such as luni-solar precession and nutation of the earth's orbit, stellar aberration, refraction by the atmosphere, and parallax are considered. However, for most applications, including mirrors tracking for a solar tower generator, an accuracy of 0.05° is quite adequate (Vant-Hult and Hildebrandt, 1976) and hence, a simplified algorithm has been developed by Walraven (1978), which computes the position of the sun to within 0.01°. In the present case this has been adopted. The theory behind the algorithm has been described by Walraven (1978) and the slightly modified version of the programme TPSUN with a sample set of results for 24 February 1984 are given in Appendix A7. This programme evaluates the solar altitude, azimuth and EWV angle (these terms have been described in Appendix A3.2) of the sun for a given location, date and time. The EWV angle from

FIGURE 4.15a Basic Components of an Incident Ray

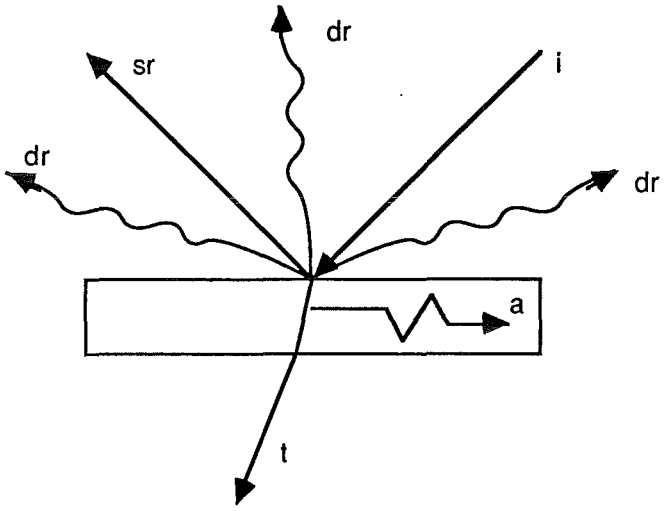

FIGURE 4.15b Basic Componets of Solar Radiation Entering a HSA-SCCR Collector

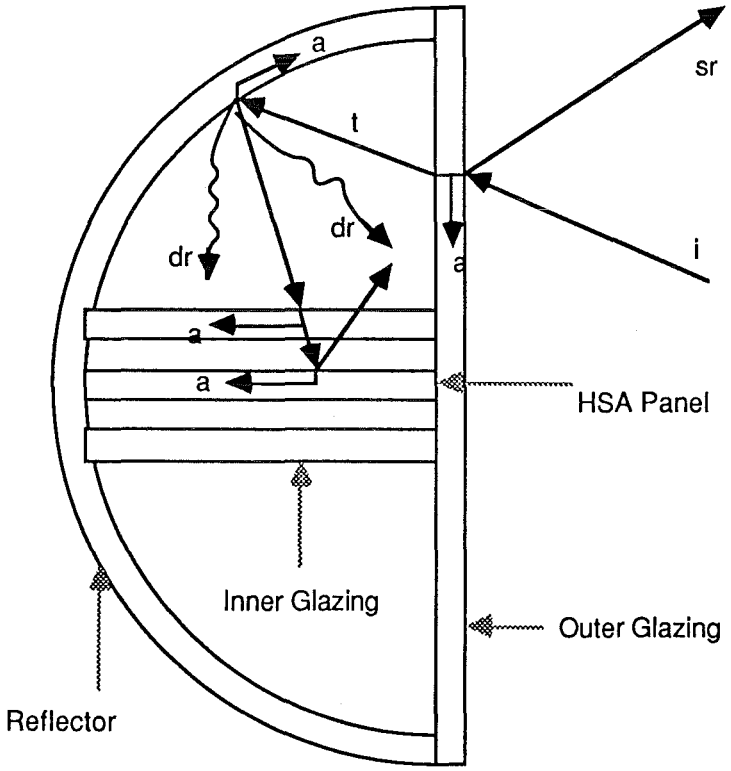

Notes: i = incident ; t = transmitted; sr = specularly reflected;

dr = diffusely reflected; a = absorbed radiation

this programme is fed to the second programme (analysing the short wave radiation), which in turn uses this to evaluate the angle of incidence.

4.5.2 Short wave radiation analysis

When radiation strikes a surface, it may be devided into a maximum of four components depending on the surface characteristics as shown in Fig. 4.15a: (1) transmitted radiation, (2) absorbed radiation, (3) specularly reflected radiation and (4) diffusely reflected radiation. Although all the surfaces do reflect diffusely, in the present case, except the reflector and the end walls, the other surfaces have been assumed to reflect specularly.

Solar radiation strikes the outer glazing first, of which a part is refleted, a part is absorbed and the rest is transmitted (Fig. 4.15b). A part of the transmitted radiation falls directly on the inner glazing and the rest is incident on the reflector, of which a part is absorbed and the rest is reflected specularly or diffusely. The specularly reflected radiation and a part of the diffusely reflected radiation falls on the inner glazing, which absorbs and reflects a part and transmits the rest to the absorber panel. The panel absorbs most of the radiation and the rest is reflected. Thus following the path of the individual rays as they enter the collector and reflected to the absorber panel, the amounts of radiation absorbed by by different parts of the collector and the collector's optical efficiency can be evaluated.

Short wave analysis is based on the ray trace techniques, which are introduced in Appendix A3.3. The rest of the theory is described in Appendix A8, which also includes the computer programme TPSWR. The programme TPSWR evaluates firstly the angle of incidence (θ) from EWV angle (supplied as an input from the programme TPSUN), then evaluates the specular and diffuse components of radiation incident, absorbed reflected and transmitted by various parts of the collector (such as outer glazing, inner glazing, reflector and absorber) as the rays strike them. It also calculates the collector's optical efficiency and the average number of reflections. The 13 input and 41 output parameters are given at the start of the TPSWR programme listing. The input variables include certain shape factors which are described in Appendix A9.

FIGURE 4.16 Analysis of Short Wave Radiation at 1p.m. on 24 Feb 1984
(For Top & Bottom Quadrants)

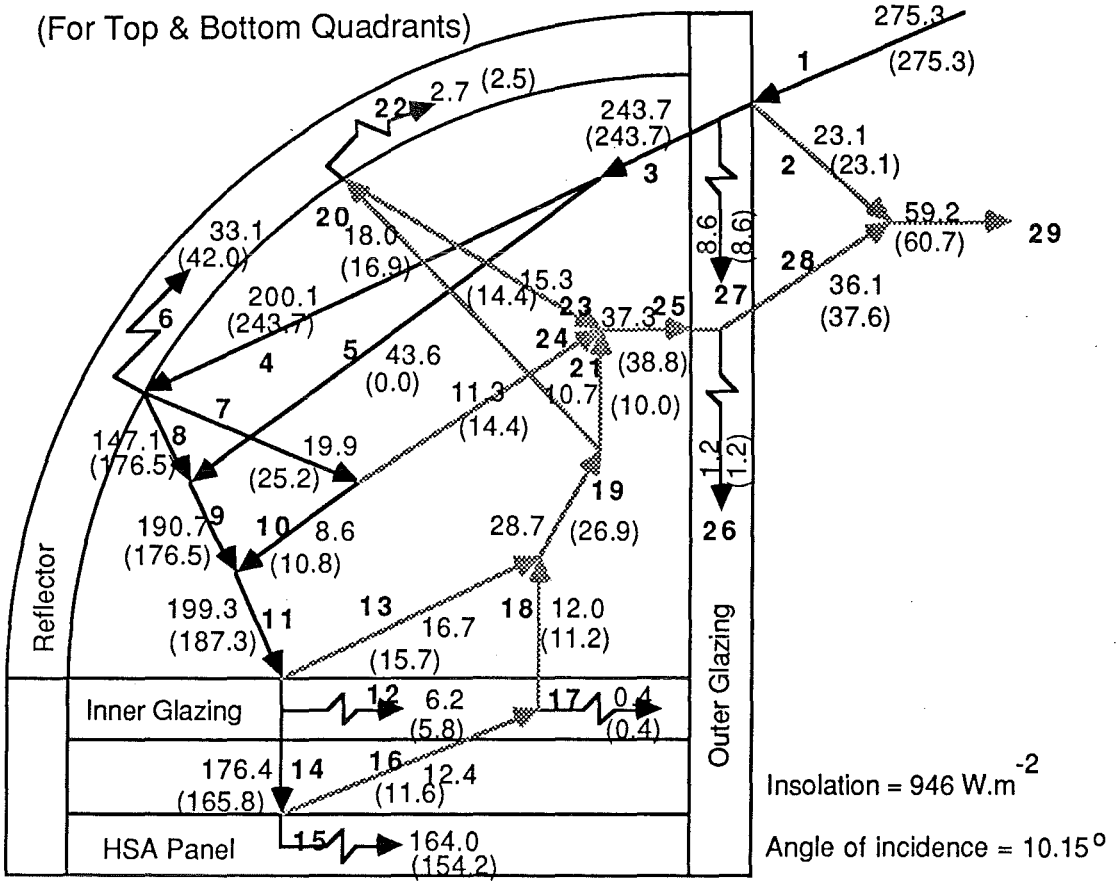

Notes: All numbers are in Watts and the numbers within brackets indicate for bottom quadrant
Only top quadrant is shown in the figure and arrows indicate energy flows
→ = primary radiation and ⇢ = secondary radiation

1.Total solar radiation incident on the outer glazing
2, 3 Primary radiation reflected and transmitted respectively by the outer glazing
4. Primary radiation incident on the reflector
5. Primary radiation directly incident on the absorber panel
6. Primary radiation absorbed by the reflector
7. Primary radiation diffusely reflected by the reflector
8. Primary radiation specularly reflected by the reflector
9. Total specular radiation incident on the inner glazing = sum of 5 and 8
10. Diffusely reflected (by the reflector) radiation incident on the inner glazing
11, 12, 13 Total primary radiation incident, absorbed and reflected resp. by the inner glazing
14. Primary radiation transmitted through the inner glazing and incident on the absorber
15. Radiation absorbed by the absorber panel
16, 17 Secondary radiation incident and absorbed respectively by the inner glazing
18. Secondary radiation transmitted through the inner glazing
19. Total secondary radiation from the inner glazing = sum of 13 and 18
20. Secondary radiation incident on the reflector
21. Secondary radiation from the inner glazing incident on the outer glazing
22, 23 Secondary radiation absorbed and reflected respectively by the reflector
24. Diffusely reflected radiation (from the reflector) incident on the outer glazing
25. Total secondary radiation incident on the outer glazing = sum of 21, 23 and 24
26. Secondary radiation absorbed by the outer glazing
27. Primary radiation absorbed by the outer glazing
28. Secondary radiation transmitted through the outer glazing
29. Total radiation lost to the atmosphere

In order to evaluate the shape factors, the collector is divided into two identical parts, top and bottom quadrants. The shape factors are evaluated for one section only as the shape factors are the same for the other section. However, it is not justified to use the same shape factors for the whole collector together, because the geometric shape factors are dependent not only on the relative areas but also on the relative positions of these areas with respect to one another. Also the energy inputs into the top and bottom quadrants are different as seen from Fig. 4.8 (except when the angle of incidence is zero). Hence, short wave and long wave analysis are carried out for each quadrant separately.

Webb's (1979) programme contained several simplifying assumptions and was written for a collector with single glazing only. Hence, TPSWR has been written for a collector with double glazing (and can also be used for collectors with single glazing) and taking into account those assumptions.

The results of short wave analysis at 1 p.m. on 24 February 1984 are given in Appendix A8 (TPSWR.DAT) and summarised in Fig. 4.16. It shows the various primary radiation (which is the radiation travelling towards the absorber panel) and secondary radiation (which is the radiation travelling towards the outer glazing) quantities for top and bottom quadrants of the collector separately. It can be seen that certain quantities for the bottom quadrant were zero (for example the primary radiation directly incident on the absorber panel), because the angle of incident of the incoming rays was about 10°. The average number of reflections was slightly more than one because of the low angle of incidence. The optical efficiency, which is the ratio of solar radiation absorbed by the panel to that incident on the outer glazing was about 58%. Of the 42% losses, 22% was lost to the atmosphere via the outer glazing (mainly due to the reflectivity of the inner and outer glazings) and the remaining 20% was absorbed by the reflector, outer and inner glazings. These losses can be minimised by using a highly specularly reflective (or less absorbing) reflector and less reflective (or less absorbing) glazing materials. The improvements in the performance of the collector with different reflector and glazing materials will be discussed in Section 4.5.4.

FIGURE 4.17 Effect of Angle of Incidence on the Optical Efficiency of the HSA-SCCR Collector

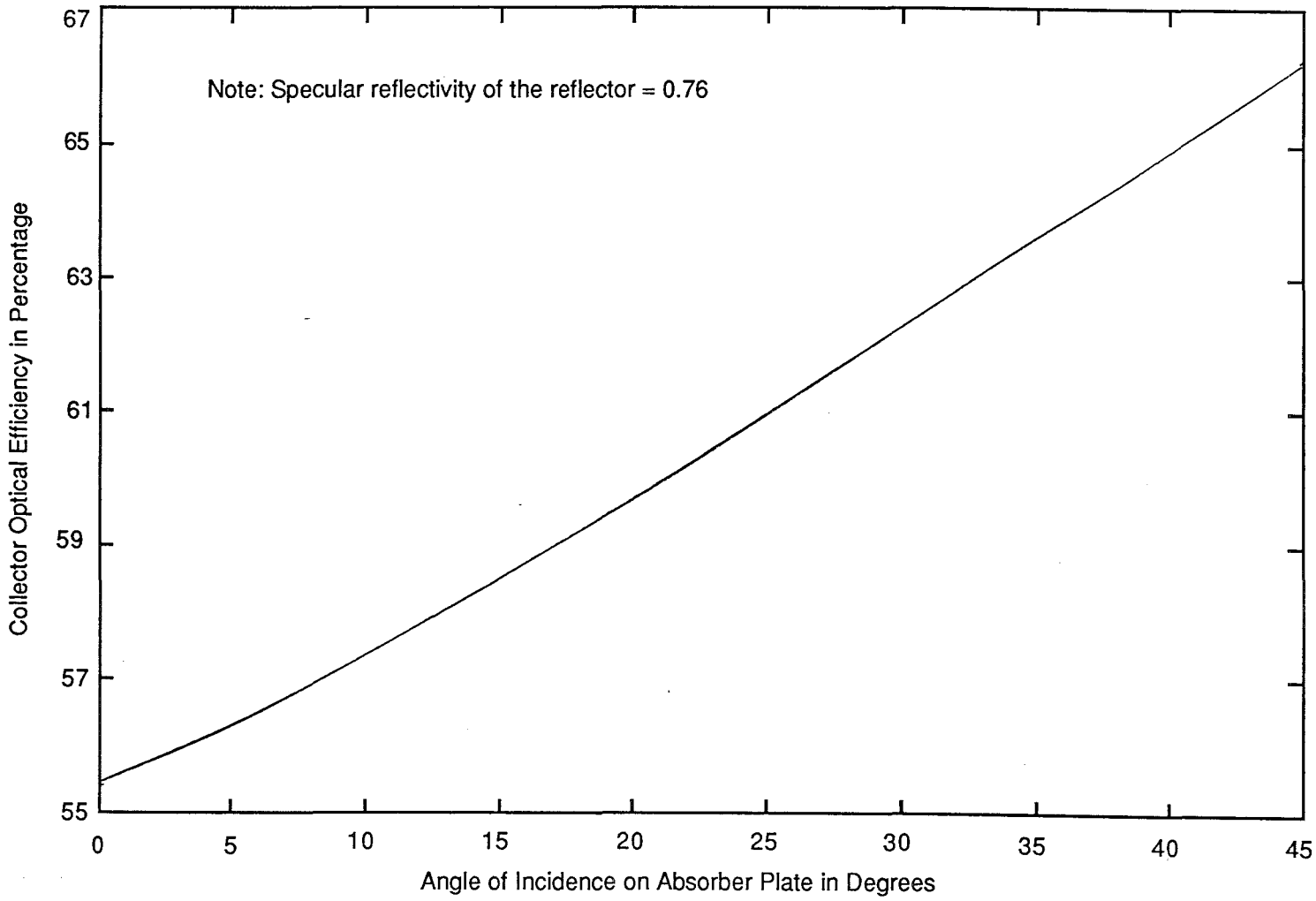

The optical efficiency of the collector changes throughout the day (Fig. 4.17) because it is dependent on the angle of incidence of the rays, which also varies during the whole day. As seen from Fig. 4.8, with the angle of incidence, the amount of direct and singly reflected radiation reaching the absorber increases, and that of multiple reflected radiation decreases. Thus, with the angle of incidence, the optical efficiency increases as shown in Fig. 4.17.

The amounts of solar radiation absorbed by the absorber panel, reflector, inner and outer glazings are introduced as inputs to the third programme, analysing the long wave radiation.

4.5.3 Long wave radiation analysis

Once the solar radiation raises the temperature of the different components of the collector above the ambient, the collector starts losing heat and this is the output energy emitted in the long wave region. At stagnation conditions when no useful energy is recovered from the collector all the input solar energy absorbed by various parts of the collector must be lost to the atmosphere by conduction, convection and radiation.Hence, by knowing the heat transfer characteristics of various surfaces and air spaces, and by conducting energy balance on each of themit is possible to determine the stagnation temperatures of these surfaces and air spaces.

Each of the important surfaces and air spaces in the collector (whose temperatures need to be evaluated) offers a resistance to the flow of thermal energy. The general expression for any resistance is given by

$$\text{Resistance} = \text{Driving force} / \text{Flow} \qquad (4.13)$$

When thermal energy q is flowing due to the temperature difference ΔT (which acts as the driving force) the resistance R can be written as

$$R = \Delta T / q \qquad (4.14)$$

For conduction through a solid according to Forrier's law of heat conduction

$$q = k A \Delta T / \Delta x \qquad (4.15)$$

where k is the thermal conductivity of the material, A is the area of heat transfer and $\Delta x$is the thickness of solid. The general expression for conduction resistance can be obtained by combining Eqs. (4.14) and (4.15).

FIGURE 4.18 Conduction/Convection Resistance Network Showing Resistances and Heat Flows at 1 p.m. on 24 February 1984

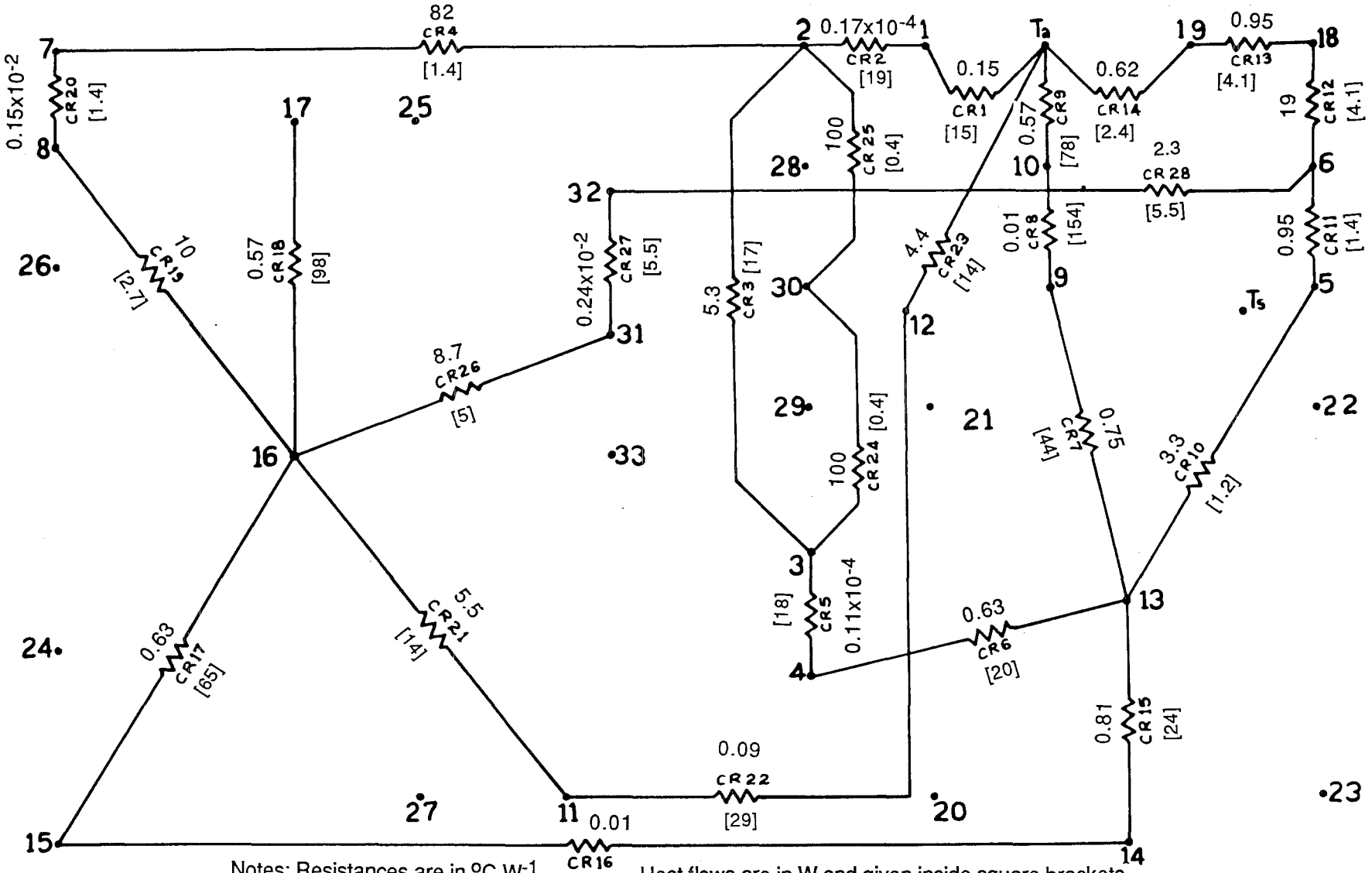

Notes: Resistances are in $^{o}C.W^{-1}$ Heat flows are in W and given inside square brackets

Conduction resistance = $\Delta x / k A$ (4.16)

The convective heat transfer can be expressed as

$q = h A \Delta T$ (4.17)

where h is the convective heat transfer coefficient, which is evaluated for a particular situation.

The general expression for convection resistance can be obtained by combining Eqs. (4.14) and (4.17).

Convection resistance = $1 / h A$ (4.18)

The radiation heat transfer is very complicated due to the geometry and presence of specular non-planar surfaces. It is difficult to give a general expression for radiation resistance, although general guidelines can be given. The general methods of analyses have been described by Holman (1972) and modified where necessary to meet the local requirements. (Appendix A10.2.1). Each surface offers a surface resistance and air gap a space resistance. With specular surfaces multiple reflections and with air spaces the absorptivity & emissivity of air have to be taken into consideration. With the help of Stefan-Boltzman law emissive power can be exprssed as the fourth power of the absolute temperature, which can then be put into the general form (as given by Eqn. 4.14) for the radiation resistance with ΔT as the driving force.

Various conduction, convection and radiation resistances can then be evaluated with the help of these general expressions. For the sake of convenience all the resistances can be divided into two main groups based on the mode of heat transfer.

(1) Conduction and convection resistances

(2) Radiation resistances

Thus the whole collector can be transformed conveniently, into these two resistance networks as shown in Figs. 4.18 and 4.19. They have the same junctions or nodal points as shown in Fig. 4.20 (which represent temperatures of surfaces and air spaces) and hence they can be superimposed to obtain a resultant combined network. From this network. Simultaneous equations can be derived for each of the nodes by conducting an energy balance at that particular node, thus obtaining the same number of simultaneous equations as the number of unknown temperatures. These equations are then solved in a matrix form using the Gauss elimination technique. A FORTRAN programme TPLWR (the flow chart of which is shown in Fig. 4.21) has been written to do all the

FIGURE 4.19 Radiation Resistance Network Showing Resistances and Heat Flows at 1 p.m. on 24 February 1984

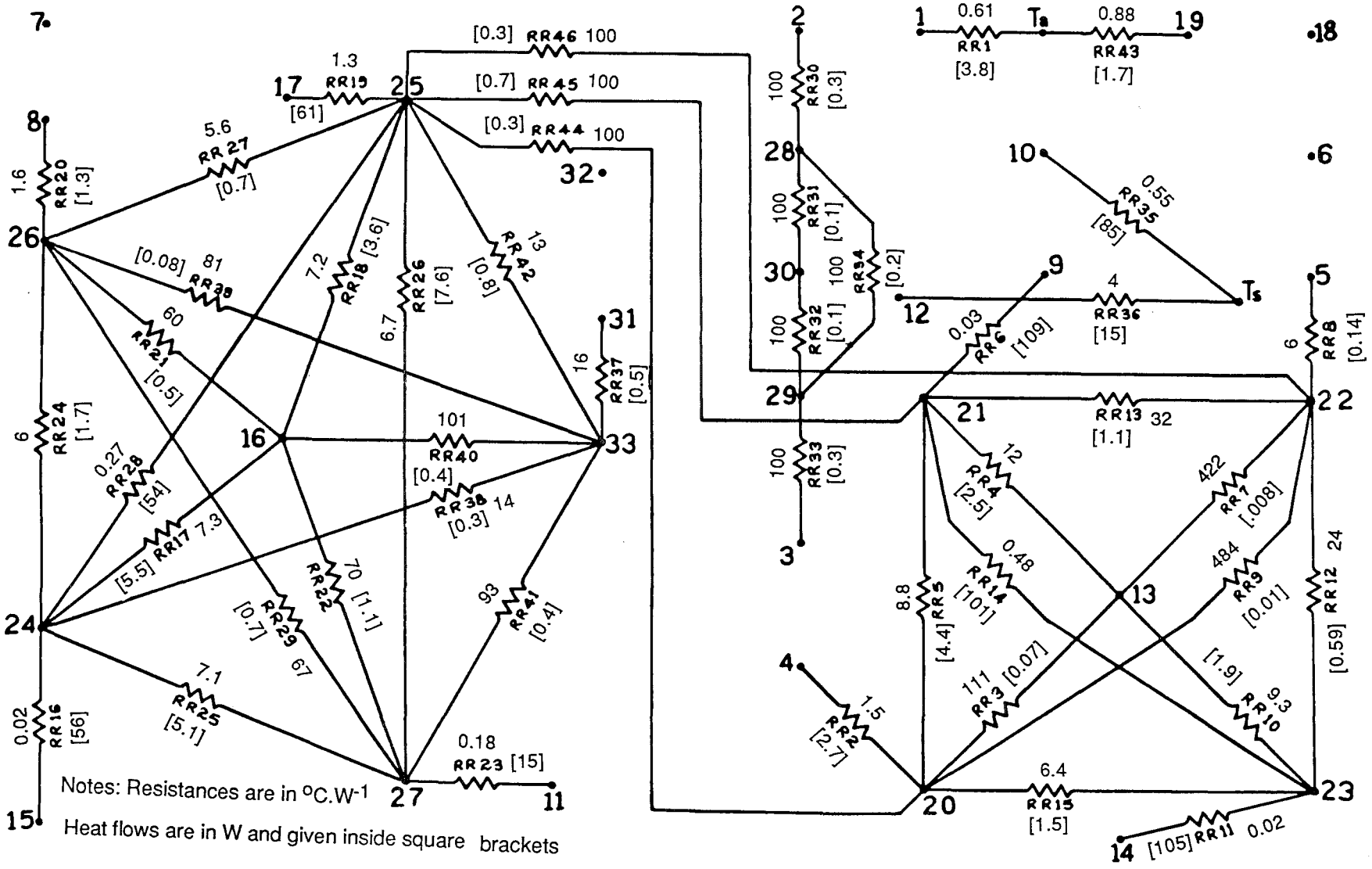

FIGURE 4.20 Cross Section of the HSA-SCCR Collector C2 with the Temperature Measuring Points (at Stagnation Conditions)

(Not to Scale)

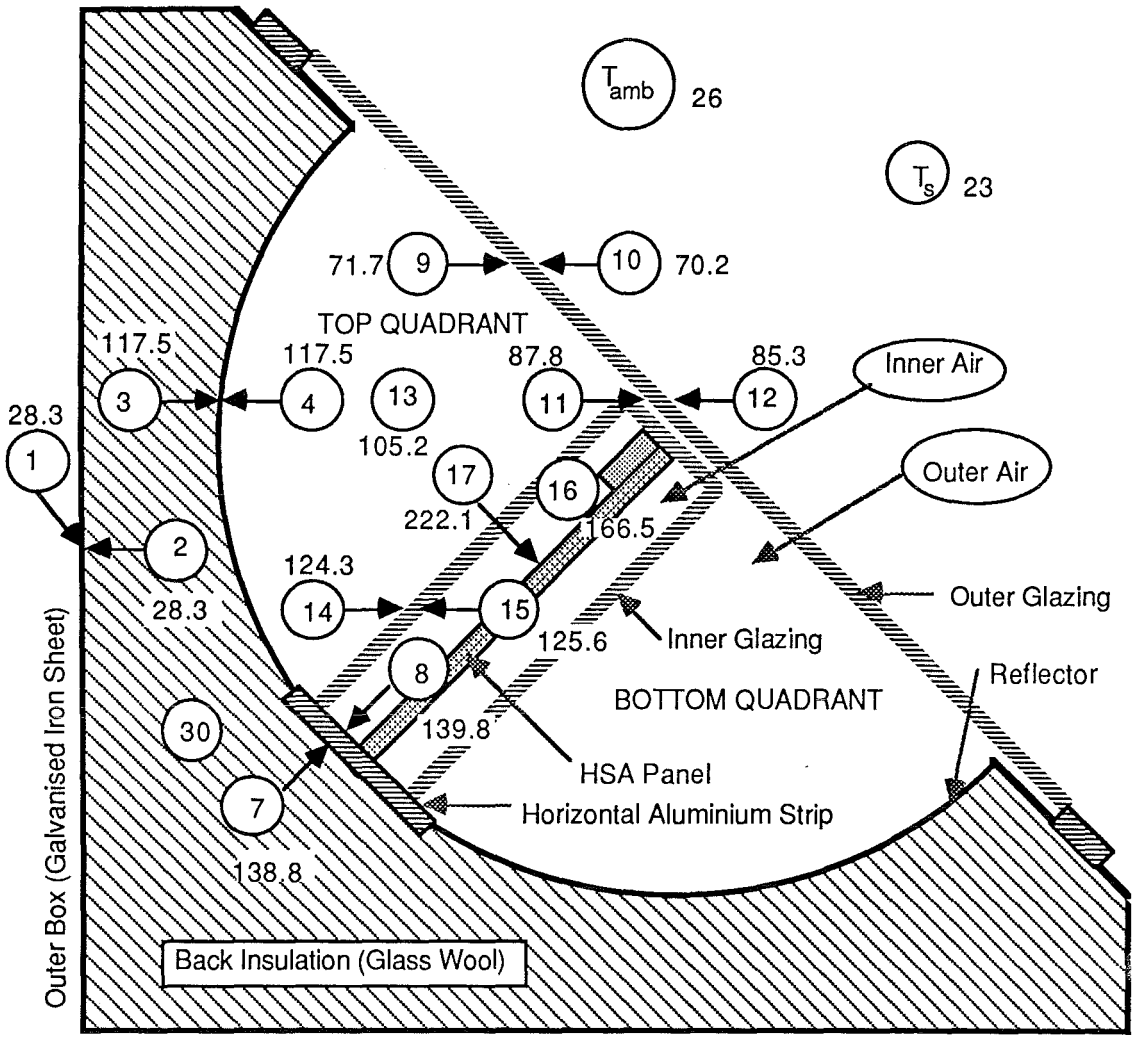

Notes:

Nembers inside the circles ndicate the temperature measuring points, which also correspond to the numbers used in the computer programme TPLWR and the numbers outside are the corresponding PREDICTED temperatures at 1pm on 24 Feb 1984 with solar insolation of 946 W/Sq.m .

T_{amb} = Ambient temperature

T_s = Sky temperature

20 to 29,33 = Dummy temperatures

Cross Section of the End Wall

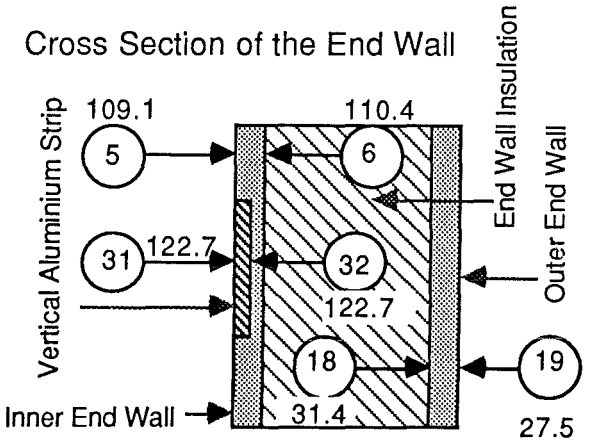

FIGURE 4.21 Flow Chart for the Computer Programme TPLWR

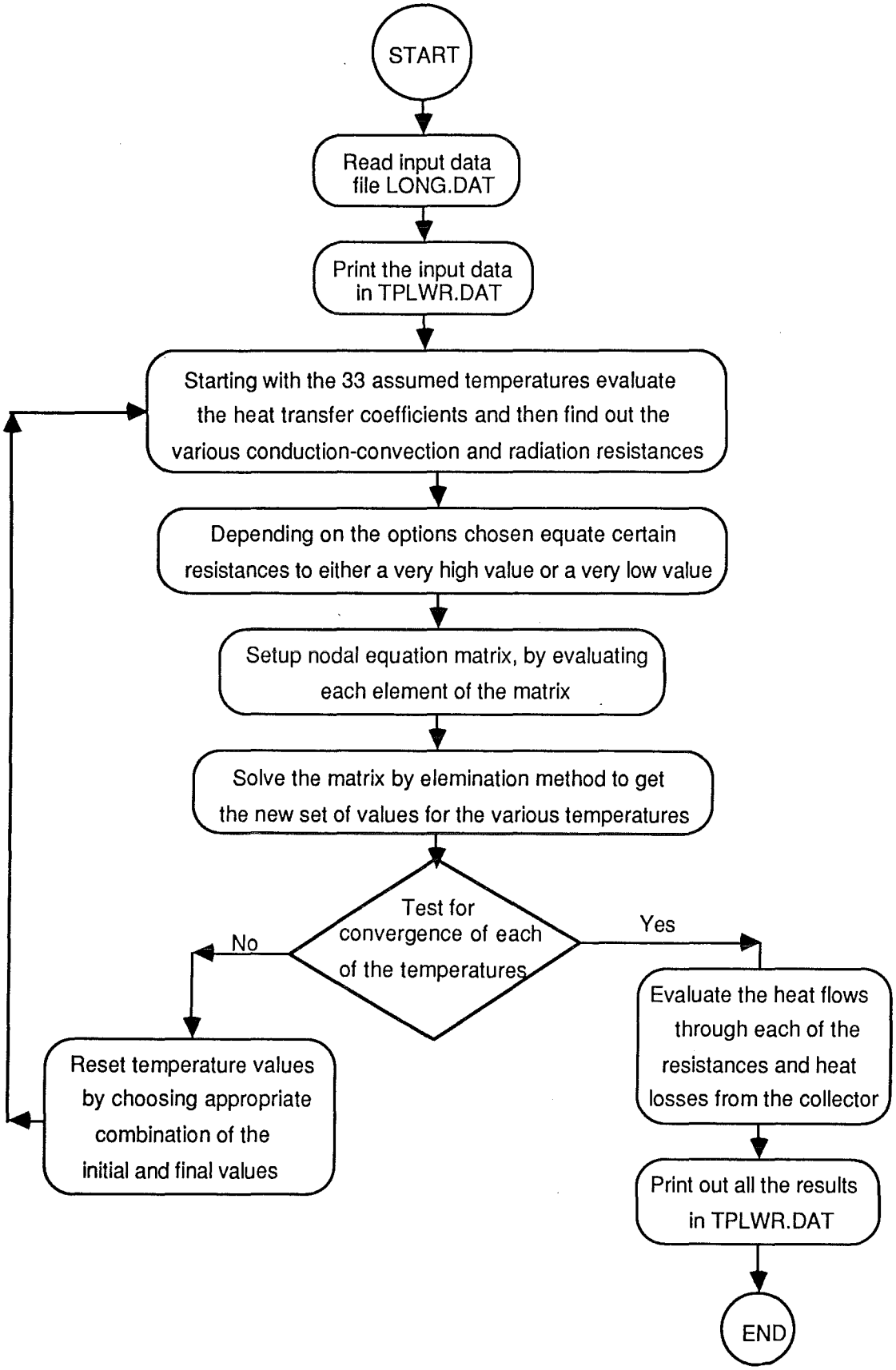

calculations and solve the matrix, to evaluate the 33 temperatures (Fig. 4.20) including 11 dummy temperatures. These dummy temperatures have been introduced to solve the radiation network. An iterative process has been employed because of the complicated equations with radiation terms containing temperatures raised to the power of four. Initially approximate values are given to all the nodes (that is, the temperatures), then various heat transfer coefficients and resistances are calculated and the equations are solved to get a new set of temperatures. A suitable combination of the new and old temperatures is used to start the next iteration. This process is continued until the required degree of convergence is achieved.

The present model actually incorporates various possible modifications in its network analysis. So, while solving for a particular case certain unwanted resistances are either equated to a very high value (to make that particular path virtually impossible for energy flow) or a very low value (to make that particular resistance virtually disappear, that is transparent to energy flow). This gives the flexibility to study the modifications without actually having to change the network or programme. To avoid the problems of changing the main programme for each modification of the model, a master data file LONG.DAT has been created. It stores all the input variables and any change can be carried out using this data file.

The description of conduction/convection and radiation networks, background theory and expressions to evaluate different resistances, formation and solving the nodal equations, the data file LONG.DAT, listing of the programme TPLWR and typical set of results (TPLWR.DAT) are given in Appendix A10. The 142 input variables to the programme (as listed in LONG.DAT) include various dimensions and properties of different parts of the collector; radiation shape factors; properties of air; various constants; and the power absorbed by the outer glazing, inner glazing, reflector and absorber panel (which are output variables of the programme TPSWR). The 200 output variables of the programme (as listed in TPLWR.DAT) include the heat transfer coefficients; conduction, convection and radiation resistances, heat flow paths and various temperatures of the surfaces and air spaces in the collector under no load or stagnation conditions and a summary of heat losses from the collector.

As discussed in the next section other parameters have been either measured or obtained from various references, while the shape factors have been evaluated in Appendix A9. The radiation shape factors are not easy to estimate, as the geometries of various parts of the collector are complicated. Because it is extremely difficult and time consuming to evaluate the shape factors accurately from basic definitions, simplying assumptions have been made and standard charts (Holman, 1972; Wiebelt, 1966; Incropera and Dewitt, 1981) have been used to evaluate the shape factors.

The results of the computer programme TPLWR, predicting the performance of the collector at stagnation conditions, at 1 p.m. on 24th February 1984 are shown in Figs. 4.18 to 4.20.

The heat flows and resistances are shown separately for conduction/convection and radiation networks in Figs. 4.18 and 4.19 respectively. By following the heat flow paths via various resistances one can decide on the components or paths of heat flow which result in major heat losses. The situation can then be improved by introducing extra resistances, or by increasing the existing resistances in those heat flow paths. One can use the modelling programme to test different materials or methods by estimating the changes in the collector performance for each modification. It can be seen from the listing of the results (TPSWR.DAT) that the total heat lost from the outer glazing and the box is equal to the total heat absorbed by different components of the collector. The convection and radiation losses from the outer glazing contribute nearly 89% of the total heat losses at stagnation conditions. This is an area where significant improvements in the collector performance are possible, for example by using convection suppressors such as "honeycombs".

The stagnation temperatures of various components of the collector are shown in Fig. 4.20. It can be noticed that all temperatures are in agreement with the physical expectations except the inner end wall inner temperature T5 which should have been closer to the reflector temperature or perhaps slightly lower, but not below T6 (the outer temperature of the inner end wall). This discrepancy is due to the fact that the radiation is supposed to strike end walls, but not get absorbed by them. However, in the actual case, a certain amount of radiation does

FIGURE 4.22 HWB Plots for Selected HSA-SCCR Collector Designs from the Model Predictions

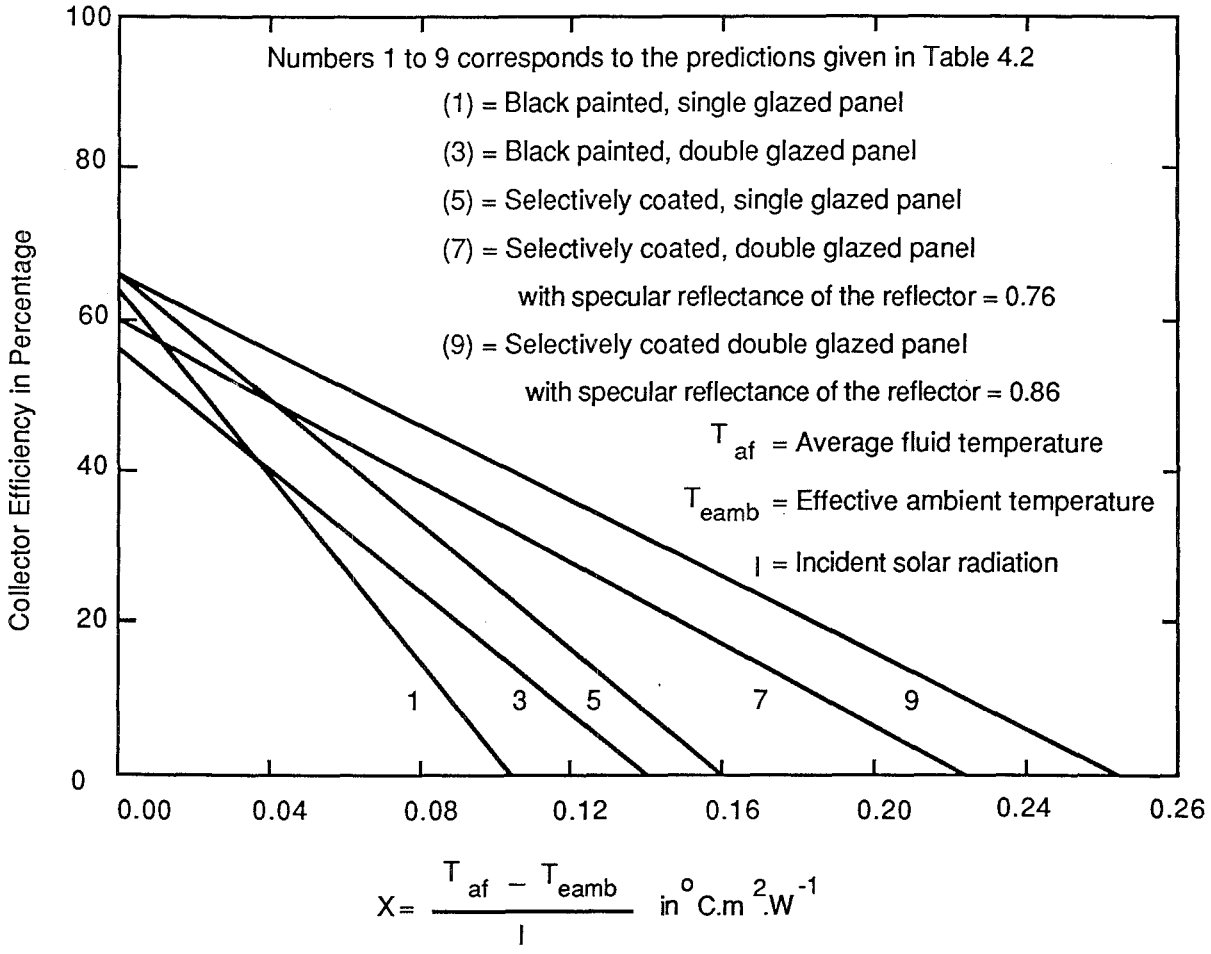

get absorbed, which would automatically increase the end wall temperature. In fact it was found (from the programme) that, by allocating part of radiation absorbed by the reflector to the end walls, the inner end wall temperature T5 goes up.

By knowing the panel stagnation temperature, the collector's figure of merit X_s can be evaluated from the Eq. (4.12) and it is equal to 0.211, at the conditions mentioned in Fig. 4.20. On combining this with the collector's optical efficiency calculated from the short wave analysis (58%), the collector's performance curve or the HWB plot can be drawn and this plot is shown along with the experimental results in Section 4.9. The HWB plots for various collector modifications can be evaluated in this way, and the plots for a few modifications described in Table 4.2 are shown in Fig. 4.22. These plots are useful in several ways as described earlier.

4.5.4 Parameters and sensitivity test

Several input parameters are used in the collector simulation and modelling. The short wave and the long wave analyses require 13 and 142 input parameters respectively. Certain parameters, such as the dimensional parameters can be easily measured with reasonably good and known accuracy. The errors involved with different measurable quantities are listed in Appendix A17. Certain parameters, such as the shape factors (Appendix 9) and the heat transfer coefficients (Appendix 10) are calculated from different expressions or charts, while others, such as the properties of the materials are obtained from a wide range of references (Kern, 1954; Insulation Handbook, 1959; Gubareff et al., 1960; Wiebelt, 1966; Holman, 1972; Wong, 1977; Kreith and Kreider, 1978; Duffie and Beckman, 1980; Incropera and Dewitt, 1981; Kreider and Kreith, 1982; Perry and Green, 1985). It is difficult to know the accuracy of these parameters. Furthermore parameters obtained from different sources have different values.

The radiation properties of materials are very much dependent on the surface conditions which do vary considerably, for example reflectivities of samples taken from the same sheet of material may differ by up to 50% (Appendix A11.5). Some of the radiation parameters can be checked by performing simple experiments or with the help of expressions from established theory, however accurate measurements of the radiation parameters need elaborate and

FIGURE 4.23 Ratio of Solar Absorptance to Absorptance at Normal Incidence for a Flat Black Surface.

(Beckman et al., 1977)

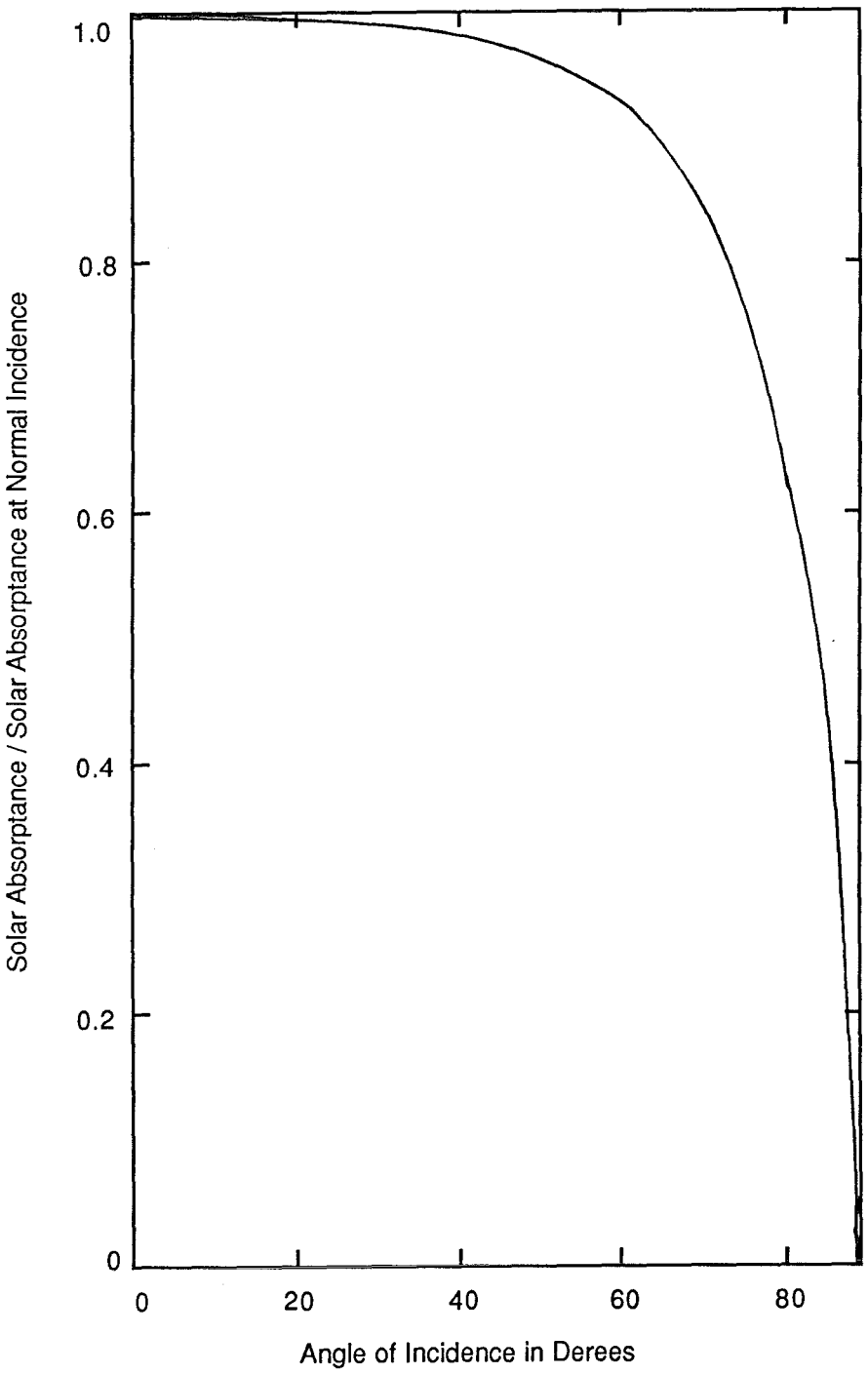

expensive equipment. Important parameters, such as the transmittance and the absorptance of the glazing were measured with a Perkin-Elmer Spectrophotometer and they were found to be within ±5% of the literature values. But the absorptance of glass (α_g) obtained from Bouger's law as given by Eq. (4.19) was found to be much higher (nearly twice the experimental value) because the extinction coefficient of glass (K_g) depends on the iron content of the glass and hence, it is not easy to estimate K_g.

$$\alpha_g = 1 - e^{-KgL} \qquad (4.19)$$

where L is the path length of the ray, which is equal to the thickness of the glazing at normal incidence.

The reflectivity of glazing (ρ_g) can be calculated from the expression obtained by combining Snell's law and Fresnel's law.

$$\rho_g = [(n_g-1) / (n_g+1)]^2 \qquad (4.14)$$

where n_g is the index of refraction for glass and it is equal to 1.5148. The reflectivity can also be found by difference, because

$$\alpha_g + \rho_g + \tau_g = 1.0 \qquad (4.21)$$

where τ_g is the transmittance of the glazing.

The reflectance of the reflector material is also an important parameter and hence a simple experiement was performed (as given in Appendix A11.5) to evaluate and compare the reflectance of various materials.

Certain radiation parameters are dependent on the angle of incidence, which varies throughout the day. The variation in absorptance of a black painted panel with angle of incidence is shown in Fig. 4.23 (Beckman et al., 1977; Hussmann & Becker, 1978). The transmittance of glass also varies in a similar way as shown in Appendix A11.2.

Hence, a sensitivity test was carried out using the simulation programme in order to determine the effects of changes in different parameters on the simulation results. It would be cumbersome, expensive, time consuming and almost impractical to carry out several experiments to test the effect of changing the value of each of the input variables, and the sensitivity test can be used as a guideline in predicting the performance of the collector for changes in various parameters.

The results of the sensitivity test are shown in Table 4.3. The significance of the change in parameter value was measured mainly as a function of change in HSA panel stagnation temperature

TABLE 4.3 Results of Sensitivity Test on Simulation Parameters

(Key to the abbreviations is provided at the end of the table)

Parameter (Modification)	VUS	VUST	ΔPar. %	ΔT17 K	Other Effects
(1) Wind velocity, $m.s^{-1}$	4.1	2.1	-49	+2.8	CLf OG = -7.6%
		6.1	+49	-2.4	CLf OG = +5.9%
(2) Emissivity of air	0.029	0.01	-66	+1.3	
		0.05	+72	-1.2	
(3) Thermal conductivity of back insulation, $W.m^{-1}.K^{-1}$	0.036	0.02	-44	+1.2	T4 = +5.7°C
					CLf OB = -2.7%
		0.06	+67	-2.0	T4 = -8.2°C
					CLf OB = +3.3%
(4) Equivalent thickness of back insulation, m	0.098	0.05	-49	-0.5	
		0.15	+53	+0.1	
(5) Without back insulation				-6.2	T4 = -31.6°C
(Using Z6 = 3 in TPLWR)					T13 = -15.1oC
					CLf OB = +11%
					RLf OB = +2.8%
(6) Emissivity of outer box	0.28	0.1	-64	0	RLf OB = -1.0%
		0.6	+114	0	RLf OB = +1.4%
(7) For long wave radiation					
For reflector ρ_{sr}	0.94	0.80	-15		
ρ_{dr}	0.02	0.06	+200	+0.3	
ε_r	0.04	0.14	+250		
(8) Aluminium strip replaced by plastic strip having same thermal conductivity as wood				+0.3	

TABLE 4.3 Results of Sensitivity Test on Simulation Parameters

(Continued) (Key is provided at the end of the table)

Parameter (Modification)	VUS	VUST	ΔPar. %	ΔT17 K	Other Effects
(9) Thermal conductivity of end wall insulation, $W.m^{-1}.K^{-1}$	0.036	0.02	-44	+0.4	
		0.06	+67	-0.5	
(10) Thickness of end wall insulation, m	0.076	0.03	-61	-1.0	T5 = -9.5°C
					T6 = -12.2°C
		0.13	+71	+0.3	
(without insulation)		0.0001		-5.0	T5 = -3.7°C
					T6 = -51.8°C
					CLf OB = +4.8%
					RLf OB = +3.9%
(11) 3 mm thick glass as end wall, without any insulation and without considering effects of short wave radiation				-15.2	T5 = -57.2°C
					T6 = -59.8°C
					CLf OB = +14%
					RLf OB = +12%
(12) Emissivity of outer end wall outer surface	0.8	0.2	-75	0	
		0.9	+13	0	
(13) Thickness of OG, mm	3	5	+67	+0.5	
(14) HSA panel emissivity	0.11	0.04	-64	+25.6	
		0.08	-27	+9.3	
		0.20	+81	-4.5	
Black paint		0.84	+664	-59.4	
		0.96	+773	-62.7	
(15) Glazing emissivity	0.94	0.82	-13	+2.1	
		0.96	+2	-0.9	

TABLE 4.3 Results of Sensitivity Test on Simulation Parameters

(*Continued*) (Key is provided at the end of the table)

Parameter (Modification)		VUS	VUST	ΔPar. %	ΔT17 K	Other Effects
(16) Panel-inner glazing gap, m		0.025	0.01	-60	-11.8	T16 = -5.4°C
			0.035	+40	+11.9	T16 = +1.5°C
(17) Shape factors				±30	±2	
(18) Heat transfer coefficients				±30	±7	
(19) For short wave radiation						
For glazing	τ_g	0.885	0.79	-11		
	ρ_g	0.0838	0.12	+43	-22.5	η_{opt} = -11.8%
	α_g	0.0312	0.09	+188		
	τ_g	0.885	0.86	-9		
	ρ_g	0.0838	0.09	+7	-5.7	η_{opt} = -3.2%
	α_g	0.0312	0.05	+60		
	τ_g	0.885	0.91	+3		
	ρ_g	0.0838	0.07	-17	+6.4	η_{opt} = +3.3%
	α_g	0.0312	0.02	-36		
(20) For short wave radiation						
For reflector	ρ_{sr}	0.76	0.7	-8		
	ρ_{dr}	0.09	0.12	+33	-6.1	η_{opt} = -3.3%
	α_r	0.15	0.18	+20		
	ρ_{sr}	0.76	0.82	+8		
	ρ_{dr}	0.09	0.07	-22	+6.3	η_{opt} = +3.7%
	α_r	0.15	0.11	-27		
	ρ_{sr}	0.76	0.93	+22		
	ρ_{dr}	0.09	0.03	-67	+17.7	η_{opt} = +10.6%
	α_r	0.15	0.04	-73		
(21) HSA panel absorptivity		0.93	0.84	-10	-12.2	η_{opt} = -5.6%
			0.96	+3	+3.9	η_{opt} = +1.8%

TABLE 4.3 Results of the Sensitivity Test on Simulation Parameters (*Continued*)

Notes:

VUS = Value used in simulation

VUST = Value used in sensitivity test

ΔPar. = Change in parameter value

ΔT17 = Change in HSA panel temperature

CLf = Convective loss from

RLf = Radiative loss from

OG = Outer glazing

OB = Outer box

T4 = Inner surface temperature of the reflector

T5 = Inner surface temperature of the inner end wall

T6 = Outer surface temperature of the inner end wall

T13 = Outer air temperature

T16 = Inner air temperature

ρ_{sr} = Specular reflectivity of the reflector

ρ_{dr} = Diffuse reflectivity of the reflector

α_r = absorptivity of the reflector

ε_r = emissivity of the reflector

(T17), because it is the most important variable from which the collector performance is estimated. HSA panel temperature was calculated for an upper and lower limit of each parameter. These limits determine the normal changes possible for that particular parameter. The table also gives certain other effects (such as the convective and radiative losses from the box or outer glazing and a few other appropriate temperatures) wherever necessary.

The panel stagnation temperature and the other effects are given as an increase (denoted as '+') or a decrease (denoted as '-') in comparison with the simulation results given by TPSWR.DAT and TPLWR.DAT. It is evident from Table 4.3 that the individual influence of most parameters is small due to the buffering effect of the rest of the network. With certain modifications where changes in other parameters are considerable, the change in the panel stagnation temperature is not appreciable. For example when the back insulation is removed, convection losses from the box are more than doubled, the reflector temperature drops by 32°C and outer air temperature drops by 15°C, while the panel temperature drops by 6°C only. The following conclusions can be arrived at from the sensitivity test.

(1) Wind velocity does not have appreciable effect, because of the double glazing.

(2) Thermal conductivity and thickness of insulation material is not crucial and hence any type of insulation (such as a less expensive one) can be used. Even total elimination of back or end wall insulation (if the savings are appreciable) can be advocated as the reduction in plate temperature is about 5% only.

(3) When the end wall is replaced by a transparent sheet of glass, the panel temperature drop is considerable (about 15°C) because of the heavy losses from the sheet of glass. It should be noted that the effects of short wave radiation have not been taken into consideration, as they will be discussed in the next section.

(4) The emissivity of the panel is very important as radiation losses dominate at high temperatures. If the emissivity is reduced from 11% to 4%, keeping the short wave absorptance same, the plate temperature may go up by about 26°C.

(5) The gap between the inner glazing and absorber panel has considerable effect, because the mode of heat transfer changes (from convection to conduction and vice versa) and the free convection pattern also changes.

(6) Heat transfer coefficients have to be changed by about ±30% to get ±3% change in the panel temperature.

(7) Glazing transmittance for short wave radiation has a considerable effect on the panel temperature and optical efficiency. Low iron content glass or special coatings are available; however, one should bear in mind the extra costs involved.

(8) Good reflectors with high specular reflectance values for short wave radiation can improve the optical efficiency and panel temperature, but they are generally very expensive.

(9) Absorptivity of the panel is also important for increasing the optical efficiency and panel temperature. Hence a better selective coating, with high α/ε values, is desirable.

Having understood the analytical model, we can proceed to the detailed design and fabrication of the collector in the following sections.

4.6 Design of HSA-SCCR Collector

The design of the collector involves several steps, the important ones being: optimum ratio of panel width to reflector radius, optimum length of the collector, collector tilt angle, type of end walls, panel plate material, collector cover system, reflector material, heat pipe fluid, condenser fluid and condenser tube details. These are described in the following sections.

4.6.1 Optimum ratio of HSA panel width to reflector radius

The width of the absorber panel may be less than, equal to, or greater than the radius of the reflector. If the width is greater than the radius, then construction problems may arise in mounting the glazing and hence, this option was discarded. Other options were considered and their performances evaluated as described in Appendix A11.1. Truncating the absorber results in lowering the performance of the collector, and hence it was decided to have the width of the absorber equal to the radius of the reflector.

4.6.2 Optimum length of the collector

The optimum length of the collector depends on the practical considerations, end wall effects and angle of incidence of solar radiation as explained in Appendix A11.2. Longer collectors reduce

the end wall effects by decreasing the ratio of the collector box surface area to the absorber area. However, practical considerations set a limit to the maximum length. When the angle of incidence exceeds 60° the glazing transmittance decreases drastically. Hence the minimum length should be such that the reflected ray (from the reflector) strikes the absorber panel when the angle of incidence is 60°, which means that the minimum length should be about three and half times the radius.

4.6.3 Collector tilt angle

The optimum orientation for the collector is decided in such a way as to maximise the amount of solar radiation and the number of hours of solar collection in a year. As mentioned in Section 4.1.1, the optimum collector tilt angle for the year-round operation of flat plate collectors is equal to the latitude of its location (Kern and Harris, 1975). Neville (1978) has shown that fixed collectors may receive only half as much energy as an ideal dual axis tracking unit over a period of one year. The optimum orientations for double exposure flat plate collectors and their reflectors, has been discussed by Souka and Safwat (1966). However, the HSA-SCCR collctor mounted in an East-West direction, is capable of receiving solar radiation for at least 8 hours on all days of the year. On the other hand, it behaves like a flat plate collector, and hence the HSA panel tilt angle may be chosen to be equal to the latitude of the location (43.5° South for these tests), but for the sake of convenience in building the collector, it was chosen to be 45°.

4.6.4 Type of end walls

The end walls can be made either transparent or reflecting as described in Appendix A11.3. Reflective end walls are preferable as they make the semi-cylinder infinitely long optically, and also, the heat losses from the end walls can be minimised by insulating the end walls.

4.6.5 HSA plate material

As described in Section 4.3 it was necessary to have a selective surface on the absorber panel, as it introduces the closest resistance to the panel and thus provides the most effective improvement. Appendix A11.4. gives the selection

procedure for HSA plate material including the important characteristics and different types of selective surfaces. Coloured stainless steel (in particular blue steel), a relatively recent introduction into the group of selective surfaces, appears to be best suited in the present investigation because it possesses almost all the requirements for the HSA panel. Yazaki blue steel has a solar absorptance of about 0.93 and thermal emittance of about 0.1. It has a high thermal stability (which is important as it should withstand collector stagnation temperatures and hence, it was checked experimentally and found to withstand temperatures up to 300°C), excellent resistance to corrosion, wear and scratching and good adherence of the film even while cold pressing (checked by dimpling the sheet).

4.6.6 Collector cover system

The designing of a collector cover system consists of choosing an appropriate glazing material, number of glazings and their arrangement. Glass is one of the best glazing materials as it is highly transperant to solar radiation, opaque to thermal radiation and, unlike plastics, not affected by ultravoilet rays. Although highly transmitting glass (or low iron content glass) and anti-reflective coatings are available, they are expensive and hence ordinary window glass was chosen.

Double glazing was needed due to the high operating temperature of the collector. Double glazing the aperture reduces the overall heat transfer coefficient considerably; at the same time solar radiation entering the collector is also reduced. This arrangement is most effective when radiation losses dominate, that is, with black painted absorbers whose emissivities are very high. Double glazing, with one each on the absorber and the aperture is more effective than double glazing the aperture as the resistance is closer to the heat source (which is the absorber panel). This arrangement is most effective when convective losses dominate, that is, with selectively coated absorbers, and hence this arrangement was chosen.

It is necessary to choose an optimum width of the air space between the panel and the inner glazing. The thermal resistance offered by the air space should be a maximum in order to minimise the losses. Anderson (1981) presented the thermal resistance as a function of the width and the length of the air space, and

concluded that the thermal resistance attains almost a constant value for widths greater than 25 mm for any length of air space. Also, Jordan (1969) recommended a value of 25 mm as the optimum width and hence the same value was chosen. In order to reduce the convective losses further, the inner air (between the inner glazings and the absorber panel) and the outer air (between the outer glazing and the inner glazings) should not be interconnected so as to stop the air flow from one compartment to the other.

4.6.7 Reflector material

An appropriate reflector material had to be chosen and then a method determined for attaching it to a backing material which gives structural strength, and the required shape (semi-cylindrical); these are described in Appendix A11.5. The requirements of a good reflector include: high specular reflectivity, high temperature resistance, durability, high strength, flexibility and easy availability at low cost. Based on these criteria, five commercially available reflectors: RFM and RFH (by ROSCO, England), space blanket (King-Seeley Thermos Co., USA), aluminised mylar and cooking foil were selected. A simple experiment was performed with a light source giving red light of wave length 0.63 microns to compare the reflectivities of these five materials and the results are given in Appendix A11.5. It was found that RFM was the best of the five materials tested. The temperature resistance of RFM was experimentally verified, and it was found to withstand about 150°C. Galvanised iron sheet was chosen as the backing material, which was pre-formed into the required shape before attaching the reflector in order to avoid damage to the reflector surface while forming it into a semi-cylindrical shape. Several contact and spray adhesives and pipe cements of different brands were tested for strength, temperature resistance, application and curing times and vapours expelled. "Ados" pipe cement was found to be best suited for this purpose. In order to avoid vapour bubbles, resulting from the expulsion of solvent vapours during the curing process, the reflector was attached in longitudinal strips. Aluminised mylar was used with the first collector as the pipe cement was not tested at that stage.

4.6.8 Heat pipe fluid

It is important to select an appropriate heat pipe fluid and find out the amount of fluid required by each panel. The selection of HSA working fluid including the criteria of selection, and properties of fluids considered, is described in Appendix A4. Based on the operating range of the collector (which was anticipated to be about 150°C to 160°C) and maximum attainable temperature of the collector at stagnation conditions (which could be about 225°C), Dowtherm A, water and Flutec PP9 (a patented fluid by the Imperial Smelting company) were selected. Of these Dowtherm A was found to be most suitable, based mainly on the compatability with stainless steel and vapour pressure characteristics. However, with the second panel, a small amount of toluene was added (as described in Section 4.9) to increase the vapour pressure at lower temperatures.

Lee & Mital (1972); Lee & Bedrossian (1978); Cohen & Bayley (1955) found that the performance of a thermosyphon heat pipe is independent of the liquid level, provided it is above a certain minimum level. Webb (1979) found that 100 cc of the working fluid or 12% of the total envelope volume was insufficient (and resulted in hot spots in the HSA panel), and 200 cc or 25% was adequate. In the present case, 200 cc representing about 30% of the envelope volume was used.

4.6.9 Condenser fluid

It was necessary to select a condenser fluid which would also meet the criteria for a thermal storage media, because the same fluid was to be employed for both purposes. The selection of a suitable condenser fluid is described in Appendix A12, which explains the selection criteria and lists the properties of the fluids considered. Once again, based on the operating temperature range and maximum working temperature, three heat transfer oils: Mobiltherm 603, Shell Thermia Oil E and Shell Thermia Oil G-68 were considered. On comparison of the various desirable properties, Mobiltherm was found to be most appropriate, mainly because of the heat transfer and vapour pressure characteristics. However, at a later stage Soya bean oil was tested in an attempt to avoid carbon deposition on the heating element (as described in Section 4.9), but was discarded because of its poor heat transfer characterisrics.

FIGURE 4.24 Methods of Attaching the Condenser Tube to the HSA Panel

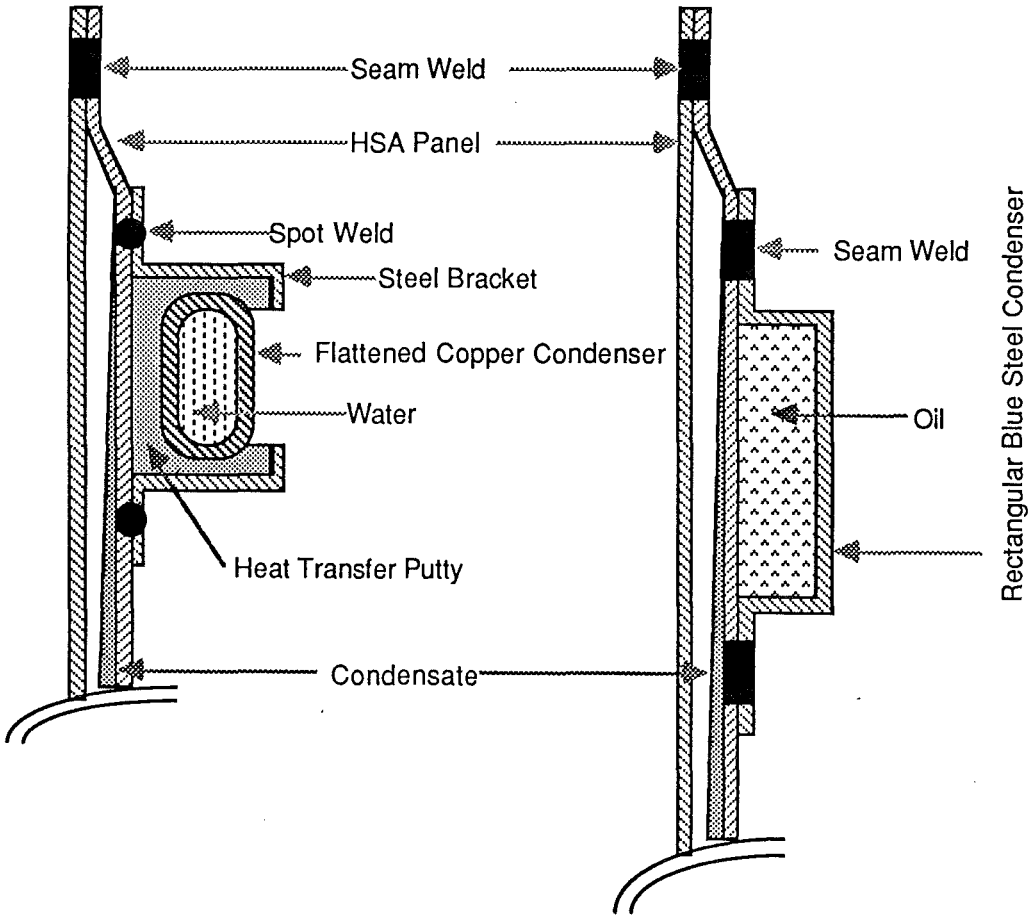

4.6.10 Condenser tube

In almost all heat pipe collectors, the condenser tube offers major resistance to heat flow, which is usually 75% of the total resistance (Bienert and Wolf, 1976). Hence, one of the most important steps in the design of the HSA panel is the design of the condenser tube. It includes the determination of the method of attaching the condenser tube to the absorber panel and the optimum condenser tube dimensions.

4.6.10.1 Method of attachment

It is necessary to find out the major resistance in the condenser tube to determine the best method of attachment of the condenser tube to the panel. In several heat pipe collectors, including Webb's (1979) HSA panel the major resistance was due to the condenser tube wall or more precisely condenser-absorber panel interface because of the method of attachment of the condenser tube. Mesman (1979) reported that, for an HSA having a three pass copper tube (10 mm diameter) condenser, the resistances offered by the bonding filler, water-side film and condensate film were 80%, 13% and 5% respectively. The condenser tube must be in good thermal contact with the panel to decrease the interface resistance. Webb (1979) used a flattened copper tube held by a steel bracket with heat transfer sealant to enhance the heat transfer (Fig. 4.24). To minimise the interface resistance, a rectangular condenser tube (more precisely a rectangular trough) made of blue steel was seam welded to the absorber panel. In the present case the interface resistance was that offered by the absorber plate only and thus eleminating the resistances offered by the heat transfer sealant and the copper tube.

The thermal resistances of the HSA panel in the present case have been evaluated in Appendix A6. According to this analysis the condenser tube resistance is 82% of the total resistance. The various resistances in decreasing order of magnitude are: the oil-side film resistance (80.7%), the vapour flow pressure drop resistance (11.5%), the condensation film resistance (7%), the condenser tube wall resistance (0.8%), the plate resistance and the evaporator resistance. Thus, the oilside film resistance constitutes the major resistance and it can be decreased in two ways. The first method is to increase the oil-side film

coefficient, which is discussed in the following section. The second method is to increase the oil-side heat transfer area. This can be achieved by increasing the condenser tube dimensions (which is also discussed in the following section), or by having internal fins, which also results in higher oil-side film coefficient. However, mechanical and practical suitability needs to be considered. In the second panel this improvement has been incorporated.

4.6.10.2 Optimum tube dimensions

The next step in the designing of the condenser tube is to determine its optimum dimensions (length, width and height). Various calculations needed to estimate these three parameters along with the background theory, the equations employed, the computer programmes and the summary of results are presented in Appendix A13, while the selection criterion and the important conclusions are given below.

The optimum length of the condenser tube, based mainly on practical considerations was found to be equal to the panel length (Appendix A13.1). The criteria for the selection of the width and the height of the condenser tube include:

(1) high condensation film coefficient,
(2) high oilside film coefficient,
(3) high overall heat transfer coefficient,
(4) low temperature drop on the oilside,
(5) low temperature drop across the condensate film,
(6) high value of net heat transfer and
(7) low pressure drop on the oilside.

The effects of changes in width and height on these variables have been evaluated in Appendix A13 and summarised below. The condenser tube widths considered are 20,30,40 and 50 mm, while the heights considered are 5,10,15 and 20 mm. The other variables taken into consideration include: oil mass flow rate, net heat transferred, panel tilt angle, oil inlet and oulet temperatures and condensate film or vapour temperature. These variables are included for the sake of comparison to evaluate their significance in determining the condenser tube dimensions.

The evaluation of the condensation film coefficient CFC (using Nusselt's equation), the correction for fin effect and the temperature drop across the condensate film (ΔT_f) are described in

Sections A13.3 to A13.7. The computer programme TPCFC does all these calculations for various conditions such as different condenser tube widths and heights, collector tilt angles and condensate film temperatures. The CFC and ΔT_f decrease as the width increases because of the increase in the film thickness. There is no direct effect of height on CFC. As the panel tilt angle increases from 30° to 60°, the gravity component increases resulting in an increase in CFC. With the increase in condensate film temperature, a slight increase in CFC occurs due to the changes in the properties of the fluid. But this temperature is decided by the collector operating temperature or the insolation.

The oil side film coefficient OFC (using Sieder & Tate correlation), the corrections for free convection and fin effect, the overall heat transfer coefficient and the computer programme TSPQFC have been described in Sections A13.8 to A13.13. As the width increases the OFC changes very little, or increases depending on the temperature rise of the oil through the condenser tube. This behaviour results because of the changes in the free convection factor and the equivalent diameter act in opposite directions. As the height increases the OFC decreases. The overall heat transfer coefficient decreases with the increase in the width or the height.

The temperature drop across the oil film ΔT_{ow} may be estimated either directly (from the condenser tube wall temperature and the average oil temperature) or indirectly (from the film coefficients, areas and ΔT_f) as described in Section A13.14. The direct method has been adapted in this case. The effects of the width and the height on ΔT_{ow} are given later in this section.

The pressure drop calculations for the condenser tube are based on the expressions given by Perry and Green (1985) for laminar flow in ducts with liquid flowing full (Sections A13.15 and A13.16). As the width and the height increase, the pressure drop ΔP_c decreases. However, ΔP_c is quite small at all times, except at cold conditions when the viscosity is very high (the ratio of kinematic viscosities of oil at 20°C and 150°C is about 25).

Overview of heat transfer calculations:

In order to find the optimum dimensions of the condenser tube (and other optimum variables of the system) one should consider

the requirements of the solar refrigeration system as a whole (including the collector, the refrigerator, the storage tank, the circulating pump and the interconnecting pipe work) because each component has certain operating or economic limits, which in turn, impose restrictions on the input variables to the other components of the system. However, the optimisation of the whole system is an enormous task by itself (Chapter 6) and hence in this investigation, the optimisation of the condenser tube has been considered in isolation.

The overview of heat transfer calculations is given in Sections A13.17 to A13.19. Certain variables employed in these calculations are interdependent. The only independent input variables include: the oil mass flow rate m_o, the vapour or condensing film temperature T_f (or the panel operating temperature, which depends on the solar input to the panel), the oil inlet temperature T_{io}, the condenser and panel dimensions and the properties of the working fluids. The three unknown variables including the condenser tube wall temperature T_w, the oil outlet temperature T_{oo} and the net heat transferred to the oil Q_{net}, can be evaluated from basic energy balance equations. Starting with an assumed value of T_w various calculations are done and employing the bisection method, convergence is achieved. In order to reduce the effects of variations in fluid properties, due to the continuous temperature rise of oil through the condenser tube, the tube along with the panel can be divided into a number of segments. The calculations can be performed for each segment, and by summing up, the final results for the entire condenser tube can be obtained. The computer programme TPHTC does these calculations for various conditions.

It is impossible to fulfil all the criteria while choosing any set of condenser tube dimensions and hence one has to choose intermediate values giving appropriate weightage to the selection criterion or conduct an optimisation of the whole system. On the other hand, there is a lot of interdependency of different variables on one another due to the complicated nature of the problem. Hence the optimum value for the condenser width was chosen to be 30 mm with the first panel, which was later increased to 40 mm with the second panel. Although the optimum value of the condenser tube width was 5 mm (to achieve maximum heat transfer)

FIGURE 4.25 Condenser Tube Details

(a) Cross Section of HSA1 Condenser Tube (Scale 1 : 1)

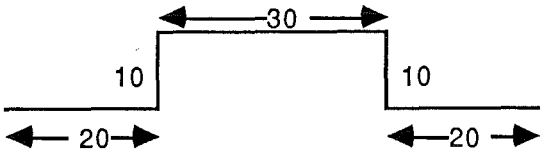

(b) Cross Section of HSA2 Condenser Tube (Scale 1 : 1)

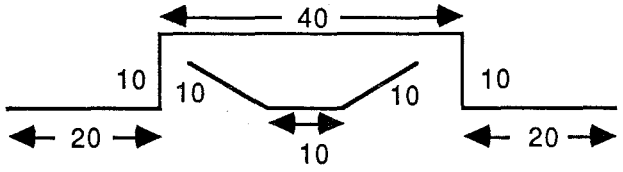

(c) Condenser Tube Attached to HSA1 (Top View) (Not to Scale)

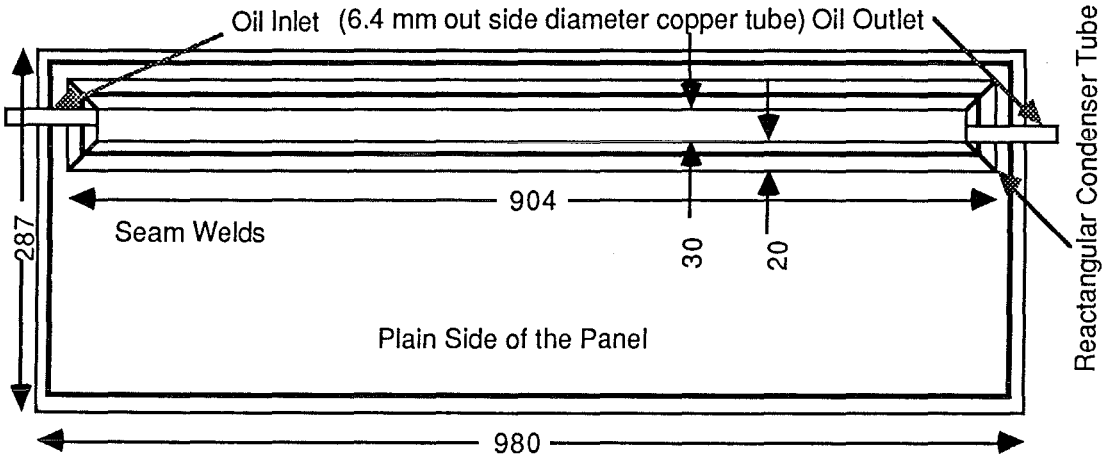

it was decided to make it 10 mm to avoid blockage problems due to carbonisation and to facilitate easy flow in cold conditions.

4.7 Fabrication of HSA-SCCR Collector

Based on the information gathered in the previous section (design of the collector), the fabrication of the collector was carried out. The first collector-1 (C1) was fabricated, tested and then the second collector (C2) was built incorporating several modifications, some of which have already been mentioned. The others will be mentioned in appropriate sections. In this section, the common details in the fabrication of both the collectors are described, although the dimensions are given for the first collector.

Yazaki blue steel sheet of 1 m wide and 2.34 m long was available and to make effective use of the sheet the length of the panel was taken as 1 m. As the optimum length is about 3.5 times the width, the appropriate width was chosen as 0.3 m, which was also equal to the radius of the reflector. This would give a total absorber area or total aperture area of about 0.6 m^2. Two sheets of the required size were cut, of which one was cold pressed, to obtain the dimple pattern (Plate 2). A third piece of blue steel 90 mm wide (or 100 mm for the second panel) and about 1 m long was used to make the condenser tube with a channel cross section as shown in Figs. 4.25a,b. Two copper tubes of 6 mm diameter (oil inlet and outlet connections to the condenser tube) were attached to the two ends of the trough. This rectangular trough was then seam welded at the top of the plain sheet leaving enough space for seam welding the panel. In the case of the second panel, an internal fin made of blue steel was seam welded first and then the rectangular trough. After that, the plain sheet and the dimpled sheet were seam welded.

After the HSA panel was ready, it was charged with an appropriate amount of working fluid, through a small diameter copper tube attached to the dimpled sheet. This was accomplished with a vacuum system as described in Appendix A14. The vacuum line was used to evacuate and degas the working fluid, to load the HSA with the required amount of fluid and finally to seal the panel hermetically. The panel was degassed in stages to about 10^{-4} mm Hg with the help of a diffusion pump backed by a rotary pump. The panel was baked (at about 225°C, which was the expected stagnation

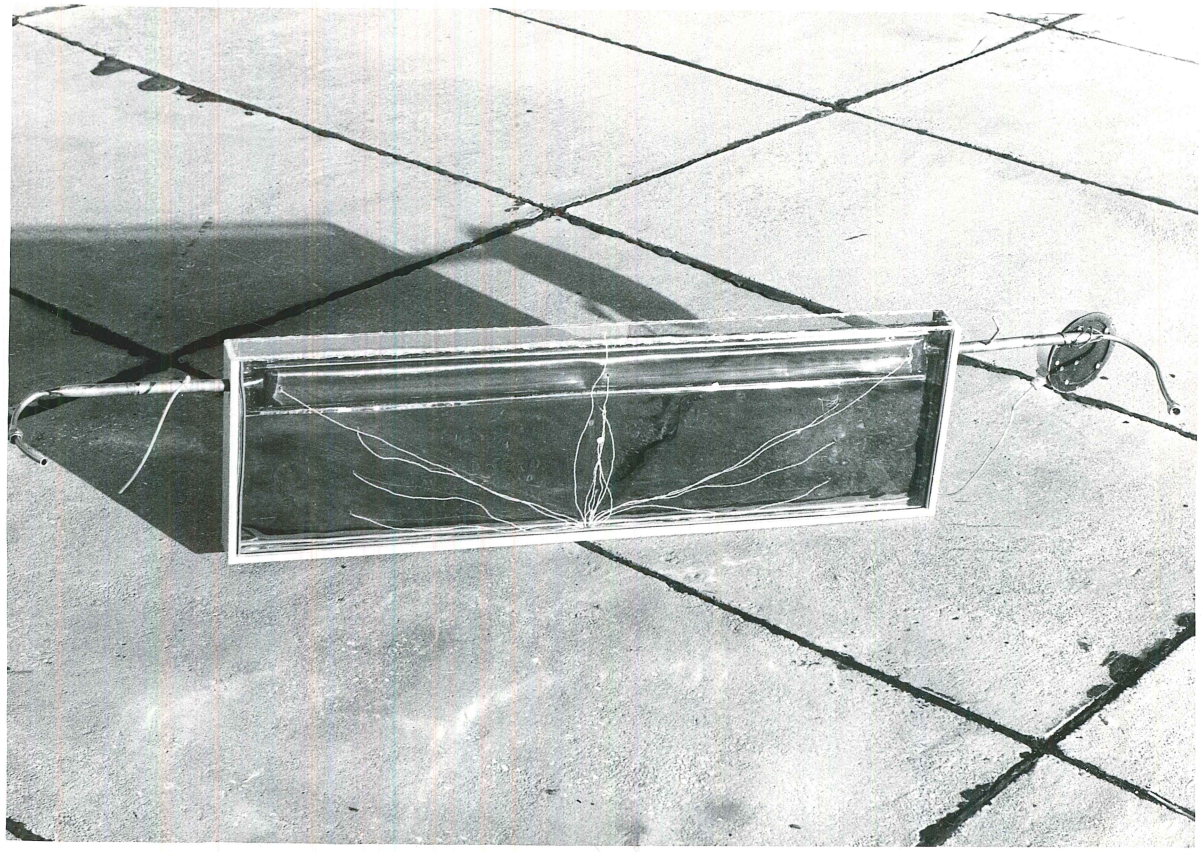

(a) Plain Side

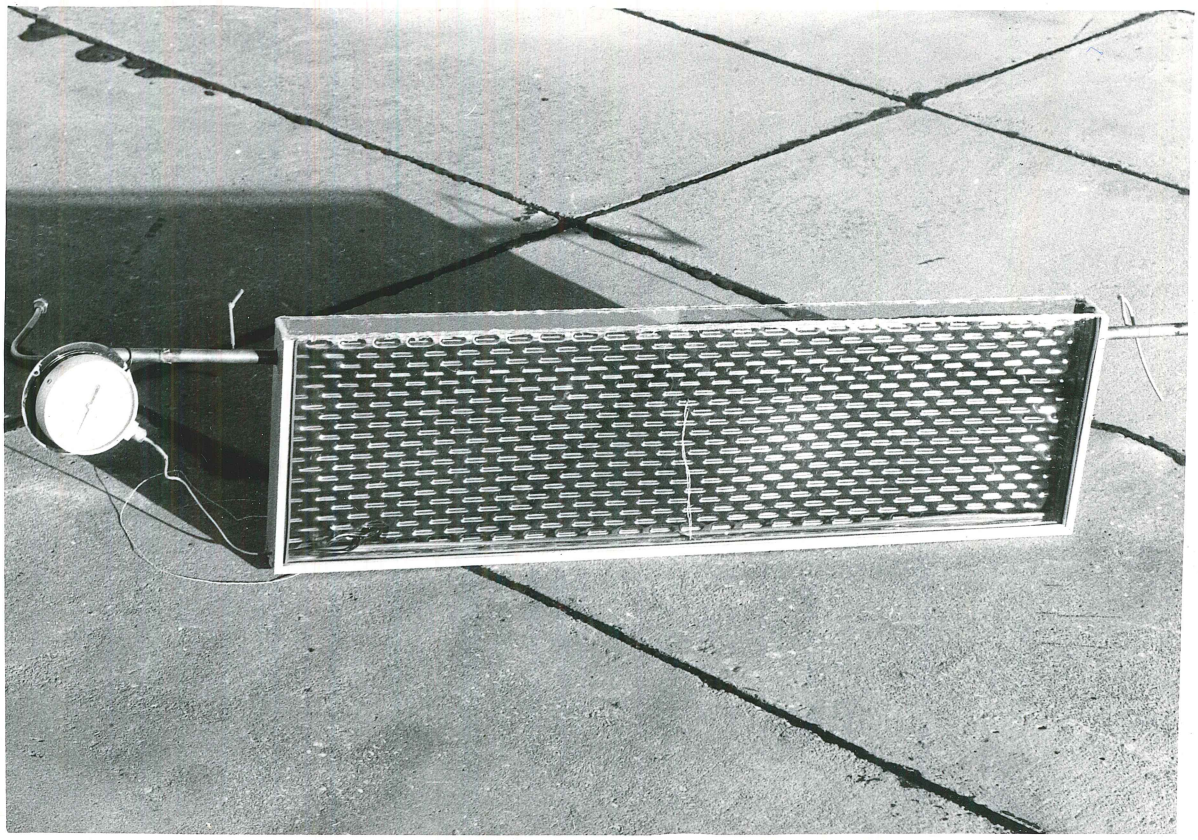

(b) Dimple Side

PLATE 2 Heat Sheet Absorber Panel

temperature of the panel) to drive away non-condensibles and to check the seam welds at high temperature. The working fluid was degassed and introduced into the panel. In the case of the second panel, two fluids were degassed separately and introduced into the panel. At this stage, the delicate task of sealing the copper tube (through which working fluid was introduced into the panel) was performed carefully in stages, avoiding any leakage of air into the panel.

The Plate 2 shows the heat sheet absorber (HSA 2) panel, after it was fitted inside the 'inner air box' comprising of the two inner glazings, one top glazing strip, two vertical and one horizontal aluminium strips. The plain side, with the condenser tube and a few thermocouples is shown in Plate 2a. The dimple side with the vacuum gauge is shown in Plate 2b.

The collector box was built to exactly fit the HSA panel. While fabricating the panel its size was reduced due to dimpling, and trimming off the edges and hence, even though the initial blue sheets were 1000 x 300 mm, the final panel was 980 x 287 mm as shown in Fig. 4.25c. The outside box was formed from a single sheet of galvanised iron(GI) of 1 mm thickness to a shape shown in Fig. 4.26a,b. This particular shape provides good stability, is easy to form and allows the HSA panel to sit in its axial plane, at 45° to the horizontal. The two 40 mm wide portions of this box perpendicular to the axial plane provide the base for the outer glazing frame. The two 10 mm wide portions parallel to the axial plane provide support to the reflector backing and extend to a length of 980 mm, which is the length of the reflector. The back of the box was provided with an opening (200 x 200 mm) to give access to the backside of the reflector for insulating the back and attaching the thermocouples.

The end wall arrangement (Figs. 4.27a,b) consisted of three layers: outer end wall of 18 mm thick Customwood, end wall insulation of 76 mm thick glass wool and inner end wall of 18 mm thick Customwood. A rectangular piece of GI sheet covering the top of the end wall arrangement provided support to the outer glazing frame. The outer end wall outer surface was painted to make it weather resistant. The inner end wall had a rectangular slot of 287 x 68 x 10 mm (Fig. 4.27b) for the vertical aluminium strip which holds the absorber panel and inner glazings.

FIGURE 4.26 Outer Galvanised Iron Sheet Box

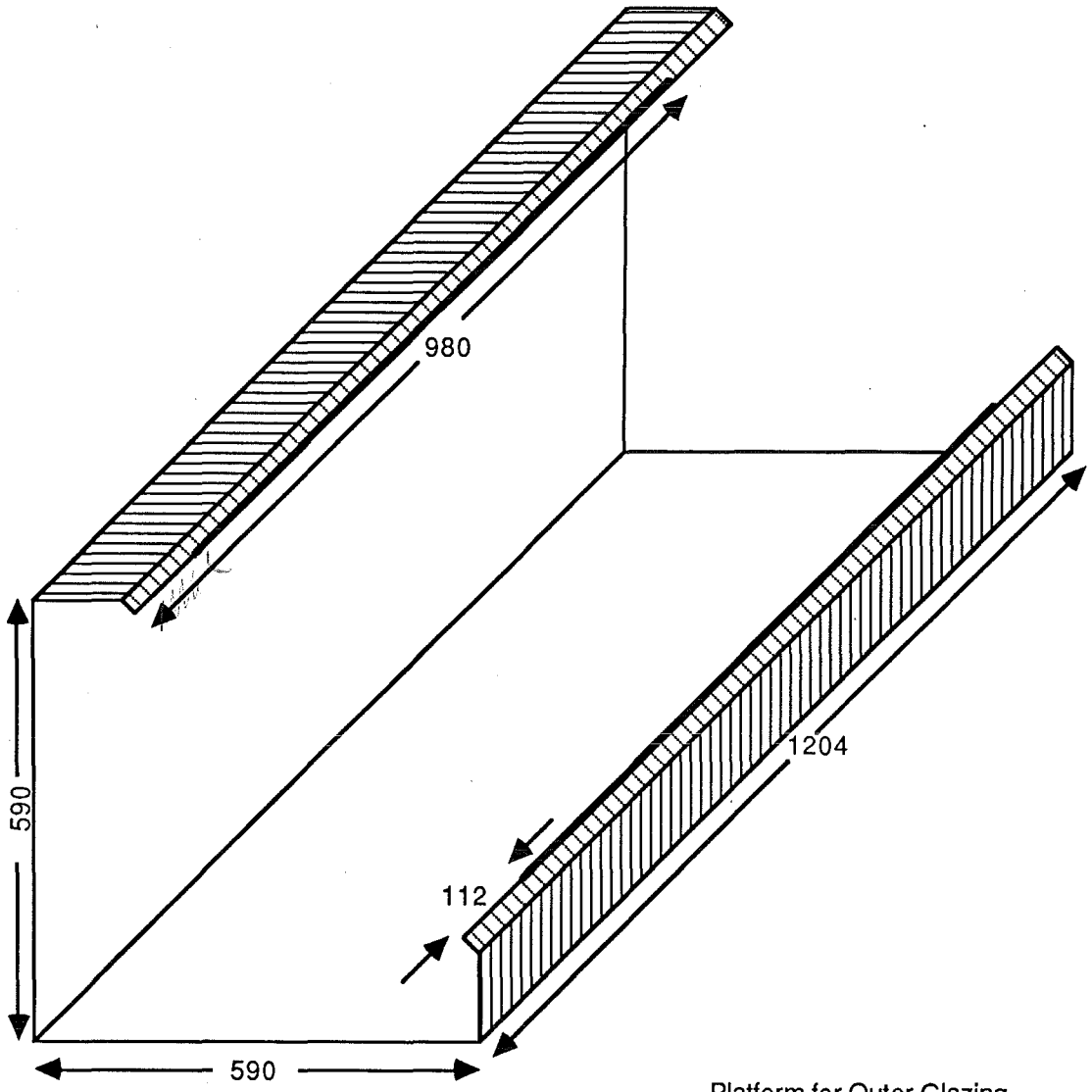

Notes: All dimensions are in mm

Scale 1 : 10

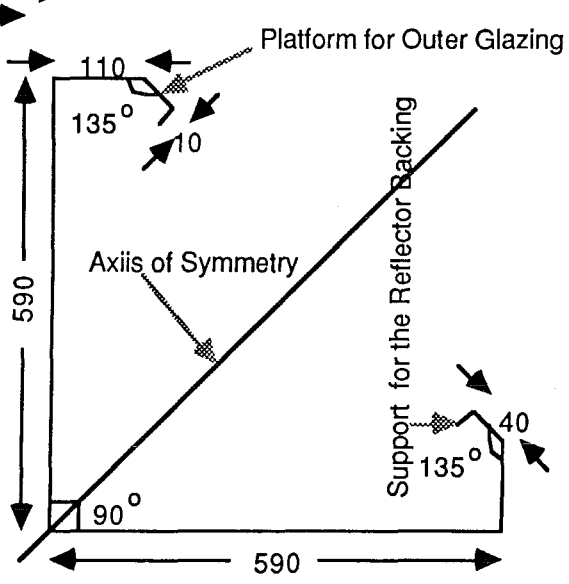

(b) Cross Section

FIGURE 4.27 End Wall Arrangement

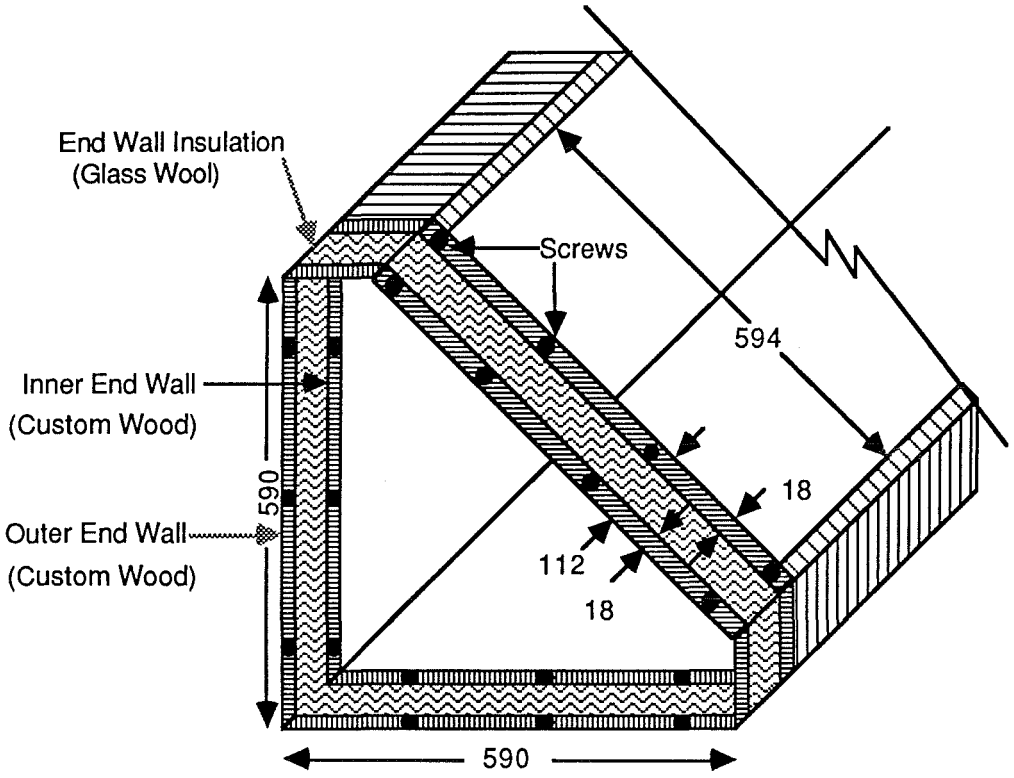

(b) Inner End Wall

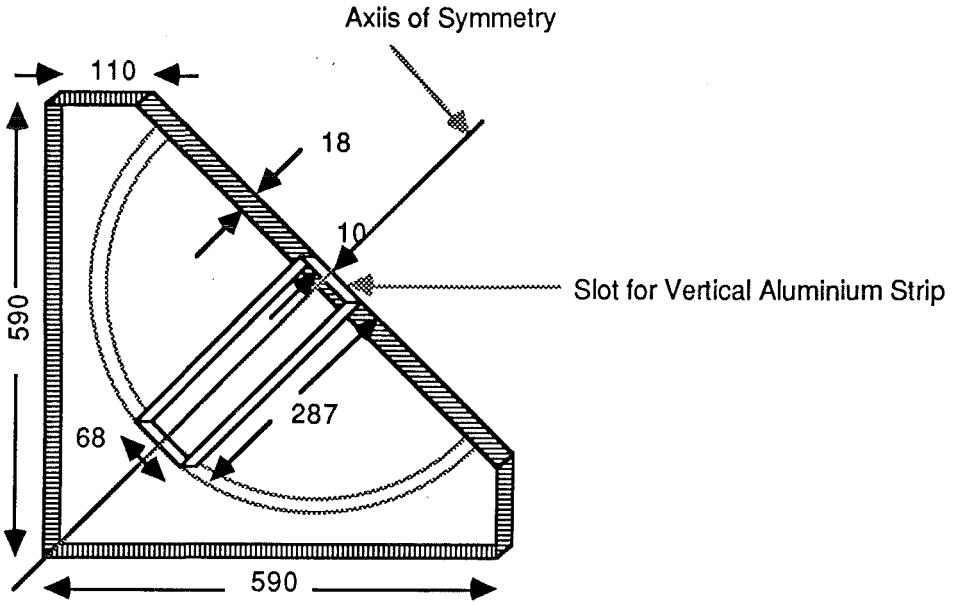

Notes: All dimensions are in mm

Scale 1 : 10

FIGURE 4.28 Reflector Arrangement

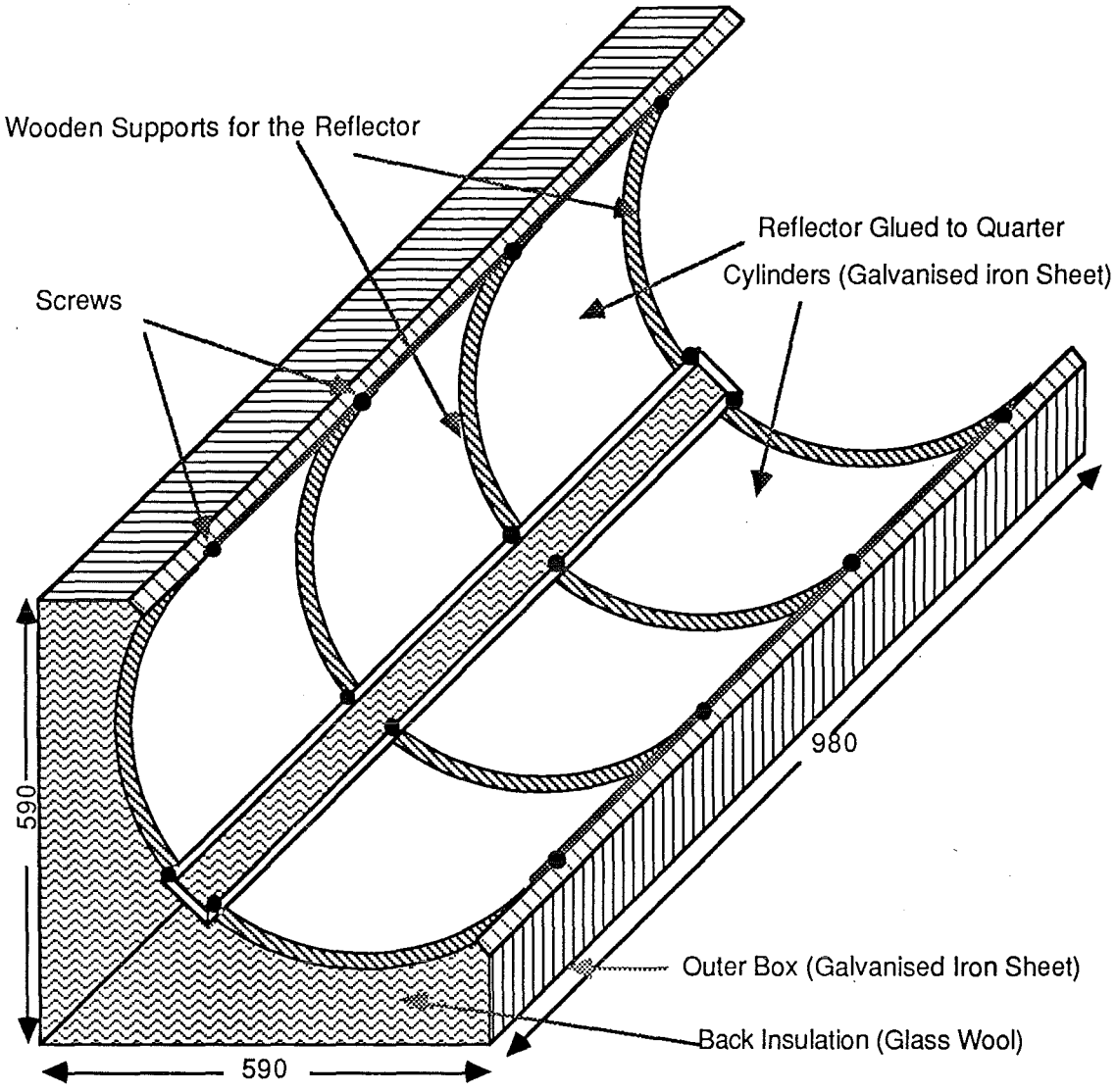

Notes: All dimensions are in mm

Scale 1 : 10

The reflector surface (RFM) was carefully glued to two preformed quarter cylindrical GI sheets. These two pieces of reflector were fixed to form a semicylindrical shape (leaving a gap of 68 mm for horizontal aluminium strip holding the panel and inner glazings) with the help of four wooden supports (Fig. 4.28). The reflector was screwed at the top and bottom ends to the outer GI box and the other two ends to the wooden supports to make sure that the reflector was semicylindrical.

The HSA panel, along with the two inner glazings on either side of the panel, could be slid into the collector as a single unit so that, if necessary, it could be removed easily. The panel and the inner glazings (3 mm thick) were held parallel to one another (leaving the required gap of about 25 mm in between) with the help of one horizontal aluminium strip (of 980 x 68 x 10 mm) and two vertical aluminium strips (each of 287 x 68 x 10 mm) as shown in Fig. 4.29. Three solid bars of aluminium were taken and three grooves of required size (leaving enough gap for the silicon rubber seals, which allow for thermal expansion) were milled out of each of them. The panel and inner glazings were slid into these grooves, (after fixing the required number of thermocouples with RTV or high temperature solder) along with the silicone rubber seals. Then the vertical aluminium strips were screwed to the two ends of the horizontal aluminium strip. In the second collector, the inner air chamber (between the two inner glazings) was made air-tight by fixing another strip of glass with RTV on the top of the inner glazings (Fig. 4.29).

The outer glazing is shown in Fig.4.30. It consisted of 4 mm thick glass placed in an aluminium frame with rubber seal to allow for thermal expansion. The frame was hinged at the top of the outer box and at the other three edges it was latched to the outer box. The arrangement was made air-tight with the help of a silicon rubber seal between the aluminium frame and the outer box. To further reduce the heat losses, the hatched portions (Fig.4.30) were painted black (in the second collector).

The Plate 3 shows the HSA-SCCR collector 2. The collector box, before the reflector and the HSA panel were fitted, is shown in Plate 3a. The back insulation, the end walls with the reflecting surface and the solarimeter can also be seen in 3a. The Plate 3b shows the fully assembled collector in operation.

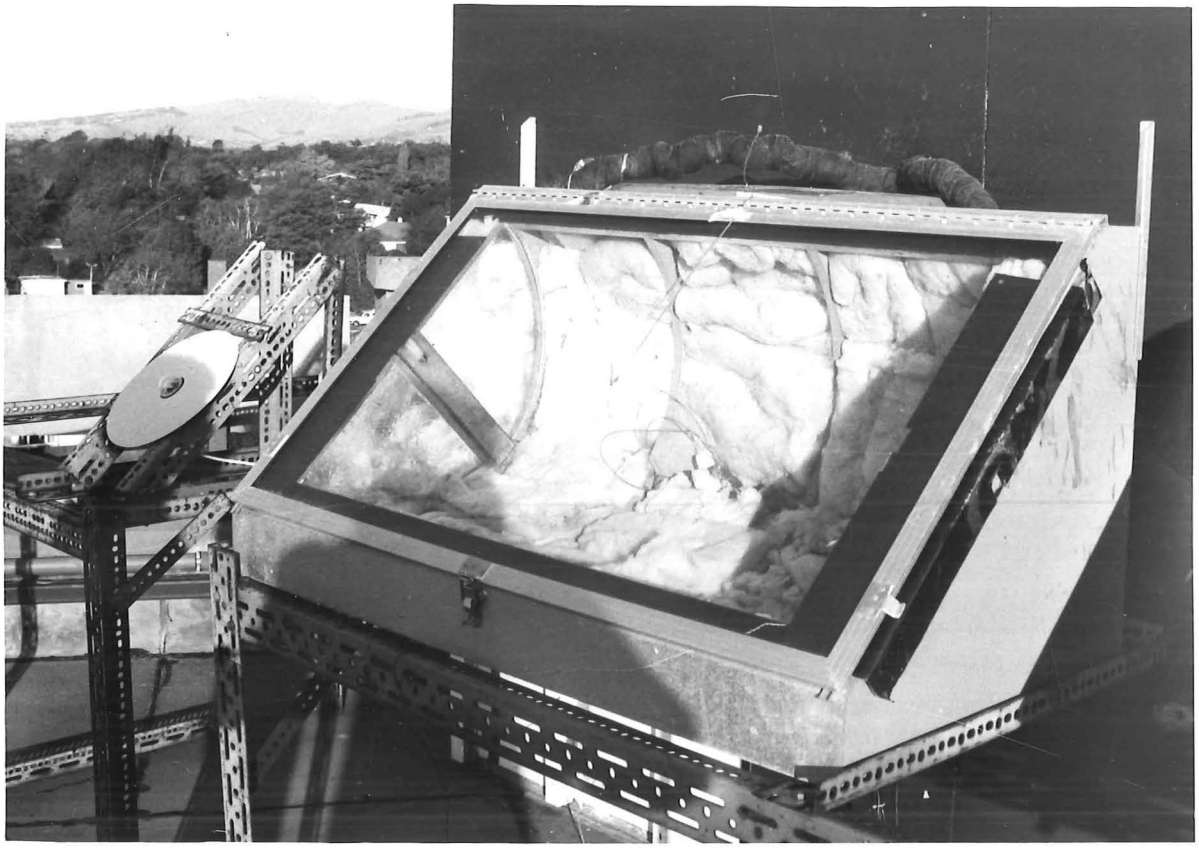

(a) Before Fitting the Reflector

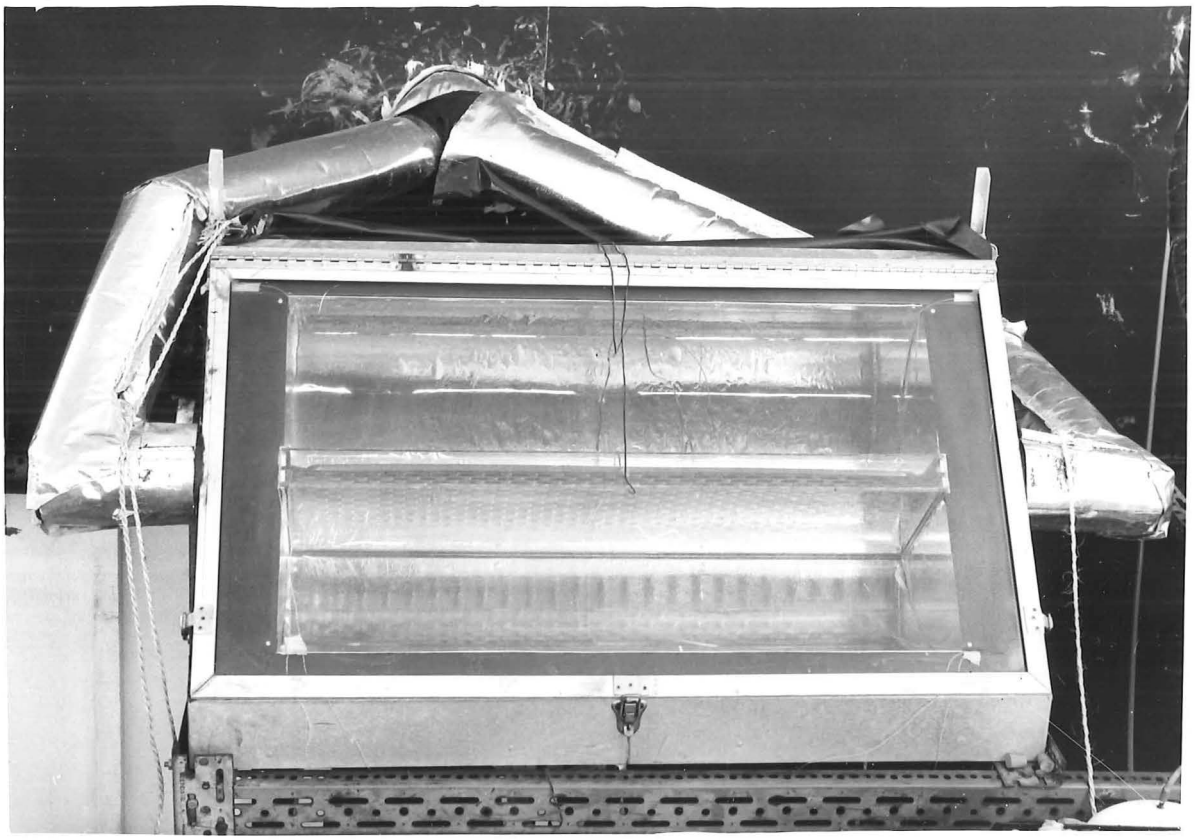

(b) Fully Assembled

PLATE 3 HSA-SCCR Collector 2

FIGURE 4.29 HSA Panel and Inner Glazing Arrangements (Not to Scale)

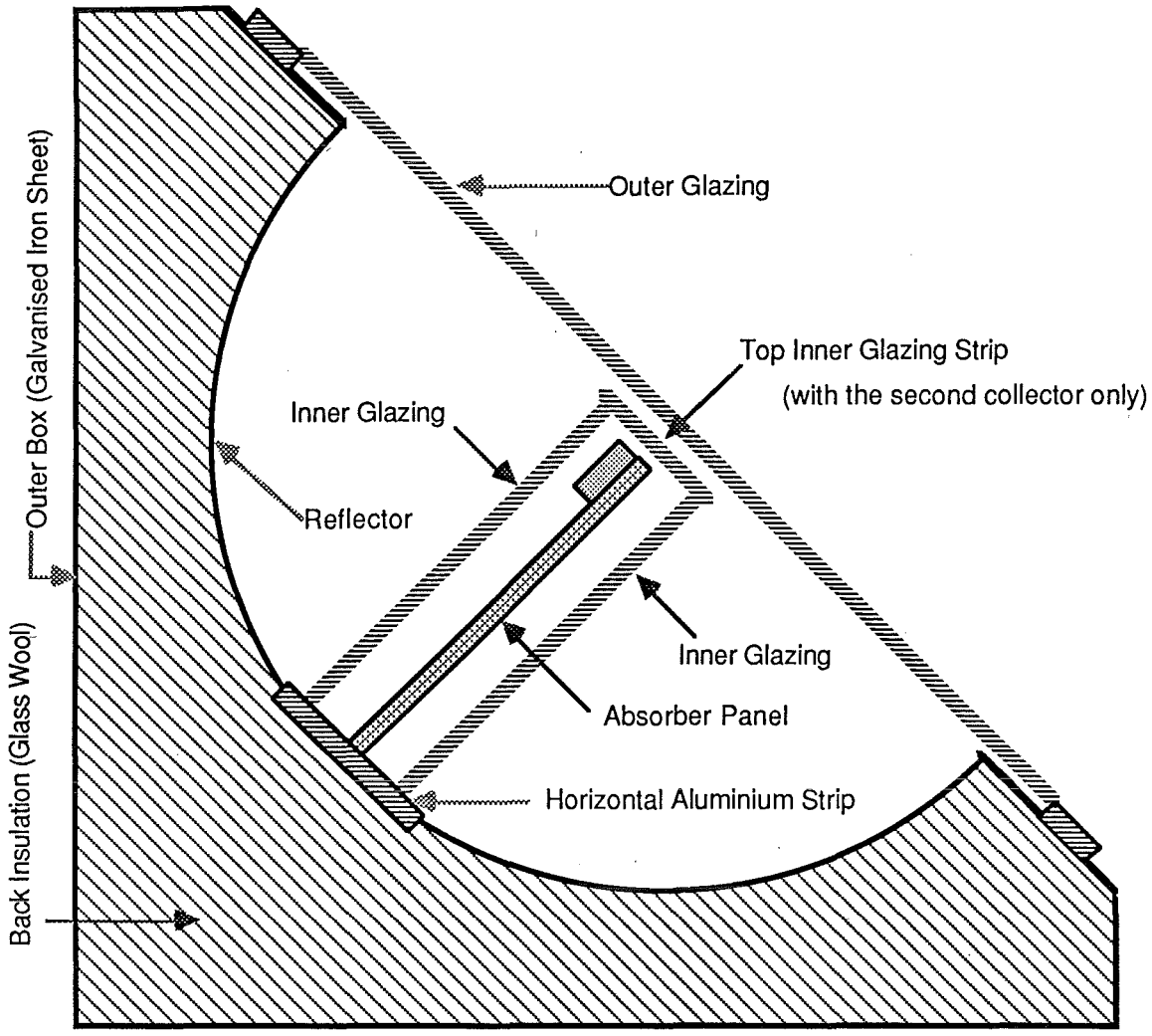

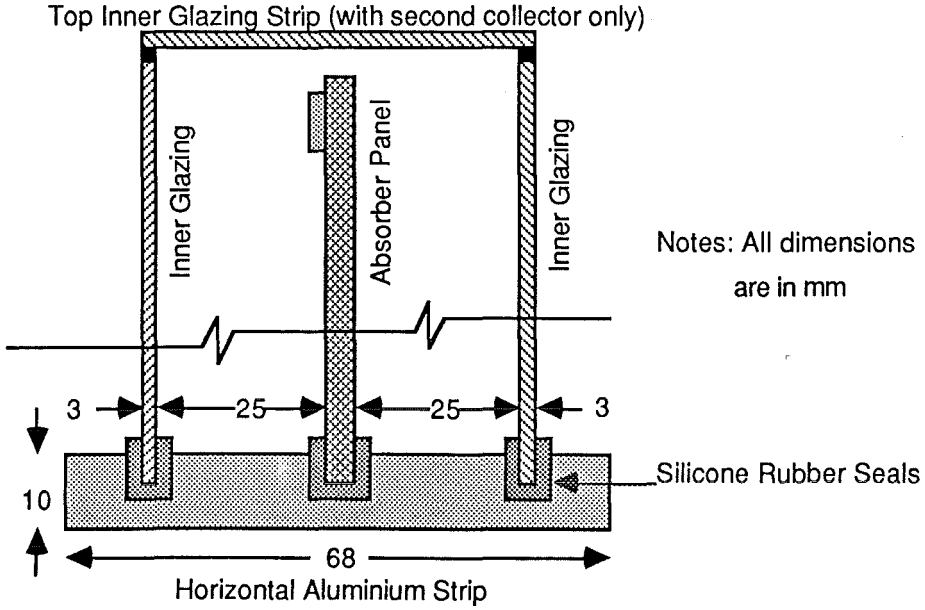

FIGURE 4.30 Outer Glazing Arrangement

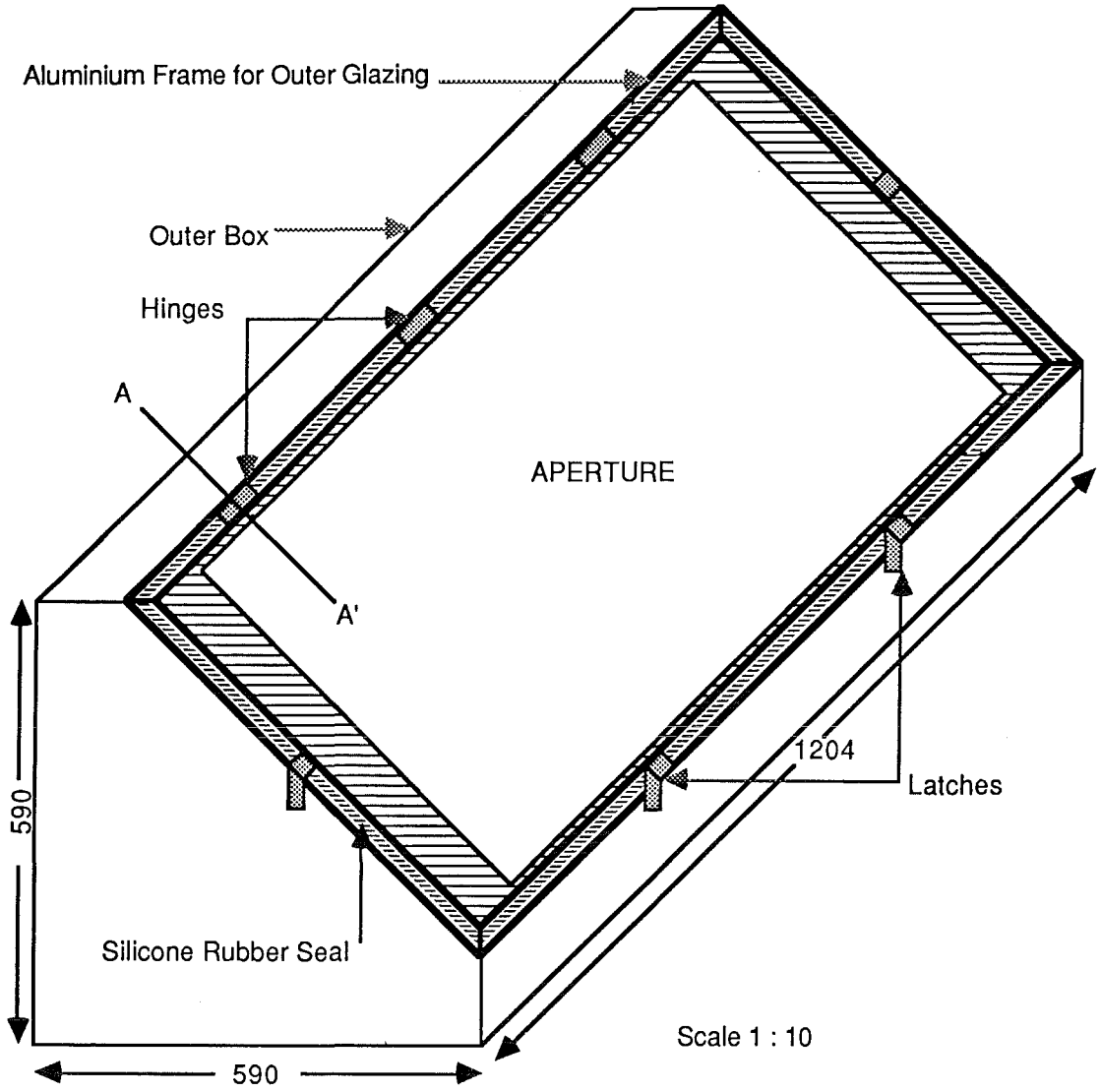

Notes: All dimensions are in mm

(b) Cross Section AA' Scale 1 : 1

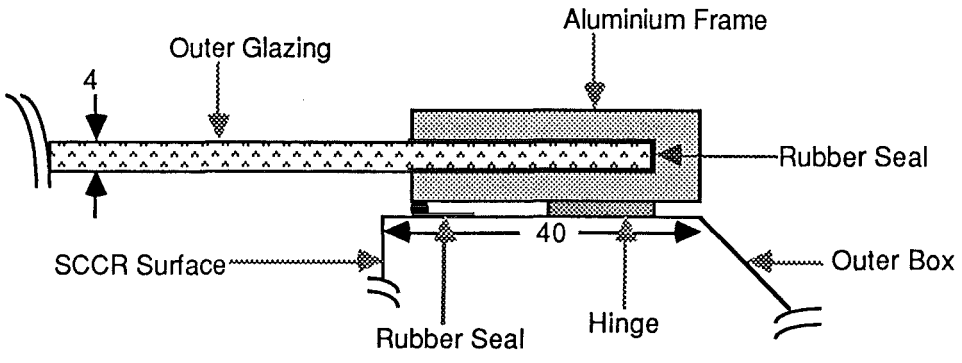

It was necessary to attach thermocouples to various surfaces prior to the assembly of the collector. Copper-constantan thermocouples were attached using either RTV or high temperature solder. For measuring higher temperatures (>100°C), teflon-coated thermocouples were employed and for measuring lower temperatures ordinary PVC coated ones were used.

4.8 Experiments on Collector C1

Several experiments were conducted to evaluate the performance of the collector C1, under stagnation conditions and with oil flow through the collector.

4.8.1 Experimental setup and experiments conducted

The schematic diagram of the experimental setup, is shown in Fig.4.31. Oil at the desired temperature could be pumped through the collector from a constant temperature oil bath. The oil bath consisted of a 28 l capacity stainless steel tank provided with 25 mm thick glass wool insulation. The oil temperature was raised, with a 2000 W base heater and it was controlled with a 500 W heating element from an on/off temperature controller. The heaters and the pump were connected separately via a variac, ammeter and voltmeter as shown in Fig. 4.31. A cooling coil was provided to reduce the oil temperature. A variable speed stirrer for mixing, and a funnel for recycling the oil were also provided. Thermocouples were provided for measuring the temperature at different depths of the oil. The flow rate of oil could be controlled with the "Danfoss" shut-off valves V1 and V2 or by varying the power input to the pump. The oil flow rate was measured by diverting the oil through the valves V3,V4 and V5 to a measuring cylinder. All parts were well insulated. The part of the insulation, which was in the open atmosphere was made weather proof with "Denso" tape. The thermocouples attached to various parts of the collector are shown in Figs.4.32a,b,c. Thermocouples were fixed at two different points along the central axis of each surface and air space in both top and bottom quadrants. They were attached to the panel in four rows and three columns. Thermocouples were also attached to measure the inlet and outlet oil temperatures to the collector and temperature rise of oil across the collector. A solarimeter (Kipp and Zonen, model CM5-6-

FIGURE 4.31 Schematic Diagram of the Experimental Setup to Find the Performance of Collector C1

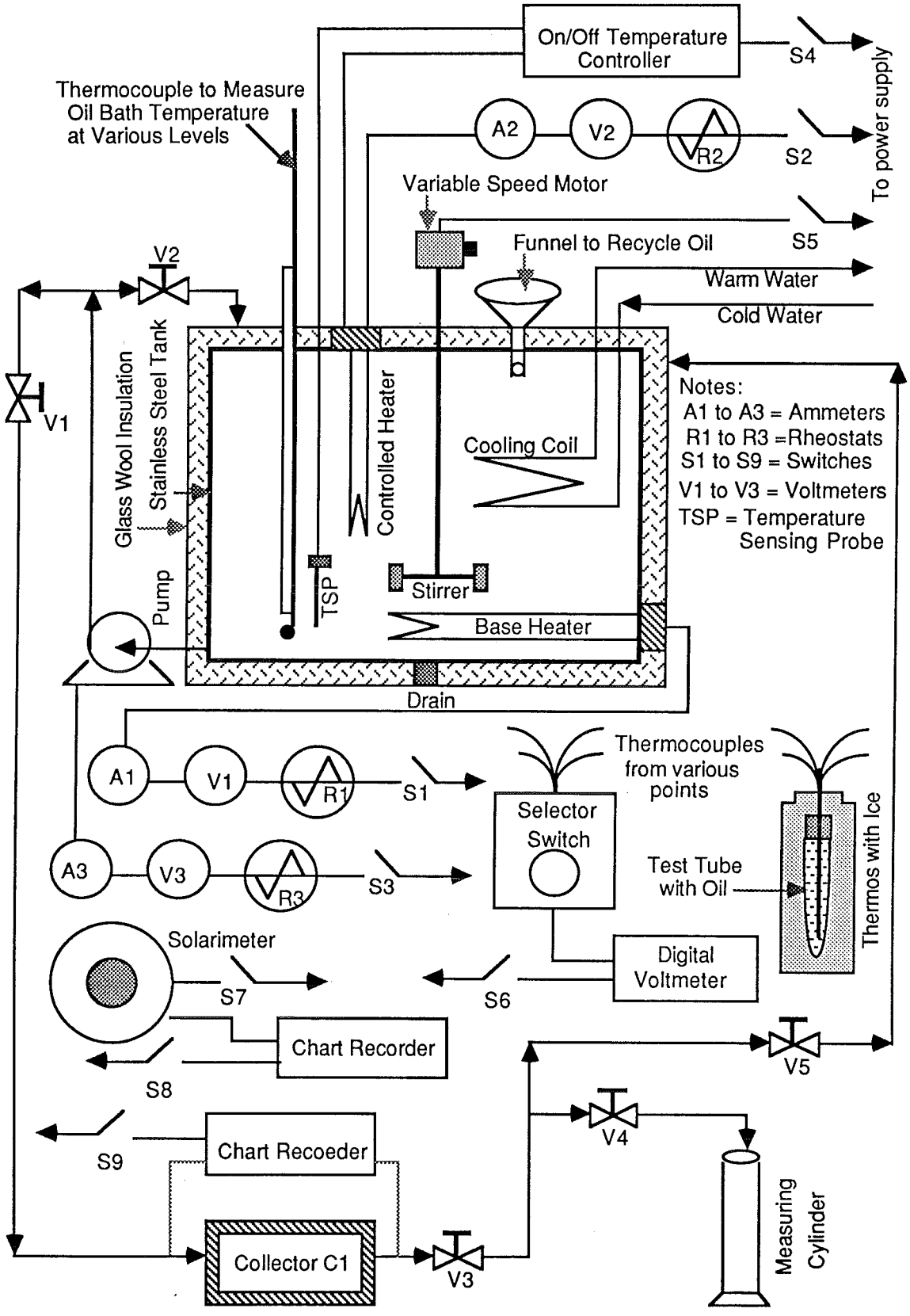

694) was fixed besides the panel at the same inclination for measuring the insolation.

Oil was pumped through the collector at any desired temperature. During operation of the system temperatures, oil flow rate and insolation were recorded at hourly intervals. The procedure was repeated for various inlet temperatures and oil flow rates. The stagnation test was conducted by taking the readings without the oil flow to the collector.

4.8.2 Results and discussions

A sample set of results for the stagnation test (at 1pm on 24 November 1982) are shown in Figs.4.32a,b,c. Typical results of experiments with oil flowing through the collector are given in Table 4.4. These points are shown in Fig.4.36, for comparison, along with the performance curve for collector 2. The thermal efficiency of the collector was evaluated from Eqn. (4.9). It was assumed that the density and specific heat capacity of oil were constant, within the inlet and outlet temperature limits for each run, and were equal to the corresponding values at the average temperature. The collector's figure of merit X_s was evaluated from Eqn. (4.12) and the X value for oil flow through the collector was calculated from Eqn. (4.7). The error analysis in evaluating the thermal efficiency and X values was conducted as described by Webb (1979); the errors involved in measuring various quantities are listed in Appendix A17. After deciding whether the error was random or systematic, the standard statistical methods were used in evaluating these errors.

According to Webb's predictions (Table 4.2), the panel should attain a stagnation temperature of 265°C, at an insolation of 850 $W.m^{-2}$ and an ambient of 17°C. However, in the present case, the maximum panel temperature achieved was only 170°C at an insolation of 851 $W.m^{-2}$ and an ambient of 26°C (Fig.4.32c). There could be two reasons for this discrepancy: the first one being inherent defects in the collector and the second one being over estimation of the collector's stagnation temperature by Webb's model. Attempts were made to attack this problem from both fronts. As shown in Table 4.2, Webb's model, indeed predicted stagnation temperatures which were upto 23% or 62°C higher than the present model predictions. In spite of this discrepancy, the collector should have attained a stagnation temperature of about 200°C, which suggested possible

FIGURE 4.32a Cross Section of the HSA-SCCR Collector C1 with the Temperature Measuring Points (at Stagnation Conditions)

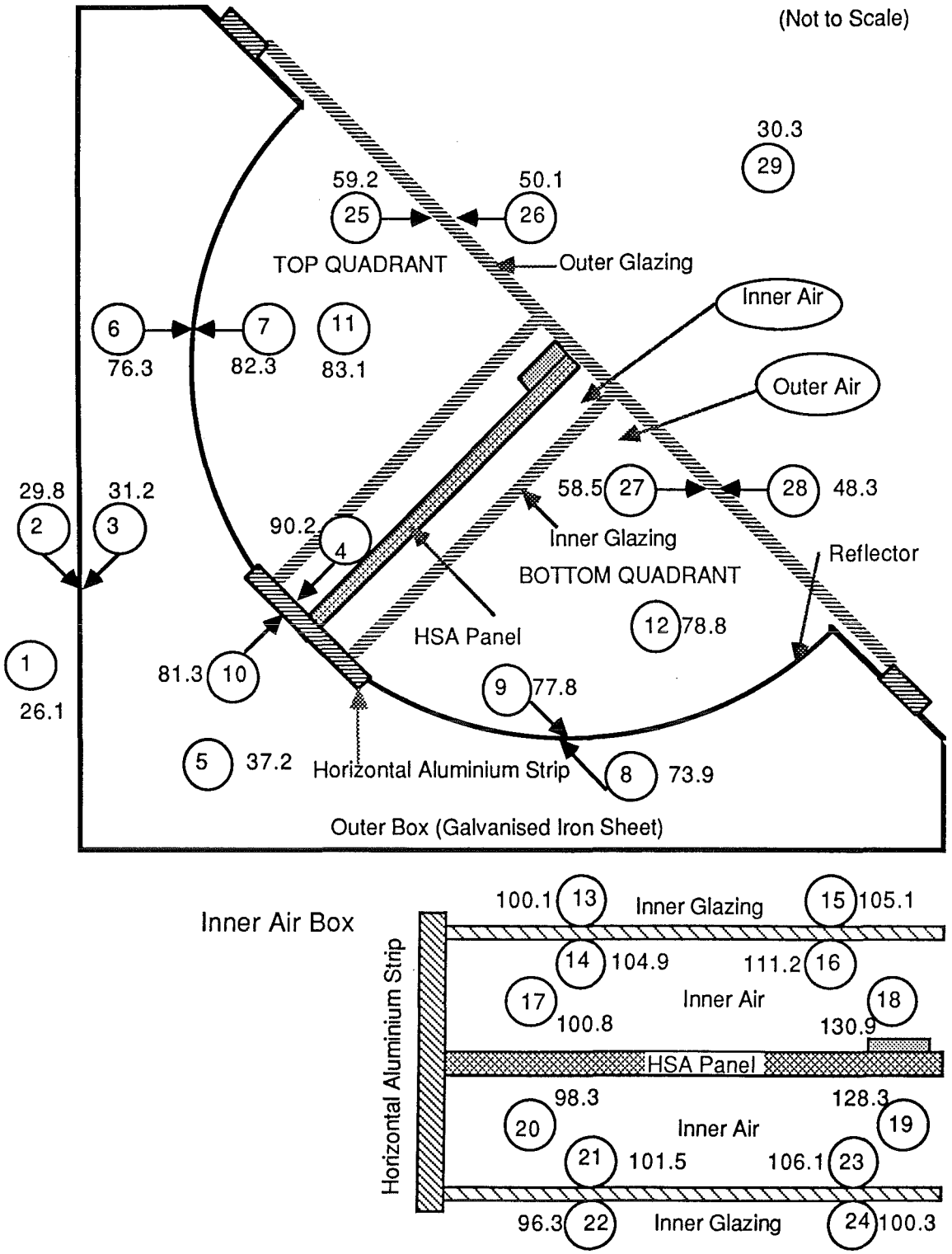

Notes: Numbers inside the circles indicate thermocouple numbers (either surface or air temperatures) and the numbers outside indicate the MEASURED temperature values in deg. Celcius at 1p.m. on 24 Nov 1982 with an insolation of 851 W/Sq.m and ambient of 26 ^{o}C

FIGURE 4.32b End Wall Temperature Measuring Points (at Stagnation Conditions)

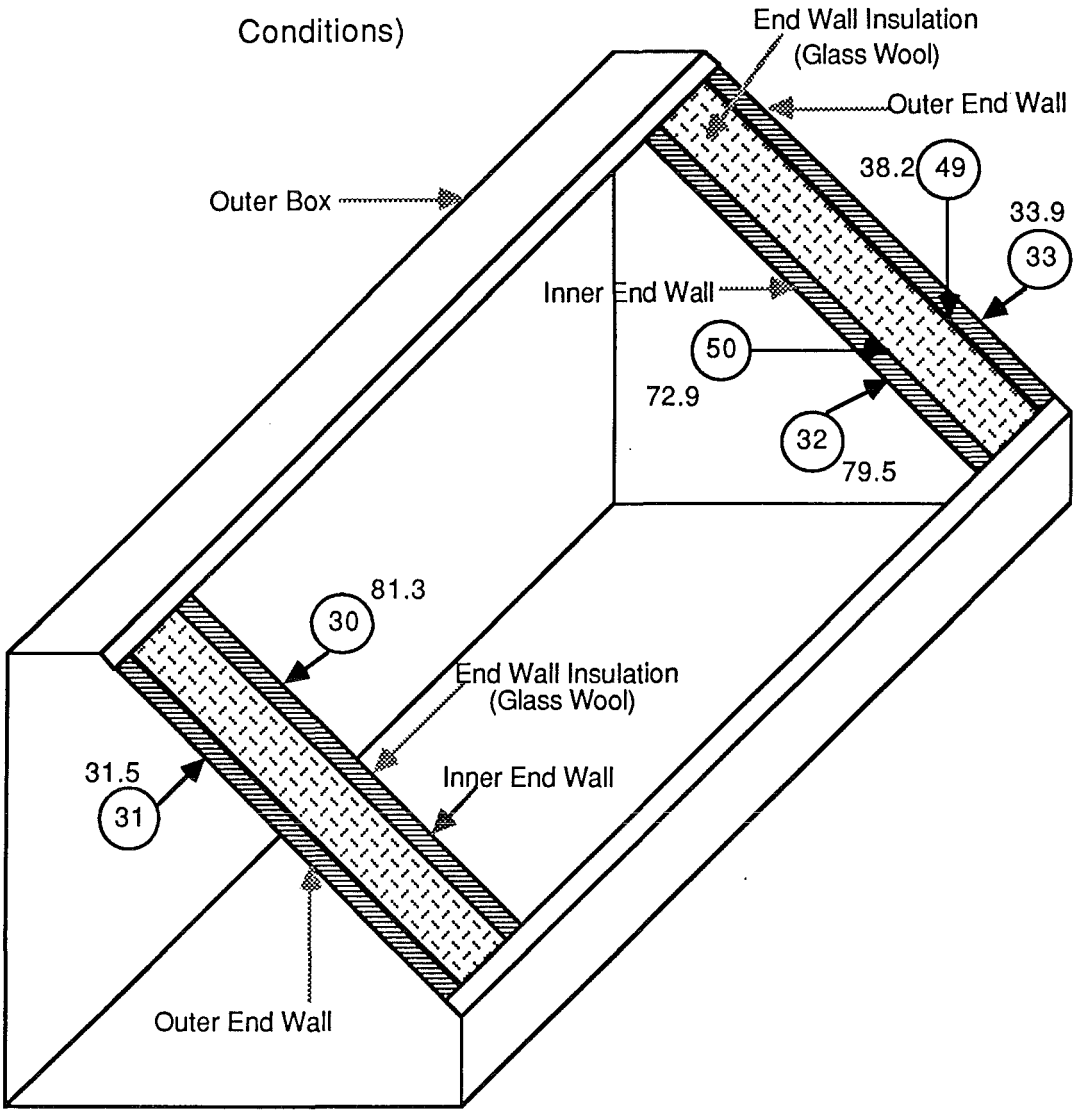

(c) HSA Panel Temperature Measuring Points

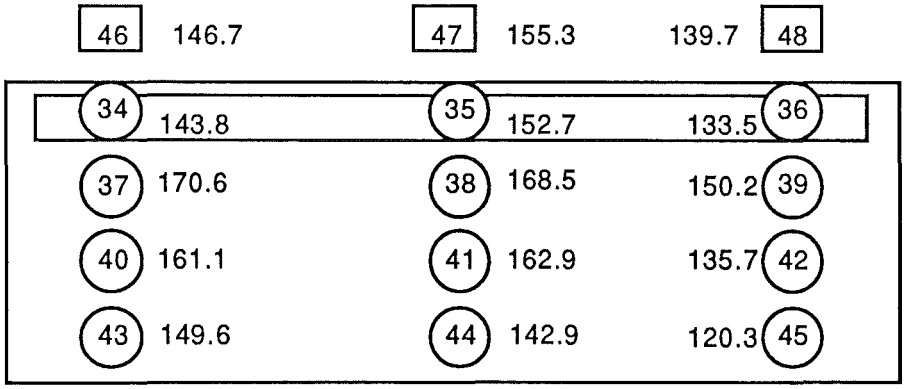

Notes: Numbers inside the circles indicate thermocouple numbers (either surface or air temperatures) and the numbers outside indicate the MEASURED temperature values in deg. Celcius at 1pm on 24 Nov 1982 with an insolation of 851 W/Sq.m and ambient of 26°C. The numbers inside the rectangular boxes indicate the condenser temperatures on the dimpled side of the panel.

TABLE 4.4 Typical Results of Experiments with Collector 1

	Run Number	
	1	2
Ambient temperature (T_{eamb} + 3) in °C	25.6	27.3
Oil inlet temperature in °C	83.7	143.5
Temperature rise in oil in °C	14.3	3.4
Oil flow rate x 10^6 in $m^3.s^{-1}$	4.5	10.2
Solar insolation (I) in $W.m^{-2}$	843.5	929.6
Thermal efficiency (η_{th}) in %	24.5	12.5
Error in η_{th} + or - in %	2.1	1.3
X = (T_{ao} - T_{eamb}) / I in $m^2.°C.W^{-1}$	0.081	0.130
Error in X in $m^2.°C.W^{-1}$	0.004	0.007

Notes: T_{eamb} = Effective ambient temperature

T_{ao} = Average oil temperature

defects in the collector system or in the techniques of temperature measurement, both of which are discussed below.

4.8.2.1 Temperature measurement

In order to interpret the results correctly, the reliability of the measurements, especially of the temperatures, should be known. The errors associated with temperature measurement, calibration of thermocouples, and methods of attachment of the thermocouples are discussed in detail in Appendix A1.

Although ASTM (1974) specifies a maximum error limit of ±0.7% with copper-constantan thermocouples, calibration of all the thermocouples was necessary. Of the various methods of calibration, comparison method with a standard thermometer (in this case a quartz thermometer) in a stirred liquid bath was chosen for its simplicity. A constant temperature bath was employed and calibration was conducted for all the 109 thermocouples between 20°C and 190°C at an interval of about 10°C. Instead of preparing a calibration chart for eacb thermocouple a different technique was used to interpret the results. Thermocouples were divided into four categories with variations of ±0.2, ±0.5, ±1.0 and ±2.0°C as compared to the average value. Thus the reliability and consistency of each thermocouple was found at various temperatures. Thermocouples with very narrow error band widths were used to measure critical temperatures such as oil inlet and outlet temperatures, while the thermocouples with the highest error band widths were discarded. Although this precaution was not taken with the first collector the error introduced was small (maximum of ±2°C).

Air or liquid temperatures can be measured comparatively easily but it is difficult to measure surface temperatures accurately and methods of attachment become important in this case. Silicone based sealants RTV and Araldite were used for attaching the thermocouples in the first collector. Welding and brazing were discarded, because of the high temperatures involved, which may damage the selective surface of the panel. Soldering was discarded as it would make an electric contact with the panel, in which case, stray currents could result in errors.

However, it was decided to investigate the method of attachment with high temperature solder ("Plumber's solder" capable of withstanding 230°C), RTV and Araldite and the amount of

each of these materials used. It was also decided to find out the effect of shade and the best method to measure the oil temperature. An outdoor test was conducted for this purpose (Appendix A1.1). The thermostat bath was used to pump oil at a specified temperature through a copper tube fixed with several thermocouples and placed in a box with reflector surface and outer glazing. The experiment was repeated at various oil temperatures ranging from ambient to about 190°C, at intervals of 10°C. It was found that the soldered thermocouples showed minimum deviation (7° to 8°C lower than the actual oil temperature of 173°C), while Araldite showed the maximum deviation (22° to 37°C) and RTV an intermediate value (15° to 30°C). However, the tests were conducted at most severe conditions; for example with an oil temperature of 173°C the temperature drop was about 120°C between the oil and the surrounding air. In the actual collector the temperature difference between a surface and surrounding medium was seldom that high.

This test clearly indicated that solder was better than RTV or Araldite. Where soldering can not be used (with the glazing and the reflector) RTV was preferable to Araldite. It was also noticed that with the increase in amounts of solder, RTV or Araldite the deviation became more pronounced. The errors became more pronounced with shading the thermocouple junctions, because of the decrease in the air temperature. The best method to measure the oil temperature accurately, was by brazing a small diameter copper tube at the inlet and the outlet to the collector and inserting thermocouples directly into the oil stream, and then sealing the small diameter tube with RTV. Precautions (Appendix A1.1) were taken to minimise the errors with the second collector.

4.8.2.2 Defects in the collector system

Keeping these errors in temperature measurement in mind, the results shown in Figs. 4.32a,b,c and Table 4.4 can be discussed. The thermocouples were attached to HSA1 with RTV and hence, some errors may be expected. However, the panel was very non-isothermal and the maximum temperature difference was about 50°C. The maximum and minimum temperatures were recorded by the thermocouples 37 and 45 respectively, indicating the possibility of hot spots in the panel. It was observed that the panel temperature decreased in general from left to right, till about the solar noon, after which

the trend became reversed gradually. This indicates the influence of the angle of incidence of solar radiation on the panel or the thermocouple junctions. It was also observed that the panel temperature decreased from top to bottom throughout the day. This behaviour can be explained from the inner air temperatures. The temperature of the inner air at the top was about 30°C more than the bottom temperature (This trend can be expected with high aspect ratios or narrow air cavities), which results in greater losses from bottom portion as compared to the top.

The reasons for the non-isothermal behaviour of the panel include: high pressure drop/low vapour density, limitations to heat transport and the presence of noncondensible gases.

(1) Pressure drop/low vapour density

The pressure drops in liquid and vapour phases, and the gravitational head, have been estimated (Appendix A15.1) with correlations available in the literature for circular heat pipes and modifying them for HSA panel. It has been assumed that the HSA panel consists of 26 separate channels (as there are 25 dimples in each row) each with an equivalent diameter of 4.8 mm, although in the actual case, the channels are non-circular, inter-connected and zigzag. However, this may alter the absolute values but the trend remains the same. It has been found that the liquid pressure drop is negligible, as compared to vapour pressure drop and the vapour pressure drop increases rapidly as the temperature goes down. The gravitational head is generally greater than the vapour pressure drop at all times ensuring proper circulation of fluids within the heat pipe. However, at low temperatures (about 100°C) the vapour pressure loss becomes excessively high tending to violate the above condition, resulting in hot spots and non-isothermal behaviour of the panel. The vapour density and vapour pressure of Dowtherm A are low at temperatures below 150°C, which results in excessive temperature drop. Thus, Dowtherm is not very suitable at lower temperatures.

The vapour pressure loss can be reduced, either by selecting an alternative working fluid with high vapour pressure and vapour density or by increasing the equivalent diameter (or decreasing the vapour flow resistance) of the flow channels by redesigning the panel pattern. The former method will be discussed in the next section and the latter method may bring only marginal improvements and since it involves major alterations, it was discarded.

FIGURE 4.33 Resistances in Flow Measurement

(a) Unequal Resistance Between the Points A,B and B,C

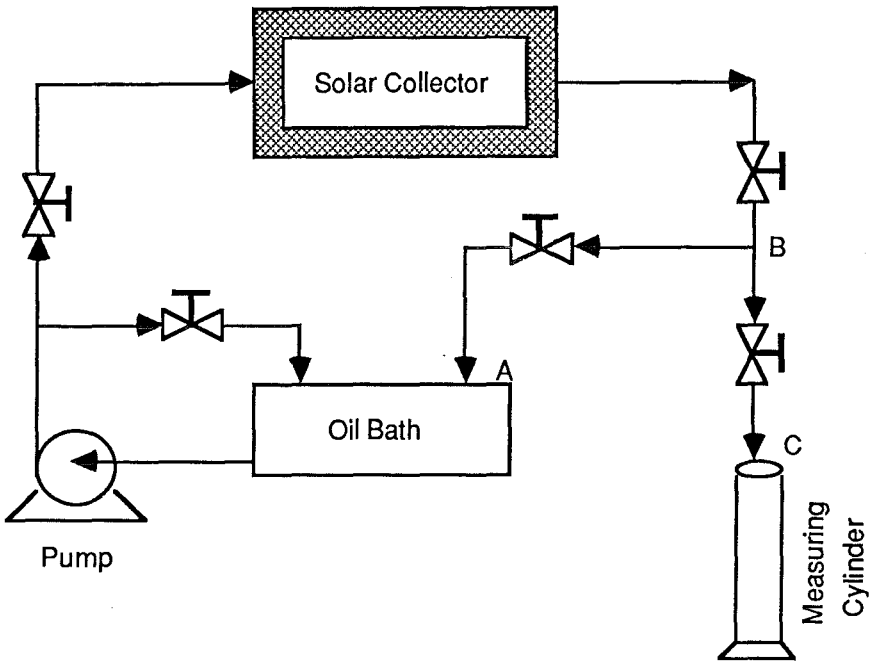

(b) Equal Resistance Between the Points A,B and B,C

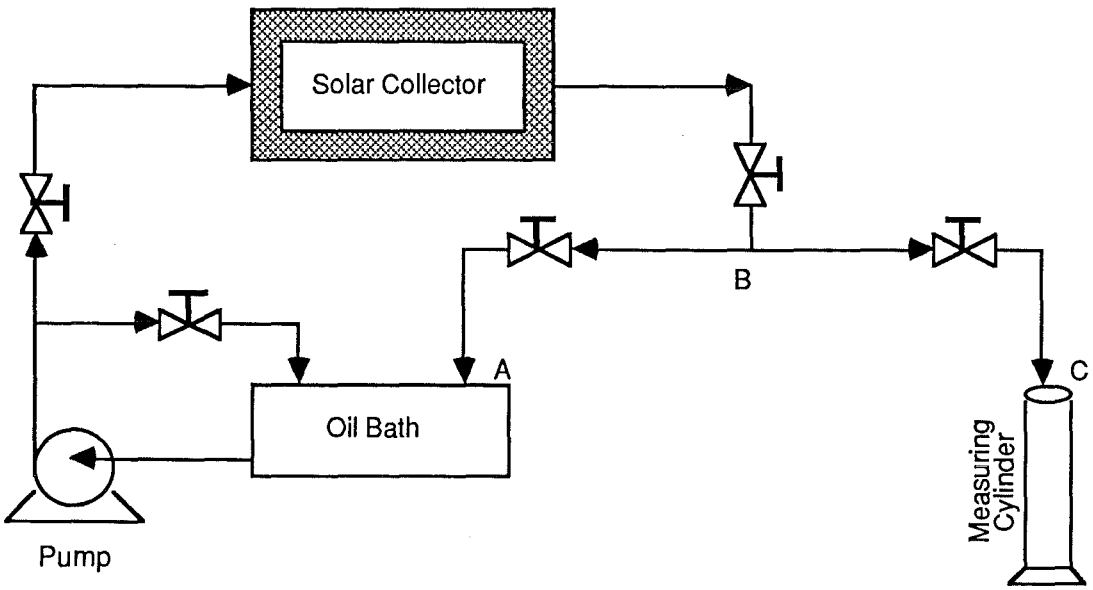

(2) Limitations to heat transport

The various limitations to heat transport are: sonic limit, viscous limit, entrainment limit, circulation limit and boiling limit (Appendix A15.3). At low vapour presures, sonic, viscous and circulation limits may be present, but the other two limits are not present with Dowtherm A. Merit number combines the important fluid properties for the efficient operation of a heat pipe and Dowtherm A has been found to have reasonably high Merit number at about 200° to 250°C and much lower values at lower temperatures, confirming once again the unsuitability of Dowtherm A at lower temperatures.

(3) Presence of noncondensible gases

The presence of noncondensible gases does result in steep temperature gradients. Though there is no clear indication of their presence it is, however, advisable to take precautions while degassing, baking, and loading the panel.

Other defects

The lower thermal efficiency (Table 4.4) may be attributed partly to the inefficiency of the panel and the collector, and partly to the condenser tube design.

The other defects in the first collector include poor reflector surface, large air cavities in the reflector surface, absence of back insulation, poor quality seals used with the absorber panel and inner glazing (which were melted, damaged or broken after a few days use) and free circulation of air between the inner air compartment and the outer air compartment (as there were gaps between the outer glazing and tops of inner glazing).

There were a few defects in other parts of the solar collection system such as fluctuating tank oil temperature (which was about 5 to 10°C), improper and insufficient insulation for the tank as well as the connecting piping, poor quality valves and uneven flow resistance between the return leg of the piping and the piping connected with the flow measurement as shown in Fig. 4.33a,b. The flow resistance between points A,B and B,C can be either unequal or equal. It was unequal with collector 1 and when calibration was made, differences up to 20% in flow rates were observed.

4.9 Experiments on Collector C2

It is evident from the analysis given in the previous section, that it was required to fabricate the second collector C2, an improved version of the collector C1. The improvements in the system are described below.

4.9.1 Improvements in the solar collector system

Several improvements were incorporated in the solar collector and the other parts of the system, some of which have already been mentioned, while the others are described below.

4.9.1.1 Alternate working fluid for the HSA panel

From the analysis of the experiments with collector C1, the major problem was found to be the low vapour pressure and vapour density of Dowtherm A, especially at temperatures below 150°C. Hence, a search was conducted for an alternative working fluid which has reasonably high vapour pressure at lower temperatures, but still has vapour pressures lower than atmospheric pressure at panel stagnation temperature, as otherwise, the panel may be ruptured. It is not easy to find a fluid with reasonably high vapour pressures (but lower than atmospheric pressure) in the whole working temperature range of 20° to 220°C and which, at the same time, meets the requirements of the heat pipe fluid (Appendix A4) especially compatability with stainless steel. In general, the vapour pressure requirements can only be met by a binary or multicomponent mixture.

Although heavier freons or their mixtures may be prospective candidates, their long term compatability with stainless steel is not known. As Dowtherm and toluene are both compatable with stainless steel (toluene compatability tests were conducted by Saski, 1978) and both fluids possess reasonably good qualities as heat pipe working fluids, it was decided to use a mixture of the two fluids. By adding a small quantity of the more volatile toluene (which has an atmospheric boiling point of 111°C), the vapour pressure in the low temperature range can be enhanced considerably. However, it is crucial to know the amount of toluene necessary for this purpose, keeping in mind the limitation of maximum vapour pressure of about 100 kPa at about 220°C.

The vapour pressure of the ternary mixture (as Dowtherm A is already a mixture) is difficult to estimate and hence, it was

TABLE 4.5 Comparison of Vapour Pressures of Pure Dowtherm A and a Mixture of Dowtherm A and Toluene (15% by Volume of Toluene)

Temperature in °C	Vapour Pressure in kPa	
	Dowtherm A	Dowtherm A and Toluene
100	1	22
150	5	42
200	25	86
210	32	92

decided to find it experimentally as described in Appendix A16. Different combinations of Dowtherm A and toluene were introduced into an evacuated glass flask, which was partly immersed in the constant temperature oil bath. At several temperatures, the vapour pressures of the mixture were noted down, once steady state was attained. The most appropriate mixture was found to contain about 15% by volume (or 0.2 mole fraction) of toluene, which gave high vapour pressures even at low temperatures, but, at the same time the vapour pressure was below atmospheric pressure even at 210°C. The superiority of the mixture over pure Dowtherm A is evident from Table 4.5. The vapour pressures mentioned for pure Dowtherm A are also experimental values. As seen from the Table 4.5 near the operating temperature of the collector (about 150°C) pure Dowtherm A has a vapour pressure of only 5kPa as compared to the mixture with a vapour pressure of 42 kPa. Hence, this combination was used with HSA2. In order to guard against possible rupture of the panel due to excessive inside pressure, a vacuum gauge was attached to the panel so that, if necessary, the solar aperture could be covered to stop further increase in pressure.

4.9.1.2 Other improvements

The various other improvements in the second collector and the whole solar collection system are described below.

(1) The thermal efficiency of the collector can be increased by improving the condenser tube design. In order to enhance the heat transfer coefficients as well as the heat transfer area on the oil side (which is the controlling side) the condenser tube width was increased from 30 mm to 40 mm, and two internal fins were provided as shown in Fig. 4.25. This would nearly double the area of heat transfer. Also, the fin effect on oil side film coefficient increases.

(2) The intermixing of the inner air and the outer air was eliminated by fixing a top glazing strip on the two inner glazings (Fig. 4.29), thus totally encapsulating the absorber panel in the inner glazing assembly. To further avoid any leaks due to damage to the poor quality seals with the absorber panel and the inner glazings, high quality silicon rubber seals were used.

(3) To improve the reflector performance RFM was used instead of aluminised mylar, which was found to have better reflectivity (Appendix A11.5). The spray adhesive was difficult to handle and

FIGURE 4.34 The Layout of the "Haake" Constant Temperature Circulator

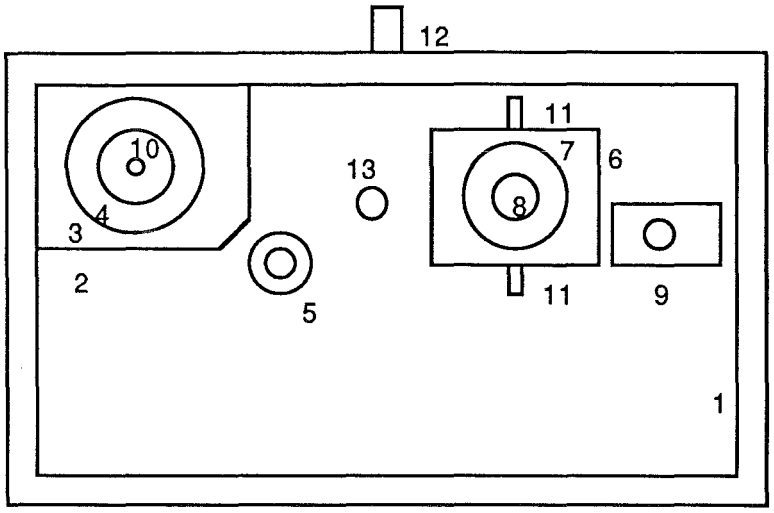

Notes 1 = Stainless steel tank

2 = Heating chamber

3 = Electric heating element

4 = Copper cooling coil

5 = Thermoregulator

6 = On/off controller

7 = Submerged pump

8 = Stirrer

9 = Level sensor

10 = Fluid inlet

11 = Fluid outlet

12 = Drain

13 = Temperature sensor

hence Ados pipe cement was employed. The reflector surface was applied in 3 to 4 strips to avoid large vapour pockets developing during the curing process.

(4) Back insulation (of glass wool) was provided to reduce the heat losses. Better seals and a better frame were employed with the outer glazing.

(5) In search for a better temperature control of the tank oil, a "Haake" constant temperature circulator (model FS2) was employed, the details of which are given below. This tank gave better temperature control (oil temperature could be controlled within a narrow range of ±0.5°C), better agitation, resulting in uniform tank temperature.

The layout of the Haake bath is shown in Fig. 4.34. It has a double layer tank (to reduce the heat losses) with an inner layer of stainless steel (1). It has a small heating chamber (2) with a 1000 W electric element (3) and a copper coil (4) through which a coolant, if necessary can be circulated. The oil inlet (10) is attached to this chamber. A thermoregulator (5) which can be set at any desired temperature controls the temperature of the oil coming out from the bottom of the heating chamber (with the help of a temperature sensor (13) by controlling the input power with an on-off controller (6). A submerged pump (7) with two outlets (11) is provided for the circulation of oil. A stirrer (8) is provided along with the pump for proper mixing. The level sensor (9) cuts off the power automatically if the liquid level falls below the minimum level. A drain (12) is provided at the bottom of the tank. The Plate 4 shows the bath with all its components.

(6) Mobiltherm produced carbon deposits on the heating element surface, which eventually caused fouling problems. In a bid to choose a better condenser fluid, soya bean oil was examined first. The whole system was emptied, thoroughly cleaned with acetone and trichloromethane and charged with soya bean oil. Although it did not produce carbon deposits, it had poor heat transfer characteristics and hence it was discarded. The system was once again cleaned and recharged with a fresh batch of Mobiltherm.

(7) The tank and piping insulation was improved and the thickness was increased to at least 50 mm. There was considerable loss from valves and hence these were also insulated. A double layer of weather resistant and water proof "Denso" tape was used

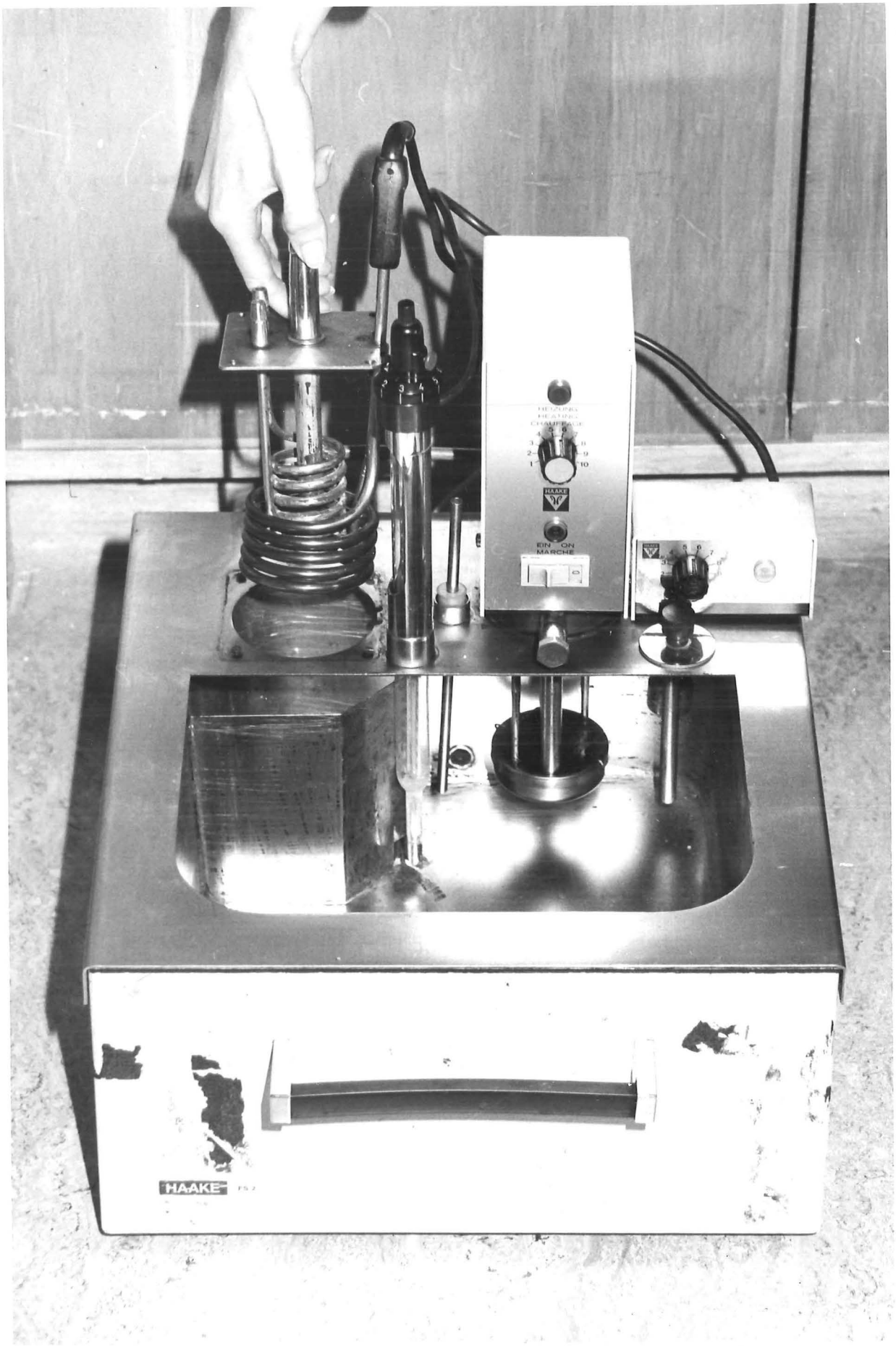

PLATE 4 "Haake" Constant Temperature Circulator

to avoid damage or water leaks into the outside insulation. A thick aluminium foil was employed on the top of the insulation to minimise radiation losses.

(8) Oil flow control and measurements were improved by employing better quality valves (quarter turn ball valves) and equalising the flow resistance as shown in Fig. 4.33.

(9) Finally the temperature measurement was improved by following all the procedures as discussed earlier. The inlet and outlet oil temperatures to the collector and the temperature rise across the collector were measured by actually immersing the thermocouple junctions in the oil stream. Wherever possible soldering was employed to attach the thermocouples. In order to reduce the contact resistance, the contact points inside the thermocouple selector switch were cleaned.

Incorporating all these improvements the second collector and the collector testing apparatus were constructed. The schematic diagram of the experimental setup is similar to that of collector 1 (Fig. 4.31), but incorporating the changes such as the Haake bath and flow control valves. The thermocouples were attached only in the top quadrant of the collector because, with collector 1 the temperatures in top and bottom quadrants differred within reasonable limits (±5°C). The same experimental procedure, calculations and error analysis as with collector 1 were followed.

4.9.2 Results and discussions

A sample set of results for a stagnation test (at 1 pm on 24 February 1984) are shown in Fig. 4.35. The summary of results of the experiments with oil flow through the collector are given in Table 4.6 and plotted in Fig. 4.36, along with the computer model predicted results.

The stagnation test results (Fig. 4.35) are in good agreement with the predictions of the computer model (Fig. 4.20, from Section 4.5.3). The model predictions are in general higher with a maximum deviation of about 11°C, which occured with the inner air. As the inner air cavity has a very high aspect ratio this behaviour may be expected. However, the difference in outer glazing outside temperature at the centre of the aperture (as indicated by thermocouple point 12) is about 17°C. This is because of the introduction of top glazing strip (between the tops of inner glazings and the outer glazing) in collector C2, which has

FIGURE 4.35 Cross Section of the HSA-SCCR Collector C2 with the Temperature Measuring Points (at Stagnation Conditions)

(Not to Scale)

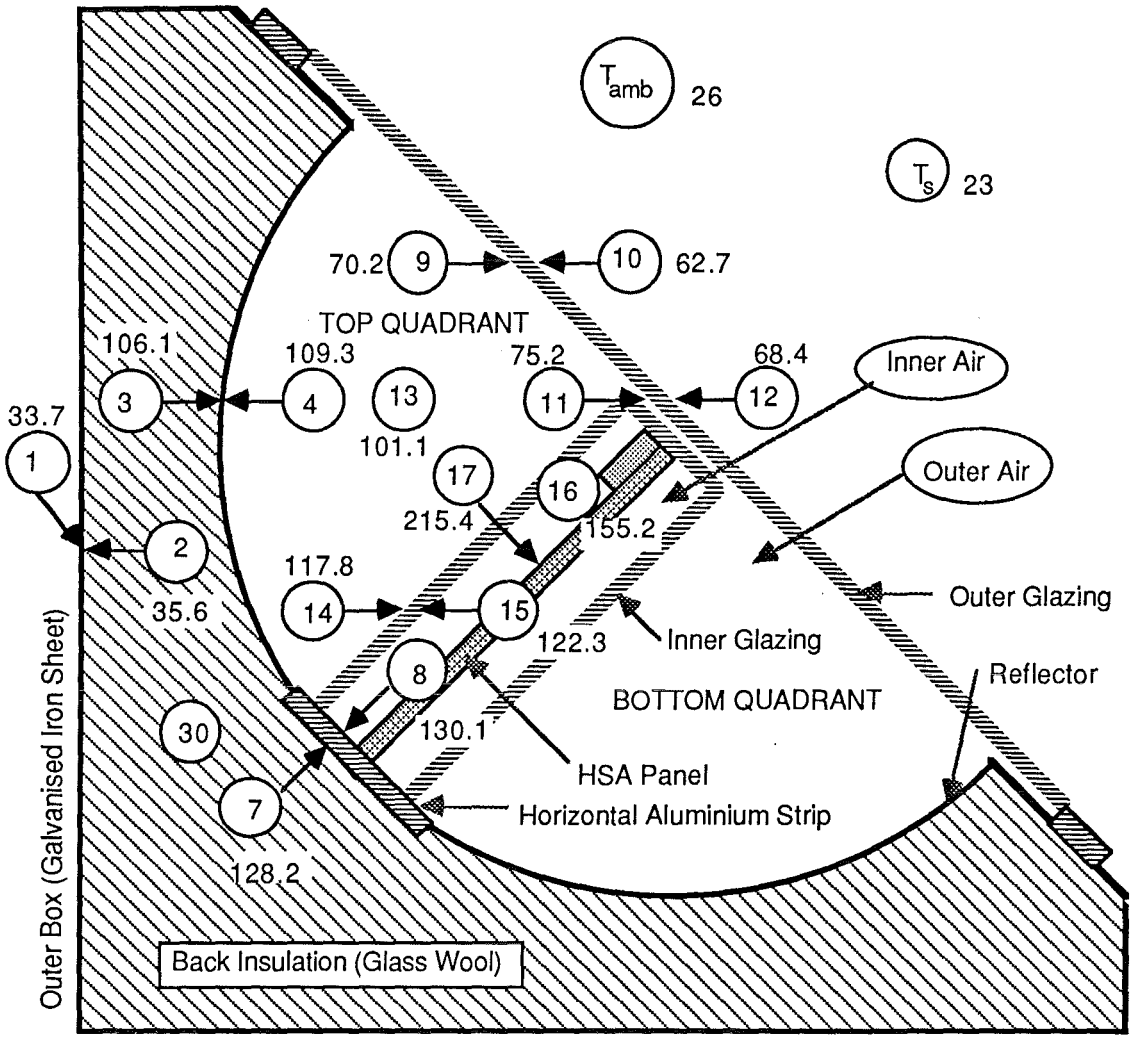

Notes:

Nembers inside the circles indicate the temperature measuring points, which also correspond to the numbers used in the computer programme TPLWR and the numbers outside are the corresponding MEASURED temperatures at 1pm on 24 Feb 1984 with an insolation of 946 W/Sq.m .

T_{amb} = Ambient temperature

T_s = Sky temperature

20 to 29,33 = Dummy temperatures

Cross Section of the End Wall

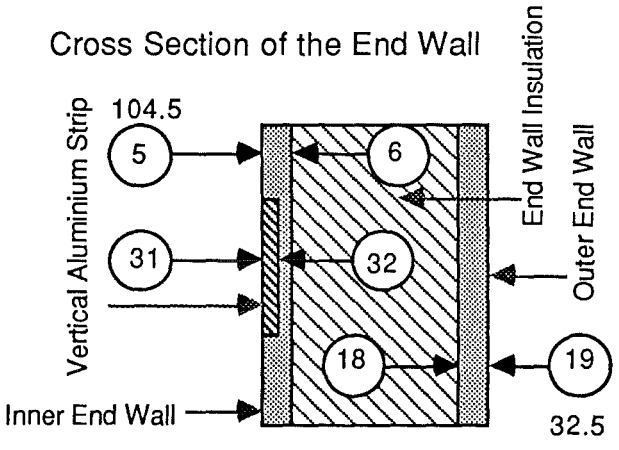

TABLE 4.6 Typical Results of Experiments with Collector 2

	Run Number					
	1	2	3	4	5	6
Ambient temperature (T_{eamb} + 3) in °C	29.1	27.3	28.2	26.5	25.0	25.7
Oil inlet temperature in °C	137.2	128.3	151.2	115.1	155.1	150.0
Temperature rise in oil in °C	19.3	14.4	4.6	8.3	3.5	3.4
Oil flow rate x 10^6 in $m^3.s^{-1}$	2.82	4.35	10.9	8.9	14.3	11.2
Solar insolation (I) in $W.m^{-2}$	964.5	942.4	936.5	898.3	946.4	883.5
Thermal efficiency (η_{th}) in %	20.5	23.8	19.5	28.8	19.3	15.6
Error in η_{th} + or - in %	1.2	1.5	1.2	1.9	1.1	1.1
$X = (T_{ao} - T_{eamb}) / I$ in $m^2.°C.W^{-1}$	0.125	0.118	0.137	0.102	0.139	0.146
Error in X in $m^2.°C.W^{-1}$	0.007	0.006	0.008	0.004	0.008	0.009

Notes: T_{eamb} = Effective ambient temperature

T_{ao} = Average oil temperature

FIGURE 4.36 Performance Curve of HSA-SCCR Collector

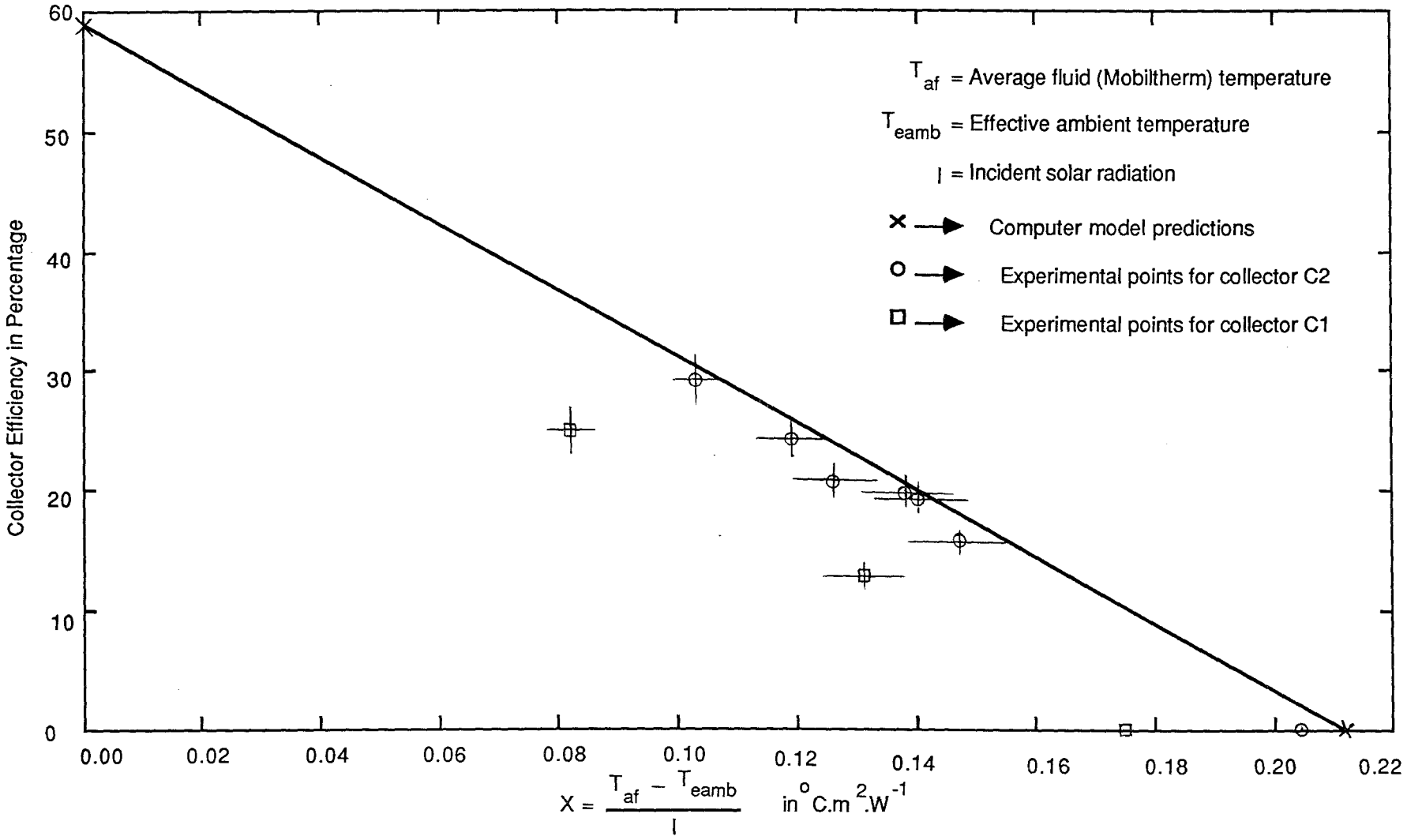

not been taken into consideration in computer model. Also, the estimated heat transfer coefficients due to the wind seem to be lower than the actual coefficients as evident from the outer glazing out side temperature (indicated by thermocouple point 10). The panel temperature (indicated by thermocouple point 17) shown in Fig. 4.35 is the maximum temperature. It was observed that the maximum variation in the apparent panel temperature was about 20°C as compared to 50°C in collector C1. This improvement was due to various modifications with collector C2, especially the addition of toluene to Dowtherm A.

The thermal efficiency of the collector has been tested mainly in the operating temperature region of the generator of the Electrolux refrigerator (Table 4.6). It may be seen from Fig. 4.36, that the thermal efficiency of collector C2 is in reasonably good agreement with the computer predicted HWB plot. The superiority (in thermal efficiency) of collector C2 over collector C1 is also evident from Fig. 4.36.

FIGURE 5.1 Generator Tube Assembly

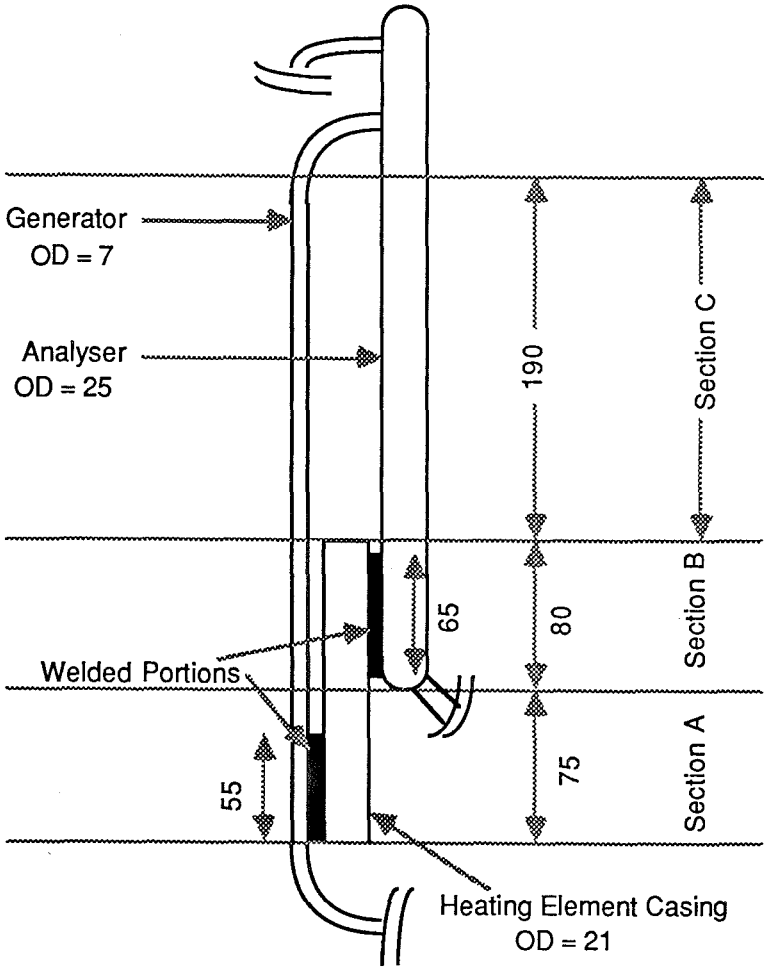

Notes: OD = Outside diameter

All dimensions are in mm
Scale 1:4

FIGURE 3.24 Schematic Diagram of Electrolux Refrigerator ER2

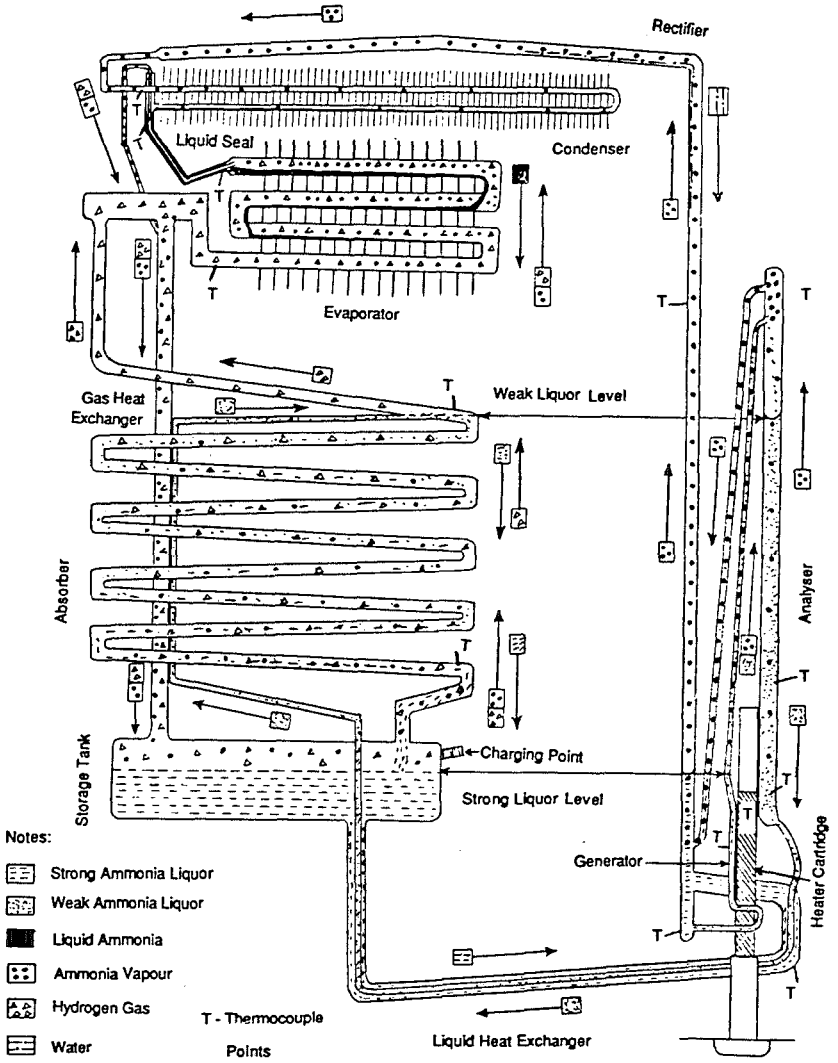

CHAPTER 5

LINKING THE COLLECTOR WITH THE REFRIGERATOR

As seen from the previous chapters it has been found that the solar collection systemis capable of producing temperatures high enough to operate the Electrolux refrigerator ER2. Before linking the collector with the refrigerator it is necessary to modify the latter in order to substitute electric heating with thermal heating.The methods of supplying the required amount of thermal energy to the generator tube of the refrigerator are discussed in the following section and in Chapter 6. Irrespective of the method, a heat exchanger has to be built surrounding the generator and the solar heated fluid has to be circulated through this heat exchanger. It is more efficient and convenient to use the same heat transfer fluid (Mobiltherm) as was employed in the solar collection system.

5.1 Modifications of ER2 to Operate on Hot Oil

As discussed in Chapter 3, it was necessary to supply 75 W of electrical energy to the generator tube to bring it to a temperature of 165°C. This energy was adequate to bring down the freezer temperature to -12°C and the cabinet temperature to about 3°C. The heating element casing external temperature corresponding to a generator temperature of 165°C was 235°C (Table A2.2). However, with solar heated oil such a large temperature difference was not desirable as it would mean a very low collector efficiency. However, the point in our favour was that the area of heat transfer between the generator tube and heating element tube was very small with electric heating: 9 mm wide and 55 mm long welded portion (Fig. 5.1). Hence, it should be possible to bring down the temperature drop in the oil loop by increasing the area of heat transfer.

5.1.1 Methods of increasing the heat transfer area

The heat transfer area could be increased in several ways, but there were a few problems associated with each. The generator tube assembly was already part of an existing unit, and so it

FIGURE 5.2 Methods of Increasing the Heat Transfer Area of the Generator Tube Assembly

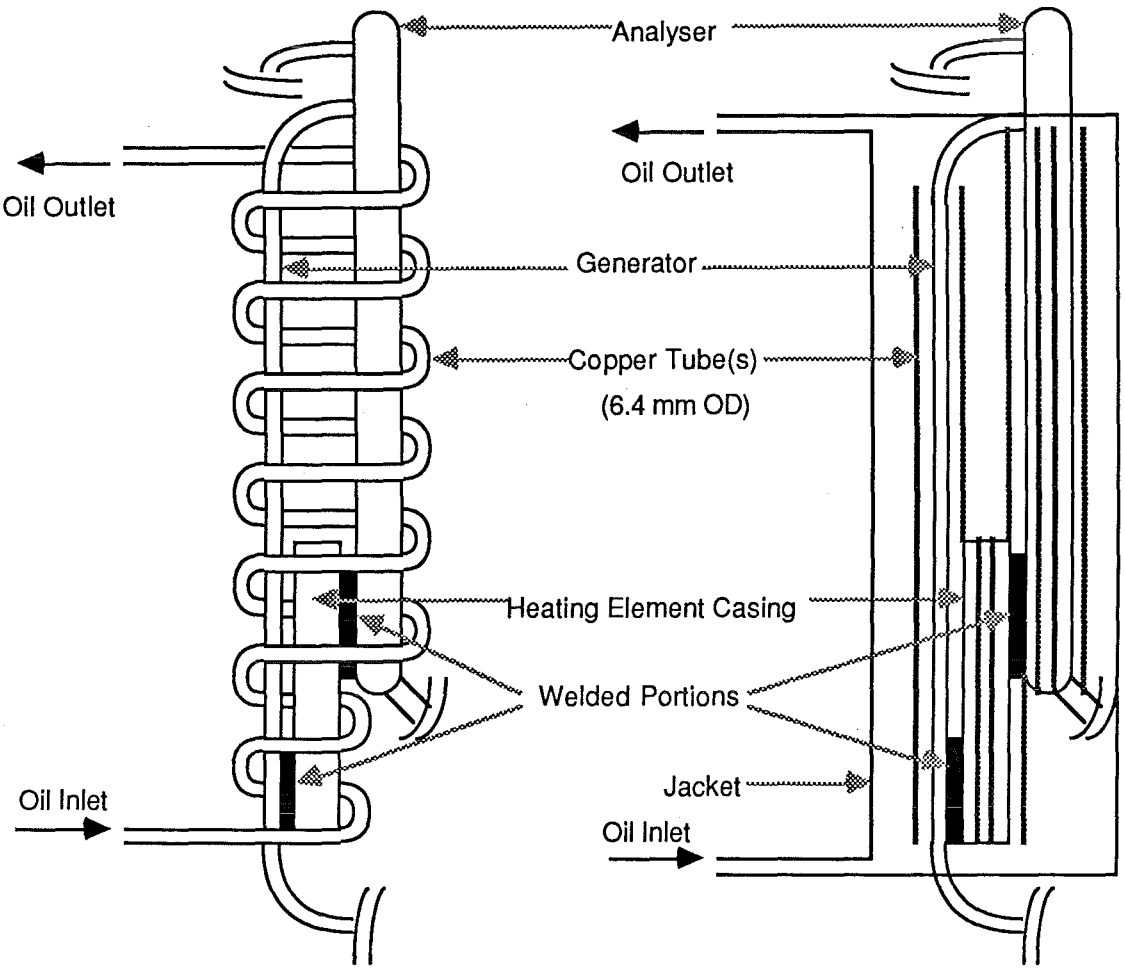

(a) Wrap Around Coil Arrangement
Scale 1:4

(b) Vertical Tube and Jacket Arrangement (Scale 1:4)

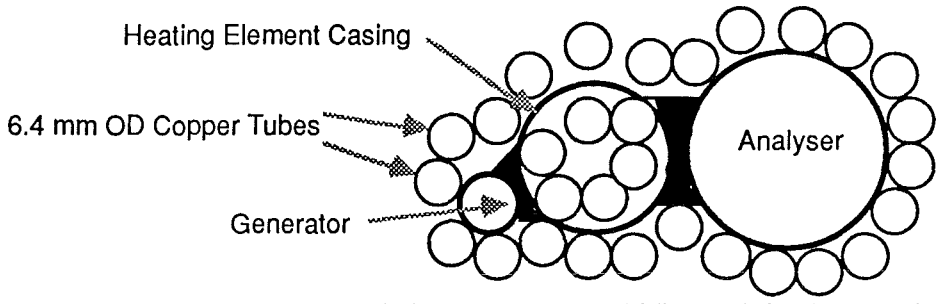

(c) Cross Sectional View of the Vertical Tube and Jacket Arrangement (Scale 1:1)

Notes: OD = Outside diameter

For better understanding please refer to Fig. 5.1

could not be cut out from the system, which left very little freedom to modify it or substitute it with extended areas like finned tubes. There were limitations imposed due to the shortage of available working space, because of the proximity of other parts of the system. There were limitations on the maximum allowable temperatures, as the system was at high pressure, and was loaded with ammonia and water, which might have decomposed if high temperature techniques such as welding were employed.

With these problems in perspective, two suitable methods of increasing the heat transfer area are shown in Fig. 5.2. One way was to wrap around the generator tube assembly a copper tubing of appropriate diameter (6.4 mm) and pump the oil through it (Fig. 5.2a). The heat transfer could be improved further by the application of heat transfer putty between the copper tubing and the generator. Another way of increasing the heat transfer area was by attaching a number of vertical copper tubes (Fig. 5.2b) with a jacket surrounding the whole assembly, through which hot oil could be pumped. Once again the heat transfer could be improved further by soldering or by the use of heat transfer putty. The heat transfer areas had been calculated for these two cases and for the bare generator tube. The bare tube area of the whole generator tube assembly including sections A, B and C (Fig. 5.1) was 0.39 m^2, the area with wrap around coil was increased to 0.2 m^2 and the area with vertical tube and jacket assembly was 0.277 m^2. However, the latter two areas needed to be multiplied with appropriate fin efficiency factors, which depend on the method of attachment. It may be observed that the area can be increased by 5 to 6 times resulting in proportionate reduction in the temperature drop.

Another major problem arised from the fact that the extended areas were calculated for the entire generator tube assembly, which included all three sections A, B and C (Fig. 5.1) but in actual situation the major portion of the heat was supplied at section A and a small fraction supplied at section B (to the analyser tube). However, section A constituted only a small fraction of the total area (about one sixth), and hence, it was decided to find out the maximum extent (of area) to which the heat can be supplied without hampering the performance of the refrigerator. In order to investigate this fact some experiments were conducted with the help of an electric heating tape (commonly

FIGURE 5.3 Schematic Diagram of the Electric Heating Tape Experimental Setup for the Generator Tube Assembly

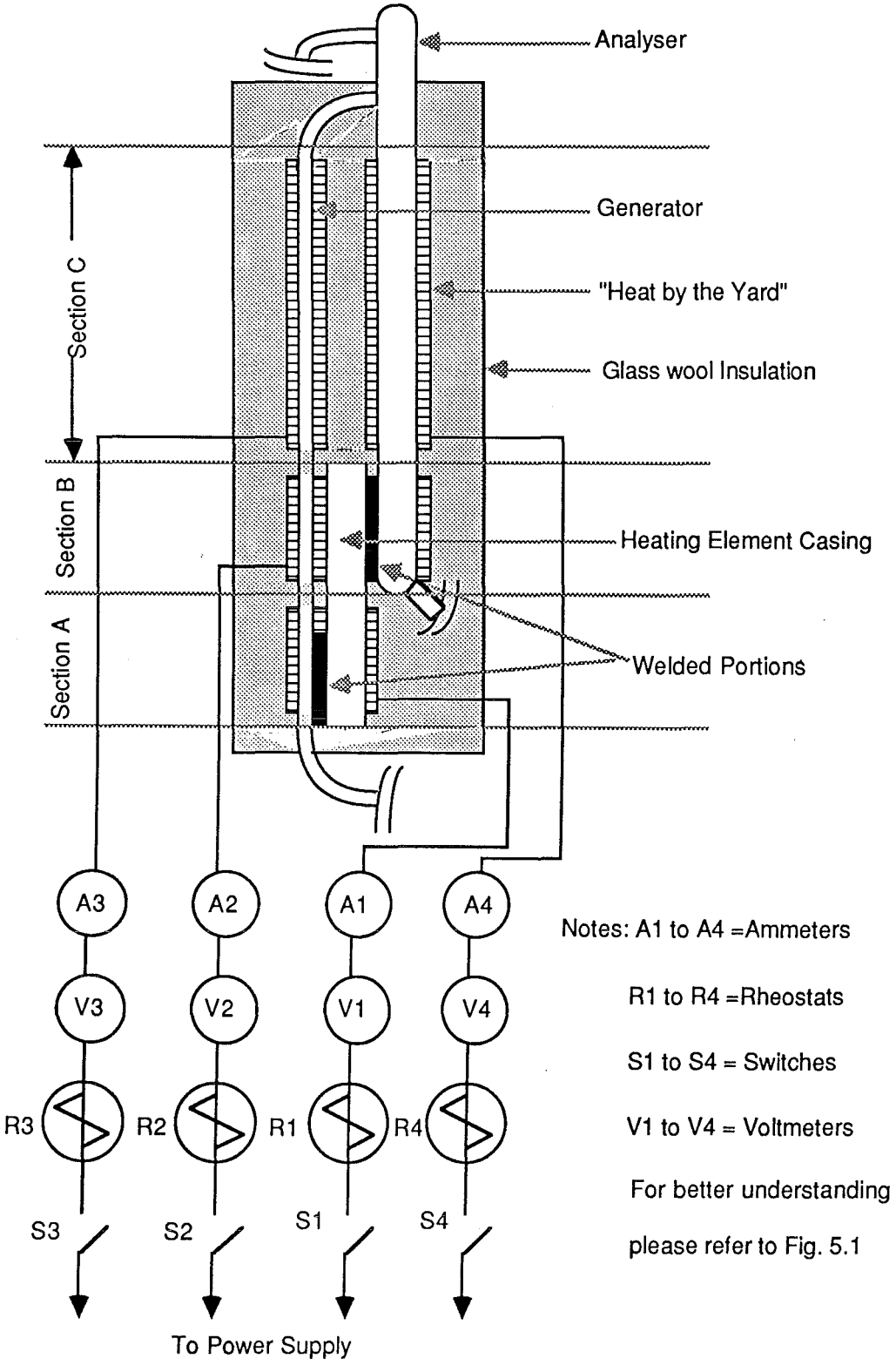

know as "heat by the yard"), which is a 25 mm wide flexible woven cloth tape embedded with resistance wire. Four pieces of such tape were wrapped around the generator tube assembly, one each in sections A and B and two in section C (one for the generator tube and one for the analyser tube separately) as shown in Fig. 5.3. Each tape was connected with a rheostat to control, and an ammeter and voltmeter, to measure the input energy. Then several experiments were conducted with different amounts of input energy to different heating tapes, ranging from 5 to 100 W. The system was allowed to come to steady state and various temperatures were noted down. It was concluded from these experiments that the major portion of the energy needs to be supplied at section A alone in order to make the refrigerator work.

5.1.2 Secondary heat pipe study

As the available area of the generator tube was not adequate to reduce the temperature drop to reasonable limit, the installation of a secondary heat pipe was suggested. The secondary heat pipe consists of a shell and tube heat exchanger connected to a jacket surrounding the generator tube, via a condensate return tube (Fig. 5.4). This arrangement in effect moves the extra area needed down to a convenient location, where there is plenty of working space. The shell and tube heat exchanger can be built of any required size. Oil can be pumped through the copper tubes of the shell and tube heat exchanger, which supplies the necessary heat to boil the secondary heat pipe fluid on shell side. The resulting vapours raise to the top of the shell, proceed upwards, condense on the generator tube, and the condensate flows back to the heat exchanger via the condensate return tube, thus completing the cycle. Inside the generator tube ammonia liquor boils, while outside the tube the secondary heat pipe working fluid condenses, and because the heat transfer coefficients connected with these two processes are very high, extra area, if needed, is small and a few fins can be incorporated inside the jacket. A small amount of energy needs to be supplied to the analyser and so a solid piece of copper can be inserted between the jacket and the analyser, with heat transfer putty, for better heat transfer.

FIGURE 5.4 Schematic Diagram of Secondary Heat Pipe

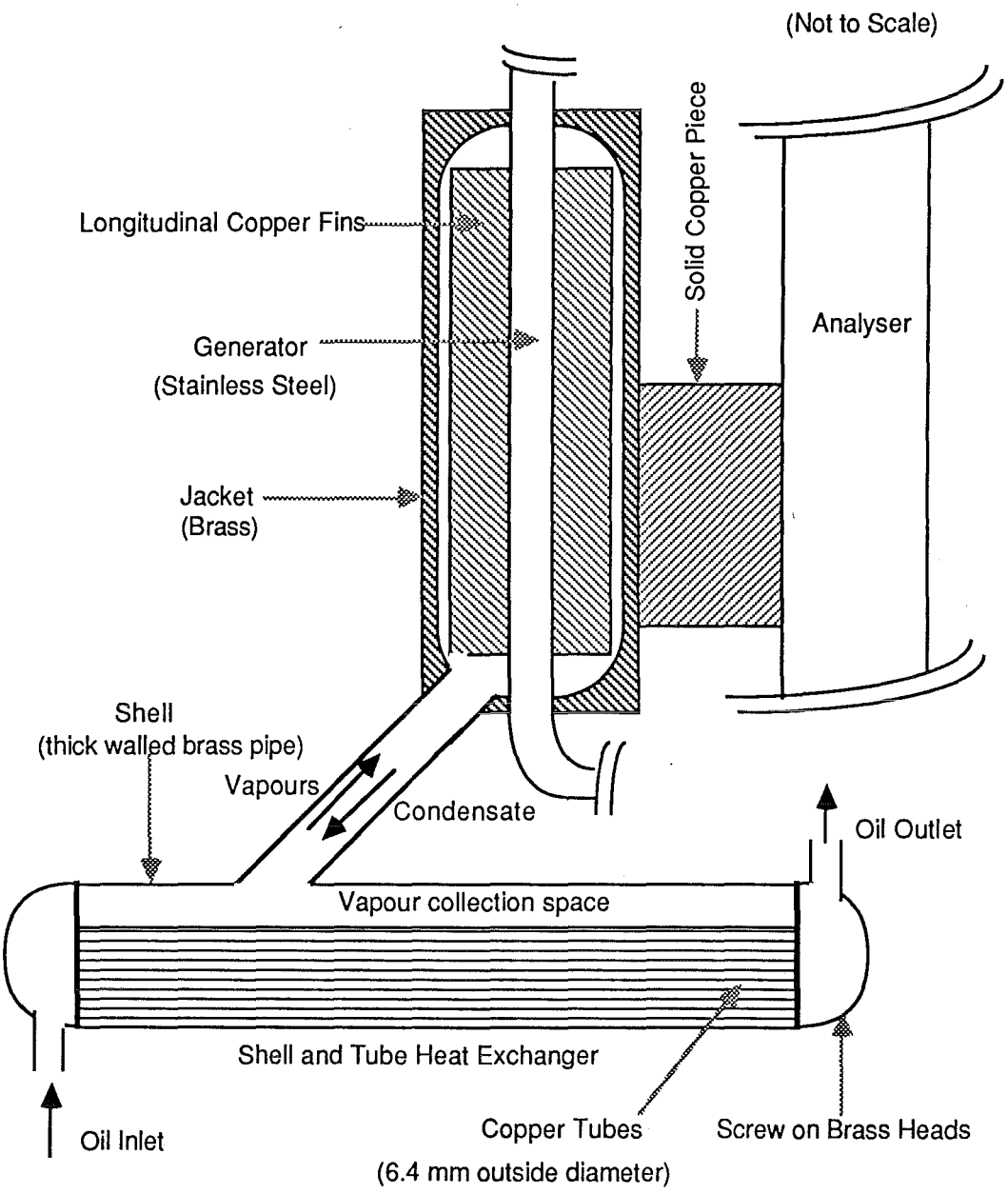

5.1.3 Selection of secondary heat pipe working fluid

The desirable properties of heat pipe working fluids have been discussed in Appendix A4. Keeping these properties in mind, the four candidates selected are: Dowtherm A, xylene, toluene and water. The important criteria for selection are discussed below.

(a) Vapour pressure

The vapour pressure of the fluid at the operating temperature should be below the safe operating pressure. The heat exchanger can be built to withstand any required working pressure, but the jacket has to be built in two sections and attached together with NZIG "Easy-Flo" (a low temperature silver brazing alloy) surrounding the generator tube, which imposes a limit on the working pressure based on the strength of the joint. In the present case the safe working pressure is approximately 700 kPa, and hence the vapour pressure should be below this limit. The vapour pressures in kPa of Dowtherm A, xylene, toluene and water at 175°C are 11, 259, 468 and 898 kPa respectively.

(b) Heat transfer characteristics

It is necessary to select a fluid which will give a high condensation film coefficient, so that the temperature drop across the condensate film is very small. The minimum overall heat transfer coefficient needed to supply 75 W, to the generator tube, with a temperature drop of 10 K, and without the addition of fins is 2200 $W.m^{-2}.K^{-1}$. It can be noticed from Kern (1954) that such overall coefficients are possible with water only. The overall heat transfer coefficient is a function of the boiling film coefficient of ammonia liquor and the condensing film coefficient of the heat pipe working fluid. The minimum value of boiling film coefficient is about 3800 $W.m^{-2}.K^{-1}$ (Kreith, 1973). Hence, the condensing film coefficient is the controlling factor (except in case of water) in the overall heat transfer. The condensation film coefficient at the generator tube can be evaluated for each of the four working fluids, at a film temperature of 175°C, a film length of 0.15 m, and net energy input of 75 W. For water it is maximum (21400 $W.m^{-2}.K^{-1}$), resulting in minimum temperature drop (1 K), and for the other three fluids it ranges from 1400 to 1500 $W.m^{-2}.K^{-1}$, with temperature drops of 15 K to 17 K.

The controlling factor for heat transfer in the shell and tube heat exchanger is the oil side film coefficient, as the

FIGURE 5.5 Fin-Jacket Arrangement for the Generator Tube

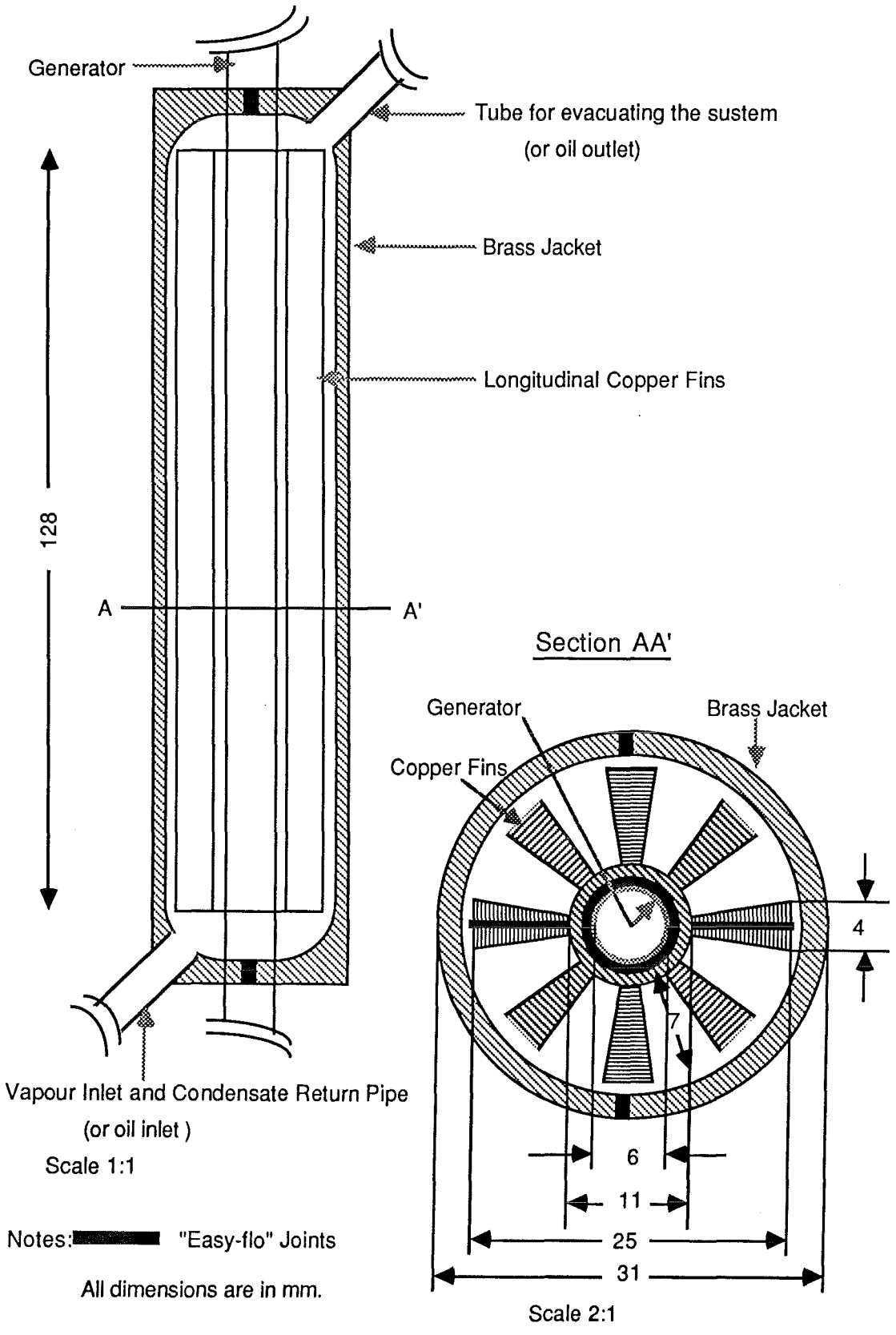

boiling film coefficient on shell side is several times larger than the oil side coefficient.

(c) Compatibility

The generator tube is made up of stainless steel and from the past experience Dowtherm A, toluene and xylene are compatable, but water results in hydrogen production at high temperatures. Also "Easy-flo" contains silver, zinc, copper and cadmium and water may attack zinc.

From the above discussion it is evident that although water has very good heat transfer characteristics, it is not compatable and it has high vapour pressure (at the working temperature of 175°C), which may exceed the safe working pressure and hence the next best candidate toluene would need to be used for the secondary heat pipe.

5.1.4 Design and construction of the jacket

The temperature drop across the condensate film for toluene was found to be 15 K, which was higher than the desirable value of about 5 K. Hence it was necessary to extend the area of heat transfer of the generator tube. However, the methods described in the previous section to extend the areas were not suitable for heat pipes. Longitudinal fins were very suitable in this case, as they facilitate easy flow of toluene vapours and condensate return. Welding of fins on to the generator surface was too dangerous to use, because of the high temperatures involved, which might decompose the inside fluids or damage the generator tube. Hence, "Easy-flo" containing 50% silver was preferred with much lower application temperatures as compared to welding. On the other hand it was possible to get different grades of "Easy-flo" with different melting points, so that the one with higher melting point could be used frist to attach the fins and then the one with lower melting point to attach the jacket. A solid copper cylinder was cut into two semi cylindrical pieces and exact fitting fins were cut out from each of them. Three full fins and two half fins (Fig. 5.5) were milled from each semicylindrical piece, which could then be attached on to the generator tube. The fins were thicker at the ends as compared to the bottom portions as they were easier to mill.

The jacket was made out of two semicylindrical brass pieces. These were also milled into the required shape (Fig. 5.5), to

enclose the fins. The clearance between the fins and jacket was very small which would need precise milling. The inner edges of the jacket were curved to facilitate easy flow of condensate and avoid any hold up of liquid. A copper tube (9.5 mm outside diameter) was connected to the bottom of the jacket for the vapour flow upwards and condensate flow downwards. A smaller diameter tube (3.2 mm) was connected to the top of the jacket for evacuating the secondary heat pipe before charging it with the working fluid.

The Plate 5 shows the three stages in fabricating the jacket. The generator tube assembly after the removal of the electric heating element is shown in Plate 5a. The generator tube fixed with the copper fins is shown in Plate 5b, and Plate 5c shows the same after fixing the external jacket.

It was necessary to lie down the refrigerator in order to work on the generator tube. Also this would drain the liquid to other parts of the refrigerator so that the heat applied is not dissipated quickly by the liquid. The Electrolux refrigerators are dependent on gravity flows within the system, and hence before the work was started on the generator tube the refrigerator was tilted on to its side, left it in that position for some time, heat applied to the generator tube before tilting back to the upright position and checking that it still worked. Then the heating element tube was cut off from the generator tube, copper fins were attached first and then the brass jacket. A solid piece of copper inserted between the jacket and analyser as shown in Fig. 5.4.

5.1.5 Shell and tube heat exchanger

The next important part of the secondary heat pipe was the design of the shell and tube heat exchanger. It was found that 42 copper tubes (each of 0.3 m long and 6.4 mm outside diameter) and a brass shell (0.1 m insude diameter), with screw on ends were required. In an attempt to buy a shell and tube heat exchanger off the shelf, "Savage" heat exchanger was tested for this purpose and an experiment was conducted with the actual fluids (toluene and Mobiltherm) to estimate the practical overall heat transfer coefficient. However, the secondary heat pipe idea was discarded, as discussed in the following section.

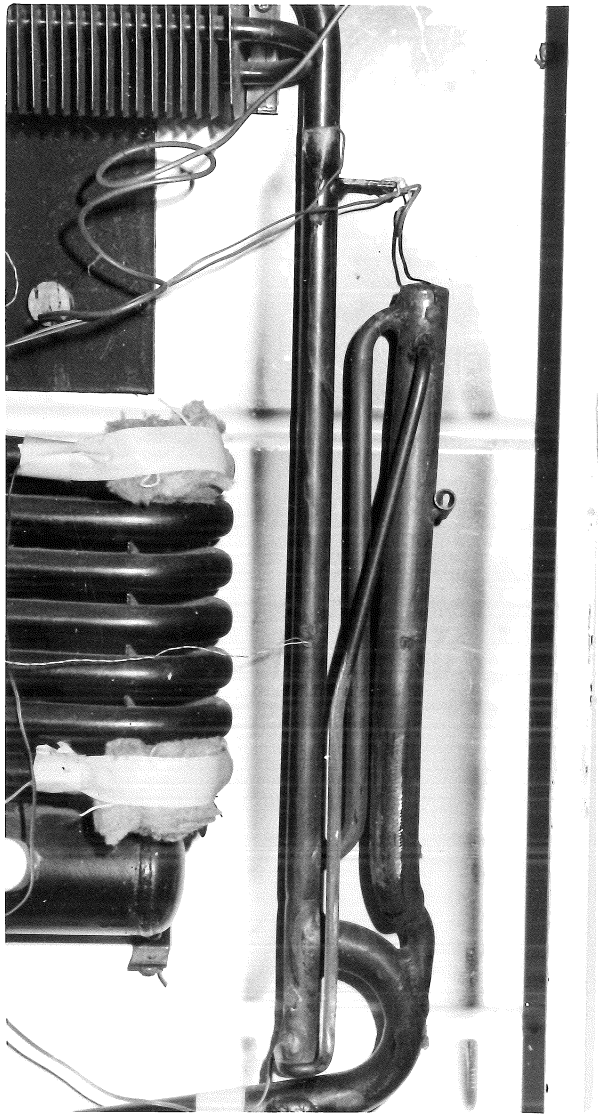

(a) Electric Element Removed

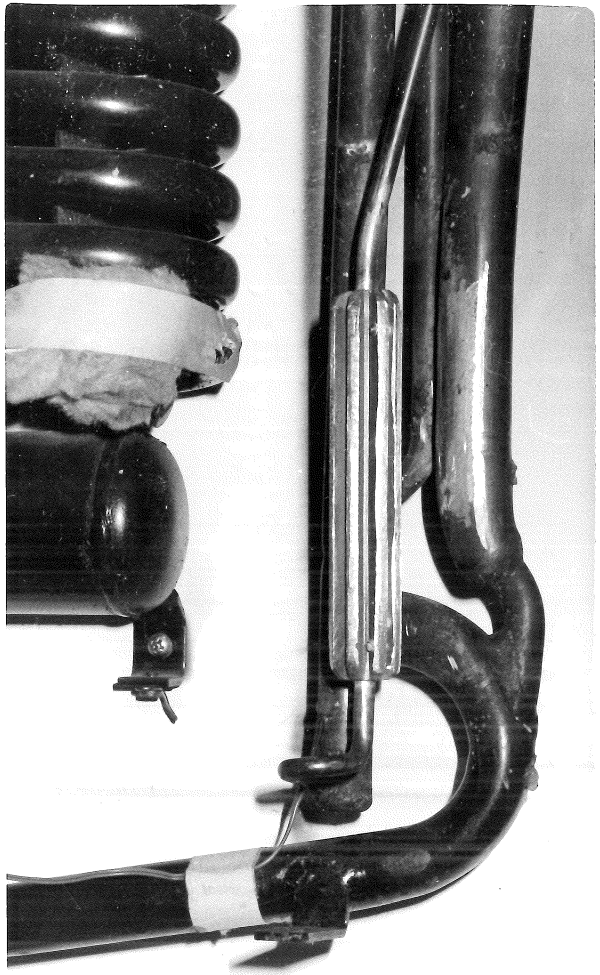

(b) Copper Fins Fitted

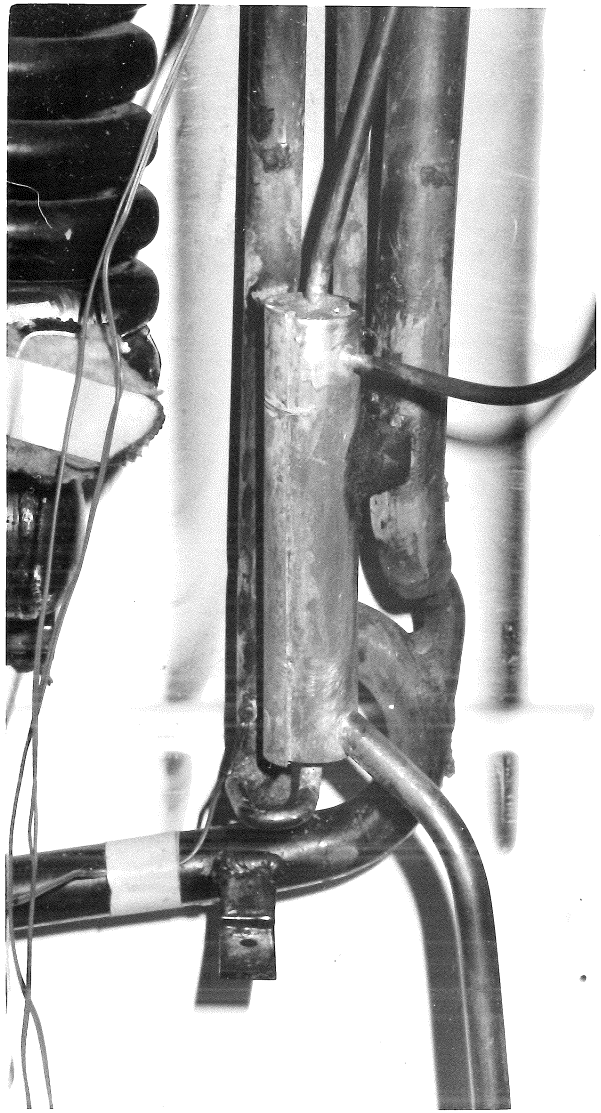

(c) Jacket Fitted

PLATE 5 Generator Tube Assembly

5.1.6 Conclusions

The introduction of a secondary heat pipe changes the path of the energy flow, so that the extra area necessary can be provided at a convenient location. It is still necessary to supply the required amount of energy to the generator tube, in fact even more to account for the extra heat losses, which would also increase the temperature drop of the oil. Moreover there are certain other complications involved with the introduction of a secondary heat pipe such as the evacuation and the charging of the heat pipe. Hence at this stage a second thought was given about the installation of the secondary heat pipe.

It is possible to eliminate the secondary heat pipe, if the oil pumped through the jacket, can provide the required numbers of watts to the generator. The calculations needed to verify this fact are given in Appendix A2.3. Once again, in this case, the oil side film coefficient is the controlling factor in heat transfer. At an oil flow rate of 3 $kg.hr^{-1}$ (which would give the necessary temperature rise of oil while passing through the collector) oil side coefficient is 265 $W.m^{-2}.K^{-1}$. The finned jacket provides a heat transfer area of 0.02 m^2 and because the overall heat transfer coefficient is nearly equal to the oil side coefficient, this results in a temperature drop across the oil film of 14 K. It is possible to bring down the temperature drop by increasing the oil flow rate. For example, by increasing the oil flow rate to 8.5 $kg.hr^{-1}$, the oil side coefficient rises to 375 $W.m^{-2}.K^{-1}$ and the corresponding temperature drop comes down to 10 K. With the present set up it is possible to get oil flow rates up to 60 $kg.hr^{-1}$. A buffer tank (or oil storage tank) is necessary between the collector and the refrigerator in the final set up in order to even out the fluctuations in solar energy collection and to add auxiliary energy. Hence this change in flow rate should not affect the collector performance. Because of the above reasons and because of the extra work involved with the secondary heat pipe it was decided to verify the performance of the refrigerator with oil passing through the jacket.

5.2 Experiments with Refrigerator ER2 Operating on Hot Oil

After fitting the finned jacket to the generator tube of the refrigerator ER2, the experiments were conducted at different inlet oil temperatures to check its performance.In order to test the performance of the refrigerator ER2 with hot oil at different

FIGURE 5.6 Schematic Diagram of the Experimental Setup to Find Out the Performance of ER2 Running with Oil

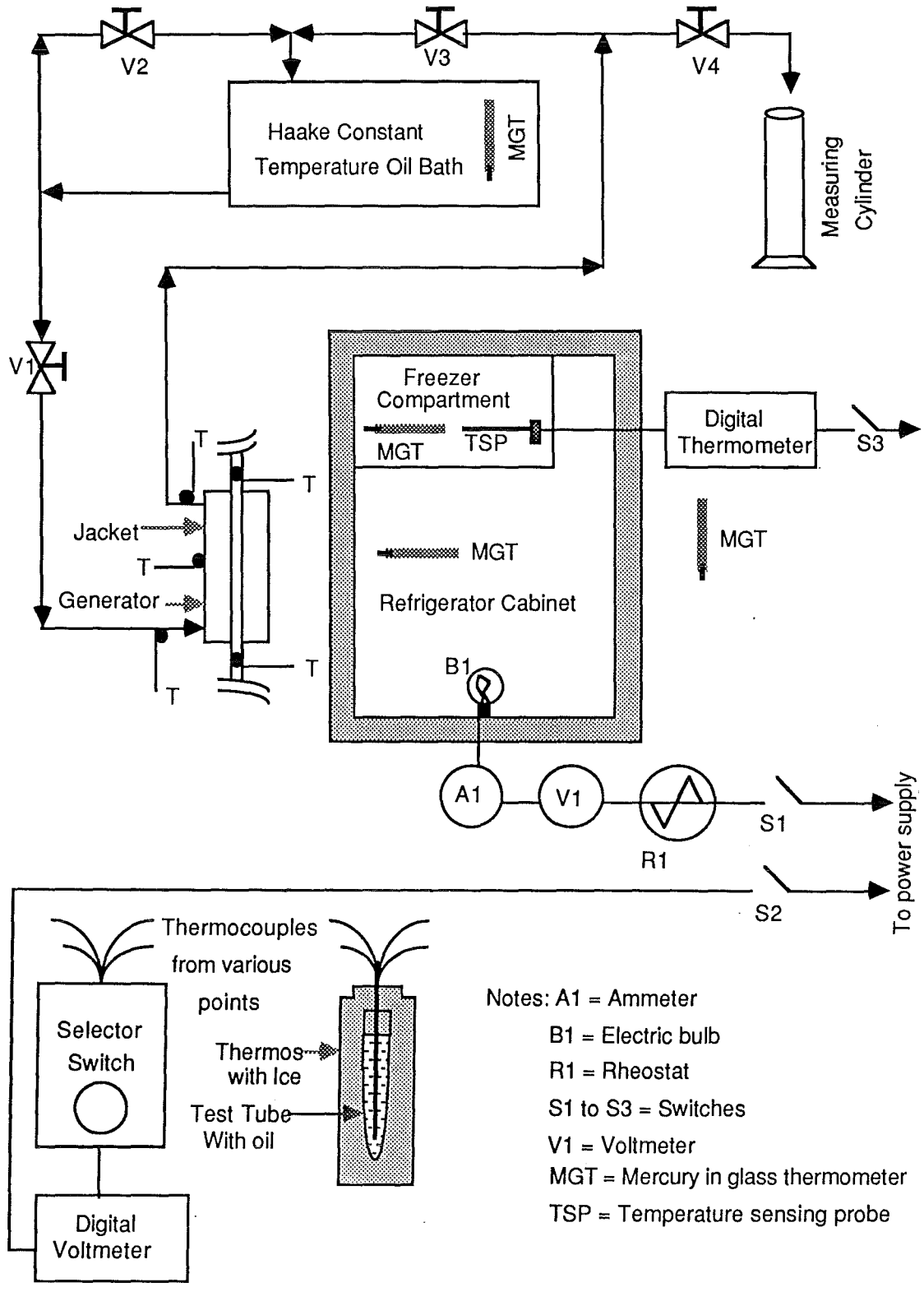

temperatures it was necesary to have a constant temperature oil bath which could provide oil at any required temperature. For this purpose the Haake bath was employed, the details of which are given in Section 4.9.

5.2.1 Description of the experimental setup

The schematic diagram of the experimental setup to determine the performance of ER2 working on oil, is shown in Fig. 5.6. The constant temperature bath provided oil at any set temperature. The flow rate of oil was controlled by valves V1 and V2, while it was measured by diverting the oil through valves V3 and V4 to a measuring cylinder. All parts were well insulated with glass wool. The copper-constantan thermocouples shown in Fig. 3.24 were left intact except the ones on the generator tube and the heating element casing. Additional thermocouples were attached to the jacket, oil inlet and outlet tubes, and both ends of the generator tube (Fig. 5.6). A digital voltmeter was used to measure the temperatures indicated by the thermocouples. Mercury-in-glass thermometers were used to measure the tank oil, freezer, cabinet and ambient temperatures.

5.2.2 Experimental procedure

After the oil in the tank reached a specified temperature, it was pumped through the jacket. The system was left for at least 12 hours to come to steady state. Then all the temperature readings and oil flow rate were measured hourly, during the day, and the average readings were used in calculations.

Problems were encountered while starting up of the refrigerator. This was alleged to be common with Electrolux refrigerators after they have been shifted around and left unused for long periods of time (a few weeks). Chari (1958) and Fraser (1970) mentioned such problems with Electrolux refrigerators. It was found that shutting off the system and restarting, or increasing the oil temperature helped in this process.

5.2.3 Results and discussions

The heat loss characteristics of the refrigerator ER2 had already been evaluated (as described in section 3.4). So by knowing the cabinet and ambient temperatures the heat leak into the refrigerator cabinet (Q_l) was evaluated. By knowing the mass

Table 5.1 Summary of the Results of the Experiments with ER2 Working on Hot Oil

T_{oi}	T_{amb}	T_{cab}	T_{fzr}	ΔT	U_o	Q_l	ΔT_o	Q_o	COP = Q_l/Q_o
°C	°C	°C	°C	K	$W.m^{-2}.K^{-1}$	W	°C	W	
193	14.5	-11.5	-25	26	0.675	25.3	1.8	63.7	0.400±0.036
182	14	-10	-24	24	0.646	22.4	1.5	53	0.423±0.041
172	13	-11	-23.5	24	0.646	22.4	1.3	46	0.487±0.045
163	10.5	-9	-22	19.5	0.640	18.0	1.2	42	0.429±0.042
154	11	-4.5	-19.5	15.5	0.545	12.2	0.8	28	0.436±0.043
144	13.5	2.5	-8.5	11	0.53	8.4	0.5	18	0.466±0.044

Notes: T_{oi} = Oil inlet temperature
T_{amb} = Ambient temperature
T_{cab} = Refrigerator cabinet temperature
T_{fzr} = Freezer temperature
ΔT = Temperature drop $T_{amb}-T_{cab}$
U_o = Overall heat transfer coefficient between the refrigerator cabinet and the ambient
Q_l = Heat leak into the cabinet
ΔT_o = Oil temperature drop
Q_o = Heat supplied by the oil

flow rate of oil and the temperature drop of the oil across the jacket of the generator tube, the heat supplied to the generator tube (Q_g) was determined. The real COP (Q_l/Q_g) was then evaluated.

Important results are summarised in Table 5.1. It is evident from the table that the real COP reaches a peak value of about 0.49 at an oil inlet temperature of about 172°C. It is comparable to the results obtained with electric heating (Fig. 3.26) but the real COP values with oil are slightly higher. This is mainly because of the lower ambient temperature of about 13°C as compared 26°C with electric heating. Another important observation is that the heat source temperature is considerably reduced. It can be noticed that oil supply temperature of 145°C and supply energy of 18 W seem to be sufficient (but, bearing in mind the low ambient temperature) to run the refrigerator with satisfactory performance. This could have resulted due to the improved method of energy supply to the generator tube. Previously the energy was supplied with a very high temperature heat source (resulting in higher heat losses) and through a very small area. But now the heat is supplied at a lower temperature through a much larger area. Moreover one should bear in mind that Electrolux refrigerators are very sensitive to the locations (area) of energy supply and the energy flux distribution within that particular area.

5.3 Linking the Solar Collection System to the refrigerator ER2

It has been found that the Electrolux refrigerator works from the hot oil at the specified temperature, which can be produced by the solar collector. Hence the next step towards achieving solar refrigeration is to link the solar collector with the refrigerator via an energy storage system which is needed due to the intermittent nature of solar energy. The energy storage options are discussed later in this chapter.

The energy storage unit (when it is hot storage) can also be used as the point where auxiliary heating, if necessary, is introduced into the system. In the present case, the oil tank serves as a storage unit. Although the energy requirements of the refrigerator alone are well within the limits of the supply capacity of a single collector, when the heat losses from the interconnecting piping and the storage tank are included, a single

FIGURE 5.7 Heat Loss Calculation Modes

(a) Mode A Tank only (T)

Oil is circulated through the small closed loop by the Haake submerged pump. The losses are from the tank and the small closed loop.

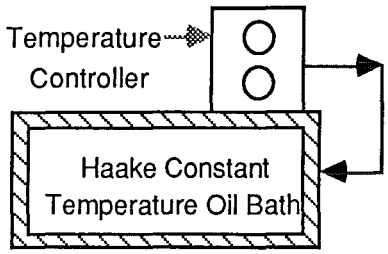

(b) Mode B Tank and refrigerator piping (T + Rp)

Oil is circulated through the piping connected with the refrigerator, but not including the oil jacket.

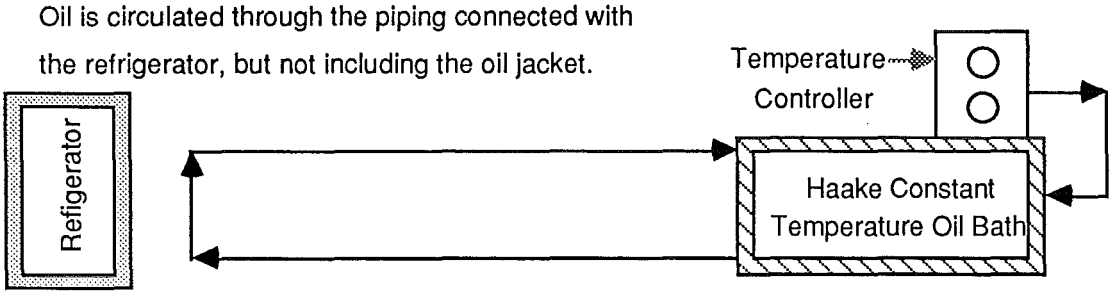

(c) Mode C Tank, refrigerator piping and collector (covered) piping (T + Rp + Cp + Cc)

Oil is circulated through the covered collector and refrigerator piping without including the jacket.

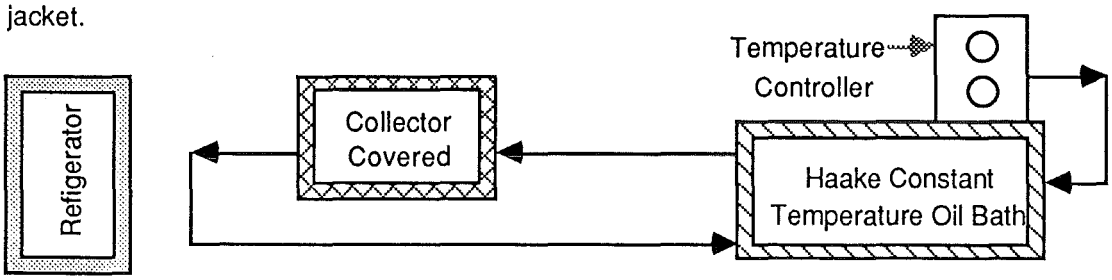

(d) Mode D Night time operation without solar input (T + Rp + R)

Oil is circulated through the jacket, but without including the collector.

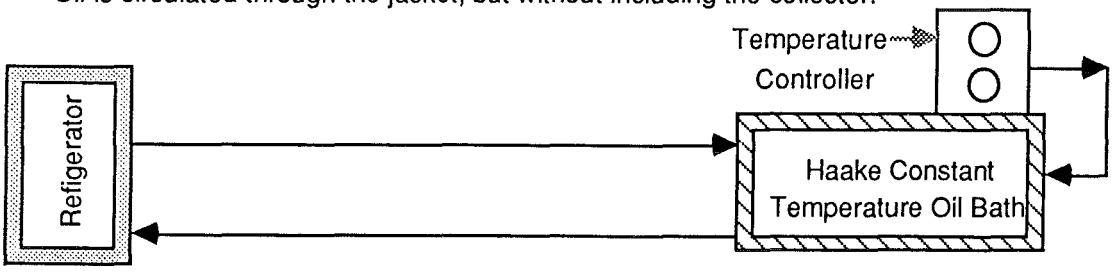

(e) Mode E Day time operation with solar input (T + Rp + Cp + R)

Oil is circulated through the jacket with solar input

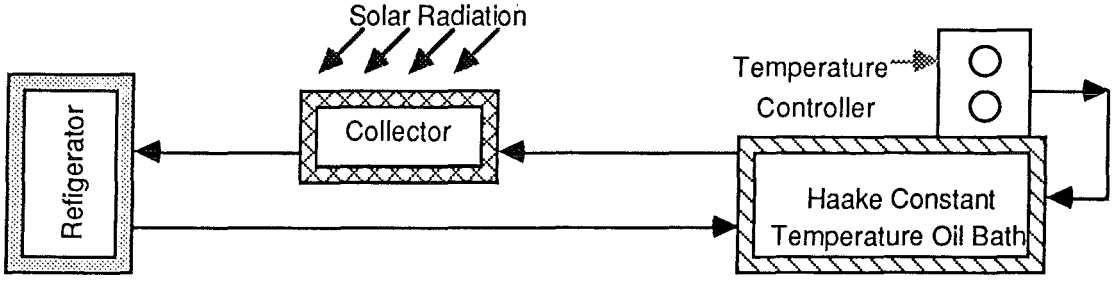

collecor cannot cope with the energy demands of the entire experimental system. In order to evaluate the solar component of the input energy into the system, the heat losses from each component of the system (such as the tank and inter connecting piping with the refrigerator and the solar collector) should be known first. Hence, the system was built in such a way that it was possible to operate it under different modes. The five modes of operation Mode A to Mode E are shown in Fig. 5.7. Each mode included only certain parts of the experimental setup. The heat loss calculation Modes A,B and C were necessary to evaluate the heat losses from the tank (T), the piping connected with the refrigerator (R_p) for night operation (or without solar input), the piping connected with the collector (C_p) and the losses from the covered collector (C_c). The Modes D and E were required for night time (without solar input) and day time (with solar input) operations of the refrigerator (R), to evaluate the solar fraction of the input energy into the oil.

5.3.1 Description of the experimental setup

The schematic diagram of the experimental set up is shown in Fig. 5.8. The constant temperature bath provided oil at any required temperature. The bath pump was not capable of providing the necessary oil flow rates and hence an external centrifugal pump was used for the circulation of the oil. As the stirrer and bath pump were operated from the same switch, and the stirrer was necesssary for proper mixing of the oil, the outlet from the pump was short circuited to the oil tank. The connecting piping and the valves V1 to V11 were arranged in such a way that the system could be operated in any of the five modes as illustrated in Fig. 5.7. Apart from the thermocouples attached to the collector and the refrigerator, several others were incorporated at different points (Fig. 5.8). The thermocouples were connected to a digital voltmeter. A digital thermometer and mercury-in-glass thermometers were used for measuring the ambient, refrigerator cabinet and freezer temperatures. A chart recorder was connected to the solarimeter to record insolation. A kilowatt-hour meter was used to measure the power input to the auxiliary heating element. The oil flow rate was controlled either by changing the power input to the pump via the variac R1, or, by controlling the flow through the recycle line via the valve V3. Provisions were made for measuring

FIGURE 5.8 Schematic Diagram of the Experimental Setup for Linking the Solar Collector with the Electrolux Refrigerator

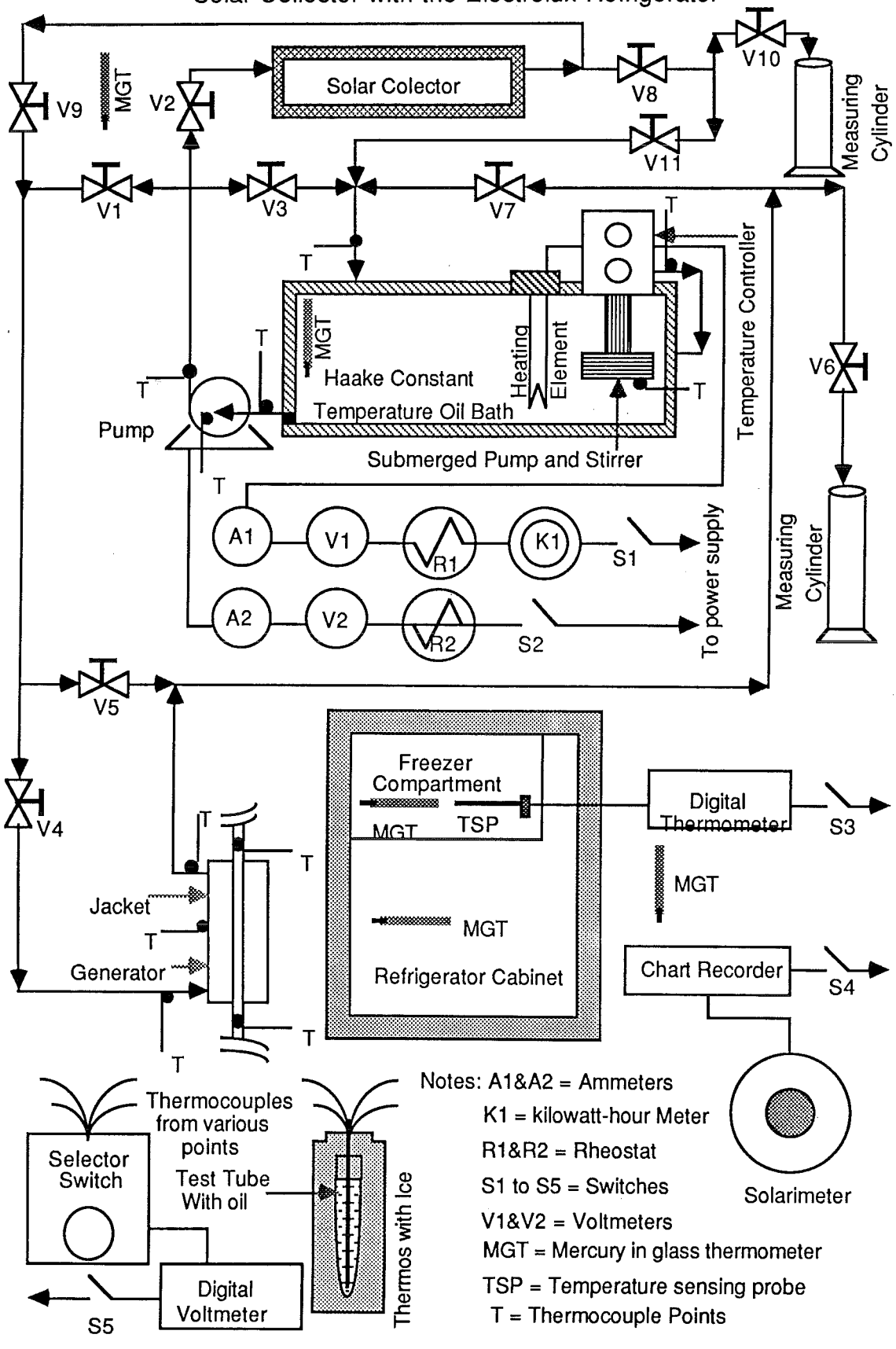

TABLE 5.2 Heat Losses Under Modes A, B & C

Tank Oil Temperature = 160°C and Ambient Temperature = 20°C

Component	Auxiliary Power Input in Watts Under		
	Mode A T	Mode B T + R_p	Mode C T+R_p+C_p+C_c
Length of connected piping			
(a) Actual	Nil	3 m	8 m
(b) Fictitious	Nil	5.5 m	13 m
(1) Without any insulation			
(a) Actual	324	632	1371
(b) Calculated	345	665	1445
(2) With 25 mm insulation			
(a) Actual total	128	222	460
(b) Actual piping&collector	-	222-128=94	460-128=332
(c) Calculated Piping only at 19 $W.m^{-1}$	-	5.5x19=104.5	13x19=247
(d) Approx.collector(covered)	-	-	332-247=85
(3) With 50 mm insulation			
(a) Actual total	67	148	347
(b) Actual piping&collector	-	148-67=81	347-67=280
Check: ΔT across the tank		1.4 K	5.2 K
Oil flow rate $m_o x10^6$		3.24 $m^{-3}.s^{-1}$	2.84 $m^{-3}.s^{-1}$
$Q = m_o\ c_{po}\ \Delta T$		88	287
(c) Calculated Piping only at 15.3 $W.m^{-1}$	-	5.5x15.3=84	13x15.3=199
(d) Approx.collector(covered)	-	-	280-199=81
Check: ΔT across collector			1.5 K
Oil flow rate $m_o x10^6$			2.84 $m^{-3}.s^{-1}$
$Q = m_o\ c_{po}\ \Delta T$			82.8

Notes: T = Tank only; R_p = Piping connectd with the refrigerator; and C_p = Piping connected with the collector; C_c = Covered collector; Q = Net heat transferred; m_o = Oil mass flow rate; cp_o = Specific heat capacity of oil; ΔT = Temperature difference.

the flow rate of oil in different modes by manipulating appropriate valves. Initially, 25 mm thick glass wool insulation was provided for all the pipe work and the tank. This was later increased to 50 mm, to lower the heat losses further. Aluminium foil was wrapped outside the insulation to reduce the radiation losses.

5.3.2 Experiments conducted

Five sets of experiments were conducted under five different modes of operation by manipulating the necessary valves. Under each mode, the system was allowed to come to steady state by maintaining the same conditions for at least 16 hours. Then hourly readings of various temperatures, oil flow rates and kilowatt-hour meter readings were noted for the day. The average readings were used in the calculations. The heat loss calculation modes were repeated for the system without any insulation, with 25 mm thick insulation and with 50 mm thick insulation, while the modes D and E were carried out only with 50 mm thick insulation.

5.3.3 Calculations and results

As the individual performances of the collector and the refrigerator have already been studied in detail, the main focus now is on the energy consumption under different modes of operation of the system. The power needed (or more precisely the power supplied to the auxiliary heating element) to maintain the oil in the tank at a given temperature (in this case 160°C) under different heat loss modes A, B & C is shown in Table 5.2 and the calculations for modes D & E are given in Table 5.3.

The power supplied to the auxiliary heating element was obtained by subtracting the power consumed by the bath pump and the stirrer (54 W) from the total power supplied to the tank (as indicated by the kilowatt-hour meter), because bath pump and the stirrer were in operation during all the experiments. The power consumed by the bath pump and stirrer was measered from the kilowatt-hour meter, while the auxiliary heating element was off. The energy input back into the oil due to the bath pump was found to be minimal, because small electric motors have low efficiencies. Similarly, the temperature rise of the oil, due to the external pump was also small. The power consumption of the external pump was found to be 20 W to 50 W as the supply voltage

TABLE 5.3 Calculations for Modes D and E

Power consumed in Mode D (without solar input and including T, R_p and R) at a freezer temperature of -14°C and cabinet temperature of 2°C	= 199 W
Power consumed in Mode B (including T and R_p, from Table 5.2)	= 148 W
The power input to the refrigerator (R)	= 199 - 148 = 51 W
Power consumed in Mode C (includes T, R_p, C_p, C_c, from Table 5.2)	= 347 W
Hence the total power needed to operate the experimental refrigeration system without solar input (includes T, R_p, C_p, C_c, R)	= 347 + 51 = 398 W
Power consumed in Mode E (With solar input Q_{solar} and includes T, R_p, C_p and R	= 227 W
Therefore, the sum of Q_{solar} and C_c	= 398 - 227 =171 W
Q_{solar} at an oil flow rate of 1.4×10^{-6} $m^3.s^{-1}$ and ΔT of 3.5 K	= 96.6 W
Hence, the losses from the covered collector	= 171 - 96.6 = 74.4 W

was increased from 150 V to 230 V respectively. The supply voltage to the external pump was different under different modes, which ranged from 160 V to 190 V depending on the resistance to flow.

As the air was almost stagnant inside the shed, the convective coefficient from the tank was taken to be 5 W/m^2K (Eq. A10.18). The theoretical heat losses per unit length of the pipe (Q_l), from the connecting pipes (neglecting the resistance offered by the oil film and the tube wall) was found using the following expression (Kern, 1954).

$$Q_l = \frac{\pi\ (T_{oa} - T_{amb})}{(1/2k_i)\ \{\ln(D_{oi}/D_{ii})\} + (1/h_{cr}D_{oi})} \qquad (5.1)$$

where T_{oa} and T_{amb} are the average oil and ambient temperatures respectively; k_i is the thermal conductivity of the insulation; D_{ii} and D_{oi} are the inside and ouside diameters of the insulation respectively; h_{cr} is the combined heat transfer coefficient due to convection and radiation as obtained from Kern (1954) for a particular outside diameter and temperature difference (T_{osi}-T_{amb}); T_{osi} is the outside surface temperature of the insulation, which was initially assumed and by iterative process converged.

In order to find out the total losses Q_l should be multiplied by the length of the piping. However, several fittings and valves of much larger diameter than the actual piping (6.4 mm outside diameter) were used. Hence, a fictitious length of piping was estimated which would give the same surface area as the existing piping, fittings and valves all together.

5.3.4 Discussions and conclusions

The final step in achieving solar refrigeration in this project involved combining the solar collector with the Electrolux refrigerator via a buffer tank to even out the fluctuations in the energy supply and add the required auxiliary power. Experiments were conducted in five different modes in order to break down the heat losses and, to evaluate the fraction of solar energy supplied, so that recommendations could be made for further experimentation, towards achieving solar refrigeration without any auxiliary source of energy.

It is evident from Table 5.2 that by increasing the thickness of the insulation from 25 mm to 50 mm the heat losses from various

parts of the system were reduced by about 30%. Heat losses should be minimised not only from the tank and the connecting piping, but also from various fittings such as valves and the pump. The break down of heat losses from different parts of the system (for 50 mm thickness insulation) are summarised below.

The heat losses from

- the tank (T) = 67 W
- the piping connected with the refrigerator alone (R_p)= 81 W
- the piping connected with the collector alone (C_p) = 118 W
- the total piping (R_p + C_p) = 81+118 = 199 W

It is also evident from Table 5.2 that the theoretical estimates of the losses were in close approximation to the measured values. The heat losses were also cross checked by measuring the temperature drop of the oil between the inlet and the outlet oil connections from the tank, and they were also found in good agreement with the losses measured from the kilowatt-hour meter.

In order to make the solar refrigeration system entirely dependent on solar energy, (except for the circulation pump), the solar collector needs to supply not only the power required to run the refrigerator (51 W), but also the losses from the tank (67 W) and the connecting piping (199 W). The covered collector losses are not accounted for, in these calculations because they are included while evaluating the solar input power into the system. Although the refrigerator power requirements (51 W) are well within the capabilities of a single solar collector (as net solar input is 97 W on a reasonably good day), the heat losses from the other parts of the system dominate the picture, as they constitute about 84% of the total power requirements. Hence, significant reductions need to be achieved in the heat losses from the system and they are discussed in the next chapter. If the present system is to rely completely on solar energy, (other than the pump) about four collectors of similar size to the present one are needed on a sunny day. However, the number of collectors or the total collector area should be determined on the basis of several factors of which the important ones are:

(1) the place or location which would determine the insolation and the number of sunshine hours available in a day and in a year,

(2) the storage type, capacity and efficiency,

(3) the operating temperature of the collector (as it determines the efficiency of the collector) which would depend on the heat losses from the entire system and

(4) the reliability with which cooling should be achieved.

All these factors are self explanatory or explained earlier, except for the storage of the thermal energy.

Solar energy storage

Solar energy is a time dependent energy resource and so, for a continuous supply of energy, storage is essential. Solar energy storage must be considered in the light of the entire solar system. There are three main types of thermal storage systems (Boer, 1976).

(1) Sensible heat storage: In this most common type, solar energy is stored as "sensible heat" of the material. A number of materials can be used depending mainly upon the temperatuer of storage. For low temperatures (of less than 100°C) water and rock pebbles are widely used, and for high temperatures petroleum oils, oxides of aluminium, magnesium and silica are used.

(2) Latent heat storage: In this type, energy is stored in the form of "latent heat of fusion". Materials that undergo a change of phase in a suitable temperature range are used. Salt hydrates, eutectic mixtures of various salts and pure metals are employed for energy storage at low, intermediate and high temperatures respectively. Weight and volume of storage material are very much less as compared to the sensible heat storage.

(3) Thermochemical storage: In this type of storage, several reversible chemical reactions are exploited. The temperature of storage is once again taken as the criterion for choosing a particular reaction. A number of oxides are employed in this type of storage.

It is hard to give general guidelines for the selection of a particular type of storage system as it can only be decided after considering all other parts of the specific application. For example, in the present case, the most convenient method would be to store solar energy as "hot oil", which is used as the working fluid in the system.

However, in the case of refrigeration and air conditioning applications, it is possible to store solar energy below ambient temperatures by cooling a tank of water or other storage medium,

during operational hours. The main advantage of this approach is the temperature difference and subsequently lower heat transfer between cold storage and ambient as compared to the temperature difference between hot storage and ambient. As a result less cooling effect is lost from cold storage than from hot storage. As night time temperatures are generally lower than day time temperatures, the losses from hot storage are more as compared to cold storage. Moreover, cold storage is preferable to hot storage because losses from cold storage are not losses in the real sense, if the cold storage is situated inside the cabinet or the cooled space. However, the storage volume needs to be accommodated within refrigerator (or cooled space), or in other words refrigerator has to be oversized. In addition, 1 KJ of cold storage is 1 KJ of cooling; 1KJ of hot storage is equivalent to less than 1KJ of cooling due to the heat losses and COP of less than one. This would result in larger storage volumes in the case of hot storage, resulting in higher heat losses. Hence, in the present case cold storage has been suggested.

The most convenient way to have the cold storage is to convert water into ice during sunshine hours and store the ice inside the refrigerator, which can absorb heat from the surrounding space during night time. The latent heat of fusion of ice is 333 $kJ.kg^{-1}$, hence one kg of ice is sufficient to extract 333 kJ of energy. At a rate of 22 W heat flow, over a period of 24 hours the heat leak into the refrigerator amounts to only 1900 kJ, which can be absorbed by six kg of ice. As latent heat storage is used the storage volume is very less (about six litres). Water being the cheapest storage material, the extra costs involved are also less.

CHAPTER 6

SUGGESTIONS FOR FUTURE WORK

The present work demonstrated beyond doubt the possibility of achieving a solar refrigeration system involving an Electrolux refrigerator, which can be operated completely from solar energy and a non-tracking collector. From this point one can proceed in several directions towards making a commercial unit. The areas of improvement in the present system can be studied under two categories:

(1) improvements without involving radical changes in the present system and

(2) improvements with radical changes in the present system.

Let us first consider simpler modifications in the existing system and then go into more radical changes.

6.1 System Heat Losses

Of the total power requirements of the system, (except for the pump) only 16% goes to run the refrigerator while the rest is lost to the surroundings. It is possible to reduce the heat losses considerably. As the refrigeration system and the solar collector system have been fully studied, the extra piping and several valves can be eliminated. Crampton (1985) worked on the same system and managed to bring down the piping heat losses from 199 W to 116 W (by reducing the length of piping by 57%), and tank heat losses from 67 W to 53 W (by reducing the tank surface area by 43%), and also suggested that further reductions are possible by improving the insulation. Thus, the total heat losses were reduced by 37%.

6.2 Condenser Heat Transfer Fluid

Mobiltherm 603 was used as heat transfer fluid. At elevated temperatures, on frequent exposure to air, this oil becomes oxidised and forms carbon deposits on the auxiliary heating element. It was observed that the carbon deposits hampered the flow and reduced the heat transfer efficiency. To prevent the oil deposition, thought to have been the result of very high heat transfer rates over small surface areas, Crampton (1985) increased the surface area of the heating element by 78%, but still could

FIGURE 6.1 Improved Dimple Pattern of the HSA Panel

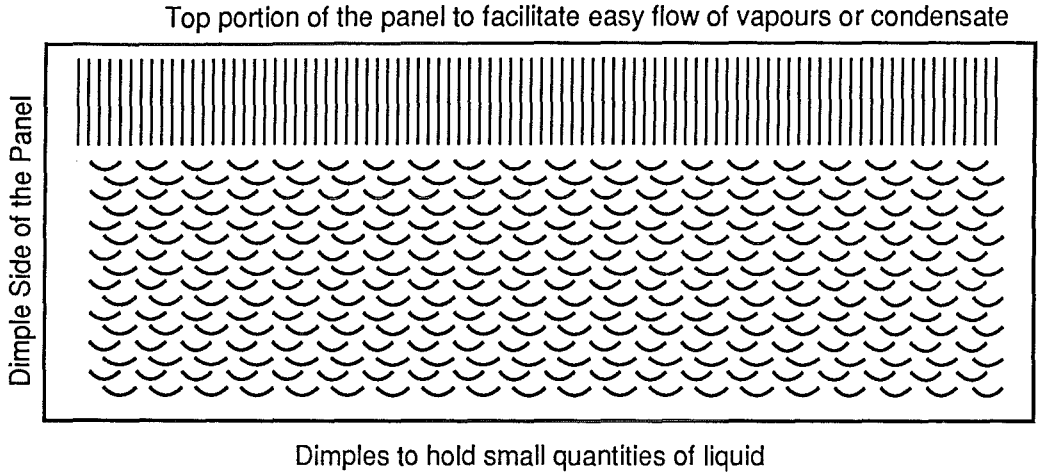

not totally eleminate the carbon deposition. On the other hand, if the viscosity of the fluid is less, it would lower the carbon deposition and blockage problems, decrease the power required for pumping and condenser tube height can be reduced from 10 mm to 5 mm, which would increase the oil side film coefficient by 46%.

In a search for a substitute for Mobiltherm, soya bean oil was examined. As it was difficult to get the heat transfer properties of soya bean oil, the system was actually charged with it and experiments were conducted. Although it was found to decompose very little, the heat transfer characteristics were not suitable and so it was discarded. Hence, it would be worthwhile to search for an alternative fluid, or find suitable additives to prevent decomposition.

6.3 HSA Working Fluid

The heat sheet absorber of the first collector was charged with Dowtherm A, which was replaced with a mixture of Dowtherm A and toluene in the second colector, in order to improve the vapour pressure characteristics. Although the improvement was substantial, there is still some room for further improvement and a search for a more suitable fluid is warranted.

The biggest hurdle in selecting the HSA working fluid has been imposed by the vapour pressure limit of 100 kPa at the collector stagnation temperature to avoid rupture of the panel. This problem may be overcome by spot welding the entire panel in place of the dimples. However this method may pose certain mechanical problems during the fabrication.

6.4 HSA Panel Design

Another interesting area of pursuit is in the design of HSA panel, including the condenser tube design. Several improvements are possible such as the dimple pattern. As the solar radiation strikes the entire area of the panel, it would be preferable to have the liquid distributed inside the whole panel instead of the bottom portion alone. This would make the panel start up easily and improve the performance. One of the ways of achieving this goal is by choosing an appropriate dimple pattern as shown in Fig. 6.1. This arrangement would allow small pockets of liquid distributed all over the panel. At the top a different pattern is chosen for free and easy movement of vapour and condensate. This

pattern has already been tried in this Department and improvements have been observed.

6.5 Refrigeration System

It would be beneficial to redesign the refrigeration system as a whole and in particular the generator tube, for solar application. The surface area of the generator tube needs to be increased (by using a coiled or finned tube). A proper heat exchanger, for the analyser tube, (in place of a solid piece of copper connecting the generator tube heat exchanger) would enhance the heat transfer. However, these changes require further experimentation and greater understanding of the system. The insulation for the refrigerator cabinet appears to be inadequate for solar applications, where heat losses are of prime concern, and hence it should be increased.

6.6 Optimisation of Solar Refrigeration System

Another interesting area for further pursuit of this project, is in the computerised optimisation of the entire solar refrigeration system. In this project, several computer simulation programmes have been used, of which a few were interlinked. However, as explained earlier various components in the system are interdependent on one another (such as the collector, storage system and the refrigerator) and each component has some operational boundaries (which depend on the type, dimensions, geometry and working fluids of that particular component). Hence, the optimisation of the whole system is possible, only if all the components of the system, are included in the optimisation programme. Such a programme, would enable one, not only to determine the optimum operating conditions and dimensions of different components, but also to find out the effects of making changes in the dimensions, geometry, type and working fluids of those components. Each component can be optimised individually and then joined together to get an overall optimisation of the system. There are several economic optimisation charts available in the literature (one such is given by Kreider and Kreith, 1982) and one of them can be incorporated in the overall optimisation to evaluate the economic feasibility of the system.

FIGURE 6.2 Methods of Linking HSA Panel to Electrolux Refrigerator

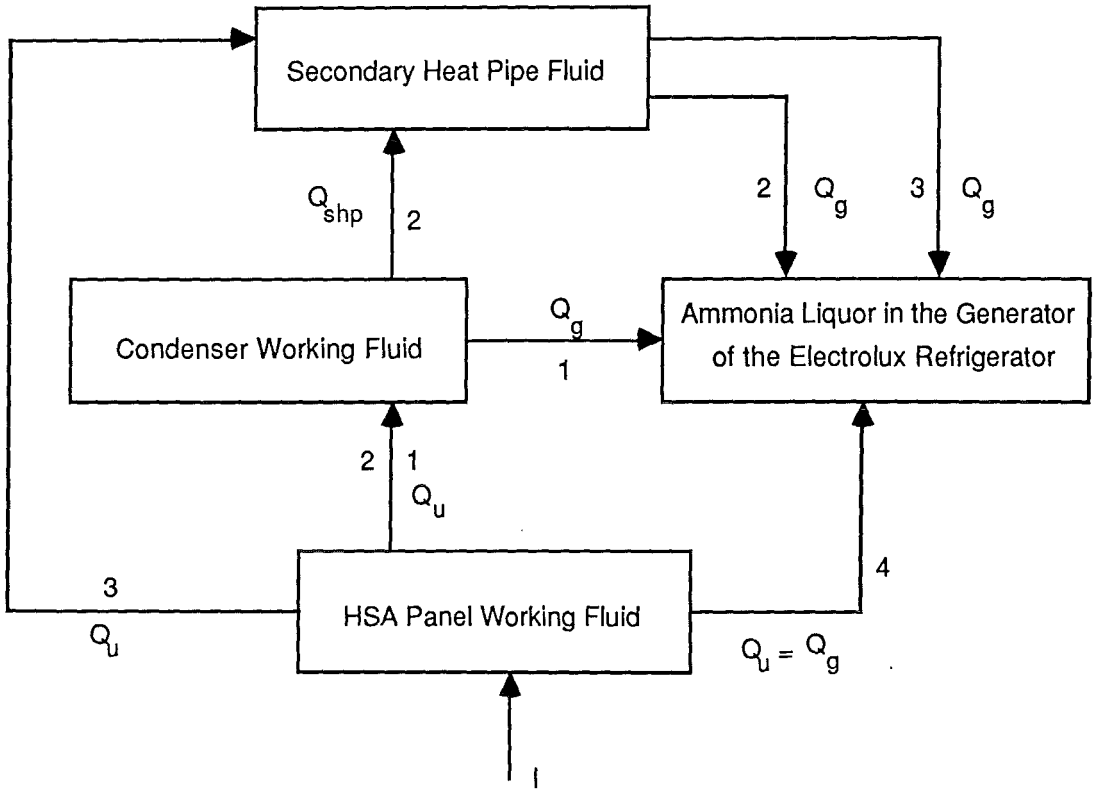

Notes: I = Solar radiation incident on the panel

Q_u = Useful energy transfered from the panel to the condenser working fluid

Q_g = Net energy transfered to the generator

Q_{shp} = Net energy tranfered to the secondary heat pipe working fluid

6.7 Energy Storage

The advantages and disadvantages of cold and hot storage have been discussed in the previous chapter. It is difficult to choose the storage type without performing optimisation study. It thus poses another interesting area of pursuit.

As seen from Chapter 5, the total power required to operate the refrigerator during night is 199 W, which includes the losses from the tank (67 W) and the refrigerator piping (81 W) and the power supplied to the refrigerator (51 W). At an average real COP of 0.4, the heat leak into the refrigerator then becomes 20 W. It is possible to store 199 W of hot storage and obtain 20 W of cooling at night time, or convert the 199 W during the day and store 20 W of cold storage, which can be used during night. Although approximately the same amount of energy (199 W) is required for either cold or hot storage the final choice of the storage type can be made only after consideration of several factors such as storage volume, heat losses, storage and ambient temperatures, day-night temperature differences, storage efficiency, storage medium, location of storage and overall costs.

6.8 Methods of Linking the Collector to the Refrigerator

There are several ways of combining the solar collector to the Electrolux refrigerator (as shown in Fig. 6.2), keeping in perspective the path of heat transfer and a few important ones are discussed below.

6.8.1 Option(1)

Heat sheet absorber (HSA) working fluid-condenser working fluid-ammonia liquor : This is the present option (Fig. 6.3) that has been studied in detail, where solar energy is first absorbed by HSA working fluid (via the metallic sheet), which is then transfered to the condenser working fluid and finally to the generator containing ammonia liquor.

This option has the following advantages. It has two independent loops, one with the refrigerator in it and the other with the solar collector. Both the loops are joined to the storage tank and hence they can be tested independently and can be modified without affecting each other. This aspect is very important during the development and testing stage of the system because, in the process, several modifications are usually needed.

FIGURE 6.3 Collector-to-Refrigerator Linking Option (1)

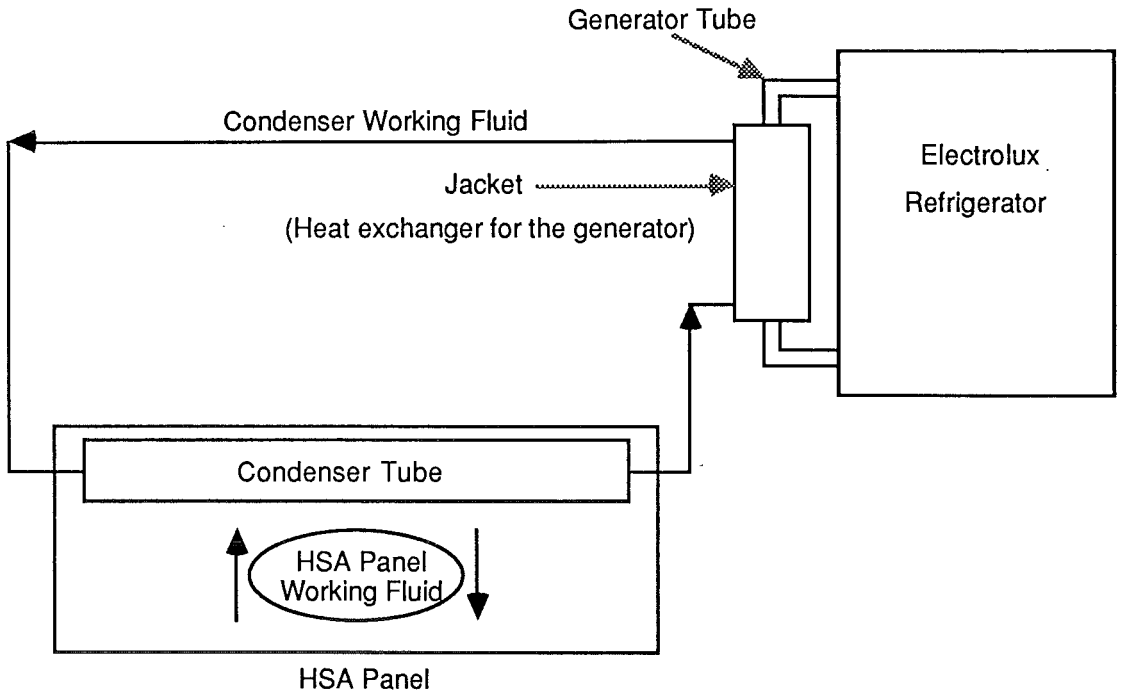

FIGURE 6.4 Collector-to-Refrigerator Linking Option (2)

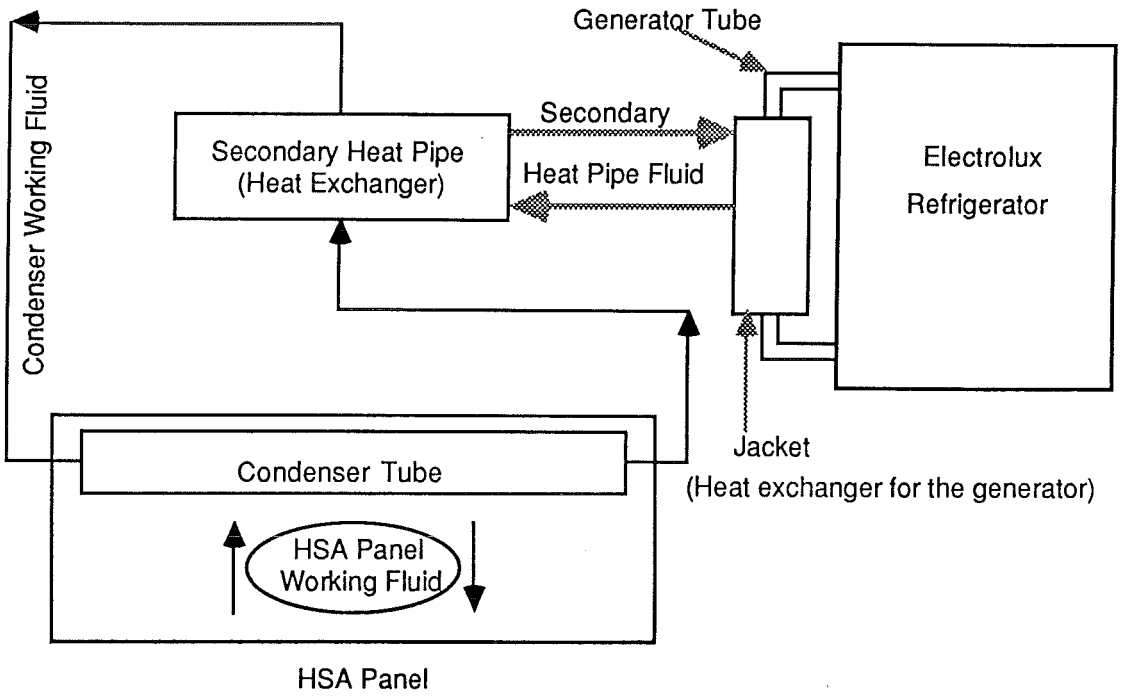

Thermal energy storage above ambient temperature is convenient, as the working fluid can also be used as the storage material. Even when the energy is stored below ambient temperature, some hot storage is beneficial (and often needed) because of the fluctuations in solar energy supply during the energy collection time. Another advantage is that, it is not necessary to redesign the whole refrigeration unit, and commercially available refrigerators can be used with slight modification. Last advantage is that the relative positioning of various components of the system is not crucial, which allows for a lot of flexibility.

The main disadvantage of this type, is the necessity of external power source for the circulation pump. It is hard to achieve thermosyphoning with HSA, especially using oil as the heat transfer fluid. Also, it is very difficult to achieve thermosyphoning in two different loops- one from the collector to the storage and the other from the storage to the refrigerator. An alternative is to use solar cells to supply the necessary power to the pump, but this was not our objective. Heat transfer oils are usually the best candidates for the condenser working fluid. But the disadvantages of systems using oil are the low oil side heat transfer coefficients and consequently large temperature drops, which would force the collector operating temperature to higher levels, thus reducing the solar energy collection efficiency. Also heat transfer oils tend to decompose after some time, especially when hot oil comes in contact with air.

6.8.2 Option(2)

HSA working fluid- condenser working fluid-secondary heat pipe fluid-ammonia liquor : This option (Fig. 6.4), utilising a secondary heat pipe, has also been described earlier. It is similar to option(1), except that the energy from condenser fluid is first transfered to the secondary heat pipe fluid and then to the ammonia liquor. The main advantage of this option over the previous one is that it introduces another heat exchanger at a convenient location where extra area can be easily provided to counter the effect of a low oil side film coefficient. Thus the area restriction of the generator tube heat exchanger (of commercial Electrolux refrigerators), is no longer a problem, as the overall heat transfer is controlled by the condensing film of

FIGURE 6.5 Collector-to-Refrigerator Linking Option (3)

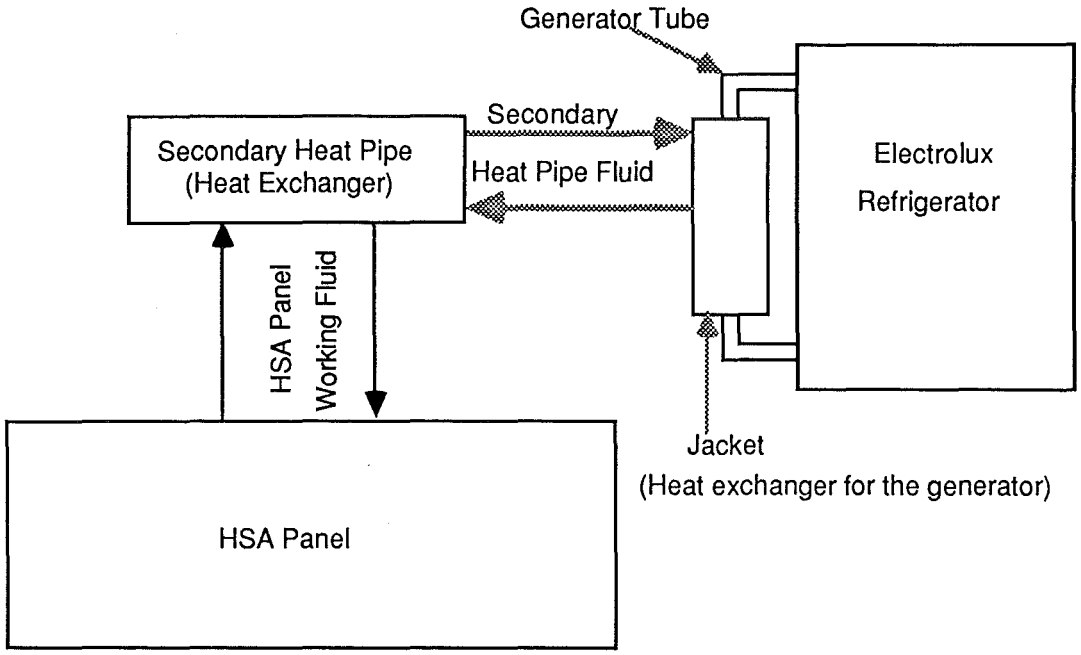

FIGURE 6.6 Collector-to-Refrigerator Linking Option (4)

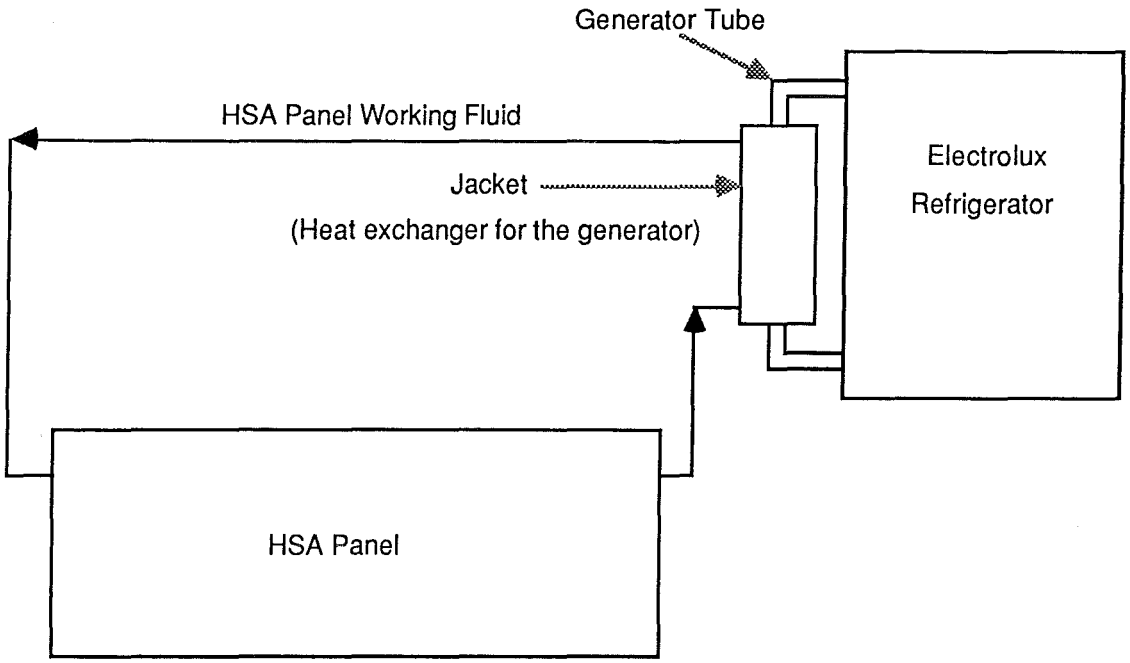

the secondary heat pipe fluid (which has a very high heat transfer coefficient), and not the oil film.

The disadvantages of this option as compared to the previous one are the extra resistances introduced in the path of heat flow due to the secondary heat pipe and the introduction of an extra heat exchanger which adds to the cost and complexity and which has to be located below the generator tube heat exchanger if the secondary heat pipe works on thermosyphoning. Also, because the generator tube heat exchanger becomes a part of the secondary heat pipe, it has to be built vacuum tight and should be compatable to the secondary heat pipe fluid. In selecting a secondary heat pipe fluid the compatability can be a big problem as there is no choice in selecting the construction materials for the generator tube (because it is a part of the commercial unit). The other advantages and disadvantages of this option are same as option(1).

6.8.3 Option(3)

HSA working fluid - secondary heat pipe fluid - ammonia liquor : In this option (Fig. 6.5), the condenser tube becomes part of the secondary heat pipe, thus the condenser working fluid is eliminated from option(2). Solar energy is transferred from HSA working fluid directly to secondary heat pipe fluid, which then delivers the energy to the ammonia liquor. The main advantage of this option over the other two options is the elimination of the circulation pump, and thus, the external power source. Other advantages are the removal of oil as the working fluid and the associated problems with it and also reducing the number of resistances in the path of heat flow.

The main disadvantage is the geometry of the system, as the solar collector has to be placed below the refrigerator in order to make the secondary heat pipe thermosyphoning. This problem may be overcome with the introduction of wick material in the secondary heat pipe, but it may prove to be a very hard task because of the geometry of the condenser tube, which in turn is dependent on the geometry of the HSA panel. The other disadvantage is the elimination of the buffer tank (or hot storage tank), which evens out the fluctuations in solar energy during the day. Also it is not possible to have hot storage of thermal energy and the two loops are interconnected which makes it impossible to test or

modify the solar collection system and refrigeration system independently.

6.8.4 Option(4)

HSA working fluid - ammonia liquor : In this option (Fig. 6.6), the secondary heat pipe, including the condenser tube is eleminated from the previous option and the whole system has to be built as a single unit. Solar energy is directly transferred from the HSA working fluid to ammonia liquor. This option can be implemented in two ways: firstly by modifying the collector so that vapours from HSA panel condense outside the generator tube (without modifying the refrigerator), and secondly by modifying the refrigerator so that the condenser tube becomes the generator tube (without modifying the solar collector). This option has all the advantages and the disadvantages of option(3). It has the added advantage (as compared to the previous options), of having a least number of resistances, in the path of heat flow, and so the over all temperature drop is minimum, which would allow the collector to operate at lower temperatures or higher efficiencies.

As seen from the above discussion, options (3 & 4) seem attractive, mainly because of the elimination of the circulation pump but, however, more work is warranted in studying these options, for which all the basic work has already been carried out in this project.

NOMENCLATURE

Symbol	Description
a	Cross section area [m^2]
A	Area [m^2]
COP	Coefficient of performance
c_p	Specific heat [$J.kg^{-1}.K^{-1}$]
C_p	Piping connected with the collector
CR	Concentration ratio or conduction/convection resistance
C1,C2	Collectors 1 and 2 respectively
D	Diameter [m]
E	Emissive power [$W.m^{-2}$] or fin efficiency factor
EWV	East-West view angle
f	Weighting function
Fij	Shape factor between ith and jth wall
F'	Efficiency factor for collector plate
g	Acceleration due to gravity [$m.s^{-2}$]
g_c	Gravitational constant
G	Irradiation [$W.m^{-2}$]
Gr	Grashof number
Gz	Greatz number
h	Heat transfer coefficient [$W.m^{-2}.K^{-1}$]
H	Height [m]
I	Insolation [$W.m^{-2}$]
J	Radiosity [$W.m^{-2}$]
k	Thermal conductivity [$W.m^{-1}.K^{-1}$]
K	Extinction coefficient [m^{-1}] or kWhr meter reading [kWhr]
L	Length [m]
Lc	Characteristic length [m]
m	Mass flowrate [$kg.s^{-1}$]
M_n	Figure of merit
n	Index of refraction
n	Number of days from vernal equinox
N	Number of reflections
Nu	Nusselt number
p	Perimeter [m]
P	Pressure [kPa] or radiative power [W]
Pr	Prandtl number

q Volumetric flowrate [$m^3.s^{-1}$]
q_{ij} Net energy exchange between ith and jth surfaces [W]
Q Thermal energy [W]
Q_l Heat leakage into the evaporator or heat loss per unit length [W]
R Radius [m] or heat transfer resistance [$K.W^{-1}$]
Ra Rayleigh number
Re Reynold's number
R_o Universal gas constant [$J.K^{-1}.kgmol^{-1}$]
t Time [s or hr] or thickness [m]
T Temperature [°C or K]
U_L Overall heat loss coefficient from collector [$W.m^{-2}$]
U_o Overall heat loss coefficient from fluid [$W.m^{-2}$]
V Velocity [$m.s^{-1}$]
W Work input to pump [J], Width [mm or m]
x Thickness [mm]
X_s Collector's figure of merit

Greek Symbols

α Absorptance or absorptivity or collector tilt angle
β Altitude angle [deg] or coefficient of thermal expansion
β_r COP of Carnot refrigerating cycle
γ Azimuthal angle [deg] or kinematic viscosity [$m^2.s^{-1}$]
δ Average film thickness [m]
Δ Difference
ε Emittance
ϕ Latitude or angle of inclination [deg]
ϕ_v Viscosity correction factor
η Efficiency
λ Angular direction [deg] or latent heat [$J.kg^{-1}$]
μ Viscosity [$kg.m^{-1}.s^{-1}$]
Ω Fin efficiency
θ Angle of incidence [deg]
ρ Reflectivity or density [$kg.m^{-3}$]
ψ Rim angle [deg] or correction for free convection
σ Surface tension [$N.m^{-1}$] or Stefan Boltzmann constant [$W.m^{-2}.K^{-4}$]
τ Transmittivity or tilt angle

Subscript

a	absorber or absorbed or average or air
ab	absorber panel
amb	ambient
ap	aperture
av	average
b	bulb or box or black body
bf	boiling film
c	condenser or condenser tube or convective or condensation or collector or critical
cf	condensate film
cr	convective and radiative
d	diffuse
e	evaporator or effective or end wall
eq	equivalent
ew	end wall
f	fin or fluid or film
g	generator or glass or glazing or gravitational
hp	heat pipe
hral	horizontal aluminium strip
i	inlet or insulation or inner
ig	inner glazing
i(j)	Mirror image of surface 'i' in surface 'j'
i(j,k)	Mirror image of surface 'i' in surface 'j' first and then in surface 'k'
itg	inner top glazing
j	jacket
l	leak into evaporator or cabinet or liquid
L	log mean or overall loss
max	maximum
min	minimum
o	outlet or oil or overall or outer
og	outer glazing
ogia	outer glazing in contact with air
opt	optical
p	absorber panel or piping
r	refrigerator or rectifier or reflector or reflected
ref	reflector or reference junction
s	specular or stagnation or surface

S	secondary
th	thermal
T	total
u	useful
v	vapour flow
vl	vapour liquid interface
vral	Vertical aluminium strip
vs	vapour sonic
w	tube wall

REFERENCES

Akinsete, V.A. and Coleman, T.A. (1982) Int. J. of Heat and Mass Transfer. Vol. 25. No. 7: 991-998.

Alefeld, G. (1980) Int. Seminar on Thermochemical Storage. Stockholm. Sweden.

Ali, A.F.M.A. (1977) Ph.D. Engg. Thesis. University of Windsor. Ontario.

Ali, M.G. and Patel, V. (1979) Solar Energy. Vol. 22: 483-491.

Alizadeh, S. et al. (1979) Solar Energy. Vol. 22: 149-154.

Anderson, B.R. (1981) Building and Environment. Vol. 16. No. 1: 35-39.

Anderson, H. (1975) ISES. Extended Abstract.

Anderson, P.P. (1976) ASHRAE Trans. Vol. 82: 959-965.

Arnold, J.N. et al. (1974) Proc. of the 1974 Heat Transfer and Fluid Mechanics Institute. Stanford University Press: 321-329.

Arnold, J.N. et al. (1975) ASME Paper 75-HT-62.

ASHRAE (1977) Fundamentals Handbook : 1.18-1.24.

ASHRAE (1978) Standards. No. 93-97.

ASTM (1974) Special Technical Publication. 470A.

Ayyaswamy, P.S. and Catton, I. (1973) J. of Heat Transfer. Vol. 95: 543p.

Baker, H.D. et al. (1953) Temperature Measurement in Engineering. Vol. 1. John Wiley and Sons, Inc. New York.

Baker, H.D. et al. (1961) Temperature Measurement in Engineering. Vol. 2. John Wiley and Sons, Inc. New York.

Basiulis, A. and Filler, M. (1971) 6th AIAA Thermophys. Conf. Tullahoma. Tennessee. Paper No. 71-409.

Bauks, R. (1974) Proc. of Workshop on Solar Cooling for Buildings. Los Angeles.

Baum, V.A. and Kakabayev, A. (1978) Proc. of ISES Conf. New Delhi. Vol. 3: 1556p.

Bayley, F.J. and Lock, G.S.H. (1964) ASME Paper 64-HT-6.

Beckman, W.A. et al. (1977) Solar Heating Design. John Wiley and Sons. NY.Beekley, D.C. and Mather, G.R. (1975) Analysis and Experimental Tests of a High performance Evacuated Tubular Collector. Owens-Illonois, Toledo, Ohio.

Bezrodnyi, M.K. and Alekseenko, D.B. (1977) High Temp. Soviet Research. Vol. 15: 309-313.

Bhardwaj, R.K. and Gupta, B.K. (1967) Solar Energy. Vol. 11. No. 3.

Bienert, W.B. (1973) Proc. of First Int. Heat Pipe Conf. Stuttgart. Germany.

Bienert, W.B. (1974) Report on Heat Pipes Applied to Flat Plate Solar Collectors. Dynatherm Corp. Cockeysville. Maryland.

Bienert, W.B. and Wolf, D.A. (1975) Annual Progress Report on Heat Pipes Applied to Flat Plate Solar Collectors. Dynatherm Corp. Cockeysville. Maryland. Report No. NSF/RANN/SE/AER 74-09164/PR/75/1

Bienert, W.B. and Wolf, D.A. (1976) Final Report on Heat Pipes Applied to Flat Plate Solar Collectors. Dynatherm Corp. Cockeysville. Maryland. Report No. COO/2604-76/1.

Bienert, W.B. and Wolf, D.A. (1976) ASME Winter Annual Meeting. New York.

Bird, R.B. et al. (1960) Transport Phenomena. John Wiley. New York.

Bliss, R.W. Jr. (1959) Solar Energy. Vol. 3. No. 4: 55-64.

Blower, R. and Evans, T.E. (1974) Introducing Coloured Stainless Steel - a Noval Product and a New Process. Int. Nickel Ltd. Thames House. Millbank. London.

Boer, K. (1975) ISES Conf. Paris.

Brinkworth, B.J. (1974) Nature. Vol. 249. No. 5459. 21p.

Buchberg, H. and Edwards, D.K. (1976) Solar Energy. Vol. 18: 193-204.

Buchberg, H. et al. (1971) Solar Energy. Vol. 13: 193-221.

Buchberg, H. et al. (1976) Trans. ASME. J. of Heat Transfer. May: 182-188.

Busse, C.A. (1967) Thermionic Conversion Specialists Conf. Palo Alto. California.

Busse, C.A. et al. (1968) Int. Conf. on Thermionic Electrical Power Generation. 2nd Stresa. Italy. Available from EURATOM Centre. Luxembourg. EUR No. 4210 f,e: 495-506.

Busse, C.A. et al. (1973) First Int. Heat Pipe Conf. Stuttgart. Paper No. 4-2.

Cathro, K.J. (1978) Selective Surfaces for Flat Plate Collectors - a Brief Review. Div. of Mineral Chemistry. CSIRO. Aust.

Catton, I. (1966) The Physics of Fluids. Vol. 9. No. 12: 2521-2522.

Catton, I. (1978) Proc. 6th Int. Heat Transfer Conf. Toronto. Vol. 6: 13p.

Catton, I. et al. (1974) Int. J. of Heat Mass Transfer. Vol. 17: 173p.

Chari, R.K. (1958) M.Sc. in Engineering Thesis. University of Florida. U.S.A.

Chinnappa, J.C.V. and Martin, H.A. (1976) Solar Energy. Vol.18 : 337-342.

Chinnappa, J.C.V. (1974) Solar Energy. Vol. 16: 165-170.

Chisholm, D. (1971) The Heat Pipe. Mills and Boon. London.

Churchill, S.W. and Chu, H.H.S. (1975) Int. J. of Heat Mass Transfer. Vol. 18: 1049p.

Churchill, S.W. and Chu, H.H.S. (1975) Int. J. of Heat Mass Transfer. Vol. 18: 1323p.

Clever, R.M. (1973) J. of Heat Transfer. Vol. 95: 407p.

Close, D.J. (1965) Mech. and Chem. Engg. Trans. I.E. Aust. :11-22.

Cohen, H. and Bayley, F.S. (1955) Proc. of Inst. of Mech. Engineers. Vol. 169: 1063p.

Cook, E. (1976) Man, Energy, Society. W.H.Freeman Company. San Francisco.

Cotter, T.P. (1965) Las Alamos Scientific Laboratory. Report No. LA-3246-MS.

Cottingham, J.G. (1977) U.S. Patent No. 4,044,819.

Crampton, H.E. (1985) B.E. Thesis. Chem. Engg. Dept. University of Canterbury. Christchurch.

Curran, H.M. (1975) Final Report on Assessment of Solar Powered Cooling of Buildings. ERDA Report No. NSF-RA-N-75-012.

Dao, K. (1976) Annual Report of Lawrence Berkley Lab. Univ. of California :1-63.

Dao, K. et al. (1977) ERDA Solar Heating and Cooling R&D Contractors' Meeting. Reston. Virginia.

Das, A.K. and Wibulswas, P. (1983) RERIC News. 9p. AIT. Bankok.

Davison, R.M. et al. (1979) Climax Molybdenum Co. 3072 One Oliver Plaza. Pittsburg. Pennsylvania 15222.

Delyannis, A.A. and Delyannis, E.A. (1978) Proc. of the ISES Conf. New Delhi. Vol. 2: 942-944.

Didion, D. et al. (1979) NTIS Data Base. NBS Washington D.C. Citation No. 240800.

Dornier System (1978) GMDH. Abtlg. VCC 7990. Friedrichshafen. FRG.

Dow Chemical U.S.A. Midland. Michigan. 48640.

Duffie, J.A. and Beckman, W.A. (1980) Solar Engineering of Thermal Processes. John Wiley and Sons. New York.

Dunkerley, J. (1978) International Comparisons of Energy Consumption - Resources for the Future. Washington D.C.

Dunkle, R.V. (1965) Mech. and Chem. Engg. Trans. I.E. Aust. :73-78.

Dunn, P.D. and Reay, D.A. (1978) Heat Pipes. Pergamon Press. NY.

Eckard, S.E. and Bond, J.A. (1976) Proc. 2nd ERDA Workshop: Use of Solar Energy for Cooling of Buildings. NTIS :110-136.

Eckert, E.R. and Sparrow, E.M. (1961) Int. J. of Heat Mass Transfer. Vol. 3: 42-54.

Edwards, D.K. et al. (1960) Report No. 60-93 Dept. of Engg. University of California at Los Angeles.

Electrotechnical Laboratory (1978) Technocrat. Vol. 11. No. 4:57p.

Espy, P.N. (1978) Proc. of the ISES Conf. New Delhi. Vol. 2: 1038-1042.

Evans, L.B. and Stefany, N.E. (9166) CEP Symp. Series. Heat Transfer. Vol. 62. No. 64: 209-215.

Evans, T.E. et al. (1972) A New Process for Colouring Stainless Steel. Int. Nickel Ltd. Thames House. Millbank. London.

Farber, E.A. (1970) Engineering Progress at the University of Florida. Vol. 27: 17p.

Farber, E.A. (1970) ASME Annual Winter Meeting. Paper No. 70-WA/S-4.

Farber, E.A. et al. (1975) ISES Congress and Exposition. University of California. Los Angeles.

Farber, E.A. et al. (1976) Proc. of 22nd Inst. of Environ. Sci. Annual Tech. Meeting. Philadelphia: 319-321.

Farber, E.A. et al. (1978) Proc. ISES Conf. New Delhi: 1561-1563.

Ferrell, J.K. et al. (1973) Int. Heat Pipe Conf. Stuttgart. FGR.

Francken, J.C. (1975) Proc. of the ISES Conf. Los Angeles. Paper 34/48.

Francken, J.C. (1978) Proc. of the ISES Conf. New Delhi. Vol. 2: 885-889.

Fraser, I.A. (1970) B.E. Thesis. Mech. Engg. Dept. University of Canterbury, Christchurch.

Fujii, S. et al. (1977) J. of Chem. Engg. Japan. Vol. 10:224-228.

Gani, R. (1979) Aust. Energy R&D and Demonstration Projects. No. 5.1.29.

Gaugler, R.S. (1944) US Patents 2,350,347 and 2,350,348.

Geoola, F. et al. (1977) Design of Ammonia-Water Absorption Refrigeration System Utilising Solar Energy. Report from Materials and Energy Res. Centre Sharif Univ. Tehran. Iran.

Geoola, F. et al. (1977) Design of Water-Lithium Bromide Absorption Refrigeration System Utilising Solar Energy. Report from Materials and Energy Res. Centre Sharif Univ. Tehran. Iran.

Globe, S. and Dropkin, D. (1959) J. Heat Transfer. Vol. 81C. 24p.

Goldstein, R.J. and Chu, T.Y. (1969) Progress in Heat and Mass Transfer. Vol. 2: 55-75.

Goldstein, R.J. et al. (1973) Int. J. Heat Mass Transfer. Vol. 16: 1025p.

Grossman, G. et al. (1979) Proc. ISES Conf. Atlanta. Georgia. Vol. 1: 720-727.

Grossman, G. and Johannsen, A. (1981) Prog. Energy Combust. Sci. Vol. 7: 185-228.

Grover, G.M. et al. (1964) J. of Appl. Phys. Vol. 35: 1990-1991.

Gruen, D.M. et al. (1978) Solar Energy. Vol. 21: 153-156.

Gruen, D.M. et al. (1978) 4th Annual Heat Pump Technology Conf. Stillwater.

Gruen, D.M. et al. (1978) Chemical Hydrogen Energy Systems Contracts Review. Washington D.C. NTIS: Conf-781142-7.

Gubareff, G.G. (1960) Thermal Radiation Properties Survey. Honeywell Research Centre. Minniapolis. 299p.

Hainsworth, W.R. (1944) Refrig. Engg. Vol. 48. Aug:97-100. Sept:201-205.

Hall, C.A. and Howerton, M.T. (1976) ISES Conf. on Solar Technology in Seventies: Sharing the Sun. Vol. 8.

Hay, H.R. and Yellott J.I. (1970) Mech. Engg. Vol. 94: 19p.

Hermann, W. et al. (1978) Proc. on the ISES Conf. New Delhi.

Hernandez, P. (1974) Proc.of Workshop on Solar cooling for Buildings. Los Angeles.

Hickok, F. (1975) Handbook of Solar and Wind Energy. Cahners Books International Inc. Boston, U.S.A.

Hill, J.E. et al. (1976) NBS Tech. Note 899.

Hill, J.E. and Streed, E.R. (1976) Solar Energy. Vol. 18: 421-431.

HMSO (1961) Explanatory Supplement to the Astronomical Ephemeris and The American Ephemeris and Nautical Almanac.

Hollands, K.G.T. (1965) Solar Energy. Vol. 9: 159p.

Hollands, K.G.T. et al. (1975) Int. J. Heat Mass Transfer. Vol. 18: 879p.

Hollands, K.G.T. et al. (1976) J. of Heat Transfer. Vol. 98: 189p.

Holman, J.P. (1972) Heat Transfer. McGraw-Hill. New York.

Hottel, H.C. (1954) Proc. of a Symposium held at M.I.T. Aug. 1950. M.I.T. Press.

Hottel, H.C. and Sarofim, A.F. (1967) Radiative Transfer. McGraw-Hill. New York.

Hottel, H.C. and Whillier, A. (1955) Trans. of the Conf. on the Use of Solar Energy. Arizona. Vol. 2. Part 1: 74-104.

Hottel, H.C. and Woertz, B.B. (1942) ASME Trans. Vol. 64: 91-104.

Hussman, E.K. and Becker, H.J. (1978) Proc. of the ISES Conf. New Delhi. Vol. 2: 1029-1031.

IGT (1964) Physical and Thermodynamic Properties of Ammonia-Water Mixtures. IGT Res. Bulletin No. 34.

Incropera, F.P. and Dewitt, D.P. (1981) Fundamentals of Heat Transfer, John Wiley and Sons. New York.

Insulation Handbook (1959) Editor Shepherd, G. Erskin and Co. London.

Ion, D.C. (1975) Availibility of World Energy Resources. Graham and Toronto Ltd. U.K.

Jacob, M. (1949) Heat Transfer. Vol. 1. John Wiley and Sons. New York.

Jacob, Y. et al. (1969) ASHRAE Trans. Vol. 75. No. 2098: 103-110.

Jenkins, L.A. (1978) B.E. Thesis. Chem. Engg. Dept. University of Canterbury, Christchurch.

Johannsen, A. (1979) Proc. ISES Conf. Atlanta. Georgia. Vol. 1: 681-685.

Johnston, A.M. (1980) Solar Energy. Vol. 25: 243-254.

Johnston, A.M. and O'Sullivan, C.H. (1981) Trans. of the ASME Vol. 103: 42-46.

Jong de B. (1973) Net Radiation Received by a Horizontal Surface on Earth. Delft Univ. Press. Delft.

Jordan, R.C. (1967) Low Temperature Engg. Applications of Solar Energy. ASHRAE. New York.

Jordan, R.C. et al. (1973) Int. Conf. on the Sun in the Service of Mankind. Paris. Paper No. E137.

Karaki, S. and Armstrong P.R. (1978) Proc. of Workshop. The Use of Solar Energy fo the Cooling of Buildings. San Francisco.

Kays, W.M. (1966) Convective Heat and Mass Transfer. McGraw-Hill. New York.

Kern, D.Q. (1954) Process Heat Transfer. McGraw-Hill. New York.

Kern, D.Q. and Othmer, D.E. Trans. AIChE. Vol. 39: 517p.

Kern, J. and Harris, I. (1975) Solar Energy. Vol. 17: 97-102.

King, H.M. (1973) Canadian Mining and Metallurgical Bull. Vol. 66: 37-54.

King, H.M. (1975) Committee on Interior and Insular Affairs. House of Representatives U.S. 93rd Congress.

Klein, S.A. et al. (1974) Trans. ASME J. of Engg. for Power. Vol. 96A: 109-113.

Klein, S.A. (1975) Solar Energy. Vol. 17: 79-80.

Kooi, C.F. (1978) Solar Energy. Vol. 20: 69-73.

Kreeb, H. et al. (1973) First Int. Heat Pipe Conf. Stuttgart. Paper No. 4-1.

Kreider, J.F. and Kreith, F. (1982) Solar Heating and Cooling. McGraw-Hill. New York.

Kreith, F. (1976) Principles of Heat Transfer. Intext Educational Publishers. New York.

Kreith, F. and Kreider, J.F. (1978) Principles of Solar Engineering. McGraw-Hill. New York.

Kupler, M. and Kogles, K. (1973) Int. Conf. on the Sun in the Service of Mankind. Paris. Paper No. E104.

Larson, D.C. and Savery, C.W. (1978) Proc. of the ISES Conf. New Delhi. Vol. 2:1033-1037.

Lee, Y. and Bedrossian, A. (1978) Int. J. of Heat and Mass Transfer. Vol. 21: 221-229.

Lee, Y. and Mital, U. (1972) Int. J. of Heat and Mass Transfer. Vol. 15: 1695-1707.

Liu, B.Y.H. and Jordon, R.C. (1963) Solar Energy. Vol. 7: 53p.

Lloyd, J.R. and Moran, W.P. (1974) Trans. of ASME J. of Heat Transfer. Vol. 96: 443p.

Lof, G.O.G. (1955) Proc. of the World Symp. on Applied Solar Energy. Phoenix. Arizona.

Lof, G.O.G. (1955) Solar Energy Research. Univ. of Wisconsin Press. Wisconsin.

Lof, G.O.G. and Tybout, R.A. (1973) ISES Conf. Paris.

MacGregor, R.K. and Emery, A.P. (1969) J. of Heat Transfer. Vol. 91: 391p.

Macriss, R.A. (1976) ASHRAE Trans. Vol. 82: 975-988.

Mahdjuri, F. (1978) SolarEnergy and Conservation Symposium-Workshop. Miami Beach. Florida.

Mann-Russell Electronics, Inc. 1401 Thorne Road. Tacoma. WA 98421.

Mather, G.R.Jr. (1980) J. of Solar Energy Engg. Vol. 102: 294-304.

McAdams, W.H. (1954) Heat Transmission. McGraw-Hill. New York.

McCabe, W.L. et al. (1985) Unit Operations of Chemical Engineering. McGraw-Hill. New York.

McDaniels, D.K. et al. (1975) Solar Energy. Vol. 17: 277-283.

Mei, V. et al. (1979) Proc. ISES Conf. Atlanta. Georgia. Vol. 1: 671-675.

Meinel, A.B. and Meinel, M.P. (1977) Applied Solar Energy : An Introduction. Addison Wesley Publishing Co. California. U.S.A.

Mesman, P.J.R. (1979) B.E. Thesis. Chem. Engg. Dept. University of Canterbury. Christchurch.

M.I.T. (1979) Optimisation of Photovoltaic/Thermal Collector Heat Pump Systems. Lincoln Lab. Lexington. MA.

Mitchell, J.W. (1976) Biophysical Journal. Vol. 16: 561p.

Morgan, V.T. (1975) Advances in Heat Transfer. Vol. 11. Academic Press. New York: 199-264.

Neville, R.C. (1978) Solar Energy. Vol. 20: 7-11.

Newcomb (1898) Tables of the Sun. Astronomical Papers prepared for the use of the American Ephemeris and Nautical Almanac. Vol. 6.

Newell, M.E. and Schmidt, F.W. (1970) ASME Trans. J. of Heat Transfer. Vol. 92: 159-168.

Newton, A.B. (1965) ASHRAE Trans. Vol. 71 II. 133p.

Nicholas, J.V. and White, D.R. (1982) Traceable Temperatures. DSIR Bulletin. New Zealand.

Offenhartz, P.O. (1976) ISES Conf. on Solar Technology in Seventies: Sharing the Sun. Vol. 8. Winnipeg.

Offenhartz, P.O. (1979) Solar Energy Storage Options Workshop. San Antonia. NTIS Conf. 790328: 11603-607.

Ong, K.S. (1978) Proc. of ISES Conf. New Delhi. Vol. 2: 993-997.

Ortabassi, U. (1976) COMPLES. Revue Int. d'Heliotechnique. 2nd Sem. 14-17.

Ostrach, S. (1952) NASA Report TN 2635.

Ostrach, S. (1972) Advances in Heat Transfer. Vol. 8. Academic Press. New York. : 161-227.

O'Toole, J.L. and Silveston, P.L. (1961) CEP Symp. Series. Vol. 57. No. 32.

Ozoe, H. et al. (1974) Int. J. of Heat and Mass Transfer. Vol. 17: 401-406.

Ozoe, H. et al. (1974) Int. J. of Heat and Mass Transfer. Vol. 17: 1209-1217.

Patton, A.R. (1975) Solar Energy for Heating and Cooling of Buildings. Noyes Data Corp. U.S.A.

Pedroso, R.I. (1976) Extended Abstract. Proc. of Solar Heating and Cooling: A National Forum. Florida.

Perry, R.H. and Green, D. (1985) Chemical Engineers' Handbook. McGraw-Hill. New York.

Philco Italiana S.p.A. - Brembate Sopra - Italy.

Philips, B.A. (1976) ASHRAE Trans. Vol. 82: 966-971.

Picking, J.W. Appliance Engineer. Feb: 61-63.

Pott, P. and Cooper, P.I. (1976) CSIRO Tech. Report No. TR-9. Div. of Mech. Engg. CSIRO Aust.

Prasad, T.S. (1980) M.Tech. Thesis. Dept. of Chem. Engg. I.I.T. Bombay. India.

Prasad, T.S. and Williamson, A.G. (1982) Paper Presented at the Tenth Australian Chem. Engg. Conf. Sydney.

Rabl, A. (1976) Solar Energy. Vol. 18: 93-111.

Rabl, A. (1976) Solar Energy. Vol. 18: 497-511.

Raithby, G.D. and Hollands, K.G.T. (1975) Advances in Heat Transfer. Vol. 11. Academic Press. New York: 265-315.

Rao, D.P. and Rao, K.S. (1976) Solar Energy. Vol. 18: 405p.

Redmond, J.D. et al. (1977) ISES Meeting. June 7. Orlando. Florida.

Redmond, J.D. et al. (1978) ISES Meeting. Aug. Denver. Colorado.

Redpoint Associates Ltd. (1977) Lynton Road. Cheney Manor. Swinddon. SN2 2QN. England.

Robertson, H.S. (1978) Dept. of Phys. University of Miami. Private Communication.

Rohsenow, W.M. and Hartnett, J.P. (1973) Handbook of Heat Transfer. McGraw-Hill. New York.

Ruedisili, L.C., and Firebaugh, M.W. (1975) Perspectives on Energy. Oxford Univ. Press. U.K.

Rush, C.K. and Sendall, R.F. (1977) Report on Performance of a Boiling-Condensing Flat Plate Collector. Queen's University. Kingston. Ontario. No. E 13 - M - am 7.

Russell, G.F. (1978) Solar Energy and Conservation Symposium Workshop. Dec. Miami Beach. Florida.

Saaski, E.W. (1977) Final Report on Two Phase Working Fluids. NASA Report No. N78-16329/2GA.

Sagar, J.C. et al. (1978) Proc. ISES Conf. New Delhi. Vol. 2: 912-916.

Satcunanathan, S. and Kochhar, G.S. (1975) ISES Congress and Exposition. University of California. Los Angeles.

Satcunanathan, S. and O'Brien, G.C. (1977) Solar Technology for Buildings. Proc. of Conf. London. 454p.

Savery, C.W. et al. (1976) ASME Winter Annual Meeting. NY. Paper No. 76-WA/HT-16.

SERVEL INC. (1946) The Miracle of Ice from Heat: The Scientific Marvel of Gas Refrigeration. Evansville, Indiana.

Seitel, S.C. (1975) Solar Energy. Vol. 17: 291-295.

Shelpuk, B.C. (1974) Proc. on Workshop : Solar Coolings for Buildings. Los Angeles.

Shelpuk, B.C. (1979) ASHRAE Meeting in June. Detroit. Michigan.

Sheridan, N.R. (1972) Solar Energy. Vol. 13: 395-401.

Simon, F.F. (1976) Solar Energy. Vol. 18: 451-466.

Smith, G.B. (1977) Aust. Inst. of Metal Finishing Annual Conf. Sydney.

Soin, R.S. et al. (1979) Solar Energy. Vol. 23: 69-73.

Solar Energy Handbook (1979) Power Systems Group/AMETEK Inc. Chilton Book Co. Radnor. Pennsylvania.

Solar Energy Research Group (1982) Solar Research Projects. Dept. of Mech. Engg. University of Sydney. Aust.

Solar Research. 525 North Fifth Street. Brighton. Michigan.

Souka, A.F. and Safwat, H.H. (1966) Solar Energy. Vol. 10. No. 4: 170-174.

Sparrow, E.M. et al. (1972) J. of Heat Transfer. Ser. C. Vol. 84: 294-299.

Sparrow, E.M. et al. (1979) Trans. ASME J. of Heat Transfer. Vol. 101: 2p.

Sparrow, E.M. and Gregg, J.L. (1956) Trans. ASME Vol. 78: 1823p.

Sparrow, E.M. and Gregg, J.L. (1956) Trans. ASME Vol. 78: 435p.

Speyer, F. (1965) J. of Engg. Power. Vol. 87: 270p.

Stickford, G.H. (1976) Sharing the Sun. Vol. 4: 295-315

Stoecker, W.F. and Reed, L.D. (1971) ASHRAE Trans. Vol.77 I: 163-170.

Swaminathan, C. and Swartman, R.K. (1970) ISES Conf. Paper No. 6/114. Melbourne.

Symons, J.G. and Cooper, P.I. (1978) Proc. of ISES Conf. New Delhi. Vol. 2: 1004-1008.

Symons, J.G. and Cathro, K.J. (1979) Aust. Energy R&D and Demonstration Projects. No. 5.1.8.

Tabor, H. (1955) Trans. of the Conf. on the Use of Solar Energy. Arizona. Vol. 2. Part 1: 1-23.

Tabor, H. (1958) Solar Energy. Vol. 2: 27-33.

Tabor, H. (1966) Solar Energy. Vol. 10. No. 3: 111-118.

Tabor, H. (1967) Low Temperature Engg. Applications of Solar Energy. ASHRAE. New York.

Tabor, H. (1977) Proc. of the First Conf. on Solar Building Technology. RIBA Publications. London. Vol. 2: 424-427.

Tabor, H. (1977) Applications of Solar Energy for Heating and Cooling of Buildings. ASHRAE. GRP-170.

Tabor, H. (1978) Solar Energy. Vol. 20: 293-303.

Tabor, H. and Zeimer, H. (1962) Solar Energy. Vol. 6. No. 2: 55-59.

Teagen, W.P. and Sargent, S.L. (1975) ISES Conf. Paris. Paper No. EH-94-1.

Trombe, F. et al. (1977) Solar Age. Vol. 2. 13p.

Vant-Hult. L.L. and Hildebrandt, A.F. (1976) Solar Energy. Vol. 18.

Vella, G.J. et al. (1976) Solar Energy. Vol.18:355-359.

Vries, H.F.W. de. et al. (1980) Solar Energy. Vol. 24: 209-213.

Walraven, R. (1978) Solar Energy. Vol. 20: 393-397.

Ward, D.S. (1979) Solar Energy. Vol. 22: 259-268.

Webb, K.L.J. (1979) M.E. Thesis. Chem. Engg. Dept. University of Canterbury. Christchurch.

Webb, K.L.J.; Prasad, T.S. and Williamson, A.G. (1984) UNESCO-KMITT-USAID Regional Seminar on Simulation and Design in Solar Energy Applications. Bankok.

Webb, K.L.J.; Prasad, T.S. and Williamson, A.G. (1984) Paper Presented at the ISES Conf. of Aust. and New Zealand Section . Auckland.

Webb, K.L.J.; Prasad, T.S. and Williamson, A.G. (1985) ASSET Vol. 7. No. 1: 25-28.

Whitlow, E.P. (1971) ASHRAE Trans. Vol. 77 II: 166-173.

Whitlow, E.P. (1976) ASHRAE Trans. Vol. 82 I: 950-958.

Wiebelt, J.A. (1966) Engineering Radiation Heat Transfer. Holt, Winchart and Winston. New York.

Wijeysundera, N.E. (1978) Solar Energy. Vol. 21: 517p.

Wilber, P.J. and Mitchell, C.E. (1975) Solar Energy. Vol. 17: 193-199.

Wilber, P.J. and Mancini, T.R. (1976) Solar Energy. Vol. 18: 337-342.

Winston, R. (1974) Solar Energy. Vol. 16: 89-95.

Wong, H.Y. (1977) Heat Transfer for Engineers. Longman. London.

WORLD ENERGY CONFERENCE. (1978) World Energy Resources 1985 - 2020. IPC Science and Technology Press. New York.

Wozniak, S.J. (1977) U.K. ISES Conf. London.

Yanagimachi, M. (1964) Proc. of the U.N. Conf. New Sources of Energy. Vol. 5. 233p.

Zeren, F. et al. (1978) ASME Paper 78-WA/Sol-15.

APPENDIX A1

THERMOCOUPLE CALIBRATION AND METHOD OF ATTACHMENT

The first section of this appendix describes the calibration technique, the experimental setup, the experiments conducted and the method of interpretation of the experimental results. The second section describes the various methods of attachment of the thermocouples, errors involved, procedures to minimise the errors and experiments conducted to compare different methods of attachment.

There are several methods for measuring temperature, however thermocouples are convenient and less expensive to use in measuring temperatures over a very wide range (Nicholas and White, 1982). Copper constantan thermocouples are suitable for the temperature range encountered in the present investigation.

A1.1 Calibration of Thermocouples

The practical use of thermocouples requires that they conform to an established temperature-electromotive force or emf relationship within acceptable limits of error. Most manufacturers supply thermocouple wire to certain limits of error depending on the materials used and the temperature range. American Society for Testing Materials ASTM (1974) specifies for copper constantan thermocouples, a maximum error limit of ±0.7% in the temperature range of 93 to 371°C and ±0.7°C in the temperature range of -59 to 93°C. However calibration is necessary in order to find out the accuracy of individual thermocouples as it does vary from one to the other depending on various factors including the type and size of the junction and homogeneity of the material. A beaded junction of very small size gives least errors (Baker et al., 1953) and hence in the present case the wires were fused with gas flame.

A1.1.1 Theory

The calibration of a thermocouple consists of determination of its emf at a sufficient number of known temperatures so that on interpolation its emfs will be known over the entire temperature range in which it is to be used. The process requires a standard thermometer to indicate temperatures on a standard scale, a means for measuring the emf of the thermocouple and a controlled

FIGURE A1.1 Schematic Diagram of the Experimental Setup for Calibration of Thermocouples

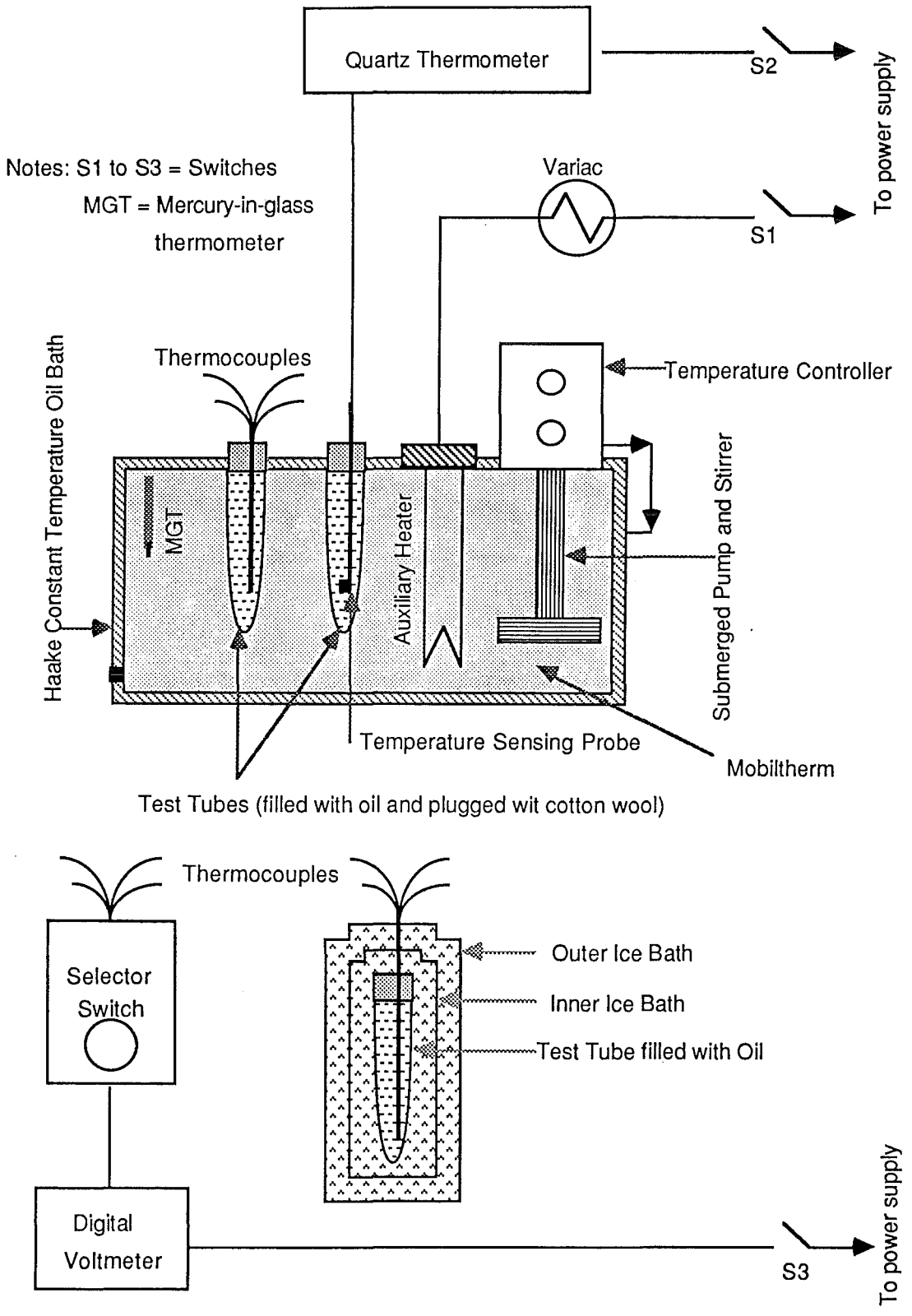

environment in which the thermocouple and the standard can be brought to the same temperature. Based on this principle there are several calibration techniques as described by ASTM (1974) and in particular in solar applications by Wozniak (1977). However calibration of a thermocouple by comparison with a working standard is sufficiently accurate for most purposes. The success of this method usually depends on the ability to bring the thermocouple and standard to the same temperature. Stirred liquid baths are best suited for this purpose. Also the accuracy depends on the standard thermometer employed and the reference junction. The reference junction can be at a fixed temperature (such as in an ice bath) or allowed to vary in which case a compensation is applied. An ice bath is convenient to use and very easy to maintain within ±0.5°C provided care is taken in preparing the ice bath, such as using distilled water and maintaining the ice water equilibrium. With ice baths "immersion error" occurs due to heat leak from the ambient via the wires, which is very small(a maximum value of 0.05°C). Also, "galvanic error" may result due to contact of water with copper wires, but it can be eliminated by proper insulation and using a heat transfer oil as an intervening medium. Another important factor in the accuracy of calibration is the accuracy of the instrument used to measure the emf. Slide wire potentiometers can give an accuracy of $\pm 5 \times 10^{-6}$ V. In the present case a digital voltmeter was employed which had similar accuracy.

A1.1.2 Experiments

The experimental setup used in the calibration of the thermocouples is shown in Fig. A1.1. The constant temperature bath described in Section 4.9 was filled with Mobiltherm heat transfer oil. A base heating element of 1000 W was provided to reduce the temperature fluctuations. Fibre glass sleeves were put on both hot and cold junctions of each thermocouple to avoid coming in contact with one another. The hot junctions were put in a test tube filled with Mobiltherm (to provide uniform temperature to all the thermocouples) which in turn was immersed in the oil bath. A quartz thermometer (by Hewlett Packard, model 2801A) was employed as the standard thermometer, which was calibrated against Rosmount thermometer by DSIR (New Zealand) and which had an accuracy of ±0.01°C. The cold junctions of the thermocouples were immersed in a test tube containing transformer oil, which in turn was put in

FIGURE A1.2 A Typical Calibration Chart for the Thermocouples

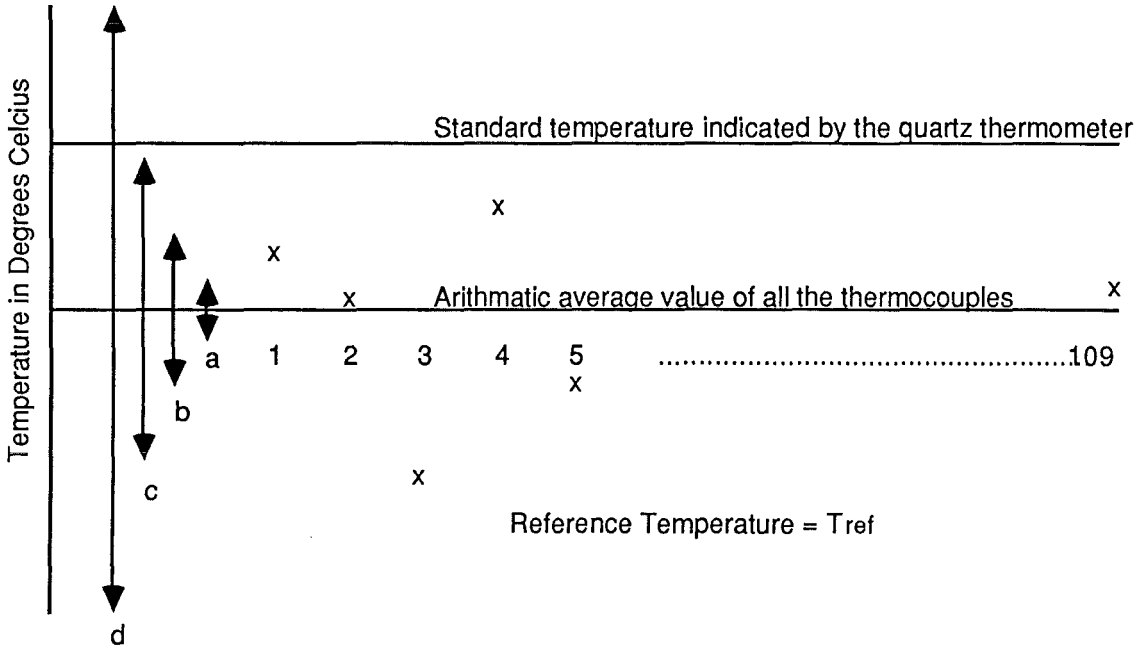

Notes: 1 to 109 represent thermocouple numbers

a = ±0.2 °C

b = ±0.5 °C

c = ±1.0 °C

d = ±2.0 °C

put in an ice bath. The oil was brought to a required temperature and readings of all the thermocouples were taken at hourly intervals during the day. The oil and ice bath temperatures were measured by the quartz thermometer. The average values of these hourly readings were used in calculations. This procedure was repeated for temperatures ranging from 20°C to about 190°C, at intervals of about 10°C.

A1.1.3 Analysis of results

It is very cumbersome to prepare calibration charts for each thermocouple because more than a hundred were calibrated and hence a different approach was followed. In the present investigation, it was sufficient to know how consistent each thermocouple was in the temperature range tested and what was the approximate accuracy of each thermocouple. The thermocouples were divided into four different categories based on their accuracies (or variations in comparison with the average value) and they are: ±0.2°C, ±0.5°C, ±1.0°C and ±2.0°C. For each temperature setting, the arithmetic average reading of all the emfs was evaluated, and the emfs of the thermocouples were plotted as shown in Fig. A1.2. This figure also shows the standard temeprature, (and ice reference temperature) which gives an indication of the absolute errors involved. It was found that the quartz thermometer always showed a higher value (up to 2.5°C), as compared to the values indicated by the thermocouples. In order to find the consistency, or the reliability of each thermocouple the Table A1.1 was prepared from the Fig.A1.2.

As shown in the Table A1.1, the thermocouples were categorised under the four accuracy limits, for each temperature setting. Different colours were used for different categories for easy identification. From this table, one could easily identify the behaviour of each thermocouple at various temperatures. The thermocouples behaving consistently within small temperature ranges, were employed at important locations. The actual figures (18 of them similar to Fig. A1.2) and tables (18 of them similar to Table A1.1) have not been included as they are too big and too many.

TABLE A1.1 Thermocouple Calibration

Average Temperature in °C	Accuracy Category	Thermocouple Numbers 1	2	3	.....	109
T_{av} 1	± 0.2 °C		x			x
	± 0.5 °C	x				
	± 1.0 °C			x		
	± 2.0 °C					
T_{av} 2	± 0.2 °C		x			x
	± 0.5 °C	x				
	± 1.0 °C			x		
	± 2.0 °C					
T_{av} 3	± 0.2 °C		x			x
	± 0.5 °C	x				
	± 1.0 °C			x		
	± 2.0 °C					
.....						
.....						
.....						
T_{av} 18	± 0.2 °C		x			x
	± 0.5 °C	x				
	± 1.0 °C			x		
	± 2.0 °C					

A1.2 Methods of Attachment

Air or liquid temperatures can be easily measured by locating hot junctions in the middle of the air cavity, or the centre of the liquid flow, but surface temperatures are very hard to measure accurately. There is no easy method of attaching a thermocouple to a surface so that it can be guaranteed to indicate the true surface temperature, which is possible only if the measuring junction attains but does not affect the surface temperature. In most cases, the presence of a thermocouple will cause a perturbation of the temperature distribution at the point of attachment, and thus, it will only indicate the perturbed temperature. In many cases, a significant difference exists between the indicated and the true surface temperatures. Hence, it was decided to perform an experiment to check the errors involved in attaching the thermocouples, and to find the best method of attachment.

A1.2.1 Theory

There are several methods of attaching thermocouples to various surfaces (Baker et al., 1953,1961). For thin materials the thermocouple junction is attached directly to the surface by welding, brazing, cementing or clamping to the surface. In the present case, they were attached either by soldering or using RTV or Araldite. In order to minimise the errors one should follow certain procedures (ASTM, 1974).

(1) To avoid perturbation errors smallest possible beads were used, which were made by fusing the thermocouple wires.

(2) To reduce conduction errors the thermocouple wires were brought away from the junction along an isotherm (parallel to the measuring surface) for at least 20 wire diameters.

(3) The measuring junction was located as close to the surface as possible rather than above or below it, thus maintaining very good contact.

(4) The installation was designed such that it causes minimum disturbance of any fluid flow or change in the emissivity of the surface, to avoid changes in convective or radiative heat transfer. Small diameter thermocouple wires were chosen to minimise disturbances to convective currents. Wherever possible, efforts were made to regain the emissivity of the surface, such as

FIGURE A1.3 Schematic Diagram of the Experimental Setup to Study the Method of Attachment of the Thermocouples

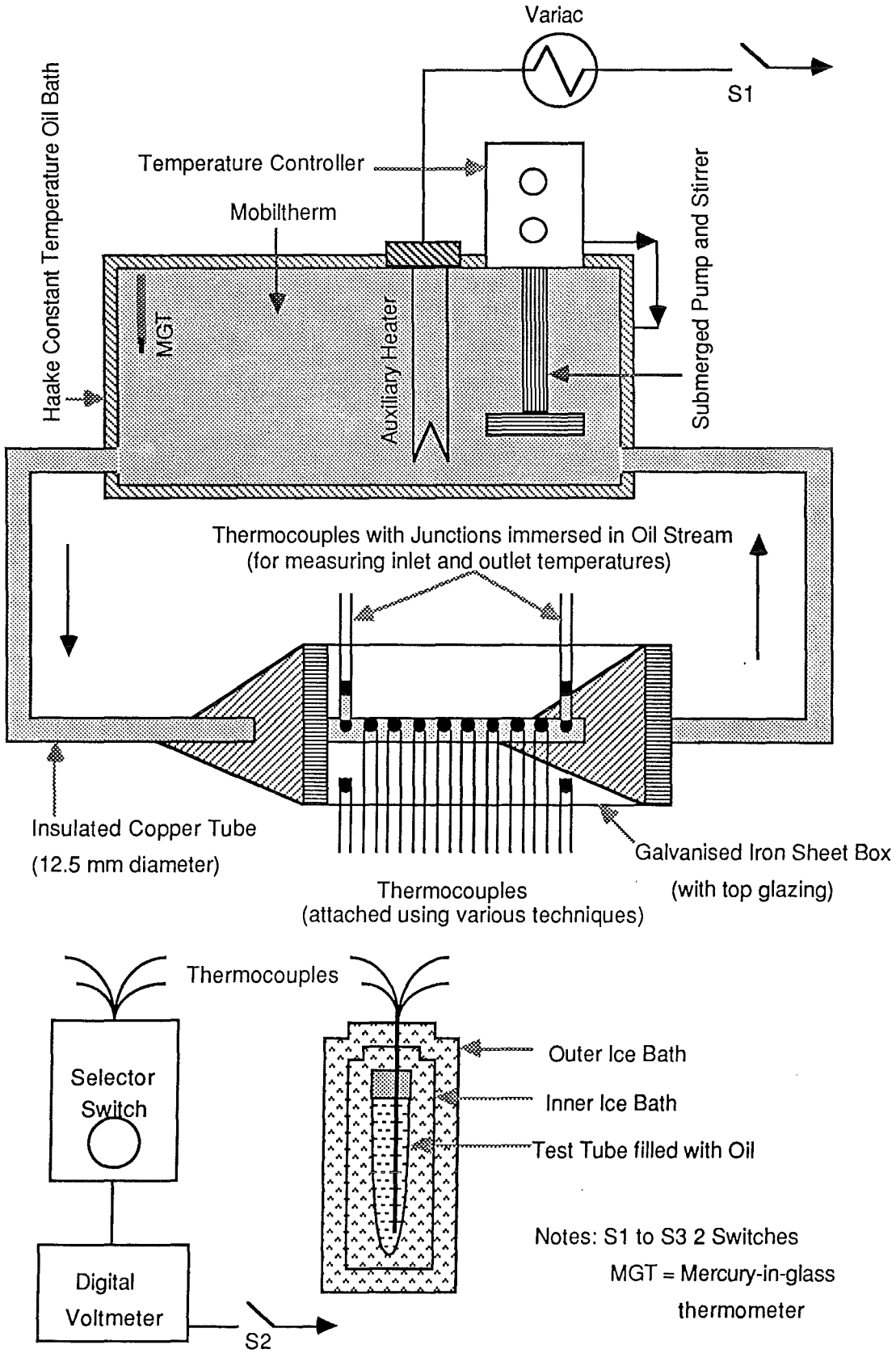

attaching a piece of reflector on the hot junction for measuring reflector temperature.

(5) The installation was designed, such that the total response is fast enough to cause negligible lag for the transient conditions.

(6) The thermal resistance and the thermal mass were reduced between the measuring junction and the surface.

(7) Wherever possible the junctions were well insulated from the ambient. For measuring the collector temperatures it was not possible to do so, as it would affect the radiation characteristics of the surface.

(8) The bare thermocouple wire, between the junction and the insulation was kept to a minimum.

A1.2.2 Experiments

An experiment was designed to study and compare the methods of attachment employed in the present investigation. The schematic diagram of the experimental setup is shown in Fig. A1.3. An outdoor test was designed with similar conditions to those experienced by the collector. The best 13 thermocouples from the previous calibration test were employed in this test in order to minimise the errors due to calibration.

A galvanised iron sheet box (0.25 m long) of triangular cross section was taken. A RFM reflector was fixed to the inside surface of the box and the glazing was fixed to the box opening. A copper tube (12.5 mm diameter) was passed through the box and connected to Haake's constant temperature oil bath. The bath and copper tube were insulated, to reduce the temperature fluctuations. Two small diameter copper tubes (just enough to pass a thermocouple) were brazed at the inlet, and the outlet of the box, but within the box (Fig. A1.3). Thermocouples were passed through each of these holes positioning them in such a way, that the junction remains at the centre of the tube and RTV sealant was used, to fill the gaps in order to avoid oil leaks. These two thermocouples provide the actual temperature of the oil. The other thermocouples were attached to the tube surface in between the inlet and the outlet connections, employing various quantities of high temperature solder, RTV and Araldite. A couple of thermocouples were fixed to the reflector surface, with RTV and one of them was covered with a piece of reflector material.

TABLE A1.2 Typical Set of Results for Testing the Method of Attachment of Thermocouples

Thermocouple Description	Thermocouple Readings in °C			
	Aperture Not Covered		Aperture Covered	
(1) Inlet oil temperature	173.1	88.0	169.0	85.6
(2) Outlet oil temperature	173.0	87.9	168.8	85.5
(3) TC soldered, a	165.9	84.0	159.0	84.1
(4) TC soldered, b	164.8	83.1	157.7	83.2
(5) TC soldered, c	165.4	83.3	158.3	83.7
(6) TC attached with RTV, a	158.4	81.7	150.8	82.6
(7) TC attached with RTV, b	143.1	73.9	134.3	76.3
(8) TC attached with RTV, c	147.2	76.4	139.7	78.2
(9) TC attached with RTV, and junction covered with reflector	151.2	77.9	144.3	79.7
(10) TC attached with Araldite, a	136.5	71.9	128.0	76.1
(11) TC attached with Araldite, b	150.7	77.7	142.8	79.3
(12) TC attached to reflector	37.9	29.3	33.4	32.1
(13) TC attached to reflector and junction covered with reflector	36.0	29.0	33.1	31.8
(14) Box air temperature	55.0	36.0	46.0	40.5

Notes: TC stands for thermocouple and
a, b, c stand for different amounts of the material used between the thermocouple junction and the surface.

The oil was pumped through the copper tube at a specified temperature, and hourly readings of the temperatures indicated by the thermocouples, and the air temperature in the box were noted down during the day, the averages were used for interpretation. This experiment was repeated at different temperatures ranging from about 20°C to 190°C at intervals of 10°C. The experiment was also repeated, with the box aperture covered with a cardboard, to find the effect of solar radiation on the temperature measurement. Typical results, at a couple of temperatures, (with and without covering the aperture) are shown in the Table A1.2.

A1.2.3 Analysis of results

As seen from the Table A1.2, the oil temperature indicated by the thermocouples actually immersed in oil, were much higher than the temperatures indicated by any other thermocouple. The closest ones to the true oil temperatures, were indicated by the thermocouples soldered to the copper tube, which showed 7° to 8°C lower values (at an oil temperature of 173°C) depending on the amount of solder used. However it may be noticed that the amount of solder was not very critical because of its high thermal conductivity. The temperatures indicated by the thermocouples attached with RTV, were much lower. (15° to 30°C at an oil temperature of 173°C). Also, the amount of RTV, did influence the thermocouple reading (up to 15°C) and hence, it was hard to find the effect of covering the junction with a reflector. The effect was more pronounced with Araldite attached thermocouples (22° to 37°C lower than the actual oil tempeature of 173°C) indicating lower thermal conductivity as compared to RTV. There was a small temperature drop by covering the junction of the thermocouple attached to the reflector. As seen from the Table A1.2, when the actual oil temperature drops to about 88°C, the errors with soldered, RTV and Araldite joints drop to 4°-5°C, 6°-14°C and 10°-16°C respectively. When the aperture was covered with cardboard, the errors with solder, RTV and Araldite increase to 10°-11°C, 18°-35°C and 26°-41°C respectively for an oil temperature of 169°C. This shows that when the thermocouples were in shade the air temperature and the temperatures indicated by the thermocouples decreased.

However, one should remember, that the tests were performed under most severe conditions, such as, very large temperature

difference between the air and the surface temperatures (about 120°C). In the actual situation, such large temperature drops, are seldom encountered. Hence, the absolute values of errors, can not be taken, as it depends on the testing conditions. However, this test did serve its purpose which was intended mainly for comparison.

APPENDIX A2

CALCULATIONS AND RESULTS OF EXPERIMENTS WITH ER1 AND ER2

This appendix gives calculations for ER1 and the summary of results for different runs for ER1 and ER2. In the final section, the heat transfer calculations for oil passing through the jacket are given.

A2.1 Calculations for ER1

The real COP can be evaluated from

$$COP_{real} = Q_l / Q_g \qquad (A2.1)$$

where Q_l is the energy leak into the cabinet and Q_g is the totral energy supplied to the generator.

In the case of the ambient controlled room Q_l can be found from

$$Q_l = U_o A_o (T_{amb} - T_{cab}) \qquad (A2.2)$$

where U_o is the overall heat transfer coefficient based on the outside area A_o of the refrigerator, T_{amb} the ambient temperature and T_{cab} the cabinet temperature.

In the case of the ambient controlled box, Q_l consists of two parts

(i) The first part Q_{l1} is from the backside of the refrigerator and it is given by $Q_{l1} = U_o A_1 (T_{abox} - T_{cab})$ (A2.3)

where T_{abox} is the ambient box temperature and A_1 is the area of the cabinet exposed to the ambient box (0.18 m^2)

(ii) The second part Q_{l2} is from the other parts of the cabinet and is given by $Q_{l2} = U_o A_2 (T_{amb} - T_{cab})$ (A2.4)

where A_2 is the area of the cabinet exposed to the external ambient (0.868 m^2). In these two cases U_o is assumed to be tha same for all surfaces of the refrigerator.

The heat leak Q_l can also be evaluated from the cabinet surface temperature measurements. As we know T_{amb}, T_{cab} and outside surface temperature T_{os} , the approximate inside surface temperature of the cabinet T_{is} can be found from (assuming the heat transfer coefficients and the areas to be the same for the inside and outside of the cabinet)

$$(T_{amb} - T_{os}) = (T_{is} - T_{cab}) \qquad (A2.5)$$

Then, Q_l can be calculated from

$$Q_l = \{k_i A_l (T_{os} - T_{is})\} / \Delta x_i \quad \text{(A2.6)}$$

where k_i is the thermal conductivity of the insulation material; A_l is the log mean area of the refrigerator; and Δx_i is the average thickness of the insulation.

It was found that the values of Q_l calculated from these two methods were in good agreement with each other (within ±5%) and the former method was adopted in the present case.

Q_g can be evaluated in three ways:

(1) from the voltmeter reading V1 volts and the ammeter reading A1 amperes as Q_g = V1 A1 Watts (A2.7)

(ii) from the time taken for 10 revolutions of the kilowatt-hour meter dial (t seconds) as 750 revolutions is equal to 1 kWhr and Q_g is given by

$$Q_g = 48000 / t \quad \text{Watts} \quad \text{(A2.8)}$$

(iii) from the kilowatt-hour meter reading K1 and K2 (in kWhrs) at different times t1 and t2 (in hours) Q_g is given by

$$Q_g = 1000 (K2 - K1) / (t2 - t1) \quad \text{(A2.9)}$$

It was found that Q_g found from these methods were within ±2%. However, the long term power consumption as obtained from the kWhr meter was used as it was the most reliable one.

As seen from Eq. (A2.2) it was necessary to know the overall heat transfer coefficient U_o, in order to evaluate the heat leak into the refrigerator. To find the actual value of U_o, the refrigerator was turned off, and the bulb B1 in the cabinet (Fig. 3.13) was turned on, maintaining the external ambient temperature at 30°C. The inside cabinet temperature and the power input to the bulb B1 were noted down at different times of the day, and average values were used in the calculations. It was assumed that the same value of U_o holds for heat flow in both directions. U_o can be evaluated from

$$U_o = 1 / (2/h_c + \Delta x_i/k_i) \quad \text{(A2.10)}$$

where h_c is the free convective film coefficient, at the refrigerator cabinet surface. It was assumed that the value of h_c was same at the inside and outside surfaces of the refrigerator cabinet and it can be evaluated from

$$T_{ia} - T_{oa} = (Q_b/A_o) (2/h_c + \Delta x_i/k_i) \quad \text{(A2.11)}$$

where T_{ia} and T_{oa} are the inside air and outside air temperatures respectively and Q_b is the power input to the bulb B1.

Substituting Q_b = 12.5 W, A_o = 1.048 m^2, Δx_i = 0.04 m, T_{oa} = 30°C, T_{ia} = 45.2°C and k_i = 0.036 $W.m^{-2}.K^{-1}$ in Eq. (A2.11) we get

h_c = 12.7 $W.m^{-2}.K^{-1}$

From Eq. (A2.10) we get U_o = 0.79 $W.m^{-2}.K^{-1}$

A2.2 Summary of Results for ER1 and ER2

The summary of results of the experiments conducted with Electrolux refrigerators ER1 and ER2 are given in Tables A2.1 and A2.2 respectively. They list the ideal and real COP values, temperatures of the various components of the system and ambient temperature for different runs with ER1 and ER2.

A2.3 Calculations for Oil Passing Through the Jacket

Instead of having to use a secondary heat pipe, the oil can be directly pumped through the jacket, provided the necessary amount of energy (75 W) can be transferred to the ammonia solution in the generator tube, and this aspect is verified in this section.

As seen from Fig. 5.5 there are 8 fins and total area of heat transfer A_{Tf} = 200 cm^2

The oil side film coefficient is the controlling factor and it may be evaluated from Sieder-Tate relationship for laminar flow in circular tubes (McCabe and Smith, 1956).

$$Nu = 2\ (Gz)^{1/3}\ \phi_v \qquad \text{(A2.12)}$$

where Nu is the Nusselt number, Gz is the Greatz number and ϕ_v is the viscosity correction factor and they are given by

$$Nu = h_o\ D_{eq} / k_o \qquad \text{(A2.13a)}$$

$$Gz = 2\ \{(m_o\ c_{po})\ /\ (k_o\ L_j)\}^{1/3} \qquad \text{(A2.13b)}$$

$$\phi_v = (\ \mu_o\ /\ \mu_w)^{0.14} \qquad \text{(A2.13c)}$$

where h_o is the oil side film coefficient; k_o, c_{po}, and m_o are the thermal conductivity, specific heat capacity and mass flow rate, respectively, of the oil; L_j is the effective length of the jacket, which is equal to the length of the fin; μ_o and μ_w are the viscosities of the oil at average oil temperature T_{oa} and the tube wall temperature T_w, respectively; D_{eq} is the equivalent diameter of the jacket and it is given by

D_{eq} = 4 (Cross sectional area / Wetted perimeter) (A2.14)

D_{eq} can be evaluated from Fig. 3.33 and it is equal to 4.7 mm.

TABLE A2.1 Summary of Results of Experiments with Electrolux Refrigerator ER1

(a) Experiments with ambient box

Quantity to be varied:- Supply voltage to the heating element (at an ambient of about 30°C)

Supply Voltage to Heating Element, V	260	250	240	230	220	210	200	190	180	170
(1) Power to heating element, W	132	122	117	104	101	90	85	80	74	69
(2) Element casing temperature, °C	214	209	203	192	188	185	179	174	169	165
(3) Generator temperature, °C	156	155	153	151	150	149	147	145	143	140
(4) Cabinet temperature, °C	12.7	12.3	10.7	9.6	9.1	10.4	11.4	13.2	13.6	27.5
(5) Evaporator temperature, °C	-8.3	-8.0	-9.4	-9.9	-10.1	-8.9	-6.5	-2.0	-0.3	27.4
(6) Condenser temperature, °C	46	45	41	38	37	36	36	34	31	29
(7) Absorber temperature, °C	43	42	39	36	34	34	33	32	29	28
(8) Ambient box temperature, °C	33	33	32	31	30	30	30	30	27	28
(9) External ambient temperature, °C	28	29	26	27	26	27	27	27	26	30
(10) Total heat leak into cabinet, W	13.4	14.5	13.3	14.6	14.9	14.5	13.2	11.9	10.1	0.5
(11) Ideal COP	1.29	1.33	1.34	1.49	1.54	1.61	1.64	2.01	2.38	-
(12) Real COP	.102	.118	.114	.139	.147	.162	.155	.148	.136	.006

TABLE A2.1 Summary of Results of Experiments with Electrolux Refrigerator ER1 *(Continued)*

(b) Experiments with ambient box

Quantity to be varied:- Supply voltage to the heating element (at an ambient of about 26°C)

Supply Voltage to Heating Element, V	230	220	210	200	190	180	170
(1) Power to heating element, W	104	101	90	85	80	74	69
(2) Element casing temperature, °C	194	183	180	178	176	172	167
(3) Generator temperature, °C	152	150	149	146	143	141	139
(4) Cabinet temperature, °C	8.4	7.9	9.6	10.2	12.7	14.2	16.6
(5) Evaporator temperature, °C	-11.5	-11.8	-9.8	-8.2	-2.8	0.1	3.3
(6) Condenser temperature, °C	39	37	37	36	33	31	30
(7) Absorber temperature, °C	35	34	34	33	31	29	28
(8) Ambient box temperature, °C	25	24	25	25	28	27	26
(9) External ambient temperature,°C	25	25	26	26	28	28	28
(10) Total heat leak into cabinet, W	13.7	13.5	13.0	12.2	12.2	10.5	8.7
(11) Ideal COP	1.43	1.48	1.54	1.64	2.06	2.39	2.79
(12) Real COP	0.132	0.133	0.145	0.144	0.153	0.141	0.127

TABLE A2.1 Summary of Results of Experiments with Electrolux Refrigerator ER1 *(Continued)*

(c) Experiments with ambient room

Quantity to be varied:- Supply voltage to the heating element and ambient temperature

Supply Voltage to Heating Element, V	250	200	180	170	230	230	230	230
(1) Power to heating element, W	106	68	55	50	90	88	84	87
(2) Element casing temperature, °C	221	190	181	180	211	208	203	204
(3) Generator temperature, °C	159	152	147	140	160	158	155	154
(4) Cabinet temperature, °C	18	17	19	27	29	22	16	13
(5) Evaporator temperature, °C	-4.2	-4.9	2.1	21.8	6.2	-1.4	-5.6	-9.1
(6) Condenser temperature, °C	62	52	47	41	68	62	56	51
(7) Absorber temperature, °C	56	48	45	37	64	58	52	47
(8) Ambient box temperature, °C	-	-	-	-	-	-	-	-
(9) External ambient temperature, °C	30	30	30	30	40	35	30	25
(10) Total heat leak into cabinet, W	9.7	10.7	9.3	2.2	9.4	11.1	11.2	10.3
(11) Ideal COP	0.971	1.16	1.49	5.1	1.01	0.992	1.05	1.10
(12) Real COP	0.092	0.158	0.167	0.044	0.105	0.125	0.133	0.117

TABLE A2.2 Summary of Results of Experiments with Electrolux Refrigerator ER2

Quantity to be varied:- Supply voltage to the heating element (at an ambient of about 26°C)

Supply Voltage to Heating Element, V	260	250	240	230	220	210	200	190	180
(1) Power to heating element, W	165	154	143	132	120	110	99	91	82
(2) Element casing temperature, °C	333	331	317	304	294	277	262	262	249
(3) Generator temperature, °C	195	192	188	186	183	180	175	173	168
(4) Cabinet temperature, °C	-1	-2	-5	-6	-6.2	-6.4	-2.1	-2.2	1.0
(5) Freezer temperature, °C	-15	-16.6	-17	-18.3	-18.4	-19.0	-17.1	-15.7	-13.5
(6) Condenser temperature, °C	38	37	38	36	37	35	37	34	35
(7) Absorber temperature, °C	46	43	46	38	40	36	39	35	35
(8) Ambient temperature,°C	26	26	26	26	26	26	27	26	26
(9) Overall heat transfer coefficient between cabinet and ambient, $W.m^{-2}.K^{-1}$	.754	.700	.754	.754	.765	.754	.700	.700	.660
(10) Total heat leak into cabinet, W	39	33	39	41	42	41	36	33	28
(11) Ideal COP	1.55	1.52	1.45	1.52	1.45	1.50	1.45	1.56	1.62
(12) Real COP	.189	.217	.274	.312	.344	.373	.367	.362	.337

TABLE A2.2 Summary of Results of Experiments with Electrolux Refrigerator ER2 *(Continued)*

Quantity to be varied:- Supply voltage to the heating element (at an ambient of about 26°C)

Supply Voltage to Heating Element, V	170	160	150	140	130	120	110	100
(1) Power to heating element, W	76	67	61	52	46	36	30	24
(2) Element casing temperature, °C	235	233	209	197	185	171	163	157
(3) Generator temperature, °C	165	161	154	150	141	135	129	126
(4) Cabinet temperature, °C	3.6	8.0	9.2	12	15	20	23	26
(5) Freezer temperature, °C	-12.1	-7.6	-3.9	1.5	8.6	14.2	18.8	23
(6) Condenser temperature, °C	34	34	34	33	32	27	30	30
(7) Absorber temperature, °C	34	35	33	33	31	30	30	28
(8) Ambient temperature, °C	26	27	26	26	26	26	26	26
(9) Overall heat transfer coefficient between cabinet and ambient, $W.m^{-2}.K^{-1}$	.646	.565	.56	.54	.53	.47	.44	.42
(10) Total heat leak into cabinet, W	24.2	20.6	18.1	13.2	9.8	5.4	2.2	.35
(11) Ideal COP	1.67	1.84	1.97	2.34	3.18	5.80	6.67	10.7
(12) Real COP	.321	.305	.259	.256	.215	.150	.074	.015

TABLE A2.2 Summary of Results of Experiments with Electrolux Refrigerator ER2 *(Continued)*

Quantity to be varied:- Ambient temperature

Supply Voltage to Heating Element, V	230	230	230	230
(1) Power to heating element, W	132	132	132	132
(2) Element casing temperature, °C	289	290	291	294
(3) Generator temperature, °C	174	175	177	178
(4) Cabinet temperature, °C	-7	-1	2	7
(5) Freezer temperature, °C	-21	-16	-12	-9
(6) Condenser temperature, °C	34	41	45	49
(7) Absorber temperature, °C	38	46	50	56
(8) Ambient temperature, °C	22	31	35	41
(9) Overall heat transfer coefficient between cabinet and ambient, $W.m^{-2}.K^{-1}$	0.72	0.76	0.775	0.79
(10) Total heat leak into cabinet, W	35.1	40.9	42.6	45.2
(11) Ideal COP	1.37	1.32	1.28	1.21
(12) Real COP	0.260	0.309	0.320	0.343

As the temperature difference between T_{oa} and T_w is not high, ϕ_v can be taken as one. Substituting the oil properties at 175°C, L_j = 130 mm, D_{eq} = 4.7 mm and m_o = 3 kg.hr^{-1} in Eq. (A2.12) we get the oil side film coefficient h_o = 265 W.m^{-2}.K^{-1}

As the major resistance to heat transfer is due to the oil film, the overall heat transfer coefficient based on the outside area U_o is approximately equal to h_o. The temperature drop across the oil film ΔT_{of} may be obtained from

$$Q_{net} = U_o A_{tf} \Delta T_{of} \qquad \text{(A2.15)}$$

where Q_{net} is the net heat transferred, which is equal to 75W.

Hence, we obtain from Eq. (A2.15) ΔT_{of} = 14 K. If the temperature drop is to be controlled at a lower value say 10 K, the mass flow rate of the oil can be increased, which in turn enhances h_o. It can be found from Eqs. (A2.12) and (A2.15) that, by increasing m_o to 8.5 kg.hr^{-1}, h_o increases to 375 W.m^{-2}.K^{-1} and ΔT_{of} reduces to 10 K.

FIGURE A3.1 Top Half of HSA-SCCR Collector

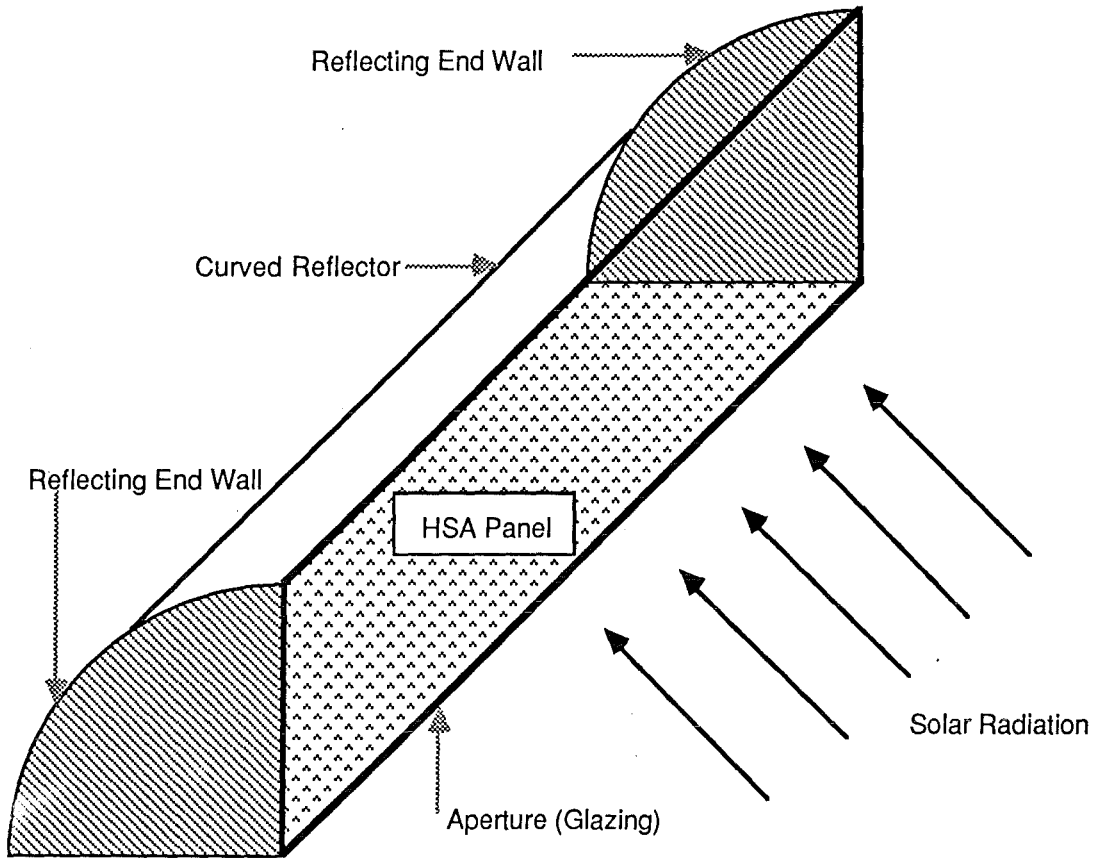

APPENDIX A3

HSA-SCCR COLLECTOR GEOMETRY EVALUATION

In order to evaluate the actual geometry of the HSA-SCCR collector the following questions need to be answered.

(1) What happens to a ray entering the aperture of the collector ?

(2) How many hours of solar radiation can the colector collect in a day ?

(3) What is the energy flux distribution on the absorber plate at different incidence angles and how can it be evaluated for a particular set of collector dimensions, properties of materials used and solar insolation ?

(4) How to evaluate the performance of the SCCR ?

The methods of determining the answers to each of these questions are described in the Sections A3.1 to A3.4 which follow.

A3.1 Solar Radiation Entering the Aperture of SCCR

The top quadrant of the collector is shown in Fig. A3.1 Any point inside the quadrant may be represented by the three coordinates in L, R and λ directions.

Consider an arbitrary ray crossing the aperture plane in a minus λ angular direction. The ray can be resolved into two components: one in the λ-R plane and another in the L direction. For specular reflections (assuming that a specular reflector is chosen as the reflector material), each of these components can be considered independently (Kooi, 1978). The component in the λ-R plane strikes the absorber directly or is reflected at the curved reflector. Its component in the $-\lambda$ angular direction is unchanged, by the reflection, since the angles of reflection and incidence are equal. The same agrument holds for any subsequent reflection so that the ray eventually proceeds to the absorbing plane. This is also true for the L component. Thus, the end planes can impart only longitudinal momentum and the cylindrical surface can impart only radial momentum to a photon upon reflection. Therefore, it can be concluded that any radiation entering the aperture which is specularly reflected, must eventually reach the absorber, provided

FIGURE A3.2 Perspective View of Sun's Daily Motion Relative to Equatorial Plane

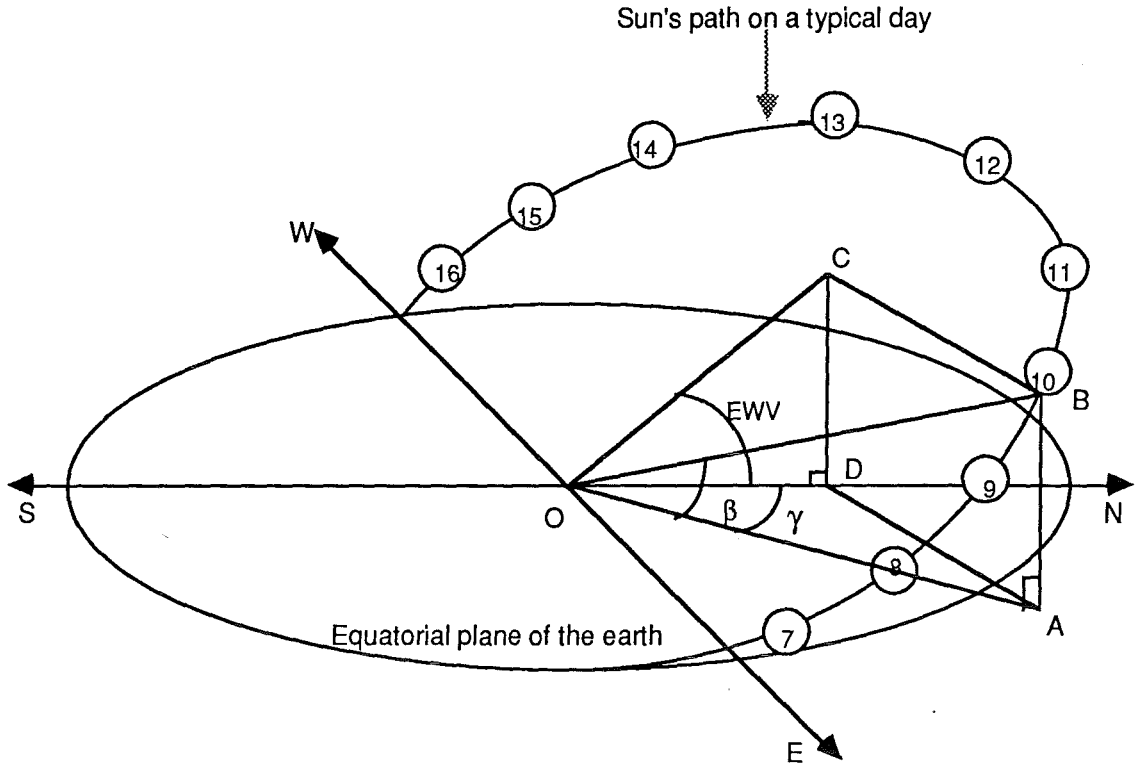

Notes: The numbers represent the position of sun at different times of the day

O = Site of interest (origine)

B = Position of the sun at 10-00 hours

OB = Sun's ray

OA = Projection of OB on the horizontal plane

OC = Projection of OB on the N-S vertical plane

OD = Projection of OC on the horizontal plane

γ = Solar altitude angle

β = Solar azimuth angle

EWV = East west view angle

it is not absorbed by the reflector or the medium (which is air) or the inner glazing.

If a collector is chosen with reflecting end walls, it becomes optically infinitely long and the flux component in the L direction is always accepted provided the sun is not behind the collector. It is the λ-R component which determines the number of hours a day, that the SCCR collects solar radiation. When the longitudinal axis of the collector is in the East-West direction and the collector facing the equator, the λ-R plane becomes the North-South vertical plane and the λ-L plane becomes the East-West vertical plane. So the limiting factor determining collection time is the component of the solar flux on the North-South vertical plane.

A3.2 Collection Time of SCCR in a Day

In order to determine the collection time of any fixed concentrator it is necessary to know the motion of the sun. Since all motion is relative, it is convenient to call the earth fixed and to describe the sun's virtual motion in a coordinate system fixed to the earth with its origin at the site of interest. Keeping this in mind the perspective view of the sun's daily motion relative to the equatorial plane is shown in Fig. A3.2. The sun is constrained to move with two degrees of freedom on the celestial sphere and as a result the location of the sun can be specified by two angles

(a) The solar altitude angle β is the angle in the vertical plane between the sun's rays and the projection of the sun's rays on the horizontal plane.

(b) The azimuth angle γ is the angle in the horizontal plane, between a line running due North-South, and the projection of the sun's rays on the horizontal plane. The sign convention for azimuth angle is positive east of the North-South line and negative West of it.

As seen in the previous section, the component of solar flux in the North-South vertical plane determines the collection time, and this projection of solar altitude in the North-South vertical plane is called EWV angle, which can be evaluated using the following equation (Tabor, 1958).

$$EWV = \tan^{-1} (\tan \beta \sec \gamma) \qquad (A3.1)$$

FIGURE A3.3 EWV Angle Versus Date Parametric in Time (Tabor, 1958)

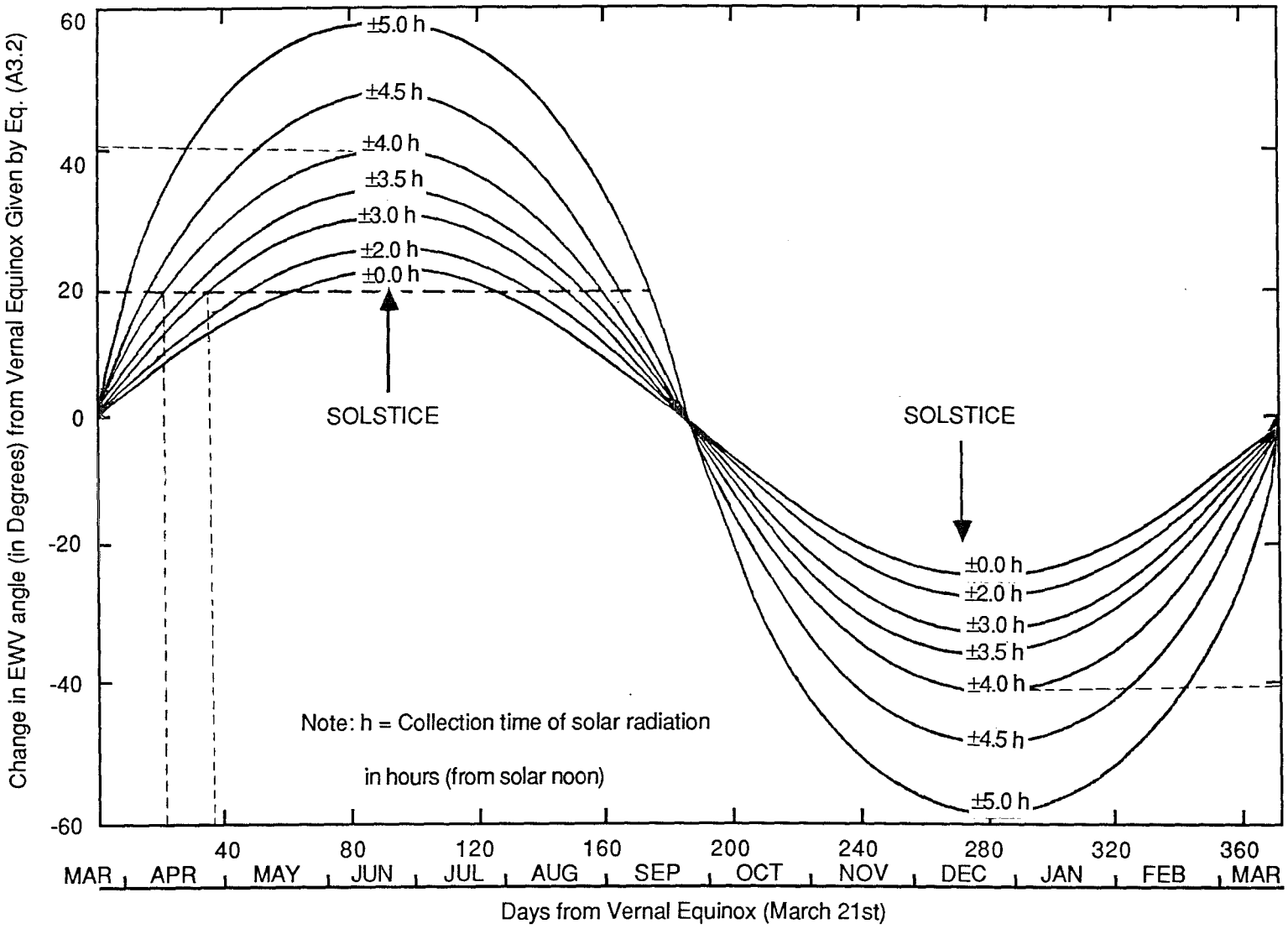

If the EWV angle lies within the acceptance angle of the collector (which is defined as the angle within which all the incident radiation is reflected to the absorber), the sun's beam and diffused radiation will be accepted. The change in EWV with time is the angle which must be accommodated by any cylindrical reflector systems mounted in the east-west direction. If this change (denoted by V) is measured from the equinox position, it becomes independent of latitude and is given by

$$V = EWV - (90^\circ - \phi) \qquad (A3.2)$$

where ϕ is the latitude in degrees.

It may be shown (Liu and Jordan, 1963; Jordan, 1967) that to a first approximation

$$\tan V = \tan \{23.5 \sin (360n/365)\} / \cos (15t) \qquad (A3.3)$$

where n is the number of days from vernal equinox (March 21) and t is the time in hours measured from solar noon. 23.5° is the "half swing" of the noon solar altitude during a year.

The values of V are plotted in Fig. A3.3 against days from equinox. This figure may be used to determine how many hours a day a cylindrical collector mounted in the East-West direction, with a given acceptance angle will accept beam radiation without any tracking aid. For example, a cylindrical collector with an acceptance angle of ±20° will accept beam radiation from the sun for four hours either side of solar noon on the 23rd day after the equinox (April 13), but will only accept beam radiation for three hours either side of noon 39 days after the equinox (April 29th) and would not collect any on the solstice (June 21). It also shows that to accept direct radiation for at least four hours either side of solar noon all year requires an acceptance angle of ±41° or 82°. The acceptance angles of some common cylindrical reflectors are shown in Fig. A3.4. The SCCR collector has an acceptance angle of ±45° (90°) and so it will accept direct radiation for at least four hours and 17 minutes, on either side of solar noon, every day of the year and hence, does not require tracking. Fig. A3.3 also shows that except for days near the equinox, the collector will be subjected to widely varying angles of incidence during the course of a single day.

Sometimes it is convenient to replot Fig. A3.3, as a function of time and parametric in the number of days from the equinox as shown in Fig. A3.5. In order to illustrate the use of Fig. A3.5, the dotted line has been added corresponding to the collector with

FIGURE A3.4 Accepted Angles for a Few Selected Solar Reflectors

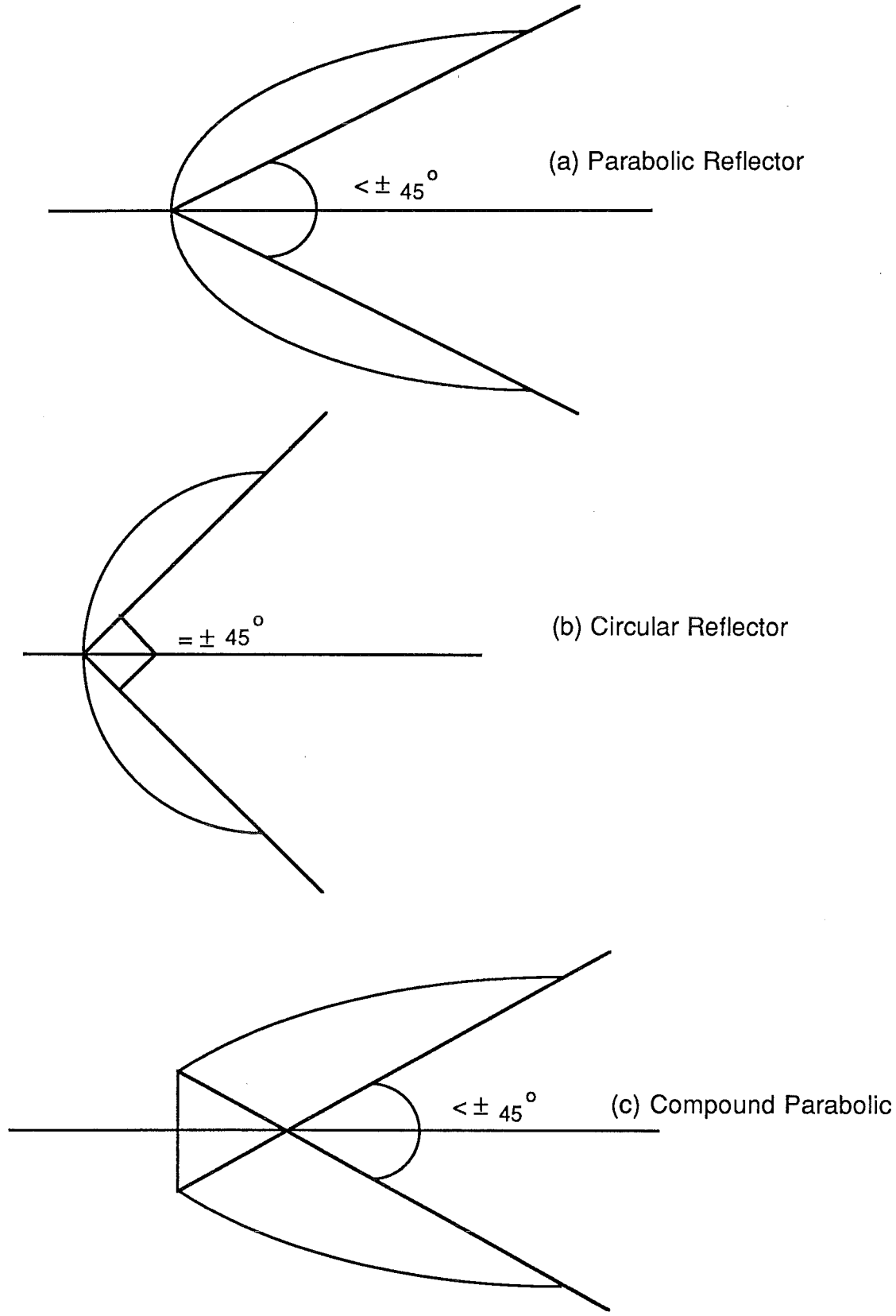

FIGURE A3.5 EWV Angle Versus Time Prametric in Number of Days from Vernal Equinox (March 21st)

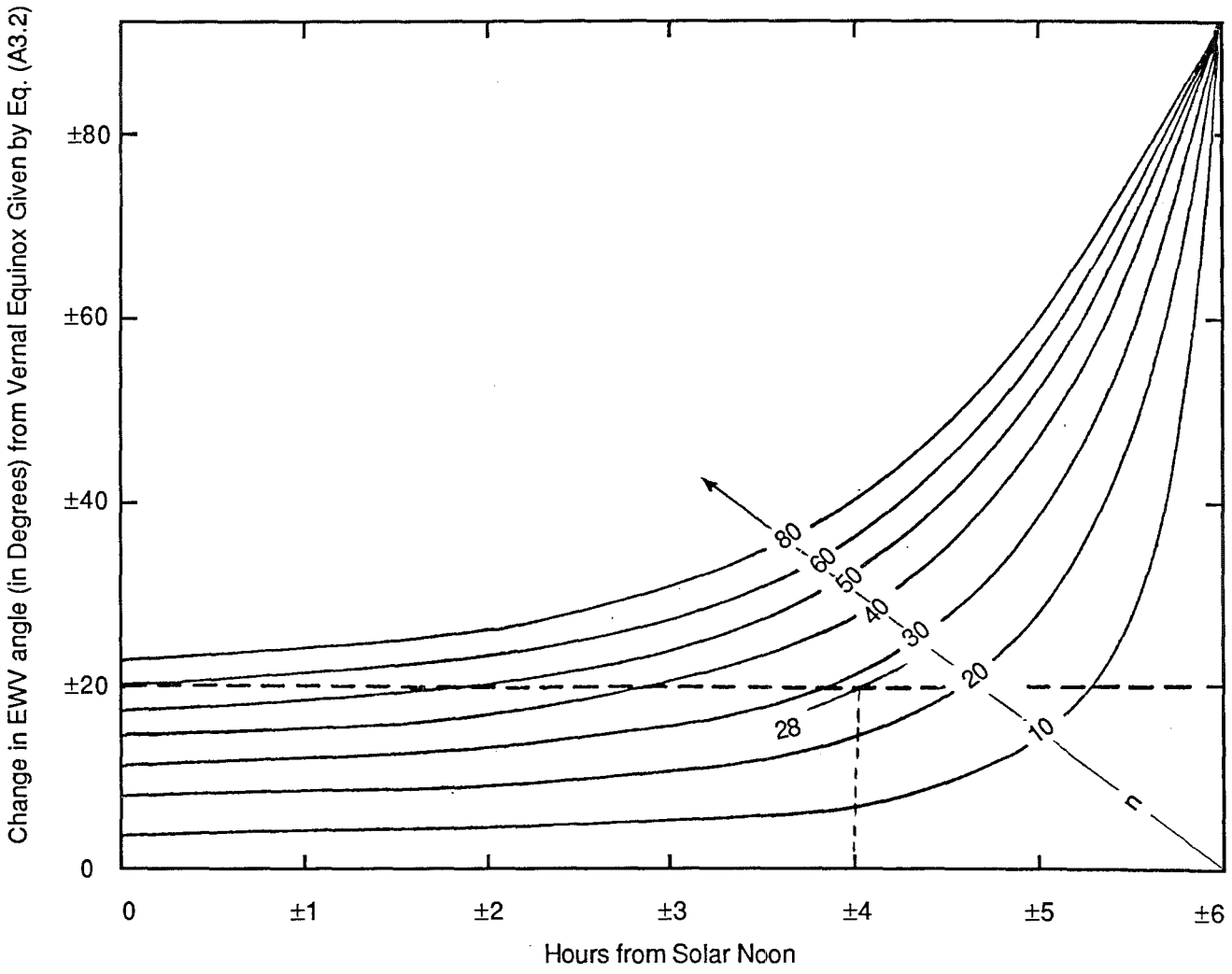

FIGURE A3.6 Reflection Path for Incident Rays (for Bottom Quadrant)

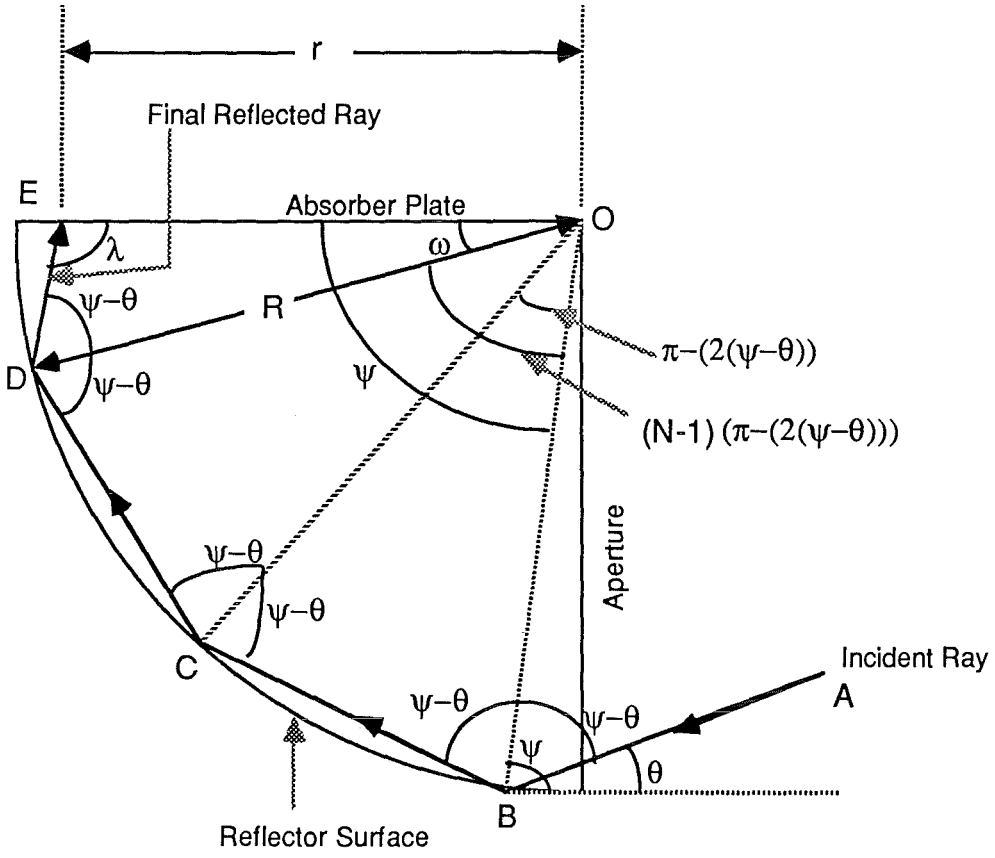

Notes: N = Number of times ray is reflected (3 in the present case)

Ψ = Rim angle at the point of first contact with the reflector

θ = Angle of incidence

R = Radius of the reflector

r = Distance on the absorber where the ray AB finally lands

λ = angle between the final reflected ray and the absorber

ω = angle subtended by the final reflected ray at the centre

O = centre of curvature

AB = Incident ray

an acceptance angle of ±20° mounted in the East-West direction. From Fig. A3.5, it can be seen that the collector will be collecting less than four hours on either side of noon, on all days farther than 28 days from the equinox, and that it will not collect at all outside of 60 days from the equinox.

At this stage it is necessary to distinguish between the acceptance angle of the SCCR with the HSA panel and without the panel. Acceptance angle denotes coverage of the angular zone within which radiation is accepted (that is "seen") by the receiver and so in the case of a flat plate collector it is ±90° (180°), neglecting the effect of angle of incidence on glazing transmissivity. The acceptance angle of SCCR, without the panel remains the same that is 45°, because the trough type reflectors normally have a line of focus and hence, the receivers employed are usually tubes. However, SCCR with the panel in its axial plane has an acceptance angle of much more than ±45°, in fact equal to ±90° because, as shown in Appendix A3.1, any ray entering the aperture must strike the panel. This makes it behave exactly like a flat plate collector, with the only difference being uneven and time dependent flux distribution on the panel (this however is taken care of by the isothermal nature of the HSA panel).

A3.3 Energy Flux Distribution on the Absorber Plate

The energy flux may be determined by following the paths of individual rays as they enter the collector and are reflected to the absorber. These ray traces are used to develop analytical equations, which in turn are solved using the computer programme TPEFD to get the flux distribution.

Fig. A3.6 shows the bottom half of the reflector along with the nomenclature used. Consider a ray AB incident on the reflector at B at an angle of incidence of θ. Angle of incidence is defined as the angle made by an incoming ray and the absorber plate (or plane parallel to the absorber plate). The ray AB is reflected at points B, C, D on the reflector surface, before finally reaching the absorber plate at E, which is at a distance of 'r' (defined positive in minus X direction) from the centre 'O'. The angle between the final reflected ray and the absorber plate is λ. The rim angle ψ is defined as the angle betwen the line OB and the absorber plate, where the line OB is the line joining the first point of contact B of the incident ray with the reflector and the

centre 'O'. As the angle of incidence is equal to the angle of reflection we have

$$\angle ABO = \angle OBC = \angle BCO = \angle OCD = \angle CDO = \angle ODE = \psi - \theta \quad (A3.4)$$

By the application of sine rule to the triangle ODE we have

$$r / \sin(\psi - \theta) = R / \sin \lambda \quad (A3.5)$$

If ω is the angle subtended by the final reflected ray at the centre and if all the angles are expressed in radians, from triangle ODE we have

$$\lambda = \pi - (\psi - \theta) - \omega \quad (A3.6)$$

Similarly from triangle OBC

$$\angle BOC = \pi - 2(\psi - \theta) \quad (A3.7)$$

If N represents the total number of reflections before the ray strikes the absorber plate, we have from Eq. (A3.7)

$$\angle BOD = (N - 1)\{\pi - 2(\psi - \theta)\} \quad (A3.8)$$

$$\text{Also } \angle DOE = \angle BOE - \angle BOD \quad (A3.9)$$

From Eqs. (A3.8) and (A3.9) we get

$$\omega = \psi - (N - 1)\{\pi - 2(\psi - \theta)\} \quad (A3.10)$$

On rearranging Eq. (A3.10)

$$\omega = \pi(1 - N) + \psi(2N - 1) + 2\theta(1 - N) \quad (A3.11)$$

Substituting Eq. (A3.11) into (A3.6) and rearranging gives

$$\lambda = N\pi - 2N\psi + (2N - 1)\theta \quad (A3.12)$$

By substituting Eq. (A3.12) into (A3.5), we get

$$(r/R) = \frac{\sin(\psi - \theta)}{\sin\{N\pi - 2N\psi + (2N - 1)\theta\}} \quad (A3.13)$$

Equation (A3.13) gives the location along the absorber, where a reflected ray terminates, as a function of the angle of incidence (θ), the number of reflections made (N), the rim angle (ψ), which describes the position of incident ray upon the reflector and the radius of the reflector (R). For the special case of r = R, the rim angle ψ attains a maximum valve of ψ_{max}, we get from Eq. (A3.13)

$$\sin(\psi_{max} - \theta) = \sin\{N\pi - 2N\psi_{max} + (2N - 1)\theta\} \quad (A3.14)$$

Solving Eq. (A3.14) gives the maximum rim angle for N reflections.

$$\psi_{max} - \theta = N\pi - 2N\psi_{max} + (2N - 1)\theta + 2I\pi \quad (A3.15)$$

where I is any integer or zero. By rearranging Eq. (A3.15) we have

$$\psi_{max} = \{N\pi + 2N\theta + 2I\pi\} / (2N + 1) \quad (A3.16)$$

It can be seen from the Eq. (A3.16), that for each value of N there will be (2N+1) solutions because of the last term in the

FIGURE A3.7 Reflection Path for Incident Rays (for Top Quadrant)

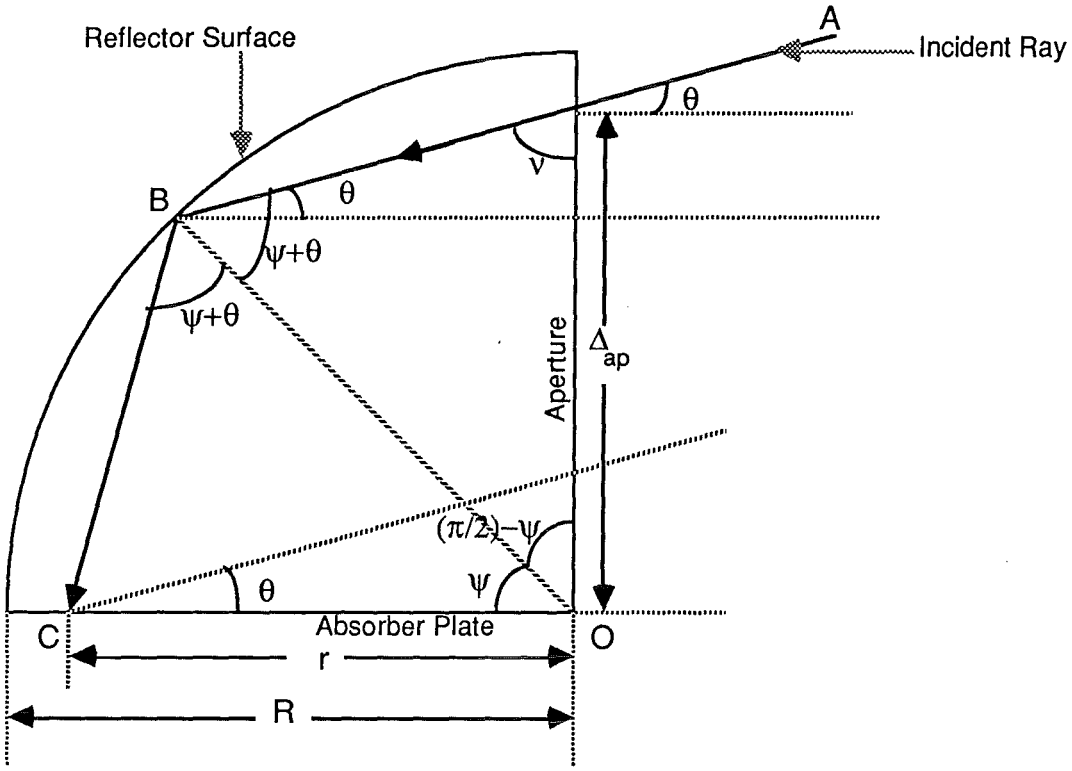

Notes: Ψ = Rim angle at the point of first contact with the reflector

θ = Angle of incidence

R = Radius of the reflector

r = Distance on the absorber where the ray AB finally lands

O = centre of curvature

AB = Incident ray

$\frac{W_{ap}}{\Delta_{ap}}$ = Fracti0on of aperture corresponding to rim angle

numerator $(2I\pi)$. However, there are only two meaningful solutions, one for the top quadrant and one for the bottom quadrant. The other solutions relate to radiation originating from the opaque (convex) side of the reflector which does not enter the real collector, or to the radiation which is absorbed by the absorber and incident directly on it.

For the bottom quadrant the required solution is for I = 0 and from Eq. (A3.16) we have

$$\psi_{max,b} = \{N\pi + 2N\theta\} / \ (2N + 1) \qquad (A3.17)$$

A similar analysis of the top quadrant yields

$$(r/R)_t = \frac{\sin(\psi + \theta)}{\sin\{N\pi - 2N\psi - (2N - 1)\theta\}} \qquad (A3.18)$$

Solving Eq. (A3.18) for ψ_{max}, we get

$$\psi_{max,t} = \{N\pi - 2N\theta\} / \ (2N + 1) \qquad (A3.19)$$

As we know the maximum rim angle for an SCCR, for a particular value of the angle of incidence, we can determine using Eqs. (A3.17) and (A3.19), the number of reflections any ray incident on the reflector will make, before striking the absorber. Eqs. (A3.13) and (A3.18) show where on the absorber the reflected radiation lands.

Now we can divide the reflector into a large number of small segments (Δ_{ap}) each subtending a rim angle of $\Delta\psi$. Also correspondingly the absorber can be divided into a large number of small segments (Δ_{ab}) and the amount of incident energy reflected by $\Delta\psi$ can be placed in the appropriate segment Δ_{ab}, if the fraction of the aperture through which the radiation striking $\Delta\psi$ passes, can be determined.

Fig. A3.2 shows an incident ray AB in the top half of the reflector, which is complementary to the bottom half shown in Fig. A3.6. As shown in Fig. A3.7, θ is the angle of incidence, ψ is the rim angle, BC is the reflected ray, 'O' is the centre and aperture segment covered by AB is Δ_{ap}. In the triangle OAB, when all the angles are expressed in radians

$$\angle ABO = \psi + \theta \text{ and } \angle AOB = (\pi/2) - \psi \qquad (A3.20)$$

If $\angle OAB = \nu$ then

$$\pi = \nu + (\psi + \theta) + \{(\pi/2) - \psi\} \qquad (A3.21)$$

By solving Eq. (A3.21) for ν we have

$$\nu = (\pi/2) - \theta \qquad (A3.22)$$

Applying the sine rule to the triangle ABO

$$R / \sin \nu = \Delta_{ap} / \sin (\psi + \theta) \qquad \text{(A3.23)}$$

Substituting ν value from Eq. (A3.22) and rearranging Eq. (A3.23) we have

$$\Delta_{ap} / R = \sin (\psi + \theta) / \sin \{(\pi/2) - \theta\} \qquad \text{(A3.24)}$$

$$\text{But } R = 0.5\ W_{ap} \qquad \text{(A3.25)}$$

where W_{ap} = aperture width

Substituting Eq. (A3.25) into (A3.24)

$$\Delta_{ap} / W_{ap} = [\sin (\psi + \theta) / \sin \{(\pi/2) - \theta\}]\ 0.5 \qquad \text{(A3.26)}$$

where Δ_{ap} / W_{ap} may be recognised as the fraction of the aperture corresponding to a rim angle ψ. But the fraction of the aperture corresponding to each element is required, and to obtain this two corrections need to be applied to Eq. (A3.26). The first correction is to subtract the sum of the aperture fractions for all the preceding $\Delta\psi$'s from Eq. (A3.26) and the second correction is to subtract from the same equation the fraction of the aperture corresponding to radiation, which is directly incident on the absorber (that is $\psi = 0$). Incorporating these two corrections in Eq. (A3.26) we have

$$(\Delta_{ap}/W_{ap})_{\Delta\psi=k} = (A3.26) - \sum_{\Delta\psi=1}^{\Delta\psi=k-1} (A3.26) - (\Delta_{ap}/W_{ap})_{\Delta\psi=0} \qquad \text{(A3.27)}$$

By substituting $\psi = 0$ in Eq. (A3.26) we get

$$(\Delta_{ap}/W_{ap})_{\Delta\psi=0} = (\tan \theta) / 2 \qquad \text{(A3.28)}$$

Combining the Eqs. (A3.27) and (A3.28) we get

$$(\Delta_{ap}/W_{ap})_{\Delta\psi=k} = (A3.26) - \sum_{\Delta\psi=1}^{\Delta\psi=k-1} (A3.26) - (\tan \theta)/2 \qquad \text{(A3.27)}$$

As $\Delta\psi$, Δ_{ab} and Δ_{ap} are made very small, the continuous function of the energy flux distribution on the absorber is produced as a function of θ. This function appears discontinuous, as it consists of an overlay of several continuous functions, one for each value of N.

It can be noticed that Figs. A3.1 and A3.2 show the relationships between incident and reflected rays lying in the plane of the diagram; however, the same relationships apply to incident rays tilted out of the plane of the diagram. The reflected rays give the same projection on to the plane of the diagram as produced by the corresponding projection of the incident rays. Thus for a given EWV altitude the pattern of the

reflection of solar radiation is established and this pattern remains the same for all rays with the same EWV altitude with only a drift along its own length. This is a result of the universal equality of angle of reflection and angle of incidence.

The computer programme TPEFD calculates the energy flux as a function of absorber width for a given value of the angle of incidence. The input parameters to the programme include the angle of incidence (θ); the specular reflectivity of the reflector material ($\rho_{ref,s}$); the aperture area (A_{ap}); the solar insolation (I) the rim angle increment ($\Delta\psi$); and the number of absorber plate segments (that is, R/Δ_{ab}). The output parameters include - the maximum value of the number of reflections (N) in each quadrant; the energy flux on each segment; and the integrated total energy on the absorber plate. A listing of the programme TPEFD and a set of results on 24th February, 1984 at 1 p.m., for $\Delta\psi = 0.05°$, $\Delta_{ab} = R/75$, $\theta = 10.15°$, $I = 946.6\ W.m^{-2}$, $A_{ap} = 0.56212\ m^{-2}$ and $\rho_{ref,s} = 0.76$, are included at the end of this appendix. It should be noted that glazing transmittance is not taken into consideration as that would reduce all the flux quantities by the same proportion, thus not affecting the comparison.

A3.4 Reflector Performance

The performance of the reflector may be determined by obtaining the energy flux on the absorber plate as a function of angle of incidence and this has been done in Section A3.3 of this appendix. Using the computer programme TPEFD, the energy flux distributions on the absorber plate, for three angles of incidence 0°, 22.5° and 45° were calculated. These are diagramatically represented in Fig. 4.8.

A3.5 Programme Listing of TPEFD

```
100 REM **********     COMPUTER PROGRAMME TPEFD     **********
110 REM                ************************
120 REM
130 REM THIS PROGRAMME CALCULATES THE ENERGY FLUX
140 REM DISTRIBUTION ALONG THE ABSORBER PLATE OF THE SEMI
150 REM CIRCULAR CYLINDRICAL REFLECTOR - HEAT SHEET ABSORBER
160 REM COLLECTOR BY USING THE RAY TRACE TECHNIQUES
170 REM
180 REM THE EFFECT OF THE ANGLE OF INCIDENCE AND OTHER INPUT
190 REM VARIABLES CAN BE FOUND BY SIMPLY CHANGING THE SAME
200 REM
210 REM THE INPUT VARIABLES TO THE PROGRAMME ARE:
220 A$="(1) THE APERTURE AREA OF THE COLLECTOR A1 IN SQ.M"
230 B$="(2) THE SPECULAR REFLECTANCE OF THE REFLECTOR R1"
240 C$="(3) THE SOLAR INSOLATION E IN W/SQ.M"
250 D$="(4) THE ANGLE OF INCIDENCE B IN DEGREES"
260 E$="(5) THE RIM ANGLE INCREMENT X IN DEGREES"
270 F$="(6) THE NUMBER OF ABSORBER PLATE SEGMENTS Z"
280 REM
290 REM THE OUTPUT VARIABLES OF THE PROGRAMME ARE:
300 G$="(1) THE PERCENTAGE OF THE APERTURE COVERED"
310 H$="(2) THE MAXIMUM VALUE OF THE NUMBER OF REFLECTIONS"
320 REM (3) THE ENERGY FLUX ON EACH SEGMENT IN W/SQ.M
330 REM (4) THE INTEGRATED TOTAL ENERGY ON THE ABSOBER PLATE
340 REM NOTE: THE OUTPUT VARIABLES ARE GIVEN FOR-
350 REM       (a) THE TOP QUADRANT
360 REM       (b) THE BOTTOM QUADRANT
370 REM       (c) THE TOTAL COLLECTOR
380 REM
390 DIM G(100),W(100),S(100),V(100),U(100),M(100),D(100)
400 OPEN "TPEFD.DAT" FOR OUTPUT AS FILE #5
410 REM
420 REM TO READ THE INPUT DATA
430 REM
440 READ A1,R1,E,X,Z,B
450 DATA 0.56212,0.76,946.4,0.05,75,10.15
460 Y=1/Z
470 A2=B
480 REM
490 REM TO RESET REGISTERS TO ZERO
500 REM
510 FOR C=0 TO 100
520 S(C)=0
530 G(C)=0
540 V(C)=0
550 U(C)=0
560 M(C)=0
570 W(C)=0
580 D(C)=0
590 NEXT C
600 H=0
610 REM
620 REM TO CONVERT THE ANGLE OF INCIDENCE TO RADIANS
630 REM
640 A2=A2*2*PI/360
650 REM
660 REM CALCULATIONS FOR THE TOP QUADRANT
670 REM --------------------------------
```

```
680 REM
690 REM TO CALCULATE THE MAXIMUM RIM ANGLE AS A FUNCTION OF
700 REM THE ANGLE OF INCIDENCE
710 REM
720 P1=(PI/2)-(2*A2)
730 REM
740 REM TO CONVERT THE MAXIMUM RIM ANGLE TO DEGREES
750 REM
760 Q1=P1*180/PI
770 FOR I=0 TO Q1 STEP X
780 IF I>0 THEN  GO TO 1030
790 REM
800 REM TO CALCULATE THE FRACTION OF THE APERTURE COVERED BY
810 REM THE RADIATION WHICH IS NOT REFLECTED
820 REM BUT DIRECTLY INCIDENT ON THE ABSORBER PLATE
830 REM
840 G(I)=(SIN(A2)/COS(A2))*.5
850 REM
860 REM TO SUM THE FRACTION OF APERTURE COVERED
870 REM
880 H=H+G(I)
890 REM
900 REM TO CALCULATE THE POWER RECIEVED IN THAT FRACTION
910 REM
920 F(I)=G(I)*A1*E
930 REM
940 REM TO CALCULATE THE INTENSITY ON EACH ABSORBER SEGMENT
950 REM
960 FOR J=0 TO Z-1
970 S(J)=S(J)+F(I)*Y
980 NEXT J
990 GO TO 1340
1000 REM
1010 REM TO CONVERT THE COUNTER TO RADIANS
1020 REM
1030 C=I*2*PI/360
1040 REM
1050 REM TO CALCULATE THE FRACTION OF APERTURE COVERED BY
1060 REM THE RADIATION
1070 REM CORRESPONDING TO THE CURRENT RIM ANGLE INTERVAL
1080 REM
1090 G(I)=((SIN(C+A2)/SIN((PI/2)-A2))*.5)-H
1100 H=H+G(I)
1110 IF I=X THEN N=1
1120 REM
1130 REM TO CALCULATE MAXIMUM RIM ANGLE FOR N REFLECTIONS
1140 REM
1150 P2=(N*PI)/(2*N+1)-(2*N*A2)/(2*N+1)
1160 REM
1170 REM TO CHECK TO SEE WHICH REFLECTION REGION WE ARE IN
1180 REM
1190 IF C>P2 THEN N=N+1
1200 REM
1210 REM TO CALCULATE THE DISTANCE ALONG THE ABSORBER PLATE
1220 REM IN MINUS X DIRECTION
1230 REM THAT THE RADIATION LANDS
1240 REM
1250 R=SIN(C+A2)/SIN(PI*N-(2*N*C)-(2*N-1)*A2)
1260 REM
1270 REM TO PLACE THE INTENSITY IN TO PROPER ABSORBER PLATE
```

```
1280 REM SEGMENT
1290 REM
1300 FOR J=0 TO Z-1
1310 IF (Z*R)<=J THEN S(J)=S(J)+G(I)*R1^N*E*A1 \ GO TO 1340
1330 NEXT J
1340 NEXT I
1350 PRINT #5,"* RESULTS OF THE COMPUTER PROGRAMME TPEFD *"
1360 PRINT #5,"  ***************************************"
1370 PRINT #5
1380 PRINT #5
1390 PRINT #5,"THE INPUT VARIABLES TO THE PROGRAMME ARE:"
1400 PRINT #5,"----------------------------------------"
1410 PRINT #5
1420 PRINT #5,A$;" = ";A1
1430 PRINT #5,B$;" = ";R1
1440 PRINT #5,C$;" = ";E
1450 PRINT #5,D$;" = ";B
1460 PRINT #5,E$;" = ";X
1470 PRINT #5,F$;" = ";Z
1480 PRINT #5
1490 PRINT #5,"THE OUTPUT VARIABLES TO THE PROGRAMME ARE:"
1500 PRINT #5,"-----------------------------------------"
1510 PRINT #5
1520 PRINT #5,"(A) RESULTS FOR THE TOP QUADRANT"
1525 PRINT #5,"--------------------------------"
1530 PRINT #5
1540 PRINT #5,G$;" = ";H*100
1550 PRINT #5,H$;" = ";N
1560 PRINT #5
1570 REM
1580 FOR K=0 TO Z-1
1590 IF K=0 THEN V(K)=S(K) \ GO TO 1630
1610 V(K)=V(K-1)+S(K)
1620 REM
1630 REM TO CALCULATE THE FLUX
1640 REM
1650 S(K)=S(K)/(.39/Z)
1660 NEXT K
1670 I$="THE ENERGY FLUX ON                    INTEGRATED"
1680 J$="   EACH SEGMENT                         TOTAL"
1690 K$="    IN W/SQ.M                          IN WATTS"
1700 L$="-----------------------------------------------"
1710 PRINT #5,L$
1720 PRINT #5,I$
1730 PRINT #5,J$
1740 PRINT #5,K$
1750 PRINT #5,L$
1760 PRINT #5
1770 FOR K=0 TO Z-1
1780 PRINT #5," SEG";K+1;"=";S(K);"                    ";V(K)
1790 NEXT K
1800 PRINT #5,L$
1810 PRINT #5
1820 REM
1830 REM CALCULATIONS FOR THE BOTTOM QUADRANT
1840 REM ------------------------------------
1850 REM
1860 H=0
1870 REM
1880 REM TO CONVERT THE ANGLE OF INCIDENCE TO DEGREES FOR
```

```
1890 REM COUNTER
1900 REM
1910 A3=A2*180/PI
1920 FOR I=A3+X TO 90 STEP X
1930 IF I=A3+X THEN N=1
1940 REM
1950 REM TO CALCULATE MAXIMUM RIM ANGLE FOR N REFLECTIONS
1960 REM
1970 P2=(N*PI)/(2*N+1)+(2*N*A2)/(2*N+1)
1980 REM
1990 REM TO CONVERT THE COUNTER TO RADIANS
2000 REM
2010 C=I*2*PI/360
2020 REM
2030 REM TO CHECK TO SEE WHICH REFLECTION REGION WE ARE IN
2040 REM
2050 IF C>P2 THEN N=N+1
2060 REM
2070 REM TO CALCULATE THE DISTANCE ALONG THE
2080 REM ABSORBER IN THE MINUS X
2090 REM DIRECTION WHERE THE RADIATION LANDS
2100 REM
2110 R=SIN(C-A2)/SIN(PI*N-(2*N*C)+(2*N-1)*A2)
2120 REM
2130 REM TO CALCULATE THE FRACTION OF THE
2140 REM APERTURE COVERED BY RADIATION
2150 REM CORRESPONDING TO THE CURRENT RIM ANGLE INTERVAL
2160 REM
2170 G(I)=(SIN(C-A2)/SIN(PI/2+A2))*.5-H
2180 REM
2190 REM TO SUM THE FRACTION OF THE APERTURE COVERED
2200 REM
2210 H=H+G(I)
2220 REM TO PLACE THE POWER RECEIVED IN TO THE
2230 REM APPROPRIATE SEGMENT REGISTER
2240 REM
2250 FOR J=Z-1 TO 0 STEP -1
2260 IF (Z*R)>=J THEN M(J)=M(J)+(G(I)*R1^N*E*A1) \
     GO TO 2290
2280 NEXT J
2290 NEXT I
2300 PRINT #5
2310 PRINT #5,"(B) RESULTS FOR THE BOTTOM QUADRANT"
2320 PRINT #5,"-----------------------------------"
2330 PRINT #5
2340 PRINT #5,G$;" = ";H*100
2350 PRINT #5,H$;" = ";N
2360 FOR K=0 TO Z-1
2370 IF K=0 THEN U(K)=M(K) \ GO TO 2410
2390 U(K)=U(K-1)+M(K)
2400 REM
2410 REM TO CALCULATE THE FLUX
2420 REM
2430 M(K)=M(K)/(.39/Z)
2440 NEXT K
2450 PRINT #5,L$
2460 PRINT #5,I$
2470 PRINT #5,J$
2480 PRINT #5,K$
2490 PRINT #5,L$
```

```
2500 PRINT #5
2510 FOR K=0 TO Z-1
2520 PRINT #5," SEG";K+1;"=";M(K);"                    ";U(K)
2530 NEXT K
2540 PRINT #5,L$
2550 PRINT #5
2560 REM
2570 REM TO SUM UP FOR TOP AND BOTTOM QUADRANTS
2580 REM
2590 FOR K=0 TO Z-1
2600 D(K)=M(K)+S(K)
2610 W(K)=U(K)+V(K)
2620 NEXT K
2630 PRINT #5
2640 PRINT #5,"(C) FOR THE WHOLE COLLECTOR"
2650 PRINT #5,"--------------------------"
2660 PRINT #5
2670 PRINT #5,L$
2680 PRINT #5,I$
2690 PRINT #5,J$
2700 PRINT #5,K$
2710 PRINT #5,L$
2720 PRINT #5
2730 FOR K=0 TO Z-1
2740 PRINT #5," SEG";K+1;"=";D(K);"                    ";W(K)
2750 NEXT K
2760 PRINT #5,L$
2770 CLOSE #5
2780 END
```

A3.6 Results File TPEFD.DAT

```
**** RESULTS OF THE COMPUTER PROGRAMME TPEFD ****
     ***************************************

THE INPUT VARIABLES TO THE PROGRAMME ARE:
-----------------------------------------
(1) THE APERTURE AREA OF THE COLLECTOR A1 IN SQ.M =  .56212
(2) THE SPECULAR REFLECTANCE OF THE REFLECTOR R1 =  .76
(3) THE SOLAR INSOLATION E IN W/SQ.M =  946.4
(4) THE ANGLE OF INCIDENCE B IN DEGREES =  10.15
(5) THE RIM ANGLE INCREMENT X IN DEGREES =  .05
(6) THE NUMBER OF ABSORBER PLATE SEGMENTS Z =  75

THE OUTPUT VARIABLES TO THE PROGRAMME ARE:
------------------------------------------

(A) RESULTS FOR THE TOP QUADRANT
--------------------------------
(1) THE PERCENTAGE OF THE APERTURE COVERED =  49.9999
(2) THE MAXIMUM VALUE OF THE NUMBER OF REFLECTIONS =  4

-----------------------------------------------
THE ENERGY FLUX ON          INTEGRATED
   EACH SEGMENT               TOTAL
    IN W/SQ.M                IN WATTS
-----------------------------------------------
 SEG 1 = 122.104              0.63494
 SEG 2 = 122.104              1.26988
 SEG 3 = 122.104              1.90482
 SEG 4 = 122.104              2.53976
 SEG 5 = 122.104              3.1747
 SEG 6 = 122.104              3.80964
 SEG 7 = 122.104              4.44458
 SEG 8 = 122.104              5.07952
 SEG 9 = 122.104              5.71446
 SEG 10 = 122.104             6.3494
 SEG 11 = 122.104             6.98434
 SEG 12 = 122.104             7.61928
 SEG 13 = 122.104             8.25422
 SEG 14 = 122.104             8.88916
 SEG 15 = 122.104             9.5241
 SEG 16 = 122.104             10.159
 SEG 17 = 122.104             10.794
 SEG 18 = 122.104             11.4289
 SEG 19 = 122.104             12.0639
 SEG 20 = 122.104             12.6988
 SEG 21 = 122.104             13.3337
 SEG 22 = 122.104             13.9687
 SEG 23 = 122.104             14.6036
 SEG 24 = 122.104             15.2386
 SEG 25 = 122.104             15.8735
 SEG 26 = 122.104             16.5084
 SEG 27 = 122.104             17.1434
 SEG 28 = 122.104             17.7783
 SEG 29 = 122.104             18.4133
 SEG 30 = 122.104             19.0482
 SEG 31 = 122.104             19.6831
 SEG 32 = 122.104             20.3181
 SEG 33 = 122.104             20.953
```

SEG 34 = 122.104	21.588
SEG 35 = 122.104	22.2229
SEG 36 = 122.104	22.8578
SEG 37 = 122.104	23.4928
SEG 38 = 122.104	24.1277
SEG 39 = 122.104	24.7626
SEG 40 = 122.104	25.3976
SEG 41 = 122.104	26.0325
SEG 42 = 122.104	26.6675
SEG 43 = 122.104	27.3024
SEG 44 = 122.104	27.9373
SEG 45 = 122.104	28.5723
SEG 46 = 122.104	29.2072
SEG 47 = 122.104	29.8422
SEG 48 = 122.104	30.4771
SEG 49 = 122.104	31.112
SEG 50 = 122.104	31.747
SEG 51 = 7841.11	72.5208
SEG 52 = 3254.19	89.4426
SEG 53 = 2361.36	101.722
SEG 54 = 1890	111.55
SEG 55 = 1641.88	120.087
SEG 56 = 1392.65	127.329
SEG 57 = 1238.48	133.769
SEG 58 = 1088.75	139.431
SEG 59 = 987.002	144.563
SEG 60 = 953.045	149.519
SEG 61 = 811.804	153.74
SEG 62 = 802.684	157.914
SEG 63 = 719.993	161.658
SEG 64 = 678.734	165.188
SEG 65 = 632.793	168.478
SEG 66 = 626.613	171.737
SEG 67 = 568.322	174.692
SEG 68 = 511.026	177.349
SEG 69 = 539.888	180.157
SEG 70 = 483.897	182.673
SEG 71 = 462.66	185.079
SEG 72 = 1283.15	191.751
SEG 73 = 866.233	196.256
SEG 74 = 783.265	200.329
SEG 75 = 903.537	205.027

(B) RESULTS FOR THE BOTTOM QUADRANT

(1) THE PERCENTAGE OF THE APERTURE COVERED = 49.9923
(2) THE MAXIMUM VALUE OF THE NUMBER OF REFLECTIONS = 5

THE ENERGY FLUX ON EACH SEGMENT IN W/SQ.M	INTEGRATED TOTAL IN WATTS
SEG 1 = 68.9305	0.358439
SEG 2 = 103.396	0.896096
SEG 3 = 103.395	1.43375
SEG 4 = 137.856	2.1506
SEG 5 = 103.39	2.68823
SEG 6 = 137.846	3.40503

SEG 7 = 137.839	4.12179
SEG 8 = 137.828	4.8385
SEG 9 = 137.817	5.55515
SEG 10 = 172.254	6.45087
SEG 11 = 172.229	7.34646
SEG 12 = 206.64	8.42099
SEG 13 = 172.166	9.31625
SEG 14 = 240.975	10.5693
SEG 15 = 240.898	11.822
SEG 16 = 240.814	13.0742
SEG 17 = 275.1	14.5048
SEG 18 = 309.326	16.1132
SEG 19 = 343.468	17.8993
SEG 20 = 343.208	19.684
SEG 21 = 411.463	21.8236
SEG 22 = 445.225	24.1387
SEG 23 = 478.803	26.6285
SEG 24 = 546.265	29.4691
SEG 25 = 579.193	32.4809
SEG 26 = 645.701	35.8385
SEG 27 = 711.458	39.5381
SEG 28 = 776.278	43.5748
SEG 29 = 839.941	47.9425
SEG 30 = 902.195	52.6339
SEG 31 = 929.668	57.4681
SEG 32 = 988.738	62.6096
SEG 33 = 1013.02	67.8773
SEG 34 = 1035.67	73.2627
SEG 35 = 1024.68	78.5911
SEG 36 = 1012.9	83.8582
SEG 37 = 1000.32	89.0599
SEG 38 = 956.337	94.0328
SEG 39 = 882.67	98.6227
SEG 40 = 870.526	103.149
SEG 41 = 828.458	107.457
SEG 42 = 787.191	111.551
SEG 43 = 718.275	115.286
SEG 44 = 707.72	118.966
SEG 45 = 641.499	122.302
SEG 46 = 604.741	125.446
SEG 47 = 595.85	128.545
SEG 48 = 533.784	131.321
SEG 49 = 526.089	134.056
SEG 50 = 492.515	136.617
SEG 51 = 459.932	139.009
SEG 52 = 428.326	141.236
SEG 53 = 422.347	143.432
SEG 54 = 367.622	145.344
SEG 55 = 386.855	147.356
SEG 56 = 333.962	149.092
SEG 57 = 353.07	150.928
SEG 58 = 301.976	152.499
SEG 59 = 298.196	154.049
SEG 60 = 294.387	155.58
SEG 61 = 268.325	156.975
SEG 62 = 265.014	158.353
SEG 63 = 240	159.601
SEG 64 = 237.168	160.835
SEG 65 = 234.318	162.053
SEG 66 = 210.527	163.148

SEG 67 = 208.138	164.23
SEG 68 = 1093.68	169.917
SEG 69 = 772.045	173.932
SEG 70 = 592.431	177.013
SEG 71 = 508.9	179.659
SEG 72 = 634.001	182.956
SEG 73 = 635.489	186.26
SEG 74 = 662.126	189.703
SEG 75 = 553.345	192.581

(C) FOR THE WHOLE COLLECTOR

THE ENERGY FLUX ON EACH SEGMENT IN W/SQ.M	INTEGRATED TOTAL IN WATTS
SEG 1 = 191.034	0.993379
SEG 2 = 225.499	2.16598
SEG 3 = 225.499	3.33857
SEG 4 = 259.96	4.69036
SEG 5 = 225.493	5.86293
SEG 6 = 259.95	7.21467
SEG 7 = 259.943	8.56637
SEG 8 = 259.932	9.91802
SEG 9 = 259.921	11.2696
SEG 10 = 294.357	12.8003
SEG 11 = 294.333	14.3308
SEG 12 = 328.744	16.0403
SEG 13 = 294.27	17.5705
SEG 14 = 363.079	19.4585
SEG 15 = 363.002	21.3461
SEG 16 = 362.918	23.2333
SEG 17 = 397.204	25.2987
SEG 18 = 431.43	27.5422
SEG 19 = 465.572	29.9631
SEG 20 = 465.311	32.3828
SEG 21 = 533.567	35.1573
SEG 22 = 567.329	38.1074
SEG 23 = 600.907	41.2321
SEG 24 = 668.368	44.7076
SEG 25 = 701.296	48.3544
SEG 26 = 767.805	52.347
SEG 27 = 833.562	56.6815
SEG 28 = 898.381	61.3531
SEG 29 = 962.045	66.3557
SEG 30 = 1024.3	71.6821
SEG 31 = 1051.77	77.1513
SEG 32 = 1110.84	82.9277
SEG 33 = 1135.12	88.8303
SEG 34 = 1157.77	94.8507
SEG 35 = 1146.79	100.814
SEG 36 = 1135	106.716
SEG 37 = 1122.43	112.553
SEG 38 = 1078.44	118.161
SEG 39 = 1004.77	123.385
SEG 40 = 992.63	128.547
SEG 41 = 950.562	133.49

SEG 42 = 909.295	138.218
SEG 43 = 840.379	142.588
SEG 44 = 829.824	146.903
SEG 45 = 763.603	150.874
SEG 46 = 726.845	154.654
SEG 47 = 717.954	158.387
SEG 48 = 655.888	161.798
SEG 49 = 648.192	165.168
SEG 50 = 614.618	168.364
SEG 51 = 8301.05	211.53
SEG 52 = 3682.51	230.679
SEG 53 = 2783.71	245.154
SEG 54 = 2257.63	256.894
SEG 55 = 2028.73	267.443
SEG 56 = 1726.61	276.422
SEG 57 = 1591.55	284.698
SEG 58 = 1390.72	291.929
SEG 59 = 1285.2	298.612
SEG 60 = 1247.43	305.099
SEG 61 = 1080.13	310.716
SEG 62 = 1067.7	316.268
SEG 63 = 959.993	321.26
SEG 64 = 915.902	326.022
SEG 65 = 867.111	330.531
SEG 66 = 837.141	334.884
SEG 67 = 776.46	338.922
SEG 68 = 1604.71	347.267
SEG 69 = 1311.93	354.089
SEG 70 = 1076.33	359.686
SEG 71 = 971.56	364.738
SEG 72 = 1917.16	374.707
SEG 73 = 1501.72	382.516
SEG 74 = 1445.39	390.032
SEG 75 = 1456.88	397.608

TABLE A4.1 Heat Pipe Working Fluids (Dunn and Reay, 1978)

Medium	Melting point (°C)	Boiling point at atmos.press. (°C)	Useful range (°C)
Helium	-272	-269	-271 - -269
Nitrogen	-210	-196	-203 - -160
Ammonia	-78	-33	-60 - 100
Freon 11	-111	24	-40 - 120
Pentane	-130	28	-20 - 120
Freon 113	-35	48	-10 - 100
Acetone	-95	57	0 - 120
Methanol	-98	64	10 - 130
Flutec PP2*	-50	76	10 - 160
Ethanol	-112	78	0 - 130
Heptane	-90	98	0 - 150
Water	0	100	30 - 200
Flutec PP9*	-70	160	0 - 225
Thermex	12	257	150 - 395
Mercury	-39	361	250 - 650
Caesium	29	670	450 - 900
Potassium	62	774	500 - 1000
Sodium	98	892	600 - 1200
Lithium	179	1340	1000 - 1800
Silver	960	2212	1800 - 2300

* Included for cases where electrical insulation is a requirement

The useful operating temperature range is indicative only

APPENDIX A4

SELECTION OF HSA WORKING FLUID

For a given set of operating conditions the performance of a thermosyphon heat pipe depends mainly on the heat pipe fluid. Hence the selection of a proper working fluid for the HSA is very important. Saski (1978) reviewed both organic and inorganic working fluids, available for use in heat pipes, in the temperature range of 50°C to 350°C, and concluded that aromatics and metal halides are suitable. Jenkins (1978) investigated specifically fluids to be used in HSA panels, but in the low temperature range. A selection of working fluids is shown in Table A4.1, with melting points and boiling points at atmospheric pressure, and useful temperature ranges (Dunn & Raey, 1978).

The first consideration in the identification of a suitable working fluid is the operating temperature range. As indicated in Chapter 3, the operating temperature of the collector was anticipated to be 150° to 160°C. From Table A4.1 the three fluids water, Flutec PP9 (a patented fluid produced by the Imperial Smelting Co. Ltd.) and Thermex (or Dowtherm A) can be chosen based on their useful temperature range. Various properties of these three fluids at different temperatures are listed in Tables A4.2a,b,c.

In order to determine the most acceptable of these fluids, a variety of characteristics must be examined. Dowtherm A was found to be appropriate in the present situation, as evident from the following discussion.

(1) Compatibility : This is an important property, as incompatibility with the HSA wall material might result in the generation of non-condensible gas or corrosion problems. The presence of non condensible gas, which accumulates in the condenser section, can be identified by a sharp temperature drop at the gas/vapour interface. Corrosion causes damage of the panel or degradation of the fluid. It results in local hot spots, or reduction in thermal conductivity due to the deposition of solid materials, in the evaporator section. Exhaustive compatibility tests have been carried out with various fluids (mainly organic)

TABLE A4.2a Properties of Water

(Dunn and Reay, 1978)

Temp.	Latent Heat of Vapo-risation	Liquid Density	Vapour Density	Liquid Thermal Conduc-tivity	Liquid Viscos.	Vapour Viscos.	Vapour Press.	Vapour Specific Heat	Liquid Surface Tension
^{o}C	kJ/kg	kg/m^3	kg/m^3	$W/m^{o}C$	cP	$cPx10^2$	$kPax10^{-2}$	$kJ/kg^{o}C$	$N/mx10^2$
20	2448	998.2	0.01	0.612	1.00	0.96	0.02	1.85	7.40
40	2402	992.3	0.05	0.630	0.65	1.04	0.07	1.86	6.96
60	2359	983.0	0.14	0.649	0.47	1.12	0.20	1.87	6.62
80	2309	972.0	0.29	0.668	0.36	1.19	0.47	1.88	6.26
100	2258	958.0	0.60	0.680	0.28	1.27	1.01	1.88	5.89
120	2200	945.0	1.12	0.682	0.23	1.34	2.02	1.89	5.50
140	2139	928.0	1.99	0.683	0.20	1.41	3.90	1.90	5.06
160	2074	909.0	3.27	0.679	0.17	1.49	6.44	1.91	4.66
180	2003	888.0	5.16	0.669	0.15	1.57	10.04	1.92	4.29
200	1967	865.0	7.87	0.659	0.14	1.65	16.19	1.93	3.89

TABLE A4.2b Properties of Flutec PP9

(a patented fluid by Imperial Smelting Co. Ltd.) (Dunn and Reay, 1978)

^{o}C	kJ/kg	kg/m^3	kg/m^3	$W/m^{o}C$	cP	cPx10	Bar	$kJ/kg^{o}C$	$N/mx10^2$
-30	103.0	2098	0.01	0.060	5.77	0.82	0.00	0.80	2.36
0	98.4	2029	0.01	0.059	3.31	0.90	0.00	0.87	2.08
30	94.5	1960	0.12	0.057	1.48	1.06	0.01	0.94	1.80
60	90.2	1891	0.61	0.056	0.94	1.18	0.03	1.02	1.52
90	86.1	1822	1.93	0.054	0.65	1.21	0.12	1.09	1.24
120	83.0	1753	4.52	0.053	0.49	1.23	0.28	1.15	0.95
150	77.4	1685	11.81	0.052	0.38	1.26	0.61	1.23	0.67
180	70.8	1604	25.13	0.051	0.30	1.33	1.58	1.30	0.40
225	59.4	1455	63.27	0.049	0.21	1.44	4.21	1.41	0.01

TABLE A4.2c Properties of Dowtherm A or Thermex

(Diphenyl-Diphenyl Oxide Eutectic) (Dunn and Reay, 1978)

^{o}C	kJ/kg	kg/m^3	kg/m^3	$W/m^{o}C$	cP	cPx10	Bar	$kJ/kg^{o}C$	$N/mx10^2$
100	354.0	992.0	0.03	0.131	0.97	0.67	0.01	1.34	3.50
150	338.0	951.0	0.22	0.125	0.57	0.78	0.05	1.51	3.00
200	321.0	905.0	0.94	0.119	0.39	0.89	0.25	1.67	2.50
250	301.0	858.0	3.60	0.113	0.27	1.00	0.88	1.81	2.00
300	278.0	809.0	8.74	0.106	0.20	1.12	2.43	1.95	1.50
350	251.0	755.0	19.37	0.099	0.15	1.23	5.55	2.03	1.00
400	219.0	691.0	41.89	0.093	0.12	1.34	10.90	2.11	0.50
450	185.0	625.0	81.00	0.086	0.10	1.45	19.00	2.19	0.03

TABLE A4.3 Compatibility Data for Low Temperature Working Fluids

(Basiulis and Filler, 1971)

Wick Material	Working Fluids					
	Water	Acetone	Ammonia	Methanol	Dow-A	Dow-E
Copper	RU	RU	NR	RU	RU	RU
Aluminium	GNC	RL	RU	NR	UK	NR
Stainless Steel	GNT	PC	RU	GNT	RU	RU
Nickel	PC	PC	RU	RL	RU	RL
Refrasil Fibre	RU	RU	RU	RU	RU	RU

RU Recommended by past successful usage

RL Recommended by literature

PC Probably compatible

NR Not recommended

UK Unknown

GNC Generation of gas at all temperatures

GNT Generation of gas at elevated temperatures, when oxide present

over long periods of time (up to 20,000 hours) by Basiulis & Filler (1971), Kreeb et al. (1973) and Busse et al. (1973), and a few selected ones are shown in Table A4.3.

As the HSA material of construction was chosen to be stainless steel, the working fluid should be compatible with it. It is evident from the Table A4.3 that water results in severe gas generation which increases with temperature. It can be seen from the same table that Dowtherm A is compatible with copper, stainless steel and Nickel (with aluminium it is unknown) and recommended from past successful usage. As Flutec PP9 is not a commonly used fluid, no tests have been conducted on its compatibility, on the other hand its use is restricted to cases, where electrical insulation is a requirements. Dow Chemicals (1976) lists various properties of Dowtherm A, and it recommends Dowtherm A based on 30 years of continuous service.

(2) Thermal stability : The fluid should be thermally stable at the anticipated stagnation temperature of the collector (of about 225°C) and should not break down to form noncondensible gases such as hydrogen, which drastically decreases the efficiency of the HSA panel. Water and Flutec PP9 have maximum operating temperature of 225°C, while Dowtherm A can be used up to 395°C (as seen from Table A4.1). The degradation rate of Dowtherm A, at 315°C has been found to be only 0.18% per year (Dow Chemicals, 1976). Dowtherm A, a clear colourless liquid, after a short period of use, turns dark as a result of the formation of colour complexes. But this discolouration has no effect on the operation of the system.

(3) Vapour Pressure : It should not be too high or too low over the operating temperature range. If the vapour pressure is too low, it sets up larger temperature difference due to lower vapour densities resulting in higher vapour volocities. This may entrain the refluxing condensate, in the counter current flow, or cause flow instabilities associated with compressibility. The upper limit to vapour pressure is not very crucial with ordinary heat pipes as all it necessitates is a thick walled container. However, in case of an HSA if the internal pressure exceeds the external atmospheric pressure, the panel may be ruptured. For example, even if the internal pressure exceeds the atmospheric pressure by only 10 kPa, for a HSA panel of 1 m^2 area that works out to be about 1000 kg force, acting on the seam weld. From Table

A4.2 it can be seen that water has high vapour pressure at the collector stagnation temperature, while Dowtherm A and Flutec have vapour pressure lower than 100 kPa.

(4) Freezing point : This should be compatable with the range of operation. Chisholm (1971) has pointed out that difficulty can be encountered in starting up, if a completely or partly frozen heat pipe (having a wick) as the temperature of the condenser, remains the same even if the evaporator temperature increases to a quite high value, because of the blockage of capillaries in the wick structure. However, this problem may not arise with the HSA as it is a wickless heat pipe. In ordinary heat pipes heat is generally supplied to a relatively small area of the heat pipe whereas in the case of HSA, radiation strikes over almost the entire area and this is especially so in the mornings, when the angle of incidence is high. Although Dowtherm A has higher freezing point as compared to the other two fluids, freezing problem should not arise due to the above mentioned reasons and because the liquid occupies only 18% of the total envelope volume of the HSA.

(5) Surface tension : In ordinary heat pipes high surface tension is desirable to provide good capillary forces for condensate return, but in the HSA surface tension is not an important factor as it operates by gravity. Dowtherm A has a surface tension value intermediate between water and Flutec.

(6) Wettability : It is desirable to have the contact angle zero or very small to improve condensate return, but in the case of wickless heat pipes this is not a major criterion. On the other hand, if the liquid is nonwetting it helps in nucleate boiling and dropwise condensation, both of which improves heat transfer characteristics of a heat pipe.

(7) Latent heat of vaporization : It is desirable to have high latent heat, as it helps to maintain minimum fluid flow and hence lower pressure drops within the heat pipes. Also it helps in increasing the condensation film coefficient. As seen from Table A4.2, Dowtherm A has a value inbetween those of water and Flutec.

(8) Thermal conductivity : Higher thermal conductivity minimises radial temperature gradients and helps to reduce boundary layer effects. It also helps in increasing the

condensation film coefficient. Dowtherm has a value intermediate between the other two fluids.

(9) Viscosity : The resistance to flow is minimised by choosing fluids with low values of vapour and liquid viscosity. Thus it helps to prevent large pressure drops in HSA and results in quick return of condensate to the evaporator. On the other hand low viscosity helps in increasing the condensation film coefficient. It can be noticed from Table A4.2 that Dowtherm A has high liquid viscosity, but intermediate vapour viscosity.

(10) Density : High density is desirable to reduce flow resistance and to increase condensation film coefficient. As seen from Table A4.2, Dowtherm A has an intermediate value.

(11) Toxicity : Low toxicity is desirable to prevent any health hazards mainly while charging the panel. Water is completely non-toxic and Dowtherm A is also very safe, except that prolonged and repeated exposure to high concentrations (more than 10 ppm in air), may be detrimental to health.

(12) Flammability : For safe operating conditions, it is necessary to have low flammability. Water is non flammable while Flutec is highly flammable. Dowtherm A has relatively high flash point (116°C) and fire point (135°C) and hence it is safe to handle it.

(13) Purity : It is preferable to have the working fluid free of dissolved gases and other liquids like water, which tend to decrease the panel efficiency. It is possible to obtain all the three fluids in pure form. Dowtherm A has a maximum water solubility of 2800 ppm at 100°C and falling on either side (to 20 ppm at 250°C and 500 ppm at 20°C).

(14) Thermodynamic considerations : The selection of the working fluid must also be based on thermodynamic considerations which are concerned with the various limitations to heat flow occuring within the heat pipe. These are discussed in Appendix A15.3 and are the viscous, sonic, capillary, entrainment and nucleate boiling limitations.

(15) Cost and availability : The working fluid should be easily available at reasonable cost. Water is best from this point of view, but Dowtherm A is also readily available (at reasonable cost) because it is extensively used as a heat transfer fluid in several industries.

It is evident from the above discussion that Dowtherm A meets most of the requirements and hence it was chosen. However, it should be mentioned that in the second panel HSA2 a small quantity of toluene was added, the reasons for this have been described in Section 4.9.

APPENDIX A5

HEAT CAPACITY OF THE HSA PANEL

The operation of most solar energy systems is transient, and the heat capacity of the collector is one of the main parameters in determining the transient effects, which tend to lower the collector overall performance. Klein et al. (1974) and Wijeysundera (1978) analysed these effects in flat plate collectors. In this appendix the heat capacity of the two HSA panels (HSA1 and HSA2) are evaluated, along with that of a typical flat plate collector for comparison. The glazings, the collector box and the insulation are common to both types and hence, they are discarded, as the purpose is to compare the two. On the other hand, the absorber is the main part in a collector, and is at the highest temperature. The heat capacity of the absorber is determined, by summing the heat capacities of its individual elements, assuming that all the elements are heated to the same degree above the ambient temperature.

A5.1 Flat Plate Collector Heat Capacity

The most common type of flat plate collector (tubes on sheet or pipe and fin) has been chosen. The area of the collector is taken as double that of the HSA panel as both sides of HSA are used, while only one side of flat plate collector is used. The absorber specifications follows.

Plate, tubes and header are made of copper.	
Absorber plate length	0.98 m
Absorber plate width	0.574 m
Abosrber plate thickness	0.0005 m
(Duffie & Beckman 1980)	
Length of the tube	0.98 m
Inside diameter of the tube	0.0127 m
Outside diameter of the tube	0.0151 m
Wall thickness of the tube	0.0012 m
Number of tubes	4
Tube spacing (Solar Energy Handbook, 1979)	0.115 m

TABLE A5.1 Heat Capacity of the Absorber Panel of the Flat Plate Collector

Absorber Panel Component	Heat Capacity in $J.K^{-1}$
Absorber Plate	970
Headers	302
Tubes	708
Working Fluid in Tubes	2077
Working Fluid in Headers	1368
TOTAL	5425

Length of the header	0.574 m
Inside diameter of the Header	0.01905 m
Outside diameter of the header	0.02145 m
Wall thickness of the header	0.0012 m
Number of headers	2
Density of copper (Wong, 1977)	8930 $kg.m^{-3}$
Specific heat capacity of copper	386 $J.kg^{-1}.K^{-1}$

Water is the most common heat transfer fluid in flat plate collectors, and hence, it has been chosen.

Density of water = 1000 $kg.m^{-3}$

Specific heat capacity of water = 4182 $J.kg^{-1}.K^{-1}$

The heat capacities of different components of the absorber panel (neglecting the bonding material) are shown in Table A5.1.

A5.2 HSA Panel Heat Capacity

The specifications of HSA1 and HSA2 are given below.

	HSA1	HSA2
Absorber plate length	0.98m	0.96m
Absorber plate width	0.287m	0.27m
Absorber plate thickness	0.00056m	0.00056m
Condenser tube length	0.904m	0.884m
Condenser tube width	0.03m	0.04m
Condenser tube height	0.01m	0.01m
Thickness of condenser tube wall	0.00056m	0.00056m
Condenser fin length	-	0.860m
Condenser fin width	-	0.01m
Condenser fin thickness	-	0.00056m
Number of condenser fins	-	2
Heat sheet working fluid	Dow-A	Dow-A + toluene
Amount of working fluid	200 ml	200 ml + 28 ml
Condenser fluid	Mobiltherm 603	

The properties of fluids and metal are given below.

Desnity of Dowtherm A = 1056 $kg.m^{-3}$

TABLE A5.2 Heat Capacity of HSA Panel

HSA Panel Components	Heat Capacity in $J.K^{-1}$	
	HSA1	HSA2
Absorber Plate	1133	1044
HSA Working Fluids	333	378
Condenser Tube	128	177
Condenser Fluid	443	578
TOTAL	2037	2177

Specific heat capacity of Dowtherm A = 1577.4 $J.kg^{-1}.K^{-1}$

Density of toluene = 866 $kg.m^{-3}$

Specific heat capacity of toluene = 1841 $J.kg^{-1}.K^{-1}$

Density of Mobiltherm 603 = 860 $kg.m^{-3}$

Specific heat capacity of Mobiltherm 603 = 1900 $J.kg^{-1}.K^{-1}$

Density of stainless steel = 78.20 $kg.m^{-3}$

Specific heat capacity of stainless steel = 460 $J.kg^{-1}.K^{-1}$

The heat capacities of different components of HSA panels (HSA1 and HSA2) are shown in Table A5.2. On comparing the total heat capacities of the absorber of a conventional flat plate collector and HSA panel, it becomes evident that the heat capacity ratio, in the same order becomes 2.6:1, which is a clear advantage of HSA over flat plate collector.

FIGURE A6.1 Magnified Picture of the Cross Section of the HSA1 Panel Showing Various Resistances (Not to Scale)

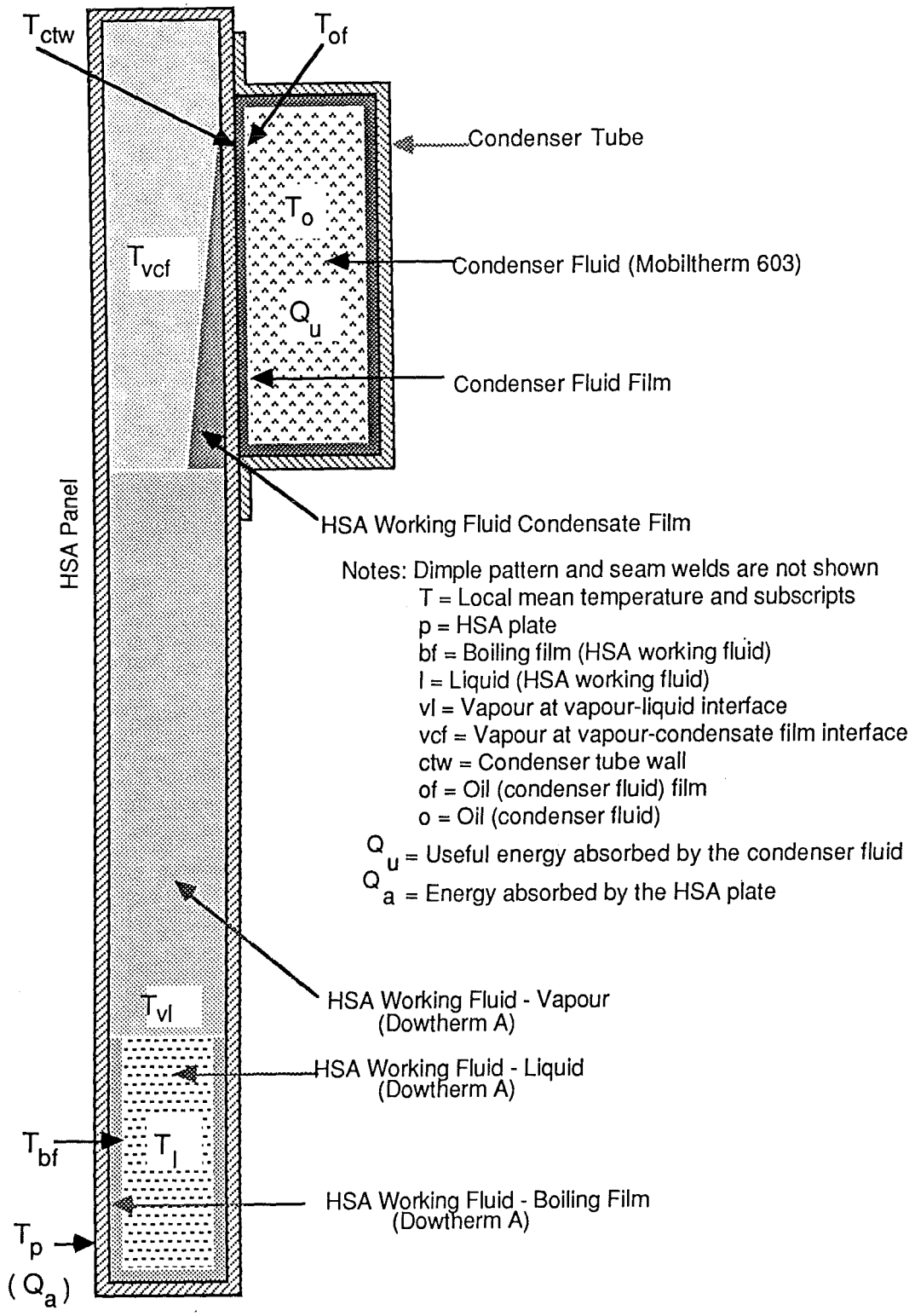

APPENDIX A6

HSA PANEL RESISTANCES

It is important to evaluate the various resistances of the HSA panel, to be able to find out the major and minor resistances, so that efforts can be made to minimise the major resistances. It also helps in choosing the design criteria for the panel, and the components of the panel and indicating where the maximum attention needs to be given, and, where appropriate modifications are required. Various heat pipe resistances for an array of heat pipes with a common condensor are given by Francken (1978). However, the resistance network of an HSA is different, and is shown in Figs. A6.1 and A6.2. The magnified picture of HSA with the inner elements and working fluids is shown in Fig. A6.1. This figure illustrates qualitatively, the physical resistances that exist in the path of heat flow as the solar radiation is absorbed by the plate, and is transferred to the condenser fluid (which is heat transfer oil Mobiltherm 603, in this case). It also shows the temperature of various elements of the system, which are helpful in understanding the resistance network shown in Fig. A6.2, and the temperature drop across each resistance. Q_a amount of solar energy is absorbed by the panel of which the useful energy Q_u is transferred to the oil after passing through the resistances shown in Fig. A6.2. These resistances in sequence are: plate resistance (R_p), boiling film resistance (R_{bf}), evaporator resistance (R_e), vapour flow pressure drop resistance (R_v), condensation resistance (R_c), condenser tube wall resistance (R_w) and condenser fluid film resistance (R_o).

The resistance due to dirt or scale inside the condenser tube is neglected. The boiling film coefficient is generally of the order of a few thousand $W.m^{-2}.K^{-1}$ and so, the boiling film resistance R_{bf} may be assumed to be negligible at this stage, which becomes apparent after the evaluation of the other resistances (Webb, 1979). The evaluation of other resistances is given in the following sections.

FIGURE A6.2 Resistance Network of HSA Panel

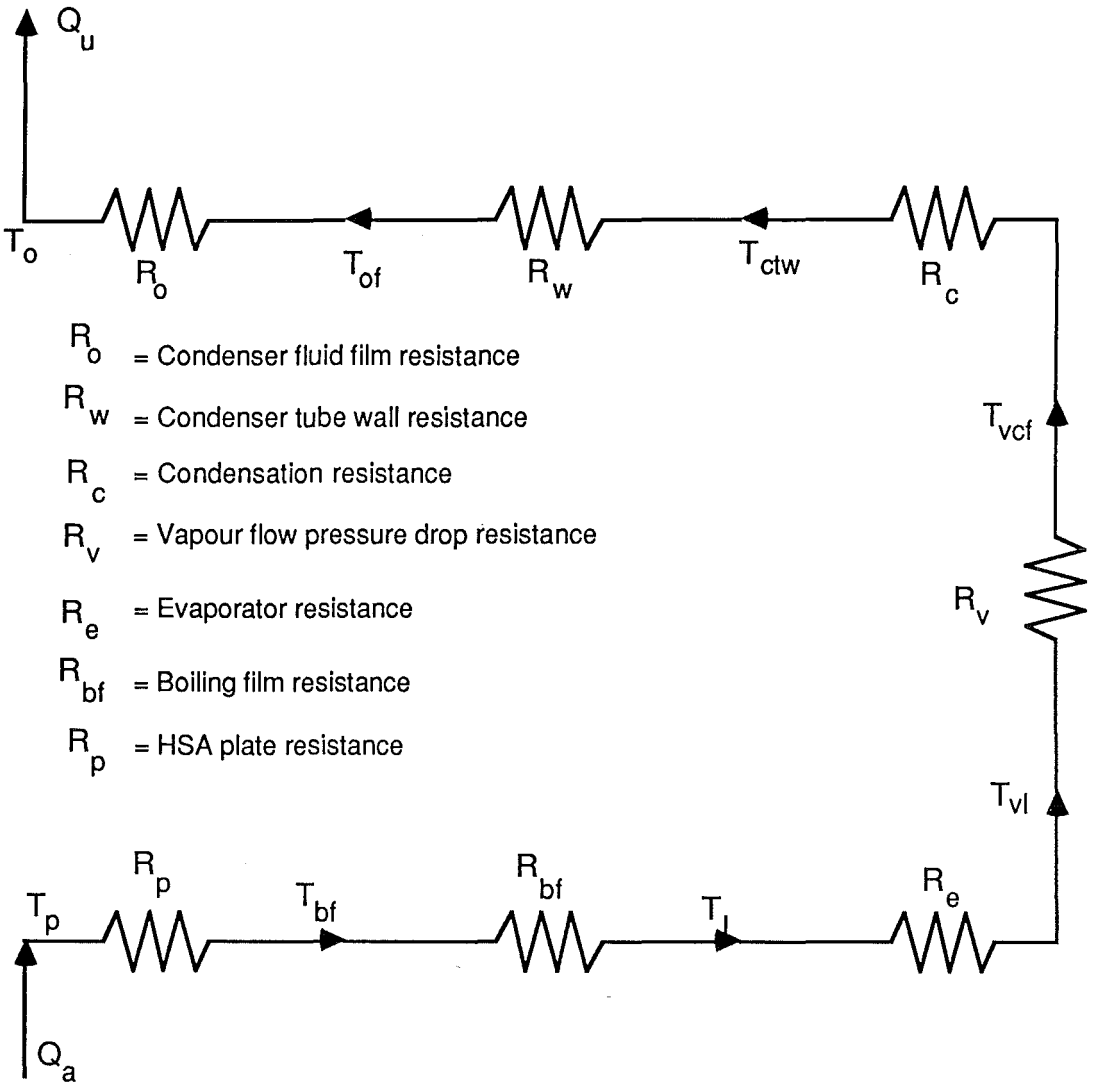

R_o = Condenser fluid film resistance

R_w = Condenser tube wall resistance

R_c = Condensation resistance

R_v = Vapour flow pressure drop resistance

R_e = Evaporator resistance

R_{bf} = Boiling film resistance

R_p = HSA plate resistance

Notes: T = Local mean temperature and subscripts

p = HSA plate

bf = Boiling film (HSA working fluid)

l = Liquid (HSA working fluid)

vl = Vapour at vapour-liquid interface

vcf = Vapour at vapour-condensate film interface

ctw = Condenser tube wall

of = Oil (condenser fluid) film

o = Oil (condenser fluid)

Q_u = Useful energy absorbed by the condenser fluid

Q_a = Energy absorbed by the HSA plate

A6.1 The Plate Resistance (R_p)

The resistance offered by the HSA plate can be obtained from the standard heat conduction equation, and is given by

$$R_p = t_p/(k_p\ A_p) \qquad \text{(A6.1)}$$

where t_p is the thickness of the plate, k_p is the thermal conductivcity of the plate material and A_p is the area of the plate, including both sides as solar radiation is absorbed from both sides.

Substituting k_p = 16.3 $W.m^{-1}.K^{-1}$, A_p = 0.6 m and t_p = 0.5 x 10^{-3} m, we get R_p = 5.1 x 10^{-5} $K.W^{-1}$.

This resistance can usually be neglected.

A6.2 The Evaporator Resistance (R_e)

In the evaporator, the liquid boils continuously, giving off vapours and a temperature drop exists between the liquid vapour interface. If the liquid is in equilibrium with the vapour above its surface, an equal flux of molecules should return to the liquid from the vapour, and there will be no net loss or gain of mass. But when a surface is losing mass by evaporation, clearly, the vapour pressure, and hence, the temperature of the vapour above the surface, must be less than the equilibrium value. In the same way, for net condensation to occur, the vapour pressure and temperature must be higher than the equilibrium value. The liquid vapour interface resistance offerred in the evaporator, can be estimated from Rohsenhow's corelation (Dunn and Reay 1978).

$$R_{ev} = \frac{R\ T_{vl}^2\ (2\pi\ R\ T_{vl})^{0.5}}{\lambda_f^2\ P_v\ A_e} \qquad \text{(A6.2)}$$

where R is the gas constant for the HSA working fluid vapours (Dowtherm A) and $R = R_o/M$; R_o is the universal gas constant; M is the molecular weight of heat sheet working fluid; T_{vl} is the absolute vapour temperature; λ_f is the latent heat of vaporisation at T_{vl}; P_v is the vapour pressure of the liquid at T_{vl}; A_e is the area of the evaporator and $A_e = A_p - A_c$; A_c is the condensation area.

For a particular set of dimensions and operating conditions, R_e can be evaluated. For a condenser width of 30 mm, panel width of 300 mm and panel length of 1000 m, A_c = 0.03 m^2 , A_p = 0.6 m^2 and hence, A_e = 0.57 m^2.

For a vapour temperature of 448 K, substituting molecular weight of Dowtherm A (166), R_o = 8300 $J.K^{-1}.kg\ mol^{-1}$, λ_f = 332.9 x 10^3 $J.kg^{-1}$, P_v = 1.1 x 10^4, in Eq. (A6.2) we get,

R_e = 5.4 x 10^{-6} $K.W^{-1}$

This resistance can also be neglected.

A6.3 The Vapour Flow Pressure Drop Resistance (R_v)

There is a certain temperature drop along the vapour column, and this is related to the vapour pressure drop, by the Clapeyron equation and combining this with the gas equation, the expression for R_v can be obtained (Dunn and Reay, 1978).

$$R_v = \frac{R\ T_v^2\ \Delta P_v}{Q_{net}\ \lambda_f\ P_v} \qquad (A6.3)$$

where Q_{net} = net heat transferred from the evaporator, to the condenser. It can be assumed that, Q_{net} is nearly equal to the heat transferred to the oil passing through the condenser. Usually in heat pipes Q_{net} is high, and ΔP_v is very low. Hence, R_v can be neglected. However, ΔP_v depends a lot on the working fluid vapour pressure P_v at the collector operating temperature T_v. As shown in Appendix A15, at a temperature of 175°C ΔP_v is 525 Pa.

Substituting these quantities in Eq. (A6.3) we get,

R_v = 1.4 x 10^{-2} $K.W^{-1}$

A6.4 The Condensation Resistance (R_c)

This resistance is offered by the condensate film, and usually it is small, due to the high condensation film coefficient. It can be evaluated from

$$R_c = 1 / (h_{cf}\ A_c) \qquad (A6.4)$$

where h_{cf} = condensation film coefficient corrected for fin effect. From Table A13.1 in Appendix A13, for a condenser width of 30 mm and a height of 10 mm, we have h_{cf} = 3921 $W.m^{-2}.K^{-1}$

Substituting values of h_{cf} and A_c in Eq. (A6.4), we get,

R_c = 8.5 x 10^{-3} $K.W^{-1}$

A6.5 The Condensor Tube Wall Resistance (R_w)

This is offered by the metallic wall of the condenser, and it is similar to R_p, as given by Eq. (A6.1), except that A_p is replaced by A_c. R_w is given by

$$R_w = t_p / (k_p\ A_c) \qquad (A6.5)$$

TABLE A6.1 HSA Panel Resistances

Source of Resistance	Resistance $K.W^{-1}$	Percentage
(1) The plate resistance	5.1×10^{-5}	0.04
(2) The evaporator resistance	5.4×10^{-6}	0.005
(3) The vapour flow pressure drop resistance	1.4×10^{-2}	11.5
(4) The condensation film resistance	8.5×10^{-3}	7.0
(5) The condenser tube wall resistance	1.0×10^{-3}	0.8
(6) The oil side film resistance	9.8×10^{-2}	80.7
TOTAL	12.15×10^{-2}	100

Substituting the appropriate quantities in Eq. (A6.5), we get,

$R_w = 1.0 \times 10^{-3}$ K.W^{-1}

This resistance is also small in the present case. However, it is a major resistance in several types of heat pipe solar collectors, including Webb's HSA-SCCR collector.

A6.6 The Oil Side Film Resistance (R_o)

This resistance is due to the oil film in the condenser tube and it is given by

$$R_o = 1 / (h_{ocf} A_o) \qquad (A6.6)$$

Where, h_{ocf} is the oil side film coefficient, corrected for free convection and fin effect, and A_o is the effective heat transfer area on oil side. For a condenser width of 300 mm and a height of 10 mm, the effective area $A_o = 0.08$ m^2, assuming that the whole tube area is equally effective in heat transfer. From Table A13.2 in Appendix A13, the value of h_{ocf} for the above mentioned conditions is 127 W.m^{-2}.K^{-1}. Substituting these quantities in Eq. (A6.6), we get,

$R_o = 9.8 \times 10^{-2}$ K.W^{-1}

This constitutes the major resistance in the panel.

The various resistances, and their percentage contributions towards the total resistance of the HSA panel are given in Table A6.1. The major resistance to heat flow is from the oil side film, the next one is due to the vapour flow pressure drop, and finally, the condensate film resistance. However, the latter two are not very high and hence, more attention can be given to the oil side film resistance.

APPENDIX A7

COMPUTER PROGRAMME TPSUN

A7.1 Programme Listing of TPSUN

```
100 REM **********    COMPUTER PROGRAMME TPSUN    **********
110 REM THIS PROGRAMME CALCULATES THE LOCAL AZIMUTH,
120 REM ELEVATION AND THE EWV ANGLE OF THE SUN AT A
130 REM SPECIFIC LOCATION, DATE  AND TIME USING AN
140 REM APPROXIMATION TO THE EQUATIONS USED TO GENERATE
150 REM THE NAUTICAL ALMANAC
160 REM IT HAS BEEN ADAPTED FROM A PROGRAM BY R. WALRAVEN
170 REM FROM SOLAR ENERGY, 1978, VOL.20,PP 393-397
180 REM
190 REM INPUT PARAMETERS:
200 REM 1. Y1=YEAR=YEAR NUMBER (EX.1984)
210 REM 2. D1=DAY=DAY NUMBER OF YEAR STARTING WITH 1 FOR
220 REM       FIRST OF JANUARY EXCEPT IN LEAP YEAR WHEN 1
230 REM       SHOULD BE SUBTRACTED FROM ALL DAYS TILL MARCH
              FIRST
240 REM 3. H1:M1:S1=HOURS:MINUTES:SECONDS - TIME OF THE DAY
250 REM 4. Z1=ZONE=LOCAL INTERNATIONAL TIME ZONE
260 REM 5. D2=1 IF DAYLIGHT SAVING TIME,ELSE=0
270 REM 6. L1=LOCAL LATITUDE IN DEGREES (NORTH POSITIVE)
280 REM 7. L2=LOCAL LONGITUDE IN DEGREES WEST OF GREENWICH
290 REM 8. Z5=TIME INCREMENT REQUIRED IN MINUTES
300 REM 9. Z6=NUMBER OF TIMES THE LOOP TO BE INCREMENTED
310 REM
320 REM OUTPUT PARAMETERS:
330 REM 1. A3=AZIMUTAL ANGLE (POSITIVE IS EAST OF SOUTH)
340 REM 2. E1=ELEVATION
350 REM 3. X6=EWV ANGLE
360 REM
370 OPEN "TPKW4.DAT" FOR OUTPUT AS FILE #5
380 REM
390 READ Y1,Z1,D2,L1,L2
400 DATA 1984,-12,1,-43.5269,-172.582
410 PRINT "WHAT DAY OF THE YEAR IS IT (NUMBER AND DATE)?"
420 INPUT D1,A$
430 Z$="*****  RESULTS OF THE COMPUTER PROGRAMME TPSUN
    *****"
440 PRINT #5,Z$
450 PRINT #5
460 PRINT #5
470 PRINT #5,"YEAR:";Y1
480 PRINT #5
490 PRINT #5,"DAY:";D1;"(";A$;")"
500 PRINT #5
510 PRINT #5,"LATITUDE:";-L1;"DEGREES SOUTH"
520 PRINT #5
530 PRINT #5,"LONGITUDE:";-L2;"DEGREES EAST OF GREENWICH"
540 PRINT #5
550 PRINT #5,"TIME","AZIMUTH","ELEVATION","EWV ANGLE"
560 REM
570 REM R1=NUMBER OF RADIANS IN ONE DEGREE
580 REM
```

```
590 R1=.0174533
600 D3=Y1-1980
610 L3=INT(D3/4)
620 REM
630 PRINT "INPUT STARTING TIME(HR,MIN,SEC),INCREMENT(MIN)"
640 PRINT "AND NUMBER OF TIMES TO REPEAT THE LOOP"
650 INPUT H1,M1,S1,Z5,Z6
660 FOR L=0 TO Z6
670 IF L=0 GO TO 750
680 REM
690 REM TO FIND THE CORRECT TIME T2 WIRH RESPECT TO 1 JAN
700 REM 1980 GREENWICH MEAN NOON
710 REM
720 M1=M1+Z5
730 IF M1>=60 THEN H1=H1+1
740 IF M1>=60 THEN M1=M1-60
750 T1=H1+(M1+S1/60)/60
760 T2=D3*365+L3+D1-1+T1/24
770 IF D3=(L3*4) GO TO 800
780 IF D3=0 GO TO 850
790 IF D3<>(L3*4) GO TO 850
800 T2=T2-1
810 REM
820 REM TO FIND THE LONGITUDE E4 IN RADIANS, WHICH GIVES
830 REM EXACT POSITION OF THE SUN ON THE CELESTIAL SPHERE
840 REM
850 T3=(360*T2/365.25)*R1
860 G1=-.031271-4.53963E-07*T2+T3
870 E2=4.90097+3.67470E-07*T2
880 E3=(.033434-2.30000E-09*T2)*SIN(G1)
890 E4=E2+E3+3.49000E-04*SIN(2*G1)+T3
900 REM
910 REM TO FIND THE ANGLE BETWEEN THE PLANE OF THE ECLIPTIC
920 REM AND THE PLANE OF THE CELESTIAL EQUATOR E5
930 REM
940 E5=.40914-6.21490E-09*T2
950 REM
960 REM TO FIND THE RIGHT ASCENSION R2 WHICH IS THE ANGLE
970 REM BETWEEN THE HOUR CIRCLE OF VERNAL EQUINOX AND
980 REM THE HOUR CIRCLE OF THE SUN
990 REM
1000 S2=SIN(E4)
1010 A1=S2*COS(E5)
1020 A2=COS(E4)
1030 R2=ATN(A1/A2)
1040 REM
1050 REM TO FIND THE DECLINATION D4 , WHICH IS THE
1060 REM ANGULAR POSITION OF THE SUN AT SOLAR NOON WITH
1070 REM RESPECT TO THE PLANE OF THE EQUATOR, NORTH POSITIVE
1080 REM
1090 IF A2<0 THEN R2=R2+PI
1100 IF R2<0 THEN M=1
1110 IF R2<0 THEN R2=R2+(2*PI)
1120 X4=(S2*SIN(E5))
1130 D4=ATN(X4/(SQR(1-X4^2)))
1140 REM
1150 REM TO FIND THE SIDERIAL TIME S3, WHICH GIVES THE
1160 REM POSITION OF THE CELESTIAL SPHERE WITH
1170 REM RESPECT TO THE EARTH AT THAT TIME
1180 REM
```

```
1190 S3=1.75933+(2*PI)*(T2/365.25-D3)+3.69400E-07*T2
1200 IF S3>(2*PI) THEN S3=S3-(2*PI)
1210 REM
1220 REM TO FIND THE LOCAL SIDERIAL TIME S4 WHICH COMBINES
1230 REM THE EFFECT OF LOCAL LONGITUDE ON S3
1240 REM
1250 S4=S3-L2*R1+1.00274*(Z1-D2+T1)*15*R1
1260 IF S4>(2*PI) THEN S4=S4-(2*PI)
1270 REM
1280 REM TO FIND THE HOUR ANGLE H2
1290 REM
1300 H2=R2-S4
1310 REM
1320 REM P1 IS THE LOCAL LATITUDE IN RADIANS
1330 REM
1340 P1=L1*R1
1350 REM
1360 REM TO FIND THE ELEVATION OF THE SUN E1
1370 REM
1380 X1=(SIN(P1)*SIN(D4)+COS(P1)*COS(D4)*COS(H2))
1390 E1=ATN(X1/(SQR(1-X1^2)))
1400 REM
1410 REM TO FIND THE AZIMUTAL ANGLE A3, WHICH IS THE ANGLE
1420 REM BETWEEN THE LOCAL CELESTIAL MERIDIAN AND THE LINE
1430 REM BETWEEN THE ZENITH AND THE SUN
1440 REM
1450 X3=(COS(D4)*SIN(H2)/COS(E1))
1460 A3=ATN(X3/(SQR(1-X3^2)))
1470 X5=COS(A3)
1480 A3=A3/R1
1490 IF SIN(E1)>(SIN(D4)/SIN(P1)) GO TO 1560
1500 IF A3<0 THEN A3=A3+360
1510 A3=180-A3
1520 REM
1530 REM TO FIND THE EWV ANGLE X6
1540 REM
1550 X4=SIN(E1)/COS(E1)
1560 X4=SIN(E1)/COS(E1)
1570 E1=E1/R1
1580 X6=ATN(X4/X5)
1590 X6=X6/R1
1600 PRINT #5
1610 PRINT #5,H1;":";M1;":";S1,A3,E1,X6
1620 NEXT L
1630 CLOSE #5
1640 END
```

A7.2 Results File TPSUN .DAT

***** RESULTS OF THE COMPUTER PROGRAMME TPSUN *****

YEAR: 1984
DAY: 54 (24 FEBRUARY)
LATITUDE: 43.5269 DEGREES SOUTH
LONGITUDE: 172.582 DEGREES EAST OF GREENWICH

TIME	AZIMUTH	ELEVATION	EWV ANGLE
1 : 0 : 0	-166.326	-35.3094	-36.0901
2 : 0 : 0	175.438	-36.1945	-36.2812
3 : 0 : 0	157.62	-33.6597	-35.7594
4 : 0 : 0	141.58	-28.1433	-34.3234
5 : 0 : 0	127.719	-20.3926	-31.285
6 : 0 : 0	115.697	-11.1301	-24.4045
7 : 0 : 0	104.895	-.921892	-3.58199
8 : 0 : 0	94.6371	9.80252	64.9244
9 : 0 : 0	84.2044	20.6831	75.0256
10 : 0 : 0	72.7355	31.3461	64.0228
11 : 0 : 0	59.0517	41.2857	59.6437
12 : 0 : 0	41.547	49.6794	57.5778
13 : 0 : 0	18.8475	55.1874	56.6527
14 : 0 : 0	-7.54801	56.258	56.4879
15 : 0 : 0	-32.3028	52.4919	57.0261
16 : 0 : 0	-51.9522	45.1366	58.4757
17 : 0 : 0	-67.0555	35.7245	61.541
18 : 0 : 0	-79.2969	25.2842	68.5365
19 : 0 : 0	-90.0443	14.4289	89.828
20 : 0 : 0	-100.267	3.57046	19.2945
21 : 0 : 0	-110.733	-6.9382	-18.9701
22 : 0 : 0	-122.132	-16.709	-29.4403
23 : 0 : 0	-135.128	-25.2423	-33.6345
24 : 0 : 0	-150.242	-31.8767	-35.6157

APPENDIX A8

ANALYSIS OF SHORT WAVE RADIATION

The computer programme TPSWR analyses the short wave radiation entering the collector, using ray trace techniques and calculates the amounts of power incident, absorbed, transmitted and reflected by the various parts of the collector. It also evaluates the average number of reflections and the collector's optical efficiency. Part of the theory underlying this has been explained in Appendix A3.3 and the remainder is described here.

A8.1 Theory

As shown in Appendix A3.3 the top and bottom quadrants are treated separately and then combined to get the final results. Any ray entering the aperture reaches the absorber after a certain number of reflections as shown in Fig. A3.6. Let N-reflected radiation refer to radiation which is reflected N times by the reflector before striking the absorber. So N can only be a positive integer, or zero in the case of radiation directly incident on the absorber. Let f_N correspond to the fraction of the aperture corresponding to each group of N-reflected rays. As shown in Appendix A3.3 the angle of incidence, the maximum rim angle, the fraction of aperture corresponding to radiation directly incident on the absorber (through the inner glazing) and the fraction of aperture for N-reflected radiation are calculated from equations A3.2, A3.19, A3.28 and A3.29 respectively. The average number of reflections N_{av} is the value of N for each group of N-reflected radiation weighted by f_N and is evaluated using the following expression.

$$N_{av} = \frac{\sum_{N=0}^{N=N_{max}} (N\ f_N\ A_{ap})}{A_{ap}} \qquad \text{(A8.1)}$$

where A_{ap} area of the aperture.

By assuming that the solar flux incident on the aperture is uniform, the amount of power delivered by the N-reflected

FIGURE A8.1 Analysis of Short Wave Radiation

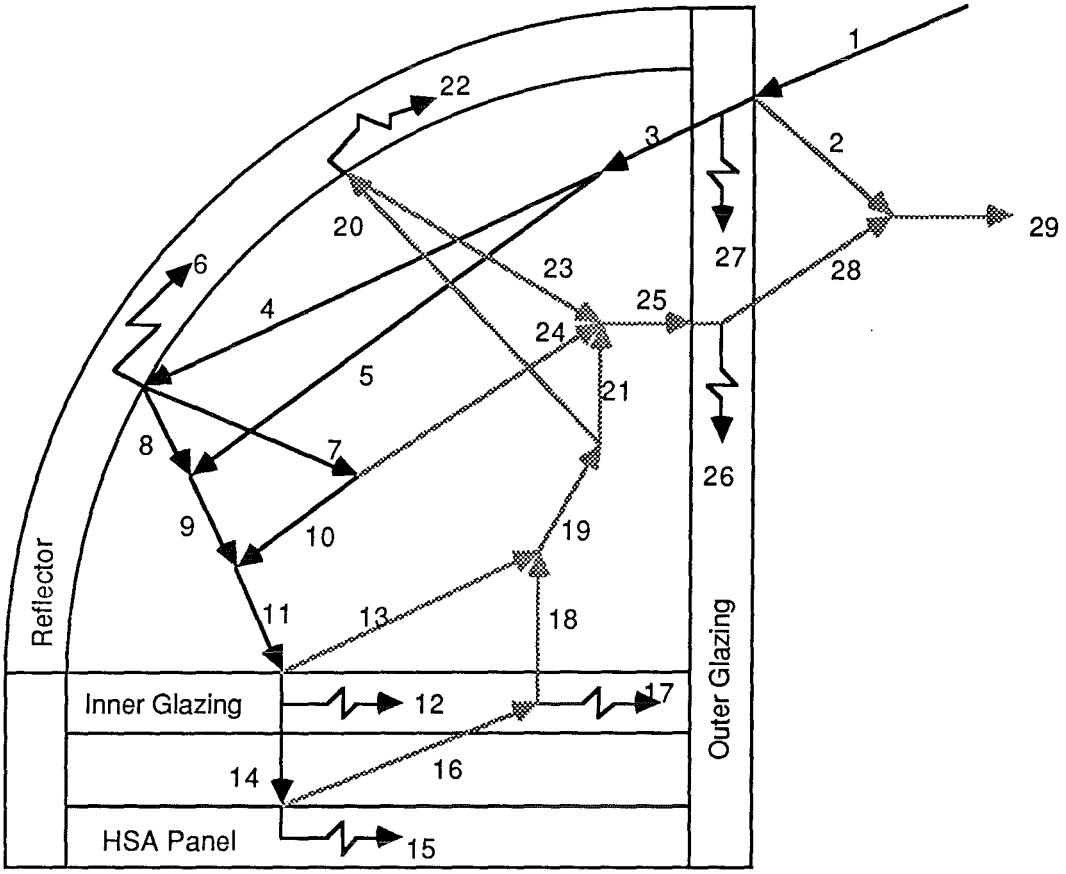

Notes: Only top quadrant is shown in the figure and arrows indicate energy flows
→ = primary radiation and ⇢ = secondary radiation

1.Total solar radiation incident on the outer glazing
2, 3 Primary radiation reflected and transmitted respectively by the outer glazing
4. Primary radiation incident on the reflector
5. Primary radiation directly incident on the absorber panel
6. Primary radiation absorbed by the reflector
7. Primary radiation diffusely reflected by the reflector
8. Primary radiation specularly reflected by the reflector
9. Total specular radiation incident on the inner glazing = sum of 5 and 8
10. Diffusely reflected (by the reflector) radiation incident on the inner glazing
11. Total primary radiation incident on the inner glazing
12, 13 Primary radiation absorbed and relected respectively by the inner glazing
14. Primary radiation transmitted through the inner glazing and incident on the absorber
15. Radiation absorbed by the absorber panel
16, 17, 18 Secondary radiation incident, absorbed and transmitted resp. by the inner glazing
19. Total secondary radiation from the inner glazing = sum of 13 and 18
20. Secondary radiation incident on the reflector
21. Secondary radiation from the inner glazing incident on the outer glazing
22, 23 Secondary radiation absorbed and reflected respectively by the reflector
24. Diffusely reflected radiation (from the reflector) incident on the outer glazing
25. Total secondary radiation incident on the outer glazing = sum of 21, 23 and 24
26. Secondary radiation absorbed by the outer glazing
27. Primary radiation absorbed by the outer glazing
28. Secondary radiation transmitted through the outer glazing
29. Total radiation lost to the atmosphere

radiation can be calculated and the amounts of power incident, absorbed, reflected and transmitted by different surfaces can be determined and these amounts summed up for different values of N.

In order to determine various power quantities consider a ray entering the top quadrant as shown in Fig.A8.1. Primary radiation refers to the rays entering the outer glazing and travelling towards the absorber, while the rays reflected from the absorber and finding their way out towards the outer glazing is referred to as secondary radiation.

The N-reflected radiation incident on outer glazing is given by

$$P_{iNog} = I\ f_N\ A_{ap} \qquad (A8.2)$$

where I = total solar insolation

The total radiation falling on the outer glazing is assumed to be beam radiation only. Of the radiation P_{iNog}, amounts of power reflected (P_{rNog}), abosrbed(P_{aNog}), and transmitted(P_{tNog}), by the N-reflected radiation are given by

$$P_{rNog} = P_{iNog}\ \rho_g \qquad (A8.3)$$

$$P_{aNog} = P_{iNog}\ \alpha_g \qquad (A8.4)$$

$$P_{tNog} = P_{iNog}\ \tau_g \qquad (A8.5)$$

where ρ_g, α_g, τ_g are the reflectivity, absorptivity and transmissivity respectively of glass. The total amounts of power incident reflected, absorbed and transmitted by the glazing are given by

$$P_{iog} = \sum_{N=0}^{N_{max}} P_{iNog} = I \qquad (A8.6)$$

$$P_{rog} = P_{iog}\ \rho_g = I\ \rho_g \qquad (A8.7)$$

$$P_{aog} = P_{iog}\ \alpha_g = F\ \alpha_g \qquad (A8.8)$$

$$P_{tog} = P_{iog}\ \tau_g = I\ \tau_g \qquad (A8.9)$$

where N_{max} is the maximum number of reflections undergone by any radiation in that quadrant.

Also because $\rho_g + \alpha_g + \tau_g = 1$,

we have, $P_{iog} = P_{rNog} + P_{aNog} + P_{tNog}$ (A8.10)

The radiation transmitted through the outer glazing strikes the reflector. When the radiation strikes the reflector the major portion of it is specularly reflected, while minor amounts are diffusely reflected and absorbed. The diffuse reflectivity is the result of irregularities in the reflector surface. Of the radiation which is diffusely reflected by the reflector, parts are

reflected to the outer glazing, the inner glazing, the end walls and other parts of the reflector depending upon the various shape factors.

The amounts reflected to the end walls and to the reflector are ignored, as they together account for less than one fifth of the diffusely reflected radiation from the reflector, which itself is quite small for a good reflector. The incident ray undergoes a few reflections before striking the inner glazing as shown in Fig. A3.6. At the first reflection of the N-reflected radiation the amounts of power absorbed (P_{a1r}), specularly reflected (P_{rs1r}) and diffusely reflected (P_{rd1r}) are given by

$$P_{a1r} = P_{tNog}\ \alpha_r \qquad \text{(A8.11)}$$

$$P_{rs1r} = P_{tNog}\ \rho_{rs} \qquad \text{(A8.12)}$$

$$P_{rd1r} = P_{tNog}\ \rho_{rd} \qquad \text{(A8.13)}$$

where α_r = absorptivity of the reflector

ρ_{rs} = specular reflectivity of the reflector

ρ_{rd} = diffuse reflectivity of the reflector

At the second reflection the power striking the reflector is the amount which is specularly reflected at the previous reflection. The amounts absorbed (P_{a2r}) specularly reflected (P_{rs2r}) and diffusely reflected (P_{rd2r}) by the reflector are given by

$$P_{a2r} = P_{rs1r}\ \alpha_r = P_{tNog}\ \rho_{rs}\ \alpha_r \qquad \text{(A8.14)}$$

$$P_{rs2r} = P_{rs1r}\ \rho_{rs} = P_{tNog}\ \rho_{rs}\ \rho_{rs} \qquad \text{(A8.15)}$$

$$P_{rd2r} = P_{rs1r}\ \rho_{rd} = P_{tNog}\ \rho_{rs}\ \rho_{rd} \qquad \text{(A8.16)}$$

Similarly at the N^{th} reflection the three components are given by

$$P_{aNr} = P_{rs(N-1)r}\ \alpha_r = P_{tNog}\ \rho_{rs}^{N-1}\ \alpha_r \qquad \text{(A8.17)}$$

$$P_{rsNr} = P_{rs(N-1)r}\ \rho_{rs} = P_{tNog}\ \rho_{rs}^{N} \qquad \text{(A8.18)}$$

$$P_{rdNr} = P_{rs(N-1)r}\ \rho_{rd} = P_{tNog}\ \rho_{rs}^{N-1}\ \rho_{rd} \qquad \text{(A8.19)}$$

As seen from Fig. A8.1 the total amounts of power absorbed and diffusely reflected by the reflector for N-reflected radiation (indicated by the subscript N) are given by summing up individual components at all the N-reflections.

$$(P_{ar})_N = P_{a1r} + P_{a2r} + P_{a3r} + \ldots\ldots\ldots + P_{aNr} \qquad \text{(A8.20)}$$

Substituting values of P_{a1r}, P_{a2r} and P_{aNr} from Eqs.(A8.11), (A8.14) and (A8.17).

$$(P_{ar})_N = P_{tNog}\ \alpha_r + P_{tNog}\ \alpha_r\ \rho_{rs} + P_{tNog}\ \alpha_r\ \rho_{rs}^2 + \ldots\ldots$$
$$\ldots\ldots\ldots\ldots\ldots + P_{tNog}\ \alpha_r\ \rho_{rs}^{N-1} \qquad \text{(A8.21)}$$

$$(P_{rdr})_N = P_{rd1r} + P_{rd2r} + P_{rd3r} + \ldots\ldots\ldots + P_{rdNr} \qquad \text{(A8.22)}$$

Substituting values of P_{rd1r}, P_{rd2r} and P_{rdNr} from Eqs.(A8.13), (A8.16), and (A8.19).

$$(P_{rdr})_N = P_{tNog}\,\rho_{rd} + P_{tNog}\,\rho_{rd}\,\rho_{rs} + P_{tNog}\,\rho_{rd}\,\rho_{rs}^2 + \ldots\ldots\ldots + P_{tNog}\,\rho_{rd}\,\rho_{rs}^{N-1} \qquad (A8.23)$$

Eqs.(A8.21) and (A8.23) are in geometric progression with a common ratio of ρ_{rs} and hence they can be summed up and the sums are given below.

$$(P_{ar})_N = \frac{P_{tNog}\,\alpha_r\,(1-\rho_{rs}^N)}{(1-\rho_{rs})} \qquad (A8.24)$$

$$(P_{rdr})_N = \frac{P_{tNog}\,\rho_{rd}\,(1-\rho_{rs}^N)}{(1-\rho_{rs})} \qquad (A8.25)$$

Eqs.(A8.24) and (A8.25) are used to calculate the amounts of power absorbed and diffusely reflected by the reflector for N-reflected radiation and the corresponding total amounts (indicated by the subscript T) for all possible values of N can be summed up as shown below.

$$(P_{ar})_T = \sum_{N=1}^{N_{max}} (P_{ar})_N \qquad (A8.26)$$

$$(P_{rdr})_T = \sum_{N=1}^{N_{max}} (P_{rdr})_N \qquad (A8.27)$$

The radiation incident on the inner glazing consists of specular and diffuse radiation originating from the reflector.

As seen from Fig. A8.1 the specular radiation incident on the inner glazing is from N-reflected radiation from the reflector and is given by Eq.(A8.18).

$$(P_{isig})_N = P_{rsNr} = P_{tNog}\,\rho_{rs}^N \qquad (A8.28)$$

The total specular radiation incident on the inner glazing can be obtained by summing up the individual components for all possible values of N and it is given by,

$$(P_{isig})_T = \sum_{N=0}^{Nmax} P_{tNog}\,\rho_{rs}^N \qquad (A8.29)$$

$(P_{isig})_T$ includes the radiation that is directly incident (N=0) on the inner glazing. The total diffused radiation incident on the inner glazing can be obtained from Eq.(A8.27) and is given by

$$P_{idig} = (P_{rdr})_T F_{rig} \quad (A8.30)$$

where F_{rig} is the radiation shape factor between the reflector and inner glazing. The diffuse radiation which is not incident on the inner glazing is assumed to strike only the outer glazing (but not the end walls) and it is accounted for along with the secondary radiation. The total radiation P_{iTig} incident on the inner glazing can be obtained from Eq.(A8.29) and (A8.30).

$$P_{iTig} = (P_{isig})_T + P_{idig} \quad (A8.31)$$

The radiation incident on the inner glazing is transmitted, or absorbed or reflected as given below.

$$P_{tig} = P_{iTig} \tau_g \quad (A8.32)$$

$$P_{aig} = P_{iTig} \alpha_g \quad (A8.33)$$

$$P_{rig} = P_{iTig} \rho_g \quad (A8.34)$$

The reflected radiation from the inner glazing is considered as the secondary radiation, because its direction is also outward from the absorber. The radiation transmitted through the inner glazing finally strikes the absorber panel, and the major portion is absorbed and the rest is reflected back onto the inner glazing as secondary radiation. The secondary radiation is assumed to consist of only diffuse radiation. As the shape factor between the absorber and inner glazing is nearly equal to one (because of the high aspect ratio, that is kept close to each other), it is assumed that the secondary radiation incident on other parts of the collector (other than inner glazing) is negligible. Also it is assumed that no secondary radiation is reflected back to the absorber from the inner glazing, which means that it is either transmitted or absorbed. The specular and diffuse components and the total radiation incident on the absorber panel are given by

$$P_{isab} = (P_{isig})_T \tau_g \quad (A8.35)$$

$$P_{idab} = P_{idig} \tau_g \quad (A8.36)$$

$$P_{iTab} = P_{tig} = P_{isab} + P_{idab} \quad (A8.37)$$

It can be seen that all radiation transmitted through the inner glazing is assumed to be incident on the absorber. This introduces negligible error because the spacing between the panel and inner glazing is small compared to the panel dimensions.

The total radiation absorbed by the absorber is given by

$$P_{aTab} = P_{iTab} \alpha_{ab} \quad (A8.38)$$

where α_{ab} = absorptivity of the absorber panel.

As the radiation which is not absorbed by the absorber is reflected, the radiation reflected by the absorber is given by

$$P_{rab} = P_{iTab}(1-\alpha_{ab}) \quad \text{(A8.39)}$$

P_{aTab} has two components - one is specular and the other one is diffuse and they are given by

$$P_{asab} = P_{isab}\ \alpha_{ab} \quad \text{(A8.40)}$$

$$P_{adab} = P_{idab}\ \alpha_{ab} \quad \text{(A8.41)}$$

The secondary radiation incident on the inner glazing is given by $(P_{iig})_S = P_{rab}$ (A8.42)

Henceforth 'S' is used as subscript to denote secondary radiation. The secondary radiation absorbed and transmitted by the inner glazing are given by,

$$(P_{aig})_S = (P_{iig})_S\ \alpha_g \quad \text{(A8.43)}$$

$$(P_{tig})_S = (P_{iig})_S\ (1-\alpha_g) \quad \text{(A8.44)}$$

The secondary radiation transmitted by the inner glazing is assumed to fall only on the reflector (not the end walls) before striking the outer glazing. The total secondary radiation incident on the reflector includes the primary radiation reflected by the inner glazing, and is given by

$$(P_{ir})_S = [(P_{tig})_S + P_{rig}]\ F_{ig-r} \quad \text{(A8.45)}$$

where F_{ig-r} is the shape factor between inner glazing and reflector.

The secondary radiation incident on the reflector is either absorbed or reflected to the outer glazing and these components are given by

$$(P_{ar})_S = (P_{ir})_S\ \alpha_r \quad \text{(A8.46)}$$

$$(P_{rdr})_S = (P_{ir})_S\ (1-\alpha_r) \quad \text{(A8.47)}$$

The total secondary radiation incident on the outer glazing (including the primary diffuse radiation originating from the reflector and not incident on the inner glazing) is given by

$$(P_{iog})_S = (P_{rdr})_S + [(P_{tig})_S + P_{rig}]\ (1-F_{ig-r}) \quad \text{(A8.48)}$$

The secondary radiation incident on the outer glazing is either absorbed or transmitted (but not reflected) to the atmosphere.

$$(P_{aog})_S = (P_{iog})_S\ \alpha_g \quad \text{(A8.49)}$$

$$(P_{tog})_S = (P_{iog})_S(1-\alpha_g) \quad \text{(A8.50)}$$

At this stage the primary and secondary radiations can be added to give the total quantities for each of the components as shown below. The total power absorbed by the outer glazing is given by

$$P_{aTog} = P_{aog} + (P_{aog})_S \quad \text{(A8.51)}$$

substituting Paog and $(P_{aog})_S$ from Eqs.(A8.4) and (A8.49)

$$P_{aTog} = [P_{iog} + (P_{iog})_S]\ \alpha_g \qquad \text{(A8.52)}$$

The total radiation reflected by outer or inner glazings is not affected as the secondary reflection has been assumed to be absent. The total radiation absorbed by the reflector is given by (from Eqs. A8.26 and A8.46).

$$P_{aTr} = (P_{ar})_T + (P_{ar})_S \qquad \text{(A8.53)}$$

The total radiation absorbed by the inner glazing is given by (from Eqs. A8.33 and A8.43)

$$P_{aTig} = P_{aig} + (P_{aig})_S \qquad \text{(A8.54)}$$

The total radiation lost to the atmosphere via the outer glazing can be obtained from Eqs.(A8.3) and (A8.50) and is given by

$$P_{lTatm} = P_{rog} + (P_{tog})_S \qquad \text{(A8.55)}$$

A8.2 Computer Programme TPSWR

TPSWR has been written to do all the above calculations and to find out the various primary and secondary radiations quantities for the top quadrant, the bottom quadrant and the whole collector individually. The various input and output variables to the programme are listed at the beginning of the programme. The listing of the programme and typical results for 1 p.m. on 24 February 1984 follows this section.

A8.3 Programme Listing of TPSWR

```
100 REM  **********   COMPUTER PROGRAMME TPSWR   **********
110 REM
120 REM
130 REM THIS PROGRAMME ANALYSES THE SHORT WAVE RADIATION OR
140 REM SOLAR RADIATION BY FOLLOWING THE PATH OF THE
150 REM INCOMING RAYS OF THE SUN
160 REM
170 REM IT EVALUATES FIRSTLY THE ANGLE OF INCIDENCE AND THEN
180 REM BY FOLLOWING THE RAY TRACE TECHNIQUES CALCULATES
190 REM THE SPECULAR AND DIFFUSED COMPONENTS OF RADIATION
200 REM INCIDENT, ABSORBED, REFLECTED AND TRANSMITTED BY
210 REM VARIOUS PARTS OF THE COLLECTOR (SUCH AS OUTER
      GLAZING,
220 REM REFLECTOR, INNER GLAZING, ABSORBER PANEL)
230 REM IT ALSO CALCULATES THE AVERAGE NUMBER OF REFLECTIONS
240 REM AND THE COLLECTOR'S OPTICAL EFFICIENCY
250 REM
260 REM NOTE THAT IF THE INCOMING RAYS MAKE A NEGATIVE ANGLE
270 REM WITH THE AXIS THEN THE SAME CALCULATIONS ARE MADE,
280 REM BUT ONLY THE QUADRANTS ARE REVERSED. THAT MEANS A
290 REM NEGATIVE ANGLE IN THE BOTTOM QUADRANT FOLLOWS THE
      SAME
300 REM PATH AS THE SAME POSITIVE ANGLE IN THE TOP QUADRANT
310 REM
320 REM
330 REM THE INPUT VARIABLES TO THE POGRAMME ARE GIVEN BELOW
340 REM
350 A1$=" 1. THE TOTAL SOLAR INSOLATION ON A SURFACE"
360 A2$="    INCLINED AT THE SAME ANGLE AS THE OUTER"
370 A3$="    GLAZING IN W/SQ.M                          I ="
380 A4$=" 2. THE TRANSMITTANCE OF GLAZING MATERIAL     T2 ="
390 A5$=" 3. THE REFLECTIVITY OF GLAZING MATERIAL      R9 ="
400 A6$=" 4. THE ABSORPTIVITY OF GLAZING MATERIAL      A7 ="
410 A7$=" 5. THE SPECULAR REFLECTANCE OF THE REFLECTOR R1 ="
420 A8$=" 6. THE DIFFUSE REFLECTANCE OF THE REFLECTOR  R2 ="
430 A9$=" 7. THE ABSORPTANCE OF THE REFLECTOR          A5 ="
440 B1$=" 8. THE ABSORPTANCE OF THE ABSORBER PANEL     A6 ="
450 B2$=" 9. THE APERTURE AREA IN SQ.M                 A4 ="
460 B3$="10. THE SHAPE FACTOR BETWEEN REFLECTOR AND"
470 B4$="    INNER GLAZING                             S1 ="
480 B5$="11. THE SHAPE FACTOR BETWEEN INNER GLAZING"
490 B6$="    AND REFLECTOR                             S2 ="
500 B7$="12. THE LATITUDE OF THE PLACE IN DEGREES      A2 ="
510 B8$="13. THE EWV ANGLE IN DEGREES                  A1 ="
520 REM
530 REM
540 REM THE OUTPUT VARIABLES OF THE PROGRAMME ARE GIVEN
BELOW
550 REM
560 C1$=" 1. ANGLE OF INCIDENCE OF THE INCOMING RAYS   AI ="
570 C2$=" 2. THE FRACTION OF THE APERTURE COVERED    C(N) ="
580 C3$=" 3. PR INCIDENT ON THE OUTER GLAZING         PR1 ="
590 C4$=" 4. PR REFLECTED BY THE OUTER GLAZING        PR2 ="
600 C5$=" 5. PR ABSORBED BY THE OUTER GLAZING         PR3 ="
610 C6$=" 6. PR TRANSMITTED THROUGH THE OUTER GLAZING PR4 ="
620 C7$=" 7. PR INCIDENT ON THE REFLECTOR             PR5 ="
630 C8$=" 8. PR ABSORBED BY THE REFLECTOR             PR6 ="
640 C9$=" 9. PR SPECULARLY REFLECTED BY THE REFLECTOR PR7 ="
```

```
650 D1$="10. PR DIFFUSELY REFLECTED BY THE REFLECTOR  PR8 ="
660 D2$="11. PR INCIDENT ON THE INNER GLAZING         PR9 ="
670 D3$="12. PR REFLECTED BY THE INNER GLAZING       PR10 ="
680 D4$="13. PR ABSORBED BY THE INNER GLAZING        PR11 ="
690 D5$="14. PR TRASMITTED THROUGH THE INNER GLAZING PR12 ="
700 D6$="15. PR (SPECULAR) INCIDENT ON THE PANEL     PR13 ="
710 D7$="16. PR (DIFFUSE) INCIDENT ON THE PANEL      PR14 ="
720 D8$="17. PR (SPECULAR+DIFFUSE) INCIDENT ON PANEL PR15 ="
730 D9$="18. PR ABSORBED BY THE ABSORBER PANEL       PR16 ="
740 E1$="19. PR REFLECTED BY THE ABSORBER PANEL      PR17 ="
750 E2$="20. SR INCIDENT ON THE INNER GLAZING         SR1 ="
760 E3$="21. SR ABSORBED BY THE INNER GLAZING         SR2 ="
770 E4$="22. SR TRASMITTED BY THE INNER GLAZING       SR3 ="
780 E5$="23. SR INCIDENT ON THE REFLECTOR             SR4 ="
790 E6$="24. SR ABSORBED BY THE REFLECTOR             SR5 ="
800 E7$="25. SR REFLECTED BY THE REFLECTOR            SR6 ="
810 E8$="26. SR (TOTAL) INCIDENT ON THE OUTER GLAZING SR7 ="
820 E9$="27. SR ABSORBED BY THE OUTER GLAZING         SR8 ="
830 F1$="28. SR TRANSMITTED BY THE OUTER GLAZING      SR9 ="
840 F2$="29. TR INCIDENT ON THE OUTER GLAZING         TR1 ="
850 F3$="30. TR REFLECTED BY THE OUTER GLAZING        TR2 ="
860 F4$="31. TR ABSORBED BY THE OUTER GLAZING         TR3 ="
870 F5$="32. TR ABSORBED BY THE REFLECTOR             TR4 ="
880 F6$="33. TR REFLECTED BY THE INNER GLAZING        TR5 ="
890 F7$="34. TR ABSORBED BY THE INNER GLAZING         TR6 ="
900 F8$="35. TR (SPECULAR) INCIDENT ON THE PANEL      TR7 ="
910 F9$="36. TR (DIFFUSE) INCIDENT ON THE PANEL       TR8 ="
920 G1$="37. TR (SPECULAR+DIFFUSE) INCIDENT ON PANEL  TR9 ="
930 G2$="38. TR ABSORBED BY THE ABSORBER PANEL       TR10 ="
940 G3$="39. TR LOST TO THE ATMOSPHERE               TR11 ="
950 G4$="40. AVERAGE NUMBER OF RELECTIONS             ANR ="
960 G5$="41. OPTICAL EFFICIENCY OF THE COLLECTOR IN % OEC ="
970 REM
980 REM
990 H1$="*****  RESULTS OF THE COMPUTER PROGRAMME TPSWR
    *****"
1000 H2$="THE INPUT VARIABLES TO THE PROGRAMME ARE GIVEN
     BELOW"
1010 H3$="THE OUTPUT VARIABLES OF THE PROGRAMME ARE GIVEN
     BELOW"
1020 H4$="NOTE: PR = PRIMARY RADIATION, WHICH IS THE
     RADIATION"
1030 H5$="            TRAVELLING TOWARDS THE ABSORBER PANEL"
1040 H6$="      SR = SECONDARY RADIATION, WHICH IS THE
     RADIATION"
1050 H7$="            TRAVELLING AWAY FROM THE ABSORBER
     PANEL"
1060 H8$="      TR = TOTAL RADIATION, WHICH IS THE SUM OF
     THE"
1070 H9$="            PRIMARY AND SECONDARY RADIATIONS"
1080 I1$="      ALL THE RADIATION QUANTITIES ARE IN WATTS"
1090 I2$="DATE = "
1100 I3$="FOR THE WHOLE COLLECTOR"
1110 REM
1120 REM
1130 OPEN "TPSWR.DAT" FOR OUTPUT AS FILE #5
1140 DIM C(20),L(20)
1150 REM
1160 REM TO READ THE INPUT DATA
1170 REM
```

```
1180 READ I,T2,A4,R1,R2,S1,S2,A2
1190 DATA 946,0.885,0.58212,0.76,0.09,0.431527,0.626716,43.5
1200 READ A5,A6,A7,R9
1210 DATA 0.15,0.93,0.0312,0.0838
1220 REM "INPUT EWV ANGLE AND DATE"
1230 READ A1,X$
1235 DATA 56.65,24 FEB 1984
1240 REM
1250 PRINT #5,H1$
1260 PRINT #5
1270 PRINT #5
1280 PRINT #5
1290 PRINT #5,H2$
1300 PRINT #5
1310 PRINT #5,A1$
1320 PRINT #5,A2$
1330 PRINT #5,A3$;I
1340 PRINT #5,A4$;T2
1350 PRINT #5,A5$;R9
1360 PRINT #5,A6$;A7
1370 PRINT #5,A7$;R1
1380 PRINT #5,A8$;R2
1390 PRINT #5,A9$;A5
1400 PRINT #5,B1$;A6
1410 PRINT #5,B2$;A4
1420 PRINT #5,B3$
1430 PRINT #5,B4$;S1
1440 PRINT #5,B5$
1450 PRINT #5,B6$;S2
1460 PRINT #5,B7$;A2
1470 PRINT #5,B8$;A1
1480 PRINT #5
1490 PRINT #5,I2$;X$
1500 PRINT #5
1510 PRINT #5
1520 PRINT #5,H3$
1530 PRINT #5
1540 PRINT #5,H4$
1550 PRINT #5,H5$
1560 PRINT #5,H6$
1570 PRINT #5,H7$
1580 PRINT #5,H8$
1590 PRINT #5,H9$
1600 PRINT #5,I1$
1610 PRINT #5
1620 PRINT #5
1630 REM
1640 REM TO CALCULATE THE ANGLE OF INCIDENCE AI IN DEGREES
1650 REM
1660 A3=ABS((A2+A1-90)*2*PI/360)
1670 AI=A3*360/(2*PI)
1680 IF (A2+A1-90)<0 THEN F5=1
1690 REM
1700 REM CALCULATIONS FOR THE TOP QUADRANT
1710 REM
1720 FOR N=0 TO 20
1730 IF N>0 GO TO 1840
1740 REM
1750 REM TO CALCULATE THE FRACTION OF APERTURE COVERED BY
1760 REM N-REFLECTED RADIATION C(N) FOR N=0
```

```
1770 REM
1780 C(N)=.5*(SIN(A3)/COS(A3))
1790 GO TO 1960
1800 REM
1810 REM TO CALCULATE THE MAXIMUM RIM ANGLE T FOR
1820 REM N-REFLECTED RADIATION
1830 REM
1840 T=((N/(2*N+1))*PI)-(((2*N)/(2*N+1))*A3)
1850 REM
1860 REM TO CALCULATE THE FRACTION OF APERATURE COVERED BY
1870 REM UP TO N-REFLECTED RADIATION, C(N)
1880 REM
1890 C(N)=.5*(SIN(T+A3)/SIN(PI/2-A3))
1900 IF C(N)>.5 THEN C(N)=.5
1910 REM
1920 REM TO  CALCULATE THE FRACTION OF APERATURE COVERED BY
1930 REM N-REFLECTED RADIATION ONLY, D
1940 REM
1950 GO TO 1980
1960 D=C(N)
1970 GO TO 2050
1980 D=C(N)-C(N-1)
1990 REM
2000 REM TO CALCULATE THE AVERAGE NUMBER OF REFLECTIONS X5
2010 REM
2020 X4=D*N
2030 X5=X5+X4
2040 REM
2050 REM TO CALCULATE THE N-REFLECTED RADIATION REACHING
2060 REM THE ABSORBER SPECULARLY, E
2070 REM K1 GIVES THE RADIATION DIRECTLY INCIDENT ON
2080 REM THE INNER GLAZING
2090 REM
2100 E=D*R1^N*I*T2*A4
2110 IF N=0 THEN K1=E
2120 E=E*T2
2130 REM
2140 REM TO CALCULATE THE TOTAL AMOUNT OF SPECULAR RADIATION
2150 REM (FOR ALL VALUES OF N) REACHING THE ABSORBER, F
2160 REM
2170 F=F+E
2180 REM
2190 REM TO CALCULATE THE AMOUNT OF N-REFLECTED RADIATION
2200 REM ABSORBED BY THE REFLECTOR, Y2
2210 REM
2220 Y2=(A5*D*I*A4*T2)*((1-R1^N)/(1-R1))
2230 REM
2240 REM TO FIND OUT THE TOTAL AMOUNT OF RADIATION ABSORBED
2250 REM (FOR ALL VALUES OF N) BY THE REFLECTOR, Y
2260 REM
2270 Y=Y2+Y
2280 REM
2290 REM TO CALCULATE THE AMOUNT OF N-REFLECTED RADIATION
2300 REM DIFFUSELY REFLECTED BY THE REFLECTOR, G
2310 REM
2320 G=(R2*D*I*A4*T2)*((1-R1^N)/(1-R1))
2330 REM
2340 REM TO FIND THE TOTAL AMOUNT OF RADIATION REFLECTED
2350 REM DIFFUSELY BY THE REFLECTOR, H
2360 REM
```

```
2370 H=H+G
2380 NEXT N
2390 REM
2400 REM TO CALCULATE THE AMOUNT OF RADIATION DIFFUSELY
2410 REM REFLECTED TO THE ABSORBER PANEL, J
2420 REM
2430 J=H*S1
2440 J=J*T2
2450 REM
2460 REM TO FIND OUT WHICH QUADRANT THE CALCULATIONS ARE
     DONE
2470 REM
2480 IF F5=1 THEN A3=-A3
2490 IF F5=1 GO TO 2520
2500 PRINT #5,"FOR THE TOP QUADRANT"
2510 GO TO 2540
2520 PRINT #5,"FOR THE BOTTOM QUADRANT"
2530 A3=ABS(A3)
2540 REM
2550 REM TO EVALUATE THE PRIMARY RADIATION QUANTITIES
2560 REM LISTED UNDER THE OUTPUT VARIABLES
2570 REM
2580 PR1=(A4/2)*I
2590 PR2=PR1*R9
2600 PR3=PR1*A7
2610 PR4=PR1*T2
2620 PR5=(F/T2)-K1+Y+H
2630 PR6=Y
2640 PR7=(F/T2)-K1
2650 PR8=H
2660 PR9=(F/T2)+(H*S1)
2670 PR10=PR9*R9
2680 PR11=PR9*A7
2690 PR12=PR9*T2
2700 PR13=F
2710 PR14=J
2720 PR15=F+J
2730 PR16=PR15*A6
2740 PR17=PR15-PR16
2750 REM
2760 REM TO EVALUATE THE VARIOUS SECONDARY RADIATION
2770 REM QUANTITIES LISTED UNDER OUTPUT VARIABLES
2780 REM
2790 SR1=PR17
2800 SR2=SR1*A7
2810 SR3=SR1*(1-A7)
2820 SR4=(SR3+PR10)*S2
2830 SR5=SR4*A5
2840 SR6=SR4*(1-A5)
2850 SR7=SR6+(SR3+PR10)*(1-S2)+H*(1-S1)
2860 SR8=SR7*A7
2870 SR9=SR7*(1-A7)
2880 REM
2890 REM TO FIND THE TOTAL RADIATION QUANTITIES LISTED
2900 REM UNDER THE OUTPUT VARIABLES
2910 REM
2920 TR1=PR1
2930 TR2=PR2
2940 TR3=PR3+SR8
2950 TR4=PR6+SR5
```

```
2960 TR5=PR10
2970 TR6=PR11+SR2
2980 TR7=PR13
2990 TR8=PR14
3000 TR9=PR15
3010 TR10=PR16
3020 TR11=PR2+SR9
3030 REM
3040 REM TO FIND THE COLLECTOR'S OPTICAL EFFICIENCY OEC AND
3050 REM THE AVERAGE NUMBER OF REFLECTIONS ANR
3060 REM
3070 OEC=(TR10/TR1)*100
3080 ANR=X5
3090 REM
3100 PRINT #5
3110 PRINT #5
3120 PRINT #5,C1$;AI
3130 PRINT #5
3140 PRINT #5,C2$;C(N)
3150 PRINT #5
3160 PRINT #5,C3$;PR1
3170 PRINT #5,C4$;PR2
3180 PRINT #5,C5$;PR3
3190 PRINT #5,C6$;PR4
3200 PRINT #5,C7$;PR5
3210 PRINT #5,C8$;PR6
3220 PRINT #5,C9$;PR7
3230 PRINT #5,D1$;PR8
3240 PRINT #5,D2$;PR9
3250 PRINT #5,D3$;PR10
3260 PRINT #5,D4$;PR11
3270 PRINT #5,D5$;PR12
3280 PRINT #5,D6$;PR13
3290 PRINT #5,D7$;PR14
3300 PRINT #5,D8$;PR15
3310 PRINT #5,D9$;PR16
3320 PRINT #5,E1$;PR17
3330 PRINT #5
3340 PRINT #5,E2$;SR1
3350 PRINT #5,E3$;SR2
3360 PRINT #5,E4$;SR3
3370 PRINT #5,E5$;SR4
3380 PRINT #5,E6$;SR5
3390 PRINT #5,E7$;SR6
3400 PRINT #5,E8$;SR7
3410 PRINT #5,E9$;SR8
3420 PRINT #5,F1$;SR9
3430 PRINT #5
3440 PRINT #5,F2$;TR1
3450 PRINT #5,F3$;TR2
3460 PRINT #5,F4$;TR3
3470 PRINT #5,F5$;TR4
3480 PRINT #5,F6$;TR5
3490 PRINT #5,F7$;TR6
3500 PRINT #5,F8$;TR7
3510 PRINT #5,F9$;TR8
3520 PRINT #5,G1$;TR9
3530 PRINT #5,G2$;TR10
3540 PRINT #5,G3$;TR11
3550 PRINT #5
```

```
3560 PRINT #5,G4$;ANR
3570 PRINT #5
3580 PRINT #5,G5$;OEC
3590 PRINT #5
3600 PRINT #5
3610 PRINT #5
3620 REM
3630 REM
3640 REM CALCULATIONS FOR THE BOTTOM QUADRANT
3650 REM
3660 FOR N=1 TO 20
3670 REM
3680 REM TO CALCULATE THE MAXIMUM RIM ANGLE B FOR
3690 REM N-REFLECTED RADIATION
3700 REM
3710 B=(N/(2*N+1))*PI+((2*N)/(2*N+1))*A3
3720 IF B<PI/2 GO TO 3760
3730 L(N)=.5
3740 GO TO 3840
3750 REM
3760 REM TO CALCULATE THE FRACTION OF APERATURE L(N) COVERED
3770 REM BY UP TO N-REFLECTED RADIATION
3780 REM
3790 L(N)=.5*(SIN(B-A3)/SIN(PI/2-A3))
3800 REM
3810 REM TO CALCULATE THE FRACTION OF APERATURE COVERED BY
3820 REM N REFLECTED RADIATION ONLY, M
3830 IF L(N)>.5 THEN L(N)=.5
3840 M=L(N)-L(N-1)
3850 REM
3860 REM TO CALCULATE THE AVERAGE NUMBER OF REFLECTIONS X7
3870 X6=M*N
3880 X7=X7+X6
3890 REM
3900 REM TO CALCULATE THE AMOUNT OF N-REFLECTED RADIATION
3910 REM REACHING THE ABSORBER PANEL SPECULARLY, O
3920 REM
3930 O=M*R1^N*T2*A4*I
3940 O=O*T2
3950 REM
3960 REM TO CALCULATE THE TOTAL AMOUNT OF SPECULAR RADIATION
3970 REM(FOR ALL VALUES OF N) REACHING THE ABSORBER, P
3980 P=P+O
3990 REM
4000 REM TO CALCULATE THE AMOUNT OF N-REFLECTED RADIATION
4010 REM ABSORBED BY THE REFLECTOR, V2
4020 REM
4030 V2=(A5*M*I*T2*A4)*((1-R1^N)/(1-R1))
4040 REM
4050 REM TO FIND THE TOTAL AMOUNT OF RADIATION ABSORBED
4060 REM (FOR ALL VALUES OF N) BY THE REFLECTOR, V
4070 REM
4080 V=V+V2
4090 REM
4100 REM TO CALCULATE THE AMOUNT OF N-REFLECTED RADIATION
4110 REM DIFFUSELY REFLECTED BY THE REFLECTOR, Q
4120 REM
4130 Q=(R2*M*A4*I*T2)*((1-R1^N)/(1-R1))
4140 REM
4150 REM TO FIND THE TOTAL AMOUNT OF RADIATION DIFFUSELY
```

```
4160 REM REFLECTED BY THE REFLECTOR, R
4170 REM
4180 R=R+Q
4190 NEXT N
4200 REM
4210 REM TO CALCULATE THE AMOUNT OF RADIATION DIFFUSELY
4220 REM REFLECTED TO THE ABSORBER PANEL, T
4230 REM
4240 T=R*S1
4250 T=T*T2
4260 IF F5=1 GO TO 4290
4270 PRINT #5,"FOR THE BOTTOM QUADRANT"
4280 GO TO 4310
4290 PRINT #5,"FOR THE TOP QUADRANT"
4300 REM
4310 REM TO EVALUATE THE PRIMARY RADIATION QUANTITIES
4320 REM LISTED UNDER THE OUTPUT VARIABLES
4330 REM
4340 PR1C=(A4/2)*I
4350 PR2C=PR1C*R9
4360 PR3C=PR1C*A7
4370 PR4C=PR1C*T2
4380 PR5C=(P/T2)+V+R
4390 PR6C=V
4400 PR7C=P/T2
4410 PR8C=R
4420 PR9C=(P/T2)+(R*S1)
4430 PR10C=PR9C*R9
4440 PR11C=PR9C*A7
4450 PR12C=PR9C*T2
4460 PR13C=P
4470 PR14C=T
4480 PR15C=P+T
4490 PR16C=PR15C*A6
4500 PR17C=PR15C-PR16C
4510 REM
4520 REM TO EVALUATE THE SECONDARY RADIATION QUANTITIES
4530 REM LISTED UNDER OUTPUT VARIABLES
4540 REM
4550 SR1C=PR17C
4560 SR2C=SR1C*A7
4570 SR3C=SR1C*(1-A7)
4580 SR4C=(SR3C+PR10C)*S2
4590 SR5C=SR4C*A5
4600 SR6C=SR4C*(1-A5)
4610 SR7C=SR6C+(SR3C+PR10C)*(1-S2)+R*(1-S1)
4620 SR8C=SR7C*A7
4630 SR9C=SR7C*(1-A7)
4640 REM
4650 REM TO FIND THE TOTAL RADIATION QUANTITIES LISTED
4660 REM UNDER THE OUTPUT VARIABLES
4670 REM
4680 TR1C=PR1C
4690 TR2C=PR2C
4700 TR3C=PR3C+SR8C
4710 TR4C=PR6C+SR5C
4720 TR5C=PR10C
4730 TR6C=PR11C+SR2C
4740 TR7C=PR13C
4750 TR8C=PR14C
```

```
4760 TR9C=PR15C
4770 TR10C=PR16C
4780 TR11C=PR2C+SR9C
4790 REM
4800 REM TO FIND THE COLLECTOR'S OPTICAL EFFICIENCY OECC
4810 REM AND THE AVERAGE NUMBER OF REFLECTIONS ANRC
4820 REM
4830 OECC=(TR10C/TR1C)*100
4840 ANRC=X7
4850 REM
4860 PRINT #5
4870 PRINT #5
4880 PRINT #5,C1$;AI
4890 PRINT #5
4900 PRINT #5,C2$;L(N)
4910 PRINT #5
4920 PRINT #5,C3$;PR1C
4930 PRINT #5,C4$;PR2C
4940 PRINT #5,C5$;PR3C
4950 PRINT #5,C6$;PR4C
4960 PRINT #5,C7$;PR5C
4970 PRINT #5,C8$;PR6C
4980 PRINT #5,C9$;PR7C
4990 PRINT #5,D1$;PR8C
5000 PRINT #5,D2$;PR9C
5010 PRINT #5,D3$;PR10C
5020 PRINT #5,D4$;PR11C
5030 PRINT #5,D5$;PR12C
5040 PRINT #5,D6$;PR13C
5050 PRINT #5,D7$;PR14C
5060 PRINT #5,D8$;PR15C
5070 PRINT #5,D9$;PR16C
5080 PRINT #5,E1$;PR17C
5090 PRINT #5
5100 PRINT #5,E2$;SR1C
5110 PRINT #5,E3$;SR2C
5120 PRINT #5,E4$;SR3C
5130 PRINT #5,E5$;SR4C
5140 PRINT #5,E6$;SR5C
5150 PRINT #5,E7$;SR6C
5160 PRINT #5,E8$;SR7C
5170 PRINT #5,E9$;SR8C
5180 PRINT #5,F1$;SR9C
5190 PRINT #5
5200 PRINT #5,F2$;TR1C
5210 PRINT #5,F3$;TR2C
5220 PRINT #5,F4$;TR3C
5230 PRINT #5,F5$;TR4C
5240 PRINT #5,F6$;TR5C
5250 PRINT #5,F7$;TR6C
5260 PRINT #5,F8$;TR7C
5270 PRINT #5,F9$;TR8C
5280 PRINT #5,G1$;TR9C
5290 PRINT #5,G2$;TR10C
5300 PRINT #5,G3$;TR11C
5310 PRINT #5
5320 PRINT #5,G4$;ANRC
5330 PRINT #5
5340 PRINT #5,G5$;OECC
5350 PRINT #5
```

```
5360 REM
5370 REM TO FIND THE OUTPUT VARIABLES FOR THE WHOLE
     COLLECTOR
5380 REM
5390 PR1T=PR1+PR1C
5400 PR2T=PR2+PR2C
5410 PR3T=PR3+PR3C
5420 PR4T=PR4+PR4C
5430 PR5T=PR5+PR5C
5440 PR6T=PR6+PR6C
5450 PR7T=PR7+PR7C
5460 PR8T=PR8+PR8C
5470 PR9T=PR9+PR9C
5480 PR10T=PR10+PR10C
5490 PR11T=PR11+PR11C
5500 PR12T=PR12+PR12C
5510 PR13T=PR13+PR13C
5520 PR14T=PR14+PR14C
5530 PR15T=PR15+PR15C
5540 PR16T=PR16+PR16C
5550 PR17T=PR17+PR17C
5560 SR1T=SR1+SR1C
5570 SR2T=SR2+SR2C
5580 SR3T=SR3+SR3C
5590 SR4T=SR4+SR4C
5600 SR5T=SR5+SR5C
5610 SR6T=SR6+SR6C
5620 SR7T=SR7+SR7C
5630 SR8T=SR8+SR8C
5640 SR9T=SR9+SR9C
5650 TR1T=TR1+TR1C
5660 TR2T=TR2+TR2C
5670 TR3T=TR3+TR3C
5680 TR4T=TR4+TR4C
5690 TR5T=TR5+TR5C
5700 TR6T=TR6+TR6C
5710 TR7T=TR7+TR7C
5720 TR8T=TR8+TR8C
5730 TR9T=TR9+TR9C
5740 TR10T=TR10+TR10C
5750 TR11T=TR11+TR11C
5760 ANRT=ANR+ANRC
5770 OECT=(TR10T/TR1T)*100
5780 FAC=C(N)+L(N)
5790 REM
5800 REM FAC REPRESENTS THE FRACTION OF APERTURE COVERED
5810 REM FOR THE WHOLE COLLECTOR
5820 REM
5830 PRINT #5
5840 PRINT #5
5850 PRINT #5,I3$
5860 PRINT #5
5870 PRINT #5
5880 PRINT #5,C1$;AI
5890 PRINT #5,C2$;FAC
5900 PRINT #5,C3$;PR1T
5910 PRINT #5,C4$;PR2T
5920 PRINT #5,C5$;PR3T
5930 PRINT #5,C6$;PR4T
5940 PRINT #5,C7$;PR5T
```

```
5950 PRINT #5,C8$;PR6T
5960 PRINT #5,C9$;PR7T
5970 PRINT #5,D1$;PR8T
5980 PRINT #5,D2$;PR9T
5990 PRINT #5,D3$;PR10T
6000 PRINT #5,D4$;PR11T
6010 PRINT #5,D5$;PR12T
6020 PRINT #5,D6$;PR13T
6030 PRINT #5,D7$;PR14T
6040 PRINT #5,D8$;PR15T
6050 PRINT #5,D9$;PR16T
6060 PRINT #5,E1$;PR17T
6070 PRINT #5
6080 PRINT #5,E2$;SR1T
6090 PRINT #5,E3$;SR2T
6100 PRINT #5,E4$;SR3T
6110 PRINT #5,E5$;SR4T
6120 PRINT #5,E6$;SR5T
6130 PRINT #5,E7$;SR6T
6140 PRINT #5,E8$;SR7T
6150 PRINT #5,E9$;SR8T
6160 PRINT #5,F1$;SR9T
6170 PRINT #5
6180 PRINT #5,F2$;TR1T
6190 PRINT #5,F3$;TR2T
6200 PRINT #5,F4$;TR3T
6210 PRINT #5,F5$;TR4T
6220 PRINT #5,F6$;TR5T
6230 PRINT #5,F7$;TR6T
6240 PRINT #5,F8$;TR7T
6250 PRINT #5,F9$;TR8T
6260 PRINT #5,G1$;TR9T
6270 PRINT #5,G2$;TR10T
6280 PRINT #5,G3$;TR11T
6290 PRINT #5
6300 PRINT #5,G4$;ANRT
6310 PRINT #5
6320 PRINT #5,G5$;OECT
6330 CLOSE #5
6340 END
```

A8.4 Results File TPSWR.DAT

***** RESULTS OF THE COMPUTER PROGRAMME TPSWR *****

THE INPUT VARIABLES TO THE PROGRAMME ARE GIVEN BELOW

1.	THE TOTAL SOLAR INSOLATION ON A SURFACE INCLINED AT THE SAME ANGLE AS THE OUTER GLAZING IN W/SQ.M	I = 946
2.	THE TRANSMITTANCE OF GLAZING MATERIAL	T2 = 0.885
3.	THE REFLECTIVITY OF GLAZING MATERIAL	R9 = 0.0838
4.	THE ABSORPTIVITY OF GLAZING MATERIAL	A7 = 0.0312
5.	THE SPECULAR REFLECTANCE OF THE REFLECTOR	R1 = 0.76
6.	THE DIFFUSE REFLECTANCE OF THE REFLECTOR	R2 = 0.09
7.	THE ABSORPTANCE OF THE REFLECTOR	A5 = 0.15
8.	THE ABSORPTANCE OF THE ABSORBER PANEL	A6 = 0.93
9.	THE APERTURE AREA IN SQ.M	A4 = 0.58212
10.	THE SHAPE FACTOR BETWEEN REFLECTOR AND INNER GLAZING	S1 = 0.43153
11.	THE SHAPE FACTOR BETWEEN INNER GLAZING AND REFLECTOR	S2 = 0.62672
12.	THE LATITUDE OF THE PLACE IN DEGREES	A2 = 43.5
13.	THE EWV ANGLE IN DEGREES	A1 = 56.65

DATE = 24 FEB 1984

THE OUTPUT VARIABLES OF THE PROGRAMME ARE GIVEN BELOW

NOTE: PR = PRIMARY RADIATION, WHICH IS THE RADIATION TRAVELLING TOWARDS THE ABSORBER PANEL
SR = SECONDARY RADIATION, WHICH IS THE RADIATION TRAVELLING AWAY FROM THE ABSORBER PANEL
TR = TOTAL RADIATION, WHICH IS THE SUM OF THE PRIMARY AND SECONDARY RADIATIONS
ALL THE RADIATION QUANTITIES ARE IN WATTS

FOR THE TOP QUADRANT

1.	THE ANGLE OF INCIDENCE OF THE INCOMING RAYS	AI = 10.15
2.	THE FRACTION OF THE APERTURE COVERED	C(N) = .5
3.	PR INCIDENT ON THE OUTER GLAZING	PR1 = 275.343
4.	PR REFLECTED BY THE OUTER GLAZING	PR2 = 23.0737
5.	PR ABSORBED BY THE OUTER GLAZING	PR3 = 8.59069
6.	PR TRANSMITTED THROUGH THE OUTER GLAZING	PR4 = 243.678
7.	PR INCIDENT ON THE REFLECTOR	PR5 = 200.053
8.	PR ABSORBED BY THE REFLECTOR	PR6 = 33.1161
9.	PR SPECULARLY REFLECTED BY THE REFLECTOR	PR7 = 147.068
10.	PR DIFFUSELY REFLECTED BY THE REFLECTOR	PR8 = 19.8696
11.	PR INCIDENT ON THE INNER GLAZING	PR9 = 199.267
12.	PR REFLECTED BY THE INNER GLAZING	PR10 = 16.6986
13.	PR ABSORBED BY THE INNER GLAZING	PR11 = 6.21713
14.	PR TRASMITTED THROUGH THE INNER GLAZING	PR12 = 176.351
15.	PR (SPECULAR) INCIDENT ON THE PANEL	PR13 = 168.763
16.	PR (DIFFUSE) INCIDENT ON THE PANEL	PR14 = 7.58824
17.	PR (SPECULAR+DIFFUSE) INCIDENT ON PANEL	PR15 = 176.351
18.	PR ABSORBED BY THE ABSORBER PANEL	PR16 = 164.007
19.	PR REFLECTED BY THE ABSORBER PANEL	PR17 = 12.3446
20.	SR INCIDENT ON THE INNER GLAZING	SR1 = 12.3446
21.	SR ABSORBED BY THE INNER GLAZING	SR2 = .385151

22.	SR TRASMITTED BY THE INNER GLAZING	SR3 = 11.9594
23.	SR INCIDENT ON THE REFLECTOR	SR4 = 17.9604
24.	SR ABSORBED BY THE REFLECTOR	SR5 = 2.69407
25.	SR REFLECTED BY THE REFLECTOR	SR6 = 15.2664
26.	SR (TOTAL) INCIDENT ON THE OUTER GLAZING	SR7 = 37.2593
27.	SR ABSORBED BY THE OUTER GLAZING	SR8 = 1.16249
28.	SR TRANSMITTED BY THE OUTER GLAZING	SR9 = 36.0968
29.	TR INCIDENT ON THE OUTER GLAZING	TR1 = 275.343
30.	TR REFLECTED BY THE OUTER GLAZING	TR2 = 23.0737
31.	TR ABSORBED BY THE OUTER GLAZING	TR3 = 9.75318
32.	TR ABSORBED BY THE REFLECTOR	TR4 = 35.8101
33.	TR REFLECTED BY THE INNER GLAZING	TR5 = 16.6986
34.	TR ABSORBED BY THE INNER GLAZING	TR6 = 6.60228
35.	TR (SPECULAR) INCIDENT ON THE PANEL	TR7 = 168.763
36.	TR (DIFFUSE) INCIDENT ON THE PANEL	TR8 = 7.58824
37.	TR (SPECULAR+DIFFUSE) INCIDENT ON PANEL	TR9 = 176.351
38.	TR ABSORBED BY THE ABSORBER PANEL	TR10 = 164.007
39.	TR LOST TO THE ATMOSPHERE	TR11 = 59.1705
40.	AVERAGE NUMBER OF RELECTIONS	ANR = .470106
41.	OPTICAL EFFICIENCY OF THE COLLECTOR IN %	OEC = 59.5645

FOR THE BOTTOM QUADRANT

1.	THE ANGLE OF INCIDENCE OF THE INCOMING RAYS	AI = 10.15
2.	THE FRACTION OF THE APERTURE COVERED	C(N) = .5
3.	PR INCIDENT ON THE OUTER GLAZING	PR1 = 275.343
4.	PR REFLECTED BY THE OUTER GLAZING	PR2 = 23.0737
5.	PR ABSORBED BY THE OUTER GLAZING	PR3 = 8.59069
6.	PR TRANSMITTED THROUGH THE OUTER GLAZING	PR4 = 243.678
7.	PR INCIDENT ON THE REFLECTOR	PR5 = 243.678
8.	PR ABSORBED BY THE REFLECTOR	PR6 = 42.0175
9.	PR SPECULARLY REFLECTED BY THE REFLECTOR	PR7 = 176.45
10.	PR DIFFUSELY REFLECTED BY THE REFLECTOR	PR8 = 25.2105
11.	PR INCIDENT ON THE INNER GLAZING	PR9 = 187.329
12.	PR REFLECTED BY THE INNER GLAZING	PR10 = 15.6982
13.	PR ABSORBED BY THE INNER GLAZING	PR11 = 5.84468
14.	PR TRASMITTED THROUGH THE INNER GLAZING	PR12 = 165.787
15.	PR (SPECULAR) INCIDENT ON THE PANEL	PR13 = 156.159
16.	PR (DIFFUSE) INCIDENT ON THE PANEL	PR14 = 9.62792
17.	PR (SPECULAR+DIFFUSE) INCIDENT ON PANEL	PR15 = 165.787
18.	PR ABSORBED BY THE ABSORBER PANEL	PR16 = 154.181
19.	PR REFLECTED BY THE ABSORBER PANEL	PR17 = 11.6051
20.	SR INCIDENT ON THE INNER GLAZING	SR1 = 11.6051
21.	SR ABSORBED BY THE INNER GLAZING	SR2 = .362078
22.	SR TRASMITTED BY THE INNER GLAZING	SR3 = 11.243
23.	SR INCIDENT ON THE REFLECTOR	SR4 = 16.8845
24.	SR ABSORBED BY THE REFLECTOR	SR5 = 2.53267
25.	SR REFLECTED BY THE REFLECTOR	SR6 = 14.3518
26.	SR (TOTAL) INCIDENT ON THE OUTER GLAZING	SR7 = 38.74
27.	SR ABSORBED BY THE OUTER GLAZING	SR8 = 1.20869
28.	SR TRANSMITTED BY THE OUTER GLAZING	SR9 = 37.5313
29.	TR INCIDENT ON THE OUTER GLAZING	TR1 = 275.343
30.	TR REFLECTED BY THE OUTER GLAZING	TR2 = 23.0737
31.	TR ABSORBED BY THE OUTER GLAZING	TR3 = 9.79938
32.	TR ABSORBED BY THE REFLECTOR	TR4 = 44.5501

33.	TR REFLECTED BY THE INNER GLAZING	TR5 = 15.6982
34.	TR ABSORBED BY THE INNER GLAZING	TR6 = 6.20675
35.	TR (SPECULAR) INCIDENT ON THE PANEL	TR7 = 156.159
36.	TR (DIFFUSE) INCIDENT ON THE PANEL	TR8 = 9.62792
37.	TR (SPECULAR+DIFFUSE) INCIDENT ON PANEL	TR9 = 165.787
38.	TR ABSORBED BY THE ABSORBER PANEL	TR10 = 154.181
39.	TR LOST TO THE ATMOSPHERE	TR11 = 60.605
40.	AVERAGE NUMBER OF RELECTIONS	ANR = .608038
41.	OPTICAL EFFICIENCY OF THE COLLECTOR IN %	OEC = 55.9962

FOR THE WHOLE COLLECTOR

1.	THE ANGLE OF INCIDENCE OF THE INCOMING RAYS	AI = 10.15
2.	THE FRACTION OF THE APERTURE COVERED	C(N) = 1
3.	PR INCIDENT ON THE OUTER GLAZING	PR1 = 550.686
4.	PR REFLECTED BY THE OUTER GLAZING	PR2 = 46.1474
5.	PR ABSORBED BY THE OUTER GLAZING	PR3 = 17.1814
6.	PR TRANSMITTED THROUGH THE OUTER GLAZING	PR4 = 487.357
7.	PR INCIDENT ON THE REFLECTOR	PR5 = 443.732
8.	PR ABSORBED BY THE REFLECTOR	PR6 = 75.1335
9.	PR SPECULARLY REFLECTED BY THE REFLECTOR	PR7 = 323.518
10.	PR DIFFUSELY REFLECTED BY THE REFLECTOR	PR8 = 45.0801
11.	PR INCIDENT ON THE INNER GLAZING	PR9 = 386.596
12.	PR REFLECTED BY THE INNER GLAZING	PR10 = 32.3968
13.	PR ABSORBED BY THE INNER GLAZING	PR11 = 12.0618
14.	PR TRASMITTED THROUGH THE INNER GLAZING	PR12 = 342.138
15.	PR (SPECULAR) INCIDENT ON THE PANEL	PR13 = 324.922
16.	PR (DIFFUSE) INCIDENT ON THE PANEL	PR14 = 17.2162
17.	PR (SPECULAR+DIFFUSE) INCIDENT ON PANEL	PR15 = 342.138
18.	PR ABSORBED BY THE ABSORBER PANEL	PR16 = 318.188
19.	PR REFLECTED BY THE ABSORBER PANEL	PR17 = 23.9496
20.	SR INCIDENT ON THE INNER GLAZING	SR1 = 23.9496
21.	SR ABSORBED BY THE INNER GLAZING	SR2 = .747229
22.	SR TRASMITTED BY THE INNER GLAZING	SR3 = 23.2024
23.	SR INCIDENT ON THE REFLECTOR	SR4 = 34.8449
24.	SR ABSORBED BY THE REFLECTOR	SR5 = 5.22674
25.	SR REFLECTED BY THE REFLECTOR	SR6 = 29.6182
26.	SR (TOTAL) INCIDENT ON THE OUTER GLAZING	SR7 = 75.9993
27.	SR ABSORBED BY THE OUTER GLAZING	SR8 = 2.37118
28.	SR TRANSMITTED BY THE OUTER GLAZING	SR9 = 73.6281
29.	TR INCIDENT ON THE OUTER GLAZING	TR1 = 550.686
30.	TR REFLECTED BY THE OUTER GLAZING	TR2 = 46.1474
31.	TR ABSORBED BY THE OUTER GLAZING	TR3 = 19.5526
32.	TR ABSORBED BY THE REFLECTOR	TR4 = 80.3603
33.	TR REFLECTED BY THE INNER GLAZING	TR5 = 32.3968
34.	TR ABSORBED BY THE INNER GLAZING	TR6 = 12.809
35.	TR (SPECULAR) INCIDENT ON THE PANEL	TR7 = 324.922
36.	TR (DIFFUSE) INCIDENT ON THE PANEL	TR8 = 17.2162
37.	TR (SPECULAR+DIFFUSE) INCIDENT ON PANEL	TR9 = 342.138
38.	TR ABSORBED BY THE ABSORBER PANEL	TR10 = 318.188
39.	TR LOST TO THE ATMOSPHERE	TR11 = 119.776
40.	AVERAGE NUMBER OF RELECTIONS	ANR = 1.07814
41.	OPTICAL EFFICIENCY OF THE COLLECTOR IN %	OEC = 57.7804

APPENDIX A9

RADIATION SHAPE FACTORS

In short wave and long wave analyses it is necessary to know radiation shape factors between different parts of the collector and in this appendix an attempt is made to evaluate them.

Radiation shape factor (also known as configuration factor, angle factor, form factor, view factor, direct exchange factor or shape modulus) between two black surfaces separated by a nonabsorbing medium, can be defined as the fraction of energy directly incident on one surface, from another surface assumed to be emitting energy diffusely. In actual practice very few surfaces are black (which means all the energy striking the surface is not absorbed, only part of it is absorbed and part reflected back to another surface) and the intervening medium is generally absorbing-emitting, which makes the analysis of the problem extremely complicated. In such cases Hottel and Sarofim (1967) define total exchange areas which take into account multiple reflections of partly specular and partly diffuse surfaces and also absorptivity of the medium. They have suggested different ways of tackling this problem as have Holman (1972) and Wiebelt (1966). In order to simplify the calculations the surfaces may be assumed to be grey (which means the monochromatic emittance is constant with respect to wave length) or have specular reflectance and diffuse emittance. Their assumptions do not bring in considerable error because short wave and long wave behaviours are analysed separately. The effect of the presence of an absorbing-emitting media is considered in the long wave analysis.

The geometries of various parts of the collector are quite complicated. In order to find relatively simple geometric shape factors such as the shape factor between the end wall and inner (or outer) glazing using the basic definition of a shape factor, one needs to solve a quadruple integration. Because it is extremely difficult and time consuming to evaluate shape factors accurately from basic definitions, simplifying assumptions are made and standard charts are used to evaluate the shape factors.

FIGURE A9.1 Shape Factor Between the Inner and Outer Glazings

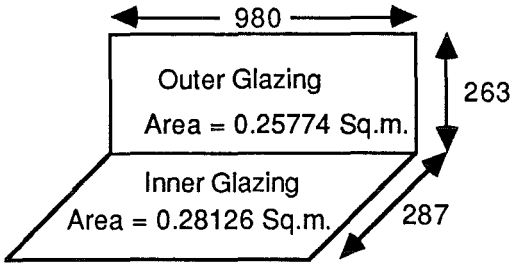

FIGURE A9.2 Shape Factor Between the End Wall and the Outer Glazing

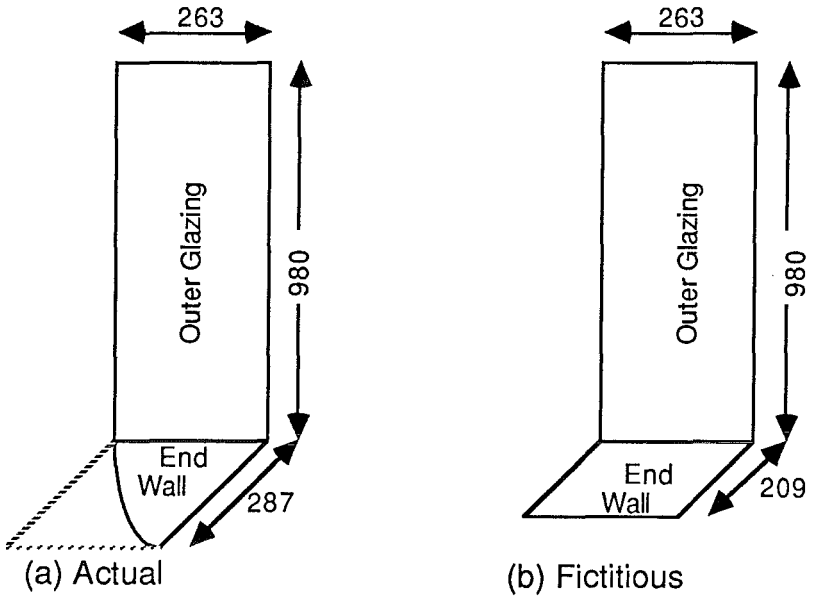

FIGURE A9.3 Shape Factor Between the End Wall and the Inner Glazing

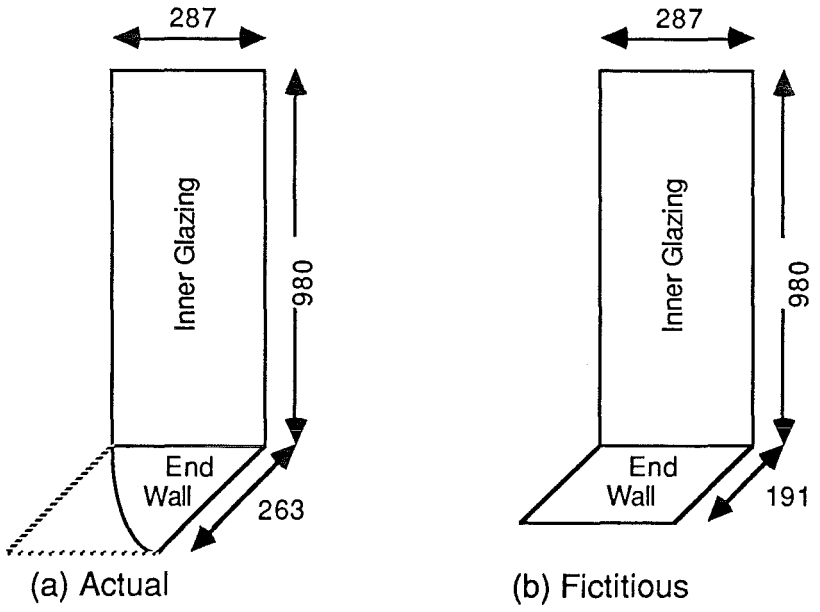

Note: All dimensions are in mm and the figures are not to scale

It should be noted that the shape factors given in this appendix are for collector C1.

The shape factors are evaluated for two specific cases, firstly for a collector with end walls and secondly for a collector without end walls, that is infinitely long (a hypothetical case).

A9.1 Shape Factors for a Collector with End Walls

Different shape factors can be evaluated as described in the following sections.

(1) Shape factor between the two end walls (e1 and e2) opposite to each other :

We can get the shape factor for two full circles each of radius equal to 275 mm and coaxial to each other and separated from each other by 980 mm (Wiebelt, 1966). $F_{4e1-4e2} = 0.075$ (because 4e1, and 4e2 represent full circles). To get the shape factor between one quadrant of each of the circles, first consider a square of length 275 mm then a square of length 550 mm (which has 4 times the area of the previous one) separated from each other by 980 mm. It can be seen that when the area is increased by 4 times, the shape factor increases by 3.74 times (Holman, 1972). Assuming the same kind of relationship holds good for a quarter circle, the shape factor $F_{e1 - e2} = 0.02$

(2) Shape factor between the inner glazing (ig) and the outer glazing (og) :

As seen from the Fig. A9.1, F_{ig-og} falls in the category of a shape factor between perpendicular rectangles with a common edge. F_{ig-og} from Holman (1972) is given by $F_{ig-og} = 0.26$

From the reciprocity theorem

$$A_{ig} F_{ig-og} = A_{og} F_{og-ig} \qquad \text{(A9.1)}$$

Therefore, $F_{og-ig} = 0.284$

(3) Shape factor between the end wall (e) and the outer glazing :

As it is very hard to evaluate the shape factor between a quarter circle and a rectangle at 90° to it, for simplicity we can assume a rectangle of same area as that of the end wall Fig. A9.2. Then the width becomes 209 mm and $F_{e1-og} = 0.27$ (from Holman, 1972). From the reciprocity theorem $F_{og-e1} = 0.058$. If both the end walls are considered, $F_{og-e} = 0.115$. From reciprocity theorem $F_{e-og} = 0.27$.

(4) Shape factor between the end wall and the inner glazing :

It is similar to finding the shape factor between the end wall and the outer glazing Fig. A9.3. The fictitious width in this case becomes 191 mm. F_{el-ig} = 0.29 (Holman, 1972). Even if the full rectangle of 263 mm x 287 mm is considered F_{el-ig} = 0.25. From the reciprocity theorem

F_{ig-el} = 0.057

If both the end walls are considered F_{ig-e} = 0.114

Therefore, $F_{e-ig} = (A_{og}/A_e)\ F_{ig-e}$ = 0.29

(5) Shape factor between reflector and inner glazing :

For a closed enclosure the shape factors with reference to any one particular surface must add up to one and this is known as summation rule. So with reference to inner glazing we have

$$F_{ig-og} + F_{ig-e} + F_{ig-r} = 1 \qquad \text{(A9.2)}$$

Substituting F_{ig-og} and F_{ig-e} values in Eq.(A9.2) we get F_{ig-r} = 0.627. From the reciprocity theorem, substituting A_{ig} = 0.28126 m^2 and A_r = 0.40848 m^2 we get F_{r-ig} = 0.432.

(6) Shape factor between reflector and outer glazing :

By the summation rule we get F_{og-r} = 0.601. From the reciprocity theorem on substituting A_{og} = 0.25774 m^2 and A_r = 0.40848 m^2 we get

F_{r-og} = 0.379

(7) Shape factor between reflector and end walls :

By the summation rule we get F_{el-r} = 0.42. By the reciprocity theorem on substituting A_{el} = 0.054935 m^2 and A_r = 0.40848 m^2 we get F_{r-el} = 0.056. If both end walls are considered then F_{r-e} = 0.112

Therefore, $F_{e-r} = (A_r/A_e)\ F_{r-e}$ = 0.42

(8) Shape factor between reflector-reflector :

By the summation rule we have

$$F_{r-r} + F_{r-ig} + F_{r-og} + F_{r-e} = 1 \qquad \text{(A9.3)}$$

On substituting F_{r-ig}, F_{r-og} and F_{r-e} values in Eq.(A9.3) we get

F_{r-r} = 0.076

(9) Shape factor between the mirror image of outer glazing in the reflector [og(r)] and the end wall :

In setting up a resistance network for the long wave radiation, the reflector and the end walls are considered specular-diffuse surfaces and hence shape factors involving mirror images need to be evaluated (Holman, 1972). It is difficult to

FIGURE A9.4 Shape Factor Between the Mirror Image of the Outer Glazing in the Reflector and the End Wall

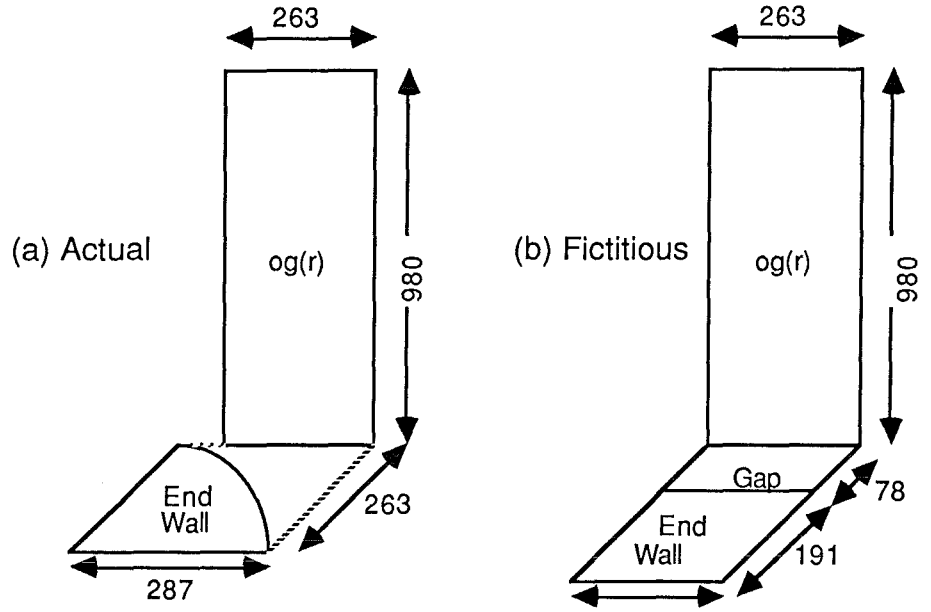

Notes: All dimensions are in mm

The figures are not to scale

og(r) = The mirror image of the outer glazing in the reflector

FIGURE A9.5 Shape Factor Between the Mirror Image of the Inner Glazing in the Reflector and the End Wall

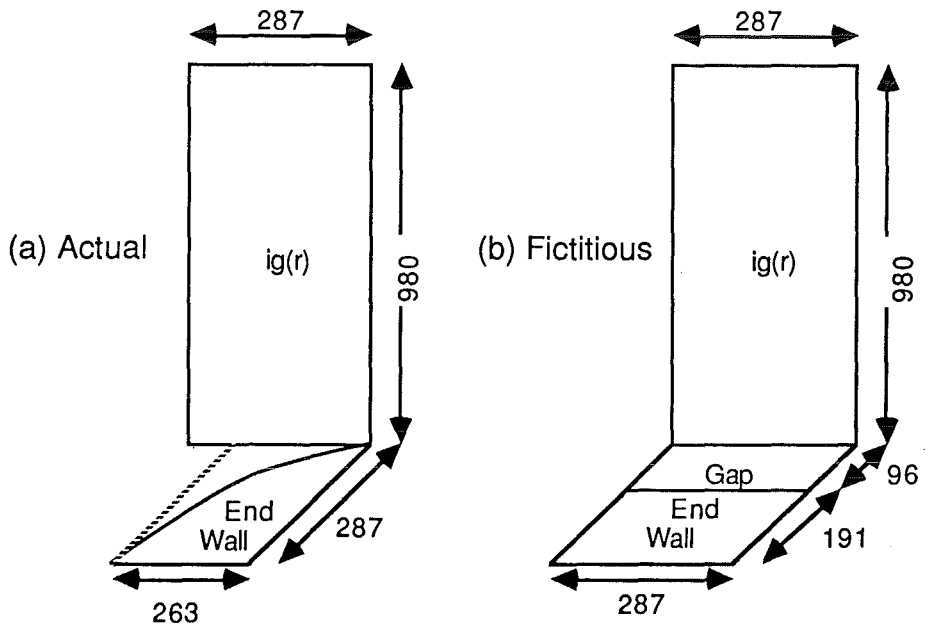

Note: ig(r) = The mirror image of the inner glazing in the reflector

find the shape factor for a curved reflector and so the reflector is assumed to be flat. To avoid complexity in the geometry a fictitious shape as shown in Fig. A9.4 is considered. For the configuration shown in Fig. A9.4 we get

$F_{og(r)-(gap + e1)} = 0.07$ and $F_{og(r)-gap} = 0.03$

Also when two retangles are adjacent and perpendicular to a third rectangle with a common edge we have

$$F_{og(r)-(gap + e1)} = F_{og(r)-gap} + F_{og(r)-e1} \qquad (A9.4)$$

from which we get $F_{og(r)-e1} = 0.04$

From the reciprocity theorem $F_{e1-og(r)} = 0.0188$. If both the end walls are considered then $F_{og(r)-e}=0.08$. From the reciprocity theorem assuming $A_{og(r)} = A_{og}$ we get $F_{e-og(r)} = 0.188$.

(10) Shape factor between the mirror image of inner glazing in the reflector [ig(r)] and the end wall :

The situation is identical to the one evaluating $F_{og(r)-e}$ and Fig. A9.5 shows the actual and fictitious shapes. For the configuration shown in Fig. A9.5 we get $F_{ig(r)-(gap + e1)} = 0.08$ and $F_{ig(r)-gap} = 0.04$.

As we have two rectangles adjacent to a third one

$$F_{ig(r)-(gap + e1)} = F_{ig(r)-gap} + F_{ig(r)-e1} \qquad (A9.5)$$

from which we get $F_{ig(r)-e1} = 0.04$. If both the end walls are considered then $F_{ig(r)-e} = 0.08$. From the reciprocity theorem assuming $A_{ig(r)} = A_{ig}$ we get $F_{e-ig(r)} = 0.205$.

(11) Shape factor between the mirror image of the end wall in the reflector [e(r)] and inner glazing or outer glazing :

Fig. A9.6 shows the mirror image of the end wall in the reflector. On comparing the Figs. A9.4, A9.5 and A9.6, it can be noticed that

$F_{e(r)-ig} = F_{e-ig(r)} = 0.205$ and $F_{e(r)-og} = F_{e-og(r)} = 0.188$

(12) Shape factor between the mirror images of the inner & outer glazings in the reflector [og(r) and ig(r)], and the outer & inner glazings respectively :

Once again the reflector is assumed to be flat. As the inner and outer glazings are of different sizes, the geometry becomes complicated and hence a fictitious shape with an average length is assumed as shown in the Fig. A9.7. The surfaces (1) and (2) represent 'ig' or 'ig(r)', while (3) represents 'og' or 'og(r)'. We have

$$F_{(1+2)-(3+4)} = F_{(1+2)-3} + F_{(1+2)-4} \qquad (A9.6)$$

where $F_{(1+2)-3} = F_{ig(r)-og} = F_{ig-og(r)}$ and hence

FIGURE A9.6 Shape Factor Between the Mirror Image of the End Wall in the Reflector and Inner or Outer Glazings

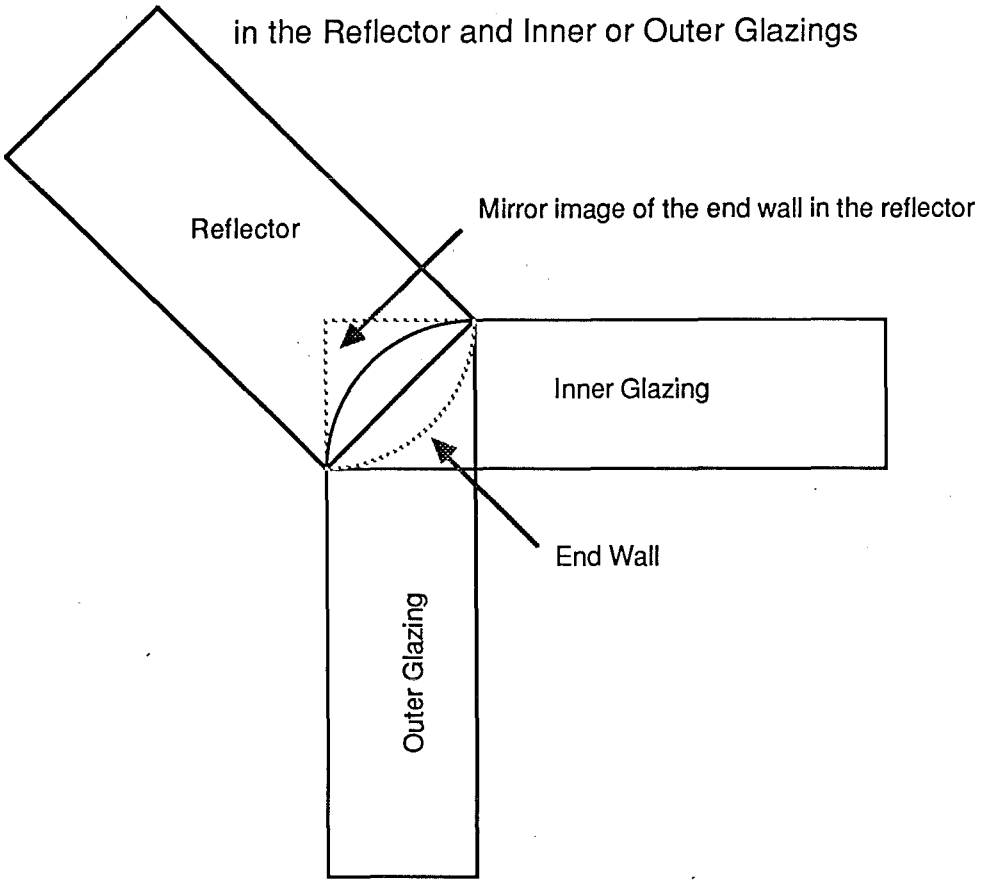

FIGURE A9.7 Shape Factors Between the Mirror Images of Inner and Outer Glazings in the Reflector, and Outer and Inner Glazings Respectively

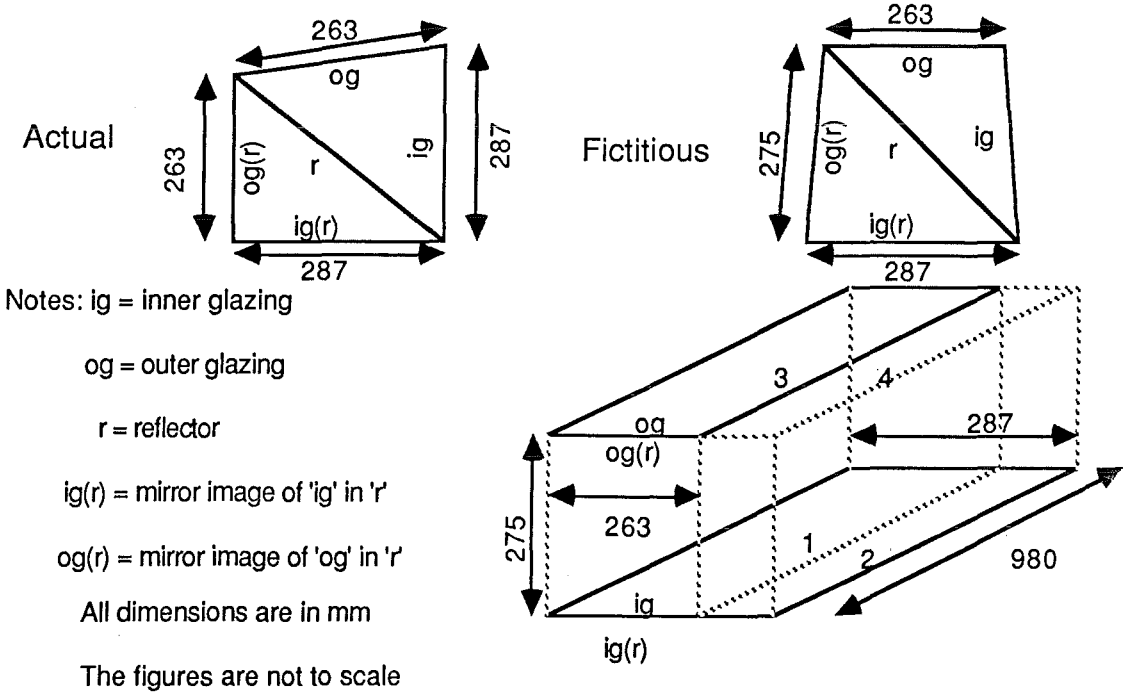

Notes: ig = inner glazing

og = outer glazing

r = reflector

ig(r) = mirror image of 'ig' in 'r'

og(r) = mirror image of 'og' in 'r'

All dimensions are in mm

The figures are not to scale

FIGURE A9.8 Shape Factors Among the Mirror Images of the Inner and Outer Glazings in the End Wall, with the Inner Glazing, the Outer Glazing and the Reflector

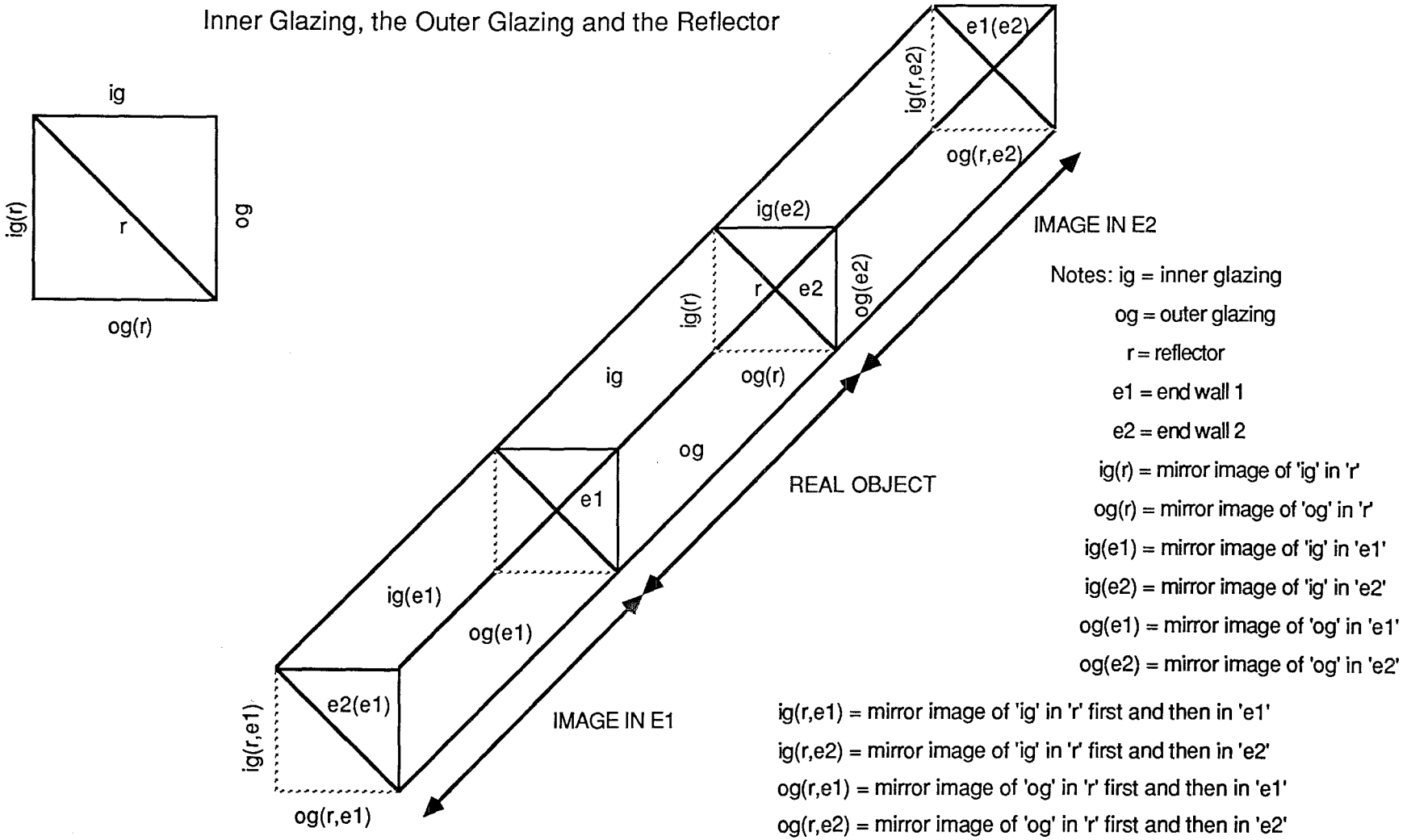

Notes: ig = inner glazing
og = outer glazing
r = reflector
e1 = end wall 1
e2 = end wall 2
ig(r) = mirror image of 'ig' in 'r'
og(r) = mirror image of 'og' in 'r'
ig(e1) = mirror image of 'ig' in 'e1'
ig(e2) = mirror image of 'ig' in 'e2'
og(e1) = mirror image of 'og' in 'e1'
og(e2) = mirror image of 'og' in 'e2'

ig(r,e1) = mirror image of 'ig' in 'r' first and then in 'e1'
ig(r,e2) = mirror image of 'ig' in 'r' first and then in 'e2'
og(r,e1) = mirror image of 'og' in 'r' first and then in 'e1'
og(r,e2) = mirror image of 'og' in 'r' first and then in 'e2'

$F_{(1+2)-3} < F_{(1+2)-(3+4)}$ and $F_{(1+2)-3} > F_{(1-3)}$

From Holman (1972) we get $F_{(1-3)} = 0.32$ and $F_{(1+2)-(3+4)} = 0.33$ which follows that $F_{(1+2)-3} = 0.325$. Therefore, $F_{ig(r)-og} = F_{ig-og(r)} = 0.325$. From the reciprocity theorem we get $F_{og(r)-ig} = 0.355$. Similarly,

$F_{og-ig(r)} = 0.355$. From Holman, (1972) we also have

$F_{ig(r)-og(r)} = F_{ig(r)-ig} = F_{ig-og} = F_{ig-ig(r)} = 0.26$.

(13) Shape factors among the mirror images of the inner & outer glazings in the end wall [ig(e) and og(e)] with the inner glazing, the outer glazing & the reflector :

Fig. A9.8 shows the real object consisting of inner glazing (ig), outer glazing (ig), reflector (r), end walls (e1 and e2) and the images of these in the end wall 1 (e1) and end wall 2 (e2). It also shows double reflections such as 'ig(r,e2)', 'og(r,e2)', 'ig(r,e1)' and 'og(r,e1)', which represent images of 'ig' and 'og' first in 'r' and then in 'e1' or 'e2'. As seen from Fig. A9.8, 'ig(e2)' can see 'og(e2)', 'r(e2)', 'og' & 'r' and not 'ig'. Also we can notice that,

$F_{ig(e2)-og(e2)} = F_{ig-og} = 0.26$ and $F_{ig(e2)-r(e2)} = F_{ig-r} = 0.627$

$F_{ig(e2)-og} + F_{ig(e2)-r} = F_{ig(e2)-e2} = F_{ig-e2} = 0.057$ (A9.7)

Similarly, 'ig(e1)' can see 'og(e1)', 'r(e1)', 'og' & 'r' (but not 'ig') and we have

$F_{ig(e1)-og(e1)} = F_{ig-og} = 0.26$ and $F_{ig(e1)-r(e1)} = F_{ig-r} = 0.627$

$F_{ig(e1)-og} + F_{ig(e1)-r} = F_{ig(e1)-e1} = F_{ig-e1} = 0.057$ (A9.8)

Adding Eqs.(A9.7) and (A9.8)

$F_{ig(e)-og} + F_{ig(e)-r} = F_{ig-e} = 0.113$

because, $F_{ig(e1)-og} + F_{ig(e2)-og} = F_{ig(e)-og}$ and

$F_{ig(e1)-r} + F_{ig(e2)-r} = F_{ig(e)-r}$ and $F_{ig-e1} + F_{ig-e2} = F_{ig-e}$

Assuming that 'ig(e)' can see 'og' and 'r' in the same ratio as 'ig' can see 'og' and 'r'. We have, $F_{ig(e)-og} = 0.033$ and $F_{ig(e)-r} = 0.08$. Applying the same logic to 'og(e)' and 'ig','og(e)' and 'r' we have

$F_{og(e)-ig} + F_{og(e)-r} = F_{og-e} = 0.115$

where $F_{og(e)-ig} = F_{og(e1)-ig} + F_{og(e2)-ig}$

and $F_{og(e)-r} = F_{og(e1)-r} + F_{og(e2)-r}$ and $F_{og-e} = F_{og-e1} + F_{og-e2}$

Assuming that 'og(e)' can see 'ig' and 'r' in the same ratio as 'og' can see 'ig' and 'r'. The ratio $F_{og-r}/F_{og-ig} = 2.1$, therefore,

$F_{og(e)-ig} = 0.037$ and $F_{og(e)-r} = 0.078$

FIGURE A9.9 Shape Factors for the Inner Air Box

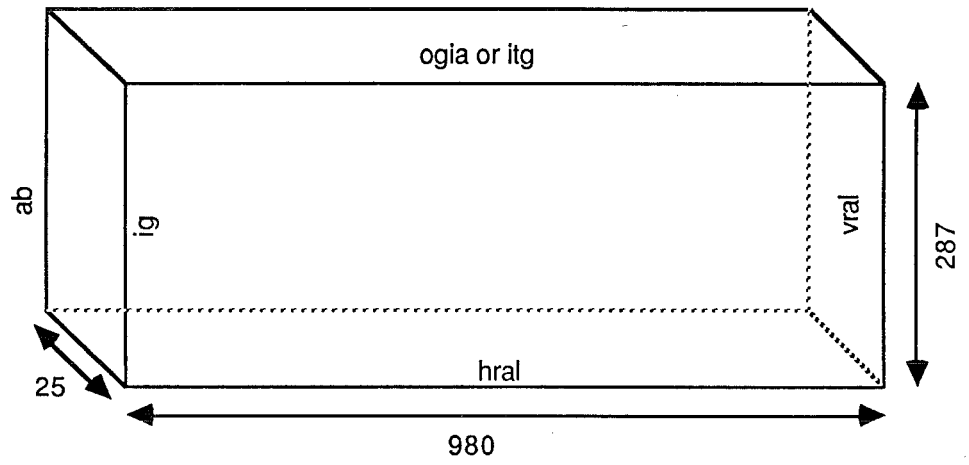

Notes: ig = inner glazing

ab = absorber panel

hral = horizontal aluminium strip

vral = vertical aluminium strip

ogia = outer glazing in contact with inner air (in the case of HSA1)

itg = inner top glazing strip (in the case of HSA2)

All dimensions are in mm

The figure is not to scale

(14) To find the shape factor between the mirror image of the inner glazing in the reflector first and then the end wall and the outer glazing ($F_{ig-r-e-og}$):

Referring to the Fig. A9.8 and considering the reflection of 'ig','og','ig(r)', 'og(r)' in 'e2' we can notice that 'ig(r,e2)' can see 'ig(e2)', 'og(e2)', 'og(r,e2)', 'ig', 'og', 'r' and 'og(r)'.

The imaginary rectangular box formed by 'ig(r,e2)', 'ig(e2)','og(e2)', 'og(r,e2)' is identical to the box formed by 'ig', 'og', 'og(r)' and 'ig(r)'. Therefore, we have

$F_{ig(r)-og(r)} = 0.26 = F_{ig(r,e2)-og(r,e2)}$

$F_{ig(r)-ig} = 0.26 = F_{ig(r,e2)-ig(e2)}$

$F_{ig(r)-og} = 0.325 = F_{ig(r,e2)-og(e2)}$

Same relationships hold good for the other end wall 'e1'. So combining both of them, applying summation rule and simplifying gives

$$F_{ig(r,e)-ig} + F_{ig(r,e)-og} + F_{ig(r,e)-0g(r)} + F_{ig(r,e)-r}$$
$$= 1-[F_{ig(r,e)-og(r,e)} + F_{ig(r,e)-ig(e)} + F_{ig(r,e)-og(e)}]$$
$$= 1-(0.26 + 0.26 + 0.325) = 0.155$$

As seen before the imaginary rectangular box formed by 'ig(r,e)','og(r,e)', 'ig(e)' and 'og(e)' is identical to the box formed by 'ig(r)', 'og(r)', 'ig' and 'og'. Hence dividing the shape factor in the same ratio (0.26:0.325:0.26:0.627) we have

$F_{ig(r,e)-ig} = 0.027$, $F_{ig(r,e)-og} = 0.342$, $F_{ig(r,e)-og(r)} = 0.027$ and

$F_{ig(r,e)-r} = 0.066$

(15) To find the shape factor between the mirror image of the inner glazing first in the end wall and then in the reflector and the outer glazing [$F_{ig(e,r)-og}$]:

We can see from the Fig. A9.8, $F_{ig(r,e)-og} = F_{ig(e,r)-og} = 0.034$

(16) Shape factor for the inner air box :

The heat sheet absorber panel is enclosed with two inner glazings, a horizontal aluminium strip and two vertical aluminium strips. In the case of the collector 2, it has also inner top glazing to make the inner box almost air tight. One half of the inner box is shown in the Fig. A9.9 as the shape factor are evaluated for only one quadrant.

As the absorber and inner glazing can be considered as two equal rectangles separated from each other by 25 mm, we can get the shape factor from the chart given by Wiebelt (1966).

FIGURE A9.10 Shape Factors for a Collector without End Walls

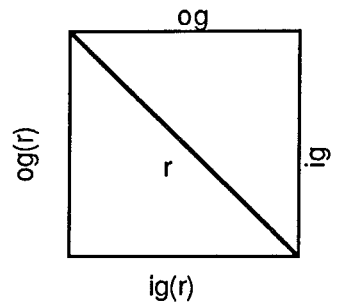

Notes: ig = inner glazing

og = outer glazing

r = reflector

ig(r) = mirror image of 'ig' in 'r'

og(r) = mirror image of 'og' in 'r'

FIGURE A9.11 Shape Factors for the Inner Air Box for a Collector without End Walls

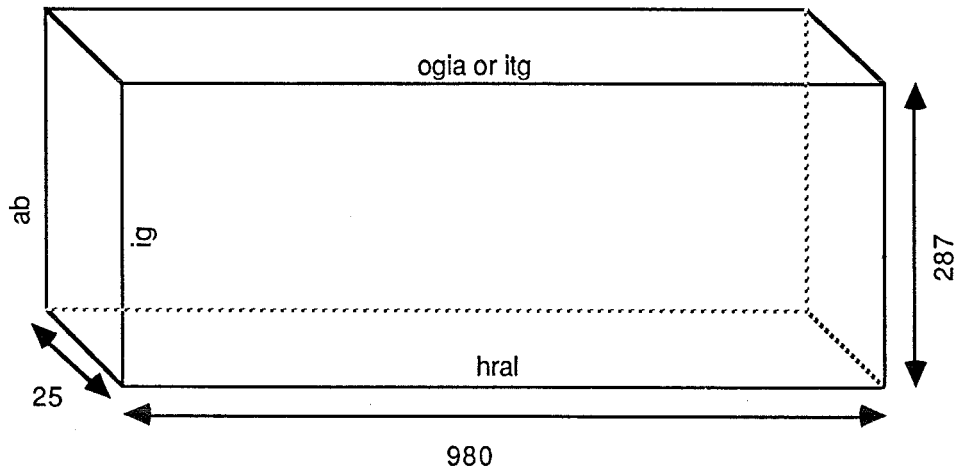

Notes: ig = inner glazing

ab = absorber panel

hral = horizontal aluminium strip

ogia = outer glazing in contact with inner air (in the case of HSA1)

itg = inner top glazing strip (in the case of HSA2)

All dimensions are in mm

The figure is not to scale

$F_{ab-ig} = F_{ig-ab} = 0.9$

The horizontal aluminium strip and the absorber are two rectangles at 90° to each other with a common edge and we have from Incropera (1981)

$F_{hral-ab} = F_{hral-ig} = 0.47$ (because $A_{ab} = A_{ig}$)

$F_{ogia-ab} = F_{ogia-ig} = 0.47$ (because $A_{ab} = A_{ig}$)

From the reciprocity theorem $F_{ab-\ hral} = 0.041$

Similarly, $F_{ig-hral} = F_{ab-ogia} = F_{ig-ogia} = 0.041$

Applying the summation rule we have

$F_{ab-ig} + F_{ab-hral} + F_{ab-ogia} + F_{ab-vral} = 1$ (A9.9)

from which we get $F_{ab-vral} = 0.018$ and $F_{ig-vral} = 0.018$

The horizontal aluminium strip and the outer glazing in contact with the inner air can be considered as two equal rectangles separated from each other by 287 mm and we have (Holman,1972), $F_{hral-ogia} = 0.035$. Similarly, $F_{ogia-hral} = 0.035$

By the summation rule we have

$F_{hral-ab} + F_{hral-ig} + F_{hral-ogia} + F_{hral-vral} = 1$ (A9.10)

from which $F_{hral-vral} = 0.025$

From the reciprocity theorem $F_{vral-hral} = F_{vral-ogia} = 0.043$

There are two vertical aluminium strips opposite to each other. However, the amount of energy exchanged between the two is very minimal as seen from Incropera (1981). By the summation rule, we have

$F_{vral-ab} + F_{vral-ig} + F_{vral-hral} + F_{vral-ogia} = 1$ (A9.11)

As $F_{vral-ab} = F_{vral-ig}$, we get $F_{vral-ab} = F_{vral-ig} = 0.457$

A9.2 Shape Factors for a Collector without End Walls :

This is a hypothetical case which is used mainly for comparison and to find out the effect of the end walls on the performance of the collector. In practice, a collector which is substantially long (as compared to its width) approaches this case. For simplicity of calculations the inner and outer glazings are assumed to be of same width and the reflector to be flat (Fig. A9.10). Hence

$A_{ig} = A_{og}$ and $(A_r/A_{ig}) = (A_r/A_{og}) = \sqrt{(2)}$

By symmetry, $F_{r-ig} = F_{r-og}$ and $F_{r-ig} + F_{r-og} = 1$ Hence, $F_{r-ig} = F_{r-og} = 0.5$. From the reciprocity theorem $F_{ig-r} = F_{og-r} = 0.707$ and by the summation rule $F_{ig-og} = 1 - F_{ig-r} = F_{og-ig} = 0.293$

From Fig. A9.10 it can noticed that,

$F_{ig-og} = F_{og-ig} = F_{ig-ig(r)} = F_{og-og(r)} = 0.293$

By the summation rule we have $F_{og-og(r)} + F_{og-ig} + F_{og-ig(r)} = 1$

Therefore, $F_{og-ig(r)} = 0.414$ and by symmetry,

$F_{og-ig(r)} = F_{ig(r)-og} = 0.414$

Shape factors for the inner air box :

For two infinitely long parallel retangular planes separated by a distance of 25 mm (Fig. A9.11) we have (Wiebelt,1966) $F_{ab-ig} = 0.91$ and $F_{ig-ab} = 0.91$

By the summation rule $F_{ab-ig} + F_{ab-hral} + F_{ab-ogia} = 1$

Because, $F_{ab-hral} = F_{ab-ogia}$, $F_{ab-hral} = 0.045$

Similarly, $F_{ab-ogia} = F_{ig-hral} = F_{ig-ogia} = 0.045$

For two infinitely long rectangular planes separated by a distance of 287 mm we have (Holman, 1972), $F_{hral-ogia} = F_{ogia-hral} = 0.04$

By the summation rule $F_{hral-ab} + F_{hral-ig} + F_{hral-ogia} = 1$

As $F_{hral-ab} = F_{hral-ig}$, we have, $F_{hral-ab} = F_{hral-ig} = 0.48$

The shape factors used in the simulation programme are tabulated in LONG.DAT (Appendix A10).

FIGURE A10.1 Cross Section of the HSA-SCCR Collector with the Temperature Measuring Points (Not to Scale)

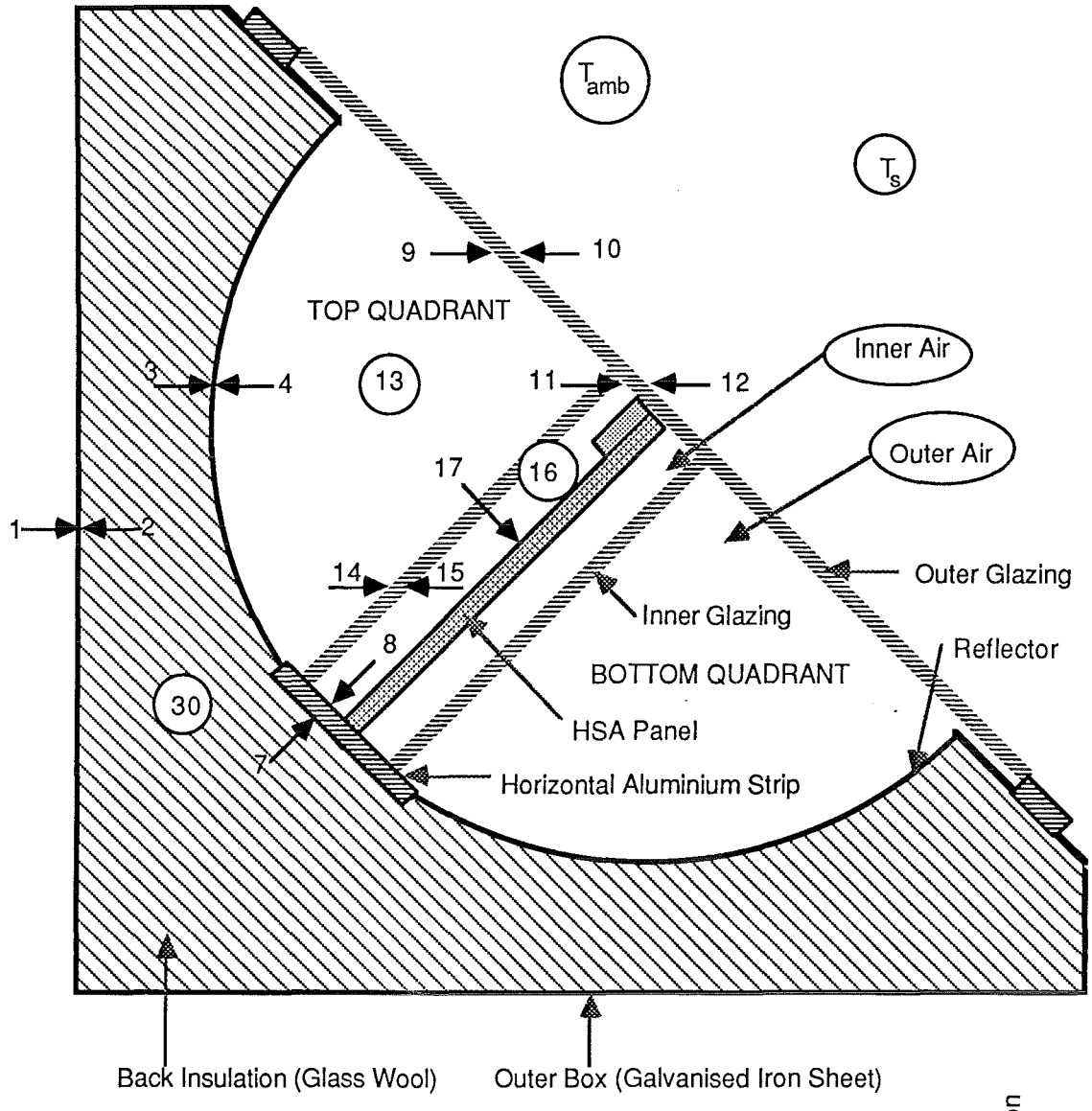

Notes: Nembers indicate temperatures

○ = Air temperature

→ = Surface temperature

T_{amb} = Ambient temperature

T_s = Sky temperature

20 to 29,33 = Dummy temperatures

Cross Section of the End Wall

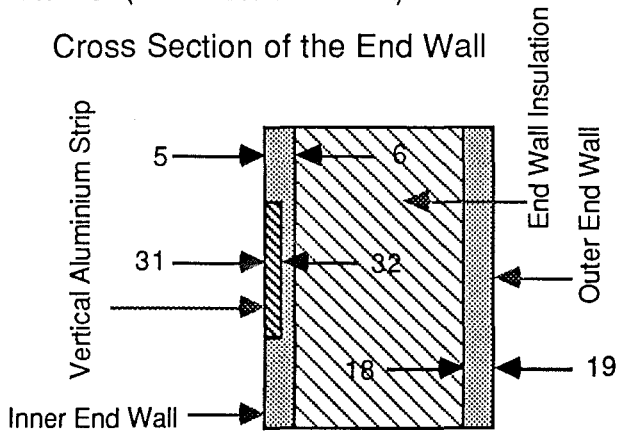

APPENDIX A10

ANALYSIS OF LONG WAVE RADIATION

The computer programme TPLWR analyses the long wave behaviour of the collector. It evaluates the temperatures, thermal resistances and heat flow paths through the collector under stagnation conditions. The model consists of two parallel networks.

(1) Conduction and convection resistance network

(2) Radiation resistance network

These two networks have the same junctions or nodal points (which are space or surface temperatures) as shown in Fig. A10.1. There are 35 temperatures (Fig. A10.1) including the ambient temperature, sky temperature and 11 dummy temperatures (which are required to solve the radiation netowrk). All the temperatures are assumed to indicate the mean values and not point values, also all the surfaces are assumed to be isothermal. Outer air denotes the air trapped between the outer glazing, inner glazing and the reflector, while the inner air denotes the air trapped between the inner glazing and the abosrber.

It should be noted that analysis of long wave radiation is also done for only one quadrant, just as was done in case of short wave radiation. While all other quantities remain the same for both the top and the bottom quadrants, the power abosrbed is different as seen from TPSWR, which implies that the top and the bottom quadrants attain slightly different set of temperatures. However due to the isothermal nature of the panel and inter mixing of the air in top and bottom quadrants, the temperatures remain more or less the same. Also Webb (1979) found from his two cell model the air temperature (in the case of a single glazed collector) remained the same for both the cells. Hence in the present programme average values of power absorbed for top and bottom quadrants has been taken as the corresponding input values to the programme.

In the first section of this appendix the conduction-convection network is analysed and expressions are formulated for evaluating each of the 28 resistances. In the second section the

FIGURE A10.2 Conduction-Convection Resistance Network

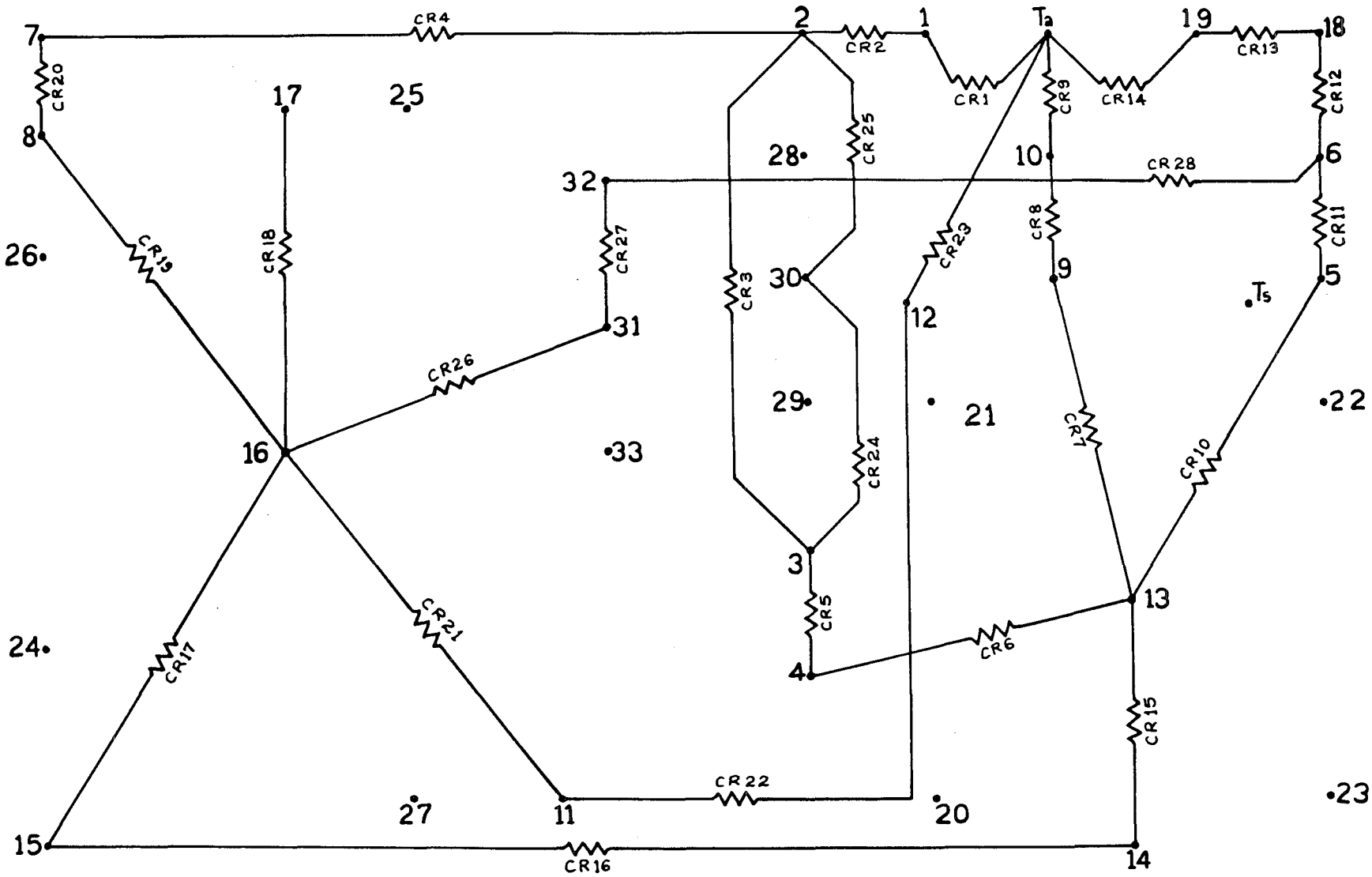

radiation network is analysed formulating the expressions for the 46 radiation resistances, after discussing the assumptions made and the background theory involved. In the third section the two networks are superimposed and energy balance equations are set up for each of the 33 nodes, which are then solved using the Gauss elimination method. The final section gives listings of computer programmes TPLWR (which is the main programme including all the subroutines), LONG.DAT (the inpout data file) and TPLWR.DAT (the output file listing all the input as well as output parameters).

A10.1 Analysis of Conduction-Convection Resistance Network

As shown in Fig. A10.2 the conduction-convection network consists of 28 resistances (CR1 to CR28) and expressions are given for each of them. This resistance network can be related to the physical model via the 33 nodal points or temperatures as shown in Fig. A10.1. The temperature differences T1 to T28 can be easily found from Fig. A10.2.For example the temperature difference to be used in conjunction with CR1 is given by

$$\Delta T1 = |T1 - T_{amb}| \qquad \text{(A10.1)}$$

The general expression for any resistance is given by

$$\text{Resistance} = \frac{\text{Driving force}}{\text{Flow}} \qquad \text{(A10.2)}$$

When thermal energy q is flowing due to the temperature difference ΔT (which acts as the driving force) the resistance R can be expressed as

$$R = \Delta T / q \qquad \text{(A10.3)}$$

Also the general expression for heat transfer is given by

$$q = h\ A\ \Delta T \qquad \text{(A10.4)}$$

where h is the heat transfer coefficient and A is the area of heat transfer. From Eqs. (A10.3) and (A10.4)) we get

$$R = 1 / (h\ A) \qquad \text{(A10.5)}$$

With the help of the general Eq. (A10.5) expressions for various resistances are derived.

(1) CR1 : Forced convection resistance from the box surface (without considering the side walls and the outer glazing) to the environment: It is given by

$$CR1 = 1 / (h_{b\text{-}atm}\ A_b) \qquad \text{(A10.6)}$$

where h_{b-atm} is the heat transfer coefficient from box to the atmosphere and A_b is the box surface area exposed to the atmosphere.

To find h_{b-atm} : The calculation of wind induced heat transfer coefficient is not well established, different authors have suggested different expressions mainly based upon wind tunnel tests (Sparrow et al., 1979; Kays, 1966; Jacob, 1949; McAdams, 1954; Kreith and Kreider, 1978).

The flow over a collector mounted on a house is not always well represented by wind tunnel tests of isolated plates. The collectors may sometimes be exposed directly to wind and at other times they can be in the wake region. The roof, nearby trees and buildings will certainly influence the flow patterns. Mitchell (1976) investigated the heat transfer due to forced convection from various shapes and showed that many shapes were well represented by a sphere when the equivalent sphere diameter is the cube root of the volume. The heat transfer coefficients obtained in this manner gives average values for stagnation and wake regions. Solar systems encounter similar situation, but Michell suggested 25% higher values for outdoor conditions and gave the following relation

$$Nu = 0.42\ Re^{0.6} \qquad \text{(A10.7)}$$

where Nu = Nusselt number $= h\ L_c\ /\ k_f$ (A10.8)

$$Re = \text{Reynolds number} = L_c\ v_f\ \rho_f\ /\ \mu_f \qquad \text{(A10.9)}$$

h = heat transfer coefficient; k_f = thermal conductivity of the fluid (air); v_f = linear velocity of the fluid (air); ρ_f = density of the fluid (air); μ_f = viscosity of the fluid (air); L_c = characteristic length, which is the cube root of the house volume.

On calm days when the wind speed is low free convection conditions may dominate. For hot horizontal plates with aspect ratios up to 7:1, Lloyd and Moran (1974) gave the following equations.

$$Nu = 0.76\ Ra^{1/4} \quad \text{for } 2.6 \times 10^4 < Ra < 10^7 \qquad \text{(A10.10)}$$

$$Nu = 0.15\ Ra^{1/3} \quad \text{for } 10^7 < Ra < 3 \times 10^{10} \qquad \text{(A10.11)}$$

where Ra = Rayleigh number $= Gr\ Pr$ (A10.12)

$$Gr = \text{Grashof number} = \rho_f^2\ g\ \beta_f\ L_c^3\ \Delta T_f\ /\ \mu_f^2 \qquad \text{(A10.13)}$$

$$Pr = \text{Prandtl number} = c_{pf}\ \mu_f\ /\ k_f \qquad \text{(A10.14)}$$

c_{pf} = specific heat capacity of the fluid (air); g = acceleration due to gravity; β_f = coefficient of thermal expansion of fluid (air); ΔT_f = mean temperature drop between the surface

FIGURE A10.3 Outer Galvanised Iron Sheet Box

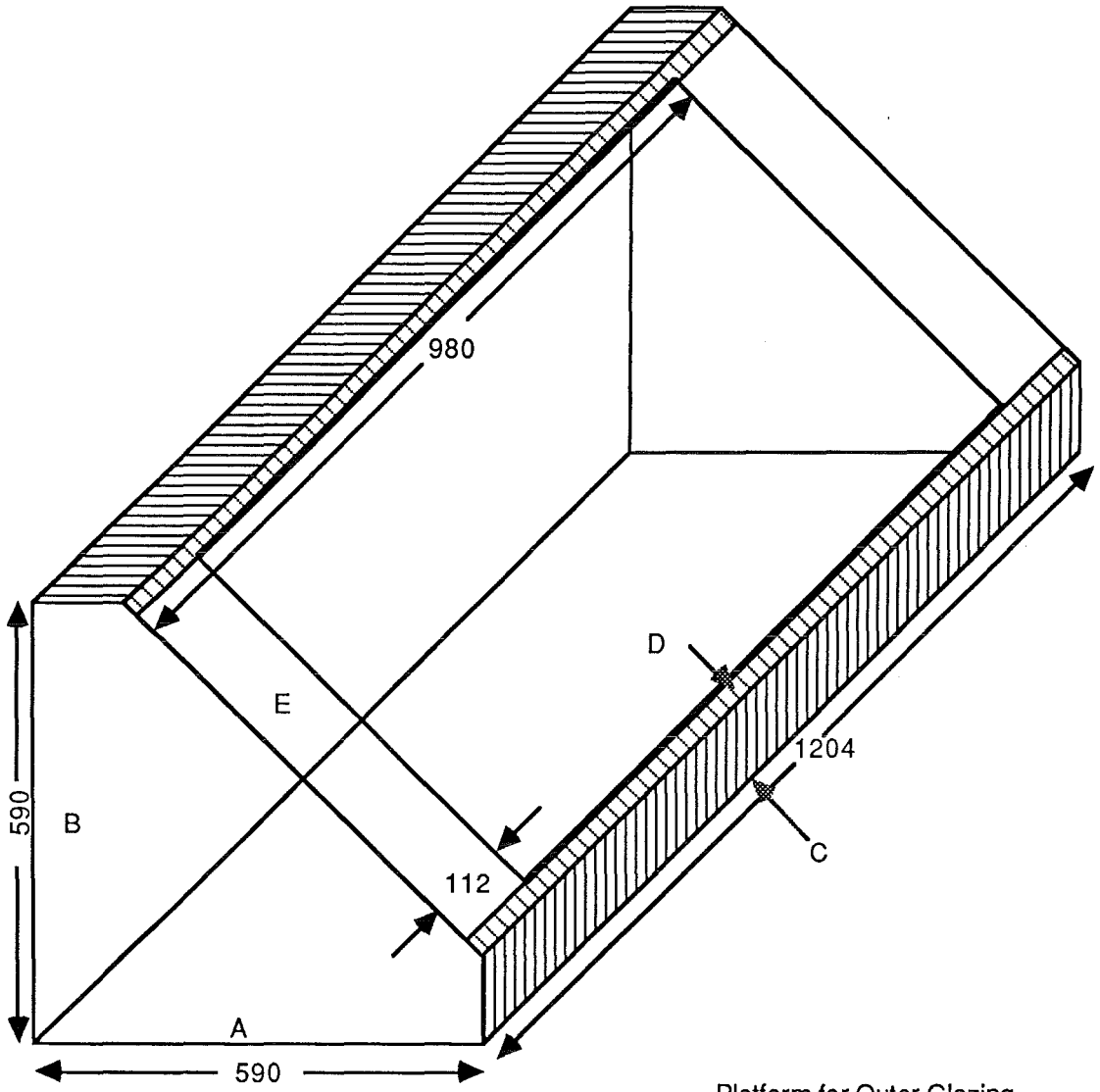

Notes: All dimensions are in mm

Scale 1 : 10

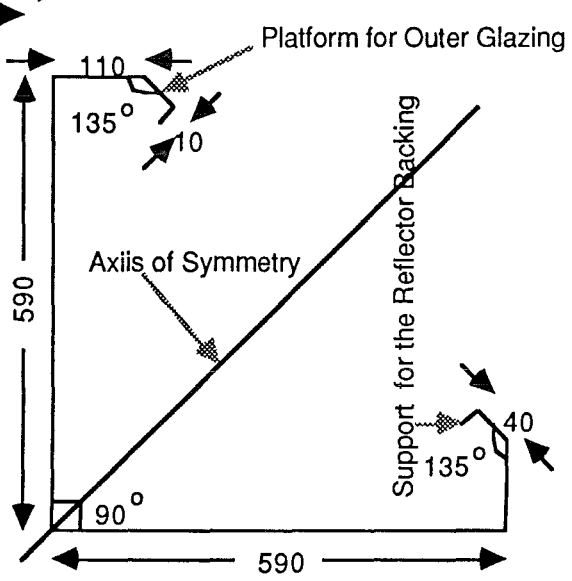

(b) Cross Section

and the fluid in contact with it (air); L_c = characteristic length, defined as four times the area divided by the perimeter of the plate.

Rohsenow and Hartnett (1973) gave the following relation for vertical plates.

$$Nu = 0.59\ Ra^{1/4} \quad \text{for} \quad 10^4 < Ra < 10^9 \qquad \text{(A10.15)}$$

$$Nu = 0.13\ Ra^{1/3} \quad \text{for} \quad 10^9 < Ra < 10^{12} \qquad \text{(A10.16)}$$

where the characteristic length is the plate height. Free convection data for hot inclined flat plates facing upwards are not available. However, for most of the solar collectors Ra is quite high and as seen from Eqs. (A10.11) and (A10.16) the heat transfer coefficients are nearly the same since the coefficient on the Rayleigh numbers differ only slightly. Hence, either of the equation may be used with an everage coefficient of 0.14 and with this, a heat transfer coefficient of 5.0 $W.m^2.K^{-1}$ is obtained for a temperature drop of 25 K.

In general both free and forced convection occurs simultaneously and hence, it is recommencded by McAdams (1954) and Kreith (1976) that both values should be calculated and the larger value used in calculations.

On substituting μ_f, ρ_f and k_f values for air (assuming that they are independant of temperature) Eq. (A10.7) reduces to

$$h = 8.6\ v_{av}^{0.6} / L_c^{0.4} \qquad \text{(A10.17)}$$

where v_{av} is the average velocity of air in $m.s^{-1}$ and L_c the characteristic length in meters.

The heat transfer coefficient for roof mounted collectors can then be expressed as

$$h_{wind} = \max\ [5,\ 8.6\ v_{av}^{0.6} / L_c^{0.4}] \qquad \text{(A10.18)}$$

Hence, $h_{b\text{-}atm}$ can be evaluated using equation (A10.18).

To find A_b : This area includes the total surface area of the outside box except the aperture area and the side area. As shown in Fig. A10.3, this includes the areas represented by the letters A, B, C, D and E and these areas are given below.

A = Bottom area = 0.71036 m^2; B = Back area = 0.71036 m^2; C = Top area = 0.26488 m^2; D = Front edge area = 0.09632 m^2; E = Front side area = 0.133056 m^2; Total area A1 = 1.91497 m^2

However, as the calculations are done for only one half of the collector, the value of A_b = A1 / 2 = 0.957488 m^2

(2) CR2 : Conduction resistance through the box walls: In the present case the box wall consists of 1mm thick galvanised

FIGURE A10.4 End Wall Arrangement

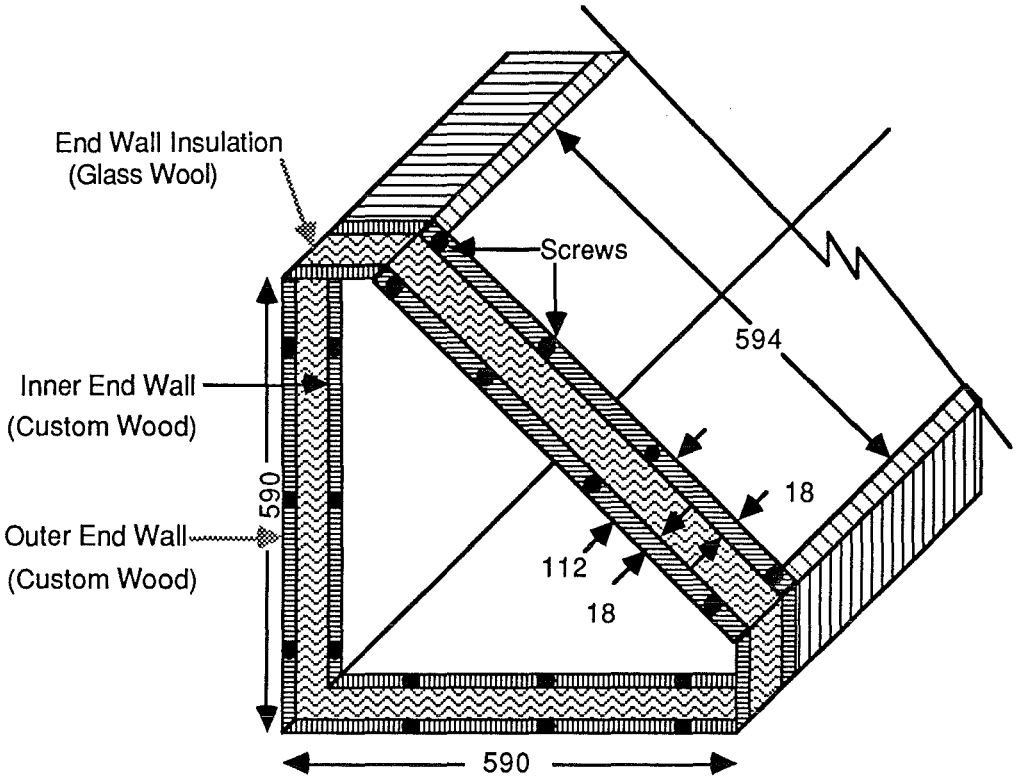

(b) Inner End Wall

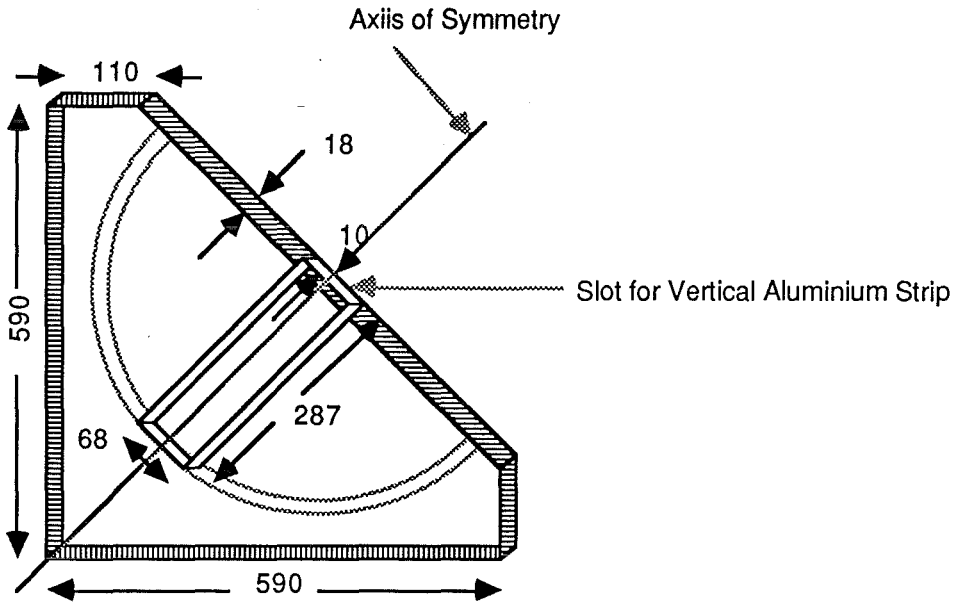

Notes: All dimensions are in mm

Scale 1 : 10

iron sheet. The side walls and outer glazing are not taken into consideration in this resistance. For conduction through a solid we have according to Fourier's law of heat conduction,

$$q = k\ A\ \Delta T\ /\ \Delta x \qquad \text{(A10.19)}$$

where Δx = thickness of the solid.

$$\text{Also } q = \text{Driving force} / \text{Resistance} \qquad \text{(A10.20)}$$

Hence, comparing Eqs. (A10.19) and (A10.20), we have

$$\text{Resistance} = \Delta x\ /\ (k\ A) \qquad \text{(A10.21)}$$

$$\text{In the present case } CR2 = t_{gi}\ /\ (k_{gi}\ A_b) \qquad \text{(A10.22)}$$

where t_{gi} = thickness of glavanised iron sheet = 1×10^{-3} m

k_{gi} = thermal conductivity of galvanised iron = 59.9 $W.m^{-1}.K^{-1}$

A_b = area of the box = 0.957488 m^2

(3) CR3 : conduction resistance through the back insulation to the reflector back: For conduction through hollow cylinders Eq. (A10.19) can be modified to

$$q = k\ A_L\ \Delta T\ /\ (R_o - R_i) \qquad \text{(A10.23)}$$

where R_o and R_i are the outer and inner radii of the cyliner respectively. A_L = log mean area and is given by

$$A_L = \{2\ \pi\ L\ (R_o - R_i)\}\ /\ \{\ln\ (R_o\ /\ R_i)\} \qquad \text{(A10.24)}$$

In the present case the reflector is semicircular cylindrical and the area is to be evaluated for only one quadrant. Hence the log mean area should be divided by 4 and by combining Eqs. (A10.23) and (A10.24) and comparing with Eq. (A10.20) expression for CR3 can be obtained.

$$CR3 = \{2\ \ln\ (R_o\ /\ R_i)\}\ /\ \{\pi\ k\ L\} \qquad \text{(A10.25)}$$

In the present case $k = k_i$ = thermal conductivity of the insulating material (glass wool) = 0.036 $W.m^{-1}.K^{-1}$ (Insulation Handbook, 1959); $L = L_r$ = length of the reflector = 0.98 m (from Fig. A10.3); $R_i = R_{ir}$ = inside radius of the reflector = 0.286 m (which can be obtained from the end wall-reflector arrangement as shown in Fig. A10.4); $R_o = R_{ob}$ = outside radius of the outer box. It is difficult to determine the value of R_{ob} because of the odd shape of the box. Hence R_{ob} can be taken as a hypothetical radius which would give the same cross sectional area as the existing box.

$$R_{ob}\ /\ R_{ir} = (A_{ob}\ /A_{ir})^{1/2} \qquad \text{(A10.26)}$$

where A_{ob} = cross sectional area of the box end wall and A_{ir} = cross sectional area of the semicircle formed by the reflector.

From Fig. A10.4, A_{ob} = 0.2329 m and A_{ir} = 0.1294 m. While evaluating A_{ir}, the aluminium strip area is neglected, as it is

only 4% of the area of A_{ir}. Substituting R_{ir}, A_{ob} and A_{ir} values in Eq. (A10.26) we get R_{ob} = 0.385 m

(4) CR4 : conduction resistance through the back insulation to the bottom (or horizontal) aluminium strip: Applying the conduction formula from Eq. (A10.21)

$$CR4 = \{ \Delta x_4 \} / \{ k_i \, A_{hr-al} \} \qquad (A10.27)$$

where A_{hr-al} = area of the horizontal aluminium strip and from Fig. A10.3 it is equal to 0.06664 m^2 ; Δx_4 = thickness of the insulation = $R_{ob} - R_{ir}$ = 0.098 m. Though the thickness of the glass wool insulation is more than $(R_{ob} - R_{ir})$ between the aluminium strip and the outer box, for convenience it is assumed to be $(R_{ob} - R_{ir})$.

(5) CR5 : Conduction resistance through the reflector supporting frame and the reflector sheet materials: In the present case the reflector sheet material consists of aluminised mylar which is only a few microns thick and hence, the resistance offered by the reflector sheet is neglected. The supporting frame for the reflector consists of 1 mm thick galvernised iron sheet, whose resistance can be found in the same way as was done for CR3 and from Eq. (A10.25)

$$CR5 = \{ 2 \ln (R_{or} / R_{ir}) \} / \{ \pi \, k_{gi} \, L_r \} \qquad (A10.28)$$

where R_{or} = outside radius of the reflector = 0.287 m

(6) CR6 : Natural convection resistance from the reflector surface to the outer air: Free or natural convection exists betwen the outer air and surfaces in contact with it (Fig. A10.1) because the Rayleigh number is always greater than 1700 in such cases (Incropera and Dewitt, 1981). The connective resistance CR6 can be obtained from Eq. (A10.5)

$$CR6 = 1 / \{ h_{r-oa} \, A_r \} \qquad (A10.29)$$

where h_{r-oa} = heat transfer coefficient from the reflector to outer air and A_r = area of the reflector.

Although some work has been done on free convective heat transfer in enclosures, the evaluation of h_{r-oa} is not easy because of the complicated geometry involved and the different temperatures of the surfaces. Mostly work is done to evaluate heat transfer coefficients in triangular, rectangular or cylindrical enclosures, but in the present case the enclosure is one quarter of a cylinder with four flat surfaces and one curved surface. Also the enclosures investigated generally consisted of one hot, one cold and the rest adiabatic surfaces, but in the present case

FIGURE A10.5 Predicted Convective Flow Patterns in the Top

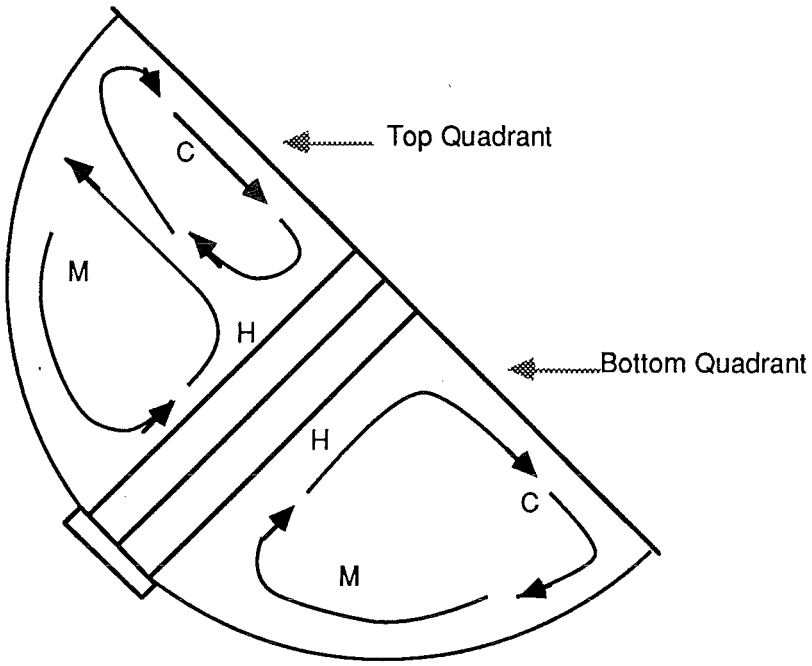

Notes: H = Hot; M = Medium; C = Cold

FIGURE A10.6 Free Convection in a Rectanglar Cavity

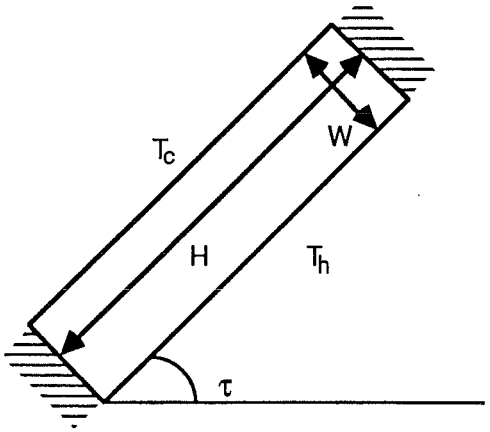

there are four different temperatures of the five surfaces as given below

1. The curved reflector surface is at T4
2. The end walls are at T5
3. The outer glazing inner surface is at T9
4. The inner glazing outer surface is at T14.

To complicate the energy flow pattern further the quarter cylinder (or the collector) is kept at 45° to the horizontal and steady state conditions are difficult to achieve with solar appliances. The predicted flow patterns in the enclosures (top and bottom) are shown in Fig. A10.5. It can be noticed that the flow patterns are different in top and bottom quadrants.

Hence, there is no expression available in the literature that can exactly represent the present situation. Evans and Stefany (1966) studied transient heat transfer to various liquids in cylindrical enclosures, while Akinsete & Coleman (1982) studied steady state laminar free convection in air contained in a long horizontal right angled triangular enclosure and Newell & Schmidt (1970) studied steady state laminar natural convection in air contained in a long vertical rectangular enclosure. However, none of these models exactly describe the present situation and hence an inclined rectangular model was chosen as it is the nearest one to the present situation.

For inclined rectangular cavities (Fig. A10.6) with small aspect ratios Catton et al. (1974) suggested a correlation as given below.

$$Nu = Nu(\tau=0^\circ) \left\{ Nu(\tau=90^\circ)/Nu(\tau=0^\circ) \right\}^{\tau/\tau^*} (\sin \tau^*)^{\tau/4\tau^*} \quad \text{(A10.30)}$$

For $H/W \leq 12$ and $0^\circ < \tau \leq \tau^*$

where $Nu(\tau=0^\circ)$ = Nusselt number for $\tau = 0^\circ$ as given by Globe and Dropkin's (1959) correlation for free convection in a horizontal cavity hated from below.

$$Nu(\tau=0^\circ) = 0.069\ Ra^{1/3}\ Pr^{0.074} \quad \text{(A10.31)}$$

for $3 \times 10^5 < Ra < 7 \times 10^9$ and tilt angle $\tau = 0^\circ$ (Fig. A10.6).

The properties are evaluated at the average temperature (T_{av}). Nu and Ra are based on the distance between the hot and cold surfaces (W), while the other surfaces are assumed adiabetic.

$Nu(\tau=90^\circ)$ = Nusselt number for $\tau = 90^\circ$ as given by Catton's (1978) correlations for free convection in vertical rectangular cavities, that is $\tau = 90^\circ$ (Fig. A10.6). Nusselt and Rayleigh numbers are based on width W.

TABLE A10.1 Critical Angle for Inclined Rectangular Cavities

(Clever, 1973)

H/W	1	3	6	12	>12
τ^* in degrees	25	53	60	67	70

$$Nu = 0.22 \{Pr\ Ra / (0.2 + Pr)\}^{0.28} (H/W)^{-1/4} \quad (A10.32)$$

For $2 < H/W < 10$; $Pr < 10^5$; $Ra < 10^{10}$

$$Nu = 0.18 \{Pr\ Ra / (0.2 + Pr)\}^{0.29} \quad (A10.33)$$

For $1 < H/W < 2$; $10^{-3} < Pr < 10^5$; $10^3 < (Ra\ Pr) < (0.2 + Pr)$

τ^* is the critical tilt angle which is related to the aspect ratio H/W as shown in Table A10.1 (Clever, 1973).

If the tilt angle τ is more than τ^*, for all aspect ratios Ayyaswamy & Catton (1973) and Arnold et al. (1975) have recommended the following correlations.

$$Nu = Nu(\tau=90^o)\ (\sin \tau)^{1/4} \quad \text{for } \tau^* < \tau < 90^o \quad (A10.34)$$

$$Nu = 1 + \{Nu(\tau=90^o)-1\} \sin \tau \quad \text{for } 90^o < \tau < 180^o \quad (A10.35)$$

Hence in the present case EQ. (A10.34) has been used to calculate h_{r-oa} because H/W = 1, $\tau^* = 25^o$ and $\tau = 45^o$

The characteristic dimension can be chosen as the radius of the reflector, on which Nusselt and Rayleigh numbers are based. In order to facilitate the use of these equations in computer programme the following cirrelations are used in evaluating propeties of air.

$$g_a = 9.11 \times 10^{-8} (T_{av}) - 1.15 \times 10^{-5} \quad (A10.36)$$

$$k_a = 7.8 \times 10^{-5} (T_{av}) + 2.88 \times 10^{-3} \quad (A10.37)$$

$$c_{pa} = 0.0004 (T_{av})^2 - 0.2\ T_{av} + 1030 \quad (A10.38)$$

$$\rho_a = \{P_{atm}\ M_a\} / \{R_{gc}\ T_{av}\} \quad (A10.39)$$

$$\beta_a = \{|\rho_1^2 - \rho_2^2|\} / \{2\ \rho_1\ \rho_2\ \Delta T\} \quad (A10.40)$$

where M_a = molecular weight of air = 28.96 ; P_{atm} = atmospheric pressure = 101330 $kg.m^{-2}.s^{-1}$; R_{gc} = Universal gas constant = 8314 $kg.m^2.s^{-2}.kmole^{-1}.K^{-1}$; γ_a = kinematic viscosity of air in $m^2.s^{-1}$; k_a = thermal conductivity of air in $W.m^{-1}.K^{-1}$; c_{pa} = heat capacity of air in $J.kg^{-1}.K^{-1}$; ρ_a = density of air in $kg.m^{-3}$; β_a = coefficient of thermal expansion of air in K^{-1} ; T_{av} = average temperature of air in K ; ΔT = temperature drop |T2 - T1| ; ρ_1 and ρ_2 are the densities of air at temperatures T1 and T2 respectively.

The total area of the reflector A_{rT} (in both the quadrants) can be calculated from Fig. A10.4 and A_{rT} = reflector area - horizontal aluminium strip area = 0.81696 m^2. Part of the aluminium strip area enclosed between the inner glazings has not been included in A_{rT}. The area of the reflector in one quadrant is therefore equal to 0.40848 m^2.

(7) CR7 : Natural convection resistance from outer air to outer glazing: The convection resistance CR7 is given by

$$CR7 = 1 / \{h_{oa-og} A_{og}\} \quad (A10.41)$$

where h_{oa-og} is the free convective heat transfer coefficient between the outer air and the outer glazing and A_{og} is the area of the outer glazing. The situation here is same as that discussed in evaluating CR6 and hence, Eq. (A10.34) can be used to calculate h_{oa-og}. The total area of the outer glazing A_{ogt} can be calculated from Fig. A10.3. It is the area of the outer glazing, in contact with the outer air, excluding the area opposite the horizontal aluminium strip.

A_{ogt} = 0.51548 m^2 and A_{og} corresponds to the outer glazing area in one quadrant and is equal to 0.25774 m^2.

(8) CR8 : Conduction resistance through outer glazing which is in contact with outer air: The conduction resistance is given by

$$CR8 = t_{og} / (k_{og} A_{og}) \quad (A10.42)$$

where t_{og} = thickness of the outer glazing = 0.003 m; k_{og} = thermal conductivity of outer glazing = 1.05 $W.m^{-1}.K^{-1}$ (Wong, 1977); A_{og} = area of outer glazing = 0.25774 m^2

(9) CR9 : Forced convection resistance from outer glazing (in contact with outer air) to the environment: This is given by

$$CR9 = 1 / (h_{og-atm} A_{og}) \quad (A10.43)$$

h_{og-atm} can be calculated using Eq. (A10.18) as the situation is very similar to that of h_{b-atm}.

(10) CR10 : Natural convection resistance from outer air to the inner side walls: The convection resistance is given by

$$CR10 = 1 / (h_{oa-ew} A_{ew}) \quad (A10.44)$$

where h_{ae-ew} is the heat transfer coefficient between the outer air and the end walls and can be evaluated from Eq. (A10.34). A_{ew} is the area of both the end walls and can be evaluated from Fig. A10.4. The total area of the end walls A_{erT} is given by A_{erT} = (area of both the end walls - area covered by the vertical aluminium strips) = 0.21974 m^2 and A_{ew} = 0.10987 m^2

(11) CR11 : Conduction Resistance through the inner side walls:

In calculating the conduction resistance CR11, the resistance offered by the aluminised mylar sheet is neglected.

$$CR11 = t_{iew} / (k_{iew} A_{iew}) \quad (A10.45)$$

where t_{iew} = thickness of inner end wall = 0.018 m; k_{iew} = thermal conductivity of inner end wall material (in the prersent case custom wood) = 0.173 $W.m^{-1}.K^{-1}$ (Kern, 1954); A_{iew} = area of

the inner end wall. In evaluating A_{iew}, only the area in contact with the outer air is considered and not the whole box end cross sectional area. Hence, $A_{iew} = A_{ew} = 0.219738\ m^2$. It is assumed that inner side wall outer temperature is T6 (Fig. A10.1) which represents the average temperature of the surface, although the temperature just behind the vertical aluminiium strip is higher than the rest of the surface.

(12) CR12 : Conduction resistance through side insulation:

It is given by $CR12 = t_{ewi} / (k_{ewi} A_{ewi})$ (A10.46)

where t_{ewi} = thickness of the end wall insulation = 0.076 m ; k_{ewi} = thermal conductivity of end wall insulation material (glass wool in the present case) = $0.036\ W.m^{-1}.K^{-1}$; A_{ewi} = area of the end wall insulation, which is once again taken equal to A_{ew} = $0.219738\ m^2$.

(13) CR13 : Conduction resistance through the outer side wall:

It is given by $CR13 = t_{oew} / (k_{oew} A_{oew})$ (A10.47)

where t_{oew} = thickness outer end wall = 0.076 m; k_{oew} = thermal conductivity of outer end wall material (custom wood in the present case) = $0.036\ W.m^{-1}.K^{-1}$; A_{oew} = area of the outer end wall, which is also taken to be equal to $A_{ew} = 0.219738\ m^2$.

(14) CR14 : Forced convection resistance from the outer side wall to the environment:

It is given by $CR14 = 1 / (h_{ew-atm} A_{ewea})$ (A10.48)

where h_{ew-atm} = heat transfer coefficient between the (outer) end wall and atmosphere, which can be calculated from Eq. (A10.18) A_{ewea} = area of the end wall exposed to the atmosphere. From Fig. A10.4, the total end wall area $A_{eweaT} = 0.4028\ m^2$ and hence, A_{ewea} = $0.2329\ m^2$.

(15) CR15 : Natural convection resistance from the inner glazing to the outer air:

It is given by $CR15 = 1 / (h_{ig-oa} A_{ig})$ (A10.49)

where h_{ig-oa} = heat transfer coefficient between inner glazing and outer air, which can be evaluated from Eq. (A10.34); A_{ig} = area of the inner glazing. The total area of the inner glazing is given by (Fig. A10.4) $A_{igt} = 0.28126\ m^2$.

(16) CR16 : Conduction resistance through the inner glazing:

It is given by $CR16 = t_{ig} / (k_{ig} A_{ig})$ (A10.50)

where t_{ig} = thickness of inner glazing = 0.003 m; k_{ig} = thermal conducitivity of the inner glazing material = 1.05 $W.m^{-1}.K^{-1}$; A_{ig}=0.28126 m^2

(17) CR17 : Natural convection resistance from inner air to the inner glazing:

It is given by $CR17 = 1 / (h_{ia-ig} A_{ig})$ (A10.51)

where h_{ia-ig} = heat transfer coefficient between inner air and inner glazing. There are numerous expressions available for free convection from vertical, horizontal and inclined plates, for both heating and cooling (Churchill & Chu, 1975; Sparrow & Gregg, 1956; Ostrach, 1952, 1972; Goldstein et al., 1973; Lloyd and Moran, 1974; Kreith and Kreider, 1978; Newell and Schmidt, 1970; McGregor and Emery, 1969) and they can be expressed in the following general form

$$Nu = f\{Ra\} \quad \text{(A10.52)}$$

However, Buchberg et al. (1976) have reported in their review paper on natural convection in enclosed spaces, as applied to solar energy, the following three different sets of correlations.

(a) Three region correlation given by Catton (1966), Goldstein & Chu (1969), O'Toole and Silverton (1961).

$$Nu = 1 + 1.446 \{1 - 1708/(Ra \cos \tau)\}^{+} \quad \text{(A10.53)}$$

For $1708 < Ra \cos \tau < 5900$

$$Nu = 0.229 (Ra \cos \tau)^{0.252} \quad \text{(A10.54)}$$

For $5900 < Ra \cos \tau < 9.23 \times 10^4$

$$Nu = 0.157 (Ra \cos \tau)^{0.285} \quad \text{(A10.55)}$$

For $9.23 \times 10^4 < Ra \cos \tau < 9 \times 10^6$

(b) Two region correlation given by Arnold et al. (1974, 1975) Ozoe et al., (1974)

$$Nu = 1 + 1.446 \{1 - 1708/(Ra \cos \tau)\}^{+} \quad \text{(A10.56)}$$

For $1708 < Ra \cos \tau < 2500$

$$Nu = 0.157 (Ra \cos \tau)^{0.285} \quad \text{(A10.57)}$$

For $2500 < Ra \cos \tau < 10^6$

(c) Hollands et al. (1975, 1976) correlation for $\tau \leq 60°$

$$Nu = 1 + 1.44 \left[\{1 - 1708/(Ra \cos \tau)\}^{+}\right] \left[1 - \{1708(\sin 1.8\tau)^{1.6}\} / \{Ra \cos \tau\}\right] + \left[\{(Ra \cos \tau)/5830\}^{1/3} - 1\right]^{+} \quad \text{(A10.58)}$$

Where the meaning of the " + exponent " is that only positive values of the terms in the brackets are to be used (that is zero is used, if the term is negative).

As τ = 45° in the present case. Holland's correlation represented by Eq. (A10.58) can be used to calculate h_{ia-ig}.

(18) CR18 : Natural convection resistance from the absorber panel to the inner air:

It is given by $CR18 = 1 / (h_{ab-ia} A_{ab})$ (A10.59)

where h_{ab-ia} = Natural convective heat transfer coefficient between the absorber panel and the inner air as calculated from Eq. (A10.58) and A_{ab} = area of the absorber panel = area of the inner glazing A_{ig}.

(19) CR19 : Natural convection resistance from the inner air to the horizontal aluminium strip:

It is given by $CR19 = 1 / (h_{ia-hral} A_{hral})$ (A10.60)

where $h_{ia-hral}$ = Natural convective heat transfer coefficient between the inner air and the horizontal aluminium strip and can be calculated from Eq. (A10.58); A_{hral} = Area of the horizontal aluminium strip = 0.06664 m^2 (Fig. A10.4)

(20) CR20 : Conduction resistance through the horizontal aluminium strip:

It is given by $CR20 = t_{hral} / (k_{al} A_{hral})$ (A10.61)

where t_{hral} = thickness of the horizontal aluminium strip = 0.01 m; k_{al} = thermal conductivity of aluminium = 205.9 $W.m^{-1}.K^{-1}$ (Kern, 1954)

(21) CR21 : Natural convective resistance from inner air to the outer glazing in contact with the inner air:

It is given by $CR21 = 1 / (h_{ia-ogia} A_{ogia})$ (A10.62)

where $h_{ia-ogia}$ = natural convective heat transfer coefficient between inner air and outer glazing in contact with the inner air, which can be calculated from Eq. (A10.58); A_{ogia} = Area of outer glazing in contact with inner air and A_{ogia} is approximately equal to A_{hral}.

(22) CR22 : Conduction resistance through the outer glazing in contact with the inner air:

It is given by $CR22 = t_{ogia} / (k_{og} A_{ogia})$ (A10.63)

where t_{ogia} = thickness of outer glazing in contact with the inner air = t_{og}.

(23) CR23 : Forced convection resistance from the outer glazing in contact with inner air to the environment:

It is given by $CR23 = 1 / (h_{ogia-atm} A_{ogia})$ (A10.64)

where h_{ogia} = forced convection heat transfer coefficient from outer glazing in contact with the inner air and the atmosphere, which can be evaluated from Eq. (A10.18)

(24) CR24 : Natural convection resistance from the box air and the reflector back: This situation arises only when there is no back insulation. The box air refers to the air trapped between the outere box and the reflector. The convective resistance is given by

$$CR24 = 1 / (h_{ba-rb} A_{rb}) \quad \text{(A10.65)}$$

where h_{ba-rb} = natural convective heat transfer coefficient between the box air and the reflector back and A_{rb} = area of the reflector back.

Churchill & Chu (1975) and Morgan (1975) have recommended a correlation, for natural convection from a long horizontal cylinder. However, the shape of the space enclosed between the outer box and the reflector is quite uncommon and the closest approximation would be concentric cylinders. The situation is similar to that described in evaluating CR3 and hence, Eqs. (A10.23) to (A10.25) are used here, except that simple thermal conductivity (k) is replaced by an effective thermal conductivity k_{eff}. The effective thermal conductivity k_{eff} is defined as the thermal conductivity that a stationery fluid should have to transfer the same amount of heat as the moving fluid. Raithby and Hollands (1975) conducted experiments to study free convective heat transfer in the annular space between long, horizontal concentric cylinders.

From Eqs. (A10.23) to (A10.25) we get, replacing k by k_{eff} and introducing effective heat transfer coefficient h_{eff}

$$CR24 = 1 / (A_L h_{eff}) \quad \text{(A10.66)}$$

where A_L = log mean area and is given by

$$A_L = \{ \pi L_r (R_{ob} - R_{ir}) \} / \{ 2 \ln (R_{ob} / R_{ir}) \} \quad \text{(A10.67)}$$

$$h_{eff} = k_{eff} / (R_{ob} - R_{ir}) \quad \text{(A10.68)}$$

$$k_{eff} = 0.386 k_a \{ Pr / (0.861 + Pr) \}^{1/4} (Ra_c)^{1/4} \quad (93)$$

where Ra_c = critical Rayleigh number which is defined as

$$Ra_c = \frac{Ra \{ \ln (R_{ob} / R_{ir}) \}^4}{(R_{ob} - R_{or})^3 (D_{ob}^{-3/5} + D_{ir}^{-3/5})^5} \quad \text{(A10.69)}$$

where D_{ob} and D_{ir} are equal to $2R_{ob}$ and $2R_{ir}$ respectively. The correlations are valid for $10^2 \leq Ra_c \leq 10^7$. On comparing Eqs.

FIGURE A10.7 Radiation Resistance Network

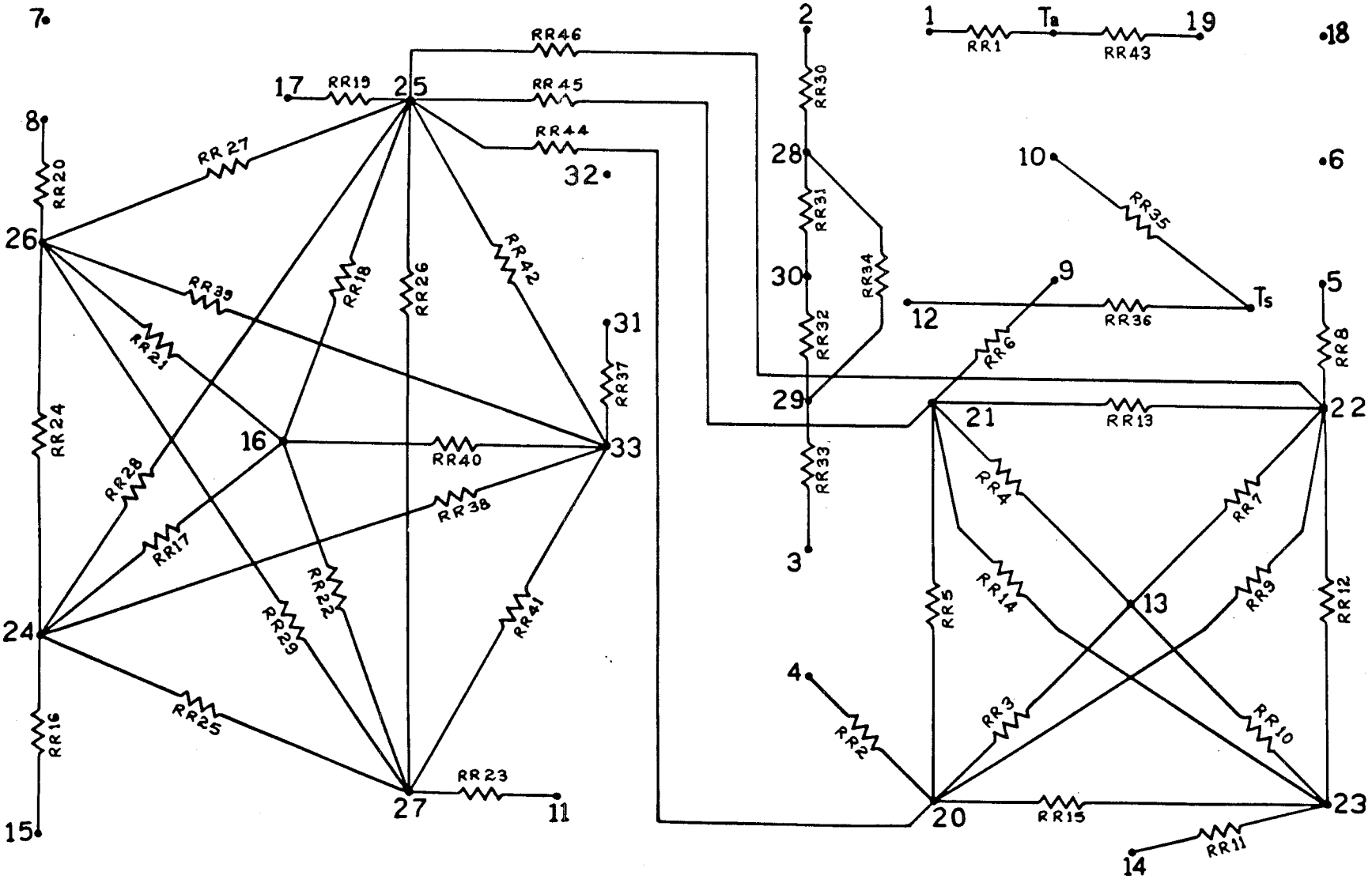

(A10.65) and (A10.66), it can be noticed that $h_{ba-rb} = h_{eff}$ and $A_{rb} = A_L$. The tmperature drop $\Delta T24$ is given by

$$\Delta T24 = |(T7 \times 0.075 + T3 \times 0.925) - T30| \qquad (A10.70)$$

A weighted average of T3 and T7 is taken because the aluminium strip area is 7.5% of the total reflector back area.

(25) CR25: Natural convection resistance from the box to the outer box:

It is given by $C25 = 1 / (h_{ba-ob} A_{ob})$ (A10.71)

Where h_{ba-ob} is the heat transfer coefficient between the box air and the outer box, which can be calculated in the same way as was done for h_{ba-rb} except with the new temperature drop

$T25 = |T30 - T2|$

A_{ob} = area of the outer box = A_L given by Eq. (A10.67)

(26) CR26 : Convection resistance between the inner air and the vertical (or side) aluminium strip: It is given by

$$CR26 = 1 / (h_{ia-vral} A_{vral}) \qquad (A10.72)$$

where $h_{ia-vral}$ is the natural convective heat transfer coefficient between the inner air and the vertical aluminium strip, which can be calculated from Eq. (A10.58); A_{vral} = Area of the vertical aluminium strip = 0.020196 m^2 (Fig. A10.4)

(27) CR27 : Conduction resistance through the vertical aluminium strip:

It is given by $CR27 = t_{vral} / (k_{al} A_{vral})$ (A10.73)

where t_{vral} = thickness of the vertical aluminium strip = 0.01 m.

(28) CR28 : Conduction resistance through part of the inner side wall: It is given by similar expression to that given by Eq. (A10.45), except that the thickness and area are different.

$$CR28 = (t_{iew} - t_{vral}) / (k_{iew} A_{vral}) \qquad (A10.74)$$

A10.2 Analysis of Radiation Resistance Network

The radiation network has been set up to take account of the thermal or long wave radiation. As shown in Fig. A10.7 the net work consists of 46 radiation resistances (RR1 to RR46). This resistance network can also be related to the physical model via the 33 nodal temperatures as shown in Fig. A10.1.

Before going into the details of the radiation network, it is necessary to summarise the background theory, some of which is common to the optical or short wave analysis.

A10.2.1 Background theory

The background theory necessary for the resistance anlysis can be explained under the following subheadings.

A10.2.1.1 Material properties

When any type of radiation strikes a material part of it can be absorbed, part reflected and part transmitted. The fraction of radiation absorbed is called the absorptivity α, the fraction reflected is known as the reflectivity ρ and the fraction teansmitted is called the transmittivity τ of that particular material.

Hence for any system $\alpha + \rho + \tau = 1$ (A10.75)

For an opaque system $\tau = 0$ and so $\alpha + \rho = 1$ (A10.76)

When a radiation strikes a surface the reflection can be either specular or diffuse. If the angle of incidence is equal to the angle of reflection, the reflection is called specular and if the incident beam is distributed uniformly in all directions after reflection, the reflection is called diffuse. No real surface is either entirely specular or entirely diffuse, but instead they are partly specular and partly diffuse. Ordinarily, a rough surface exhibits diffuse behaviour better than a highly polished surface and vice versa.

Hence for any system Eq. (A10.75) becomes

$\alpha + \tau + \rho_s + \rho_d = 1$ (A10.77)

where ρ_s = specular reflectivity and ρ_d = diffuse reflectivity

These material properties do vary with wave lengths, however for the entire thermal radiation range they can be assumed constant without introducing much error.

A10.2.1.2 Black body

In the study of real surfaces or systems it is convenient to define an ideal surface and it is called black surface or black body. For a black body all energy incident upon the body is absorbed, regardless of direction, wave length or any other identifiable energy characteristic.

Hence $\alpha_b = 1$, $\rho_b = 0$ and $\tau_b = 0$ (A10.78)

Any body emits a certain amount of thermal radiation depending on its temperature. The emissive power of a body E is defined as the energy emitted by the body per unit area per unit time. According to Stefan-Boltzman law the black body emissive

power E_b is directly proportional to the fourth power of the absolute temperature T

$$E_b = \sigma T^4 \qquad \text{(A10.79)}$$

where σ = Stefan-Bolzman constant = 5.669×10^{-8} $W.m^{-2}.K^{-4}$

The black body is not only a perfect absorber, but also a perfect emitter and hence the emissivity of any surface E is defined as

$$\varepsilon = E / E_b \qquad \text{(A10.80)}$$

Emissivity of a black body $\varepsilon_b = 1$. The emissivity of any surface varies with temperature, wave length of the radiation and the surface conditions.

A10.2.1.3 Kirchhoff's law and grey body

According to Kirchhoff's law, for a body in thermal equilibrium the ratio of its emissive power to that of a black body at the same temperature is equal to it absorptivity. So we have

$$E / E_b = \alpha \qquad \text{(A10.81)}$$

From Eqs. (A10.80) and (A10.81) we get $\varepsilon = \alpha$

Thus, at a given temperature, a body can absorb as much incident radiation as it can emit. This law unfortunately applies only to a few types of surfaces bearing the grey surface characteristics. A grey body is defined such that the momochromatic emissivity E of a body is independent of wave length. This implies that $\varepsilon_\lambda = \varepsilon = \alpha = \alpha_\lambda$ (A10.82)

For engineering application, some materials can be approximated to grey body conditions.

A10.2.1.4 Shape factor and receiprocity theorem

Radiation shape factor F_{m-n} is defined as the fraction of energy leaving surface m and arriving at surface n. The net energy exchanged between two black surfaces A1 and A2 is given by

$$q_{1-2} = E_{b1} A_1 F_{12} - E_{b2} A_2 F_{21} \qquad \text{(A10.83)}$$

Where F_{12} and F_{21} are the shape factors. At equilibrium (or when the surfaces are at the same temperature) there can be no heat exchange and $q_{1-2} = 0$ and also if the comissivities are equal, $E_{b1} = E_{b2}$ and Eq. (A10.83) reduces to

$$A_1 F_{12} = A_2 F_{21} \qquad \text{(A10.84)}$$

$$\text{Hence } q_{12} = A_1 F_{12} (E_{b1} - E_{b2}) \qquad \text{(A10.85)}$$

$$\text{or } q_{12} = A_2 F_{21} (E_{b1} - E_{b2}) \qquad \text{(A10.86)}$$

FIGURE A10.8 Surface Resistance

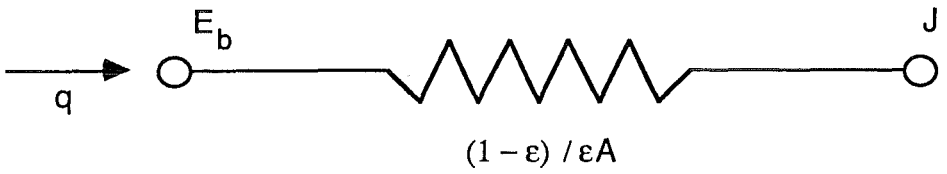

FIGURE A10.9 Space Resistance

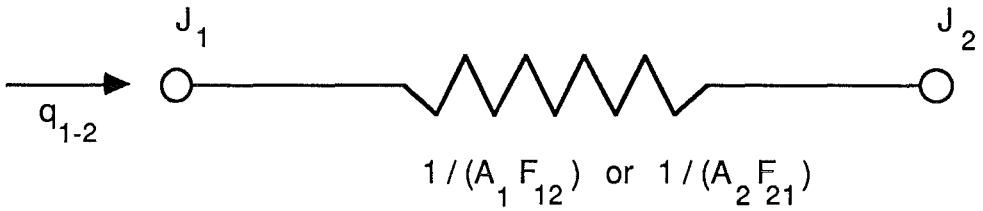

FIGURE A10.10 Resistance Network for a Two Surface System

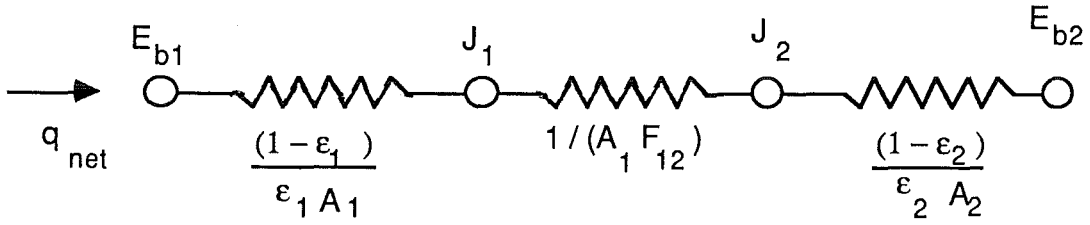

This is known as the reciprocity theorem.

A10.2.1.5 Irradiation and radiosity

With heat exchange between non black bodies two more new terms need to be defined, because unlike black bodies, only part of the incident radiation is absorbed, while part is reflected. Irradiation (G) is defined as the total radiation incident upon a surface per unit time and per unit area. Radiosity (J) is defined as the total radiation which leaves a surface per unit time and per unit area. Radiosity is the sum of the energy emitted and the energy reflected when no energy is transmitted and so

$$J = \varepsilon E_b + \rho G \qquad \text{(A10.87)}$$

$$\text{As } \tau = 0,\ \rho = 1 - \alpha = 1 - \varepsilon \qquad \text{(A10.88)}$$

Combining Eqs. (A10.87) and (A10.88) we have

$$J = \varepsilon E_b + (1-\varepsilon) G \qquad \text{(A10.89)}$$

$$\text{and } G = (J - \varepsilon E_b) / (1 - \varepsilon) \qquad \text{(A10.90)}$$

A10.2.1.6 Surface and space resistances

In the formulation of the radiation net work each surface is supposed to have a "surface resistance" and the space between the two surfaces is supposed to have a "space resistance". Hence if there are two surfaces which see each other and nothing else the radiation net work will have two surface resistances and one space resistance in series. Similarly if there are three surfaces which see each other and nothing else, the resulting radiation net work will have three surface resistances and three space resistances.

(a) Surface resistance: The net energy leaving any surface per unit area (q/A) is the difference between the radiosity J and the irradiation G

$$q / A = J - G \qquad \text{(A10.91)}$$

Substituting for G in terms of J from Eq. (A10.90) and rearranging

$$q = \{E_b - J\} / \{(1-\varepsilon) / \varepsilon A\} \qquad \text{(A10.92)}$$

Hence the heat flow q occurs across a potentail difference of $E_b - J$ with a resistance of $(1-\varepsilon) / \varepsilon A$ (Fig. A10.8)

(b) Space resistance: The amount of radiation leaving surface A_1 and reaching surface A_2 is $J_1 A_1 F_{12}$ and of the total energy leaving surface A_2 and reaching surface A_1 is $J_2 A_2 F_{21}$ and hence the net exchange

$$q_{1-2} = J_1 A_1 F_{12} - J_2 A_2 F_{21} \qquad \text{(A10.93)}$$

FIGURE A10.11 Resistance Network for a Three Surface System

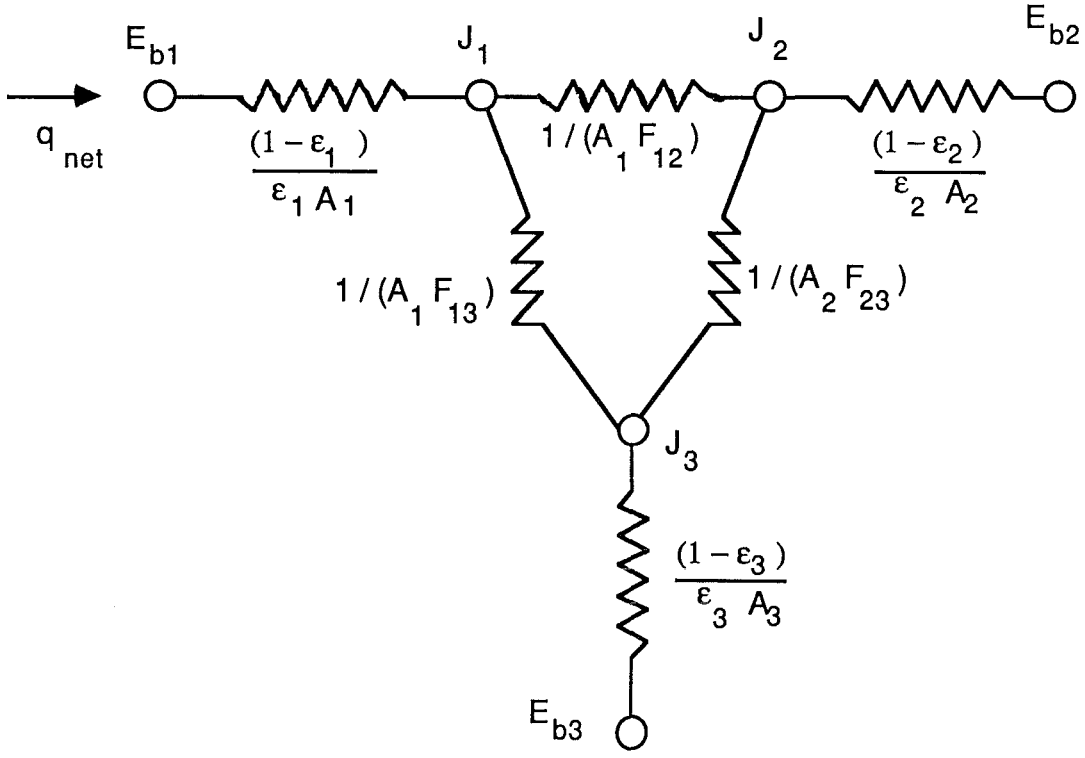

According to the reciprocity theorem

$$A_1 F_{12} = A_2 F_{21} \qquad \text{(A10.94)}$$

combining Eqs. (A10.93) and (A10.94) we have

$$q_{1-2} = (J_1 - J_2)\, A_1 F_{12} = (J_1 - J_2)\, A_2 F_{21} \qquad \text{(A10.95)}$$

$$\text{(or)}\quad q_{1-2} = \frac{J_1 - J_2}{1 / (A_1 F_{12})} = \frac{J_1 - J_2}{1 / (A_2 F_{21})} \qquad \text{(A10.96)}$$

Hence, we can see that heat flow q occurs across a potential difference of $J_1 - J_2$ with a resistance of $1/(A_1 F_{12})$ or $1/(A_2 F_{21})$, as shown in Fig. A10.9.

(c) Two surface system: Similarly for two surfaces which see each other and nothing else, the radiation network is shown in Fig. A10.10. The net heat transfer would be the overall potential difference divided by the sum of the resistances.

$$q_{net} = \{E_{b1} - E_{b2}\} / \{R_{Tot}\} \qquad \text{(A10.97)}$$

where R_{tot} = total resistance of the system and it is given by

$$R_{Tot} = \frac{1-\varepsilon_1}{\varepsilon_1 A_1} + \frac{1}{A_1 F_{12}} + \frac{1-\varepsilon_2}{\varepsilon_2 A_2} \qquad \text{(A10.98)}$$

E_{b1} and E_{b2} can be expressed in temperature terms using

$$E_{b1} = \sigma\, T1^4 \qquad \text{(A10.99)}$$

$$E_{b2} = \sigma\, T2^4 \qquad \text{(A10.100)}$$

Combining Eqs. (A10.97) to (A10.100)

$$q_{net} = \{\sigma\, (T1^4 - T2^4)\} \,/\, R_{Tot} \qquad \text{(A10.101)}$$

In order to superimpose the radiation net work on the conduction-convection net work, the nodes have to be same, that is the potential differences have to be in terms of temperature differences. On rearranging Eq. (A10.101)

$$q_{net} = \{\sigma\, (T1^2 + T2^2)\, (T1 + T2)\, (T1 - T2)\} \,/\, R_{Tot} \qquad \text{(A10.102)}$$

In the above equation (T1 -T2) represents the driving force and so combining the other terms with R_{Tot} , the total effective resistance R_{Teff} can be obtained.

$$q_{net} = (T1 - T2) \,/\, R_{Teff} \qquad \text{(A10.103)}$$

$$\text{where } R_{Teff} = R_{Tot} \,/\, \{\sigma\, (T1^2 + T2^2)\, (T1 + T2)\} \qquad \text{(A10.104)}$$

This is the general form that will be used for the radiation net work analysis.

(d) Three surface system: Radiation net work for three surfaces which see each other and nothing else can be represented as shown in Fig. A10.11. In this case each of the bodies exchange heat with the other two by applying the same principle as in two

FIGURE A10.12 Surface Resistance of a Specular-Diffuse Surface

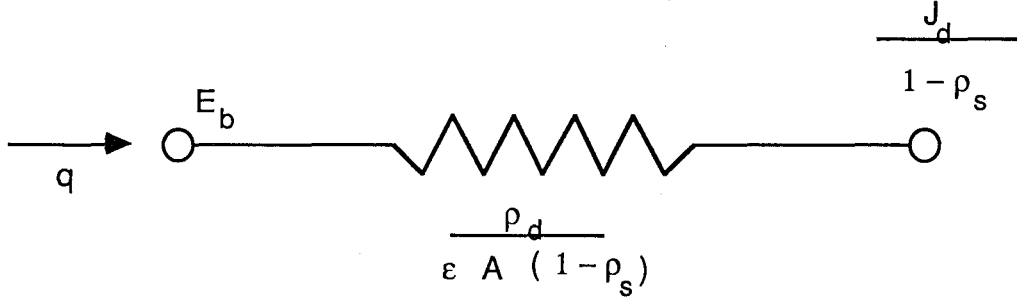

FIGURE A10.13 System with Two Specular-Diffuse Surfaces

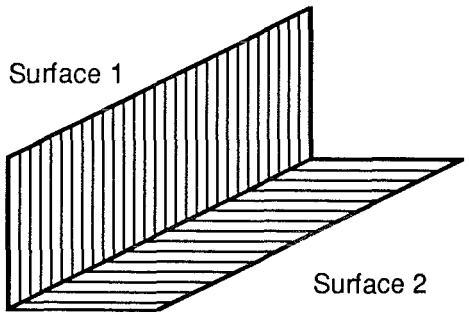

surface system, we can find out the net heat exchange between each set of two surfaces.

A10.2.1.7 Radiation exchange with specular surfaces

It is assumed that all but the reflector and the end walls emit diffusely and reflect diffusely, whereas reflector and abosrber emit diffusely but reflect partly specularly and partly diffusely (for thermal radiation). In fact no real surface is completely diffuse or completely specular, but the analysis becomes extremely complicated if all surfaces are treated like that.

(a) Surface resistance of a partly specular and partly diffuse surface: The total reflectivity of a surface ρ is given by

$$\rho = \rho_s + \rho_d \qquad \text{(A10.105)}$$

where ρ_s = specular component and ρ_d = diffuse component

Assuming Kirchhoffs law still applies, we have

$$\varepsilon = \alpha = 1 - \rho \qquad \text{(A10.106)}$$

The net heat lost by a surface is the difference between the energy emitted and absorbed.

$$q/A = \varepsilon E_b - \alpha G \qquad \text{(A10.107)}$$

This actually follows from the original definition of J, G and q/A from Eqs. (A10.89), (A10.90) and (A10.91) respectively.

The diffuse radiosity J_d is defined as the total diffuse energy leaving the surface per unit area and per unit time.

$$J_d = \varepsilon E_b + \rho_d G \qquad \text{(A10.108)}$$

Combining the Eqs. (A10.107) and (A10.108) and rearranging,

$$q = \frac{E_b - \{J_d / (\varepsilon + \rho_d)\}}{\rho_d / \{A \varepsilon (\varepsilon + \rho_d)\}} \qquad \text{(A10.109)}$$

Because $(\varepsilon + \rho_d) = (1 - \rho_s)$ Eq. (A10.109) can be written as

$$q = \frac{E_b - \{J_d / (1 - \rho_s)\}}{\rho_d / \{A \varepsilon (1 - \rho_s)\}} \qquad \text{(A10.110)}$$

When represented as a network element (Fig. A10.12), it gives the surface resistance for a partly specular - partly diffuse surface. If $\rho_s = 0$, that is, when a surface reflects in diffuse manner alone, it reduces to the same form as shown in Fig. (A10.8)

(b) Space resistance between two specular - diffuse surfaces: For simplicity, first of all assume that the two

FIGURE A10.14 Space Resistance Between Two Specular-Diffuse Surfaces

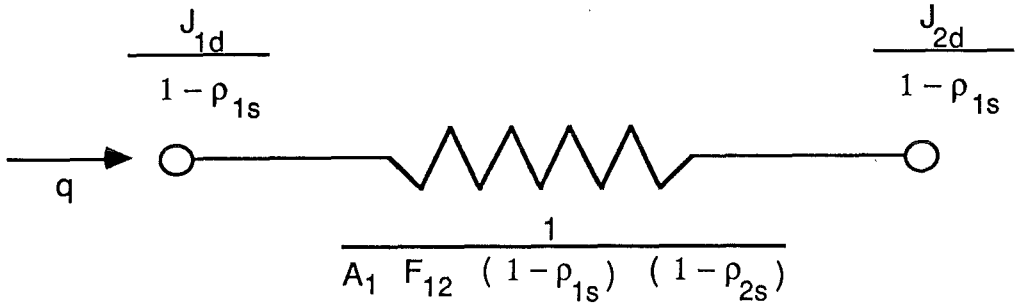

FIGURE A10.15 System with One Specular-Diffuse Surface

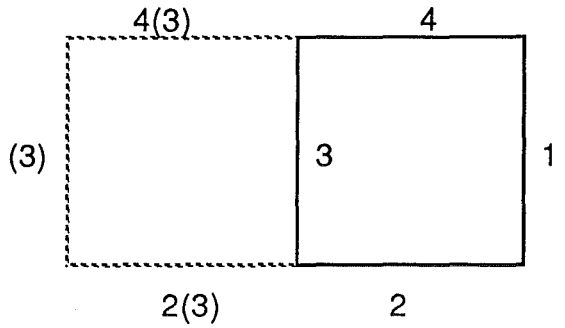

Notes: 1,2 and 4 are diffuse reflecting; 3 specular-diffuse reflecting

FIGURE A10.16 Space Resistance Between Two Specular-Diffuse Surfaces

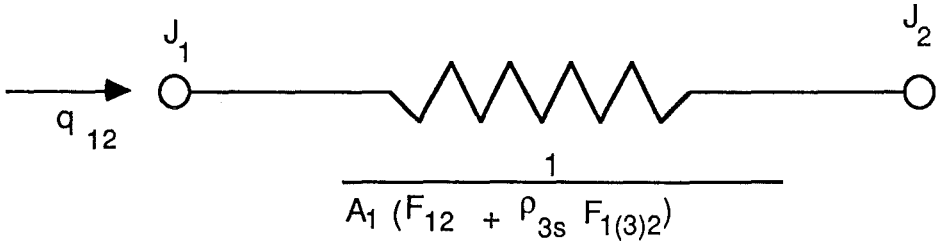

surfaces are perpendicular to each other as shown in Fig. A10.13. In this arrangement any diffuse radiation leaving 1, which is specularly reflected by 2 will not be reflected directly back to 1. This means that specular reflections need not be considered at this stage and only direct diffuse exchange between the two surfaces is to be taken into account and they are given by

$$q_{1\to2} = J_{1d}\, A_1\, F_{12}\, (1 - \rho_{2s}) \qquad \text{(A10.111)}$$

$$q_{2\to1} = J_{2d}\, A_2\, F_{21}\, (1 - \rho_{1s}) \qquad \text{(A10.112)}$$

Where $q_{1\to2}$ represents the diffuse radiation leaving 1 which arrives at 2 and which may contribute to a diffuse radiosity of surface 2 and $q_{2\to1}$ can be defined in the same way. The factor $(1-\rho_s)$ represents the fraction absorbed plus the fraction reflected diffusely because $\rho_s + \rho_d + \alpha = 1$

Thus the specular reflection is not considered at the moment. The net exchange between the two surfaces is given by

$$q_{1-2} = q_{1\to2} - q_{2\to1} \qquad \text{(A10.113)}$$

Combining the Eqs. (A10.111) to (A10.113) and rearranging gives

$$q_{1-2} = \frac{\{J_{1d} / (1 - \rho_{1s})\} - \{J_{2d} / (1 - \rho_{2s})\}}{1 / \{A_1\, F_{12}\, (1 - \rho_{1s})\, (1 - \rho_{2s})\}} \qquad \text{(A10.114)}$$

So it can be represented as shown in Fig. A10.14.

(c) System with one specular-diffuse surface:

Sparrow's technique (Eckert and Sparrow 1961, Sparrow et al., 1962) can be used to find out the radiation net work of an enclosure with 4 long surfaces, as shown in Fig. A10.15. The surfaces 1, 2, 4 reflect diffusely, while surface 3 reflects both specularly and diffusely. As the specular reflection produces mirror image, the mirror image is shown by dashed lines. The nomenclature is that 2(3) designates the mirror image of surface 2 in mirror 3.

Consider the radiation exchange between 1 and 2. The radiation leaving 2 and arriving at 1

$$q_{2\to1} = (q_{2\to1})_{\text{direct diffuse}} + (q_{2\to1})_{\text{specular reflected}} \qquad \text{(A10.115)}$$

The first part on the right hand side is given by

$$(q_{2\to1})_{\text{direct diffuse}} = J_2\, A_2\, F_{21} \qquad \text{(A10.116)}$$

Part of the diffuse radiation from 2 is specularly reflected in 3 and strikes 1. This specularly reflected radiation acts like diffuse energy coming from the image surface 2(3). Therefore,

$$(q_{2\to1})_{\text{specular reflected}} = J_2\, A_{2(3)}\, F_{2(3)1}\, \rho_{3s} \qquad \text{(A10.117)}$$

FIGURE A10.17 Resistance Network for a Four Surface System with Specular-Diffuse and Three Diffuse Surfaces

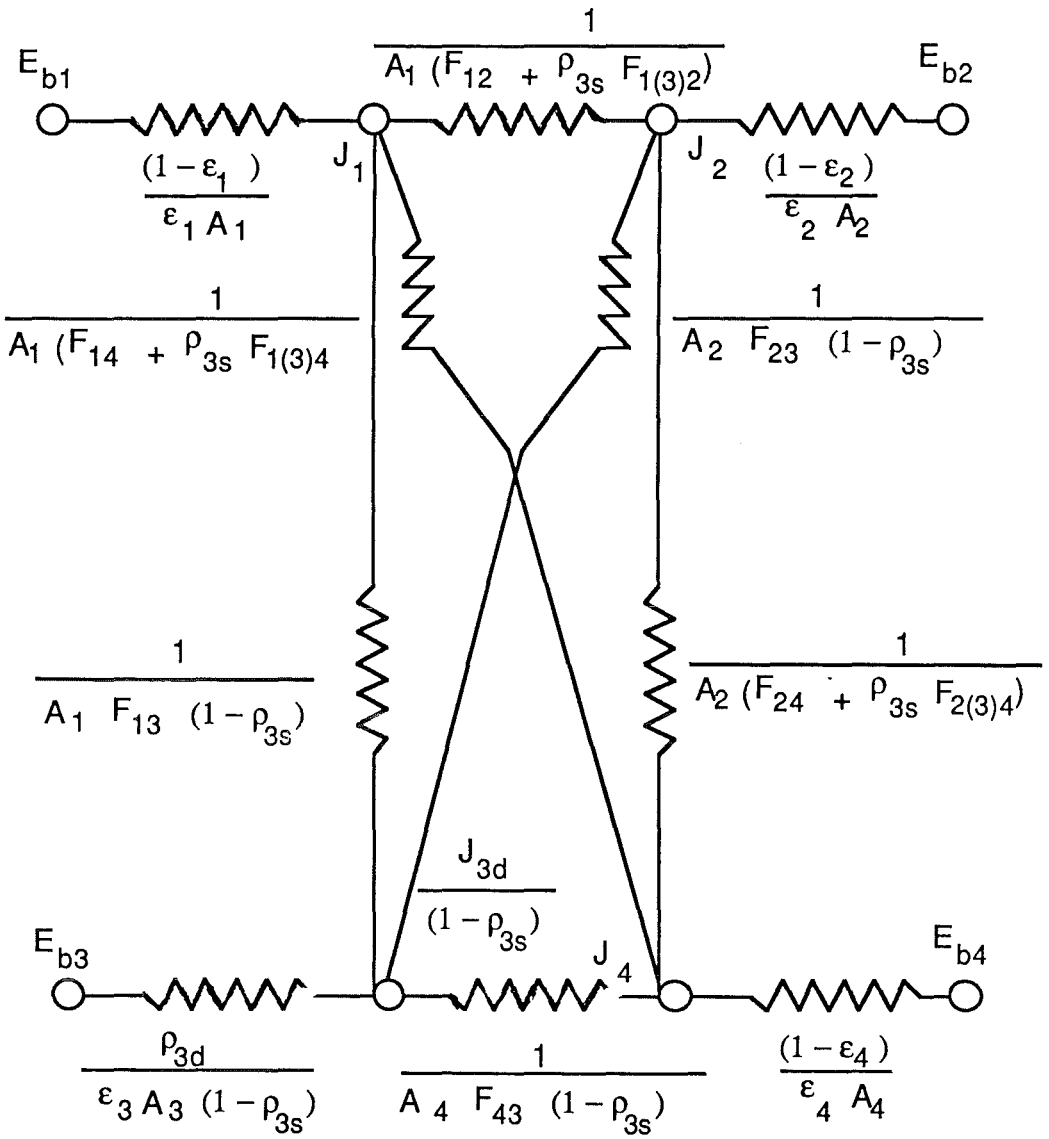

where $F_{2(3)1}$ is the radiation shape factor between 2(3) and 1. ρ_{3s} is inserted because only this fraction of the radiation gets to 1. As $A_2 = A_{2(3)}$, combining the Eqs. (A10.115) to (A10.117) we have

$$q_{2\to1} = J_2 A_2 \{F_{21} + \rho_{3s} F_{2(3)1}\} \quad \text{(A10.118)}$$

Similarly

$$q_{1\to2} = J_1 A_1 \{F_{12} + \rho_{3s} F_{1(3)2}\} \quad \text{(A10.119)}$$

The net exchange $q_{1-2} = q_{1\to2} - q_{2\to1}$ (A10.120)

By reciprocity theorem $A_1 F_{12} = A_2 F_{21}$ (A10.121)

and $A_1 F_{1(3)2} = A_2 F_{2(3)1}$ (A10.122)

Combining Eqs. (A10.118) to (A10.122)

$$q_{1-2} = \frac{J_1 - J_2}{1 \,/\, \{A_1 (F_{12} + \rho_{3s} F_{1(3)2})\}} \quad \text{(A10.123)}$$

This can be expressed as the net work element shown in Fig. A10.16. Similarly expressions can be developed for radiation exchange between other surfaces and the final network is shown in Fig. A10.17.

(d) System with two specular diffuse surfaces:

A system with two specular diffuse reflecting surfaces is shown in Fig. A10.18. Surfaces 1, 4 are diffuse reflecting while surfaces 2, 3 are specular - diffuse reflecting. 1(3,2) represents the image of 1(3) in mirror 2. In this case multiple reflections need to be considered.

Now considering the exchange between surfaces 1 and 4, the diffuse energy leaving 1 and arriving at 4 is given by

$J_1 A_1 F_{14}$ - direct

$+ J_1 A_1 F_{1(2)4} \rho_{2s}$ - reflection in 2 only

$+ J_1 A_1 F_{1(3)4} \rho_{3s}$ - reflection in 3 only

$+ J_1 A_1 \rho_{2s} \rho_{3s} F_{1(3,2)4}$ - reflection first in 2 and then in 3.

The last term is zero as it is not possible for any ray coming from 1, reflecting in 3, first to be reflected to 4 via 2. This can also be noticed from the fact that surface 1(3,2) cannot see surface 4 when looking through mirror 2, and so $F_{1(3,2)4} = 0$. Therefore

$$q_{1\to4} = J_1 A_1 \{F_{14} + \rho_{2s} F_{1(2)4} + \rho_{3s} F_{1(3)4} + \rho_{3s} \rho_{2s} F_{1(2,3)4}\} \quad \text{(A10.124)}$$

Similarly

$$q_{4\to1} = J_4 A_4 \{F_{41} + \rho_{2s} F_{4(2)1} + \rho_{3s} F_{4(3)1} + \rho_{3s} \rho_{2s} F_{4(2,3)1}\} \quad \text{(A10.125)}$$

FIGURE A10.18 System with Two Specular-Diffuse Surfaces

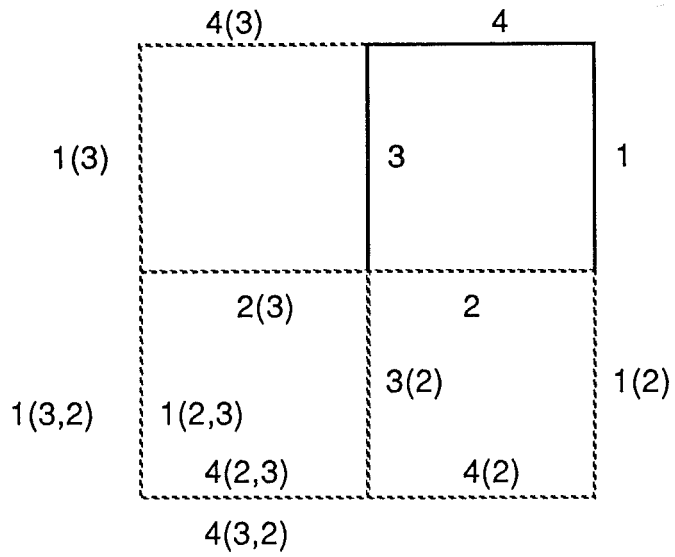

Notes: 1 and 4 are diffuse reflecting; 2 and3 are specular-diffuse reflecting

FIGURE A10.19 Energy Exchange Between the Surfaces One and Four from Figure A10.18

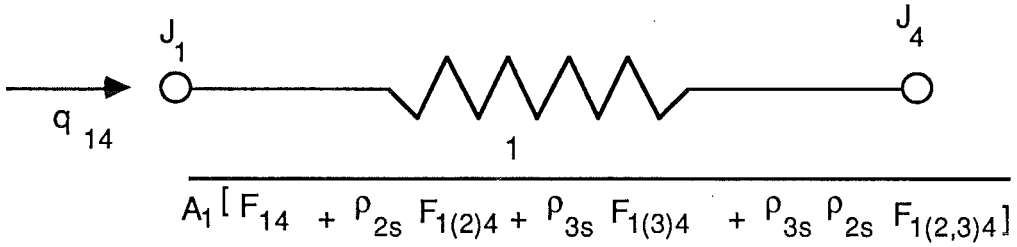

FIGURE A10.20 Space Resistance Between Surfaces One and Three from Figure A10.18

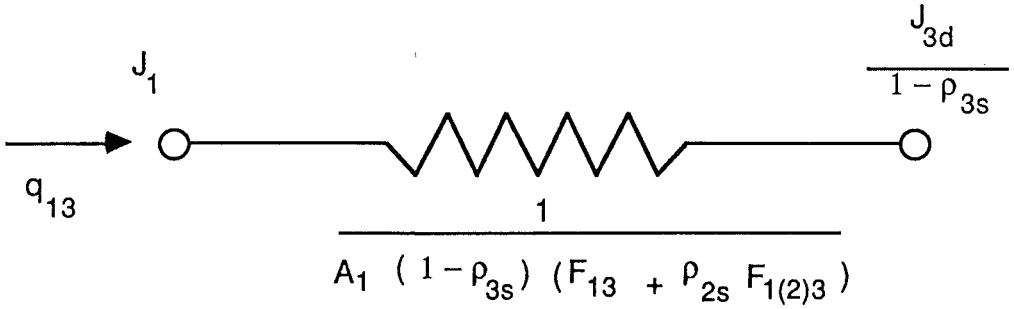

FIGURE A10.21 Resistance Network for a Four Surface System with Two Specular-Diffuse and Two Diffuse Surfaces

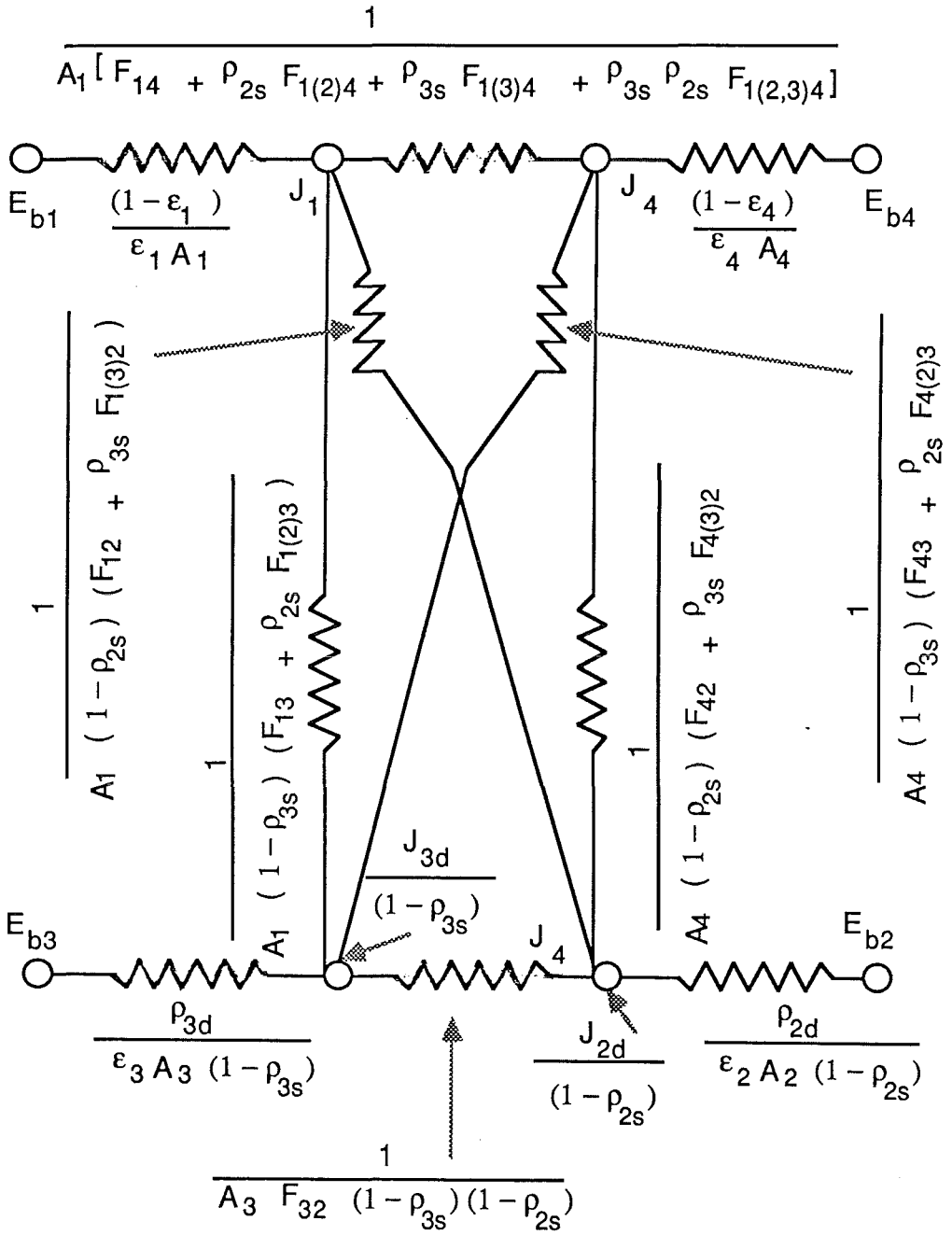

The heat exchange q_{1-4} can be obtained by substracting the Eq. (A10.125) from Eq. (A10.124) and applying the receiprocity theorem we get the resistance as shown in Fig. A10.19.

Now considering the diffuse energy leaving 1 and the amount which contributes to the diffuse radiosity of surface 3 is

$$q_{1\to3} = \{J_1\ A_1\ F_{13}\ (1 - \rho_{3s})\} + \{J_1\ A_1\ \rho_{2s}\ F_{1(2)3}(1 - \rho_{3s})\} \qquad \text{(A10.126)}$$

The first term is the direct exchange and 2nd one after reflection in 2. The factor $(1 - \rho_{3s})$ is used to leave out the specular reflection from 3, which is taken into account in other terms. The diffuse energy going from 3 to 1 is

$$q_{1\to3} = J_{3d}\ A_3\ F_{31} + J_{3d}\ A_3\ \rho_{2s}\ F_{3(2)1} \qquad \text{(A10.127)}$$

The resulting resistance term is shown in Fig. A10.20. The whole network is given in Fig. A10.21.

A10.2.1.8 Radiation exchange in an absorbing-transmitting medium

Considering the system shown in Fig. A10.22 in which a transmitting, absorbing medium is held by two non-transmitting surfaces which see each other and nothing else. A practical example of medium can be either a gas or a transparent sheet of glass or plastic. Assuming the medium to be non-reflecting, and applying Kirchhoff's law,

$$\alpha_m + \tau_m = 1 = \varepsilon_m + \tau_m \qquad \text{(A10.128)}$$

So the medium can emit and transmit radiation. The transmitted radiation is analysed first.

$$(q_{1\to2})_{\text{transmitted}} = J_1\ A_1\ F_{12}\ \tau_m \qquad \text{(A10.129)}$$

$$(q_{2\to1})_{\text{transmitted}} = J_2\ A_2\ F_{21}\ \tau_m \qquad \text{(A10.130)}$$

From reciprocity theorem $A_1\ F_{12} = A_2\ F_{21}$ (A10.131)

Combining Eqs. (A10.128) to (A10.131) and rearranging gives

$$(q_{1-2})_{\text{transmitted}} = \frac{J_1 - J_2}{1\ /\ \{A_1\ F_{12}\ (1 - \varepsilon_m)\}} \qquad \text{(A10.132)}$$

which can be represented as a resistance element as shown in Fig. A10.23. Now, the emitted radiation is considered, which is the exchange process between surface 1 and the medium. As the medium is nonreflective, the energy leaving the medium is that which is emitted by the medium.

$$J_m = \varepsilon_m\ E_{bm} \qquad \text{(A10.133)}$$

FIGURE A10.22 System with Absorbing Transmitting Media

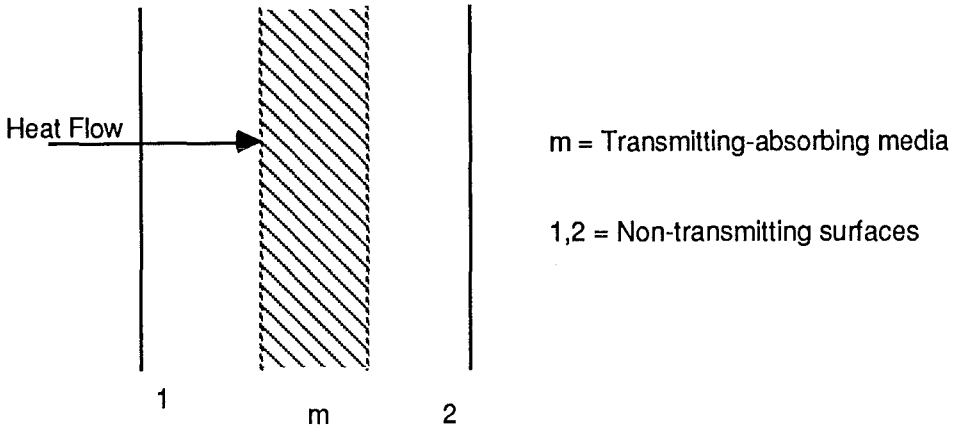

FIGURE A10.23 Energy Exchange Between the Surfaces One and Two from Figure A10.22

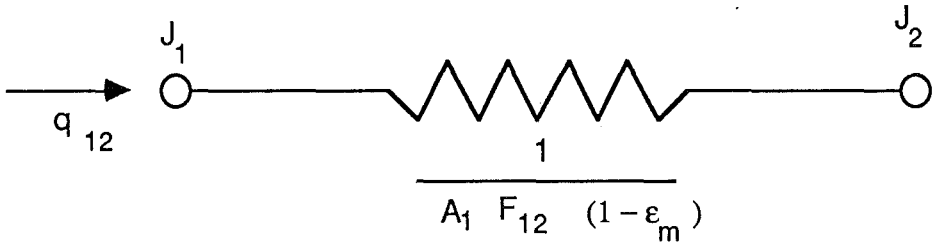

FIGURE A10.24 Resistance Between the Surface One and the Medium from Figure A10.22

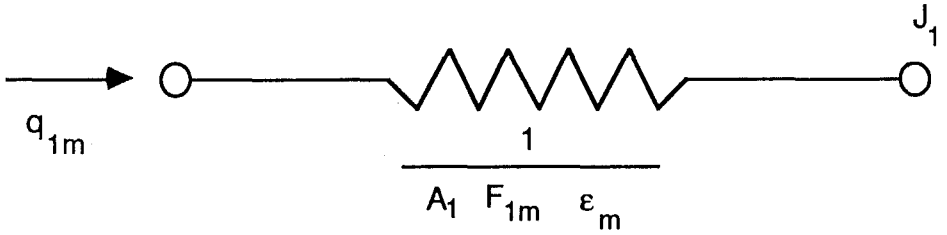

FIGURE A10.25 Resistance Network for the System Shown in Fig. A10.22

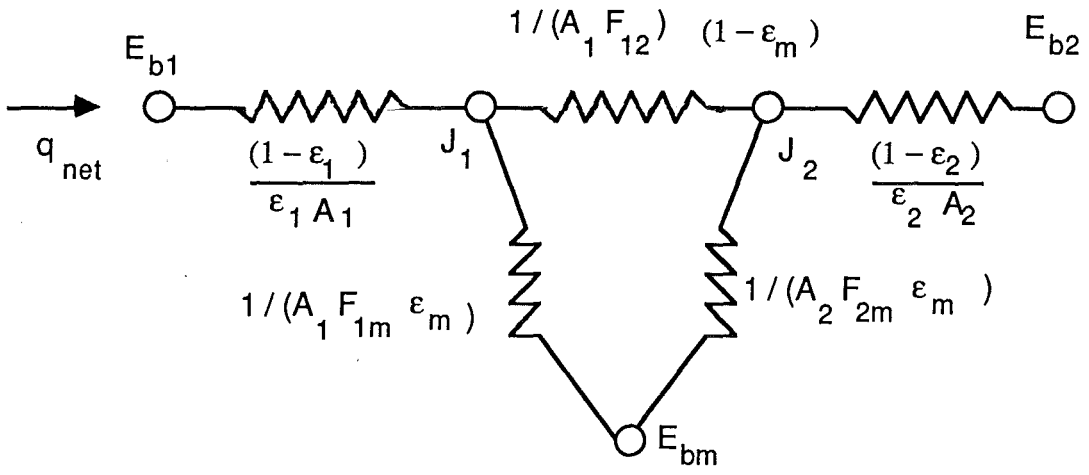

The energy leaving the medium and reaching surface 1 is given by

$$(q_{m\rightarrow 1})_{emitted} = A_m F_{m1} J_m = A_m F_{m1} \varepsilon_m E_{bm} \qquad (A10.134)$$

The energy which leaves the surface 1 and reaches the transparent medium is

$$(q_{m\rightarrow 1})_{emitted} = J_1 A_1 F_{1m} \alpha_m = J_1 A_1 F_{1m} \varepsilon_m \qquad (A10.135)$$

The net exchange is given by

$$(q_{m-1})_{emitted} = A_m F_{m1} \varepsilon_m E_{bm} - J_1 A_1 F_{1m} \varepsilon_m \qquad (A10.136)$$

Applying reciprocity theorem, $A_1 F_{1m} = A_m F_{m1}$, Eq. (A10.136) gives

$$(q_{m-1})_{emitted} = \{E_{bm} - J_1\} / \{1 / (A_1 F_{1m} \varepsilon m)\} \qquad (A10.137)$$

This is shown as a network element in Fig. A10.24. Similarly the radiation exchange between the medium and surface 2 can be evaluated and so the total network can be represented as shown in Fig. A10.25. F_{1m} and F_{2m} are always unity as the whole surface is in contact with the medium.

A10.2.2 Assumptions

Several assumptions have to be made before proceeding to the complete radiation net work, the important ones are listed below, (the others are mentioned at appropriate places).

(1) The glazings are opaque to thermal radiation.

(2) All surfaces are grey.

(3) All surfaces emit diffusely and reflect diffusely for thermal radiation.

(4) Sky is a black body at some equivalent sky temperature.

(5) Reflector and the end walls are the only specular-diffuse surfaces.

(6) Surface temperatures are uniform.

(7) Radiosity and irradiation are uniform over each surface.

(8) Kirchoff's law applies to the thermal radiation properties that is $\alpha = \varepsilon$

(9) Emittivity is independent of wave length, temperature and surface condition and assumed constant.

(10) Reflective and emittive properties are constant all over the surface.

(11) Air is assumed to be non-reflecting, transmitting and absorbing media.

(12) Glazing is assumed to be non-reflecting, non-transmitting but asborbing media.

(13) Material properties such as absorptivity, transmissivity and reflectivity are constant over the wave length range (of thermal radiation) under consideration.

A10.2.3 Expressions for radiation resistances

Now different elements of the radiation network can be analysed.

(1) RR1 : Surface resistance of the outer surface of the outer galvanised iron sheet box (without considering the end walls and the outer glazing) and the space resistance between the box and the environment:

The end walls and the outer glazing are accounted for separately in other resistances. In this case there is only one surface resistance, that of the box, as the environment is assumed to be a black body. Hence taking surface 1 as box and surface 2 as sky, from Eq. (A10.98), $(1 - \varepsilon_2) / (\varepsilon_2 A_2)$ reduces to zero and F_{12} becomes unity. Since all energy leaving the box reaches the environment, the fraction of energy leaving the box and arriving at the sky equals unity.

$$E_{b1} = \sigma T1^4 \qquad \text{(A10.138)}$$

where T1 is the absolute temperature of the outer box surface.

$$E_{b2} = \sigma T_{amb}^4 \qquad \text{(A10.139)}$$

The ambient temperature T_{amb} is used instead of the sky temperature T_{sky} because the box mainly exchanges radiation with the environment (except for a small top portion of the box and the glazing which is considered separately). $\varepsilon_1 = \varepsilon_{bo}$ = emissivity of the box outer surface and it is 0.28 (Kreith and Kreider, 1978). $A_1 = A_{bo}$ = box outer surface area = 0.957488 m^2 (from the calculation of CR1). For galvanised iron sheet long wave emittance = 0.28 (Kreith and Kreider, 1978). Substituting for ε_1, A_1 & F_{12} and combining Eqs. (A10.97), (A10.98), (A10.102), (A10.138) & (A10.139) and rearranging gives

$$RR1 = 1 \; / \; \{\varepsilon_{bo} A_{bo} \sigma (T1^2 + T_{amb}^2) (T1 + T_{amb})\} \qquad \text{(A10.140)}$$

(2) RR2 : Surface resistance of the inner surface of the reflector: The reflector is supposed to reflect both specularly and diffusely. Hence, from the Eq. (A10.110) substituting the following quantities for the reflector (r) the expression for 'q' can be obtained. $E_b = E_r$; $\varepsilon = \varepsilon_r$; $A = A_r$; $J_d = J_{dr} / (1 - \rho_{sr})$, where ρ_{sr} is the specular reflectivity of the reflector.

$$q = \frac{E_r - J_{dr} / (1 - \rho_{sr})}{\rho_{dr} / \varepsilon r\ A_r\ (1 - \rho_{sr})} \qquad \text{(A10.141)}$$

E_r can be related to the reflector inner surface temperature T4 as

$$E_r = \sigma\ T4^4 \qquad \text{(A10.142)}$$

Defining a dummy temperature T20 such that

$$J_{dr} / (1 - \rho_{sr}) = \sigma\ T20^4 \qquad \text{(A10.143)}$$

Combining Eqs. (A10.141) to (A10.143) gives

$$q = (T4 - T20) / RR2 \qquad \text{(A10.144)}$$

where RR2 is given by

$$RR2 = \rho_{dr} / \{\varepsilon_r\ A_r\ \sigma\ (1 - \rho_{sr})\ (T4^2 + T20^2)\ (T4 + T20)\} \qquad \text{(A10.145)}$$

(3) RR3 : Space resistance between the reflector and the outer air: Air is supposed to be an absorbing and transmitting media, hence the analysis given in Section A10.2.1.8 applies, but keeping in mind that the reflector is a specular-diffuse surface, the node J_d changes to

$J_d / (1 - \rho_s)$, as per the analysis given in Section A10.2.1.7 . The resistance will also change from $1 / (A_1\ F_{1m}\ \varepsilon_m)$ to

$$1 / \{A_1\ F_{1m}\ \varepsilon_m\ (1 - \rho_{sr})\}$$

In the present case substituting corresponding quantities for the outer air (oa) and the reflector (r) the expression for 'q' can be obtained. $A_1 = A_r$; $F_{1m} = F_{r\text{-}oa} = 1$; $\varepsilon_m = \varepsilon_{oa}$; $J_1 = J_{dr}$; $E_{bm} = E_{oa}$

$$q = \frac{\{J_{dr} / (1 - \rho_{sr})\} - E_{oa}}{1 / \{A_r\ \varepsilon_{oa}\ F_{r\text{-}oa}\ (1 - \rho_{sr})\}} \qquad \text{(A10.146)}$$

E_{oa} can be related to the outer air temperature T13 by

$$E_{oa} = \sigma\ T13^4 \qquad \text{(A10.147)}$$

Combining Eqs. (A10.143), (A10.146) and (A10.147) gives

$$q = (T20 - T13) / RR3 \qquad \text{(A10.148)}$$

where RR3 is given by

$$RR3 = 1 / \{\varepsilon_{oa}\ A_r\ \sigma\ (1 - \rho_{sr})\ (T13^2 + T20^2)\ (T13 + T20)\} \qquad \text{(A10.149)}$$

(4) RR4 : Space resistance between the outer air and the outer glazing: This situation is same as that described in Section A10.2.1.8 and by substituting the appropriate quantities for the outer glazing (og) and outer air (oa) we have

$A_2 = A_{og}$; $F_{2m} = F_{og\text{-}oa} = 1$; $\varepsilon_m = \varepsilon_{oa}$; $J_2 = J_{og}$; $E_{bm} = E_{oa}$

From Eq. (A10.137) we get

$$E_{oa} - J_{og}$$

$$q = \frac{}{1 \;/\; (\varepsilon_{oa}\, A_{og}\, F_{og\text{-}oa})} \qquad \text{(A10.150)}$$

Defining a dummy temperature T21 such that

$$J_{og} = \sigma\, T21^4 \qquad \text{(A10.151)}$$

Combining Eqs. (A10.147), (A10.150) and (A10.151) gives

$$q = (T13 - T21) \;/\; RR4 \qquad \text{(A10.152)}$$

$$RR4 = 1 \Big/ \{\varepsilon_{oa}\, A_{og}\, \sigma\, (T13^2 + T21^2)\,(T13 + T21)\} \qquad \text{(A10.153)}$$

(5) RR5 : Space resistance between the reflector and the outer glazing: The expression given in Section A10.2.1.7d can be used except for the fact that the transmissivity of air should be taken into account. In the present case we have $A_4 = A_{og}$; $F_{4(2)3} = F_{og\text{-}e\text{-}r}$; $\rho_{3s} = \rho_{sr}$; $J_4 = J_{og}$; $J_{3d} = J_{dr}$; $F_{43} = F_{og\text{-}r}$; $\rho_{2s} = \rho_{se}$, where ρ_{se} = specular reflectivity of the end wall. Combining with Eqs. (A10.143) and (A10.151) gives

$$q = (T20 - T21) \;/\; RR5 \qquad \text{(A10.154)}$$

$$RR5 = 1 \Big/ \{A_{og}\, \sigma\, (1 - \rho_{sr})\, (F_{og\text{-}r} + \rho_{se}\, F_{og\text{-}e\text{-}r})\, (1 - \varepsilon_{oa})\, (T20^2 + T21^2)\, (T20 + T21)\} \qquad \text{(A10.155)}$$

(6) RR6 : Surface resistance of the inner surface of the outer glazing: By substituting $A = A_{og}$; $\varepsilon = \varepsilon_{og}$; $J = J_{og}$; $E_b = E_{og}$; $E_{og} = \sigma\, T9^4$, where T9 is the inner surface temperature of the outer glazing; and $J_{og} = \sigma\, T21^4$ in Eq. (A10.92) we get

$$q = (T9 - T23) \;/\; RR6 \qquad \text{(A10.156)}$$

$$RR6 = (1 - \varepsilon_{og}) \Big/ \{\varepsilon_{og}\, A_{og}\, \sigma\, (T9^2 + T21^2)\,(T9 + T21)\} \qquad \text{(A10.157)}$$

(7) RR7 : Space resistance between the outer air and the end walls: The expression is similar to the one used for RR3 as the end walls are also reflecting specularly-diffusely, except that T20 is replaced by another dummy temperature T22 and the area & reflectivity terms are changed to that of the end walls.

$$q = (T22 - T13) \;/\; RR7 \qquad \text{(A10.158)}$$

$$RR7 = 1 \Big/ \{\varepsilon_{oa}\, A_e\, \sigma\, (1 - \rho_{se})\,(T13^2 + T22^2)\,(T13 + T22)\} \qquad \text{(A10.159)}$$

(8) RR8 : Surface resistance of the end walls: The expression is similar to the one used for RR2 except that T20 is replaced by T22 and the area & emissivity terms are changed to that of the end walls.

$$q = (T5 - T22) \;/\; RR8 \qquad \text{(A10.160)}$$

$$RR8 = \rho_{dr} \Big/ \{\varepsilon_e\, A_e\, \sigma\, (1 - \rho_{se})\,(T5^2 + T22^2)\,(T4 + T22)\} \qquad \text{(A10.161)}$$

(9) RR9 : Space resistance between the end walls and the reflector: The expression is similar to the one used for RR5 except that this time both the surfaces are specular - diffuse and we have

$J_2 = J_{dr} / (1 - \rho_{sr})$; $J_1 = J_{de} / (1 - \rho_{se})$; $A_1 = A_e$; $F_{12} = F_{e-r}$; $\varepsilon_m = \varepsilon_{oa}$; $J_{dr} / (1 - \rho_{sr}) = \sigma\ T20^4$; $J_{de} / (1 - \rho_{se}) = \sigma\ T22^4$

The expression for 'q' is given by

$$q = (T22 - T20) / RR9 \qquad \text{(A10.162)}$$

$$RR9 = 1 / \{A_e\ \sigma\ F_{e-r}\ (1 - \rho_{sr})\ (1 - \rho_{se})\ (1 - \varepsilon_{oa})\ (T20^2 + T22^2)\ (T20 + T22)\} \qquad \text{(A10.163)}$$

(10) RR10 : Space resistance between the outer air and the inner glazing: The expression is similar to the one used for RR4 except that T20 is replaced by another dummy temperature T23 and the area term is changed to that of the inner glazing.

$$q = (T13 - T23) / RR10 \qquad \text{(A10.164)}$$

$$RR10 = 1 / \{\varepsilon_{oa}\ A_{ig}\ \sigma\ (T13^2 + T23^2)(T13 + T23)\} \qquad \text{(A10.165)}$$

(11) RR11 : Surface resistance of the outer surface of the inner glazing: The expression is similar to the one used for RR6 except that the temperature, the area and the emissivity terms are changed to that of the inner glazing.

$$q = (T14 - T23) / RR11 \qquad \text{(A10.166)}$$

$$RR11 = (1 - \varepsilon_{ig}) / \{\varepsilon_{ig}\ A_{ig}\ \sigma\ (T14^2 + T23^2)(T14 + T23)\} \qquad \text{(A10.167)}$$

(12) RR12 : Space resistance between the end walls and the inner glazing: The expression is similar to the one used for RR5 except that the temperatures and the other properties are changed to that of the end wall and the inner glazing.

$$q = (T22 - T23) / RR12 \qquad \text{(A10.168)}$$

$$RR12 = 1 / \{A_e\ \sigma\ (1 - \rho_{se})\ (F_{e-ig} + \rho_{sr}\ F_{e-r-ig})\ (1 - \varepsilon_{oa})\ (T22^2 + T23^2)\ (T22 + T23)\} \qquad \text{(A10.169)}$$

(13) RR13 : Space resistance between the end walls and the outer glazing: The expression is similar to the one used for RR12 except that the temperatures and the other properties are changed to that of the outer glazing.

$$q = (T22 - T21) / RR13 \qquad \text{(A10.170)}$$

$$RR13 = 1 / \{A_e\ \sigma\ (1 - \rho_{se})\ (F_{e-og} + \rho_{sr}\ F_{e-r-og})\ (1 - \varepsilon_{oa})\ (T22^2 + T21^2)\ (T22 + T21)\} \qquad \text{(A10.171)}$$

(14) RR14 : Space resistance between the outer glazing and the inner glazing: The expression for the resistance between the surfaces 1 and 4, shown in Fig. A10.21, in Section A10.2.1.7d can be used. In the present case we have $A_1 = A_{ig}$; $\rho_{3s} = \rho_{se}$; $\rho_{2s} = \rho_{sr}$; $J_4 = J_{og}$; $J_1 = J_{ig}$; $F_{14} = F_{ig-og}$; $F_{1(2)4} = F_{ig-r-og}$; $F_{1(3)4} = F_{ig-e-og}$; $F_{1(2,3)4} = F_{ig-r-e-og}$; $F_{1(3,2)4} = F_{ig-e-r-og}$, this shape factor is

included to make the programme (resistance) a more general one. Also we have,

$J_{ig} = \sigma\ T23^4$ and $J_{og} = \sigma\ T21^4$ and hence

$$q = (T23 - T21) / RR14 \qquad \text{(A10.172)}$$

$$RR14 = 1 \Big/ \{A_{ig}\ \sigma\ (F_{ig\text{-}og} + \rho_{sr}\ F_{ig\text{-}r\text{-}og} + \rho_{se}\ F_{ig\text{-}e\text{-}og} + \rho_{se}\ \rho_{sr}\ F_{ig\text{-}r\text{-}e\text{-}og} + \rho_{se}\ \rho_{sr}\ F_{ig\text{-}e\text{-}r\text{-}og})\ (1 - \varepsilon_{oa})\ (T23^2 + T21^2)\ (T23 + T21)\} \qquad \text{(A10.173)}$$

(15) RR15 : Space resistance between the reflector and the inner glazing: The expression is similar to the one used for RR5 except that the temperatures and the other properties are changed to that of the inner glazing.

$$q = (T20 - T23) / RR15 \qquad \text{(A10.174)}$$

$$RR15 = 1 \Big/ \{A_{ig}\ \sigma\ (1 - \rho_{sr})\ (F_{ig\text{-}r} + \rho_{se}\ F_{ig\text{-}e\text{-}r})\ (1 - \varepsilon_{oa})\ (T20^2 + T23^2)\ (T20 + T23)\} \qquad \text{(A10.175)}$$

(16) RR16 : Surface resistance of the inner surface of the inner glazing: The expression is similar to the one used for RR11 except that the temperatures are changed accordingly.

$$q = (T15 - T24) / RR16 \qquad \text{(A10.176)}$$

$$RR16 = (1 - \varepsilon_{ig}) \Big/ \{\varepsilon_{ig}\ A_{ig}\ \sigma\ (T15^2 + T24^2)(T15 + T24)\} \qquad \text{(A10.177)}$$

(17) RR17 : Space resistance between the inner air and the inner glazing: The expression is similar to the one used for RR10 except that T23 is replaced by another dummy temperature T24; T13 replaced by the inner air temperature T16; and the area & emissivity terms are changed accordingly.

$$q = (T16 - T24) / RR17 \qquad \text{(A10.178)}$$

$$RR17 = 1 \Big/ \{\varepsilon_{ia}\ A_{ig}\ \sigma\ (T16^2 + T24^2)(T16 + T24)\} \qquad \text{(A10.179)}$$

(18) RR18 : Space resistance between the inner air and the absorber panel: The expression is similar to the one used for RR17 except that T24 is replaced by another dummy temperature T25 and the area term changed accordingly.

$$q = (T16 - T25) / RR18 \qquad \text{(A10.180)}$$

$$RR18 = 1 \Big/ \{\varepsilon_{ia}\ A_{ab}\ \sigma\ (T16^2 + T25^2)(T16 + T25)\} \qquad \text{(A10.181)}$$

(19) RR19 : Surface resistance of the absorber panel: The expression is similar to the one used for RR16 except that T15 & T24 are to be replaced by T17 & T25 respectively. Also the area and emissivity terms are changed accordingly.

$$q = (T17 - T25) / RR19 \qquad \text{(A10.182)}$$

$$RR19 = (1 - \varepsilon_{ab}) \Big/ \{\varepsilon_{ab}\ A_{ab}\ \sigma\ (T17^2 + T25^2)(T17 + T25)\} \qquad \text{(A10.183)}$$

(20) RR20 : Surface resistance of the horizontal aluminium strip:

The expression is similar to the one used for RR19 except that T17 & T25 are to be replaced by T8 & T26 (T26 being another dummy temperature) respectively. Also the area and emissivity terms are changed accordingly.

$$q = (T8 - T26) \;/\; RR20 \qquad \text{(A10.184)}$$

$$RR20 = (1 - \varepsilon_{al}) \Big/ \{\varepsilon_{al}\, A_{hral}\, \sigma\, (T8^2 + T26^2)(T8 + T26)\} \qquad \text{(A10.185)}$$

where A_{hral} is the area of the horizontal aluminium strip and ε_{al} is the emissivity of aluminium = 0.18 (Wong, 1977)

(21) RR21 : Space resistance between the inner air and the horizontal aluminium strip: The expression is similar to the one used for RR18 except that T25 is replaced by T26 and the area term changed accordingly.

$$q = (T16 - T26) \;/\; RR21 \qquad \text{(A10.186)}$$

$$RR21 = 1 \Big/ \{\varepsilon_{ia}\, A_{hral}\, \sigma\, (T16^2 + T26^2)(T16 + T26)\} \qquad \text{(A10.187)}$$

(22) RR22 : Space resistance between the inner air and the outer glazing in contact with the inner air: The expression is similar to the one used for RR21 except that T26 is replaced by another dummy temperature T27 and the area term changed accordingly.

$$q = (T16 - T27) \;/\; RR22 \qquad \text{(A10.188)}$$

$$RR22 = 1 \Big/ \{\varepsilon_{ia}\, A_{og\text{-}ia}\, \sigma\, (T16^2 + T27^2)(T16 + T27)\} \qquad \text{(A10.189)}$$

where Aog-ia is the area of the outer glazing in contact with the inner air.

(23) RR23 : Surface resistance of the outer glazing in contact with the inner air: The expression is similar to the one used for RR20 except that T8 & T26 are to be replaced by T11 & T27 (T27 being another dummy temperature) respectively. Also the area and emissivity terms are changed accordingly.

$$q = (T11 - T27) \;/\; RR23 \qquad \text{(A10.190)}$$

$$RR23 = (1 - \varepsilon_{og}) \Big/ \{\varepsilon_{og}\, A_{og\text{-}ia}\, \sigma\, (T11^2 + T27^2)(T11 + T27)\} \qquad \text{(A10.191)}$$

(24) RR24 : Space resistance between the inner glazing and the horizontal aluminium strip: The expression for the resistance between the surfaces 1 and 2 seperated by a medium, shown in Fig. A10.21, in Section A10.2.1.7d can be used, after making appropriate changes.

$$q = (T24 - T26) \;/\; RR24 \qquad \text{(A10.192)}$$

$$RR24 = 1 / \{A_{ig} F_{ig\text{-}hral} \sigma (1 - \varepsilon_{ia}) (T24^2 + T26^2) (T24 + T26)\} \quad (A10.193)$$

(25) RR25 : Space resistance between the inner glazing and the outer glazing in contact with the inner air: The expression is similar to the one used for RR24 except that T26 is to be replaced by T27 and the shape factor changed accordingly.

$$q = (T24 - T27) / RR25 \quad (A10.194)$$

$$RR25 = 1 / \{A_{ig} F_{ig\text{-}ogia} \sigma (1 - \varepsilon_{ia}) (T24^2 + T27^2) (T24 + T27)\} \quad (A10.195)$$

where $F_{ig\text{-}ogia}$ is the shape factor between 'ig' and 'ogia'.

(26) RR26 : Space resistance between the absorber panel and the outer glazing in contact with the inner air: The expression is similar to the one used for RR25 except that T24 is to be replaced by T25 and the area & the shape factor changed accordingly.

$$q = (T25 - T27) / RR26 \quad (A10.196)$$

$$RR26 = 1 / \{A_{ab} F_{ab\text{-}ogia} \sigma (1 - \varepsilon_{ia}) (T25^2 + T27^2) (T25 + T27)\} \quad (A10.197)$$

where $F_{ab\text{-}ogia}$ is the shape factor between 'ab' and 'ogia'.

(27) RR27 : Space resistance between the absorber panel and the horizontal aluminium strip: The expression is similar to the one used for RR26 except that T27 is to be replaced by T26 and the shape factor changed accordingly.

$$q = (T25 - T26) / RR27 \quad (A10.198)$$

$$RR27 = 1 / \{A_{ab} F_{ab\text{-}hral} \sigma (1 - \varepsilon_{ia}) (T25^2 + T26^2) (T25 + T26)\} \quad (A10.199)$$

(28) RR28 : Space resistance between the inner glazing and the absorber panel: The expression is similar to the one used for RR25 except that T27 is to be replaced by T25 and the area & shape factor terms changed accordingly.

$$q = (T24 - T25) / RR28 \quad (A10.200)$$

$$RR28 = 1 / \{A_{ab} F_{ab\text{-}ig} \sigma (1 - \varepsilon_{ia}) (T24^2 + T25^2) (T24 + T25)\} \quad (A10.201)$$

where $F_{ab\text{-}ig}$ is the shape factor between 'ab' and 'ig'.

(29) RR29 : Space resistance between the horizontal aluminium strip and the outer glazing in contact with the inner air: The expression is similar to the one used for RR28 except that T24 & T25 are to be replaced by T26 & T27 respectively and the area & shape factor terms changed accordingly.

$$q = (T26 - T27) / RR29 \quad (A10.202)$$

$$RR29 = 1 / \{A_{hral} F_{hral\text{-}ogia} \sigma (1 - \varepsilon_{ia}) (T26^2 + T27^2)$$

$$(T26 + T27)\} \qquad \text{(A10.203)}$$

(30) RR30 : Surface resistance of the inner surface of the outer box: The expression for the surface resistance of the surface 1 shown in Fig. A10.25, in Section A10.2.1.8 can be used, after making appropriate changes.

$$q = (T28 - T2) \,/\, RR30 \qquad \text{(A10.204)}$$

$$RR30 = (1 - \varepsilon_{bi}) \,/\, \{\varepsilon_{bi}\, A_{bi}\, \sigma\, (T28^2 + T2^2)\, (T28 + T2)\} \qquad \text{(A10.205)}$$

where A_{bi} = area of the outer box inner surface = 0.791728 m^2, for half the collector as obtained from Fig. A10.3; ε_{bi} = emissivity of the outer box inner surface, which in the present case is galvanised iron sheet = 0.17 (Kreith and Kreider, 1978)

(31) RR31 : Space resistance between the inner surface of the outer box and the box air in contact with it: The expression for the resistance of the surfaces 1 shown in Fig. A10.25, in Section A10.2.1.8 can be used, after making appropriate changes.

$$q = (T28 - T30) \,/\, RR31 \qquad \text{(A10.206)}$$

$$RR31 = 1 \,/\, \{\varepsilon_{ba}\, A_{bi}\, F_{bi\text{-}ba}\, \sigma\, (T28^2 + T30^2)\, (T28 + T30)\} \qquad \text{(A10.207)}$$

where ε_{ba} = emissivity of the box air; $F_{bi\text{-}ba}$ = shape factor between the inner surface of the outer box and box air.

(32) RR32 : Space resistance between the outer surface of the reflector and the air in contact with it: The expression is similar to the one used for RR31 except that T28 is to be replaced by T29 and the area term changed accordingly.

$$q = (T29 - T30) \,/\, RR32 \qquad \text{(A10.208)}$$

$$RR32 = 1 \,/\, \{\varepsilon_{ba}\, A_{ro}\, F_{ro\text{-}ba}\, \sigma\, (T29^2 + T30^2)\, (T29 + T30)\} \qquad \text{(A10.209)}$$

where A_{ro} = reflector outside surface area = A_r; $F_{ro\text{-}ba}$ = shape factor between the reflector outer surface and the box air.

(33) RR33 : Surface resistance of the outer surface of the reflector: The expression is similar to the one used for RR30 except that T28 & T2 are to be replaced by T29 & T3 respectively and the area & shape factor terms changed accordingly. But T3 is modified as

T3 = 0.075 T7 + 0.925 T3, because 7.5% of the reflector area is covered by the horizontal aluminium strip.

$$q = (T29 - T3) \,/\, RR33 \qquad \text{(A10.210)}$$

$$RR33 = (1 - \varepsilon_{ro}) \,/\, \{\varepsilon_{ro}\, A_{ro}\, \sigma\, (T29^2 + T3^2)\, (T29 + T3)\} \qquad \text{(A10.211)}$$

where ε_{ro} = emissivity of the reflector outer surface, which in the present case is galvanised iron sheet = 0.17 (Kreith and Kreider, 1978).

(34) RR34 : Space resistance between the inner surface of the outer box and the outer surface of the reflector: The expression for the resistance of the surfaces 1 shown in Fig. A10.25, in Section .8 can be used, after making appropriate changes.

$$q = (T28 - T29) / RR34 \qquad (A10.212)$$

$$RR34 = 1 / \{\varepsilon_{ba} A_{ro} F_{ro-bi} \sigma (1-\varepsilon_{ba}) (T28^2 + T29^2) (T28 + T29)\} \qquad (A10.213)$$

where F_{ro-bi} = shape factor between the reflector outer surface and the inner surface of the outer box, which is approximately equal one.

(35) RR35 : Surface resistance of the outer surface of the outer glazing and the space resistance between the outer glazing and the sky: It is similar to RR1 except that this time the radiation exchange is not with the environment, but with the sky and hence T_{amb} is to be replaced by T_{sky} and T1 by T10.

$$q = (T10 - T_{sky}) / RR35 \qquad (A10.214)$$

$$RR35 = 1 / \{\varepsilon_{ogo} A_{ogo} \sigma (T10^2 + T_{sky}^2) (T10 + T_{sky})\} \qquad (A10.215)$$

where ε_{ogo} and A_{ogo} are the emissivity and the area of the outer glazing outside suface, which are equal to ε_{og} and A_{og} respectively. For smooth glass emissivity is 0.94 (Wong, 1977).

(36) RR36 : Surface resistance of the outer surface of the outer glazing and the space resistance between the outer glazing and the sky: It is similar to RR35 except that T10 is to be replaced by T12 and the area term changed accordingly.

$$q = (T12 - T_{sky}) / RR36 \qquad (A10.216)$$

$$RR36 = 1 / \{\varepsilon_{ogo} A_{ogo} \sigma (T12^2 + T_{sky}^2) (T12 + T_{sky})\} \qquad (A10.217)$$

(37) RR37 : Surface resistance of the vertical aluminium strip: The expression is similar to the one used for RR20 except that temperatures and area terms changed accordingly.

$$q = (T31 - T33) / RR37 \qquad (A10.218)$$

$$RR37 = (1 - \varepsilon_{al}) / \{\varepsilon_{al} A_{vral} \sigma (T31^2 + T33^2) (T31 + T33)\} \qquad (A10.219)$$

where A_{vral} is the area of the vertical aluminium strip.

(38) RR38 : Space resistance between the inner glazing and the vertical aluminium strip: The expression is similar to the one used for RR24 except that the temperature and the shape factor changed accordingly.

$$q = (T24 - T33) / RR38 \qquad (A10.220)$$

$$RR38 = 1 / \{A_{ig} F_{ig-vral} \sigma (1 - \varepsilon_{ia}) (T24^2 + T33^2)$$

$$(T24 + T33)\} \qquad \text{(A10.221)}$$

(39) RR39 : Space resistance between the horizontal aluminium strip and the vertical aluminium strip: The expression is similar to the one used for RR38 except that the temperature, the area and the shape factor changed accordingly.

$$q = (T26 - T33) / RR39 \qquad \text{(A10.222)}$$

$$RR39 = 1/\{A_{hral}\, F_{hral\text{-}vral}\, \sigma\, (1 - \varepsilon_{ia})\, (T26^2 + T33^2)$$
$$(T26 + T33)\} \qquad \text{(A10.223)}$$

(40) RR40 : Space resistance between the vertical aluminium strips and the inner air: The expression is similar to the one used for RR21 except that the temperature and the area terms changed accordingly.

$$q = (T16 - T33) / RR40 \qquad \text{(A10.224)}$$

$$RR40 = 1/\{A_{vral}\, \varepsilon_{ia}\, \sigma\, (T16^2 + T33^2)\, (T16 + T33)\} \qquad \text{(A10.225)}$$

(41) RR41 : Space resistance between the vertical aluminium strip and the outer glazing in contact with the inner air: The expression is similar to the one used for RR29 except that the temperature, the area and the shape factor terms changed accordingly.

$$q = (T33 - T27) / RR41 \qquad \text{(A10.226)}$$

$$RR41 = 1/\{A_{vral}\, F_{vral\text{-}ogia}\, \sigma\, (1 - \varepsilon_{ia})\, (T33^2 + T27^2)$$
$$(T33 + T27)\} \qquad \text{(A10.227)}$$

(42) RR42 : Space resistance between the absorber panel and the vertical aluminium strip: The expression is similar to the one used for RR27 except that the temperature and the shape factor changed accordingly.

$$q = (T25 - T33) / RR42 \qquad \text{(A10.228)}$$

$$RR42 = 1/\{A_{ab}\, F_{ab\text{-}hral}\, \sigma\, (1 - \varepsilon_{ia})\, (T25^2 + T33^2)$$
$$(T25 + T33)\} \qquad \text{(A10.229)}$$

(43) RR43 : Surface resistance of the outer surface of the outer end walls and the space resistance between the outer end walls and the atmosphere: It is similar to RR1 except that the temperature, emissivity and the area terms changed accordingly.

$$q = (T19 - T_{amb}) / RR43 \qquad \text{(A10.230)}$$

$$RR43 = 1 / \{\varepsilon_{ewos}\, A_{ewos}\, \sigma\, (T19^2 + T_{amb}^2)\, (T19 + T_{amb})\} \qquad \text{(A10.231)}$$

where ε_{ewos} and A_{ewos} are the emissivity and the area of the end wall outside suface, which are equal to 0.8 (Wong, 1977) and A_e respectively.

(44) RR44 : Space resistance between the reflector and the absorber panel: The expression is similar to the one used for RR15

FIGURE A10.26 Conduction-Convection-Radiation Resistance Network

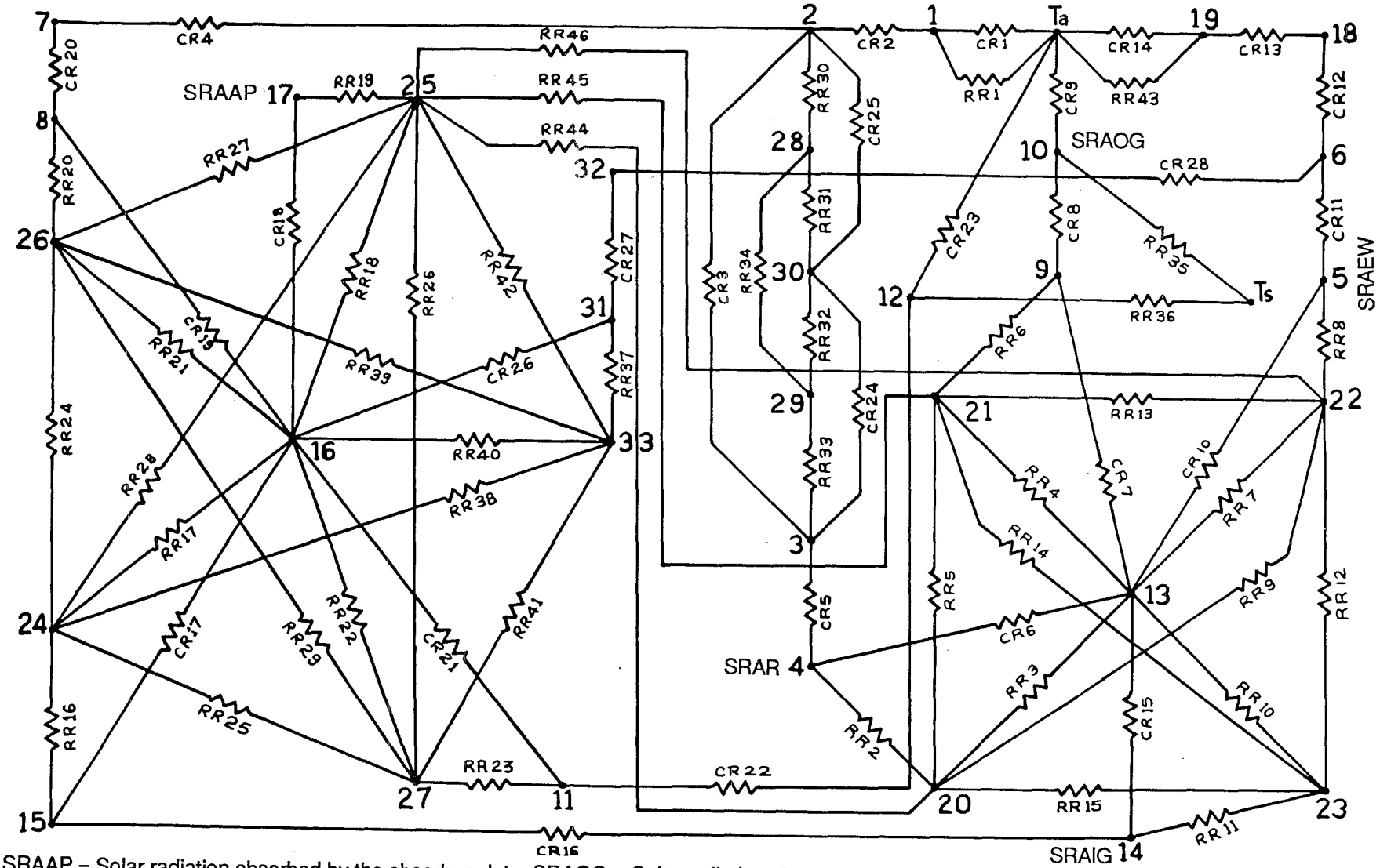

SRAAP = Solar radiation absorbed by the absorber plate; SRAOG = Solar radiation absorbed by the outer glazing

SRAEW = Solar radiation absorbed by the end walls SRAR = Solar radiation absorbed by the reflector; SRAIG = Solar radiation absorbed by the inner glazing

except that the temperatures and the other properties are changed to that of the inner glazing.

$$q = (T20 - T25) \;/\; RR44 \qquad \text{(A10.232)}$$

$$RR44 = 1 \;/\; \{A_{ab}\, \sigma\, (1 - \rho_{sr})\, (F_{ab\text{-}r} + \rho_{se}\, F_{ab\text{-}e\text{-}r})\, (1 - \varepsilon_{oa})\, (T20^2 + T25^2)\, (T20 + T25)\} \qquad \text{(A10.233)}$$

where $F_{ab\text{-}r} = F_{ig\text{-}r}$ and $F_{ab\text{-}e\text{-}r} = F_{ig\text{-}e\text{-}r}$

(45) RR45 : Space resistance between the absorber panel and the inner surface of the outer glazing: The expression is similar to the one used for RR14 except that the temperatures and the other properties are changed accordingly.

$$q = (T25 - T21) \;/\; RR45 \qquad \text{(A10.234)}$$

$$RR45 = 1 \;/\; \{A_{ab}\, \sigma\, (F_{ab\text{-}og} + \rho_{sr}\, F_{ab\text{-}r\text{-}og} + \rho_{se}\, F_{ab\text{-}e\text{-}og} + \rho_{se}\, \rho_{sr}\, F_{ab\text{-}r\text{-}e\text{-}og} + \rho_{sr}\, \rho_{se}\, F_{ab\text{-}e\text{-}r\text{-}og})\, (1 - \varepsilon_{oa})\, (T25^2 + T21^2)\, (T25 + T21)\} \qquad \text{(A10.235)}$$

where $F_{ab\text{-}og} = F_{ig\text{-}og}$; $F_{ab\text{-}r\text{-}og} = F_{ig\text{-}r\text{-}og}$; $F_{ab\text{-}e\text{-}og} = F_{ig\text{-}e\text{-}og}$; $F_{ab\text{-}r\text{-}e\text{-}og} = F_{ig\text{-}r\text{-}e\text{-}og}$; and $F_{ab\text{-}e\text{-}r\text{-}og} = F_{ig\text{-}e\text{-}r\text{-}og}$.

(46) RR46 : Space resistance between the end walls and the inner glazing: The expression is similar to the one used for RR12 except that the temperatures and the other properties are changed accordingly.

$$q = (T22 - T25) \;/\; RR46 \qquad \text{(A10.236)}$$

$$RR46 = 1 \;/\; \{A_e\, \sigma\, (1 - \rho_{se})\, (1 - \varepsilon_{oa})\, (F_{e\text{-}ab} + \rho_{sr}\, F_{e\text{-}r\text{-}ab})\, (T22^2 + T25^2)\, (T22 + T25)\} \qquad \text{(A10.237)}$$

A10.3 Solving the Conduction-Convection-Radiation Network by Nodal Method

The conduction-convection network shown in Fig. A10.2 and the radiation network shown in Fig. A10.7 have the same nodal points represented by 33 temperatures shown in Fig. A10.1. Hence the two networks can be superimposed and the resultant network is shown in Fig. A10.26. This network is analogous to an electrical resistance network, where the current flows due to the voltage difference and in the present case heat flows due to the difference in temperatures. The heat can flow either by conduction or convection or radiation and hence all three modes of heat transfer are considered. An energy balance equation can be written for each mode considering the heat flowing into the nodes as positive and out of the nodes as negative. Thus 33 different equations can be written for 33 different temperatures as described below. It should be noted that the solar radiation absorbed by various

surfaces (as calculated from the short wave analysis explained in Appendix A8) are introduced as inputs at the corresponding nodes.

A10.3.1 Expressions for nodal equations

(1) Node 1 : Conducting energy balance on node 1 we have,

$(T_{amb} - T1)/RR1 + (T_{amb}-T1)/CR1 + (T2-T1)/CR2 = 0$

$\Rightarrow -T1(1/RR1 + 1/CR1 + 1/CR2) + T2/CR2 = -Tamb(1/RR1 + 1/CR)$

(2) Node 2 : Conducting energy balance on node 2 we have,

$(T1-T2)/CR2 + (T7-T2)/CR4 + (T3-T2)/CR3 + (T30-T2)/CR25 + (T28-T2)/RR30 = 0$

$\Rightarrow T1(1/CR2) - T2(1/CR2 + 1/CR3 + 1/CR4 + 1/CR25 + 1/RR30) + T3/CR3 + T7/CR4 + T28/RR30 + T30/CR25 = 0$

(3) Node 3 : Conducting energy balance on node 3 we have,

$(T2-T3)/CR3 + (T4-T3)/CR5 + (T29-T3)/RR33 + (T30-T3)/CR24 = 0$

$\Rightarrow T2/CR3 - T3(1/CR3 + 1/CR5 + 1/CR24 + 1/RR33) + T4/CR5 + T29/RR33 + T30/CR24 = 0$

(4) Node 4 : Conducting energy balance on node 4 we have,

$(T3-T4)/CR5 + (T13-T4)/CR6 + (T20-T4)/RR2 + SRAR = 0$

$\Rightarrow T3/CR5 - T4(1/CR5 + 1/CR6 + 1/RR2) + T13/CR6 + T20/RR2 = -SRAR$

where SRAR = solar radiation absorbed by the reflector.

(5) Node 5 : Conducting energy balance on node 5 we have,

$(T6-T5)/CR11 + (T13-T5)/CR10 + (T22-T5)/RR8 + SRAEW = 0$

where SRAEW = solar radiation absorbed by the end walls.

$-T5(1/CR10 + 1/CR11 + 1/RR8) + T6/CR11 + T13/CR10 + T22/RR8 = -SRAEW$

(6) Node 6 : Conducting energy balance on node 6 we have,

$(T5-T6)/CR11 + (T18-T6)/CR12 + (T32-T6)/CR28 = 0$

$\Rightarrow T5/CR11 - T6(1/CR11 + 1/CR12 + 1/CR28) + T18/CR12 + T32/CR28 = 0$

(7) Node 7 : Conducting energy balance on node 7 we have,

$(T8-T7)/CR20 + (T2-T7)/CR4 = 0$

$\Rightarrow T2/CR4 - T7(1/CR4 + 1/CR20) + T8/CR20 = 0$

(8) Node 8 : Conducting energy balance on node 8,

$(T7-T8)/CR20 + (T16-T8)/CR19 + (T26-T8)/RR20 = 0$

$\Rightarrow T7/CR20 - T8(1/CR19 + 1/CR20 + 1/RR20) + T16/CR19 + T26/RR20 = 0$

(9) Node 9 : Conducting energy balance on node 9,

$(T10-T9)/CR8 + (T13-T9)/CR7 + (T21-T9)/RR6 = 0$

$\Rightarrow -T9(1/CR7 + 1/CR8 + 1/RR6) + T10/CR8 +$

$T13/CR7 + T21/RR6 = 0$

(10) Node 10 : Conducting energy balance on node 10,

$(T9-T10)/CR8 + (T_{amb}-T10)/CR9 + (T_{sky}-T10)/RR35 + SRAOG = 0$

$\Rightarrow T9/CR8 - T10(1/CR8 + 1/CR9 + 1/RR35)$

$= - (T_{amb}/CR9 + T_{sky}/RR35 + SRAOG)$

(11) Node 11 : Conducting energy balance on node 11,

$(T12-T11)/CR22 + (T16-T11)/CR21 + (T27-T11)/RR23 = 0$

$\Rightarrow - T11(1/CR21 + 1/CR22 + 1/RR23) + T12/CR22 +$

$T16/CR21 + T27/RR23 = 0$

(12) Node 12 : Conducting energy balance on node 12,

$(T11-T12)/CR22 + (T_{amb}-T12)/CR23 + (T_{sky} + T12)/RR36 = 0$

$\Rightarrow T11/CR22 - T12(1/CR22 + 1/CR23 + 1/RR36)$

$= -(T_{amb}/CR23 + T_{sky}/RR36)$

(13) Node 13 : Conducting energy balance on node 13,

$(T20-T13)/RR3 + (T14-T13)/CR15 + (T23-T13)/RR10 +$

$(T22-T13)/RR7 + (T5-T13)/CR10 + (T21-T13)/RR4 +$

$(T9-T13)/CR7 + (T4-T13)/CR6 = 0$

$\Rightarrow T4/CR6 + T5/CR10 + T9/CR7 - T13(1/CR6 + 1/CR7 + 1/CR10 +$

$1/CR15 + 1/RR3 + 1/RR4 + 1/RR7 + 1/RR10) + T14/CR15 +$

$T20/RR3 + T21/RR4 + T22/RR7 + T23/RR10 = 0$

(14) Node 14 : Conducting energy balance on node 14,

$(T13-T14)/CR15 + (T23-T14)/RR11 + (T15-T14)/CR16 + SRAIG = 0$

$\Rightarrow T13/CR15 - T14(1/CR15 + 1/CR16 + 1/RR11) + T15/CR16 +$

$T23/RR11 = -SRAIG.$

(15) Node 15 : Conducting energy balance on node 15,

$(T14-T15)/CR16 + (T24-T15)/RR16 + (T16-T15)/CR17 = 0$

$\Rightarrow T14/CR16 - T15(1/CR16 + 1/CR17 + 1/RR16) +$

$T16/CR17 + T24/RR16 = 0$

(16) Node 16 : Conducting energy balance on node 16,

$(T26-T16)/RR21 + (T24-T16)/RR17 + (T15-T16)/CR17 +$

$(T27-T16)/RR22 + (T11-T16)/CR21 + (T25-T16)/RR18 +$

$(T17-T16)/CR18 + (T8-T16)/CR9 +$

$(T33-T16)/RR40 + (T31-T16)/CR26 = 0$

$\Rightarrow T8/CR19 + T11/CR21 + T15/CR17 - T16(1/CR17 + 1/CR18 +$

$1/CR19 + 1/CR21 + 1/CR26 + 1/RR17 + 1/RR18 + 1/RR21 + 1/RR22$

$+ 1/RR40) + T17/CR18 + T24/RR17 + T25/RR18 + T26/RR21 +$

$T27/RR22 + T31/CR26 + T33/RR40 = 0$

(17) Node 17 : Conducting energy balance on node 17,

$(T16-T17)/CR18 + (T25-T17)/RR19 + SRAAP = 0$

$\Rightarrow T16/CR18 - T17(1/CR18 + 1/RR19) + T25/RR19 = -SRAAP$

where SRAAP = solar radiation absorbed by the absorber plate.

(18 Node 18 : Conducting energy balance on node 18 we have,

(T6-T18)/CR12 + (T19-T18)/CR13 = 0

$\Rightarrow$ T6/CR12 - T18(1/CR12 + 1/CR13) + T19/CR13 = 0

(19) Node 19 : Conducting energy balance on node 19,

(T18-T19)/CR13 + (T_{amb}-T19)/CR14 + (T_{amb}-T19)/RR43 = 0

$\Rightarrow$ T18/CR13 - T19(1/CR13 + 1/CR14 + 1/RR43)

= - T_{amb}(1/CR14 + 1/RR43)

(20) Node 20 : Conducting energy balance on node 20,

(T4-T20)/RR2 + (T23-T20)/RR15 + (T13-T20)/RR3 +

(T22-T20)/RR9 + (T21-T20)/RR5 + (T25-T20)/RR44 = 0

$\Rightarrow$ T4/RR2 + T13/RR3 - T20(1/RR2 + 1/RR3 + 1/RR5 + 1/RR9 +

1/RR15 + 1/RR44) + T21/RR5 + T22/RR9 +

T23/RR15 + T25/RR44 = 0

(21) Node 21 : Conducting energy balance on node 21,

(T20-T21)/RR5 + (T13-T21)/RR4 + (T22-T21)/RR13 +

(T23-T21)/RR14 + (T9-T21)/RR6 + (T25-T21)/RR45 = 0

$\Rightarrow$ T9/RR6 + T13/RR4 + T20/RR5 - T21(1/RR4 + 1/RR5 + 1/RR6 +

1/RR13 + 1/RR14 + 1/RR45) + T22/RR13 +

T23/RR14 + T25/RR45 = 0

(22) Node 22 : Conducting energy balance on node 22,

(T13-T22)/RR7 + (T20-T22)/RR9 + (T23-T22)/RR12 +

(T5-T22)/RR8 + (T21-T22)/RR13 + (T25-T22)/RR46 = 0

$\Rightarrow$ T5/RR8 + T13/RR7 + T20/RR9 + T21/RR13 - T22 (1/RR7 +

1/RR8 + 1/RR9 + 1/RR12 + 1/RR13 + 1/RR46) +

T23/RR12 + T25/RR46 = 0

(23) Node 23 : Conducting energy balance on node 23,

(T20-T23)/RR15 + (T13-T23)/RR10 + (T22-T23)/RR12 +

(T21-T23)/RR14 + (T14-T23)/RR11 = 0

$\Rightarrow$ T13/RR10 + T14/RR11 + T20/RR15 + T21/RR14 + T22/RR12 -

T23(1/RR10 + 1/RR11 + 1/RR12 + 1/RR14 + 1/RR15) = 0

(24) Node 24 : Conducting energy balance on node 24,

(T26-T24)/RR24 + (T16-T24)/RR17 + (T27-T24)/RR25 +

(T25-T24)/RR28 + (T15-T24)/RR16 + (T33-T24)/RR38 = 0

$\Rightarrow$ T15/RR16 + T16/RR17 - T24(1/RR16 + 1/RR17 + 1/RR24 +

1/RR25 + 1/RR28 + 1/RR38) + T25/RR28 +

T26/RR24 + T27/RR25 + T33/RR38 = 0

(25) Node 25 : Conducting energy balance on node 25,

(T26-T25)/RR27 + (T16-T25)/RR18 + (T27-T25)/RR26 +

(T24-T25)/RR28 + (T17-T25)/RR19 + (T20-T25)/RR44 +

(T21-T25)/RR45 + (T22-T25)/RR46 + (T33-T25)/RR42 = 0
⇒ T16/RR18 + T17/RR19 + T20/RR44 + T21/RR45 + T22/RR46 +
T24/RR28 - T25(1/RR18 + 1/RR19 + 1/RR26 +
1/RR27 + 1/RR28 +1/RR42 + 1/RR44 +
1/RR45 + 1/RR46) + T26/RR27 + T27/RR26 + T33/RR42 = 0

(26) Node 26 : Conducting energy balance on node 26,
(T8-T26)/RR20 + (T24-T26)/RR24 + (T27-T26)/RR29 +
(T16-T26)/RR21 + (T25-T26)/RR27 + (T33-T26)/RR39 = 0
⇒ T8/RR20 + T16/RR21 + T24/RR24 + T25/RR27 - T26(1/RR20 +
1/RR21 +
1/RR24 + 1/RR27 + 1/RR29 + 1/RR39) + T27/RR29 + T33/RR39 = 0

(27) Node 27 : Conducting energy balance on node 27,
(T16-T27)/RR22 + (T26-T27)/RR29 + (T24-T27)/RR25 +
(T11-T27)/RR23 + (T25-T27)/RR26 + (T33-T27)/RR41 = 0
⇒ T11/RR23 + T16/RR22 + T24/RR25 + T25/RR26 + T26/RR29 -
T27(1/RR22
+ 1/RR23 + 1/RR25 + 1/RR26 + 1/RR29 + 1/RR41) +T33/RR41 = 0

(28) Node 28 :Conducting energy balance on node 28,
(T2-T28)/RR30 + (T30-T28)/RR31 + (T29-T28)/RR34 = 0
⇒ T2/RR30 - T28(1/RR30 + 1/RR31 + 1/RR34) + T29/RR34 +
T30/RR31 = 0

(29) Node 29 : Conducting energy balance on node 29,
(T28-T29)/RR34 + (T30-T29)/RR32 + (T3-T29)/RR33 = 0
⇒ T3/RR33 + T28/RR34 - T29(1/RR32 + 1/RR33 + 1/RR34) +
T30/RR32 = 0

(30) Node 30 : Conducting energy balance on node 30,
(T2-T30)/CR25 + (T3-T30)/CR24 + (T28-T30)/RR31 +
(T29-T30)/RR32
⇒ T2/CR25 + T3/CR24 + T28/RR31 + T29/RR32 - T30(1/CR24 +
1/CR25 + 1/RR31 + 1/RR32) = 0

(31) Node 31 : Conducting energy balance on node 31,
(T16-T31)/CR26 + (T32-T31)/CR27 + (T33-T31)/RR37 = 0
⇒ T16/CR26 - T31(1/CR26 + 1/CR27 + 1/RR37) + T32/CR27
+T33/RR37 = 0

(32) Node 32 : Conducting energy balance on node 32,
(T31-T32)/CR27 + (T6-T32)/CR28 = 0
⇒ T6/CR28 + T31/CR27 -T32(1/CR27 + 1/CR28) = 0

(33) Node 33 : Conducting energy balance on node 33,
(T24-T33)/RR38 + (T25-T33)/RR42 + (T26-T33)/RR39 +
(T27-T33)/RR41 + (T16-T33)/RR40 + (T31-T33)/RR37 = 0

$\Rightarrow$ T16/RR40 + T24/RR38 + T25/RR42 + T26/RR39 + T27/RR41 + T31/RR37 -

T33(1/RR37 + 1/RR38 + 1/RR39 + 1/RR40 + 1/RR41 + 1/RR42) = 0

A10.3.2 Gauss elimination method

The 33 nodal equations obtained in the previous section can be expressed in the form shown below

a_{11} T1 + a_{12} T2 + ...+ a_{1n} Tn = C_1

a_{21} T1 + a_{22} T2 + ...+ a_{2n} Tn = C_2

a_{31} T1 + a_{32} T2 + ...+ a_{3n} Tn = C_3

.....

.....

a_{n1} T1 + a_{n2} T2 + ...+ a_{nn} Tn = C_n

where n = 33 and a_{ij} (i = 1 to n and j = 1 to n) represents the coefficients of the temperatures; C_i (i = 1 to n) represents the constants; T1 to Tn are nodal temperatures. For example, if we consider the energy balance equation on node 1, we have

a_{11} = (1/RR1 + 1/CR1 + 1/CR2)

a_{12} = 1/CR2

a_{13} = a_{14} = ...= a_{1n} = 0

C1 = - T_{amb}(1/RR1 + 1/CR1)

Using the matrix notation we can represent the set of 33 equations as [A] [T] = [C]

where

$$[A] = \begin{bmatrix} a_{11} + a_{12} + \ldots\ldots\ldots + a_{1n} \\ a_{21} + a_{22} + \ldots\ldots\ldots + a_{2n} \\ a_{31} + a_{32} + \ldots\ldots\ldots + a_{3n} \\ \ldots\ldots\ldots\ldots\ldots\ldots\ldots \\ \ldots\ldots\ldots\ldots\ldots\ldots\ldots \\ a_{n1} + a_{n2} + \ldots\ldots\ldots + a_{nn} \end{bmatrix}_{nxn} \quad [T] = \begin{bmatrix} T1 \\ T2 \\ T3 \\ .. \\ .. \\ Tn \end{bmatrix}_{nx1} \quad [C] = \begin{bmatrix} C1 \\ C2 \\ C3 \\ .. \\ .. \\ Cn \end{bmatrix}_{nx1}$$

In order to find the solution set all the elements of the matrix [A] are converted to zero except the leading diagonal whose elements are made equal to 1. In the process, all the necessary changes are made to [C] also. Finally, [C] represents the various [T] values. Computer programme TPLWR does all the required calculations.

A10.3.3 Computer programme TPLWR

This programme does the long wave analysis of the collector to solve the conduction, convection and radiation network. As the order of the matrix is 33x33 double precision variables are used. The various input and output variables to the programme are given in the listing of the programme attached at the end of this appendix. The input variables include solar radiation absorbed by different parts of the collector, ambient temperature, initial values for 33 temperatures, various dimensions and properties of the collector parts, constants, air properties and various shape factors. All the input data are stored in the data file LONG.DAT so that any modification can be done easily without touching the main programme. Also these input variables are printed along with the output parameters in the results file PLONG1.DAT. The output variables to the programme include the heat transfer coefficients, conduction, convection and radiation resistances, temperatures of different parts of the collector, heat flows through various resistances and heat losses from the collector. The basic flow chart for this computer programme is shown in Fig. 4.21. Different subroutines are written to evaluate various heat transfer coefficients (HTC) and they include (a) HTCOA to evaluate HTC between the outer air and various surfaces in contact with it (b) HTCIA for HTC between the inner air and wider surfaces in contact with it (c) HTCBA to find HTC between the box air and the surfaces in contact with it (d) HTCATM for finding HTC from various collector surfaces to the atmosphere

A10.4 Programme Listing of TPLWR

```
C       **********    COMPUTER PROGRAMME TPLWR    **********
C
C       THIS PROGRAMME " TPLWR.FOR " SOLVES THE LONG WAVE
C       CONDUCTION, CONVECTION AND RADIATION NETWORK
C       TO FIND THE STAGNATION TEMPERATURE OF THE ABSORBER
        PLATE
C
C       THIS PROGRAMME SOLVES THE SET OF SIMULTANIOUS
        EQUATIONS
C       OBTAINED FROM NODAL SOLUTION OF THE NETWORK USING
C       MATRIX ELIMINATION METHOD
C
C       THE INPUT VARIABLES TO THE PROGRAMME ARE --
C       ------------------------------------------
C       (1) SRAAP - SOLAR RADIATION ABSORBED BY THE ABSORBER
C                   PLATE IN WATTS
C       (2) SRAR  - SOLAR RADIATION ABSORBED BY THE
C                   REFLECTOR IN WATTS
C       (3) SRAOG - SOLAR RADIATION ABSORBED BY THE OUTER
C                   GLAZING IN WATTS
C       (4) SRAIG - SOLAR RADIATION ABSORBED BY THE INNER
C                   GLAZING IN WATTS
C       (5) SRAEW - SOLAR RADIATION ABSORBED BY THE END
C                   WALLS IN WATTS
C       (6) TAMB  - AMBIENT TEMPERATURE IN DEG.CEL.
C       (7) TSKY  - SKY EQUIVALENT TEMPERATURE IN DEG.CEL.
C       (8) T(33) - ALL THE 33 INITIAL TEMPERATURE VALUES
C                   IN DEG.CEL.
C       (9) VAIR  - WIND VELOCITY IN M/S
C       (10) VARIOUS DIMENSIONS AND PROPERTIES OF THE
             COLLECTOR SYSTEM COMPONENTS
C       (11) VARIOUS CONSTANTS INCLUDING Z5,Z6,Z7 AS
             EXPLAINED IN THE DATA FILE LONG.DAT
C       (12) AIR PROPERTIES
C       (13) VARIOUS SHAPE FACTORS
C
C       NOTE: ALL THE INPUT DATA IS STORED IN THE DATA FILE
C             LONG.DAT SO THAT ANY MODIFICATION CAN BE DONE
C             EASILY WITHOUT TOUCHING THE MAIN PROGRAMME
C
C       THE OUTPUT VARIABLES ARE --
C       ------------------------
C       (1) VARIOUS HEAT TRANSFER COEFFICIENTS
C       (2) VARIOUS CONDUCTION AND CONVECTION
C           RESISTANCES - CR(28)
C       (3) VARIOUS RADIATION RESISTANCES - RR(46)
C       (4) VARIOUS TEMPERATURES IN THE COLLECTOR
C           SYSTEM - T(33)
C       (5) AMOUNTS OF HEAT FLOWING THROUGH
C           VARIOUS RESISTANCES
C       (6) VARIOUS HEAT LOSSES FROM THE COLLECTOR
C
C       NOTE:ALL THE OUTPUT RESULTS ARE STORED IN THE OUTPUT
C       FILE TPLWR.DAT, WHICH ALSO PRINTS THE INPUT DATA
C
        IMPLICIT INTEGER (I,J,K,N)
        IMPLICIT REAL*8 (A-H,L,M,O-Z)
        DIMENSION T(33),T9(33),A(33,34),B(33,34),CR(28),
```

```
     1  RR(46),QC(28),QR(46)
C
        COMMON T1,T2,ATMPRE,MOLAIR,GASCON,ACCGRA,RADREF,
     1  LIGAB,ANGTLT,RADBOX,VBUILD,VELAIR,HTC
C
C       TO OPEN AND READ DATA FILE - LONG.DAT
C       -------------------------------------
C
        OPEN (UNIT=5,FILE='LONG.DAT',STATUS='OLD')
        READ (5,361)
        READ (5,361)
        READ (5,361)
        READ (5,361)
 361    FORMAT (75X)
        READ (5,367) ITMAX,ANGTLT
 367    FORMAT (20X,I3,37X,G20.8)
 362    FORMAT (20X,G20.8,20X,G20.8)
 363    FORMAT (20X,G20.8)
        READ (5,362) ACCGRA,GASCON
        READ (5,362) ATMPRE,STBZC
        READ (5,367) N,DIFCON
        READ (5,362) VBUILD,Z5
        READ (5,362) Z6,Z7
        READ (5,362) P8,P9
        READ (5,362) P7,Z8
        READ (5,361)
        READ (5,361)
        READ (5,361)
        READ (5,361)
        READ (5,361)
        READ (5,362) VELAIR,MOLAIR
        READ (5,362) EMOAIR,EMIAIR
        READ (5,363) EMBAIR
        READ (5,361)
        READ (5,361)
        READ (5,362) ABOX,TCGIS
        READ (5,362) LGIS,TCBIM
        READ (5,362) RADBOX,LAVBI
        READ (5,362) EMBOS,EMBIS
        READ (5,363) ABOXIS
        READ (5,361)
        READ (5,361)
        READ (5,362) RADREF,LREF
        READ (5,362) AREF,DRREF
        READ (5,362) SRREF,EMREF
        READ (5,362) EMROS,AREFOS
        READ (5,361)
        READ (5,361)
        READ (5,362) AHRAL,AVRAL
        READ (5,362) LAL,TCAL
        READ (5,363) EMAL
        READ (5,361)
        READ (5,361)
        READ (5,362) TCEWIM,LEWI
        READ (5,362) AEW,LIEW
        READ (5,362) TCIEWM,LOEW
        READ (5,362) TCOEWM,AEWEA
        READ (5,362) SREW,DREW
        READ (5,362) EMEW,EMEWOS
        READ (5,361)
```

```
      READ (5,361)
      READ (5,362) AOG,LOG
      READ (5,362) TCOGM,AOGIA
      READ (5,363) EMOG
      READ (5,361)
      READ (5,361)
      READ (5,362) AIG,LIG
      READ (5,362) TCIGM,LIGAB
      READ (5,363) EMIG
      READ (5,361)
      READ (5,361)
      READ (5,362) AAB,EMAB
      READ (5,361)
      READ (5,361)
C
C     TO READ SHAPE FACTORS FOR A COLLECTOR WITHOUT
C     END WALLS
C
      READ (5,361)
      READ (5,362) SFOGR,SFIGOG
      READ (5,362) SIGROG,SFIGR
      READ (5,362) SIGHAL,SIGGIA
      READ (5,362) SABGIA,SABHAL
      READ (5,362) SFABIG,SHAGIA
      IF (Z5.EQ.1.0) GO TO 1002
C
C     TO READ SHAPE FACTORS FOR A COLLECTOR WITH END WALLS
C
      READ (5,361)
      READ (5,362) SFOGR,SFIGOG
      READ (5,362) SIGROG,SFIGR
      READ (5,362) SIGHAL,SIGGIA
      READ (5,362) SABGIA,SABHAL
      READ (5,362) SFABIG,SHAGIA
      IF (Z5.EQ.2.0) GO TO 1019
1002  READ (5,361)
      READ (5,361)
      READ (5,361)
      READ (5,361)
      READ (5,361)
      READ (5,361)
1019  READ (5,362) SFOGER,SFER
      READ (5,362) SFEIG,SFERIG
      READ (5,362) SFEOG,SFEROG
      READ (5,362) SIGEOG,SIGREG
      READ (5,362) SIGERG,SFIGER
      READ (5,362) SIGVAL,SHAVAL
      READ (5,362) SVAGIA,SABVAL
      READ (5,363) SFROBI
      READ (5,361)
      READ (5,361)
      READ (5,362) SRAAP,SRAR
      READ (5,362) SRAOG,SRAIG
      READ (5,363) SRAEW
      READ (5,361)
      READ (5,361)
      READ (5,364) (T(I),I=1,16,1)
364   FORMAT (16G5.1)
      READ (5,364) (T(I),I=17,32,1)
      READ (5,366) T(33),TAMB,TSKY
```

```
 366    FORMAT (3G5.1)
        OPEN (UNIT=6,FILE='PLONG1.DAT',STATUS='NEW')
        OPEN (UNIT=7,FILE='PLONG9.DAT',STATUS='NEW')
C
C       NOTE: PLONG9.DAT IS THE QUICK CHECKING FILE WHICH
C             STORES ONLY THE IMPORTANT DATA LIKE THE
C             ABSORBER PANEL STAGNATION TEMPERATURE
C
C       TO CONVERT THE TEMPERATURES TO ABSOLUTE SCALE
C       -------------------------------------------
C
        DO 678 I=1,33,1
        T(I)=T(I)+273.0
 678    CONTINUE
        TAMB=TAMB+273.0
        TSKY=TSKY+273.0
C
C       TO WRITE THE INPUT DATA IN TO THE OUTPUT DATA
C       FILE PLONG1.DAT
C
        WRITE (6,747)
 747    FORMAT (//,' **** RESULTS OF THE COMPUTER PROGRAMME'
     1  ,'TPLWR ****')
        WRITE (6,748)
 748    FORMAT (' ****************************************'
     1  ,'********')
        WRITE (6,10)
 10     FORMAT (///,' **** VARIOUS CONSTANTS ****')
        WRITE (6,751)
 751    FORMAT (' --------------------------')
        WRITE (6,11) ITMAX
 11     FORMAT (//,' MAXIMUM NUMBER OF ITERATIONS ALLOWED
        =',I3)
        WRITE (6,12)
 12     FORMAT (/,' TILT ANGLE OF THE ABSORBER PLATE TO
        THE')
        WRITE (6,9000) ANGTLT
 9000   FORMAT (' HORIZONTAL IN DEGREES =',G15.6)
        WRITE (6,13) ACCGRA
 13     FORMAT (/,' ACCELERATION DUE TO GRAVITY IN M/SQ.S ='
     1  ,G15.6)
        WRITE (6,14) GASCON
 14     FORMAT (/,' UNIVERSAL GAS CONSTANT'
     1  ,' IN KG.SQ.M/SQ.S.KMOLE.K =',G15.6)
        WRITE (6,15) ATMPRE
 15     FORMAT (/,' ATMOSPHERIC PRESSURE IN KG/M.SQ.S ='
     1  ,G15.6)
        WRITE (6,16) STBZC
 16     FORMAT (/,' STEFAN-BOLTZMAN CONSTANT IN W/SQ.M.QD.K
     1  =',G15.6)
        WRITE (6,17) N
 17     FORMAT (/,' NUMBER OF UNKNOWN TEMPERATURES = ',I2)
        WRITE (6,18) DIFCON
 18     FORMAT (/,' MAXIMUM ALLOWABLE DIFFERENCE FOR '
     1  ,'CONVERGENCE = ',G15.6)
        WRITE (6,19) VBUILD
 19     FORMAT (/,' VOLUME OF THE BUILDING IN CUB.M. =
        ',G15.6)
        WRITE (6,1003)
 1003   FORMAT (/,' COUNTER -- Z5=1.0 MEANS IT IS A
```

```
      COLLECTOR')
      WRITE (6,9001)
9001  FORMAT (' WITHOUT END WALLS AND Z5=2.0 MEANS
      COLLECTOR')
      WRITE (6,9002) Z5
9002  FORMAT (' WITH END WALLS Z5 =',G15.6)
      WRITE (6,1004)
1004  FORMAT (/,' COUNTER -- Z6=3.0 A COLLECTOR WITHOUT
      BACK')
      WRITE (6,9003)
9003  FORMAT (' INSULATION AND Z6=4.0 A COLLECTOR WITH
      BACK')
      WRITE (6,9004) Z6
9004  FORMAT (' INSULATION Z6 =',G15.6)
      WRITE (6,1005)
1005  FORMAT (/,' COUNTER -- Z7=5.0 A COLLECTOR WITH
      SINGLE'
     1 ,' GLAZING AND Z7=6.0')
      WRITE (6,9005) Z7
9005  FORMAT (' IS A COLLECTOR WITH DOUBLE GLAZING Z7
      =',G15.6)
      WRITE (6,1006)
1006  FORMAT (/,' IN RESETTING TEMPERATURES WEIGHT GIVEN')
      WRITE (6,9006) P8
9006  FORMAT (' FOR THE NEW VALUE =',G15.6)
      WRITE (6,1007)
1007  FORMAT (/,' IN RESETTING TEMPERATURES WEIGHT GIVEN')
      WRITE (6,9007) P9
9007  FORMAT (' FOR THE OLD VALUE =',G15.6)
      WRITE (6,1008)
1008  FORMAT (/,' THE HIGHEST VALUE ALLOTTED FOR THE')
      WRITE (6,9008) P7
9008  FORMAT (' UNWANTED RESISTANCES =',G15.6)
      WRITE (6,1009)
1009  FORMAT (/,' THE LOWEST VALUE ALLOTTED FOR THE')
      WRITE (6,9009) Z8
9009  FORMAT (' UNWANTED RESISTANCES =',G15.6)
      WRITE (6,20)
20    FORMAT (//,' **** VARIOUS PROPERTIES OF AIR ****')
      WRITE (6,752)
752   FORMAT (' ----------------------------------')
      WRITE (6,21) VELAIR
21    FORMAT (//,' AVERAGE VELOCITY OF AIR IN M/S
      =',G15.6)
      WRITE (6,22) MOLAIR
22    FORMAT (/,' MOLECULAR WEIGHT OF AIR =',G15.6)
      WRITE (6,23) EMOAIR
23    FORMAT (/,' EMISSIVITY OF OUTER AIR =',G15.6)
      WRITE (6,24) EMIAIR
24    FORMAT (/,' EMISSIVITY OF INNER AIR =',G15.6)
      WRITE (6,25) EMBAIR
25    FORMAT (/,' EMISSIVITY OF BOX AIR =',G15.6)
      WRITE (6,30)
30    FORMAT (//,' ****VARIOUS DETAILS OF THE COLLECTOR
     1 BOX',' ****')
      WRITE (6,753)
753   FORMAT (' ----------------------------------------
      ---')
      WRITE (6,31)
31    FORMAT (//,' OUTSIDE AREA OF THE BOX WITHOUT
```

```
      CONSIDERING')
      WRITE (6,9010) ABOX
9010  FORMAT (' THE END WALLS AND GLAZING , IN SQ.M.
      =',G15.6)
      WRITE (6,32)
32    FORMAT (/,' THERMAL CONDUCTIVITY OF GALVANISED
      IRON')
      WRITE (6,9011) TCGIS
9011  FORMAT (' SHEET IN W./M.K. =',G15.6)
      WRITE (6,33) LGIS
33    FORMAT (/,' THICKNESS OF GALVANISED IRON'
     1 ,' SHEET IN M. = ',G15.6)
      WRITE (6,34)
34    FORMAT (/,' THERMAL CONDUCTIVITY OF THE BACK
      INSULATION')
      WRITE (6,9012) TCBIM
9012  FORMAT (' MATERIAL IN W./M.K. =',G15.6)
      WRITE (6,35)
35    FORMAT (/,' RADIUS OF THE BOX, IF IT WERE ASSUMED TO
      BE')
      WRITE (6,9013) RADBOX
9013  FORMAT (' CYLINDRICAL, IN M =',G15.6)
      WRITE (6,36) LAVBI
36    FORMAT (/,' AVERAGE THICKNESS OF THE BACK
      INSULATION'
     1 ,' IN M =',G15.6)
      WRITE (6,37) EMBOS
37    FORMAT (/,' EMISSIVITY OF THE BOX OUTER SURFACE ='
     1 ,G15.6)
      WRITE (6,38) EMBIS
38    FORMAT (/,' EMISSIVITY OF THE BOX INNER SURFACE ='
     1 ,G15.6)
      WRITE (6,39) ABOXIS
39    FORMAT (/,' AREA OF THE BOX INNER SURFACE IN SQ.M ='
     1 ,G15.6)
      WRITE (6,40)
40    FORMAT (//,' **** VARIOUS DETAILS OF THE REFLECTOR
      ****')
      WRITE (6,754)
754   FORMAT ('      ---------------------------------')
      WRITE (6,41) RADREF
41    FORMAT (//,' INSIDE RADIUS OF THE REFLECTOR IN M ='
     1 ,G15.6)
      WRITE (6,42) LREF
42    FORMAT (/,' LENGTH OF THE REFLECTOR IN M =',G15.6)
      WRITE (6,43) AREF
43    FORMAT (/,' AREA OF REFLECTOR INNER SURFACE IN SQ.M
     1 =',G15.6)
      WRITE (6,44)
44    FORMAT (/,' DIFFUSE REFLECTIVITY OF REFLECTOR
      INNER')
      WRITE (6,9200) DRREF
9200  FORMAT (' SURFACE =',G15.6)
      WRITE (6,45) SRREF
45    FORMAT (/,' SPECULAR REFLECTIVITY OF REFLECTOR
      INNER'
     1 ,' SURFACE =',G15.6)
      WRITE (6,46) EMREF
46    FORMAT (/,' EMISSIVITY OF THE REFLECTOR INNER'
     1 ,'SURFACE =',G15.6)
```

```
      WRITE (6,47) EMROS
47    FORMAT (/,' EMISSIVITY OF THE REFLECTOR OUTER'
     1 ,' SURFACE =',G15.6)
      WRITE (6,48) AREFOS
48    FORMAT (/,' AREA OF THE REFLECTOR OUTER SURFACE'
     1 ,' IN SQ.M =',G15.6)
      WRITE (6,50)
50    FORMAT (//,' **** VARIOUS DETAILS OF THE ALUMINIUM'
     1 ,' STRIP ****')
      WRITE (6,755)
755   FORMAT (' ----------------------------------------'
     1 ,'--------')
      WRITE (6,51)
51    FORMAT (//,' AREA OF THE HORIZONTAL ALUMINIUM
      STRIP')
      WRITE (6,9201) AHRAL
9201  FORMAT (' IN SQ.M =',G15.6)
      WRITE (6,52)
52    FORMAT (/,' AREA OF THE VERTICAL ALUMINMIUM STRIP')
      WRITE (6,9202) AVRAL
9202  FORMAT (' IN SQ.M =',G15.6)
      WRITE (6,53) LAL
53    FORMAT (/,' THICKNESS OF THE ALUMINIUM STRIP IN M ='
     1 ,G15.6)
      WRITE (6,54) TCAL
54    FORMAT (/,' THERMAL CONDUCTIVITY OF ALUMINIUM'
     1 ,' IN W/M.K =',G15.6)
      WRITE (6,55) EMAL
55    FORMAT (/,' EMISSIVITY OF ALUMINIUM STRIP =',G15.6)
      WRITE (6,60)
60    FORMAT (//,' **** VARIOUS DETAILS OF THE END WALL'
     1 ,' ****')
      WRITE (6,756)
756   FORMAT ('      ---------------------------------')
      WRITE (6,61)
61    FORMAT (//,' THERMAL CONDUCTIVITY OF THE END WALL')
      WRITE (6,9014) TCEWIM
9014  FORMAT (' INSULATION MATERIAL IN W/M.K =',G15.6)
      WRITE (6,62) LEWI
62    FORMAT (/,' THICKNESS OF END WALL INSULATION IN M ='
     1 ,G15.6)
      WRITE (6,63) AEW
63    FORMAT (/,' AREA OF END WALL IN SQ.M =',G15.6)
      WRITE (6,64) LIEW
64    FORMAT (/,' THICKNESS OF THE INNER END WALL IN M ='
     1 ,G15.6)
      WRITE (6,65)
65    FORMAT (/,' THERMAL CONDUCTIVITY OF THE INNER END')
      WRITE (6,9015) TCIEWM
9015  FORMAT (' WALL MATERIAL IN W/M.K =',G15.6)
      WRITE (6,66) LOEW
66    FORMAT (/,' THICKNESS OF THE OUTER END WALL IN M ='
     1 ,G15.6)
      WRITE (6,67)
67    FORMAT (/,' THERMAL CONDUCTIVITY OF THE OUTER END')
      WRITE (6,9016) TCOEWM
9016  FORMAT (' WALL MATERIAL IN W/M.K =',G15.6)
      WRITE (6,68)
68    FORMAT (/,' AREA OF THE END WALL EXPOSED TO THE')
      WRITE (6,9017) AEWEA
```

```
9017    FORMAT (' ATMOSPHERE IN SQ.M =',G15.6)
        WRITE (6,69)
69      FORMAT (/,' SPECULAR REFLECTIVITY OF THE INNER')
        WRITE (6,9018) SREW
9018    FORMAT (' SURFACE OF THE INNER END WALL =',G15.6)
        WRITE (6,141)
141     FORMAT (/,' EMISSIVITY OF THE INNER SURFACE OF')
        WRITE (6,9019) EMEW
9019    FORMAT (' THE INNER END WALL =',G15.6)
        WRITE (6,142) DREW
142     FORMAT (/,' DIFFUSE REFLECTIVITY OF THE END WALL ='
     1  ,G15.6)
        WRITE (6,143) EMEWOS
143     FORMAT (/,' EMISSIVITY OF THE END WALL OUTER SURFACE
     1  =',G15.6)
        WRITE (6,70)
70      FORMAT (//,' **** VARIOUS DETAILS OF THE OUTER'
     1  ,' GLAZING ****')
        WRITE (6,757)
757     FORMAT (' ---------------------------------------'
     1  ,'--------')
        WRITE (6,71)
71      FORMAT (//,' AREA OF THE OUTER GLAZING IN CONTACT')
        WRITE (6,2020) AOG
2020    FORMAT (' WITH THE OUTER AIR IN SQ.M =',G15.6)
        WRITE (6,72) LOG
72      FORMAT (/,' THICKNESS OF THE OUTER GLAZING IN M ='
     1  ,G15.6)
        WRITE (6,73)
73      FORMAT (/,' THERMAL CONDUCTIVITY OF THE OUTER')
        WRITE (6,2021) TCOGM
2021    FORMAT (' GLAZING MATERIAL IN W/M.K =',G15.6)
        WRITE (6,74)
74      FORMAT (/,' AREA OF THE OUTER GLAZING IN CONTACT')
        WRITE (6,2022) AOGIA
2022    FORMAT (' WITH THE INNER AIR , IN SQ.M =',G15.6)
        WRITE (6,75) EMOG
75      FORMAT (/,' EMISSIVITY OF THE OUTER GLAZING
        =',G15.6)
        WRITE (6,80)
80      FORMAT (//,' **** VARIOUS DETAILS OF THE INNER'
     1  ,' GLAZING ****')
        WRITE (6,758)
758     FORMAT ('       ----------------------------'
     1  ,'--------')
        WRITE (6,81) AIG
81      FORMAT (//,' AREA OF THE INNER GLAZING IN SQ.M ='
     1  ,G15.6)
        WRITE (6,82) LIG
82      FORMAT (/,' THICKNESS OF THE INNER GLAZING IN M ='
     1  ,G15.6)
        WRITE (6,83)
83      FORMAT (/,' THERMAL CONDUCTIVITY OF THE INNER')
        WRITE (6,2023) TCIGM
2023    FORMAT (' GLAZING MATERIAL IN W/M.K =',G15.6)
        WRITE (6,84)
84      FORMAT (/,' THE GAP BETWEEN THE INNER GLAZING AND')
        WRITE (6,2024) LIGAB
2024    FORMAT (' THE ABSORBER PANEL IN M =',G15.6)
        WRITE (6,85) EMIG
```

```
85      FORMAT (/,' EMISSIVITY OF THE INNER GLAZING
        =',G15.6)
        WRITE (6,90)
90      FORMAT (//,' **** VARIOUS DETAILS OF THE ABSORBER'
     1  ,' PANEL ****')
        WRITE (6,759)
759     FORMAT ('      ------------------------------'
     1  ,'------')
        WRITE (6,91) AAB
91      FORMAT (//,' AREA OF THE ABSORBER PANEL IN SQ.M ='
     1  ,G15.6)
        WRITE (6,92) EMAB
92      FORMAT (/,' EMISSIVITY OF THE ABSORBER PANEL ='
     1  ,G15.6)
        WRITE (6,110)
110     FORMAT (//,' **** VARIOUS SHAPE FACTORS ****')
        WRITE (6,761)
761     FORMAT (' ------------------------------')
        WRITE (6,111) SFOGR
111     FORMAT (//,' SHAPE FACTOR - OUTER GLAZING -'
     1  ,' REFLECTOR =',G15.6)
        WRITE (6,112)
112     FORMAT (/,' SHAPE FACTOR - OUTER GLAZING - END
        WALL')
        WRITE (6,2025) SFOGER
2025    FORMAT (' - REFLECTOR =',G15.6)
        WRITE (6,113) SFER
113     FORMAT (/,' SHAPE FACTOR - END WALL - REFLECTOR ='
     1  ,G15.6)
        WRITE (6,114) SFEIG
114     FORMAT (/,' SHAPE FACTOR - END WALL - INNER GLAZING
     1  =',G15.6)
        WRITE (6,115)
115     FORMAT (/,' SHAPE FACTOR - END WALL - REFLECTOR')
        WRITE (6,2026) SFERIG
2026    FORMAT (' - INNER GLAZING =',G15.6)
        WRITE (6,116) SFEOG
116     FORMAT (/,' SHAPE FACTOR - END WALL - OUTER GLAZING
     1  =',G15.6)
        WRITE (6,117)
117     FORMAT (/,' SHAPE FACTOR - END WALL - REFLECTOR')
        WRITE (6,2027) SFEROG
2027    FORMAT (' - OUTER GLAZING =',G15.6)
        WRITE (6,118) SFIGOG
118     FORMAT (/,' SHAPE FACTOR - INNER GLAZING - OUTER'
     1  ,' GLAZING =',G15.6)
        WRITE (6,119)
119     FORMAT (/,' SHAPE FACTOR - INNER GLAZING')
        WRITE (6,2028) SIGROG
2028    FORMAT (' - REFLECTOR - OUTER GLAZING =',G15.6)
        WRITE (6,120)
120     FORMAT (/,' SHAPE FACTOR - INNER GLAZING')
        WRITE (6,2029) SIGEOG
2029    FORMAT (' - END WALL - OUTER GLAZING =',G15.6)
        WRITE (6,121)
121     FORMAT (/,' SHAPE FACTOR - INNER GLAZING -
        REFLECTOR')
        WRITE (6,2030) SIGREG
2030    FORMAT (' - END WALL - OUTER GLAZING =',G15.6)
        WRITE (6,122)
```

```
122     FORMAT (/,' SHAPE FACTOR - INNER GLAZING - END
        WALL')
        WRITE (6,2031) SIGERG
2031    FORMAT (' - REFLECTOR - OUTER GLAZING =',G15.6)
        WRITE (6,123) SFIGR
123     FORMAT (/,' SHAPE FACTOR - INNER GLAZING - REFLECTOR
     1  =',G15.6)
        WRITE (6,124)
124     FORMAT (/,' SHAPE FACTOR - INNER GLAZING - END
        WALL')
        WRITE (6,2032) SFIGER
2032    FORMAT (' - REFLECTOR =',G15.6)
        WRITE (6,125)
125     FORMAT (/,' SHAPE FACTOR - INNER GLAZING')
        WRITE (6,2033) SIGHAL
2033    FORMAT (' - HORIZONTAL ALUMINIUM STRIP =',G15.6)
        WRITE (6,126)
126     FORMAT (/,' SHAPE FACTOR - INNER GLAZING - OUTER')
        WRITE (6,2034) SIGGIA
2034    FORMAT (' GLAZING IN CONTACT WITH INNER AIR
        =',G15.6)
        WRITE (6,127)
127     FORMAT (/,' SHAPE FACTOR - ABSORBER PANEL - OUTER')
        WRITE (6,2035) SABGIA
2035    FORMAT (' GLAZING IN CONTACT WITH INNER AIR
        =',G15.6)
        WRITE (6,128)
128     FORMAT (/,' SHAPE FACTOE - ABSORBER PANEL')
        WRITE (6,2036) SABHAL
2036    FORMAT (' - HORIZONTAL ALUMINIUM STRIP =',G15.6)
        WRITE (6,129) SFABIG
129     FORMAT (/,' SHAPE FACTOR - ABSORBER PANEL - INNER'
     1  ,' GLAZING =',G15.6)
        WRITE (6,130)
130     FORMAT (/,' SHAPE FACTOR - HORIZONTAL ALUMINIUM
        STRIP')
        WRITE (6,2037) SHAGIA
2037    FORMAT (' - OUTER GLAZING IN CONTACT WITH INNER AIR
     1  =',G15.6)
        WRITE (6,131)
131     FORMAT (/,' SHAPE FACTOR - REFLECTOR OUTER SURFACE')
        WRITE (6,2038) SFROBI
2038    FORMAT (' - BOX INNER SURFACE =',G15.6)
        WRITE (6,132)
132     FORMAT (/,' SHAPE FACTOR - INNER GLAZING -
        VERTICAL')
        WRITE (6,2039) SIGVAL
2039    FORMAT (' ALUMINIUM STRIP =',G15.6)
        WRITE (6,133)
133     FORMAT (/,' SHAPE FACTOR - HORIZONTAL ALUMINIUM
        STRIP')
        WRITE (6,2040) SHAVAL
2040    FORMAT (' - VERTICAL ALUMINIUM STRIP =',G15.6)
        WRITE (6,134)
134     FORMAT (/,' SHAPE FACTOR - VERTICAL ALUMINIUM
        STRIP')
        WRITE (6,2041) SVAGIA
2041    FORMAT (' - OUTER GLAZING IN CONTACT WITH INNER AIR
     1  =',G15.6)
        WRITE (6,135)
```

```
  135    FORMAT (/,' SHAPE FACTOR - ABSORBER PANEL')
         WRITE (6,2042) SABVAL
  2042   FORMAT (' - HORIZONTAL ALUMINIUM STRIP =',G15.6)
         WRITE (6,150)
  150    FORMAT (//,' **** VARIOUS SOLAR INPUTS - IN WATTS'
     1   ,' ****')
         WRITE (6,762)
  762    FORMAT ('      --------------------------------')
         WRITE (6,151) SRAAP
  151    FORMAT (//,' SOLAR RADIATION ABSORBED BY THE
         ABSORBER '
     1   ,'PANEL =',G15.6)
         WRITE (6,152) SRAR
  152    FORMAT (/,' SOLAR RADIATION ABSORBED BY THE
         REFLECTOR '
     1   ,'=',G15.6)
         WRITE (6,153) SRAOG
  153    FORMAT (/,' SOLAR RADIATION ABSORBED BY THE OUTER'
     1   ,' GLAZING =',G15.6)
         WRITE (6,154) SRAIG
  154    FORMAT (/,' SOLAR RADIATION ABSORBED BY THE INNER'
     1   ,' GLAZING =',G15.6)
         WRITE (6,155) SRAEW
  155    FORMAT (/,' SOLAR RADIATION ABSORBED BY THE END'
     1   ,' WALLS =',G15.6)
C
C        TO SET ITERATION COUNTER - ITC
C        ------------------------------
         ITC=0
    699  ITC=ITC+1
         IF (ITC.GT.ITMAX) GO TO 2000
C
C        *****  TO EVALUATE THE CONDUCTION AND CONVECTION
C               RESISTANCES CR(1) TO CR(28)  *****
C               --------------------------
C        TO EVALUATE CR(1)
C        -----------------
         T1=TAMB
         T2=T(1)
         CALL HTCATM
C        HTCBAT = HEAT TRANSFER COEFFICIENT FROM THE BOX TO
C                 THE ATMOSPHERE, WITHOUT CONSIDERING THE
C                 END WALLS AND THE GLAZING, IN W/SQ.M.K
         HTCBAT=HTC
         CR(1)=1.0/(HTCBAT*ABOX)
C        TO EVALUATE CR(2) TO CR(5)
C        --------------------------
         CR(2)=LGIS/(TCGIS*ABOX)
         X=RADBOX/RADREF
         CR(3)=2.0*((DLOG(X))/((22.0/7.0)*TCBIM*LREF))
         CR(4)=LAVBI/(TCBIM*AHRAL)
         X=(LREF+LGIS)/LREF
         CR(5)=2.0*((DLOG(X))/((22.0/7.0)*TCGIS*LREF))
C        TO EVALUATE CR(6)
C        -----------------
         T1=T(4)
         T2=T(13)
         CALL HTCOA
C        HTCROA = HEAT TRANSFER COEFFICIENT BETWEEN THE
C                 REFLECTOR AND THE OUTER AIR , IN W/SQ.M.K
```

```
      HTCROA=HTC
      CR(6)=1.0/(HTCROA*AREF)
C     TO EVALUATE CR(7)
C     -----------------
      T1=T(9)
      T2=T(13)
      CALL HTCOA
C     HTOGOA = HEAT TRANSFER COEFFICIENT BETWEEN THE OUTER
C              GLAZING AND THE OUTER AIR, IN W/SQ.M.K
      HTOGOA=HTC
      CR(7)=1.0/(HTOGOA*AOG)
C     TOEVALUATE CR(8)
C     ----------------
      CR(8)=LOG/(TCOGM*AOG)
C     TO EVALUATE CR(9)
C     -----------------
      T1=TAMB
      T2=T(10)
      CALL HTCATM
C     HTCOGA = HEAT TRANSFER COEFFICIENT BETWEEN THE OUTER
C              GLAZING AND THE ATMOSPHERE IN W/SQ.M.K
      HTCOGA=HTC
      CR(9)=1.0/(HTCOGA*AOG)
C     TO EVALUATE CR(10)
C     ------------------
      T1=T(5)
      T2=T(13)
      CALL HTCOA
C     HTEWOA = HEAT TRANSFER COEFFICIENT BETWEEN THE END
C              WALL AND THE OUTER AIR, IN W/SQ.M.K
      HTEWOA=HTC
      CR(10)=1.0/(HTEWOA*AEW)
C     TO EVALUATE CR(11) TO CR(13)
C     ----------------------------
      CR(11)=LIEW/(TCIEWM*AEW)
      CR(12)=LEWI/(TCEWIM*AEW)
      CR(13)=LOEW/(TCOEWM*AEW)
C     TO EVALUATE CR(14)
C     ------------------
      T1=TAMB
      T2=T(19)
      CALL HTCATM
C     HTCEWA = HEAT TRANSFER COEFFICIENT FROM THE END WALL
C              TO THE ATMOSPHERE, IN W/SQ.M.K
      HTCEWA=HTC
      CR(14)=1.0/(HTCEWA*AEWEA)
C     TO EVALUATE CR(15)
C     ------------------
      T1=T(14)
      T2=T(13)
      CALL HTCOA
C     HTIGOA = HEAT TRANSFER COEFFICIENT BETWEEN THE INNER
C              GLAZING AND THE OUTER AIR, IN W/SQ.M.K
      HTIGOA=HTC
      CR(15)=1.0/(HTIGOA*AIG)
C     TO EVALUATE CR(16)
C     ------------------
      CR(16)=LIG/(TCIGM*AIG)
C
C     TO EVALUATE CR(17)
```

```
C       ------------------
        T1=T(16)
        T2=T(15)
        CALL HTCIA
C       HTIAIG = HEAT TRANSFER BETWEEN THE INNER AIR AND THE
C                INNER GLAZING IN W/SQ.M.K
        HTIAIG=HTC
        CR(17)=1.0/(HTIAIG*AIG)
C       TO EVALUATE CR(18)
C       ------------------
        T1=T(16)
        T2=T(17)
        CALL HTCIA
C       HTIAAB = HEAT TRANSFER COEFFICIENT BETWEEN THE INNER
C                AIR AND THE ABSORBER PANEL, IN W/SQ.M.K
        HTIAAB=HTC
        CR(18)=1.0/(HTIAAB*AAB)
C       TO EVALUATE CR(19)
C       ------------------
        T1=T(16)
        T2=T(8)
        CALL HTCIA
C       HTIAHA = HEAT TRANSFER COEFFICIENT BETWEEN THE INNER
C                AIR AND THEHORIZONTAL ALUMINIUM STRIP,
C                IN W/SQ.M.K
        HTIAHA=HTC
        CR(19)=1.0/(HTIAHA*AHRAL)
C       TO EVALUATE CR(20)
C       ------------------
        CR(20)=LAL/(TCAL*AHRAL)
C       TO EVALUATE CR(21)
C       ------------------
        T1=T(16)
        T2=T(11)
        CALL HTCIA
C       HTIAOG = HEAT TRANSFER COEFFICIENT BETWEEN THE INNER
C                AIR AND THE OUTER GLAZING, IN W/SQ.M.K
        HTIAOG=HTC
        CR(21)=1.0/(HTIAOG*AOGIA)
C       TO EVALUATE CR(22)
C       ------------------
        CR(22)=LOG/(TCOGM*AOGIA)
C       TO EVALUATE CR(23)
C       ------------------
        T1=TAMB
        T2=T(12)
        CALL HTCATM
C       HTAOGI = HEAT TRANSFER COEFFICIENT BETWEEN THE
C                ATMOSPHERE AND THE OUTER GLAZING IN
C                CONTACT WITH THE INNER AIR, IN W/SQ.M.K
        HTAOGI=HTC
        CR(23)=1.0/(HTAOGI*AOGIA)
C       TO EVALUATE CR(24)
C       ------------------
        T1=T(30)
        T2=T(7)*0.075+T(3)*0.925
        CALL HTCBA
C       HTCBAR = HEAT TRANSFER COEFFICIENT BETWEEN THE BOX
C                AIR AND THE REFLECTOR , IN W/SQ.M.K
        HTCBAR=HTC
```

```
      X=RADBOX/RADREF
      CR(24)=(2.0*DLOG(X))/((RADBOX-RADREF)*(22.0/7.0)*
     1  LREF*HTCBAR)
C     TO EVALUATE CR(25)
C     ------------------
      T1=T(30)
      T2=T(2)
      CALL HTCBA
C     HTCBAB = HEAT TRANSFER COEFFICIENT BETWEEN THE BOX
C              AIR AND THE OUTER BOX, IN W/SQ.M.K
      HTCBAB=HTC
      X=RADBOX/RADREF
      CR(25)=(2.0*DLOG(X))/((RADBOX-RADREF)*(22.0/7.0)*
     1  LREF*HTCBAB)
C     TO EVALUATE CR(26)
C     ------------------
      T1=T(16)
      T2=T(31)
      CALL HTCIA
C     HTIAVA = HEAT TRANSFER COEFFICIENT BETWEEN THE
C              INNER AIR AND THE VERTICAL ALUMINIUM
C              STRIP, IN W/SQ.M.K
      HTIAVA=HTC
      CR(26)=1.0/(HTIAVA*AVRAL)
C     TO EVALUATE CR(27) AND CR(28)
C     -----------------------------
      CR(27)=LAL/(TCAL*AVRAL)
      CR(28)=(LIEW-LAL)/(TCIEWM*AVRAL)
C     TO EVALUATE RADIATION RESISTANCES RR(1) TO RR(46)
C     -------------------------------------------------
      RR(1)=1.0/(EMBOS*ABOX*STBZC*(T(1)+TAMB)*(T(1)**2+
     1  TAMB**2))
      RR(2)=DRREF/(STBZC*EMREF*AREF*(1.0-
      SRREF)*(T(4)+T(20))*
     1  (T(4)**2+T(20)**2))
      RR(3)=1.0/(STBZC*AREF*EMOAIR*(1.0-
      SRREF)*(T(20)+T(13))*
     1  (T(20)**2+T(13)**2))
      RR(4)=1.0/(STBZC*EMOAIR*AOG*(T(13)+T(21))*(T(13)**2+
     1  T(21)**2))
      RR(5)=1.0/(STBZC*AOG*(1.0-SRREF)*(1.0-
      EMOAIR)*(SFOGR+
     1  SREW*SFOGER)*(T(20)+T(21))*(T(20)**2+T(21)**2))
      RR(6)=(1.0-EMOG)/(STBZC*EMOG*AOG*(T(9)+T(21))*
     1  (T(9)**2+T(21)**2))
      RR(7)=1.0/(STBZC*AEW*EMOAIR*(1.0-
      SREW)*(T(22)+T(13))*
     1  (T(22)**2+T(13)**2))
      RR(8)=DREW/(STBZC*AEW*EMEW*(1.0-SREW)*(T(5)+T(22))*
     1  (T(5)**2+T(22)**2))
      RR(9)=1.0/(STBZC*AEW*SFER*(1.0-SREW)*(1.0-SRREF)*
     1  (1.0-EMOAIR)*(T(22)+T(20))*(T(22)**2+T(20)**2))
      RR(10)=1.0/(STBZC*EMOAIR*AIG*(T(13)+T(23))*(T(13)**
     1  2+T(23)**2))
      RR(11)=(1.0-EMIG)/(STBZC*EMIG*AIG*(T(14)+T(23))*
     1  (T(14)**2+T(23)**2))
      RR(12)=1.0/(STBZC*AEW*(1.0-SREW)*(1.0-
      EMOAIR)*(SFEIG+
     1  SRREF*SFERIG)*(T(22)+T(23))*(T(22)**2+T(23)**2))
      RR(13)=1.0/(STBZC*AEW*(1.0-SREW)*(1.0-
```

```
     EMOAIR)*(SFEOG+
    1  SRREF*SFEROG)*(T(21)+T(22))*(T(21)**2+T(22)**2))
       RR(14)=1.0/(STBZC*AIG*(SFIGOG+SRREF*
    1  SIGROG+SREW*SIGEOG+SREW*
    1  SRREF*SIGREG+SREW*SRREF*SIGERG)*
    1  (1.0-EMOAIR)*(T(21)+T(23))*
    1  (T(21)**2+T(23)**2))
       RR(15)=1.0/(STBZC*AIG*(1.0-SRREF)*
    1  (1.0-EMOAIR)*(SFIGR+SREW*
    1  SFIGER)*(T(20)+T(23))*(T(20)**2+T(23)**2))
       RR(16)=(1.0-EMIG)/(STBZC*EMIG*AIG*(T(15)+T(24))*
    1  (T(15)**2+T(24)**2))
       RR(17)=1.0/(STBZC*EMIAIR*AIG*(T(16)+T(24))*
    1  (T(16)**2+T(24)**2))
       RR(18)=1.0/(STBZC*EMIAIR*AAB*(T(16)+T(25))*
    1  (T(16)**2+T(24)**2))
       RR(19)=(1.0-EMAB)/(STBZC*AAB*EMAB*(T(17)+T(25))*
    1  (T(17)**2+T(25)**2))
       RR(20)=(1.0-EMAL)/(STBZC*AHRAL*(T(8)+T(26))*
    1  (T(8)**2+T(26)**2))
       RR(21)=1.0/(STBZC*EMIAIR*AHRAL*(T(16)+T(26))*
    1  (T(16)**2+T(26)**2))
       RR(22)=1.0/(STBZC*EMIAIR*AOGIA*(T(16)+T(27))*
    1  (T(16)**2+T(27)**2))
       RR(23)=(1.0-EMOG)/(STBZC*EMOG*AOGIA*(T(11)+T(27))*
    1  (T(11)**2+T(27)**2))
       RR(24)=1.0/(STBZC*AIG*SIGHAL*(1.0-EMIAIR)*
    1  (T(26)+T(24))*
    1  (T(26)**2+T(24)**2))
       RR(25)=1.0/(STBZC*AIG*SIGGIA*(1.0-EMIAIR)*
    1  (T(24)+T(27))*
    1  (T(24)**2+T(27)**2))
       RR(26)=1.0/(STBZC*AAB*SABGIA*(1.0-EMIAIR)*
    1  (T(25)+T(27))*
    1  (T(25)**2+T(27)**2))
       RR(27)=1.0/(STBZC*AAB*SABHAL*(1.0-EMIAIR)*
    1  (T(25)+T(26))*
    1  (T(25)**2+T(26)**2))
       RR(28)=1.0/(STBZC*AAB*SFABIG*(1.0-EMIAIR)*
    1  (T(24)+T(25))*
    1  (T(24)**2+T(25)**2))
       RR(29)=1.0/(STBZC*AHRAL*SHAGIA*(1.0-EMIAIR)*
    1  (T(26)+T(27))*
    1  (T(26)**2+T(27)**2))
       RR(30)=(1.0-EMBIS)/(STBZC*EMBIS*ABOXIS*(T(28)+T(2))*
    1  (T(28)**2+T(2)**2))
       RR(31)=1.0/(STBZC*ABOXIS*EMBAIR*(T(32)+T(30))*
    1  (T(32)**2+T(30)**2))
       RR(32)=1.0/(STBZC*AREFOS*EMBAIR*(T(30)+T(29))*
    1  (T(30)**2+T(29)**2))
       T3=T(7)*0.075+T(3)*0.925
       RR(33)=(1.0-EMROS)/(STBZC*EMROS*AREFOS*(T(29)+T3)*
    1  (T(29)**2+T3**2))
       RR(34)=1.0/(STBZC*AREFOS*SFROBI*
    1  (1.0-EMBAIR)*(T(28)+T(29))*
    1  (T(28)**2+T(29)**2))
       RR(35)=1.0/(STBZC*EMOG*AOG*(T(10)+TSKY)*(T(10)**
    1  2+TSKY**2))
       RR(36)=1.0/(STBZC*EMOG*AOGIA*(T(12)+TSKY)*
    1  (T(12)**2+TSKY**2))
```

```
      RR(37)=(1.0-EMAL)/(STBZC*EMAL*AVRAL*(T(31)+T(33))*
     1  (T(31)**2+T(33)**2))
      RR(38)=1.0/(STBZC*AIG*SIGVAL*(1.0-EMIAIR)*
     1  (T(24)+T(33))*
     1  (T(24)**2+T(33)**2))
      RR(39)=1.0/(STBZC*AHRAL*SHAVAL*(1.0-EMIAIR)*
     1  (T(26)+T(33))*
     1  (T(26)**2+T(33)**2))
      RR(40)=1.0/(STBZC*EMIAIR*AVRAL*(T(16)+T(33))*
     1  (T(16)**2+T(33)**2))
      RR(41)=1.0/(STBZC*AVRAL*SVAGIA*(1.0-EMIAIR)*
     1  (T(27)+T(33))*
     1  (T(27)**2+T(33)**2))
      RR(42)=1.0/(STBZC*AAB*SABVAL*(1.0-EMIAIR)*
     1  (T(25)+T(33))*
     1  (T(25)**2+T(33)**2))
      RR(43)=1.0/(STBZC*AEWEA*EMEWOS*(T(19)+TAMB)*
     1  (T(19)**2+TAMB**2))
      RR(44)=1.0/(STBZC*AAB*(1.0-SRREF)*(1.0-EMOAIR)*
     1  (SFIGR+SREW*SFIGER)*(T(20)**2+T(25)**2)*
     1  (T(20)+T(25)))
      RR(45)=1.0/(STBZC*AAB*(SFIGOG+SRREF*SIGROG+SREW*
     1  SIGEOG+SREW*
     1  SRREF*SIGREG+SREW*SRREF*SIGERG)*(1.0-EMOAIR)*
     1  (T(21)**2+T(25)**2)*(T(21)+T(25)))
      RR(46)=1.0/(STBZC*AEW*(1.0-SREW)*(1.0-EMOAIR)*
     1  (SFEIG+SRREF*
     1  SFERIG)*(T(22)**2+T(25)**2)*(T(22)+T(25)))
C
C       TO CHOOSE THE OPTION/MODIFICATION WE WOULD LIKE TO
        HAVE
C       ------------------------------------------------
        IF (Z6.EQ.4.0) GO TO 1012
C       FOR A COLLECTOR WITHOUT A BACK INSULATION
C       CR-3 WILL VANISH, THAT
C       MEANS EQUATED TO A VERY HIGH VALUE
C       AND CR-4 IS TO BE MODIFIED
        CR(3)=P7
        CR(4)=1.0/((1.0/(1.0/HTCBAB+1.0/HTCBAR))*AHRAL)
        IF (Z6.EQ.3.0) GO TO 1013
C       FOR A COLLECTOR WITH BACK INSULATION
C       THE FOLLOWING RESISTANCES
C       VANISH, THAT MEANS EQUATED TO A VERY HIGH VALUE
 1012   CR(24)=P7
        CR(25)=P7
        RR(30)=P7
        RR(31)=P7
        RR(32)=P7
        RR(33)=P7
        RR(34)=P7
 1013   IF (Z7.EQ.5.0) GO TO 1014
C       FOR A COLLECTOR WITH A DOUBLE GLAZING
C       THE FOLLOWING RESISTANCES
C       VANISH, THAT MEANS EQUATED TO A VERY HIGH VALUE
        RR(44)=P7
        RR(45)=P7
        RR(46)=P7
C       FOR A COLLECTOR WITH SINGLE GLAZING
C       THE FOLLOWING RESISTANCES
C       MUST BE EQUATED TO A VERY SMALL VALUE
```

```
 1014    IF (Z7.EQ.6.0) GO TO 1015
         CR(15)=Z8
         CR(16)=Z8
         CR(17)=Z8
         RR(10)=Z8
         RR(11)=Z8
         RR(12)=Z8
         RR(14)=Z8
         RR(15)=Z8
         RR(16)=Z8
         RR(17)=Z8
         RR(24)=Z8
         RR(25)=Z8
         RR(28)=Z8
         RR(38)=Z8
 1015    IF (Z5.EQ.2.0) GO TO 1011
C        FOR A COLLECTOR WITHOUT THE END WALLS
C        THE FOLLOWING RESISTANCES
C        VANISH, THAT MEANS EQUATED TO A VERY HIGH VALUE
         CR(10)=P7
         CR(11)=P7
         CR(12)=P7
         CR(13)=P7
         CR(14)=P7
         CR(26)=P7
         CR(27)=P7
         CR(28)=P7
C
         RR(7)=P7
         RR(8)=P7
         RR(9)=P7
         RR(12)=P7
         RR(13)=P7
         RR(37)=P7
         RR(38)=P7
         RR(39)=P7
         RR(40)=P7
         RR(41)=P7
         RR(42)=P7
         RR(43)=P7
C
C        TO SETUP NODAL EQUATION MATRIX A(33,34)
C        ---------------------------------------
 1011    N1=N+1
         DO 560 I=1,N,1
         DO 565 J=1,N1,1
         A(I,J)=0.0
         B(I,J)=0.0
  565    CONTINUE
  560    CONTINUE
         A(1,1)=-(1.0/RR(1)+1.0/CR(1)+1.0/CR(2))
         A(1,2)=1.0/CR(2)
         A(1,34)=-TAMB*(1.0/RR(1)+1.0/CR(1))
         A(2,1)=1.0/CR(2)
         A(2,2)=-(1.0/CR(2)+1.0/CR(3)+1.0/CR(4)+1.0/CR(25)+
     1   1.0/RR(30))
         A(2,3)=1.0/CR(3)
         A(2,7)=1.0/CR(4)
         A(2,28)=1.0/RR(30)
         A(2,30)=1.0/CR(25)
```

```
      A(3,2)=1.0/CR(3)
      A(3,3)=-(1.0/CR(3)+1.0/CR(5)+1.0/CR(24)+1.0/RR(33))
      A(3,4)=1.0/CR(5)
      A(3,29)=1.0/RR(33)
      A(3,30)=1.0/CR(24)
      A(4,3)=1.0/CR(5)
      A(4,4)=-(1.0/CR(5)+1.0/CR(6)+1.0/RR(2))
      A(4,13)=1.0/CR(6)
      A(4,20)=1.0/RR(2)
      A(4,34)=-SRAR
      A(5,5)=-(1.0/CR(10)+1.0/CR(11)+1.0/RR(8))
      A(5,6)=1.0/CR(11)
      A(5,13)=1.0/CR(10)
      A(5,22)=1.0/RR(8)
      A(5,34)=-SRAEW
      A(6,5)=1.0/CR(11)
      A(6,6)=-(1.0/CR(11)+1.0/CR(12)+1.0/CR(28))
      A(6,18)=1.0/CR(12)
      A(6,32)=1.0/CR(28)
      A(7,2)=1.0/CR(4)
      A(7,7)=-(1.0/CR(4)+1.0/CR(20))
      A(7,8)=1.0/CR(20)
      A(8,7)=1.0/CR(20)
      A(8,8)=-(1.0/CR(19)+1.0/CR(20)+1.0/RR(20))
      A(8,16)=1.0/CR(19)
      A(8,26)=1.0/RR(20)
      A(9,9)=-(1.0/CR(7)+1.0/CR(8)+1.0/RR(6))
      A(9,10)=1.0/CR(8)
      A(9,13)=1.0/CR(7)
      A(9,21)=1.0/RR(6)
      A(10,9)=1.0/CR(8)
      A(10,10)=-(1.0/CR(8)+1.0/CR(9)+1.0/RR(35))
      A(10,34)=-(TAMB/CR(9)+TSKY/RR(35)+SRAOG)
      A(11,11)=-(1.0/CR(21)+1.0/CR(22)+1.0/RR(23))
      A(11,12)=1.0/CR(22)
      A(11,16)=1.0/CR(21)
      A(11,27)=1.0/RR(23)
      A(12,11)=1.0/CR(22)
      A(12,12)=-(1.0/CR(22)+1.0/CR(23)+1.0/RR(36))
      A(12,34)=-(TAMB/CR(23)+TSKY/RR(36))
      A(13,4)=1.0/CR(6)
      A(13,5)=1.0/CR(10)
      A(13,9)=1.0/CR(7)
      A(13,13)=-(1.0/CR(6)+1.0/CR(7)+1.0/CR(15)+
     1  1.0/RR(3)+1.0/RR(4)+
     1  1.0/RR(7)+1.0/RR(10)+1.0/CR(10))
      A(13,14)=1.0/CR(15)
      A(13,20)=1.0/RR(3)
      A(13,21)=1.0/RR(4)
      A(13,22)=1.0/RR(7)
      A(13,23)=1.0/RR(10)
      A(14,13)=1.0/CR(15)
      A(14,14)=-(1.0/CR(15)+1.0/CR(16)+1.0/RR(11))
      A(14,15)=1.0/CR(16)
      A(14,23)=1.0/RR(11)
      A(14,34)=-SRAIG
      A(15,14)=1.0/CR(16)
      A(15,15)=-(1.0/CR(16)+1.0/CR(17)+1.0/RR(16))
      A(15,16)=1.0/CR(17)
      A(15,24)=1.0/RR(16)
```

```
      A(16,8)=1.0/CR(19)
      A(16,11)=1.0/CR(21)
      A(16,15)=1.0/CR(17)
      A(16,16)=-(1.0/CR(17)+1.0/CR(18)+1.0/CR(19)+
     1  1.0/CR(21)+
     1  1.0/CR(26)+
     1  1.0/RR(17)+1.0/RR(18)+1.0/RR(21)+1.0/RR(22)+
     1  1.0/RR(40))
      A(16,17)=1.0/CR(18)
      A(16,24)=1.0/RR(17)
      A(16,25)=1.0/RR(18)
      A(16,26)=1.0/RR(21)
      A(16,27)=1.0/RR(22)
      A(16,31)=1.0/CR(26)
      A(16,33)=1.0/RR(40)
      A(17,16)=1.0/CR(18)
      A(17,17)=-(1.0/CR(18)+1.0/RR(19))
      A(17,25)=1.0/RR(19)
      A(17,34)=-SRAAP
      A(18,6)=1.0/CR(12)
      A(18,18)=-(1.0/CR(12)+1.0/CR(13))
      A(18,19)=1.0/CR(13)
      A(19,18)=1.0/CR(13)
      A(19,19)=-(1.0/CR(13)+1.0/CR(14)+1.0/RR(43))
      A(19,34)=-TAMB*(1.0/CR(14)+1.0/RR(43))
      A(20,4)=1.0/RR(2)
      A(20,13)=1.0/RR(3)
      A(20,20)=-(1.0/RR(2)+1.0/RR(3)+1.0/RR(5)+1.0/RR(9)+
     1  1.0/RR(15)+
     1  1.0/RR(44))
      A(20,21)=1.0/RR(5)
      A(20,22)=1.0/RR(9)
      A(20,23)=1.0/RR(15)
      A(20,25)=1.0/RR(44)
      A(21,9)=1.0/RR(6)
      A(21,13)=1.0/RR(4)
      A(21,20)=1.0/RR(5)
      A(21,21)=-(1.0/RR(4)+1.0/RR(5)+1.0/RR(6)+
     1  1.0/RR(13)+1.0/RR(14)
     1  +1.0/RR(45))
      A(21,22)=1.0/RR(13)
      A(21,23)=1.0/RR(14)
      A(21,25)=1.0/RR(45)
      A(22,5)=1.0/RR(8)
      A(22,13)=1.0/RR(7)
      A(22,20)=1.0/RR(9)
      A(22,21)=1.0/RR(13)
      A(22,22)=-(1.0/RR(7)+1.0/RR(8)+1.0/RR(9)+
     1  1.0/RR(12)+1.0/RR(13)
     1  +1.0/RR(46))
      A(22,23)=1.0/RR(12)
      A(22,25)=1.0/RR(46)
      A(23,13)=1.0/RR(10)
      A(23,14)=1.0/RR(11)
      A(23,20)=1.0/RR(15)
      A(23,21)=1.0/RR(14)
      A(23,22)=1.0/RR(12)
      A(23,23)=-(1.0/RR(10)+1.0/RR(11)+1.0/RR(12)+
     1  1.0/RR(14)+
     1  1.0/RR(15))
```

```
      A(24,15)=1.0/RR(16)
      A(24,16)=1.0/RR(17)
      A(24,24)=-(1.0/RR(16)+1.0/RR(17)+1.0/RR(24)+
     1  1.0/RR(25)+
     1  1.0/RR(28)+1.0/RR(38))
      A(24,25)=1.0/RR(28)
      A(24,26)=1.0/RR(24)
      A(24,27)=1.0/RR(25)
      A(24,33)=1.0/RR(38)
      A(25,16)=1.0/RR(18)
      A(25,17)=1.0/RR(19)
      A(25,20)=1.0/RR(44)
      A(25,21)=1.0/RR(45)
      A(25,22)=1.0/RR(46)
      A(25,24)=1.0/RR(28)
      A(25,25)=-(1.0/RR(18)+1.0/RR(19)+1.0/RR(26)+
     1  1.0/RR(27)+
     1  1.0/RR(28)+1.0/RR(42)+1.0/RR(44)+1.0/RR(45)+
     1  1.0/RR(46))
      A(25,26)=1.0/RR(27)
      A(25,27)=1.0/RR(26)
      A(25,33)=1.0/RR(42)
      A(26,8)=1.0/RR(20)
      A(26,16)=1.0/RR(21)
      A(26,24)=1.0/RR(24)
      A(26,25)=1.0/RR(27)
      A(26,26)=-(1.0/RR(20)+1.0/RR(21)+1.0/RR(24)+
     1  1.0/RR(27)+
     1  1.0/RR(29)+1.0/RR(39))
      A(26,27)=1.0/RR(29)
      A(26,33)=1.0/RR(39)
      A(27,11)=1.0/RR(23)
      A(27,16)=1.0/RR(22)
      A(27,24)=1.0/RR(25)
      A(27,25)=1.0/RR(26)
      A(27,26)=1.0/RR(29)
      A(27,27)=-(1.0/RR(22)+1.0/RR(23)+1.0/RR(25)+
     1  1.0/RR(26)+
     1  1.0/RR(29)+1.0/RR(41))
      A(27,33)=1.0/RR(41)
      A(28,2)=1.0/RR(30)
      A(28,28)=-(1.0/RR(30)+1.0/RR(31)+1.0/RR(34))
      A(28,29)=1.0/RR(34)
      A(28,30)=1.0/RR(31)
      A(29,3)=1.0/RR(33)
      A(29,28)=1.0/RR(34)
      A(29,29)=-(1.0/RR(32)+1.0/RR(33)+1.0/RR(34))
      A(29,30)=1.0/RR(32)
      A(30,2)=1.0/CR(25)
      A(30,3)=1.0/CR(24)
      A(30,28)=1.0/RR(31)
      A(30,29)=1.0/RR(32)
      A(30,30)=-(1.0/CR(24)+1.0/CR(25)+1.0/RR(31)+
     1  1.0/RR(32))
      A(31,16)=1.0/CR(26)
      A(31,31)=-(1.0/CR(26)+1.0/CR(27)+1.0/RR(37))
      A(31,32)=1.0/CR(27)
      A(31,33)=1.0/RR(37)
      A(32,6)=1.0/CR(28)
      A(32,31)=1.0/CR(27)
```

```
      A(32,32)=-(1.0/CR(27)+1.0/CR(28))
      A(33,16)=1.0/RR(40)
      A(33,24)=1.0/RR(38)
      A(33,25)=1.0/RR(42)
      A(33,26)=1.0/RR(39)
      A(33,27)=1.0/RR(41)
      A(33,31)=1.0/RR(37)
      A(33,33)=-(1.0/RR(37)+1.0/RR(38)+1.0/RR(39)+
     1 1.0/RR(40)+
     1 1.0/RR(41)+1.0/RR(42))
C
C     TO SOLVE THE MATRIX BY ELIMINATION METHOD
C     ****************************************
      I=1
      DO 455 I=1,N,1
      J=1
      DO 465 J=1,N1,1
      B(I,J)=A(I,J)/A(I,I)
  465 CONTINUE
      K=1
      DO 475 K=1,N,1
      IF (K.EQ.I) GO TO 475
      A9=A(K,I)
      J=1
      DO 485 J=1,N1,1
      B(K,J)=A(K,J)-A9*B(I,J)
  485 CONTINUE
  475 CONTINUE
      J=1
      DO 495 J=1,N,1
      K=1
      DO 497 K=1,N1,1
      A(J,K)=B(J,K)
  497 CONTINUE
  495 CONTINUE
  455 CONTINUE
      I=1
      DO 498 I=1,N,1
      T9(I)=A(I,N1)
  498 CONTINUE
C
C     TO TEST FOR CONVERGENCE
C     ***********************
      I=1
      DO 499 I=1,N,1
      T8=DABS(T9(17)-T(17))
      IF (T8.GT.DIFCON) GO TO 593
  499 CONTINUE
      GO TO 596
C
C     TO RESET INITIAL TEMPERATURES
C     _____________________________
  593 I=1
      WRITE (7,999) T(17)-273.0,T9(17)-273.0
  999 FORMAT (/,' T-17 = ',G15.6,' T9-17 = ',G15.6)
      DO 582 I=1,N,1
      T(I)=(P8*T9(I)+P9*T(I))
  582 CONTINUE
      GO TO 699
 2000 ITC=ITC-1
```

```
      WRITE (6,591) ITC
591   FORMAT(//,' THE SYSTEM DID NOT CONVERGE AFTER ',I3,
     1 ' ITERATIONS')
      GO TO 598
596   WRITE (6,597) ITC
597   FORMAT (//,' THE SYSTEM HAS CONVERGED AT ITERATION
     1 =',I3)
598   WRITE (6,701)
701   FORMAT (//,' **** VARIOUS HEAT TRANSFER
      COEFFICIENTS')
      WRITE (6,9100)
9100  FORMAT ('       IN WATTS/SQ.M.DEG.CEL. ****')
      WRITE (6,717)
717   FORMAT ('     ----------------------------------')
      WRITE (6,702)
702   FORMAT (//,' HEAT TRANSFER COEFFICIENT FROM THE')
      WRITE (6,9101)
9101  FORMAT (' OUTER BOX TO THE ATMOSPHERE WITHOUT')
      WRITE (6,9102) HTCBAT
9102  FORMAT (' CONSIDERING THE END WALLS AND THE '
     1 ,'GLAZING =',G15.6)
      WRITE (6,703)
703   FORMAT (/,' HEAT TRANSFER COEFFICIENT FROM THE')
      WRITE (6,9103) HTCROA
9103  FORMAT (' REFLECTOR TO THE OUTER AIR =',G15.6)
      WRITE (6,704)
704   FORMAT (/,' HEAT TRANSFER COEFFICIENT FROM THE')
      WRITE (6,9104) HTOGOA
9104  FORMAT (' OUTER GLAZING TO THE OUTER AIR =',G15.6)
      WRITE (6,705)
705   FORMAT (/,' HEAT TRANSFER COEFFICIENT FROM THE')
      WRITE (6,9105) HTCOGA
9105  FORMAT (' OUTER GLAZING TO THE ATMOSPHERE =',G15.6)
      WRITE (6,706)
706   FORMAT (/,' HEAT TRANSFER COEFFICIENT FROM THE
      INNER')
      WRITE (6,9106) HTEWOA
9106  FORMAT (' END WALL TO THE OUTER AIR =',G15.6)
      WRITE (6,707)
707   FORMAT (/,' HEAT TRANSFER COEFFICIENT FROM THE
      OUTER')
      WRITE (6,9107) HTCEWA
9107  FORMAT (' END WALL TO THE ATMOSPHERE =',G15.6)
      WRITE (6,708)
708   FORMAT (/,' HEAT TRANSFER COEFFICIENT FROM THE
      INNER')
      WRITE (6,9108) HTIGOA
9108  FORMAT (' GLAZING TO THE OUTER AIR =',G15.6)
      WRITE (6,709)
709   FORMAT (/,' HEAT TRANSFER COEFFICIENT FROM THE')
      WRITE (6,9109) HTIAIG
9109  FORMAT (' INNER AIR TO THE INNER GLAZING =',G15.6)
      WRITE (6,710)
710   FORMAT (/,' HEAT TRANSFER COEFFICIENT FROM THE')
      WRITE (6,9110) HTIAAB
9110  FORMAT (' INNER AIR TO THE ABSORBER =',G15.6)
      WRITE (6,711)
711   FORMAT (/,' HEAT TRANSFER COEFFICIENT FROM THE')
      WRITE (6,9111) HTIAHA
9111  FORMAT (' INNER AIR TO THE HORIZONTAL ALUMINIUM'
```

```
     1  ,' STRIP =',G15.6)
        WRITE (6,712)
712     FORMAT (/,' HEAT TRANSFER COEFFICIENT FROM THE')
        WRITE (6,9112) HTIAOG
9112    FORMAT (' INNER AIR TO THE OUTER GLAZING =' ,G15.6)
        WRITE (6,713)
713     FORMAT (/,' HEAT TRANSFER COEFFICIENT FROM THE')
        WRITE (6,9113)
9113    FORMAT (' ATMOSPHERE TO THE OUTER GLAZING')
        WRITE (6,9114) HTAOGI
9114    FORMAT (' IN CONTACT WITH THE INNER AIR =',G15.6)
        WRITE (6,714)
714     FORMAT (/,' HEAT TRANSFER COEFFICIENT FROM THE')
        WRITE (6,9115) HTCBAR
9115    FORMAT (' BOX AIR TO THE REFLECTOR =',G15.6)
        WRITE (6,715)
715     FORMAT (/,' HEAT TRANSFER COEFFICIENT FROM THE')
        WRITE (6,9116) HTCBAB
9116    FORMAT (' BOX AIR TO THE OUTER BOX =',G15.6)
        WRITE (6,716)
716     FORMAT (/,' HEAT TRANSFER COEFFICIENT FROM THE')
        WRITE (6,9117) HTIAVA
9117    FORMAT (' INNER AIR TO THE VERTICAL ALUMINIUM STRIP
     1  =',G15.6)
        WRITE (6,720)
720     FORMAT (//,' **** VARIOUS CONDUCTION AND
        CONVECTION')
        WRITE (6,9118)
9118    FORMAT ('      RESISTANCES IN DEG.CEL./WATT ****')
        WRITE (6,718)
718     FORMAT ('      ----------------------------')
        DO 721 I=1,28,1
        WRITE (6,722) I,CR(I)
722     FORMAT (/,' CONDUCTION-CONVECTION RESISTANCE CR-'
     1  ,I2,' =',G15.6)
721     CONTINUE
        WRITE (6,730)
730     FORMAT (//,' **** VARIOUS RADIATION RESISTANCES'
     1  ,' IN DEG.CEL./WATT ****')
        WRITE (6,719)
719     FORMAT ('      ------------------------------'
     1  ,'------------------')
        DO 731 I=1,46,1
        WRITE (6,732) I,RR(I)
732     FORMAT (/,' RADIATION RESISTANCE RR-',I2,' =',G15.6)
731     CONTINUE
        WRITE (6,740)
740     FORMAT (//,' **** VARIOUS NETWORK TEMPERATURES IN'
     1  ,' DEG.CEL. ****')
        WRITE (6,734)
734     FORMAT ('      --------------------------------'
     1  ,'---------')
        TAMB=TAMB-273.0
        WRITE (6,736) TAMB
736     FORMAT (//,' AMBIENT TEMPERATURE - TAMB = ',G15.6)
        TSKY=TSKY-273.0
        WRITE (6,737) TSKY
737     FORMAT (/,' EQUIVALENT SKY TEMPERATURE - TSKY = '
     1  ,G15.6)
        DO 741 I=1,33,1
```

```
      T9(I)=T9(I)-273.0
      WRITE (6,742)I,T9(I)
 742  FORMAT (/,' NETWORK TEMPERATURE  T-',I2,' = ',G15.6)
 741  CONTINUE
C
C     TO FIND OUT THE AMOUNTS OF HEAT FLOWING THROUGH
C     VARIOS RESISTANCES QC(28), QR(46) IN WATTS
C     ------------------------------------------
C     TO FIND THE AMOUNTS OF HEAT FLOWING THROUGH THE
C     CONDUCTION/CONVECTION RESISTANCES
      QC(1)=DABS(T9(1)-TAMB)/CR(1)
      QC(2)=DABS(T9(2)-T9(1))/CR(2)
      QC(3)=DABS(T9(3)-T9(2))/CR(3)
      QC(4)=DABS(T9(7)-T9(2))/CR(4)
      QC(5)=DABS(T9(4)-T9(3))/CR(5)
      QC(6)=DABS(T9(13)-T9(4))/CR(6)
      QC(7)=DABS(T9(13)-T9(9))/CR(7)
      QC(8)=DABS(T9(9)-T9(10))/CR(8)
      QC(9)=DABS(T9(10)-TAMB)/CR(9)
      QC(10)=DABS(T9(13)-T9(5))/CR(10)
      QC(11)=DABS(T9(5)-T9(6))/CR(11)
      QC(12)=DABS(T9(18)-T9(6))/CR(12)
      QC(13)=DABS(T9(18)-T9(19))/CR(13)
      QC(14)=DABS(T9(19)-TAMB)/CR(14)
      QC(15)=DABS(T9(14)-T9(13))/CR(15)
      QC(16)=DABS(T9(15)-T9(14))/CR(16)
      QC(17)=DABS(T9(16)-T9(15))/CR(17)
      QC(18)=DABS(T9(17)-T9(16))/CR(18)
      QC(19)=DABS(T9(16)-T9(8))/CR(19)
      QC(20)=DABS(T9(8)-T9(7))/CR(20)
      QC(21)=DABS(T9(16)-T9(11))/CR(21)
      QC(22)=DABS(T9(11)-T9(12))/CR(22)
      QC(23)=DABS(T9(12)-TAMB)/CR(23)
      QC(24)=DABS(T9(30)-T9(3))/CR(24)
      QC(25)=DABS(T9(30)-T9(2))/CR(25)
      QC(26)=DABS(T9(31)-T9(16))/CR(26)
      QC(27)=DABS(T9(31)-T9(32))/CR(27)
      QC(28)=DABS(T9(32)-T9(6))/CR(28)
C
C     TO FIND HEAT FLOWING THROUGH RADIATION RESISTANCES
      QR(1)=DABS(T9(1)-TAMB)/RR(1)
      QR(2)=DABS(T9(20)-T9(4))/RR(2)
      QR(3)=DABS(T9(20)-T9(13))/RR(3)
      QR(4)=DABS(T9(21)-T9(13))/RR(4)
      QR(5)=DABS(T9(21)-T9(20))/RR(5)
      QR(6)=DABS(T9(21)-T9(9))/RR(6)
      QR(7)=DABS(T9(22)-T9(13))/RR(7)
      QR(8)=DABS(T9(22)-T9(5))/RR(8)
      QR(9)=DABS(T9(22)-T9(20))/RR(9)
      QR(10)=DABS(T9(23)-T9(13))/RR(10)
      QR(11)=DABS(T9(23)-T9(14))/RR(11)
      QR(12)=DABS(T9(23)-T9(22))/RR(12)
      QR(13)=DABS(T9(22)-T9(21))/RR(13)
      QR(14)=DABS(T9(23)-T9(21))/RR(14)
      QR(15)=DABS(T9(23)-T9(20))/RR(15)
      QR(16)=DABS(T9(24)-T9(15))/RR(16)
      QR(17)=DABS(T9(24)-T9(16))/RR(17)
      QR(18)=DABS(T9(25)-T9(16))/RR(18)
      QR(19)=DABS(T9(25)-T9(17))/RR(19)
      QR(20)=DABS(T9(26)-T9(8))/RR(20)
```

```
      QR(21)=DABS(T9(26)-T9(16))/RR(21)
      QR(22)=DABS(T9(27)-T9(16))/RR(22)
      QR(23)=DABS(T9(27)-T9(11))/RR(23)
      QR(24)=DABS(T9(26)-T9(24))/RR(24)
      QR(25)=DABS(T9(27)-T9(24))/RR(25)
      QR(26)=DABS(T9(27)-T9(25))/RR(26)
      QR(27)=DABS(T9(26)-T9(25))/RR(27)
      QR(28)=DABS(T9(25)-T9(24))/RR(28)
      QR(29)=DABS(T9(27)-T9(26))/RR(29)
      QR(30)=DABS(T9(28)-T9(2))/RR(30)
      QR(31)=DABS(T9(30)-T9(28))/RR(31)
      QR(32)=DABS(T9(30)-T9(29))/RR(32)
      QR(33)=DABS(T9(29)-T9(3))/RR(33)
      QR(34)=DABS(T9(29)-T9(28))/RR(34)
      QR(35)=DABS(T9(10)-TSKY)/RR(35)
      QR(36)=DABS(T9(12)-TSKY)/RR(36)
      QR(37)=DABS(T9(33)-T9(31))/RR(37)
      QR(38)=DABS(T9(33)-T9(24))/RR(38)
      QR(39)=DABS(T9(33)-T9(26))/RR(39)
      QR(40)=DABS(T9(33)-T9(16))/RR(40)
      QR(41)=DABS(T9(33)-T9(27))/RR(41)
      QR(42)=DABS(T9(33)-T9(25))/RR(42)
      QR(43)=DABS(T9(19)-TAMB)/RR(43)
      QR(44)=DABS(T9(25)-T9(20))/RR(44)
      QR(45)=DABS(T9(25)-T9(21))/RR(45)
      QR(46)=DABS(T9(25)-T9(22))/RR(46)
      WRITE (6,9210)
 9210 FORMAT (//,' **** HEAT FLOWS THROUGH THE VARIOUS')
      WRITE (6,9211)
 9211 FORMAT ('     CONDUCTION-CONVECTION RESISTANCES'
     1 ,' IN WATTS ****')
      WRITE (6,9212)
 9212 FORMAT ('     ---------------------------------'
     1 ,'---------')
      DO 9300 I=1,28,1
      WRITE (6,9213) I,I,QC(I)
 9213 FORMAT (/,' HEAT FLOW THROUGH THE RESISTANCE CR-'
     1 ,I2,' IS QC-',I2,' =',G15.6)
 9300 CONTINUE
      WRITE (6,9214)
 9214 FORMAT (//,' **** HEAT FLOWS THROUGH THE VARIOUS')
      WRITE (6,9215)
 9215 FORMAT ('      RADIATION RESISTANCES IN WATTS ****')
      WRITE (6,9216)
 9216 FORMAT ('      ------------------------------')
      DO 9400 I=1,46,1
      WRITE (6,9217) I,I,QR(I)
 9217 FORMAT (/,' HEAT FLOW THROUGH THE RESISTANCE RR-'
     1 ,I2,' IS QR-',I2,' =',G15.6)
 9400 CONTINUE
C
C     TO CALCULATE THE HEAT LOSSES FROM THE COLLECTOR
      HLCG=QC(9)+QC(23)
      HLRG=QR(35)+QR(36)
      HLCB=QC(1)+QC(14)
      HLRB=QR(1)+QR(43)
      HLT=HLCG+HLRG+HLCB+HLRB
      HLCGP=(HLCG/HLT)*100
      HLRGP=(HLRG/HLT)*100
      HLCBP=(HLCB/HLT)*100
```

```
      HLRBP=(HLRB/HLT)*100
      WRITE (6,9301)
 9301 FORMAT (//,' **** HEAT LOSSES FROM THE COLLECTOR'
     1 ,' IN WATTS OR % ****')
      WRITE (6,9302)
 9302 FORMAT ('      ------------------------------'
     1 ,'--------------')
      WRITE (6,9303)
 9303 FORMAT (/,' HEAT LOSS DUE TO CONVECTION FROM THE'
     1 ,' OUTER GLAZING')
      WRITE (6,9304) HLCG
 9304 FORMAT (' IN WATTS =',G15.6)
      WRITE (6,9305) HLCGP
 9305 FORMAT (' IN PERCENTAGE =',G15.6)
      WRITE (6,9306)
 9306 FORMAT (/,' HEAT LOSS DUE TO RADIATION FROM THE'
     1 ,' OUTER GLAZING')
      WRITE (6,9307) HLRG
 9307 FORMAT (' IN WATTS =',G15.6)
      WRITE (6,9308) HLRGP
 9308 FORMAT (' IN PERCENTAGE =',G15.6)
      WRITE (6,9309)
 9309 FORMAT (/,' HEAT LOSS DUE TO CONVECTION FROM THE'
     1 ,' OUTER BOX')
      WRITE (6,9310) HLCB
 9310 FORMAT (' IN WATTS =',G15.6)
      WRITE (6,9311) HLCBP
 9311 FORMAT (' IN PERCENTAGE =',G15.6)
      WRITE (6,9312)
 9312 FORMAT (/,' HEAT LOSS DUE TO RADIATION FROM THE'
     1 ,' OUTER BOX')
      WRITE (6,9313) HLRB
 9313 FORMAT (' IN WATTS =',G15.6)
      WRITE (6,9314) HLRBP
 9314 FORMAT (' IN PERCENTAGE =',G15.6)
      END
      SUBROUTINE HTCOA
C     ****************
      IMPLICIT INTEGER (I,J,K,N)
      IMPLICIT REAL*8 (A-H,L,M,O-Z)
      COMMON T1,T2,ATMPRE,MOLAIR,GASCON,ACCGRA,RADREF,
     1 D3,D4,D5,D6,D7,HTC
C     SUBROUTINE HTCOA CALCULATES THE HEAT TRANSFER
C     COEFFICIENT BETWEEN THE
C     OUTER AIR AND VARIOUS SURFACES IN
C     CONTACT WITH IT FOR GIVEN T1 AND T2
C
C     TO FIND THE AVERAGE TEMPERATURE - TAVG
      TAVG=(T1+T2)/2.0
C
C     TO FIND OUT THE TEMPERATURE DIFFERENCE - TDELTA
      TDELTA=DABS(T1-T2)
C
C     TO FIND OUT THE KINEMATIC VISCOSITY OF AIR IN SQ.M/S
      VISAIR=9.11E-8*TAVG-1.15E-5
C
C     TO FIND OUT THE THERMAL CONDUCTIVITY OF AIR IN W/M.K
      TCAIR=7.8E-5*TAVG+2.88E-3
C
C     TO FIND THE AVERAGE DENSITY OF THE AIR IN KG/CUB.M
```

```
      DENAIR=(ATMPRE*MOLAIR)/(GASCON*TAVG)
C
C     TO CALCULATE THE HEAT CAPACITY OF THE AIR IN J/KG.K
      HCAIR=(0.0004*TAVG*TAVG)-(0.2*TAVG)+1030.0
C
C     TO CALCULATE THE PRANDTL NUMBER - PRANUM
      PRANUM=(HCAIR*VISAIR*DENAIR)/TCAIR
C
C     TO CALCULATE THE COEFFICIENT OF THERMAL
C     EXPANSION COTHEX IN 1/K
      D1=(ATMPRE*MOLAIR)/(GASCON*T1)
      D2=(ATMPRE*MOLAIR)/(GASCON*T2)
      COTHEX=(DABS(D1*D1-D2*D2))/(2.0*TDELTA*D1*D2)
C
C     TO CALCULATE THE GRASHOF NUMBER - GRNUM
      GRNUM=(ACCGRA*COTHEX*RADREF**3*TDELTA)/(VISAIR**2)
C
C     TO CALCULATE THE NUSSELT NUMBER - NUSNUM
      NUSNUM=0.18*(((PRANUM**2*GRNUM)/(0.2+PRANUM))**0.29)
C
C     TO CALCULATE THE HEAT TRANSFER COEFFICIENT IN
      W/SQ.M.K
      HTC=(NUSNUM*TCAIR)/RADREF
      HTC=HTC*2.0
      RETURN
      END
C
      SUBROUTINE HTCIA
C     ****************
      IMPLICIT INTEGER (I,J,K,N)
      IMPLICIT REAL*8 (A-H,L,M,O-Z)
      COMMON T1,T2,ATMPRE,MOLAIR,GASCON,ACCGRA,D3,LIGAB,
     1 ANGTLT,
     1 D4,D5,D6,HTC
C     SUBROUTINE HTCIA CALCULATES THE HEAT
C     TRANSFER COEFFICIENT BETWEEN THE
C     INNER AIR AND VARIOUS SURFACES IN CONTACT WITH IT
C     FOR A GIVEN T1 AND T2
C
C     TO FIND THE AVERAGE TEMPERATURE - TAVG
      TAVG=(T1+T2)/2.0
C
C     TO FIND OUT THE TEMPERATURE DIFFERENCE - TDELTA
      TDELTA=DABS(T1-T2)
C
C     TO FIND OUT THE KINEMATIC VISCOSITY OF AIR IN SQ.M/S
      VISAIR=9.11E-8*TAVG-1.15E-5
C
C     TO FIND OUT THE THERMAL CONDUCTIVITY OF THE AIR
C     IN W/M.K
      TCAIR=7.8E-5*TAVG+2.88E-3
C
C     TO FIND THE AVERAGE DENSITY OF THE AIR IN KG/CUB.M
      DENAIR=(ATMPRE*MOLAIR)/(GASCON*TAVG)
C
C     TO CALCULATE THE HEAT CAPACITY OF THE AIR IN J/KG.K
      HCAIR=(0.0004*TAVG*TAVG)-(0.2*TAVG)+1030.0
C
C     TO CALCULATE THE PRANDTL NUMBER - PRANUM
      PRANUM=(HCAIR*VISAIR*DENAIR)/TCAIR
```

```
C
C       TO CALCULATE THE COEFFICIENT OF THERMAL EXPANSION
C       COTHEX IN 1/K
        D1=(ATMPRE*MOLAIR)/(GASCON*T1)
        D2=(ATMPRE*MOLAIR)/(GASCON*T2)
        COTHEX=(DABS(D1*D1-D2*D2))/(2.0*TDELTA*D1*D2)
C
C       TO CALCULATE THE GRASHOF NUMBER - GRNUM
        GRNUM=(ACCGRA*COTHEX*LIGAB**3*TDELTA)/(VISAIR**2)
C
C       TO CALCULATE THE RAYLEIGH NUMBER - RALNUM
        RALNUM=PRANUM*GRNUM
C
C       TO CALCULATE THE NUSSELT NUMBER - NUSNUM
        Z1=1.0-(1708.0/(RALNUM*DCOSD(ANGTLT)))
        IF (Z1.LT.0.0) Z1=0.0
        Z2=(((RALNUM*DCOSD(ANGTLT))/5830.0)**(1.0/3.0))-1.0
        IF (Z2.LT.0.0) Z2=0.0
        NUSNUM=1.0+(1.44*Z1*(1.0-((((DSIND(1.8*ANGTLT))**
     1  1.6)*1708.0)
     1  /(RALNUM*DCOSD(ANGTLT))))))+Z2
C
C       TO CALCULATE THE HEAT TRANSFER COEFFICIENT IN
        W/SQ.M.K
        HTC=(NUSNUM*TCAIR)/LIGAB
        HTC=HTC*2
        RETURN
        END
C
        SUBROUTINE HTCBA
C       ****************
        IMPLICIT INTEGER (I,J,K,N)
        IMPLICIT REAL*8 (A-H,L,M,O-Z)
        COMMON T1,T2,ATMPRE,MOLAIR,GASCON,ACCGRA,RADREF,
     1  D3,D4,RADBOX,
     1  D5,D6,HTC
C       THE SUBROUTINE HTCBA EVALUATES THE
C       HEAT TRANSFER COEFFICIENTS
C       BETWEEN THE BOX AIR AND THE
C       SURFACES IN CONTACT WITH IT
C
C       TO FIND THE AVERAGE TEMPERATURE - TAVG
        TAVG=(T1+T2)/2.0
C
C       TO FIND OUT THE TEMPERATURE DIFFERENCE - TDELTA
        TDELTA=DABS(T1-T2)
C
C       TO FIND OUT THE KINEMATIC VISCOSITY OF THE AIR
C       IN SQ.M/S
        VISAIR=9.11E-8*TAVG-1.15E-5
C
C       TO FIND OUT THE THERMAL CONDUCTIVITY OF THE AIR
C       IN W/M.K
        TCAIR=7.8E-5*TAVG+2.88E-3
C
C       TO FIND THE AVERAGE DENSITY OF THE AIR IN KG/CUB.M
        DENAIR=(ATMPRE*MOLAIR)/(GASCON*TAVG)
C
C       TO CALCULATE THE HEAT CAPACITY OF THE AIR IN J/KG.K
        HCAIR=(0.0004*TAVG*TAVG)-(0.2*TAVG)+1030.0
```

```
C
C       TO CALCULATE THE PRANDTL NUMBER - PRANUM
        PRANUM=(HCAIR*VISAIR*DENAIR)/TCAIR
C
C       TO CALCULATE THE COEFFICIENT OF THERMAL EXPANSION
C       COTHEX IN 1/K
        D1=(ATMPRE*MOLAIR)/(GASCON*T1)
        D2=(ATMPRE*MOLAIR)/(GASCON*T2)
        COTHEX=(DABS(D1*D1-D2*D2))/(2.0*TDELTA*D1*D2)
C
C       TO CALCULATE THE GRASHOF NUMBER - GRNUM
        GRNUM=(ACCGRA*COTHEX*(RADBOX-RADREF)**3*TDELTA)/
     1  (VISAIR**2)
C
C       TO CALCULATE THE RAYLEIGH NUMBER - RALNUM
        RALNUM=PRANUM*GRNUM
C
C       TO FIND THE CRITICAL RAYLEIGH NUMBER RACNUM
        Z3=((1.0/((2.0*RADBOX)**0.6))+(1.0/((2.0*RADREF)**
     1  0.6)))**5
        X=RADBOX/RADREF
        X1=DLOG(X)
        RACNUM=(((X1)**4)/(((RADBOX-RADREF)**3)*Z3))
     1  *RALNUM
C
C       TO FIND OUT THE EFFECTIVE THERMAL CONDUCTIVITY OF
C       AIR IN W/M.K -TCEFFA
        TCEFFA=0.386*((PRANUM/(0.861+PRANUM))**0.25)*
     1  (RACNUM**0.25)*
     1  TCAIR
C
C       TO CALCULATE THE HEAT TRANSFER COEFFICIENT
C       IN W/M.K - HTC
        HTC=TCEFFA/(RADBOX-RADREF)
        RETURN
        END
C
        SUBROUTINE HTCATM
C       ******************
        IMPLICIT INTEGER (I,J,K,N)
        IMPLICIT REAL*8 (A-H,L,M,O-Z)
        COMMON T1,T2,D3,D4,D5,D6,D7,D8,D9,D10,VBUILD,VELAIR,
     1  HTC
C
C       SUBROUTINE HTCATM CALCULATES HEAT TRANSFER
        COEFFICIENT
C       FROM VARIOUS COLLECTOR SURFACES TO THE ATMOSPHERE
C       FOR A GIVEN T1 AND T2
C
C       TO FIND THE AVERAGE TEMPERATURE - TAVG
        TAVG=(T1+T2)/2.0
C
C       TO FIND OUT THE TEMPERATURE DIFFERENCE - TDELTA
        TDELTA=DABS(T1-T2)
C
C       TO FIND OUT THE KINEMATIC VISCOSITY OF AIR IN SQ.M/S
        VISAIR=9.11E-8*TAVG-1.15E-5
C
C       TO FIND OUT THE THERMAL CONDUCTIVITY OF AIR IN W/M.K
        TCAIR=7.8E-5*TAVG+2.88E-3
```

```
C
C       TO FIND THE CHARACTERISTIC LENGTH IN M - LCHAR
        LCHAR=VBUILD**(1.0/3.0)
C
C       TO CALCULATE THE REYNOLDS NUMBER - REYNUM
        REYNUM=VELAIR*LCHAR/VISAIR
C
C       TO CALCULATE THE NUSSELT NUMBER - NUSNUM
        NUSNUM=0.42*REYNUM**0.6
C
C       TO CALCULATE THE HEAT TRANSFER COEFFICIENT
C       IN W/M.K - HTC
        HTC=(NUSNUM*TCAIR)/LCHAR
        IF (HTC.LT.5.0) HTC=5.0
        RETURN
        END
```

A10.5 Results File TPLWR.DAT

```
**** RESULTS OF THE COMPUTER PROGRAMME TPLWR ****
************************************************
**** VARIOUS CONSTANTS ****
---------------------------
MAXIMUM NUMBER OF ITERATIONS ALLOWED = 10
TILT ANGLE OF THE ABSORBER PLATE TO THE
HORIZONTAL IN DEGREES =    45.0000
ACCELERATION DUE TO GRAVITY IN M/SQ.S =    9.80660
UNIVERSAL GAS CONSTANT IN KG.SQ.M/SQ.S.KMOLE.K =    8314.00
ATMOSPHERIC PRESSURE IN KG/M.SQ.S =    101330.
STEFAN-BOLTZMAN CONSTANT IN W/SQ.M.QD.K =   0.566970E-07
NUMBER OF UNKNOWN TEMPERATURES = 33
MAXIMUM ALLOWABLE DIFFERENCE FOR CONVERGENCE =    0.500000
VOLUME OF THE BUILDING IN CUB.M. =     2400.00
COUNTER -- Z5=1.0 MEANS IT IS A COLLECTOR
           WITHOUT END WALLS AND Z5=2.0 MEANS COLLECTOR
           WITH END WALLS Z5 =    2.00000
COUNTER -- Z6=3.0 A COLLECTOR WITHOUT BACK
           INSULATION AND Z6=4.0 A COLLECTOR WITH BACK
           INSULATION Z6 =    4.00000
COUNTER -- Z7=5.0 A COLLECTOR WITH SINGLE GLAZING AND Z7=6.0
           IS A COLLECTOR WITH DOUBLE GLAZING Z7 = 6.00000
IN RESETTING TEMPERATURES WEIGHT GIVEN
FOR THE NEW VALUE =   0.750000
IN RESETTING TEMPERATURES WEIGHT GIVEN
FOR THE OLD VALUE =   0.250000
THE HIGHEST VALUE ALLOTTED FOR THE
UNWANTED RESISTANCES =    100.000
THE LOWEST VALUE ALLOTTED FOR THE
UNWANTED RESISTANCES =   0.100000E-05

**** VARIOUS PROPERTIES OF AIR ****
-----------------------------------
AVERAGE VELOCITY OF AIR IN M/S =    4.10000
MOLECULAR WEIGHT OF AIR =    28.9600
EMISSIVITY OF OUTER AIR =   0.290000E-01
EMISSIVITY OF INNER AIR =   0.290000E-01
EMISSIVITY OF BOX AIR =   0.290000E-01

****VARIOUS DETAILS OF THE COLLECTOR BOX ****
----------------------------------------------
OUTSIDE AREA OF THE BOX WITHOUT CONSIDERING
THE END WALLS AND GLAZING , IN SQ.M. =   0.957488
THERMAL CONDUCTIVITY OF GALVANISED IRON
SHEET IN W./M.K. =    59.8580
THICKNESS OF GALVANISED IRON SHEET IN M. =    0.100000E-02
THERMAL CONDUCTIVITY OF THE BACK INSULATION
MATERIAL IN W./M.K. =   0.360000E-01
RADIUS OF THE BOX, IF IT WERE ASSUMED TO BE
CYLINDRICAL, IN M =   0.385039
AVERAGE THICKNESS OF THE BACK INSULATION IN M = 0.980392E-01
EMISSIVITY OF THE BOX OUTER SURFACE =   0.280000
EMISSIVITY OF THE BOX INNER SURFACE =   0.170000
AREA OF THE BOX INNER SURFACE IN SQ.M =   0.791728

**** VARIOUS DETAILS OF THE REFLECTOR ****
     --------------------------------
INSIDE RADIUS OF THE REFLECTOR IN M =   0.287000
```

```
LENGTH OF THE REFLECTOR IN M =    0.980000
AREA OF REFLECTOR INNER SURFACE IN SQ.M =    0.408480
DIFFUSE REFLECTIVITY OF REFLECTOR INNER
SURFACE =    0.200000E-01
SPECULAR REFLECTIVITY OF REFLECTOR INNER SURFACE =    0.940
EMISSIVITY OF THE REFLECTOR INNERSURFACE =    0.400000E-01
EMISSIVITY OF THE REFLECTOR OUTER SURFACE =    0.170000
AREA OF THE REFLECTOR OUTER SURFACE IN SQ.M =    0.408480

**** VARIOUS DETAILS OF THE ALUMINIUM STRIP ****
-----------------------------------------------
AREA OF THE HORIZONTAL ALUMINIUM STRIP
IN SQ.M =    0.333200E-01
AREA OF THE VERTICAL ALUMINMIUM STRIP
IN SQ.M =    0.201960E-01
THICKNESS OF THE ALUMINIUM STRIP IN M =    0.100000E-01
THERMAL CONDUCTIVITY OF ALUMINIUM IN W/M.K =     205.870
EMISSIVITY OF ALUMINIUM STRIP =    0.180000

**** VARIOUS DETAILS OF THE END WALL ****
     ----------------------------
THERMAL CONDUCTIVITY OF THE END WALL
INSULATION MATERIAL IN W/M.K =    0.360000E-01
THICKNESS OF END WALL INSULATION IN M =    0.760000E-01
AREA OF END WALL IN SQ.M =    0.109869
THICKNESS OF THE INNER END WALL IN M =    0.180000E-01
THERMAL CONDUCTIVITY OF THE INNER END
WALL MATERIAL IN W/M.K =    0.173000
THICKNESS OF THE OUTER END WALL IN M =    0.180000E-01
THERMAL CONDUCTIVITY OF THE OUTER END
WALL MATERIAL IN W/M.K =    0.173000
AREA OF THE END WALL EXPOSED TO THE
ATMOSPHERE IN SQ.M =    0.232900
SPECULAR REFLECTIVITY OF THE INNER
SURFACE OF THE INNER END WALL =    0.940000
EMISSIVITY OF THE INNER SURFACE OF
THE INNER END WALL =    0.400000E-01
DIFFUSE REFLECTIVITY OF THE END WALL =    0.200000E-01
EMISSIVITY OF THE END WALL OUTER SURFACE =    0.800000

**** VARIOUS DETAILS OF THE OUTER GLAZING ****
----------------------------------------------
AREA OF THE OUTER GLAZING IN CONTACT
WITH THE OUTER AIR IN SQ.M =    0.257740
THICKNESS OF THE OUTER GLAZING IN M =    0.300000E-02
THERMAL CONDUCTIVITY OF THE OUTER
GLAZING MATERIAL IN W/M.K =     1.05000
AREA OF THE OUTER GLAZING IN CONTACT
WITH THE INNER AIR , IN SQ.M =    0.333200E-01
EMISSIVITY OF THE OUTER GLAZING =    0.940000

**** VARIOUS DETAILS OF THE INNER GLAZING ****
     ------------------------------------
AREA OF THE INNER GLAZING IN SQ.M =    0.281260
THICKNESS OF THE INNER GLAZING IN M =    0.300000E-02
THERMAL CONDUCTIVITY OF THE INNER
GLAZING MATERIAL IN W/M.K =     1.05000
THE GAP BETWEEN THE INNER GLAZING AND
THE ABSORBER PANEL IN M =    0.250000E-01
EMISSIVITY OF THE INNER GLAZING =    0.940000
```

```
**** VARIOUS DETAILS OF THE ABSORBER PANEL ****
     -------------------------------------
AREA OF THE ABSORBER PANEL IN SQ.M =    0.281260
EMISSIVITY OF THE ABSORBER PANEL =    0.110000

**** VARIOUS SHAPE FACTORS ****
------------------------------
SHAPE FACTOR - OUTER GLAZING - REFLECTOR =    0.601178
SHAPE FACTOR - OUTER GLAZING - END WALL
- REFLECTOR =    0.779680E-01
SHAPE FACTOR - END WALL - REFLECTOR =    0.420000
SHAPE FACTOR - END WALL - INNER GLAZING =    0.290000
SHAPE FACTOR - END WALL - REFLECTOR
- INNER GLAZING =    0.204797
SHAPE FACTOR - END WALL - OUTER GLAZING =    0.270000
SHAPE FACTOR - END WALL - REFLECTOR
- OUTER GLAZING =    0.187671
SHAPE FACTOR - INNER GLAZING - OUTER GLAZING =    0.260000
SHAPE FACTOR - INNER GLAZING
- REFLECTOR - OUTER GLAZING =    0.325000
SHAPE FACTOR - INNER GLAZING
- END WALL - OUTER GLAZING =    0.333190E-01
SHAPE FACTOR - INNER GLAZING - REFLECTOR
- END WALL - OUTER GLAZING =    0.342220E-01
SHAPE FACTOR - INNER GLAZING - END WALL
- REFLECTOR - OUTER GLAZING =    0.342220E-01
SHAPE FACTOR - INNER GLAZING - REFLECTOR =    0.626716
SHAPE FACTOR - INNER GLAZING - END WALL
- REFLECTOR =    0.799650E-01
SHAPE FACTOR - INNER GLAZING
- HORIZONTAL ALUMINIUM STRIP =    0.409410E-01
SHAPE FACTOR - INNER GLAZING - OUTER
GLAZING IN CONTACT WITH INNER AIR =    0.409410E-01
SHAPE FACTOR - ABSORBER PANEL - OUTER
GLAZING IN CONTACT WITH INNER AIR =    0.409410E-01
SHAPE FACTOE - ABSORBER PANEL
- HORIZONTAL ALUMINIUM STRIP =    0.409410E-01
SHAPE FACTOR - ABSORBER PANEL - INNER GLAZING =    0.900000
SHAPE FACTOR - HORIZONTAL ALUMINIUM STRIP
- OUTER GLAZING IN CONTACT WITH INNER AIR =    0.350000E-01
SHAPE FACTOR - REFLECTOR OUTER SURFACE
- BOX INNER SURFACE =     1.00000
SHAPE FACTOR - INNER GLAZING - VERTICAL
ALUMINIUM STRIP =    0.181180E-01
SHAPE FACTOR - HORIZONTAL ALUMINIUM STRIP
- VERTICAL ALUMINIUM STRIP =    0.250000E-01
SHAPE FACTOR - VERTICAL ALUMINIUM STRIP
- OUTER GLAZING IN CONTACT WITH INNER AIR =    0.426830E-01
SHAPE FACTOR - ABSORBER PANEL
- HORIZONTAL ALUMINIUM STRIP =    0.181180E-01

**** VARIOUS SOLAR INPUTS - IN WATTS ****
     -------------------------------
SOLAR RADIATION ABSORBED BY THE ABSORBER PANEL =     159.100
SOLAR RADIATION ABSORBED BY THE REFLECTOR =     40.1800
SOLAR RADIATION ABSORBED BY THE OUTER GLAZING =     9.80000
SOLAR RADIATION ABSORBED BY THE INNER GLAZING =     6.40000
SOLAR RADIATION ABSORBED BY THE END WALLS =    0.000000E+00
```

THE SYSTEM HAS CONVERGED AT ITERATION = 5

**** VARIOUS HEAT TRANSFER COEFFICIENTS
IN WATTS/SQ.M.DEG.CEL. ****

HEAT TRANSFER COEFFICIENT FROM THE
OUTER BOX TO THE ATMOSPHERE WITHOUT
CONSIDERING THE END WALLS AND THE GLAZING = 6.91962
HEAT TRANSFER COEFFICIENT FROM THE
REFLECTOR TO THE OUTER AIR = 3.89166
HEAT TRANSFER COEFFICIENT FROM THE
OUTER GLAZING TO THE OUTER AIR = 5.19712
HEAT TRANSFER COEFFICIENT FROM THE
OUTER GLAZING TO THE ATMOSPHERE = 6.86396
HEAT TRANSFER COEFFICIENT FROM THE INNER
END WALL TO THE OUTER AIR = 2.71949
HEAT TRANSFER COEFFICIENT FROM THE OUTER
END WALL TO THE ATMOSPHERE = 6.92144
HEAT TRANSFER COEFFICIENT FROM THE INNER
GLAZING TO THE OUTER AIR = 4.38486
HEAT TRANSFER COEFFICIENT FROM THE
INNER AIR TO THE INNER GLAZING = 5.68663
HEAT TRANSFER COEFFICIENT FROM THE
INNER AIR TO THE ABSORBER = 6.29027
HEAT TRANSFER COEFFICIENT FROM THE
INNER AIR TO THE HORIZONTAL ALUMINIUM STRIP = 2.88438
HEAT TRANSFER COEFFICIENT FROM THE
INNER AIR TO THE OUTER GLAZING = 5.45066
HEAT TRANSFER COEFFICIENT FROM THE
ATMOSPHERE TO THE OUTER GLAZING
IN CONTACT WITH THE INNER AIR = 6.85058
HEAT TRANSFER COEFFICIENT FROM THE
BOX AIR TO THE REFLECTOR = 1.86593
HEAT TRANSFER COEFFICIENT FROM THE
BOX AIR TO THE OUTER BOX = 1.91179
HEAT TRANSFER COEFFICIENT FROM THE
INNER AIR TO THE VERTICAL ALUMINIUM STRIP = 5.66822

**** VARIOUS CONDUCTION AND CONVECTION
RESISTANCES IN DEG.CEL./WATT ****

CONDUCTION-CONVECTION RESISTANCE CR- 1 = 0.150933
CONDUCTION-CONVECTION RESISTANCE CR- 2 = 0.174480E-04
CONDUCTION-CONVECTION RESISTANCE CR- 3 = 5.30056
CONDUCTION-CONVECTION RESISTANCE CR- 4 = 81.7320
CONDUCTION-CONVECTION RESISTANCE CR- 5 = 0.110639E-04
CONDUCTION-CONVECTION RESISTANCE CR- 6 = 0.629063
CONDUCTION-CONVECTION RESISTANCE CR- 7 = 0.746544
CONDUCTION-CONVECTION RESISTANCE CR- 8 = 0.110854E-01
CONDUCTION-CONVECTION RESISTANCE CR- 9 = 0.565254
CONDUCTION-CONVECTION RESISTANCE CR-10 = 3.34686
CONDUCTION-CONVECTION RESISTANCE CR-11 = 0.947003
CONDUCTION-CONVECTION RESISTANCE CR-12 = 19.2148
CONDUCTION-CONVECTION RESISTANCE CR-13 = 0.947003
CONDUCTION-CONVECTION RESISTANCE CR-14 = 0.620346
CONDUCTION-CONVECTION RESISTANCE CR-15 = 0.810842
CONDUCTION-CONVECTION RESISTANCE CR-16 = 0.101584E-01
CONDUCTION-CONVECTION RESISTANCE CR-17 = 0.625226
CONDUCTION-CONVECTION RESISTANCE CR-18 = 0.565227
CONDUCTION-CONVECTION RESISTANCE CR-19 = 10.4050

CONDUCTION-CONVECTION RESISTANCE CR-20 = 0.145781E-02
CONDUCTION-CONVECTION RESISTANCE CR-21 = 5.50612
CONDUCTION-CONVECTION RESISTANCE CR-22 = 0.857486E-01
CONDUCTION-CONVECTION RESISTANCE CR-23 = 4.38094
CONDUCTION-CONVECTION RESISTANCE CR-24 = 100.000
CONDUCTION-CONVECTION RESISTANCE CR-25 = 100.000
CONDUCTION-CONVECTION RESISTANCE CR-26 = 8.73551
CONDUCTION-CONVECTION RESISTANCE CR-27 = 0.240515E-02
CONDUCTION-CONVECTION RESISTANCE CR-28 = 2.28970

**** VARIOUS RADIATION RESISTANCES IN DEG.CEL./WATT ****

RADIATION RESISTANCE RR- 1 = 0.608395
RADIATION RESISTANCE RR- 2 = 1.53550
RADIATION RESISTANCE RR- 3 = 111.155
RADIATION RESISTANCE RR- 4 = 12.3216
RADIATION RESISTANCE RR- 5 = 8.78006
RADIATION RESISTANCE RR- 6 = 0.262769E-01
RADIATION RESISTANCE RR- 7 = 421.602
RADIATION RESISTANCE RR- 8 = 6.01732
RADIATION RESISTANCE RR- 9 = 483.640
RADIATION RESISTANCE RR-10 = 9.33456
RADIATION RESISTANCE RR-11 = 0.160549E-01
RADIATION RESISTANCE RR-12 = 24.3488
RADIATION RESISTANCE RR-13 = 31.7906
RADIATION RESISTANCE RR-14 = 0.476206
RADIATION RESISTANCE RR-15 = 6.41409
RADIATION RESISTANCE RR-16 = 0.157453E-01
RADIATION RESISTANCE RR-17 = 7.32256
RADIATION RESISTANCE RR-18 = 7.19599
RADIATION RESISTANCE RR-19 = 1.33765
RADIATION RESISTANCE RR-20 = 1.56530
RADIATION RESISTANCE RR-21 = 59.6491
RADIATION RESISTANCE RR-22 = 70.0721
RADIATION RESISTANCE RR-23 = 0.177898
RADIATION RESISTANCE RR-24 = 5.94960
RADIATION RESISTANCE RR-25 = 7.08777
RADIATION RESISTANCE RR-26 = 6.67864
RADIATION RESISTANCE RR-27 = 5.63666
RADIATION RESISTANCE RR-28 = 0.266191
RADIATION RESISTANCE RR-29 = 67.1340
RADIATION RESISTANCE RR-30 = 100.000
RADIATION RESISTANCE RR-31 = 100.000
RADIATION RESISTANCE RR-32 = 100.000
RADIATION RESISTANCE RR-33 = 100.000
RADIATION RESISTANCE RR-34 = 100.000
RADIATION RESISTANCE RR-35 = 0.554581
RADIATION RESISTANCE RR-36 = 3.98642
RADIATION RESISTANCE RR-37 = 15.5877
RADIATION RESISTANCE RR-38 = 13.7658
RADIATION RESISTANCE RR-39 = 81.0501
RADIATION RESISTANCE RR-40 = 100.581
RADIATION RESISTANCE RR-41 = 93.1654
RADIATION RESISTANCE RR-42 = 13.0325
RADIATION RESISTANCE RR-43 = 0.878842
RADIATION RESISTANCE RR-44 = 100.000
RADIATION RESISTANCE RR-45 = 100.000
RADIATION RESISTANCE RR-46 = 100.000

**** VARIOUS NETWORK TEMPERATURES IN DEG.CEL. ****

AMBIENT TEMPERATURE - TAMB = 26.0000
EQUIVALENT SKY TEMPERATURE - TSKY = 23.0000

NETWORK TEMPERATURE	T- 1 =	28.2930
NETWORK TEMPERATURE	T- 2 =	28.2933
NETWORK TEMPERATURE	T- 3 =	117.490
NETWORK TEMPERATURE	T- 4 =	117.490
NETWORK TEMPERATURE	T- 5 =	109.109
NETWORK TEMPERATURE	T- 6 =	110.397
NETWORK TEMPERATURE	T- 7 =	138.842
NETWORK TEMPERATURE	T- 8 =	138.844
NETWORK TEMPERATURE	T- 9 =	71.8907
NETWORK TEMPERATURE	T-10 =	70.1895
NETWORK TEMPERATURE	T-11 =	87.7503
NETWORK TEMPERATURE	T-12 =	85.2515
NETWORK TEMPERATURE	T-13 =	105.014
NETWORK TEMPERATURE	T-14 =	124.312
NETWORK TEMPERATURE	T-15 =	125.550
NETWORK TEMPERATURE	T-16 =	166.471
NETWORK TEMPERATURE	T-17 =	222.065
NETWORK TEMPERATURE	T-18 =	31.3892
NETWORK TEMPERATURE	T-19 =	27.4953
NETWORK TEMPERATURE	T-20 =	113.284
NETWORK TEMPERATURE	T-21 =	74.7575
NETWORK TEMPERATURE	T-22 =	108.283
NETWORK TEMPERATURE	T-23 =	122.635
NETWORK TEMPERATURE	T-24 =	126.438
NETWORK TEMPERATURE	T-25 =	140.813
NETWORK TEMPERATURE	T-26 =	136.805
NETWORK TEMPERATURE	T-27 =	90.3910
NETWORK TEMPERATURE	T-28 =	61.7420
NETWORK TEMPERATURE	T-29 =	84.0412
NETWORK TEMPERATURE	T-30 =	72.8916
NETWORK TEMPERATURE	T-31 =	122.940
NETWORK TEMPERATURE	T-32 =	122.927
NETWORK TEMPERATURE	T-33 =	130.566

**** HEAT FLOWS THROUGH THE VARIOUS
CONDUCTION-CONVECTION RESISTANCES IN WATTS ****

HEAT FLOW THROUGH THE RESISTANCE	CR- 1 IS	QC- 1 =	15.1919
HEAT FLOW THROUGH THE RESISTANCE	CR- 2 IS	QC- 2 =	18.9608
HEAT FLOW THROUGH THE RESISTANCE	CR- 3 IS	QC- 3 =	16.8278
HEAT FLOW THROUGH THE RESISTANCE	CR- 4 IS	QC- 4 =	1.35258
HEAT FLOW THROUGH THE RESISTANCE	CR- 5 IS	QC- 5 =	17.6082
HEAT FLOW THROUGH THE RESISTANCE	CR- 6 IS	QC- 6 =	19.8323
HEAT FLOW THROUGH THE RESISTANCE	CR- 7 IS	QC- 7 =	44.3692
HEAT FLOW THROUGH THE RESISTANCE	CR- 8 IS	QC- 8 =	153.467
HEAT FLOW THROUGH THE RESISTANCE	CR- 9 IS	QC- 9 =	78.1763
HEAT FLOW THROUGH THE RESISTANCE	CR-10 IS	QC-10 =	1.22330
HEAT FLOW THROUGH THE RESISTANCE	CR-11 IS	QC-11 =	1.36055
HEAT FLOW THROUGH THE RESISTANCE	CR-12 IS	QC-12 =	4.11182
HEAT FLOW THROUGH THE RESISTANCE	CR-13 IS	QC-13 =	4.11182
HEAT FLOW THROUGH THE RESISTANCE	CR-14 IS	QC-14 =	2.41040
HEAT FLOW THROUGH THE RESISTANCE	CR-15 IS	QC-15 =	23.7995
HEAT FLOW THROUGH THE RESISTANCE	CR-16 IS	QC-16 =	121.873
HEAT FLOW THROUGH THE RESISTANCE	CR-17 IS	QC-17 =	65.4495
HEAT FLOW THROUGH THE RESISTANCE	CR-18 IS	QC-18 =	98.3573
HEAT FLOW THROUGH THE RESISTANCE	CR-19 IS	QC-19 =	2.65512

HEAT FLOW THROUGH THE RESISTANCE CR-20 IS QC-20 = 1.35258
HEAT FLOW THROUGH THE RESISTANCE CR-21 IS QC-21 = 14.2969
HEAT FLOW THROUGH THE RESISTANCE CR-22 IS QC-22 = 29.1407
HEAT FLOW THROUGH THE RESISTANCE CR-23 IS QC-23 = 13.5248
HEAT FLOW THROUGH THE RESISTANCE CR-24 IS QC-24 = 0.445983
HEAT FLOW THROUGH THE RESISTANCE CR-25 IS QC-25 = 0.445983
HEAT FLOW THROUGH THE RESISTANCE CR-26 IS QC-26 = 4.98317
HEAT FLOW THROUGH THE RESISTANCE CR-27 IS QC-27 = 5.47236
HEAT FLOW THROUGH THE RESISTANCE CR-28 IS QC-28 = 5.47236

**** HEAT FLOWS THROUGH THE VARIOUS
RADIATION RESISTANCES IN WATTS ****

HEAT FLOW THROUGH THE RESISTANCE RR- 1 IS QR- 1 = 3.76888
HEAT FLOW THROUGH THE RESISTANCE RR- 2 IS QR- 2 = 2.73947
HEAT FLOW THROUGH THE RESISTANCE RR- 3 IS QR- 3 = 0.7E-01
HEAT FLOW THROUGH THE RESISTANCE RR- 4 IS QR- 4 = 2.45559
HEAT FLOW THROUGH THE RESISTANCE RR- 5 IS QR- 5 = 4.38791
HEAT FLOW THROUGH THE RESISTANCE RR- 6 IS QR- 6 = 109.097
HEAT FLOW THROUGH THE RESISTANCE RR- 7 IS QR- 7 = 0.8E-02
HEAT FLOW THROUGH THE RESISTANCE RR- 8 IS QR- 8 = 0.13724
HEAT FLOW THROUGH THE RESISTANCE RR- 9 IS QR- 9 = 0.1E-01
HEAT FLOW THROUGH THE RESISTANCE RR-10 IS QR-10 = 1.88764
HEAT FLOW THROUGH THE RESISTANCE RR-11 IS QR-11 = 104.474
HEAT FLOW THROUGH THE RESISTANCE RR-12 IS QR-12 = 0.58943
HEAT FLOW THROUGH THE RESISTANCE RR-13 IS QR-13 = 1.05456
HEAT FLOW THROUGH THE RESISTANCE RR-14 IS QR-14 = 100.539
HEAT FLOW THROUGH THE RESISTANCE RR-15 IS QR-15 = 1.45788
HEAT FLOW THROUGH THE RESISTANCE RR-16 IS QR-16 = 56.4236
HEAT FLOW THROUGH THE RESISTANCE RR-17 IS QR-17 = 5.46699
HEAT FLOW THROUGH THE RESISTANCE RR-18 IS QR-18 = 3.56559
HEAT FLOW THROUGH THE RESISTANCE RR-19 IS QR-19 = 60.7427
HEAT FLOW THROUGH THE RESISTANCE RR-20 IS QR-20 = 1.30254
HEAT FLOW THROUGH THE RESISTANCE RR-21 IS QR-21 = 0.49733
HEAT FLOW THROUGH THE RESISTANCE RR-22 IS QR-22 = 1.08573
HEAT FLOW THROUGH THE RESISTANCE RR-23 IS QR-23 = 14.8439
HEAT FLOW THROUGH THE RESISTANCE RR-24 IS QR-24 = 1.74247
HEAT FLOW THROUGH THE RESISTANCE RR-25 IS QR-25 = 5.08585
HEAT FLOW THROUGH THE RESISTANCE RR-26 IS QR-26 = 7.5497
HEAT FLOW THROUGH THE RESISTANCE RR-27 IS QR-27 = 0.71095
HEAT FLOW THROUGH THE RESISTANCE RR-28 IS QR-28 = 54.000
HEAT FLOW THROUGH THE RESISTANCE RR-29 IS QR-29 = 0.69136
HEAT FLOW THROUGH THE RESISTANCE RR-30 IS QR-30 = 0.33448
HEAT FLOW THROUGH THE RESISTANCE RR-31 IS QR-31 = 0.11149
HEAT FLOW THROUGH THE RESISTANCE RR-32 IS QR-32 = 0.11149
HEAT FLOW THROUGH THE RESISTANCE RR-33 IS QR-33 = 0.33448
HEAT FLOW THROUGH THE RESISTANCE RR-34 IS QR-34 = 0.22299
HEAT FLOW THROUGH THE RESISTANCE RR-35 IS QR-35 = 85.0903
HEAT FLOW THROUGH THE RESISTANCE RR-36 IS QR-36 = 15.6159
HEAT FLOW THROUGH THE RESISTANCE RR-37 IS QR-37 = 0.4891
HEAT FLOW THROUGH THE RESISTANCE RR-38 IS QR-38 = 0.2998
HEAT FLOW THROUGH THE RESISTANCE RR-39 IS QR-39 = 0.8E-01
HEAT FLOW THROUGH THE RESISTANCE RR-40 IS QR-40 = 0.3569
HEAT FLOW THROUGH THE RESISTANCE RR-41 IS QR-41 = 0.431218
HEAT FLOW THROUGH THE RESISTANCE RR-42 IS QR-42 = 0.786272
HEAT FLOW THROUGH THE RESISTANCE RR-43 IS QR-43 = 1.70142
HEAT FLOW THROUGH THE RESISTANCE RR-44 IS QR-44 = 0.275291
HEAT FLOW THROUGH THE RESISTANCE RR-45 IS QR-45 = 0.660553
HEAT FLOW THROUGH THE RESISTANCE RR-46 IS QR-46 = 0.325300

**** HEAT LOSSES FROM THE COLLECTOR IN WATTS OR % ****

HEAT LOSS DUE TO CONVECTION FROM THE OUTER GLAZING
IN WATTS = 91.7012
IN PERCENTAGE = 42.5567
HEAT LOSS DUE TO RADIATION FROM THE OUTER GLAZING
IN WATTS = 100.706
IN PERCENTAGE = 46.7357
HEAT LOSS DUE TO CONVECTION FROM THE OUTER BOX
IN WATTS = 17.6023
IN PERCENTAGE = 8.16890
HEAT LOSS DUE TO RADIATION FROM THE OUTER BOX
IN WATTS = 5.47030
IN PERCENTAGE = 2.53866

A10.6 Input Data File LONG.DAT

```
THE DATA REQUIRED FOR TPLWR.FOR PROGRAMME
****************************************

1.CONSTANTS
-----------
1.1 ITMAX  =    10              1.2 ANGTLT =        45.0
1.3 ACCGRA =    9.8066          1.4 GASCON =        8314.0
1.5 ATMPRE =    1.0133E05       1.6 STBZC  =        5.6697E-8
1.7 N      =    33              1.8 DIFCON =        0.5
1.9 VBUILD =    2400.0          1.10 Z5    =        2.0
1.11 Z6    =    4.0             1.12 Z7    =        6.0
1.13 P8    =    0.75            1.14 P9    =        0.25
1.15 P7    =    100.0           1.16 Z8    =        1.0E-6

(NOTE:- Z5=1.0 WITHOUT END WALLS ; Z5=2.0 WITH END WALLS
Z6=3.0 WITHOUT BACK INSULATION ; Z6=4.0 WITH BACK INSULATION
Z7=5.0 WITH SINGLE GLAZING ; Z7=6.0 WITH DOUBLE GLAZING)

2.AIR PROPERTIES
----------------
2.1 VELAIR =    4.1             2.2 MOLAIR =        28.96
2.3 EMOAIR =    0.029           2.4 EMIAIR =        0.029
2.5 EMBAIR =    0.029

3.BOX DETAILS
-------------
3.1 ABOX   =    0.957488        3.2 TCGIS  =        59.858
3.3 LGIS   =    0.001           3.4 TCBIM  =        0.036
3.5 RADBOX =    0.3850392       3.6 LAVBI  =        0.0980392
3.7 EMBOS  =    0.28            3.8 EMBIS  =        0.17
3.9 ABOXIS =    0.791728

4.REFLECTOR DETAILS
-------------------
4.1 RADREF =    0.287           4.2 LREF   =        0.98
4.3 AREF   =    0.40848         4.4 DRREF  =        0.02
4.5 SRREF  =    0.94            4.6 EMREF  =        0.04
4.7 EMROS  =    0.17            4.8 AREFOS =        0.40848

5.ALUMINIUM STRIP DETAILS
-------------------------
5.1 AHRAL  =    0.03332         5.2 AVRAL  =        0.020196
5.3 LAL    =    0.01            5.4 TCAL   =        205.87
5.5 EMAL   =    0.18

6.END WALL DETAILS
------------------
6.1 TCEWIM =    0.036           6.2 LEWI   =        0.076
6.3 AEW    =    0.109869        6.4 LIEW   =        0.018
6.5 TCIEWM =    0.173           6.6 LOEW   =        0.018
6.7 TCOEWM =    0.173           6.8 AEWEA  =        0.2329
6.9 SREW   =    0.94            6.10 DREW  =        0.02
6.11 EMEW  =    0.04            6.12 EMEWOS=        0.8

7.OUTER GLAZING
---------------
7.1 AOG    =    0.25774         7.2 LOG    =        0.003
7.3 TCOGM  =    1.05            7.4 AOGIA  =        0.03332
```

7.5 EMOG = 0.94

8.INNER GLAZING

8.1 AIG =	0.28126	8.2 LIG =	0.003
8.3 TCIGM =	1.05	8.4 LIGAB =	0.025
8.5 EMIG =	0.94		

9.ABSORBER PANEL

9.1 AAB =	0.28126	9.2 EMAB =	0.11

10.SHAPE FACTORS

DATA FOR COLLECTOR WITHOUT END WALLS:-

10.1 SFOGR =	0.707107	10.2 SFIGOG =	0.292893
10.3 SIGROG =	0.414214	10.4 SFIGR =	0.707107
10.5 SIGHAL =	0.045	10.6 SIGGIA =	0.045
10.7 SABGIA =	0.045	10.8 SABHAL =	0.045
10.9 SFABIG =	0.91	10.10 SHAGIA =	0.04

DATA FOR COLLECTOR WITH END WALLS:-

10.1 SFOGR =	0.601178	10.2 SFIGOG =	0.26
10.3 SIGROG =	0.325	10.4 SFIGR =	0.626716
10.5 SIGHAL =	0.040941	10.6 SIGGIA =	0.040941
10.7 SABGIA =	0.040941	10.8 SABHAL =	0.040941
10.9 SFABIG =	0.9	10.10 SHAGIA =	0.035
10.11 SFOGER =	0.077968	10.12 SFER =	0.42
10.13 SFEIG =	0.29	10.14 SFERIG =	0.204797
10.15 SFEOG =	0.27	10.16 SFEROG =	0.187671
10.17 SIGEOG =	0.033319	10.18 SIGREG =	0.034222
10.19 SIGERG =	0.034222	10.20 SFIGER =	0.079965
10.21 SIGVAL =	0.018118	10.22 SHAVAL =	0.025
10.23 SVAGIA =	0.042683	10.24 SABVAL =	0.018118
10.25 SFROBI =	1.0		

11.SOLAR INPUTS

11.1 SRAAP =	159.1	11.2 SRAR =	40.18
11.3 SRAOG =	9.8	11.4 SRAIG =	6.4
11.5 SRAEW =	0.0		

12.INITIAL VALUES OF VARIOUS TEMPERATURES

15.0 19.0 35.0 75.0 65.0 45.0 85.0 95.0 60.0 40.0 70.0 45.0
70.0 80.0 95.0 135.
175. 30.0 20.0 80.0 65.0 70.0 85.0 100. 170. 105. 65.0 23.0
32.0 25.0 75.0 65.0
70.0 26.0 23.0

APPENDIX A11

COLLECTOR DESIGN PARAMETERS

In this appendix some of the important parameters in the design of the HSA-SCCR collector are described. They include optimum ratio of the absorber width to reflector radius, optimum length of HSA panel, type of end walls, absorber plate material and reflector material.

A11.1 Optimum Ratio of Absorber Width to Reflector Radius

As seen in Appendix A3.4 the energy flux on the absorber plate is very nonuniform and this suggests the possibility, that changes in the relative sizes of the absorber and the reflector might be advantageous. Three specific modifications have been considered (Webb, 1979).

(1) Reflector rim angle of 90° and absorber width of 0.5 R (where R is the radius of the reflector), that is, full SCCR and half HSA.

(2) Reflector rim angle of 90° and absorber width of 0.9 R, that is, full SCCR and 90% HSA.

(3) Reflector rim angle of 60° and absorber width of 0.5 R, that is, half SCCR and half HSA.

The modification incorporating truncated reflector and full absorber plate width is not considered because of the construction problems, which may arise in mounting of the glazing.

The amount of power incident on the absorber of the modified collector is shown in Table A11.1 as a percentage of the amount of power incident on the basic SCCR for different angles of incidence. It is evident from the Table A11.1 that, truncating the absorber by half of its original width seriously affects its performance for all angles of incidence greater than 0° and, during the course of a single day the collector experiences angles of incidence from 0° to 45°.

Modification 2, where the absorber width is decreased by 10% does not suffer such a great loss of performance; however, the savings resulting from such a modification are minimal. Moreover, much of the cost of fabricating the panel lies in the labour

TABLE A11.1 Power Incident on Absorber Panel (with Different Ratios of Panel Width to the Reflector Radius) as Percent of Power Incident on Absorber Panel of Complete Collector (that is, with a Rim Angle of 90° & Absorber Width of R)

Collector Description		Angle of Incidence in Degrees									
Reflector Rim Angle = 90° Absorber Width = R	(a)	0	5	10	15	20	25	30	35	40	45
Reflector Rim Angle = 90° Absorber Width =0.5 R	(b)	100	77	71	67	63	60	55	51	47	42
Reflector Rim Angle = 90° Absorber Width =0.9 R	(c)	100	99	98	97	96	95	93	92	91	89
Reflector Rim Angle = 60° Absorber Width = 0.5 R	(d)	91	65	58	53	50	46	43	43	43	43

Notes: R = Reflector radius

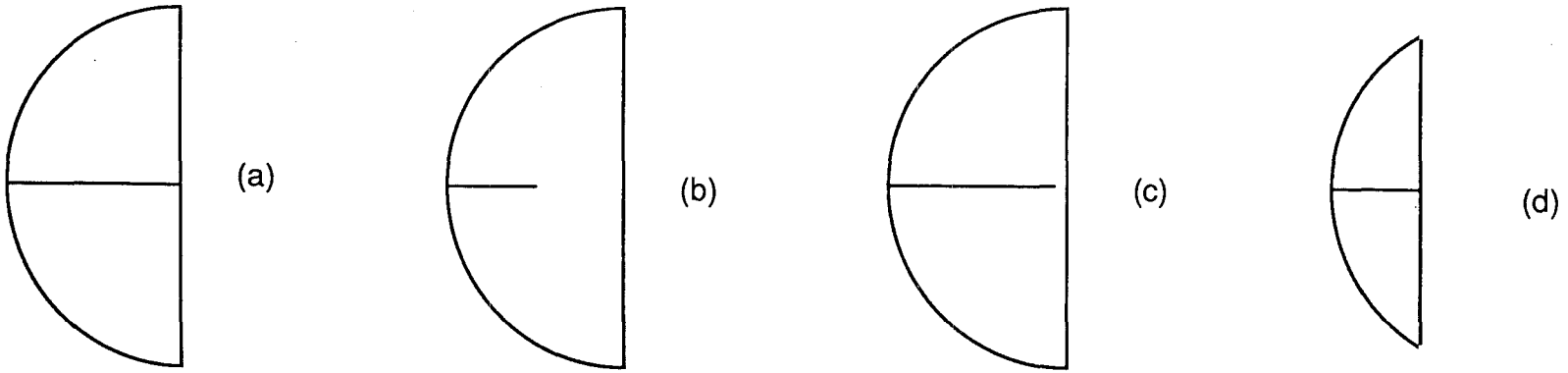

FIGURE A11.1 Effect of Angle of Incidence on Transmittance of Glass

(Duffie and Beckman, 1980)

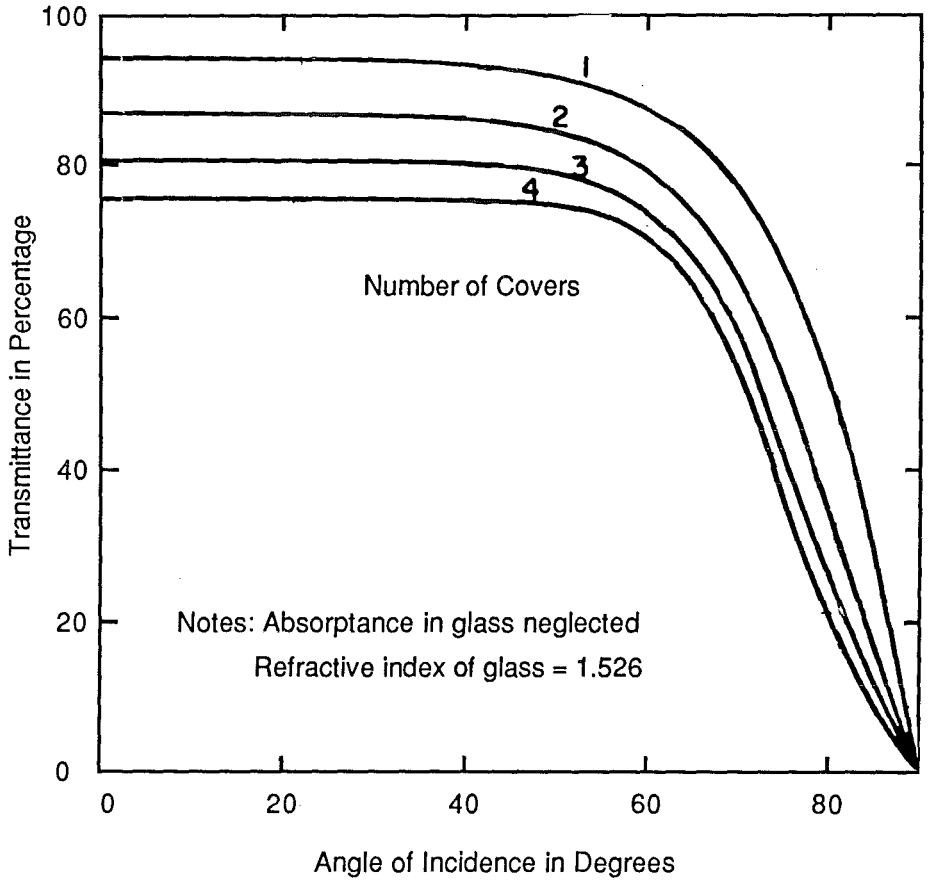

involved in making it, and not in material cost, and any size reduction of the absorber plate does not affect these labour costs. Thus it can be concluded that in an optimum collector the width of the absorber should be equal to the radius of the reflector.

A11.2 Optimum Length of the HSA Panel

It is advantageous to have the collector as long as practicable to minimize end wall losses by reducing the ratio of the box surface area to the absorber area for a given absorber width. However the upper limit is set by practical considerations of the collector fabrication. The lower limit to the collector length (L_{min}) can be derived keeping in view the angle of incidence of solar radiation on the glazing. As shown in Fig. A11.1 the transmittance of glass decreases with increase in angle of incidence, and falls off very rapidly after 60°. Fig. A11.2 shows the plan view of the collector with an incident beam of radiation making an angle of incidence of 60° with the normal to the glazing. The minimum length is chosen such that any radiation incident on the glazing at an angle greater than or equal to 60°, which is reflected from an end wall, will reach the absorber before striking the opposite end wall and thus involving another reflection loss. Fig. A11.2 shows the worst case where the beam's North-South component is such that the beam is reflected to the leading edge of the absorber and we have

$$\tan 60^\circ = 0.5\ L_{min} / R \qquad \text{(A11.1)}$$

where R is the radius of the reflector and from Eq. (A11.1),

$$L_{min} = 3.46\ R \qquad \text{(A11.2)}$$

Hence, the minimum length of the HSA panel should be about 3.5 times the reflector radius.

A11.3 End Wall Type

The end walls can be made either transparent or reflecting (Fig. A11.3). If the end walls were clear, they would gain radiation at one end and lose from the other as both ends allow incident radiation to pass through. Reflecting end walls would behave in the opposite way, but the net result would be the same, that is to lose radiation from one end and gain it from the other. However, the advantage of reflecting end walls comes from the fact that, they make the semicylinder optically infinitely long and any

FIGURE A11.2 Calculation of the MInimum Length of the Collector

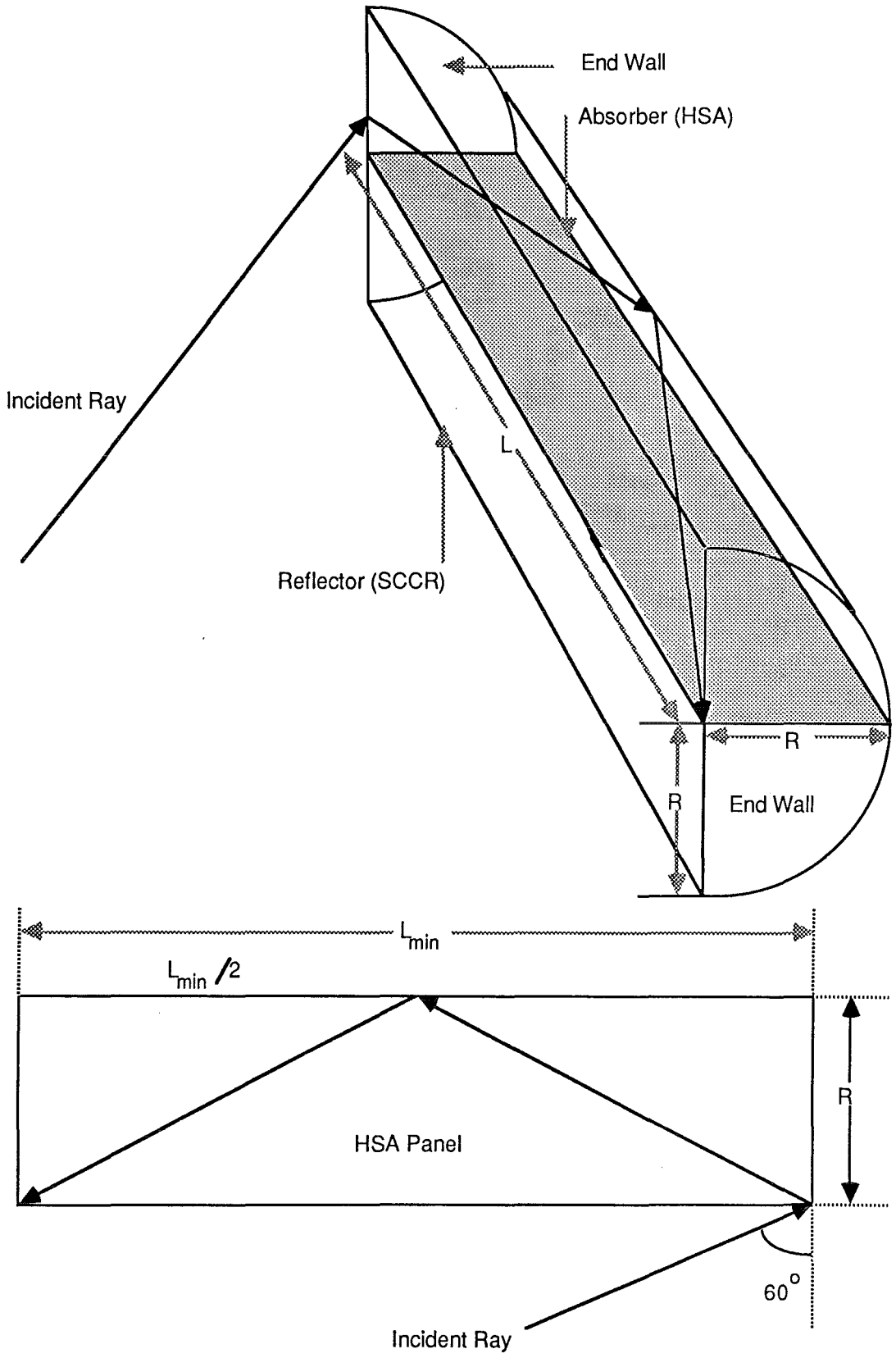

FIGURE A11.3 End Wall Type

(a) Ray Trace of Reflection Pattern for SCCR with Transmitting End Walls

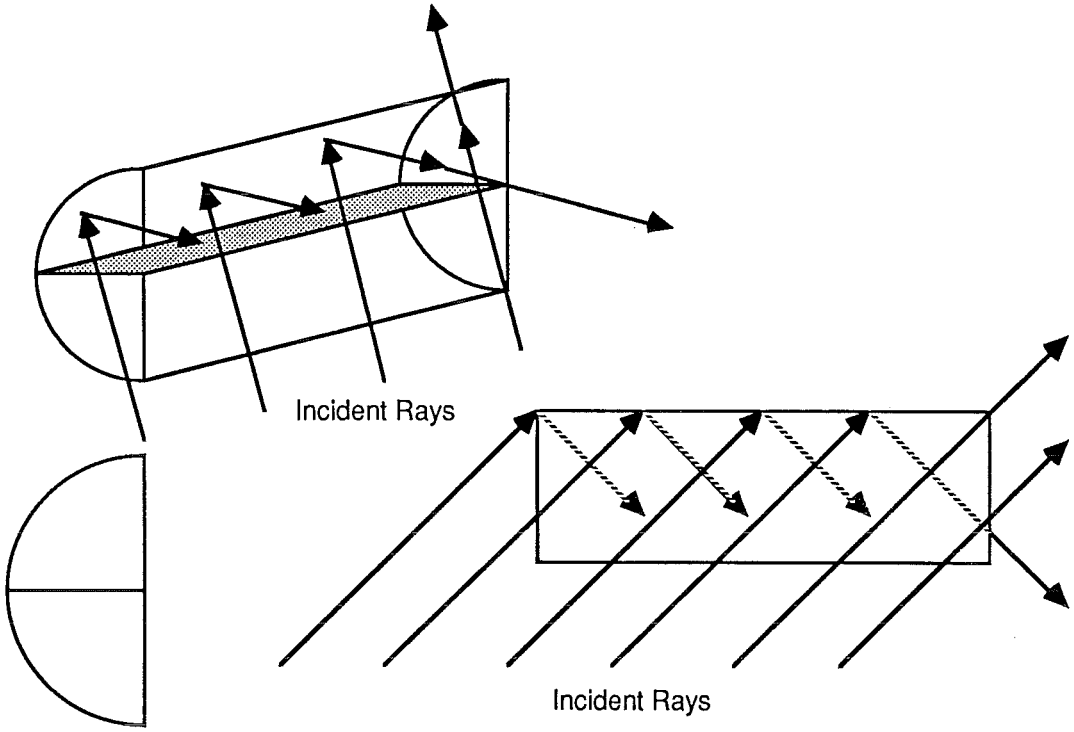

(b) Ray Trace of Reflection Pattern for SCCR with Reflecting End Walls

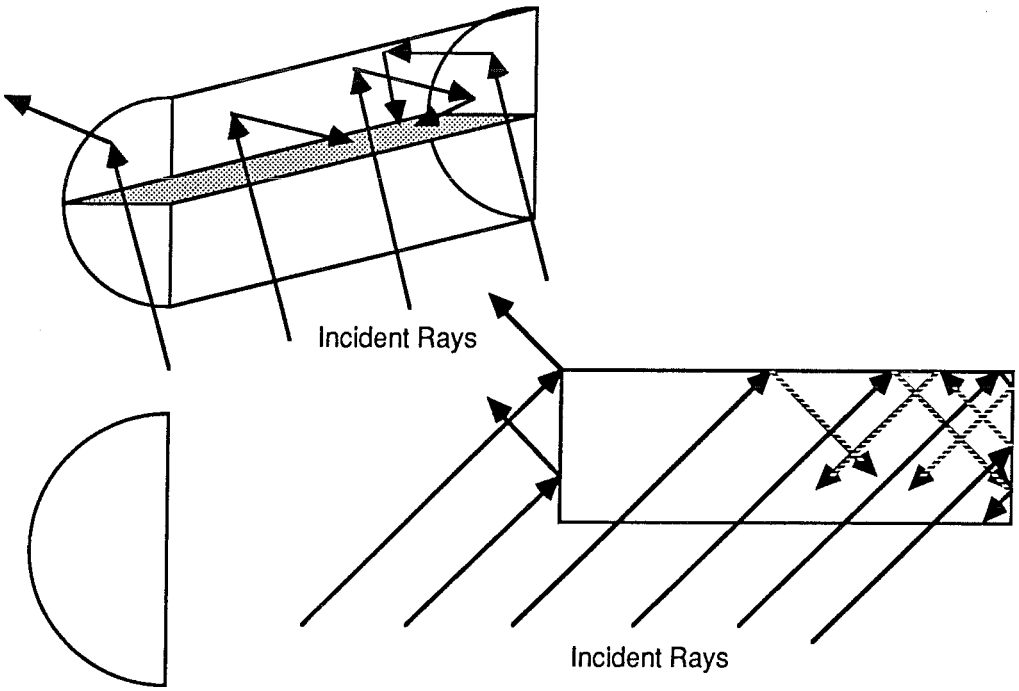

FIGURE A11.4 A Hypothetical Selective Surface with the Cutoff Wavelength at 3×10^{-6}m

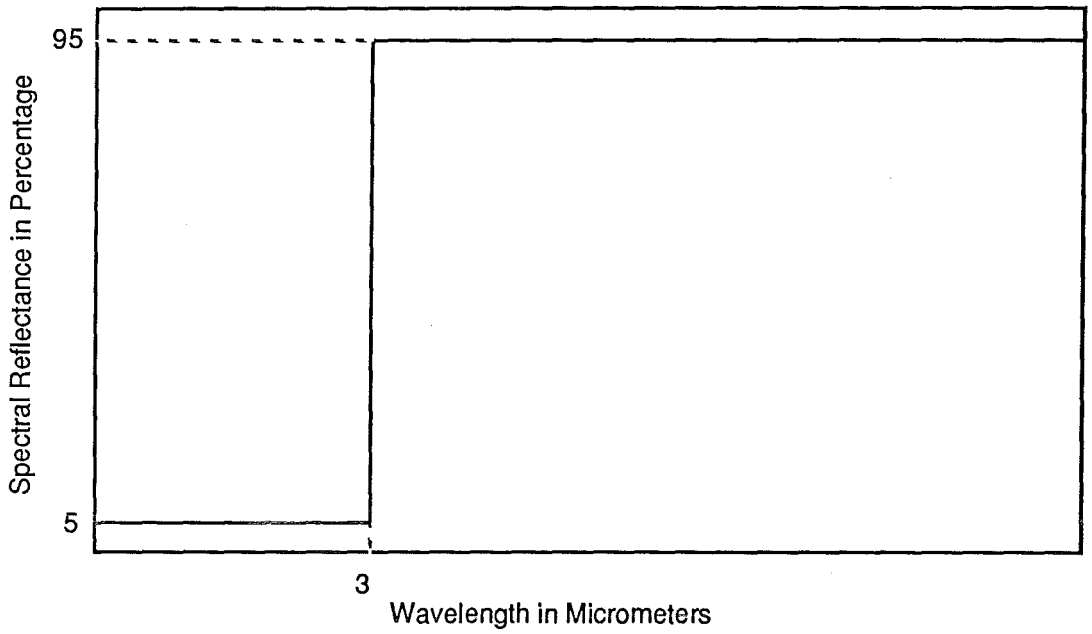

Note: 1 Micrometer = 10^{-6} m

FIGURE A11.5 Spectral Reflectance of Selected Surfaces

(Edwards et al., 1960)

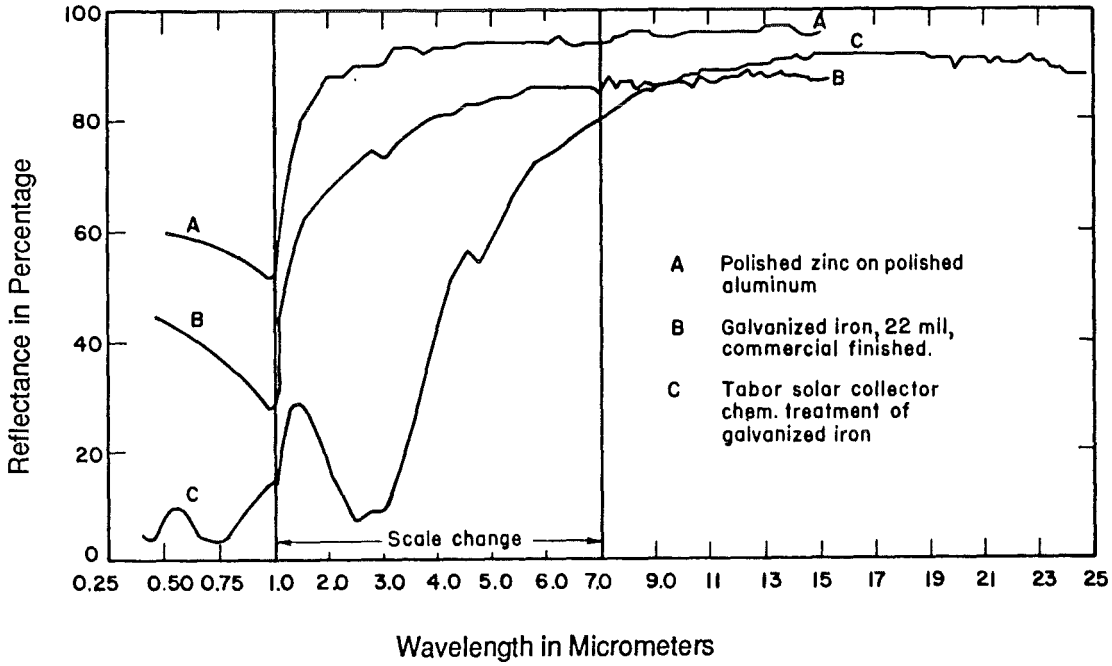

radiation entering the aperture, which is specularly reflected must strike the absorber, before leaving the collector (Winston, 1974). But with clear end walls the radiation reflected off the cylindrical reflector is also allowed to pass through the end walls before striking the absorber. Reflective end walls would also be better at keeping the thermal radiation in. They would reflect the radiation back into the collector whereas the clear end walls would transmit it to the environment. Another point in favour of reflective end walls is that they are cheaper and easier to build and hence are chosen for use in the HSA-SCCR collector.

A11.4 Absorber Plate Material

A selective surface introduces a resistance closest to the absorber plate and hence, it is one of the most effective improvements possible, with any solar collector. In the present case it is necessary to have a selective surface on the panel to achieve high temperatures.

Selective surfaces have high solar absorptance α and low thermal emittance ε, thus reducing the losses from reradiation and making convective losses more domonant. In order to achieve best results a selective surface should possess the characteristics shown in Fig. A11.4, which include high α/ε ratio and cutoff wave length at 3 microns. However, real surfaces do deviate as shown in Fig. A11.5.

Sveral methods of preparing selective surfaces have been developed, which depend on various mechanisms to achieve selectivity (Duffie and Beckman, 1980; Tabor, 1967,1977; Smith, 1977; Cathro, 1978). However, coloured stainless steel and in particular blue steel, appears to be well suited in the present investigation because of the various properties discussed below. As seen in Section 4.4.3.2, with the HSA, the panel material of construction is not very crucial, and metals with lower thermal conductivity than copper (such as stainless steel) can be used, without noticeable effect in collector performance.

When a sheet of stainless steel is immersed in a hot solution containing appropriate concentrations of chromic and sulphuric acids (200 to 300 $g.l^{-1}$ of chromic acid and 450 to 550 $g.l^{-1}$ of sulphuric acid; Evans et al., 1972) a coloured surface is formed. The colour depends on the treatment time (which varies from 5 to 15 minutes) and solution temperature (which varies from 75° to

85°C). After colouring, the steel is rinsed in cold water, and then surface hardening is done by a cathodic treatment, in another acidic solution, containing chromic and phosphoric or sulphuric acids. The film is actually an interference film (containing chromium and iron) of perfectly uniform colour, thickness and texture. The thickness of the film varies from 0.05 to 0.8 microns as the colour changes from bronze to green (the colouring order is bronze - blue - gold - red - purple - green). Blue steel has high α/ε ratios with α values from 0.9 to 0.93 and ε values from 0.06 to 0.11 (Redmond et al., 1977,1978).

Atmospheric corrosion tests over a period of seven years, accelerated corrosion tests and pitting tests on coloured steels showed excellent colour retention and stability, even better than uncoloured steel (Davison et al., 1979). Blower and Evans (1974) conducted heat resistance tests at 200°C and noticed a slight alteration in shade (due to the removal of some of the water present in the film) during the early stages of exposure, but no further change in colour was found after this initial period. However, they found that none of the other properties was affected. This property is important as the panel surface should retain selective properties at stagnation conditions. The stability was checked by placing samples of "Yazaki" blue steel in an oven over a period of a few days and no noticeable change in colour was observed at or below 300°C.

The adherence of the film and the colour intensity was tested (Blower and Evans, 1974) by subjecting the coloured sheets to various commercial cold forming processes including high pressure techniques and it was found that there was no change in adherence or colour intensity. This property is important while dimpling the sheet with the help of a die in a press and hence it was also actually checked with a sample of blue sheet. Coloured steel was found to have excellent resistance to wear and scratching (blower and Evans, 1974) by usage over a period of two years in domestic and industrial applications, which means that the HSA panel handling during its fabrication and assembly would not damage the film. Finally a sample of blue steel was checked for the strength of seam weld befor proceeding with the fabrication of the panel.

FIGURE A11.6 Schematic Diagram of the Experimental Setup to Measure the Reflectivity of Various Reflector Materials

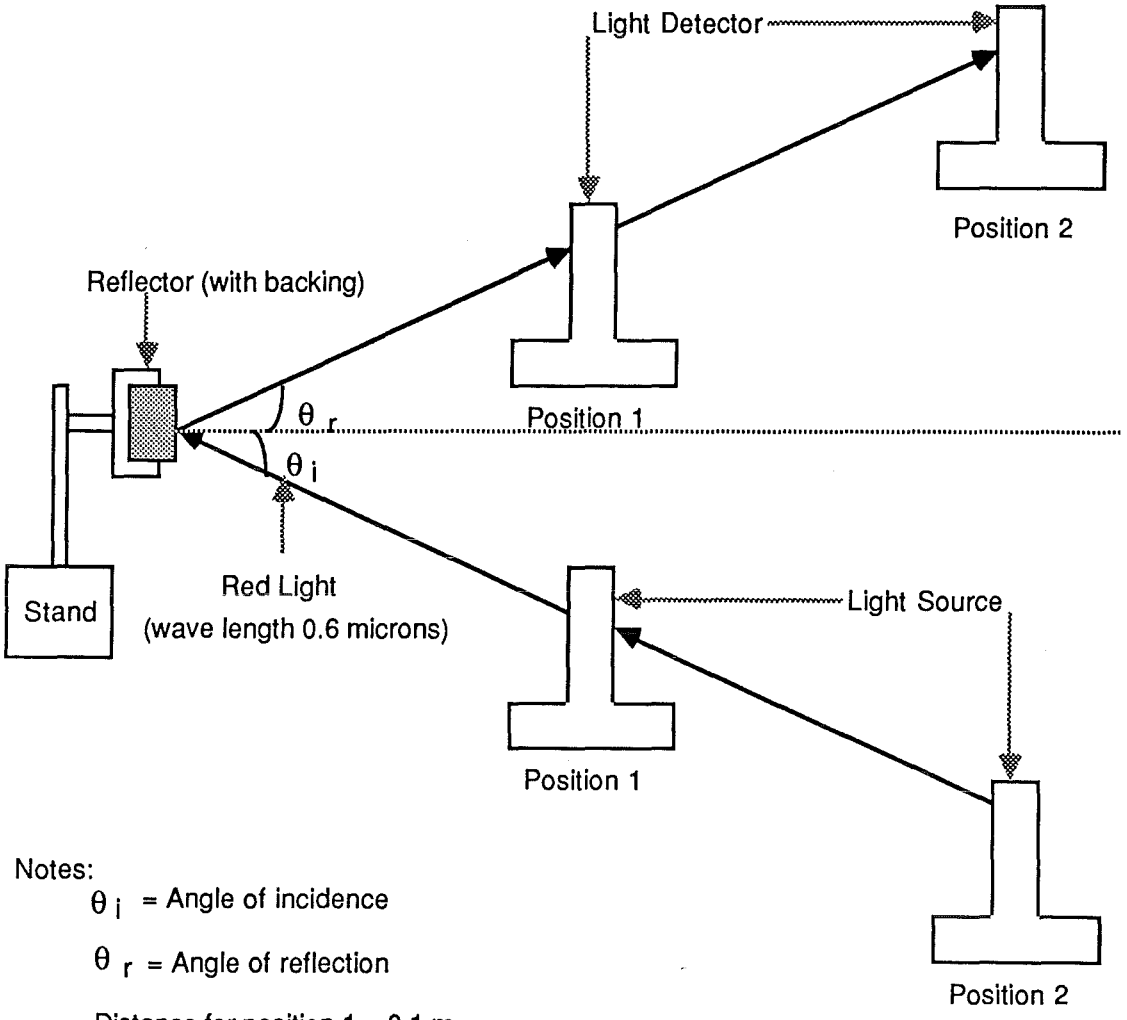

Notes:

θ_i = Angle of incidence

θ_r = Angle of reflection

Distance for position 1 = 0.1 m

Distance for position 2 = 0.6 m

A11.5 Reflector Material

The requirements of a good reflector materials are - high specular reflectivity, high temperature resistance, durability, high strength, flexibility and easy availability at low cost. Based on these criteria an appropriate reflector material must be chosen and then the method of attachment to the backing material should be determined. In order to get reasonably good performance, the reflectivity should be atleast 0.8. As the expected reflector temperature (from the computer model) is about 120°C, the reflector and its backing should be able to withstand this temperature. Also it should be able to withstand repeated heating and cooling cycles without reduction in its reflectivity or strength. The reflector material should be strong enough to be formed into semicylindrical shape or flexible enough to be able to attach to a backing material with glue.

Highly polished metals meet all the requirements except that their specular reflectivity is low. Back silvered mirrors have very high specular reflectivity but they are too expensive to form into semicylindrical shape. Hence, metalised plastics were found to be very suitable. Five such reflector materials were considered and they were - "Roscoflex-m" (RFM) and "Roscoflex-h" (RFH) manufactured by ROSCO England (and distributed by SELECON in New Zealand); "Space Energy Blanket" manufactured by King-Seeley Thermos Co., Connecticut (USA); aluminised mylar and ordinary cooking foil that can be bought locally. As the reflectivity data for these materials was not available, it was decided to perform a simple experiment to evaluate the reflectivity of these materials.

A few samples of these materials were attached to a rigid surface (such as glass pane) which can be fixed in a vertical plane with the help of a stand as shown in Fig. A11.6. A light source (Spectrophysics 120 laser with 5 mW vertically polarised output) giving red light with a wave length of 0.63 microns was used to project light on to the reflector surface. The reflected radiation was measured with a light detector (United Detector Technology Opto-techta), which was calibrated to give the reflectivity. The light source and the light detector were placed at two different positions (Fig. A11.6) in order to measure the specularity of the beam, so that the specular nature of the reflector can also be evaluated. Three samples of each materials

TABLE A11.2 Reflectivity Measurements of Various Reflector Materials (in Percentage)

Reflector Type	Position 1				Position 2			
	Point1	Point2	Point3	Average	Point1	Point2	Point3	Average
(1) Silvered Mirror	100	100	100	100	98.5	98.5	98.5	98.5
(2) RFM	100	94	93	95.7	97	75	86	86
(3) RFH	84	88	80	84	22	22	20	21.3
(4) Space Blanket-1	92	91	90	91	70	68	72	70
Space Blanket-2	84	93	91	89.3	55	68	72	65
Space Blanket-3	83	60	70	71	46	26	20	30.7
Average				83.8				55.2
(5) Aluminised Mylar-1	91	88	84	87.7	68	71	62	67
Aluminised Mylar-2	93	87	86	88.7	73	64	62	66.3
Aluminised Mylar-3	86	79	88	84.3	63	55	74	64
Average				86.9				65.8
(6) Cooking Foil-1	70	72	70	70.7	26	31	29	28.7
Cooking Foil-2	65	67	66	66	14	18	13	15
Cooking Foil-3	61	69	72	67.3	26	33	30	29.7
Average				68				24.5

(except RFM and RFH, due to nonavailability at that stage) were tested.

The reflectivity measurements were done at three different points on the same sample. For comparison a back silvered mirror was also tested and the results are given in Table A11.2. As seen from the table the reflectivity does vary from sample to sample and within the same sample from one point to the other. However the main function of this test was not to find the absolute values of the reflectivity but to compare a few selected reflectors. The extent of diffuse nature of the reflectors can be seen clearly, by comparing the average values at position 1 and position 2. The reflectors in decreasing order of their reflectivity are - RFM, aluminised mylar, space blanket, RFH and cooking foil. Although RFH has a high reflectivity (of 84%) at position 1, the reflectivity falls to a very low value (of 21%) at position 2. RFM appears to be best of the five with reflectivities of 96% and 86% at positions 1 and 2 respectively.

On the other hand RFM has a tough but flexible backing plastic which makes it very easy to handle, unlike the other four reflectors. The temperature resistance of RFM with the backing plastic material was checked in an oven and it was found to withstand temperatures as high as 150°C. Galvanised iron sheet was chosen as the backing material which was used to give a semicylindrical shape and support to the reflector. The reflector was fixed on preformed quarter cylindrical sheets to avoid damage to the reflector surface while forming into cylindrical shape. Hence, samples of RFM were glued to small quarter cylindrical iron sheets and placed in an oven to ckeck the temperature stability and formation of vapour cavities. Several contact and spray adhesives and pipe cements of different brands such as "Bostic" and "Ados" were tested for good strength, high temperature resistance (upto 150°C), reasonable application and curing times and vapours expelled during the curing process. As the reflector is not porous solvent vapours could not escape freely, resulting in formation of vapour pockets and uneven surface finish. Hence the reflector was attached in longitudinal strips and if necessary one or two pin holes were made to squeeze out the vapour from the bubbles. Ados cement was found to be best suited for this purpose.

APPENDIX A12

SELECTION OF CONDENSER FLUID

Several heat transfer fluids are available and just as in the case of the HSA working fluid, the operating temperature range of the fluid is the main criterion in selection of a suitable condenser fluid and this range should provide safe margins. The other desirable properties of the condenser fluid are given below.

(1) The condenser fluid should have high resistance to thermal cracking as it results in breaking up into lower boiling compounds which lower the flash point. Any decomposition products, if formed should be maintained in the solution. Simultaneously, under the reactive conditions (especially at high temperatures) some molecules polymerize and form coke deposits which reduce heat transfer and cause blockage.

(2) The maximum oil film temperature of the fluid should be higher than the collector stagnation temperature and the auxiliary heating element surface temperature, so that the fluid may not form a layer of coke on the heat transfer surfaces.

(3) Excellent oxidation stability is required because the reaction of the hot fluid with the atmospheric oxygen produces acidity in the fluid, together with non-soluble contaminants and an increase in viscosity. This property was essential in the present set up because of the frequent flow measurements using a measuring cylinder and stop watch, which would result in direct contact of the hot fluid with the atmospheric air.

(4) Low viscosity is desirable for the following reasons.

(a) It permits fast start-ups at lower temperatures.

(b) It prevents coking at the heat transfer surfaces.

(c) It decreases frictional losses and thus minimises the power requirements for pumping.

(d) It increases Reynold's number, thus increasing turbulence and heat transfer.

(5) Low vapour pressure helps in the following respect.

(a) It allows operation over the span of recommended temperatures at essentially atmospheric pressures.

(b) It minimizes oil vaporization which may cause pump cavitation.

(c) The storage of thermal energy becomes easier and cheaper.

(6) Higher thermal conductivity results in higher heat transfer rates. The most convenient way of comparing heat transfer efficiencies is to determine the ratio of the heat transfer coefficient to the friction energy expended pumping the fluid per unit surface area of the pipe. The most efficient fluid will show the largest ratio over a given temperature range.

(7) It is desirable to have long service life and the fluid should be able to withstand alternate heating and cooling cycles, without change in chemical composition.

(8) It should be non-corrosive and compatible with all the materials it comes in contact with.

(9) It should be non-toxic and should not cause disagreeable odours in the event of a leak.

(10) It is desirable to have the same fluid as the energy storage medium to avoid additional equipment and lowering the system efficiency. Hence, the fluid should also possess certain extra qualities such as high flash point (to avoid fire risks), high heat capacity (to lower the circulation rate and heat losses), lower density (to reduce pumping costs) and easy availability in pure form at a low price.

The desired operating temperature of the collector is about 150° to 160°C, (which fixes the fluid temperature for continuous operation) the stagnation temperature of the collector estimated is about 225°C (which fixes the maximum attainable film temperature) and the lower limit of the operating temperature in winter is about 0°C (which fixes the lowest possible operating temperature). Considering these operating temperature ranges, and other desirable properties, three heat transfer oils have been found suitable for the prescent application and they are given below.

(1) Mobiltherm 603 (a product of Mobil Oil company)

(2) Shell thermia oil - E (a product of Shell Oil Company) and

(3) Shell thermia oil - G 68 (a product of Shell Oil company)

The various properties of these three fluids are listed in the Table A12.1, along with their costs.

On comparing the various desirable properties Mobiltherm was found to be appropriate in the present situation as it has higher operating and film temperatures, higher oxidation stability, lower viscosity, higher thermal conductivity, lower density and higher heat capacity as compared to Thermia oils.

TABLE A12.1 Properties of Heat Transfer Oils

Property	Mobiltherm	Thermia Oils	
	603	E	G-68
(1) Maximum operating (or bulk oil) Temperature recommended			
(a) for continuous operation in °C	315	290	290
(b) for intermittent heating in °C	315	315	315
Maximum oil film temperature in °C	345	315	315
(2) Minimum operating temperature (without any start up problem for the pump in °C)	-15	-9	-9
(3) Initial Boiling point in °C	330		
(4) Pour point °C	-18	-26	-29
(5) Flash point, closed up in °C	206	226	185
(6) Density in $kg.m^{-3}$			
at 20 °C	858	897	896
at 150 °C	778	821	815
(7) Kinematic Viscosity in centi stokes			
at 20 °C	49	500	230
at 150 °C	2.2	3.6	2.85

TABLE A12.1 Properties of Heat Transfer Oils (*Continued*)

Property	Mobiltherm 603	Thermia Oils E	Thermia Oils G-68
(8) Specific Heat in $kJ.kg^{-1}.K^{-1}$			
at 20 °C	1.9	1.81	1.81
at 150 °C	2.46	2.27	2.27
(9) Thermal conductivity in $W.m^{-1}.K^{-1}$			
at 20 °C	0.132	0.128	0.129
at 150 °C	0.123	0.119	0.120
(10) Vapour pressure in Pascals			
at 20 °C		$1.3x10^{-4}$	$5.9x10^{-4}$
at 150 °C	170	12	48
(11) Viscosity in centi poise			
at 20 °C	42.2	451	206
at 150 °C	1.71	2.95	2.32
(12) Cost in 1984			
(a) when purchased in 20l tins in cents.l^{-1}	166	132.5	134.5
(b) when purchased in 200l drums in cents.l^{-1}	133.7	132.5	134.5

APPENDIX A13

CONDENSER TUBE DIMENSIONS

Once the shape of the condenser tube is determined, the next step in the design calculations of the HSA panel is the determination of condenser tube dimensions. A rectangular cross section has been chosen for the condenser tube and the three dimensions that need to be estimated are its length, width and height.

A13.1 Length of the Condenser Tube

The minimum length of the tube is usually equal to the length of the HSA panel. If the tube is shorter, condensation process may not be as efficient, and the vapours may have to travel extra distance in the horizontal direction. Lock & Bailey (1964) and Lee & Bedrossian (1978) have shown that, for better heat transfer in heat pipes, it is preferable to have the length of the condenser as much as practicable.

On the other hand, it is preferable to have the maximum length of the condenser tube approximately equal to the length of the HSA panel because longer tubes extending from the panel are neither convenient to construct nor efficient to operate. The other way of having a longer tube is by using multipass tubes. But multipass tubes are harder to construct, especially in rectangular cross section.If circular or elliptical cross section is used a major resistance is introduced in the path of the heat transfer due to the filler material used to attach the tube. On the other hand, the condensation area can be increased without the use of multipass tubes by increasing the width of the condenser tube.

A13.2 Width and Height of the Condenser Tube

The criteria for the selection of the width and height of the condenser tube include:

(1) high condensation film coefficient,

(2) high oil side film coefficient,

(3) high overall heat transfer coefficient,

(4) low temperature drop on the oil side,

(5) low temperature drop across the condensate film and

(6) low pressure drop on the oil side.

In the following sections the effects of changes in width and height on all these variables have been evaluated. The other variables considered include: mass flow rate of oil, net heat output from the collector, collector tilt angle, oil inlet and outlet temperatures and condensate film or vapour temperature. These variables are included for comparison, though some of them are not independent variables as explained later. The condenser tube widths considered are 20, 30, 40 and 50 mm, while the heights considered are 5, 10, 15 and 20 mm.

A13.3 Condensation Film Coefficient (CFC)

Nusselt's equation (Kern, 1954) for a film condensing on a vertical or inclined surface holds good for pure substances. It is assumed to be valid in the present case because Dowtherm A behaves almost like a pure substance, although it is a mixture. The other assumptions involved in deriving the film coefficient are listed by Kern (1954). The average condensation film coefficient h_c is given by

$$h_c = 0.943 \left[k_f^3 \rho_f^2 \lambda_f g \sin \alpha\right] / \left[\mu_f L_{cp} \Delta T_f\right] \quad \text{(A13.1)}$$

where k_f, ρ_f, μ_f, λ_f are the thermal conductivity, the density, the viscosity and the latent heat of vaporization of the fluid respectively, at the mean condensate film temperature T_f; g is the acceleration due to gravity; α is the tilt angle of the condensing surface; L_{cp} is the length of condensation path parallel to the condensate flow (which is the width of the condenser in the present case); and ΔT_f is the temperature drop across the condensate film.

A13.3.1 Fin effect

In a heat pipe, there is always a temperature gradient between the evaporator section and the condenser section (Lee and Mital, 1972). Though the condensation process is mainly isothermal, due to this difference in the wall temperature there is heat flow via the wall. This effect can be evaluated, assuming the rest of the HSA panel behaving like a longitudinal fin of uniform thickness, Kern (1954) gives the following expression for evaluating the fin efficiency Ω.

$$\Omega = (\tanh E W_f) / (E W_f) \quad \text{(A13.2)}$$

TABLE A13.1 Summary of the Results of the Computer Programme TPCFC to Calculate the Condensation Film Coefficient

T_f	α	W_c	ΔT_f	R_{cf}	h_c	h_{cf}
°C	Degrees	mm	K	$K.W^{-1}$	$W.m^{-2}.K^{-1}$	$W.m^{-2}.K^{-1}$
		20	1.63	0.01228	3666	4051
		30	1.13	0.00854	3627	3883
170	43.5	40	0.87	0.00655	3607	3798
		50	0.70	0.00531	3595	3748
	30		1.25	0.00946	3264	3507
170	45	30	1.12	0.00847	3659	3916
	60		1.05	0.00794	3912	4178
170			1.13	0.00854	3627	3883
180			1.20	0.00909	3647	3904
190	43.5	30	1.27	0.00962	3676	3935
200			1.33	0.01008	3699	3960

Notes: T_f = Condensate film temperature

α = HSA panel tilt angle

W_c = Condenser tube width

ΔT_f = Temperature drop across the condensate film

R_{cf} = Condensate film resistance

h_c = Condensation film coefficient not corrected for fin effect

h_{cf} = Condensation film coefficient corrected for fin effect

Fin efficiency factor E is given by

$$E = (h_c p_f / k_s a_f)^{0.5} \quad \text{(A13.3)}$$

where W_f, p_f and a_f are the width, the perimeter and the cross sectional area respectively of the fin, and they are given by

$$W_f = W_p - W_c \; ; \; p_f = 2 (L_p + t_s) \; ; \; a_f = L_p t_s$$

where W_p and L_p are the width and length of the panel; t_s is the thickness of the plain sheet of the panel; k_s is the thermal conductivity of the fin material. The condensation coefficient corrected for fin effect h_{cf} is given by

$$h_{cf} = (\Omega A_f + A_{cf}) h_c / A_c \quad \text{(A13.4)}$$

where A_f is the fin area; A_{cf} is the condensation area exclusive of the fin area; A_c is the heat transfer area on which h_c is based and it is equal to $L_p W_c$, where W_c is the condenser tube width.

A13.3.2 Condensate film temperature drop

It is necessary to know the condensate film temperature drop ΔT_f to evaluate the film coefficient, and hence it is assumed first and then checked in the following manner. The condensate film resistance R_{cf} is given by

$$R_{cf} = 1 / h_{cf} A_{cf} \quad \text{(A13.5)}$$

If Q_{net} is the net energy transfered to the oil,

$$\Delta T_f = Q_{net} R_c \quad \text{(A13.6)}$$

ΔT_f is assumed initially and h_{cf} is evaluated from Eqs. (A13.1) to (A13.4). Then R_{cf} and ΔT_f are evaluated for a given value of Q_{net}. This new value of ΔT_f, is in turn used to get a better estimate of h_{cf}, and the iterative process is carried out until the values converge.

A13.3.3 Computer programme TPCFC

The computer programme TPCFC estimates the condensation film coefficient corrected for fin effect and the temperature drop across the condensate film for various conditions. The input and output variables are given at the beginning of the programme listing. The computer programme and a sample set of results are included at the end of this appendix. The summary of results is given in Table A13.1.

FIGURE A13.1 Condenser Tube

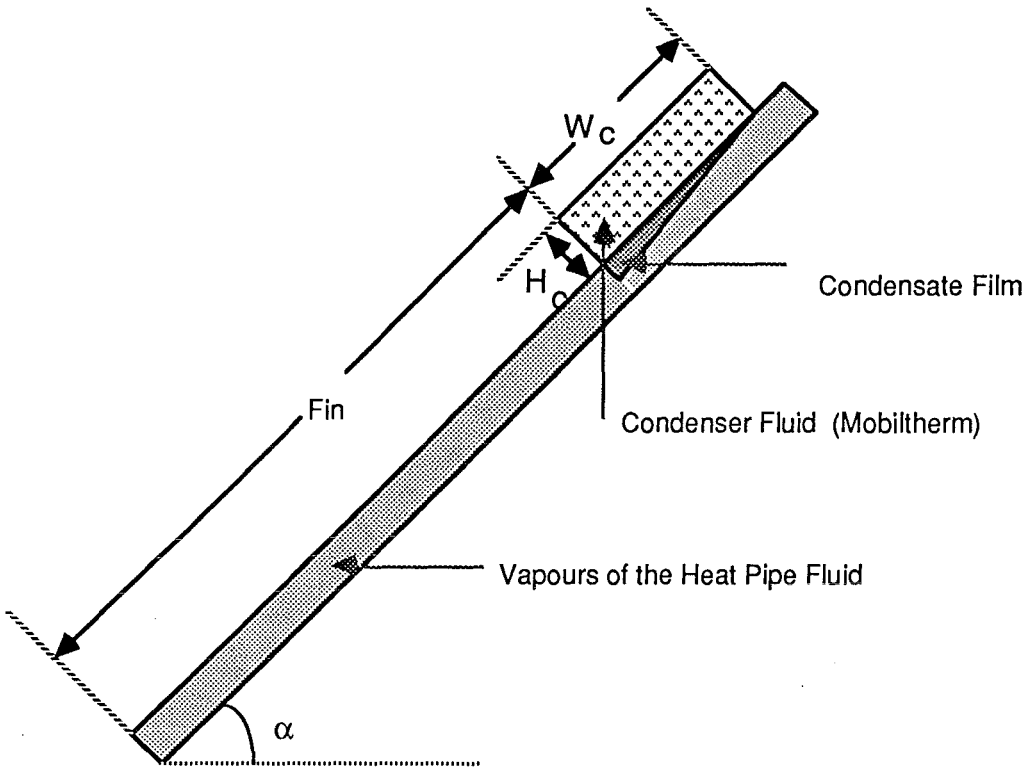

Notes:

W_c = Condenser tube width

H_c = Condenser tube height

α = Tilt angle

A13.3.4 Observations

The following observations can be made from Table A8.1 with the help of Figs. A13.1 and A6.1.

(1) Effect of condenser width Wc : As the width increases, h_{cf} decreases. It can also be noticed that R_{cf} decreases as W_c goes up, although as per Eq. (A13.5) it should increase (because h_{cf} is decreasing). This is because of the fact that the product $h_{cf}A_{cf}$ is increasing, as W_c goes up. As per Eq. (A13.6) ΔT_f also decreases with increase in W_c

(2) Effect of HSA panel tilt angle α : As α increases, the gravity component acting on the condensing film increases, thus the film thickness (and ΔT_f & R_{cf}) decreases resulting in an increase of h_{cf}.

(3) Effect of condensate film or vapour temperature Tf: As T_f increases h_{cf} increases because of the changes in the properties of the fluid.

A13.4 Oil Side Film Coefficient (OFC)

The oil side film coefficient can be evaluated from the Sieder and Tate correlation for heating and cooling of petroleum fractions in horizontal and vertical tubes for streamline flow, (the oil flow rate is generally restricted to the laminar region, in order to get an appreciable temperature rise through the collector) as given by McCabe and Smith (1956).

$$Nu = 2\ (Gz)^{1/3}\ \phi_v \qquad \text{(A13.7)}$$

where Nu is Nusselt number, Gz is Greatz number and ϕ_v is the viscosity correction factor and they are given by

$$Nu = (h_o\ D_{ec})/k_o\ ; Gz = (m_o\ c_{po})/(k_o\ L_o);\ \phi_v = (\mu_{oa}/\mu_{ow})^{0.14} \qquad \text{(A13.8)}$$

where h_o is the average OFC; D_{ec} is the equivalent diameter of the condenser tube; k_o and c_{po} are the oil thermal conductivity and the specific heat capacity at the average oil temperature T_{ao}; m_o is the oil flow rate; L_o is the length of heat transfer path before mixing of the oil occurs, and in the present case it is equal to the length of the panel L_p; μ_{oa} and μ_{ow} are the viscosities of oil at T_{ao} and T_w (tube wall temperature) respectively. D_{ec} is given by

$$D_{ec} = 4\ (a_c/p_c) = (2\ Wc\ Hc)/(W_c + H_c) \qquad \text{(A13.9)}$$

where a_c, p_c, W_c and H_c are the condenser tube cross sectional area, perimeter, width and height respectively.

A13.4.1 Correction for free convection

Just as there is a transition region and not a single point separating laminar and turbulent flow, there must be a transition region between free convection to a stationary fluid and passing in streamline flow. At low linear velocities and in horizontal tubes, both are undoubtedly operative. In the present case the flow rates may be quite small and free convection may exsist, in which case correction must be applied. The correction factor, for free convection ψ is given by Kern and Othmer (1943)

$$\psi = 2.25\ (1 + 0.010\ Gr^{1/3})\ /\ \log Re \qquad \text{(A13.10)}$$

where Gr is the Grashof number and Re is the Reynolds number and they are given by

$$Gr = (D_{ec}\ g\ \rho_o^2\ \beta_o\ \Delta T_{ow})/\mu_o^2\ ;\ Re = (\ D_{ec}\ V_o\ r_o)/\mu_o \qquad \text{(A13.11)}$$

where ρ_o, μ_o and β_o are the density, the viscosity and the coefficient of thermal expansion of the oil at T_{ao}; ΔT_{ow} is the oil side temperature drop and V_o is the linear velocity of oil, through the condenser tube and they are given by

$$\Delta T_{ow} = T_w - T_{ao} \qquad \text{and} \qquad V_o = m_o\ /\ (\rho_o\ a_c) \qquad \text{(A13.12)}$$

The OFC corrected for free convection h_{oc} is given by

$$h_{oc} = h_o\psi$$

A13.4.2 Fin effect

The fin effect for the OFC is found in the same way as it was done for CFC using the Eqs. (A13.2) to (A13.4) except that h_c is replaced by h_{oc}. Then the OFC corrected for free convection and fin effect h_{ocf} is given by

$$h_{ocf} = (\Omega\ A_f + A_{of})\ h_{oc}\ /\ A_o \qquad \text{(A13.13)}$$

where A_{of} is the bare condenser tube area, exclusive of the fin area, and A_o is the heat transfer area on which h_{oc} is based. A_o is given by

$$A_o = 2L_p(W_c + H_c) \qquad \text{(A13.14)}$$

A13.4.3 Overall heat transfer coefficient

The overall heat trasfer coefficient U_{oh} for the condenser tube can be calcaulated from the individual coefficients as given below

$$U_{oh} = 1/[\{D_{oc}/(D_{ic}\ h_{of})\} + \{(t_s\ D_{oc})/(k_s\ D_{lc})\} + (1/h_{cf})] \qquad \text{(A13.15)}$$

where D_{ic}, D_{oc} and D_{lc} are the inside, outside and log mean diameters of the condenser tube respectively.

Also the observed overall coefficient U_{oa} can be calculated, from the net heat transfer Q_{net} as given below

$$U_{oa} = Q_{net} / (A_o \Delta T_{ow}) \quad \text{(A13.16)}$$

A13.4.4 Oil film temperature drop

By conducting heat balances separately on the condensation side and the oil side of the condenser tube, we have

$$Q_{net} = h_{cf} A_c \Delta T_f \quad \text{(A13.17)}$$

$$Q_{net} = h_{ocf} A_o \Delta T_{ow} \quad \text{(A13.18)}$$

where A_c and A_o are the heat transfer areas on which h_{cf} and h_{ocf} are based, respectively; ΔT_f and ΔT_{ow} are the temperature drops across the condensate film and oil film respectively. On rearranging the Eqs. (A13.17) and (A13.18) we have

$$\Delta T_{ow} = \{h_{cf} A_c \Delta T_f\} / h_{ocf} A_o \quad \text{(A13.19)}$$

Eq. (A13.19) can be used to estimate the oil side temperature drop indirectly, if the tube wall temperature T_w is not known. However, it will be shown in Section A13.6 that T_w is evaluated first and ΔT_{ow} is estimated directly from it using,

$$\Delta T_{ow} = T_w - \{(T_{io} + T_{oo})/2\} \quad \text{(A13.20)}$$

A13.4.5 Computer programme TSPQFC

The computer programme TSPQFC estimates, the overall heat transfer coefficient, and the OFC corrected for free convection and fin effect, for various conditions. The input and output variables are given at the beginning of the programme listing. The computer programme and a sample set of results are given at the end of this appendix. The summary of the results is given in Table A13.2.

A13.4.6 Observations

The following observations can be made from the Table A13.2 and the Figs. A13.1 and A6.1.

(1) Efect of condenser tube width Wc and height Hc : As the width increases OFC changes very little because, the changes in the free convection factor and the equivalent diameter act in opposite directions. However, when the temperature rise through the condenser increases the effect of the equivalent diameter dominates, resulting in an increase in OFC with the width. As H_c increases OFC decreases for the same reasons as mentioned above.

TABLE A13.2 Summary of the Results of the Computer Programme TSPQFC to Calculate the Oil Side Film Coefficient (OFC) and the Overall Heat Transfer Coefficient

W_c	H_c	T_w	T_{io}	T_{oo}	m_o	U_{oa}	h_o	h_{oc}	h_{ocf}
mm	mm	°C	°C	°C	kg.hr^{-1} ←			W.m^{-2}.K^{-1}	→
	5					442	183	210	233
	10					442	110	149	168
20	15	175	155	165	19	442	85	130	148
	20					442	73	121	138
	5					295	171	211	234
	10					295	98	145	164
30	15	175	155	165	19	295	73	124	141
	20					295	61	114	131
	5					221	165	215	239
	10					221	92	145	164
40	15	175	155	165	19	221	61	122	140
	20					221	55	112	128
	5					177	161	220	244
	10					177	88	147	166
50	15	175	155	165	19	177	64	123	140
	20					177	51	111	128
		165			19.7	177	99	154	174
		175			19.7	126	101	163	183
30	10	185	135	145	19.7	98	102	169	190
		195			19.7	80	102	175	196

Notes: W_c = Condenser tube width; H_c = Condenser tube height
T_w = Condenser tube wall temperature
T_{io} = Oil inlet temperature
T_{oo} = Oil outlet temperature
m_o = Oil mass flow rate
U_{oa} = Overall heat transfer coefficient
h_o = OFC not corrected for free convection and fin effect
h_{oc} = OFC corrected for free convection only
h_{ocf}= OFC corrected for free convection and fin effect

TABLE A13.2 Summary of the Results of the Computer Programme TSPQFC to Calculate the Oil Side Film Coefficient (OFC) and the Overall Heat Transfer Coefficient (*Continued*)

W_c	H_c	T_w	T_{io}	T_{oo}	m_o	U_{oa}	h_o	h_{oc}	h_{ocf}
mm	mm	°C	°C	°C	$kg.hr^{-1}$ ←			$W.m^{-2}.K^{-1}$	→
				25	25.1	29	165	452	486
				45	8.2	31	106	419	451
				65	4.8	33	84	370	401
				85	3.4	35	71	329	358
30	10	175	15	105	2.6	38	62	292	319
				125	2.1	42	56	266	292
				145	1.7	47	51	246	271
				165	1.5	52	47	222	246
			15	25	25.1	29	165	452	486
			35	45	24.1	33	146	297	325
			55	65	23.2	38	130	242	267
			75	85	22.1	47	121	215	238
30	10	175	95	105	21.2	59	112	194	216
			115	125	20.4	80	106	179	200
			135	145	19.7	126	102	164	184
			155	165	18.9	295	98	145	164
					6	177	67	134	153
					10	177	79	142	161
					60	177	143	186	207
30	10	185	155	165	120	177	181	211	234
					180	177	207	229	253
					240	177	228	242	267

Notes: W_c = Condenser tube width; H_c = Condenser tube height
T_w = Condenser tube wall temperature
T_{io} = Oil inlet temperature
T_{oo} = Oil outlet temperature
m_o = Oil mass flow rate
U_{oa} = Overall heat transfer coefficient
h_o = OFC not corrected for free convection and fin effect
h_{oc} = OFC corrected for free convection only
h_{ocf}= OFC corrected for free convection and fin effect

TABLE A13.3 Values of $1/R_o$ for Various Condenser Tube Dimensions

W_c mm	H_c mm	A_o m2	h_{ocf} $W.m^{-2}.K^{-1}$	$A_o\ h_{ocf} = 1/R_o$ $W.K^{-1}$
20	5	0.05	233	11.7
	10	0.06	168	10.1
	15	0.07	148	10.3
	20	0.08	138	11.1
30	5	0.07	234	16.4
	10	0.08	164	13.1
	15	0.09	141	12.7
	20	0.10	131	13.1
40	5	0.09	239	21.5
	10	0.10	164	16.4
	15	0.11	140	15.4
	20	0.12	128	15.4
50	5	0.11	244	26.8
	10	0.12	166	19.9
	15	0.13	140	18.2
	20	0.14	128	17.9

Notes: R_o = Oil side film resistance

W_c = Condenser tube width

H_c = Condenser tube height

A_o = Area of heat transfer on the oil side

h_{ocf} = Oil side film coefficient corrected for free convection and fin effect

The aim is to decrease the oilside film resistance R_o, which is possible by increasing the area of heat transfer A_o or by increasing the OFC. The A_o increases with increase in W_c or H_c. The product $A_o h_{ocf}$ should increase in order to reduce R_o. The Table A13.3 is made from the Table A13.2 and gives $1/R_o$ values for different H_c and W_c values. It is desirable to have a maximum value of $1/R_o$ and as seen from Table A13.3, it occurs at maximum width and minimum height.

The overall heat transfer coefficient decreases with increase in both W_c and H_c because, the heat transfer area increases while the other quantities remain the same (Table A13.2).

(2) Effect of oil outlet temperature T_{oo} : For a fixed inlet temperature of the oil, as T_{oo} increases OFC decreases, even though the free convection factor increases because of the rapid decrease in oil flow rate to transfer a fixed amount of energy. However, U_{oa} increases because of the fall in temperature drop across the oil film ΔT_{ow}.

(3) Effect of the oil inlet temperature Tio : For a fixed temperature rise of the oil through the condenser, as T_{io} increases OFC drops because of the changes in oil properties, especially viscosity. Once again U_{oa} increases with T_{io} because ΔT_{ow} decreases.

(4) Effect of tube wall temperature Tw : OFC increases slightly with T_w, because the free convection factor increases. However, U_{oa} drops with T_w because ΔT_{ow} increases.

(5) Effect of oil mass flow rate mo : As expected OFC increases with m_o. However, U_{oa} remains the same, as none of the quantities affecting it are changed.

A13.5 Oil Side Pressure Drop

The pressure drop in the condenser tube can be estimated from the standard Fanning equation, for circular tubes (McCabe et al., 1985). However, simple hydraulic radius or equivalent diameter gives erroneous results, in the case of laminar flow through noncircular cross sections. Perry and Green (1985) gives the following expression to calculate the pressure drop for ducts with liquid flowing full.

$$m_o = \{W_c\, H_c^3\, \rho_o\, g_c\} \{ (g\, \rho_o \sin\alpha)/g_c + \Delta P_c/L_c \} / \{\mu_o\, K\} \quad \text{(A13.21)}$$

where, ΔP_c is the pressure drop in the condenser tube; α is the angle between the condenser tube and the horizontal (in the

TABLE A13.4 "K" Factor Values as a Function of the Ratio W_c/H_c

W_c/H_c	1	2	3	4	5	10	>10
K	28.6	17.5	15.3	14.2	13.7	12.8	12

Notes: H_c = Condenser tube height; W_c = Condenser tube width

TABLE A13.5 Summary of Pressure Drop Calculations for the Condenser Tube

Mass flow rate of the oil = 20 $kg.hr^{-1}$

Average oil temperature = 150 °C

H_c	W_c	D_{ec}	V_o	Re	K	ΔP_c
mm	mm	mm	$m.s^{-1}$	Dimensionless		Pa
	20	8.0	0.142	598	14.2	77.1
	30	8.6	0.123	556	13.5	48.9
5	40	8.9	0.115	538	13.1	36.7
	50	9.1	0.110	526	12.8	27.8
	20	13.3	0.051	360	17.5	11.9
	30	15.0	0.040	319	15.3	6.9
10	40	16.0	0.036	299	14.2	4.8
	50	16.7	0.033	287	13.7	3.7
	20	17.1	0.031	280	25.2	5.1
	30	20.0	0.023	239	17.5	2.4
15	40	21.8	0.019	219	16.0	1.6
	50	23.1	0.017	207	14.9	1.2
	20	20.0	0.023	239	28.6	2.4
	30	24.0	0.016	200	23.1	1.3
20	40	26.7	0.013	180	17.5	0.7
	50	28.6	0.011	167	16.4	0.6

Notes: H_c = Condenser tube height; W_c = Condenser tube width

D_{ec} = Equivalent diameter of the condenser tube

V_o = Velocity of the oil through the condenser tube

Re = Reynolds number

K = Factor from Eq. (A13.21)

ΔP_c = Oil pressure drop in the condenser tube

present case it is equal to zero); and K is a factor depending on the ratio of W_c/H_c as given in Table A13.4. Substititing $\alpha = 0$, and rearranging Eq. (A13.21), we get,

$$\Delta P_c = \frac{m_o \mu_o K L_c}{W_c H_c^3 \rho g_c} \quad \text{(A13.22)} \qquad \Delta P_c = \frac{m_o \gamma_o K L_c}{W_c H_c^3 g_c} \quad \text{(A13.23)}$$

where γ_o is the kinematic viscosity of oil.

From Eq. (A13.23), ΔP_c can be estimated for different heights and widths of the condenser tube (but for a specified average oil temperature and mass flow rate). The summary of results are given in Table A13.5.

It is evident from Eq. (A13.23), ΔP_c is directly proportional to oil mass flow rate m_o, and the factor K, which is dependent on the ratio W_c/H_c. It can be seen, that ΔP_c falls with increase in either W_c or H_c. However, it should be noted that the kinematic viscosity of the oil, at 20°C is about 25 times of that at 150°C (Table A12.1), and hence, at cold conditions, all ΔP_c values should be multiplied by a factor of about 25, as evident from Eq. (A13.23).

A13.6 Over View of the Heat Transfer Calculations

As mentioned earlier, while evaluating the heat transfer coefficients, certain conditions have been assumed. Some of the variables considered are interdependent, and they have been included for comparison sake. In actual practice only independent quantities can be taken as input variables and they include - the mass flow rate of the oil m_o; the vapour or condensing film temperature T_f, which is approximately equal to the operating temperature of the panel (which inturn depends on the power input to the panel); the inlet oil temperature T_{io}; the condenser tube dimensions height H_c, width W_c and length L_c; the panel dimensions width W_p and length L_p; the panel tilt angle to the horizontal α; the properties of the condenser fluid (Mobiltherm); and the properties of the HSA panel working fluid (Dowtherm A).

Recalling the expressions for the net heat transferred Q_{net}, we have,

$$Q_{net} = A_c h_{cf}(T_f - T_w) \quad \text{(A13.24)}$$

$$Q_{net} = A_o h_{of} \{T_w - (T_{io} + T_{oo})/2\} \quad \text{(A13.25)}$$

$$Q_{net} = m_o c_{po}(T_{oo} - T_{io}) \quad \text{(A13.26)}$$

We also know that

$$h_{cf} = f\ (T_f, T_w) \qquad \text{(A13.27)}$$

$$h_{of} = f\ (T_{io}, T_{oo}, T_w) \qquad \text{(A13.28)}$$

$$c_{po} = f\ (T_{io}, T_{oo}) \qquad \text{(A13.29)}$$

In these Eqs. (A13.24) to (A13.29) there are three unknown quantities T_w, T_{oo}, and Q_{net}, which have been solved employing the following procedure.

(1) First T_w value is assumed.

(2) h_{cf} is found from Eq. (A13.17).

(3) Q_{net} is evaluated from Eq. (A13.24).

(4) T_{oo} can then be evaluated from Eq. (A13.26). But c_{po} is a function of T_{io} and T_{oo}. Hence, T_{oo} is assumed, c_{po} is esimated from Eq. (A13.29), and then T_{oo} is calculated from Eq. (A13.26). This procedure is continued till T_{oo} is converged.

(5) At this stage h_{ocf} is evaluated from Eq. (A13.28).

(6) Now "Bisection Method" can be used to converge on to T_w.

From Eq. (A13.25), we have,

$$\delta = Q_{net} - A_o\, h_{of} \left\{T_w - (T_{io} + T_{oo})/2\right\} \qquad \text{(A13.30)}$$

The aim is, to reduce the value of δ to nearly zero, which can be achieved in the folowing manner. Once δ is evaluated, from Eq. (A13.30), it is checked whether δ has a positive, or negative value. Then, another value for T_w is assumed, in such a way, that a value of δ with opposite sign to the one previously obtained, can be achieved. These positive and negative values of δ, define the two boundaries for T_w. Now, an intermediate value for T_w is assumed, and δ is found out. If this δ is positive, the higher positive value is eliminated, and if it is negative, the higher negative value is eliminated. Thus, a new set of boundaries, closure than the previous one, is obtained. This procedure is repeated till δ tends to zero. The condenser tube, along with the panel can be devided into a number of segments, and these calculations can be performed for each segment, which can be summed up at the end, to get the results for the entire condenser tube.

A13.6.1 Computer programme TPHTC

The computer programme does all the heat transfer calculations mentioned in the previous section. It evaluates various heat transfer coefficients and temperature drops for different conditions as mentioned in Table A13.6. The input and output variables are listed at the beginning of the programme. The

TABLE A13.6 Summary of the Results of the Computer Programme TPHTC to Evaluate the Heat Transfer Characteristics of HSA panel (Key is provided at the end of the table)

W_c	H_c	α	m_o	T_f	T_{io}	T_{oo}	T_w	ΔT_{ow}	ΔT_f	Q_{net}	h_{ocf}	h_{cf}	U_{oa}	U_{oh}
mm	mm	Deg.	$kg.hr^{-1}$	←		^oC	→	K	K	W	←	$W.m^{-2}.K^{-1}$		→
20						166.0	173.7	13.2	1.3	108	136	4298	124	123
30						167.9	173.9	12.5	1.1	127	127	3921	117	115
40	10	43.5	14	175	155	169.6	174.0	11.7	1.0	144	123	3682	113	112
50						171.2	174.1	11.0	0.9	160	121	3512	112	110
	5					169.8	173.7	11.3	1.3	145	183	3754	164	156
	10					167.9	173.9	12.5	1.1	127	127	3921	117	115
30	15	43.5	14	175	155	167.5	174.0	12.7	1.0	123	108	3956	100	100
	20					167.6	174.0	12.6	1.1	124	98	3947	91	92
		30				167.8	173.8	12.4	1.2	126	127	3549	116	115
30	10	45	14	175	155	167.9	173.9	12.5	1.1	127	127	3954	117	115
		60				167.9	174.0	12.5	1.0	127	127	4214	117	115

(continued on the next page)

TABLE A13.6 Summary of the Results of the Computer Programme TPHTC to Evaluate the Heat Transfer Characteristics of HSA panel (*Continued*) (Key is provided on the next page)

W_c	H_c	α	m_o	T_f	T_{io}	T_{oo}	T_w	ΔT_{ow}	ΔT_f	Q_{net}	h_{ocf}	h_{cf}	U_{oa}	U_{oh}
mm	mm	Deg.	$kg.hr^{-1}$	←		°C	→	K	K	W	←	$W.m^{-2}.K^{-1}$		→
			10			170.6	174.1	11.3	0.9	109	121	4109	112	110
			20			165.4	173.7	13.5	1.3	145	134	3754	122	121
			30			162.9	173.5	14.5	1.5	166	143	3596	130	129
30	10	43.5	40	175	155	161.5	173.3	15.0	1.7	181	150	3500	135	135
			50			160.5	173.1	15.4	1.9	192	156	3434	139	140
			60			160.0	173.0	15.6	2.0	201	161	3383	143	144
				165		161.3	164.6	6.5	0.4	61	118	4918	111	108
				170		164.5	169.3	9.5	0.7	93	123	4307	114	112
30	10	43.5	14	175	155	167.9	173.9	12.5	1.1	127	127	3921	117	115
				180		171.3	178.5	15.4	1.5	161	130	3649	119	118
				185		174.7	183.1	18.2	1.9	195	134	3436	121	120
					145	164.9	173.1	18.2	1.9	193	133	3429	120	120
					150	166.4	173.5	15.4	1.5	160	130	3642	119	117
30	10	43.5	14	175	155	167.9	173.9	12.5	1.1	127	127	3921	117	115
					160	169.5	174.3	9.5	0.7	94	123	4315	114	112
					165	171.2	174.6	6.5	0.4	61	118	4941	111	108

TABLE A13.6 Summary of the Results of the Computer Programme TPHTC to Evaluate the Heat Transfer Characteristics of HSA panel (*Continued*)

Notes: W_c = Condenser tube width

H_c = Condenser tube height

α = Collector panel tilt angle

m_o = Oil mass flow rate

T_f = Condensate film temperature

T_{io} = Oil inlet temperature

T_{oo} = Oil outlet temperature

T_w = Condenser tube wall temperature

ΔT_{ow} = Temperature drop across the oil film

ΔT_f = Temperature drop across the condensate film

Q_{net} = Net heat transfer to the oil

h_{ocf} = Oil side film coefficient corrected for free convection and fin effect

h_{cf} = Condensation film coefficient corrected for fin effect

U_{oa} = Overall heat transfer coefficient calculated from the net heat transfer to the oil

U_{oh} = Overall heat transfer coefficient calculated from individual film coefficients

FIGURE A13.2 Effect of the Condenser Tube Width on the Oil Side Film Coefficient

This chart shows how the oil side film coefficient corrected for free convection and fin effect decreases by 11% as the condenser tube width is increased by 150%. The Percentages indicate the changes in the direction the arrows point; for example, $W_c \uparrow$ 150% means as the condenser tube width increases by 150%.

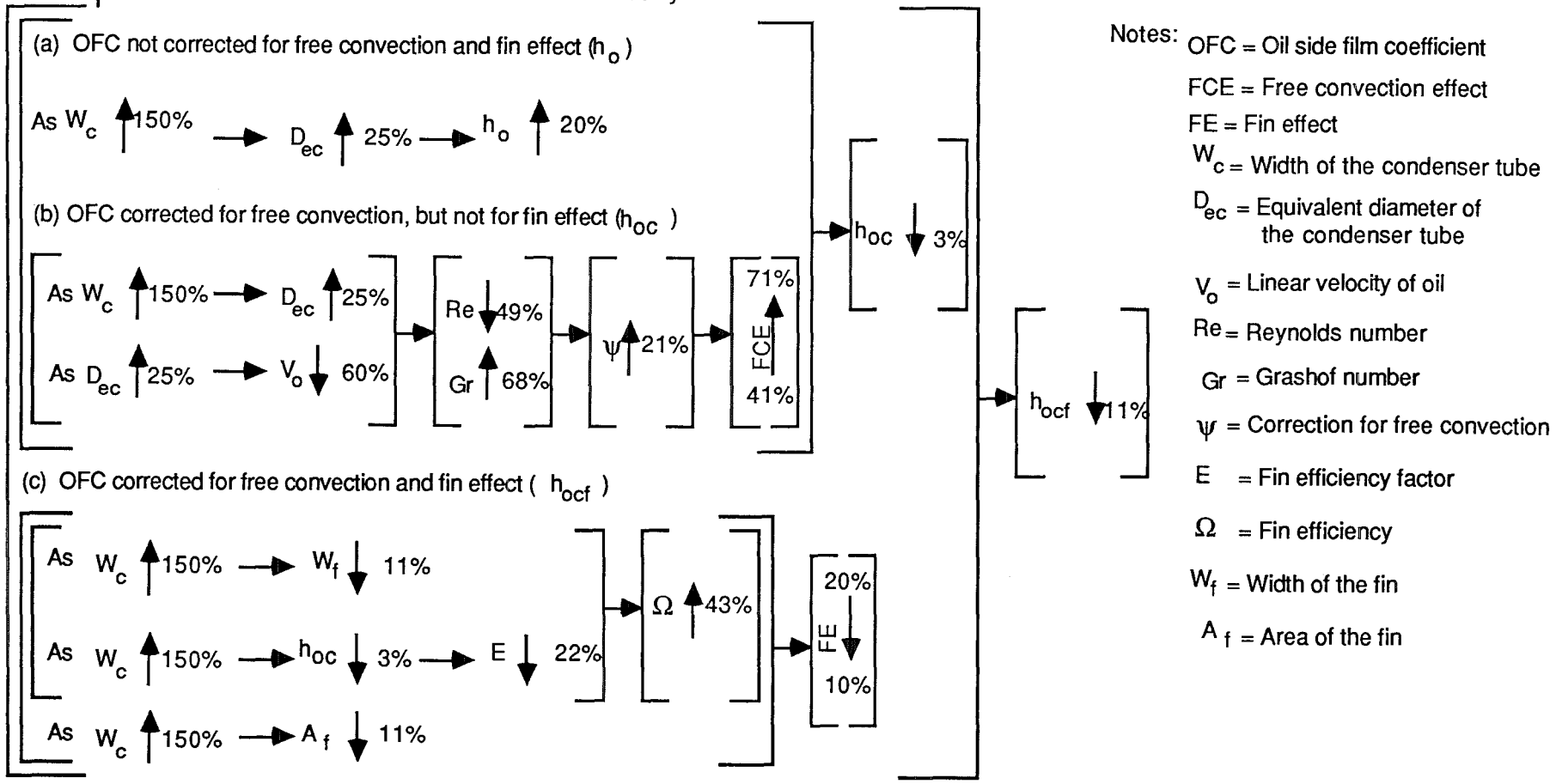

Notes:
- OFC = Oil side film coefficient
- FCE = Free convection effect
- FE = Fin effect
- W_c = Width of the condenser tube
- D_{ec} = Equivalent diameter of the condenser tube
- V_o = Linear velocity of oil
- Re = Reynolds number
- Gr = Grashof number
- ψ = Correction for free convection
- E = Fin efficiency factor
- Ω = Fin efficiency
- W_f = Width of the fin
- A_f = Area of the fin

programme listing (including subroutines, for intrapolating various properties of Mobiltherm and Dowtherm A, at any desired temperature, and for evaluating all the heat transfer coefficients) and a sample set of results are included at the end of this appendix. The summary of results is given in Table A13.6.

A13.6.2 Observations

In order to determine the optimum geometry, dimensions and operating conditions for the solar refrigeration system, one should keep in mind, the individual requirements for each of the following three important parts of the system.

(1) The collector

(2) The condenser or heat exchanger

(3) The refrigerator

Although the condenser is a part of the collector it may be considered seperately from the heat transfer point of view. In the final detailed analysis one should also consider the storage system and oil ammonia liquor heat exchanger along with the above three parts, however for the present discussion they are not included.

From the results listed in Table A13.6 the following observations can be made.

(1) Condenser tube width W_c : As W_c increases all the heat transfer coefficients, temperature drops and ΔP_c decrease, while T_{oo}, T_w and Q_{net} increase, thus some favouring lower and some favouring higher W_c values. To illustrate the inter dependency of different variables a chart is drawn (Fig. A13.2) showing the effect of changes in W_c on OFC. Hence, an intermediate value of 30 or 40 mm is recommended.

(2) Condenser tube height H_c : As H_c increases ΔT_{ow} and T_w increases, while the other quantities decrease rapidly. Hence, 5 mm is preferable

(3) Collector tilt angle α : As α increases from 30° to 60° CFC increases, while the other quantities remain the same. However, this is not an important criterion as the condensate film offers low resistance.

(4) Oil mass flow rate m_o : As m_o increases from 10 to 60 $kg.hr^{-1}$ all other quantities increase except CFC, T_{oo} and T_w. Hence, an intermediate value is preferable. On the other hand energy requirements of the generator of the refrigeration system

fixes the lower limit on m_o, while the pumping costs and the heat losses from the system impose the upper limit. Hence, the whole refrigeration system should be kept in view while deciding m_o.

(5) Condensate film or vapour temperature T_f : Except for CFC, all other quantities increase as T_f goes up. Also as T_f increases the collector efficiency falls. However, insolation on the panel controls T_f.

(6) Oil inlet temperature T_{io} : As T_{io} increases all except T_{oo}, T_w and h_{cf} increase. However, the value of T_{io} depends mainly on the generator operating temperature and various heat losses in the system.

A13.7 Programme Listing of TPCFC

```
100 REM **********    COMPUTER PROGRAMME TPCFC    **********
110 REM
120 REM THIS PROGRAMME EVALUATES THE CONDENSATION FILM
130 REM COEFFICIENT CORRECTED FOR FIN EFFECT AND CHECKS THE
140 REM LIQUID FILM TEMPERATURE TO CONVERGE ON TO THE
150 REM FINAL VALUE OF THE COEFFICIENT
160 REM
170 REM NOTE THAT IT IS POSSIBLE TO FIND THE EFFECTS OF
180 REM CONDENSER TUBE DIMENSIONS, CONDENSER TUBE WALL
190 REM TEMPERATURE, CONDENSATE FILM TEMPERATURE OR VAPOUR
200 REM TEMPERATURE, NET HEAT OUTPUT FROM THE COLLECTOR AND
210 REM HSA PANEL TILT ANGLE ON THE CONDENSATION FILM
220 REM COEFFICIENT
230 REM
240 REM THE INPUT VARIABLES TO THE PROGRAMME ARE:
250 REM 1.CONDENSER TUBE WALL TEMPERATURE IN DEG. CEL. T1
260 REM 2.CONDENSATE FILM TEMPERATURE OR VAPOUR
270 REM   TEMPERATURE IN DEG. CEL. T2
280 REM 3.LIUID THERMAL CONDUCTIVITY AT T2 IN
290 REM   BTU/(HR)(FT)(DEG.FAR) P1
300 REM 4.LIQUID DENSITY AT T2 IN LB/CUB.FT. P2
310 REM 5.LIQUID VISCOSITY AT T2 IN LB/(HR)(FT) P3
320 REM 6.LATENT HEAT OF CONDENSATION AT T2 IN BTU/LB P4
330 REM 7.LENGTH OF CONDENSATION PATH IN FT C1
340 REM 8.ACCELERATION DUE TO GRAVITY IN FT/SQ.HR. G1
350 REM 9.HSA PANEL TILT ANGLE IN DEGREES C2
360 REM 10.NET HEAT OUTPUT FROM THE COLLECTOR IN WATTS Q1
370 REM 11.FIN THICKNESS IN FT C4
380 REM 12.THERMAL CONDUCTIVITY OF THE FIN MATERIAL IN
390 REM    BTU/(HR)(FT)(DEG.FAR.) C5
400 REM 13.FIN WIDTH IN FT C6
410 REM 14.CONDENSATION AREA EXCLUDING FIN AREA IN SQ.FT A1
420 REM 15.FIN AREA IN SQ.FT A3
430 REM
440 REM THE OUTPUT VARIABLES TO THE PROGRAMME ARE:
450 REM
460 REM 1.TEMPERATURE DROP ACROSS THE CONDENSING FILM IN
470 REM   DEG. CEL. T4
480 REM 2.CONDENSATE FILM RESISTANCE IN DEG.CEL./W R1
490 REM 3.CONDENSATION FILM COEFFICIENT NOT CORRECTED FOR
500 REM   FIN EFFECT IN W/(SQ.M)(DEG. CEL.) H3
510 REM 4.CONDENSATION FILM COEFFICIENT CORRECTED FOR FIN
520 REM   EFFECT IN W/(SQ.M)(DEG. CEL.) H6
530 REM
540 OPEN "TPCFC.DAT" FOR OUTPUT AS FILE #5
550 REM
560 REM TO FIND CONDENSATION FILM COEFFICIENTS NOT
570 REM CORRECTED FOR FIN EFFECT H1,H2,H3
580 REM H1 IS IN BTU/(SQ.FT)(HR)(DEG.FAR.)
590 REM H2 IS IN KCAL/(SQ.M)(HR)(DEG.CEL.)
600 REM H3 IS IN W/(SQ.M)(DEG.CEL.)
610 REM
620 T1=165
630 T2=170
640 T3=(T2-T1)*1.8
650 P1=.071
660 P2=58.342
670 P3=1.1858
```

```
680 P4=144
685 C1=3
690 C1=C1/30.4
700 G1=4.16975E+08
710 C2=43.5
720 C3=.688355
730 C4=1.645E-3
740 C5=9.4
750 C6=(30/30.4)-C1
760 A1=C1*100/30.4
770 Q1=132.6
780 REM
790 REM NOTE THAT THE WIDTH OF THE HSA PANEL IS 30 CM AS
    USED IN C6
800 REM AND THE LENGTH OF THE PANEL (WHICH IS ASSUMED TO BE
810 REM THE LENGTH OF THE CONDENSER TUBE, THOUGH IN PRACTICE
820 REM IT IS SLIGHTLY SHORTER) IS 100CM AS USED IN A1
830 REM
840 A$="**********  RESULTS OF THE PROGRAMME TPCFC
    **********"
850 PRINT #5,A$
860 PRINT #5
870 PRINT #5
880 B$="CONDENSER TUBE WALL TEMPERATURE IN DEG.CEL. T1="
890 C$="CONDENSATE FILM OR VAPOUR TEMPERATURE IN DEG.CEL.
    T2="
900 D$="CONDENSER WIDTH OR LENGTH OF CONDENSATION PATH IN
    CM="
910 E$="HSA PANEL TILT ANGLE IN DEGREES C2="
920 F$="NET HEAT OUTPUT FROM THE COLLECTOR IN WATTS Q1="
930 G$="FIN THICKNESS IN MM="
940 H$="FIN WIDTH IN CM="
950 I$="FIN LENGTH IN CM="
960 PRINT #5,B$;T1
970 PRINT #5,C$;T2
980 PRINT #5,D$;C1*30.4
990 PRINT #5,E$;C2
1000 PRINT #5,F$;Q1
1010 PRINT #5,G$;C4*304
1020 PRINT #5,H$;C6*30.4
1030 PRINT #5,I$;(A1/C1*30.4)
1040 PRINT #5
1050 PRINT #5
1060 PRINT #5,"T4 = TEMPERATURE DROP ACROSS THE CONDENSATE"
1070 PRINT #5,"     FILM IN DEG.CEL."
1080 PRINT #5,"R1 = CONDENSATE FILM RESISTANCE IN DEG.CEL."
1090 J$="H3 = CONDENSATION FILM COEFFICIENT NOT CORRECTED"
1100 K$="     FOR FIN EFFECT IN W/(SQ.M)(DEG.CEL)"
1110 L$="H6 = CONDENSATION FILM COEFFICIENT CORRECTED"
1120 M$="     FOR FIN EFFECT IN W/(SQ.M)(DEG.CEL.)"
1130 PRINT #5,J$
1140 PRINT #5,K$
1150 PRINT #5,L$
1160 PRINT #5,M$
1170 PRINT #5
1180 PRINT #5
1190 PRINT #5
1200 PRINT #5,TAB(7);"T4";TAB(22);"R1";TAB(37);"H3";TAB(52)
     ;"H6"
1210 PRINT #5
```

```
1220 PRINT "T4","R1","H3","H4","H5","H6"
1230 PRINT
1240 H1=.943*(((P1^3*P2^2*P4*G1*C3)/(P3*C1*T3))^.25)
1250 H2=H1*4.88
1260 H3=H2/.86
1270 REM
1280 REM TO CALCULATE THE FIN EFFECT
1290 REM
1300 X1=((2*H1)/(C5*C4))^.5
1310 REM
1320 REM TO FIND THE FIN EFFICIENCY E1
1330 REM
1340 X2=X1*C6
1350 E1=1/X2
1360 REM
1370 REM NOTE THAT A2 IS THE HEAT TRANSFER AREA ON WHICH
1380 REM THE CONDENSATION FILM COEFFICIENT IS BASED ON
1390 REM
1400 A2=A1
1410 A3=((3000)/(30.4^2))-A1
1415 A3=2*A3
1420 REM
1430 REM TO FIND THE CONDENSATION FILM COEFFICIENTS
1440 REM CORRECTED FOR FIN EFFECT H4,H5,H6
1450 REM H4 IS IN BTU/(HR)(SQ.FT)(DEG.FAR.)
1460 REM H5 IS IN KCAL/(HR)(SQ.M)(DEG.CEL.)
1470 REM H6 IS IN W/(SQ.M)(DEG.CEL.)
1480 REM
1490 H4=(E1*A3+A1)*H1/A2
1500 H5=H4*4.88
1510 H6=H5/.86
1520 REM
1530 REM TO CHECK THE FILM TEMPERATURE T2
1540 REM
1550 REM TO FIND CONDENSATE FILM RESISTANCE R1 IN DEG.CEL./W
1560 REM
1570 R1=1/(H6*A2*.0929)
1580 T4=Q1*R1
1590 T5=T4*1.8
1600 X3=ABS(T3-T5)
1610 PRINT #5,TAB(4);T4;TAB(17);R1;TAB(34);H3;TAB(49);H6
1620 PRINT T4,R1,H3,H4,H5,H6
1630 T3=T5
1640 IF X3<1.00000E-04 GO TO 1670
1650 T3=T5
1660 GO TO 1240
1670 PRINT #5
1680 END
```

A13.8 Results File TPCFC.DAT

********** RESULTS OF THE PROGRAMME TPCFC **********

CONDENSER TUBE WALL TEMPERATURE IN DEG.CEL. T1= 165
CONDENSATE FILM OR VAPOUR TEMPERATURE IN DEG.CEL. T2= 170
CONDENSER WIDTH OR LENGTH OF CONDENSATION PATH IN CM= 3
HSA PANEL TILT ANGLE IN DEGREES C2= 43.5
NET HEAT OUTPUT FROM THE COLLECTOR IN WATTS Q1= 132.6
FIN THICKNESS IN MM= .50008
FIN WIDTH IN CM= 27
FIN LENGTH IN CM= 100

T4 = TEMPERATURE DROP ACROSS THE CONDENSATE
FILM IN DEG.CEL.
R1 = CONDENSATE FILM RESISTANCE IN DEG.CEL.
H3 = CONDENSATION FILM COEFFICIENT NOT CORRECTED
FOR FIN EFFECT IN W/(SQ.M)(DEG.CEL)
H6 = CONDENSATION FILM COEFFICIENT CORRECTED
FOR FIN EFFECT IN W/(SQ.M)(DEG.CEL.)

T4	R1	H3	H6
1.61982	.122158E-01	2502.15	2714.49
1.23474	.931179E-02	3316.57	3561.04
1.15638	.872082E-02	3549.45	3802.36
1.1382	.858369E-02	3608.12	3863.1
1.13384	.855086E-02	3622.44	3877.93
1.13279	.854294E-02	3625.91	3881.53
1.13254	.854103E-02	3626.75	3882.4
1.13248	.854057E-02	3626.96	3882.61
1.13246	.854046E-02	3627.01	3882.66

A13.9 Programme Listing of TSPQFC

```
10 REM ************ COMPUTER PROGRAMME TSPQFC *************
20 REM
30 REM THIS PROGRAMME EVALUATES THE OILSIDE FILM COEFFICIENT
40 REM AND OVERALL HEAT TRANSFER COEFFICIENT FOR ALL
50 REM POSSIBLE COMBINATIONS OF INLET AND OUTLET
60 REM TEMPERATURES OF OIL AND NET HEAT OUTPUT FROM THE
70 REM COLLECTOR FOR GIVEN CONDENSER TUBE DIMENSIONS
80 REM AND CONDENSER TUBE WALL TEMPERATURE
90 REM
100 REM NOTE THAT IT IS POSSIBLE TO FIND THE EFFECTS OF
110 REM CONDENSER TUBE DIMENSIONS AND CONDENSER TUBE WALL
120 REM TEMPERATURE ON THE HEAT TRANSFER COEFFICIENTS
130 REM BY SIMPLY USING THE REQUIRED INPUT DATA
140 REM
150 REM THE INPUT VARIABLES TO THE PROGRAMME ARE:
160 REM
170 REM 1. INLET OIL TEMPERATURE IN DEG.CEL. T1(I)
180 REM 2. OUTLET OIL TEMPERATURE IN DEG.CEL. T2(I)
190 REM 3. AVERAGE OIL TEMPERATURE IN DEG.CEL. T3(J)
200 REM 4. KINEMATIC VISCOSITY OF THE OIL IN CENTISTOKES
210 REM    V1(J) AT T3(J)
220 REM 5. SPECIFIC HEAT OF THE OIL IN KJ/(KG)(DEG.CEL.)
230 REM    S2(J) AT T3(J)
240 REM 6. THERMAL CONDUCTIVITY OF THE OIL IN
250 REM    W/(M)(DEG.CEL.) K1(J) AT T3(J)
260 REM 7. DENSITY OF THE OIL IN KG/CU.M. R1(J) AT T3(J)
270 REM 8. NET ENERGY TRANSFERRED TO THE OIL IN W Q2(K)
280 REM 9. CONDENSER TUBE WALL TEMPERATURE IN DEG.CEL. T4
290 REM 10. VISCOSITY OF THE OIL IN CENTISTOKES V2 AT T4
300 REM 11. CONDENSER TUBE LENGTH IN M L1
310 REM 12. CONDENSE TUBE WIDTH IN CM B3
320 REM 13. CONDENSER TUBE HEIGHT IN CM B4
330 REM
340 REM THE OUTPUT VARIABLES TO THE PROGRAMME ARE:
350 REM
360 REM 1. MASS FLOW RATE OF THE OIL IN KG/HR M1
370 REM 2. FREE CONVECTION FACTOR S3
380 REM 3. OVERALL HEAT TRANSFER COEFFICIENT BASED ON THE
390 REM    WHOLE CONDENSER TUBE AREA A1 IN W/(SQ.M)(K) H3
400 REM 4. OVERALL HEAT TRANSFER COEFFICIENT BASED ON THE
410 REM    ACTUAL CONTACT AREA A3 BETWEEN THE CONDENSER TUBE
420 REM    AND THE PANEL IN W/(SQ.M)(K) H4
430 REM 5. OILSIDE FILM COEFFICIENT NOT CORRECTED FOR FREE
440 REM    CONVECTION AND FIN EFFECT IN W/(SQ.M)(K) H6
450 REM 6. OILSIDE FILM COEFFICIENT CORRECTED FOR FREE
460 REM    CONVECTION BUT NOT FOR FIN EFFECT IN
470 REM    W/(SQ.M)(K) H8
480 REM
490 DIM T1(9),T2(9),T3(17),V1(17),S2(17),K1(17),R1(17)
500 DIM T8(45),T9(45),M9(45),S9(45),P6(45),P7(45)
510 DIM P8(45),P9(45),Q2(10)
530 REM
540 REM TO READ INLET OIL TEMPERATURES
560 REM FOR I=1 TO9
570 READ T1(I)
580 NEXT I
590 REM
600 REM TO READ OUTLET OIL TEMPERATURES
```

```
620 FOR I=1 TO 9
630 READ T2(I)
640 NEXT I
650 REM
660 REM TO READ AVERAGE OIL TEMPERATURES
680 FOR I=1 TO 17
690 READ T3(I)
700 NEXT I
710 REM
720 REM TO READ OI VISCOSITY VALUES
740 FOR I=1 TO 17
750 READ V1(I)
760 NEXT I
770 REM
780 REM TO READ OIL SPECIFIC HEAT VALUES
800 FOR I=1 TO 17
810 READ S2(I)
820 NEXT I
830 REM
840 REM TO READ OIL THERMAL CONDUCTIVITY VALUES
860 FOR I=1 TO 17
870 READ K1(I)
880 NEXT I
890 REM
900 REM TO READ OIL DENSITY VALUES
920 FOR I=1 TO 17
930 READ R1(I)
940 NEXT I
950 REM
970 REM TO READ NET OUTPUT FROM THE COLLECTOR
980 FOR I=1 TO 10
990 READ Q2(I)
1000 NEXT I
1010 REM
1020 REM INPUT DATA
1040 DATA 15,35,55,75,95,115,135,155,175
1050 DATA 25,45,65,85,105,125,145,165,185
1060 DATA 20,30,40,50,60,70,80,90,100,110,120,130,140
          ,150160,170,180
1070 DATA 49,29,19,13.5,10,7.8,6.3 5.4,3.3,2.8,2.45,
          2.15,1.9,1.7,2,1.58,1.4
1080 DATA 1.9,1.94,1.98,2.03,2.06,2.11,2.16,2.20,2.25,2.30
          ,2.34,2.38,2.42,2.47,2.52,2.56,2.6
1090 DATA 0.1320,0.1312,0.1305,0.1298,0.1290,0.1283,0.1276,
          0.1268,0.1260,0.1254,0.1248,0.1240,0.1233,0.1226,
          0.1219,0.1212,0.1205
1100 DATA 862,856,850,842,835,829,823,816,810,802,795,790
          ,785,778,766,760
1110 DATA 132.6,100,150,200,250,300,350,400,450,500
1120 READ V2,T4,B3,B4,L1
1130 DATA 1.4,185,3,1,1
1140 REM
1150 M=1
1160 Q2=Q2(M)
1170 LPRINT "CONDENSER TUBE WALL TEMPERATURE IN
     DEG.CEL,T4=";T4
1180 LPRINT "VISCOSITY OF OIL IN CENTISTOKES AT T4=";V2
1190 LPRINT "NET HEAT OUTPUT IN WATTS,Q2=";Q2
1200 LPRINT "WIDTH OF THE CONDENSER TUBE IN CM,B3=";B3
1210 LPRINT "HEIGHT OF THE CONDENSER TUBE IN CM,B4="B4
```

```
1220 LPRINT "LENGTHOF THE CONDENSER TUBE IN M,L1=";L1
1230 LPRINT
1250 LPRINT "ALL TEMPERATURES ARE IN DEGREES CELSIUS"
1260 LPRINT "MASS FLOW RATES ARE IN KGS/HR"
1270 LPRINT "HEAT TRANSFER COEFFICIENTS ARE IN W/(SQ.M)(K)"
1280 LPRINT "H3 = OVERALL HEAT TRANSFER COEFFICIENT BASED"
1290 LPRINT "     ON THE WHOLE CONDENSER TUBE AREA A1"
1300 LPRINT "H4 = OVERALL HEAT TRANSFER COEFFICIENT BASED"
1310 LPRINT "     ON THE CONTACT AREA A2"
1320 LPRINT "H6 = OILSIDE FILM COEFFICIENT NOT CORRECTED"
1330 LPRINT "     FOR FREE CONVECTION AND FIN EFFECT"
1340 LPRINT "H8 = OIL SIDE FILM COEFFICIENT CORRECTED FOR"
1350 LPRINT "     FREE CONVECTION BUT NOT FOR FIN EFFECT"
1360 LPRINT
1380 L=1
1390 I=1
1400 J=1
1410 X9=(T1(I)+T2(J))/2
1420 K=1
1430 IF X9=T3(K) THEN GOTO 1490
1440 K=K+1
1450 GOTO 1430
1460 REM
1470 REM TO FIND MASS FLOW RATE OF OIL M1 IN KG/HR
1490 Q1 = Q1*0.86
1500 S1 = S2(K)/4.1873
1510 M1=Q1/(S1*(T2(J)-T1(I)))
1520 REM
1530 REM TO FIND EQUIVALENT DIAMETER D2 IN M
1550 B1=B3/100
1560 B2=B4/100
1570 D1=(2*B1*B2)/(B1+B2)
1580 D2=D1*100
1590 REM
1600 REM TO FIND OVERALL HEAT TRANSFER COEFFICIENTS H1
1610 REM AND H2 IN KCAL/(HR)(SQ.M)(K) AND H3 AND H4
1620 REM IN W/(SQ.M)(K)
1630 REM H1 AND H3 ARE BASED ON WHOLE CONDENSER TUBE SREA A1
1640 REM H2 AND H4 ARE BASED ON CONTACT AREA A2
1650 REM
1660 T5=T4-T3(K)
1670 A1=L1*B1
1680 A2=2*L1*(B1+B2)
1690 H1=Q1/(A1*T5)
1700 H2=Q1/(A2*T5)
1710 H3=H1/0.86
1720 H4=H2/0.86
1730 REM
1750 REM TO FIND GREATZ NUMBER G1
1760 K2=K1(K)/0.86
1770 G1=(M1*S1)/(K2*L1)
1790 TO FIND VISCOSITY CORRECTION FACTOR P1
1810 P1=(V1(K)/V2)[0.14
1840 TO FIND NUSSULT NUMBER N1
1850 N1=2*PI*(G1[0.3333)
1860 REM
1870 REM TO FIND OIL SIDE FILM COEFFICIENT NOT CORRECTED
1880 REM FOR FREE CONVECTION AND FIN EFFECT H5 AND H6
1890 REM H5 IS IN KCAL/(HR)(SQ.M)(DEG.CEL)
1900 REM H6 IS IN W/(SQ.M)(DEG.CEL)
```

```
1920 H5=(N1*K2)/D1
1930 H6=H5/0/86
1940 REM TO FIND GRASSHOF NUMBER G3
1970 R2=R1(K)/1000
1980 V3=(V1(K)*R2)/100
1990 V4=V3*360
2000 B5=0.000809
2010 G2=1.2714E08
2020 G3=((D1[3)*(R1(K)[2)*G2*B5*T5)/(V4[2)
2040 REM TO FIND REYNOLDS NUMBER R3
2060 M2=M1/3.6
2070 F1=M1/R2
2080 A3=B3*B4
2090 U1=F1/A3
2100 R3=(D2*U1*R2)/V3
2120 REM TO FIND FREE CONVECTION FACTOR S3
2140 X8=LOG(R3)/LOG(10)
2150 S3=(2.25*(1+(0.01*(G3[0.333333))))/X8
2170 REM TO FIND OIL SIDE FILM COEFFICIENT CORRECTED FOR
2180 REM FREE CONVECTION BUT NOT FOR FIN EFFECT H7 & H8
2190 REM H7 IS IN KCAL/(HR)(SQ.M)(DEG.CEL)
2200 REM H8 IS IN W/(SQ.M)(K)
2220 H7=H5*S3
2230 H8=H7/0/86
2240 T8(L)=T1(I)
2250 T9(L)=T2(J)
2260 M9(L)=M1
2270 S9(L)=S3
2280 P6(L)=H3
2290 P7(L)=H4
2300 P8(L)=H6
2310 P9(L)=H8
2320 L=L+1
2330 IF J=9 GOTO 2360
2340 J=J+1
2350 GOTO 1410
2360 IF I=9 GOTO 2390
2370 I=I+1
2380 GOTO 1400
2390 LPRINT "INLET""OUTLET'"MASS FLOW""H.T.C.""H.T.C."
2400 LPRINT "TEMP-T1""TEMP-T2""RATE-M1"" H3 "" H4 "
2410 LPRINT
2420 FOR L=1 TO 45
2430 LPRINT TAB(4)T8(L);TAB(16)T9(L);TAB(26)M9(L);
          TAB(37)P6(L);TAB(49)P7(L)
2440 NEXT L
2450 LPRINT CHR$(12)
2460 LPRINT
2490 LPRINT "INLET""OUTLET""FREE CONV.""H.T.C.""H.T.C."
2500 LPRINT "TEMP-T1""TEMP-T2""FACTOR-S3"" H6 "" H8 "
2510 LPRINT
2520 FOR L=1 TO 45
2530 LPRINT TAB(4)T8(L);TAB(16)T9(L);TAB(26)S9(L);
     TAB(37)P8(L);TAB(49)P9(L)
2540 NEXT L
2550 LPRINT
2600 IF M=M+1
2620 GOTO 1160
2630 END
```

A13.10 Results File TSPQFC.DAT

CONDENSER TUBE WALL TEMPERATURE IN DEG CEL,T4= 175
VISCOSITY OF OIL IN CENTYSTOKES AT T4= 1.4
NET HEAT OUTPUT FROM THE COLLECTOR IN WATTS,Q2= 132.6
WIDTH OF THE CONDENSER TUBE IN CM,B3= 3
HEIGHT OF THE CONDENSER TUBE IN CM,B4= 1
LENGTH OF THE CONDENSER TUBE IN M,L1= 1

ALL TEMPERATURES ARE IN DEGREES CELCIUS
MASS FLOW RATES ARE IN KG/HR
HEAT TRANSFER COEFFICIENTS IN W/(SQ.M)(DEG.CEL.)

H3 = OVERALL HEAT TRANSFER COEFFICIENT
BASED ON THE WHOLE CONDENSER TUBE AREA A1
H4 = OVERALL HEAT TRANSFER COEFFICIENT
BASED ON THE CONTACT AREA A2
H6 = OIL SIDE FILM COEFFICIENT NOT CORRECTED
FOR FREE CONVECTION AND FIN EFFECT
H8 = OIL SIDE FILM COEFFICIENT CORRECTED FOR
FREE CONVECTION BUT NOT FOR FIN EFFECT

INLET TEMP.-T1	OUTLET TEMP.-T2	MASS FLOW RATE-M1	H.T.C. H3	H.T.C. H4
15	25	25.1317	28.5161	10.6936
15	45	8.20452	30.4828	11.431
15	65	4.82326	32.7407	12.2778
15	85	3.36033	35.36	13.26
15	105	2.57553	38.4348	14.413
15	125	2.05732	42.0952	15.7857
15	145	1.70051	46.5263	17.4474
15	165	1.44698	52	19.5
35	45	24.1163	32.7407	12.2778
35	65	7.84077	35.36	13.26
35	85	4.63595	38.4348	14.413
35	105	3.23292	42.0952	15.7857
35	125	2.45629	46.5263	17.4474
35	145	1.97315	52	19.5
35	165	1.63249	58.9333	22.1
55	65	23.1798	38.4348	14.413
55	85	7.54349	42.0952	15.7857
55	105	4.42132	46.5263	17.4474
55	125	3.10067	52	19.5
55	145	2.35804	58.9333	22.1
55	165	1.88736	68	25.5
75	85	22.1066	46.5263	17.4474
75	105	7.23489	52	19.5
75	125	4.24447	58.9333	22.1
75	145	2.96586	68	25.5
75	165	2.26735	80.3636	30.1364
95	105	21.2224	58.9333	22.1
95	125	6.92033	68	25.5
95	145	4.08122	80.3636	30.1364
95	165	2.86616	98.2222	36.8333
115	125	20.4061	80.3636	30.1364
115	145	6.68772	98.2222	36.8333
115	165	3.94631	126.286	47.3572
135	145	19.7315	126.286	47.3572
135	165	6.44404	176.8	66.3

155	165	18.9485	294.667	110.5

INLET TEMP.-T1	OUTLET TEMP.-T2	FREE CONV. FACTOR-S3	H.T.C. H6	H.T.C. H8
15	25	2.7476	164.566	452.161
15	45	3.96569	105.596	418.762
15	65	4.42677	83.6449	370.277
15	85	4.63593	71.0222	329.254
15	105	4.67725	62.37	291.72
15	125	4.73798	56.1363	265.973
15	145	4.78435	51.3441	245.648
15	165	4.7111	47.1957	222.344
35	45	2.07701	143.031	297.076
35	65	2.89765	94.2005	272.96
35	85	3.33135	75.8694	252.748
35	105	3.63291	65.2643	237.099
35	125	3.85052	58.0396	223.483
35	145	3.94393	52.3361	206.41
35	165	3.99618	47.7769	190.925
55	65	1.86327	129.735	241.731
55	85	2.52772	86.5634	218.808
55	105	2.93487	70.6017	207.207
55	125	3.18751	60.8461	193.948
55	145	3.36096	54.0072	181.516
55	165	3.48569	49.0143	170.849
75	85	1.7775	120.727	214.592
75	105	2.34455	80.7034	189.213
75	125	2.68001	65.6965	176.067
75	145	2.91174	56.9842	165.923
75	165	3.07539	51.0499	156.999
95	105	1.72374	112.339	193.644
95	125	2.22496	75.5812	168.165
95	145	2.517	62.0991	156.304
95	165	2.71675	54.2495	147.382
115	125	1.68119	106.188	178.522
115	145	2.1221	71.9539	152.693
115	165	2.3631	59.3641	140.283
135	145	1.61588	101.511	164.03
135	165	1.98261	68.9143	136.63
155	165	1.48297	97.6427	144.802

A13.11 Programme Listing of TPHTC

```
100 REM **********    COMPUTER PROGRAMME TPHTC    **********
110 REM               ******** ********* *****
120 REM
130 REM THIS PROGRAMME EVALUATES THE DESIGN CHARACTERISTICS
140 REM OF THE HEAT SHEET ABSORBER PLATE
150 REM
160 REM IT EVALUATES THE FOLLOWING VARIABLES FOR EACH
170 REM INTEGRATED SECTION OF THE CONDENSER TUBE AND
180 REM ABSORBER PLATE:
190 REM 1.THE OIL SIDE FILM COEFFICIENT CORRECTED FOR FREE
200 REM   CONVECTION AND FOR FIN EFFECT H5 TO H9
210 REM 2.THE CONDENSATION FILM COEFFICIENT CORRECTED
220 REM   FOR FIN EFFECT C1 TO C4
230 REM 3.THE OVERALL HEAT TRANSFER COEFFICIENTS H1 TO H4,UO
240 REM 4.CONDENSER TUBE WALL TEMPERATURE  T4
250 REM 5.NET HEAT TRANSFERED FROM THE COLLECTOR TO
260 REM   THE OIL Q1,Q2
270 REM 6.OUTLET TEMPERATURE OF THE  OIL T2
280 REM 7.TEMPERATURE DROP ACROSS THE OIL FILM TDO
290 REM 8.TEMPERATURE DROP ACROSS THE CONDENSATE FILM TCO
300 REM 9.EQUIVALENT DIAMETER OF THE CONDENSER TUBE D2
310 REM 10.REYNOLDS NUMBER OF THE OIL R3
320 REM
330 REM THE MAIN INPUT VARIABLES TO THE PROGRAMME ARE:
340 REM 1.MASS FLOW RATE OF THE OIL IN KG/HR M1
350 REM 2.DOW-A VAPOUR TEMPERATURE OR CONDENSATE FILM
360 REM   TEMPERATURE IN DEG.CEL. T8
370 REM 3.INLET OIL TEMPERATURE IN DEG.CEL. T1
380 REM 4.CONDENSER TUBE DIMENSIONS--
390 REM   (a)WIDTH IN CM B3
400 REM   (b)HEIGHT IN CM B4
410 REM   (c)INTEGRATED LENGTH IN CM L2
420 REM 5.HSA PANEL WIDTH IN M W1
430 REM 6.HSA PANEL TILT ANGLE TO THE HORIZONTAL IN DEG A4
440 REM
450 REM NOTE THAT IT IS POSSIBLE TO FIND THE EFFECTS OF
460 REM ALL THESE INPUT QUANTITIES ON VARIOUS OUTPUTS
470 REM LISTED ABOVE BY SIMPLY CHANGING THE INPUT VALUES
480 REM
490 DIM V1A(21),S2A(21),K1A(21),R1A(21),T3A(21)
500 DIM T8A(7),P2A(7),P3A(7),P4A(7),P5A(7)
510 OPEN "TPHTC.DAT" FOR OUTPUT AS FILE #5
520 REM
530 REM INPUT VALUES
540 REM
550 M1=14
560 T8=175
570 T1=155
580 B3=3
590 B4=1
600 L2=100
610 W1=.3
620 A4=43.5
630 REM
640 REM TO READ OIL PROPERTIES
650 REM
660 GOSUB 6330
670 REM
```

```
680 REM TO READ DOW-A PROPERTIES
690 REM
700 GOSUB 6750
710 REM
720 REM TO EVALUATE DOW-A PROPERTIES AT T4
730 REM
740 GOSUB 5980
750 REM
760 PRINT "T1","T2","T4","Q2","C4","H9"
770 A$="*****  RESULTS OF THE COMPUTER PROGRAMME TPHTC
    *****"
780 PRINT #5,A$
790 PRINT #5
800 PRINT #5
810 PRINT #5
820 J$="THE INPUT DATA:"
830 PRINT #5,J$
840 PRINT #5
850 B$="MASS FLOW RATE OF THE OIL IN KG/HR            M1 ="
860 C$="DOW-A VAPOUR TEMPERATURE IN DEG.CEL.          T8 ="
870 D$="INLET OIL TEMPERATURE IN DEG.CEL.             T1 ="
880 E$="CONDENSER TUBE WIDTH IN CM                    B3 ="
890 F$="CONDENSER TUBE HEIGHT IN CM                   B4 ="
900 G$="CONDENSER TUBE LENGTH IN CM                   L2 ="
910 H$="HSA PANEL WIDTH IN M                          W1 ="
920 I$="HSA PANEL TILT ANGLE TO THE HORIZONTAL IN DEG A4 ="
930 PRINT #5,B$;M1
940 PRINT #5,C$;T8
950 PRINT #5,D$;T1
960 PRINT #5,E$;B3
970 PRINT #5,F$;B4
980 PRINT #5,G$;L2
990 PRINT #5,H$;W1
1000 PRINT #5,I$;A4
1010 PRINT #5
1020 PRINT #5
1030 K$="THE RESULTS:"
1040 PRINT #5,K$
1050 PRINT #5
1060 FOR L=1 TO 1
1070 REM
1080 REM CONDENSER TUBE WALL TEMPERATURE IS FIRST ASSUMED,
1090 REM VARIOUS UNKNOWN QUANTITIES EVALUATED AND FINALLY
1100 REM IT IS CONVERGED USING BISECTION METHOD
1110 REM
1120 Y5=T8-2
1130 Y6=T8
1140 T4=(Y5+Y6)/2
1150 REM
1160 REM TO EVALUATE CONDENSATION FILM COEFFICIENT NOT
1170 REM CORRECTED FOR FIN EFFECT
1180 REM
1190 GOSUB 3810
1200 REM
1210 REM TO FIND THE CONTACT AREA BETWEEN THE CONDENSER
1220 REM AND THE HSA PANEL IN SQ.M A2
1230 REM
1240 B1=B3/100
1250 B2=B4/100
1260 L1=L2/100
```

```
1270 A2=L1*B1
1280 REM
1290 REM F2,F3,F4 REPRESENT THE FIN WIDTH, LENGTH AND
1300 REM THICKNESS RESPECTIVELY, WHILE K3 STANDS FOR THE
1310 REM THERMAL CONDUCTIVITY OF THE FIN MATERIAL
1320 REM
1330 F2=W1-B1
1340 F3=L1
1350 F4=5.00000E-04
1360 K3=16.269
1370 REM
1380 REM TO FIND THE FIN EFFECT FOR THE CONDENSATION
1390 REM FILM COEFFICIENT
1400 REM
1410 GOSUB 4520
1420 REM
1430 REM TO FIND THE KINEMATIC VISCOSITY V2 AND DENSITY R4
1440 REM OF THE OIL AT THE CONDENSER WALL TEMPERATURE T4
1450 REM
1460 T9=T4
1470 GOSUB 5520
1480 V2=V1
1490 R4=R1
1500 Q2=A2*C4*(T8-T4)
1510 REM TO FIND THE NET HEAT TRANSFER BETWEEN THE OIL AND
1520 REM DOW-A Q2 IN W AND Q1 IN KCAL/HR
1530 REM
1540 Q1=Q2*.86
1550 REM
1560 REM TO ASSUME OIL OUTLET TEMPERATURE T2 IN DEG.CEL.
1570 REM
1580 T2=T1+0.1
1590 T3=(T1+T2)/2
1600 REM
1610 REM TO FIND THE OIL SPECIFIC HEAT AT THE AVERAGE
1620 REM TEMPERATURE OF THE OIL T3
1630 REM
1640 T9=T3
1650 GOSUB 5520
1660 S1=S2/4.1873
1670 REM
1680 REM Z5=TEMPERATURE RISE IN OIL
1690 REM Z7=NEW OIL OUTLET TEMPERATURE
1700 REM
1710 Z5=Q1/(M1*S1)
1720 Z7=T1+Z5
1730 REM
1740 REM TO CONVERGE ON TO THE OIL OUTLET TEMPPERATURE T2
1750 REM
1760 X6=ABS(T2-Z7)
1770 IF X6<1.00000E-02 GO TO 1820
1780 REM
1790 REM TO FIND THE ACTUAL OIL OUTLET TEMPERATURE T2
1800 T2=T1+Z5
1810 GO TO 1590
1820 T2=T1+Z5
1830 REM
1840 REM TO FIND THE OIL SIDE FILM COEFFICIENT CORRECTED
1850 REM FOR FREE CONVECTION BUT NOT FOR FIN EFFECT
1860 REM
```

```
1870 GOSUB 3040
1880 REM
1890 REM TO FIND THE OIL SIDE FILM COEFFICIENT CORRECTED
1900 REM FOR FREE CONVECTION AND FIN EFFECT
1910 REM
1920 GOSUB 4190
1930 T3=(T1+T2)/2
1940 REM
1950 REM A1=HEAT TRANSFER AREA FOR OIL SIDE FILM COEFFICIENT
1960 REM Z6=CALCULATED NET HEAT TRANSFER (NEW)
1970 REM
1980 A1=2*L1*(B1+B2)
1990 Z6=A1*H9*(T4-T3)
2000 REM
2010 REM TO USE BISECTION METHOD TO CONVERGE ON TO THE
2020 REM CONDENSER WALL TEMPERATURE T4
2030 X7=Q2-Z6
2040 IF X7>1.00000E-02 GO TO 2070
2050 IF X7<-1.00000E-02 GO TO 2070
2060 GO TO 2130
2070 IF X7>0 GO TO 2100
2080 Y6=T4
2090 GO TO 1140
2100 Y5=T4
2110 GO TO 1140
2120 REM
2130 PRINT T1,T2,T4,Q2,C4,H9
2140 REM
2150 REM TO CALCULATE THE TEMPERATURE DROPS ON OIL SIDE
2160 REM AND CONDENSATION SIDE
2170 REM
2180 T3=(T1+T2)/2
2190 TDO=T4-T3
2200 TDC=T8-T4
2210 REM
2220 L$="OUTLET TEMPERATURE OF THE OIL IN DEG.CEL.      T2 ="
2230 M$="CONDENSER TUBE WALL TEMPERATURE IN DEG.CEL.    T4 ="
2240 X1$="TEMPERATURE DROP ACROSS OIL FILM IN DEG.CEL. TDO="
2250 X2$="TEMPERATURE DROP ACROSS THE CONDENSATE"
2260 X3$="FILM IN DEG.CEL.                              TDC="
2270 X4$="EQUIVALENT DIAMETER OF CONDENSER TUBE IN CM   D2 ="
2280 X5$="REYNOLDS OF THE OIL (DIMENSIONLESS)           R3 ="
2290 N$="NET HEAT TRANSFERRED TO THE OIL IN W           Q2 ="
2300 O$="OIL SIDE FILM COEFFICIENT NOT CORRECTED FOR FREE"
2310 P$="CONVECTION & FIN EFFECT IN W/(SQ.M)(DEG.CEL.) H6 ="
2320 Q$="OIL SIDE FILM COEFFICIENT CORRECTED FOR FREE"
2330 R$="CONVECTION BUT NOT FOR FIN EFFECT IN"
2340 S$="W/(SQ.M)(DEG.CEL.)                             H8 ="
2350 T$="OIL SIDE FILM COEFFICIENT CORRECTED FOR FREE"
2360 U$="CONVECTION  & FIN EFFECT IN W/(SQ.M)(DEG.CEL.)H9 ="
2370 V$="CONDENSATION FILM COEFFICIENT NOT CORRECTED"
2380 W$="FOR FIN EFFECT IN W/(SQ.M)(DEG.CEL.)           C3 ="
2390 X$="CONDENSATION FILM COEFFICIENT CORRECTED"
2400 Y$="FOR FIN EFFECT IN W/(SQ.M)(DEG.CEL.)           C4 ="
2410 PRINT #5,L$;T2
2420 PRINT #5,M$;T4
2430 PRINT #5,X1$;TDO
2440 PRINT #5,X2$
2450 PRINT #5,X3$;TDC
2460 PRINT #5,X4$;D2
```

```
2470 PRINT #5,X5$;R3
2480 PRINT #5,N$;Q2
2490 PRINT #5,O$
2500 PRINT #5,P$;H6
2510 PRINT #5,Q$
2520 PRINT #5,R$
2530 PRINT #5,S$;H8
2540 PRINT #5,T$
2550 PRINT #5,U$;H9
2560 PRINT #5,V$
2570 PRINT #5,W$;C3
2580 PRINT #5,X$
2590 PRINT #5,Y$;C4
2600 REM
2610 REM TO FIND OUT THE OVERALL HEAT TRANSFER COEFFICIENTS
2620 REM
2630 GOSUB 5180
2640 REM
2650 Z1$="OVERALL HEAT TRANSFER COEFFICIENT BASED ON"
2660 Z2$="THE TOTAL AREA OF THE CONDENSER TUBE A1, IN"
2670 Z3$="W/(SQ.M)(DEG.CEL.)                                    H3 ="
2680 Z4$="OVERALL HEAT TRANSFER COEFFICIENT BASED ON"
2690 Z5$="THE CONTACT AREA OF THE CONDENSER TUBE A2, IN"
2700 Z6$="W/(SQ.M.)(DEG.CEL.)                                   H4 ="
2710 Z7$="OVERALL HEAT TRANSFER COEFFICIENT CALCULATED"
2720 Z8$="FROM INDIVIDUAL FILM COEFFICIENTS"
2730 Z9$="IN W/(SQ.M)(DEG.CEL.)                                 UO ="
2740 PRINT #5,Z1$
2750 PRINT #5,Z2$
2760 PRINT #5,Z3$;H3
2770 PRINT #5,Z4$
2780 PRINT #5,Z5$
2790 PRINT #5,Z6$;H4
2800 PRINT #5,Z7$
2810 PRINT #5,Z8$
2820 PRINT #5,Z9$;UO
2830 REM
2840 T1=T2
2850 NEXT L
2860 REM
2870 REM THIS IS A SUBROUTINE TO EVALUATE THE OIL SIDE FILM
2880 REM COEFFICIENTS CORRECTED FOR FREE CONVECTION,
2890 REM BUT NOT FOR FIN EFFECT
2900 REM
2910 REM INPUT VARIBLES ARE--
2920 REM 1.MASS FLOW RATE OF THE OIL IN KG/HR M1
2930 REM 2.INLET OIL TEMPERATURE IN DEG.CEL. T1
2940 REM 3.OUTLET OIL TEMPERATUREIN DEG.CEL. T2
2950 REM 4.CONDENSER TUBE WALL TEMPERATURE IN DEG.CEL. T4
2960 REM 5.CONDENSER TUBE DIMENSIONS-
2970 REM   (a)WIDTH IN CM B3
2980 REM   (b)HEIGHT IN CM B4
2990 REM   (c)LENGTH IN CM L2
3000 REM 6.ALL THE OIL PROPERTIES AT AVERAGE TEMPERATURE T3
3010 REM
3020 REM *TO EVALUATE THE GREATZ NUMBER (G1)*
3030 REM
3040 S1=S2/4.1873
3050 K2=K1*.86
3060 L1=L2/100
```

```
3070 G1=(M1*S1)/(K2*L1)
3080 REM
3090 REM *TO EVALUATE THE VISCOSITY CORRECTION FACTOR (P1)
3100 REM
3110 R2=R1/1000
3120 V3=(V1*R2)/100
3130 V4=V3*360
3140 R5=R4/1000
3150 V5=(V2*R5)/100
3160 V6=V5*360
3170 P1=(V4/V6)^.14
3180 REM
3190 REM *TO EVALUATE THE NUSSELTS NUMBER (N1)*
3200 REM
3210 N1=2*P1*(G1^.333333)
3220 REM
3230 REM *TO EVALUATE THE OIL SIDE FILM COEFFICIENTS H5,H6
3240 REM NOT CORRECTED FOR FREE CONVECTION AND FIN EFFECT*
3250 REM H5 IS IN KCAL/(HR)(SQ.M)(DEG.CEL.)
3260 REM H6 IS IN W/(SQ.M)(DEG.CEL.)
3270 REM
3280 B1=B3/100
3290 B2=B4/100
3300 D1=(2*B1*B2)/(B1+B2)
3310 D2=D1*100
3320 H5=(N1*K2)/D1
3330 H6=H5/.86
3340 REM
3350 REM *TO EVALUATE THE GROSSHOF NUMBER G3*
3360 REM
3370 T3=(T1+T2)/2
3380 B5=8.09000E-04
3390 G2=1.27140E+08
3400 T5=T4-T3
3410 G3=((D1^3)*(R1^2)*G2*B5*T5)/(V4^2)
3420 REM
3430 REM *TO EVALUATE THE REYNOLDS NUMBER R3
3440 REM
3450 F1=M1/R1
3460 A3=B1*B2
3470 U1=F1/A3
3480 R3=(D1*U1*R1)/V4
3490 REM
3500 REM *TO EVALUATE THE FREE CONVECTION CORRECTION
3510 REM FACTOR S3*
3520 REM
3530 X1=LOG(R3)/LOG(10)
3540 X=ABS(X1)
3550 S3=(2.25*(1+(.01*(G3^.333333))))/X
3560 REM
3570 REM *TO EVALUATE THE OIL SIDE FILM COEFFICIENTS
3580 REM CORRECTED FOR FREE CONVETOIN BUT NOT FOR FIN
3590 REM EFFECT H7,H8*
3600 REM H7 IS IN KCAL/(HR)(SQ.M)(DEG.CEL.)
3610 REM H8 IS IN W/(SQ.M)(DEG.CEL.)
3620 REM
3630 H7=H5*S3
3640 H8=H7/.86
3650 RETURN
3660 REM
```

```
3670 REM ***THIS IS A SUBROUTINE TO EVALUATE THE
3680 REM CONDENSATION FILM COEFFICIENT NOT CORRECTED
3690 REM FOR FIN EFFECT***
3700 REM
3710 REM THE INPUT VARIBLES ARE--
3720 REM 1.VAPOUR TEMPERATURE OR CONDENSATE
3730 REM   FILM TEMPERATURE IN DEG.CEL.T8
3740 REM 2.CONDENSER TUBE WALL TEMPERATURE IN DEG.CEL. T4
3750 REM 3.CONDENSER TUBE WIDTH IN CM B3
3760 REM 4.THE ANGLE BETWEEN THE COLLECTOR PLATE
3770 REM   AND THE HORIZONTAL IN DEGREES A4
3780 REM 5.ALL PROPERTIES OF DOWTHERM-A AT THE
3790 REM   AVARAGE TEMPERATURE T3
3800 REM
3810 T6=T8-T4
3820 T7=T6*1.8
3830 P6=P5*2.42
3840 B6=B3/30.4
3850 A5=(A4*PI)/180
3860 G4=4.16975E+08
3870 X2=(P2^3)*(P4^2)*P3*G4*(SIN(A5))
3880 X3=P6*B6*T7
3890 REM
3900 REM C1 IS IN BTU/(HR)(SQ.FT)(DEG.FAR.)
3910 REM C2 IS IN KCAL/(HR)(SQ.M)(DEG.CEL.)
3920 REM C3 IS IN W/(SQ.M)(DEG.CEL.)
3930 REM
3940 C1=.943*((X2/X3)^.25)
3950 C2=C1*4.88
3960 C3=C2/.86
3970 RETURN
3980 REM
3990 REM ***THIS IS A SUBROUTINE TO FIND OUT THE FIN
4000 REM EFFECT FOR THE OIL SIDE FILM COEFFICIENT H8
4010 REM TO GET A CORRECTED COEFFICIENT H9***
4020 REM
4030 REM H8 AND H9 ARE IN W/(SQ.M)(DEG.CEL.)
4040 REM
4050 REM THE INPUT VARIABLES ARE--
4060 REM 1.THE OIL SIDE FILM COEFFICIENT H8
4070 REM 2.THE FIN DIMENSIONS-
4080 REM   (a)WIDTH IN M F2
4090 REM   (b)LENGTH IN M F3
4100 REM   (c)THICKNESS IN M F4
4110 REM 3.THE THERMAL CONDUCTIVITY OF THE FIN
4120 REM   MATERIAL IN W/(M)(DEG.CEL.) K3
4130 REM 4.CONDENSER TUBE DIMENSIONS-
4140 REM   (a)WIDTH IN M B1
4150 REM   (b)HEIGHT IN M B2
4160 REM
4170 REM TO FIND THE FIN EFFICIENCY E1
4180 REM
4190 P7=2*(F3+F4)
4200 A6=F3*F4
4210 M2=((H8*P7)/(K3*A6))^.5
4220 X4=M2*F2
4230 Y3=-X4
4240 IF X4>25 GO TO 4270
4250 Y1=(EXP(X4)-EXP(Y3))/(EXP(X4)+EXP(Y3))
4260 GO TO 4280
```

```
4270 Y1=1
4280 E1=Y1/X4
4290 A7=2*F2*F3
4300 A8=2*F3*(B1+B2)
4310 H9=H8+((H8*E1*A7)/A8)
4320 RETURN
4330 REM
4340 REM
4350 REM ***THIS IS A SUBROUTINE TO FIND OUT THE FIN
4360 REM EFFECT FOR THE CONDENSATION FILM COEFFICIENT C3
4370 REM TO GET A CORRECTED CONDENSATION FILM
4380 REM COEFFICIENT C4***
4390 REM
4400 REM C3 AND C4 ARE IN W/(SQ.M)(DEG.CEL.)
4410 REM
4420 REM THE INPUT VARIABLES ARE--
4430 REM 1.CONDENSATION FILM COEFFICIENT C3
4440 REM 2.THE FIN DIMENSIONS-
4450 REM    (a)WIDTH IN M F2
4460 REM    (b)LENGTH IN M F3
4470 REM    (c)THICKNESS IN M F4
4480 REM 3.THE THERMAL CONDUCTIVITY OF THE FIN MATERIAL
4490 REM    IN W/(M)(DEG.CEL.) K3
4500 REM 4.THE CONDENSER TUBE WIDTH IN M B1
4510 REM
4520 P7=2*(F3+F4)
4530 A6=F3*F4
4540 M3=((C3*P7)/(K3*A6))^.5
4550 X5=M3*F2
4560 Y4=-X5
4570 IF X5>25 GO TO 4600
4580 Y2=(EXP(X5)-EXP(Y4))/(EXP(X5)+EXP(Y4))
4590 GO TO 4640
4600 Y2=1
4610 REM
4620 REM TO FIND THE FIN EFFICIENCY E2
4630 REM
4640 E2=Y2/X5
4650 A9=B1*F3
4660 A7=2*F2*F3
4670 C4=C3+((C3*E2*A7)/A9)
4680 RETURN
4690 REM
4700 REM
4710 REM ***THIS IS A SUBROUTINE TO EVALUATE THE OVERALL
4720 REM HEAT TRANSFER COEFFICIENTS***
4730 REM
4740 REM THE INPUT VARIABLES ARE--
4750 REM 1.THE MASS FLOW RATE OF THE OIL IN KG/HR M1
4760 REM 2.THE SPECIFIC HEAT OF THE OIL IN
4770 REM    KJ/(KG)(DEG.CEL.) S2
4780 REM 3.THE INLET TEMPERATURE OF OIL IN DEG.CEL. T1
4790 REM 4.THE OUTLET TEMPERATURE OF OIL IN DEG.CEL. T2
4800 REM 5.THE TEMPERATURE DROP ACROSS THE OIL
4810 REM    FILM IN DEG.CEL. TDO
4820 REM 6.THE TEMPERATURE DROP ACROSS THE
4830 REM    CONDENSATE FILM IN DEG.CEL. TDC
4840 REM 7.EQUIVALENT DIAMETER OF THE CONDENSER
4850 REM    TUBE IN M D1
4860 REM 8.CONDENSER TUBE WALL THICKNESS IN M F4
```

```
4870 REM 9.THERMAL CONDUCTIVITY OF THE CONDENSER TUBE
4880 REM   WALL MATERIAL IN W/(M)(DEG.CEL.) K3
4890 REM 10.THE OILSIDE FILM COEFFICIENT
4900 REM    IN W/(SQ.M)(DEG.CEL.) H9
4910 REM 11.THE CONDENSATION FILM COEFFICIENT
4920 REM    IN W/(SQ.M)(DEG.CEL.) C4
4930 REM 12.THE CONDENSER TUBE DIMENSIONS-
4940 REM   (a)WIDTH IN M B1
4950 REM   (b)HEIGHT IN M B2
4960 REM   (c)LENGTH IN M L1
4970 REM
4980 REM H1 IS THE OVERALL HEAT TRANSFER COEFFICIENT
4990 REM BASED ON THE TOTAL AREA OF THE CONDENSER
5000 REM TUBE A1, IN KCAL/(HR)(SQ.M)(DEG.CEL.)
5010 REM
5020 REM H2 IS THE OVERALL HEAT TRANSFER COEFFICIENT
5030 REM BASED ON THE CONTACT AREA OF THE CONDENSER
5040 REM TUBE A2, IN KCAL/(HR)(SQ.M)(DEG.CEL.)
5050 REM
5060 REM H3 IS THE OVERALL HEAT TRANSFER COEFFICIENT
5070 REM BASED ON THE TOTAL AREA OF THE CONDENSER
5080 REM TUBE A1, IN W/(SQ.M)(DEG.CEL.)
5090 REM
5100 REM H4 IS THE OVERALL HEAT TRANSFER COEFFICIENT
5110 REM BASED ON THE CONTACT AREA OF THE CONDENSER
5120 REM TUBE A2, IN W/(SQ.M)(DEG.CEL.)
5130 REM
5140 REM UO IS THE OVERALL HEAT TRANSFER COEFFICIENT
5150 REM CALCULATED FROM THE INDIVIDUAL FILM
5160 REM COEFFICIENTS IN W/(SQ.M)(DEG.CEL.)
5170 REM
5180 S1=S2/4.1873
5190 A1=2*L1*(B1+B2)
5200 A2=L1*B1
5210 T3=(T1+T2)/2
5220 T5=TDO+TDC
5230 Q1=M1*S1*(T2-T1)
5240 H1=Q1/(A1*T5)
5250 H2=Q1/(A2*T5)
5260 H3=H1/.86
5270 H4=H2/.86
5280 DO=D1+2*F4
5290 LMD=(DO-D1)/(LOG(DO/D1))
5300 UO=1/((DO/(D1*H9))+(1/C4)+((F4*DO)/(K3*LMD)))
5310 RETURN
5320 REM
5330 REM
5340 REM ***THIS IS A SUBROUTINE TO EVALUATE THE
5350 REM    PROPERTIES OF THE OIL AT ANY GIVEN
5360 REM    TEMPERATURE T9 IN DEG.CEL.***
5370 REM
5380 REM THE PROPERTIES EVALUATED ARE--
5390 REM 1.KINEMATIC VISCOSITY OF THE OIL IN
5400 REM   CENTISTOKES V1
5410 REM 2.SPECIFIC HEAT OF THE OIL IN
5420 REM   KJ/(KG)(DEG.CEL.) S2
5430 REM 3.THERMAL CONDUCTIVITY OF THE OIL IN
5440 REM   W/(M)(DEG.CEL.) K1
5450 REM 4.DENSITY OF THE OIL IN KG/(CU.M) R1
5460 REM
```

```
5470 REM THE INPUT VARIBLES ARE--
5480 REM 1.ANY TEMPERATURE IN DEG.CEL. T9
5490 REM 2.ALL THE ABOVE PROPERTIES AT SPECIFIED
5500 REM   TEMPERATURE INTERVALS
5510 REM
5520 I=1
5530 FOR I=1 TO 21
5540 IF T9=T3A(I) GO TO 5570
5550 NEXT I
5560 GO TO 5620
5570 V1=V1A(I)
5580 S2=S2A(I)
5590 K1=K1A(I)
5600 R1=R1A(I)
5610 GO TO 5760
5620 I=1
5630 IF T9<T3A(I) GO TO 5660
5640 I=I+1
5650 GO TO 5630
5660 J=I-1
5670 T=T9-T3A(J)
5680 V=ABS(V1A(I)-V1A(J))
5690 S=ABS(S2A(I)-S2A(J))
5700 K=ABS(K1A(I)-K1A(J))
5710 R=ABS(R1A(I)-R1A(J))
5720 V1=V1A(J)-(T*V/10)
5730 S2=S2A(J)+(T*S/10)
5740 K1=K1A(J)-(T*K/10)
5750 R1=R1A(J)-(T*R/10)
5760 RETURN
5770 REM
5780 REM
5790 REM ***THIS IS A SUBROUTINE TO EVALUATE THE
5800 REM     PROPERTIES OF THE DOW-A AT ANY SPECIFIC
5810 REM     TEMPERATURE T8 IN DEG.CEL.***
5820 REM
5830 REM THE PROPERTIES EVALUATED ARE--
5840 REM 1.LIQUID THERMAL CONDUCTIVITY IN
5850 REM   BTU/(HR)(FT)(DEG.FAR.) P2
5860 REM 2.LATENT HEAT OF CONDENSATION IN
5870 REM   BTU/LB P3
5880 REM 3.LIQUID DENSITY IN LB/CU.FT P4
5890 REM 4.LIQUID VISCOSITY IN CENTIPOISE P5
5900 REM
5910 REM
5920 REM
5930 REM INPUT VARIBLES ARE--
5940 REM 1.ANY GIVEN TEMPERATURE T8 IN DEG.CEL.
5950 REM 2.ALL THE ABOVE PROPERTIES AT SPECIFIED
5960 REM   TEMPERATURE INTERVALS
5970 REM
5980 I=1
5990 FOR I=1 TO 7
6000 IF T8=T8A(I) GO TO 6030
6010 NEXT I
6020 GO TO 6080
6030 P2=P2A(I)
6040 P3=P3A(I)
6050 P4=P4A(I)
6060 P5=P5A(I)
```

```
6070 GO TO 6220
6080 I=1
6090 IF T8<T8A(I) GO TO 6120
6100 I=I+1
6110 GO TO 6090
6120 J=I-1
6130 T=T8-T8A(J)
6140 Z1=ABS(P2A(I)-P2A(J))
6150 Z2=ABS(P3A(I)-P3A(J))
6160 Z3=ABS(P4A(I)-P4A(J))
6170 Z4=ABS(P5A(I)-P5A(J))
6180 P2=P2A(J)-(T*Z1/10)
6190 P3=P3A(J)-(T*Z2/10)
6200 P4=P4A(J)-(T*Z3/10)
6210 P5=P5A(J)-(T*Z4/10)
6220 RETURN
6230 REM *** THIS IS A SUBROUTINE TO READ THE INPUT
6240 REM     DATA FOR THE PROPERTIES OF THE OIL AT
6250 REM     VARIOUS AVERAGE OIL TEMPERATURES T3A(21)***
6260 REM
6270 REM THE PROPERTIES READ ARE--
6280 REM 1.KINEMATIC VISCOSITY IN CENTISTOKES V1A(21)
6290 REM 2.SPECIFIC HEAT IN KJ/(KG)(DEG.CEL.) S2A(21)
6300 REM 3.THERMAL CONDUCTIVITY IN W/(M)(DEG.CEL.) K1A(21)
6310 REM 4.DENSITY IN KG/CU.M R1A(21)
6320 REM
6330 I=1
6340 FOR I=1 TO 21
6350 READ V1A(I)
6360 NEXT I
6370 FOR I=1 TO 21
6380 READ S2A(I)
6390 NEXT I
6400 FOR I=1 TO 21
6410 READ K1A(I)
6420 NEXT I
6430 FOR I=1 TO 21
6440 READ R1A(I)
6450 NEXT I
6460 T=0
6470 FOR I=1 TO 21
6480 T3A(I)=T+10
6490 T=T3A(I)
6500 NEXT I
6510 DATA 85,49,29,19,13.5,10,7.8,6.3,5,4,3.3,2.8,2.45,
     2.15,1.9,1.72
6520 DATA 1.58,1.4,1.3,1.2,1.13
6530 DATA 1.84,1.9,1.94,1.98,2.03,2.06,2.11,2.16,2.20,2.25
6540 DATA 2.30,2.34,2.38,2.42,2.47,2.52,2.56,
     2.6,2.64,2.69,2.72
6550 DATA 0.1326,0.1319,0.1312,0.1305,0.1298,
     0.1290,0.1283,0.1276
6560 DATA 0.1268,0.1260,0.1254,0.1248,0.1240,
     0.1233,0.1226,0.1219
6570 DATA 0.1212,0.1205,0.1196,0.1190,0.1183
6580 DATA 870,862,856,850,842,835,829,823,816,810
6590 DATA 802,795,790,785,778,772,766,760,753,747,740
6600 RETURN
6610 REM
6620 REM
```

```
6630 REM *** THIS IS A SUBROUTINE TO READ THE INPUT DATA
6640 REM     FOR THE PROPERTIES OF DOWTHERM-A AT VARIOUS
6650 REM     FILM OR VAPOUR TEMPERATURES T8A(7) ***
6660 REM
6670 REM THE PROPERTIES READ ARE--
6680 REM 1.LIQUID THERMAL CONDUCTIVITY IN
6690 REM   BTU/(HR)(FT)(DEG.FAR.) P2A(7)
6700 REM 2.LATENT HEAT OF CONDENSATION IN
6710 REM   BTU/LB P3A(7)
6720 REM 3.LIQUID DENSITY IN LB/CU.FT P4A(7)
6730 REM 4.LIQUID VISCOSITY IN CENTIPOISE P5A(7)
6740 REM
6750 T=150
6760 FOR I=1 TO 7
6770 T8A(I)=T+10
6780 T=T8A(I)
6790 NEXT I
6800 I=1
6810 FOR I=1 TO 7
6820 READ P2A(I)
6830 NEXT I
6840 FOR I=1 TO 7
6850 READ P3A(I)
6860 NEXT I
6870 FOR I=1 TO 7
6880 READ P4A(I)
6890 NEXT I
6900 FOR I=1 TO 7
6910 READ P5A(I)
6920 NEXT I
6930 DATA 0.0716,0.0710,0.0704,0.0695,0.0688,0.0681,0.0675
6940 DATA 145.8,144.0,142.14,140.4,138.48,136.6,134.72
6950 DATA 58.890,58.336,57.774,57.206,56.634,56.05,55.456
6960 DATA 0.54,0.50,0.462,0.426,0.39,0.368,0.346
6970 RETURN
6980 END
```

A13.12 Results File TPHTC.DAT

***** RESULTS OF THE COMPUTER PROGRAMME TPHTC *****

THE INPUT DATA:

MASS FLOW RATE OF THE OIL IN KG/HR	M1 = 14
DOW-A VAPOUR TEMPERATURE IN DEG.CEL.	T8 = 175
INLET OIL TEMPERATURE IN DEG.CEL.	T1 = 155
CONDENSER TUBE WIDTH IN CM	B3 = 3
CONDENSER TUBE HEIGHT IN CM	B4 = 1
CONDENSER TUBE LENGTH IN CM	L2 = 100
HSA PANEL WIDTH IN M	W1 = .3
HSA PANEL TILT ANGLE TO THE HORIZONTAL IN DEG	A4 = 43.5

THE RESULTS:

OUTLET TEMPERATURE OF THE OIL IN DEG.CEL.	T2 = 167.891
CONDENSER TUBE WALL TEMPERATURE IN DEG.CEL.	T4 = 173.924
TEMPERATURE DROP ACROSS OIL FILM IN DEG.CEL.	TDO = 12.4783
TEMPERATURE DROP ACROSS THE CONDENSATE FILM IN DEG.CEL.	TDC = 1.07605
EQUIVALENT DIAMETER OF CONDENSER TUBE IN CM	D2 = 1.5
REYNOLDS OF THE OIL (DIMENSIONLESS)	R3 = 148.346
NET HEAT TRANSFERRED TO THE OIL IN W	Q2 = 126.586
OIL SIDE FILM COEFFICIENT NOT CORRECTED FOR FREE CONVECTION AND FIN EFFECT IN W/(SQ.M)(DEG.CEL.)	H6 = 71.43
OIL SIDE FILM COEFFICIENT CORRECTED FOR FREE CONVECTION BUT NOT FOR FIN EFFECT IN W/(SQ.M)(DEG.CEL.)	H8 = 110.086
OIL SIDE FILM COEFFICIENT CORRECTED FOR FREE CONVECTION AND FIN EFFECT IN W/(SQ.M)(DEG.CEL.)	H9 = 126.811
CONDENSATION FILM COEFFICIENT NOT CORRECTED FOR FIN EFFECT IN W/(SQ.M)(DEG.CEL.)	C3 = 3664.01
CONDENSATION FILM COEFFICIENT CORRECTED FOR FIN EFFECT IN W/(SQ.M)(DEG.CEL.)	C4 = 3921.31
OVERALL HEAT TRANSFER COEFFICIENT BASED ON THE TOTAL AREA OF THE CONDENSER TUBE A1, IN W/(SQ.M)(DEG.CEL.)	H3 = 116.739
OVERALL HEAT TRANSFER COEFFICIENT BASED ON THE CONTACT AREA OF THE CONDENSER TUBE A2, IN W/(SQ.M.)(DEG.CEL.)	H4 = 311.303
OVERALL HEAT TRANSFER COEFFICIENT CALCULATED FROM INDIVIDUAL FILM COEFFICIENTS IN W/(SQ.M)(DEG.CEL.)	UO = 114.966

FIGURE A14.1 Schematic Diagram of the Vacuum System Used for Loading the HSA Panel

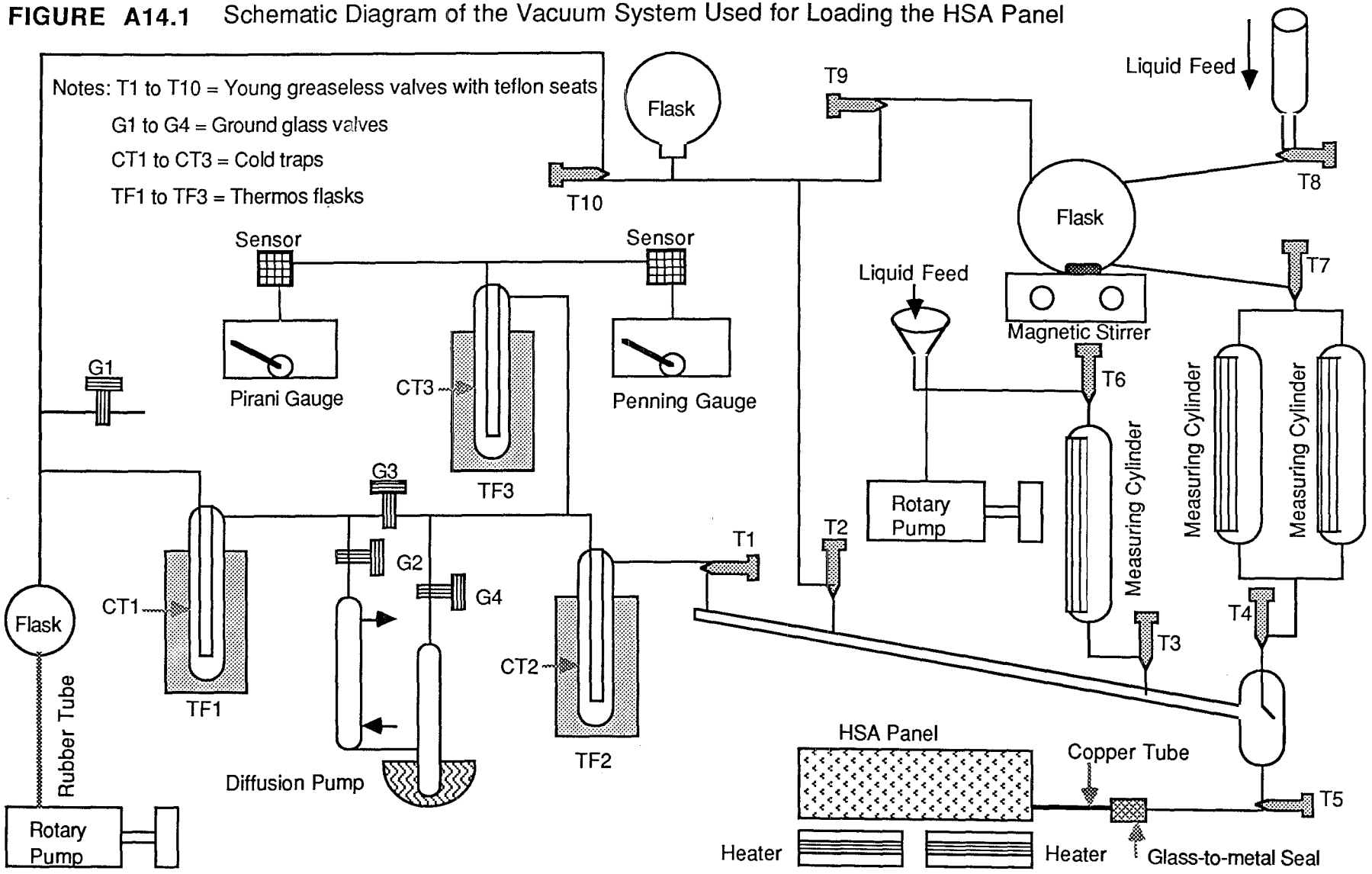

APPENDIX A14

CHARGING HSA PANEL

The HSA panel was required to be charged with an appropriate amount of working fluid, and this was accomplished with a vacuum system shown in Fig. A14.1. The vacuum line helps to perform the following four functions.

(1) To evacuate and degas the HSA
(2) To degas the working fluid
(3) To load the HSA with the required amount of the fluid
(4) To seal the panel hermetically

A14.1 Description of the Vacuum System

The vacuum line shown in the Fig. A14.1 was all made of glass for ease of fabrication, modifications and detection of leaks with a halide leak detector (Dynavac High Vacuum Leak Detector). The vacuum was created by the mercury diffusion pump (DP), backed by a two stage rotary pump (RP1). The diffusion pump was capable of getting vacuum as high as 10^{-6} mm Hg, but on a low vacuum of about 10^{-2} mm Hg created by the rotary pump (RP1). A Pirani gauge (PG1) with a range of 760 to 10^{-2} mm Hg was used to measure low vacuum, while a Penning gauge (PG2), with a range of 10^{-2} to 10^{-7} mm Hg, was used to measure high vacuum. In order to protect these gauges and to guard against their reading the vapour pressure of the mercury in the diffusion pump a cold trap CT3 was located before the vacuum gauges. The flow through various parts of the vacuum line was controlled by four ground glass values G1 to G4 and ten "Young" greaseless valves T1 to T10 with teflon seats and teflon seals. Cold trap CT1 prevents mercury vapour from getting into the rotary pump. Another cold trap CT2 was located between the diffusion pump and the panel to condense any condensables, so that vacuum gauges read only the pressure exerted by non-condensable gases. In case of power failure flask F1 prevents the oil from RP1 getting into the line due to the pressure differential.

A14.2 Degassing and Loading Procedure

The system was pumped down in stages by progressively opening valves G3, T1, T3, T4, T2, T10, T7, T9 and T5. First the whole system was evacuated to about 10^{-2} mm Hg with the rotary pump alone and then to about 10^{-4} mm Hg with the diffusion pump. However, there was no need to evacuate any further to the top portion of the line (where the working fluid is introduced) from G1 to T7 including flasks F2 and F3. So, valves G2, G3, G4, T1, T3, T4 and T5 were opened in stages and the panel was evacuated. To further drive away any condensables such as water, and non-condensable gases from the HSA panel, it was slowly and uniformly heated to about 225°C (which was the expected stagnation temperature of the panel). Using two (or more) radiative (or fan) heaters H1 and H2. It was necessary to monitor the surface temperature of the panel, with the help of a surface thermometer to avoid localized or excessive heating, which might damage the selective coating of the panel. Baking of the panel under vacuum also tested the integrity of the seam weld at the highest possible operating temperature. When the vacuum reached a steady value T5 was closed and baking stopped.

At this stage degassing of the working fluid was started. A measured amount (at least about 50 ml more than the actual amount needed as part of it was retained in LF1, F3, M1 and M2) of Dowtherm A was introduced carefully into the flask F3 via the feeder LF1 by partially opening the valve T8. In order to avoid any air entering F3, part of the liquid was retained in LF1. The magnetic stirrer MS was used to stir the liquid. As the flask F3 was under vacuum the non-condesables tend to come out and accumulate in the top portion of the flask and this process was enhanced by the stirrer. With T10 still closed T9 was opened to let the non-condensables and Dowtherm A vapours to expand and accumulate in flask F2. After a few minutes T9 was closed and T10 was opened to allow the non-condensables and vapours to be pumped out using RP1. With valves G2, G4 and T1 closed and G3 open the vacuum in F2 could be measured and when it had reached a steady value the process of expanding the degassing was repeated several times to ensure that Dowtherm A was properly degassed. Bubbles rising from the liquid was an indication of the process of degassification. If necessary, the liquid could be further degassed opening valves G2, G4, T1 and T2 and pumping down using

FIGURE A14.2 Steps in Sealing the Copper Tube

(a) Annealed portion of the Copper Tube

(b) Compressed by Modified Vice Grips

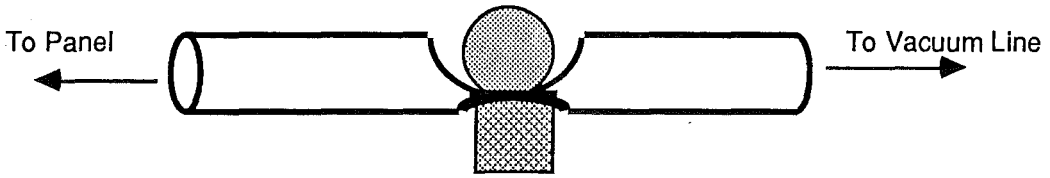

(c) Vacuum Line Connection Cut-off

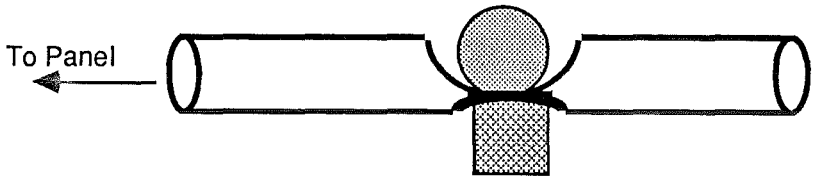

(d) Open End Filled with "Silfos"

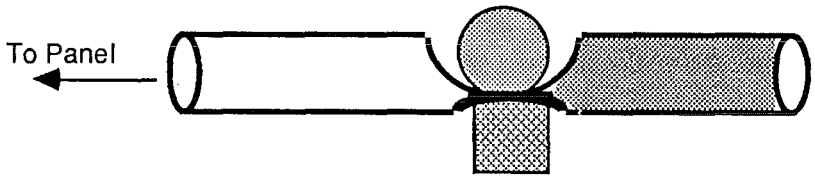

(e) Extra "Silfos" Added to Strengthen the Compressed Portion

the diffusion pump. But one should be careful not to flash boil the liquid.

When the liquid was completely degassed, with T8 and T9 closed T7 was opened slowly, to let the liquid drain into the measuring cylinders M1 and M2. Again slightly more than the required amount of 200 ml was drained into M1 and M2. Then T7 was closed and T4 and T5 opened carefully to let the liquid enter the HSA, making sure that a small amount was retained before T4.

When a secondary working fluid was also to be charged (like toluene in the case of HSA2) M3 was used. With T3 closed and T6 open, toluene was fed into the measuring cylinder M3 via the feeder LF2. Toluene could not be fed into the flask F3 and degassed because it was very hard to flush out the remaining Dowtherm A while the panel was connected at the other end. Also a mixture of Dowtherm A and toluene could not be degassed as toluene vaporises much faster during the degassing process, thus altering their ratio. Hence, a second rotary pump RP2 was directly connected to M3. Once the toluene was degassed loading was done in the same way.

After the liquid was charged into the panel the delicate task of sealing the copper tube CT was to be performed very carefully, avoiding any leakage of air into the panel, and this was done in stages as shown in Fig. A14.2. A modified vice grips as shown in Fig. A6.2 were used to compress the annealed copper tube CT as close to the panel as possible. The end was then cut off and filled with silfos (a silver brazing alloy containing phosphorous) as just closing the end would still end up in trapping some air. Then the vice grips were removed and to increase the strength of the compressed portion of the tube a small amount of silfos was added there.

This whole process was carried out and finished within a few minutes to ensure that no air diffuses into the panel. The panel was then ready to be assembled into the box.

FIGURE A15.1 Schematic Diagram of the Experimental Setup to Find the Isothermal Nature of Collector C1

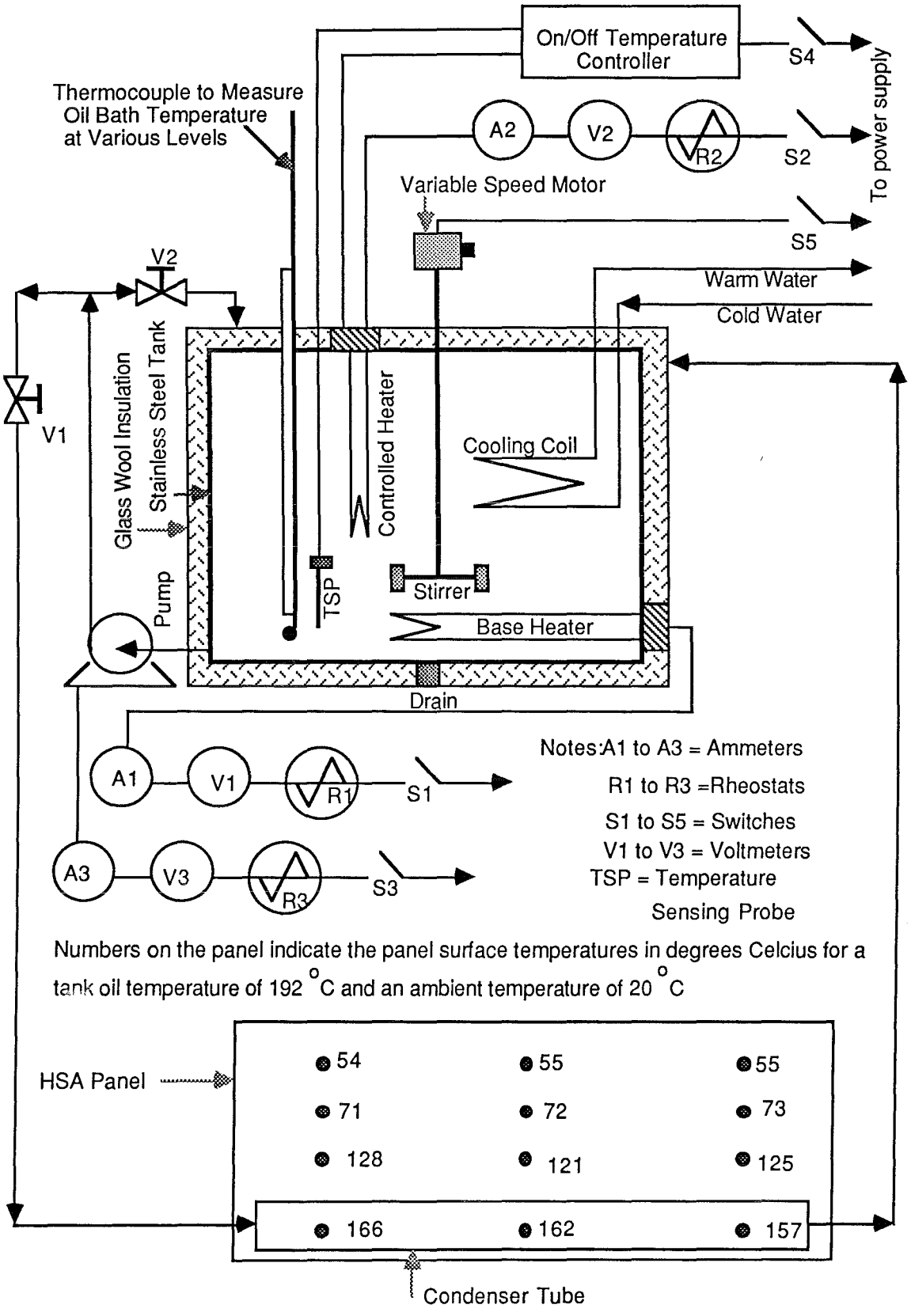

APPENDIX A15

ANALYSIS OF NONISOTHERMAL BEHAVIOUR OF HSA1

In this appendix the nonisothermal behaviour of the panel is verified and the reasons for it are discussed. A simple experiment was conducetd to check the nonisothermal nature of the panel. The schematic diagram of the experimental setup is shown in Fig. A15.1. The HSA1 was removed from the box and arranged upside down with the condenser tube at the bottom. Hot oil from the constant temperature oil bath (used with testing of collector C1) was pumped through the condenser tube of the panel, which was acting as the energy source to evaporator section. The panel temperatures at various locations were noted down with the help of a surface thermometer and are shown in Fig. A15.1. The maximum temperature drop across the panel increased to 74°C (with an oil temperature of 192°C and an ambient of 20°C) because the panel was exposed directly to the atmosphere and some heat was conducted via the blue steel plate. This confirmed the nonisothermal nature of the panel.

The reasons for the nonisothermal behaviour of the panel are: high pressure drop, low vapour density, limitations to heat transport and presence of noncondensible gases and these are discussed in detail in the following sections.

A15.1 High Pressure Drop

In an HSA panel vapours rise from the evaporator section to the condenser section, while the condensed liquid returns from the condenser to the evaporator under the action of gravity. Hence, for proper functioning of the panel the following condition must be met.

$$\Delta P_g \geq \Delta P_v + \Delta P_l \qquad \text{(A15.1)}$$

where ΔP_g is the gravitational head which is due to the hydrostatic head of the liquid; ΔP_v is the vapour pressure drop necessary to cause the vapours to flow from the evaporator to the condenser; and ΔP_l is the liquid pressure drop required to return the liquid from the condenser to the evaporator. If this condition is not met, the heat pipe can not operate efficiently resulting in hot spots and nonisothermal behaviour of the panel.

FIGURE A15.2 Estimation of the Equivalent Diameter for the Flow Paths in the HSA Panel

(a) Absorber Panel (Not to Scale)

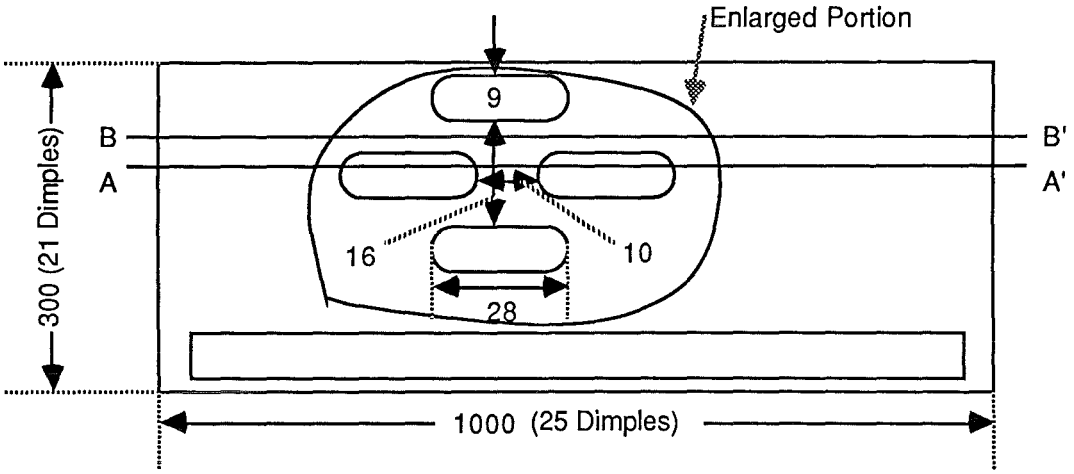

(b) Cross Section AA'

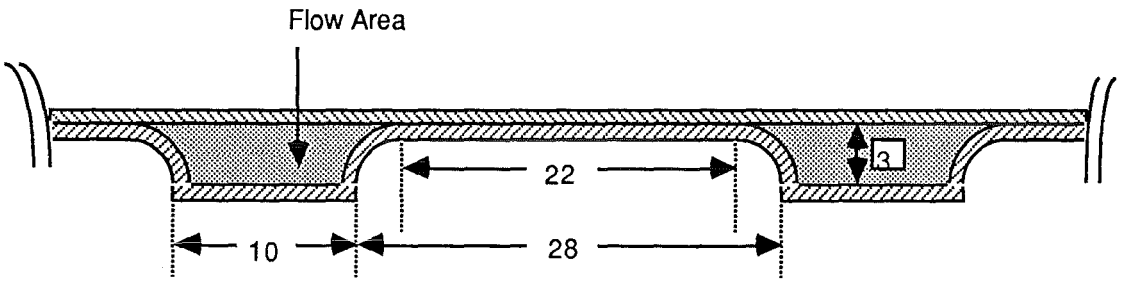

(c) Cross Section BB'

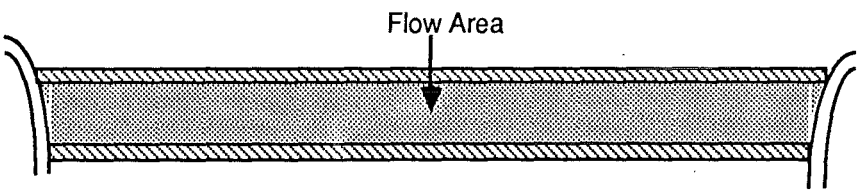

A15.1.1 To estimate the gravitational head (ΔP_g)

It is given by Dunn and Reay (1978)

$$\Delta P_g = \rho_l \; g \; L_{hp} \sin \phi \qquad \text{(A15.2)}$$

where ρ_l is the liquid density, g is the acceleration due to gravity, L_{hp} is the length of heat pipe (which is equal to panel width in the present case) and ϕ is the angle made by the panel with the horizontal.

Substituting $g = 9.81$ m.s^{-2}, $L_{hp} = 0.3$ m, $\phi = 45^{\circ}$ and ρ_l values from Table A4.2, (which depend on temperature) in Eq.(A15.2) ΔP_g can be evaluated at various temperatures as shown in Table A15.1.

A15.1.2 To estimate the vapour pressure drop (ΔP_v)

In evaluating ΔP_v the vapour can be considered either compressible or incompressible depending on its velocity. The fluid is defined as compressible when the vapour velocity V_v is small compared to the velocity of sound in the vapour C_v, that is Mach number Ma ($= V_v/C_v$) < 0.3.

If the same thing is translated into physical form ΔP_v should be small as compared to the average vapour pressure P_v of the fluid in the panel. However this condition is not met during startup or in case of high temperature heat pipes (Dunn and Reay, 1978). When the flow is incompressible it can be either in laminar region with axial Reynold's number $Re_a < 2100$ or in turbulent region with $Re_a > 2100$. Expressions are given for ΔP_v under each of these three categories by Chisholm (1971) and Dunn and Reay (1978). The axial Reynold's number is given by

$$Re_a = \{D_{eq} \; V_v \; \rho_v\} \; / \; \mu_v \qquad \text{(A15.3)}$$

where D_{eq} is the equivalent diameter of HSA, ρ_v is the vapour density and μ_v is the vapour viscosity. The HSA panel consists of several dimples (25 in each row and 21 in each column) whose cross section is shown in Figs. A15.2a,b,c. Hence D_{eq} is given by

$$D_{eq} = 4 \text{ (cross sectional area)/(wetted perimeter)} \qquad \text{(A15.4)}$$

As there are two different cross sections (Figs. A15.2) a weighted average was evaluated and found to be 4.8 mm. The average vapour velocity V_v can be estimated from

$$V_v = m_v \; / \; (26 \; \pi R_{eq}^2 \; \rho_v) \qquad \text{(A15.5)}$$

where R_{eq} is the equivalent radius and m_v is the mass flow rate of vapours travelling to the condenser (which is equal to the

TABLE A15.1 Summary of Results on Pressure Drop Calculations

Temperature in °C	100	150	200	250
(1) Mass flow rate of liquid or vapour x 10^4 in $kg.s^{-1}$	2.8	3.0	3.1	3.3
(2) Vapour velocity in $m.s^{-1}$	21.1	3.0	0.7	0.2
(3) Axial Reynolds number for vapour flow	451.0	4.0	3.7	3.4
(4) Vapour pressure loss, ΔP_v in $N.m^{-2}$	6840	1040	272	81
(5) Liquid pressure loss, ΔP_l in $N.m^{-2}$	37	27	22	18
(6) Gravitational head, ΔP_g in $N.m^{-2}$	2064	1979	1883	1786

mass flow rate of condensate flowing downwards) and it can be evaluated from

$$m_v = Q_{net} / \lambda \qquad \text{(A15.6)}$$

where λ is the latent heat of vaporisation of Dowtherm A and Q_{net} is the net heat transfered to the oil. For a typical value of Q_{net} = 100 W, the mass flow rate, vapour velocity and axial Reynold's number are shown in Table A15.1. It can be seen that Re_a lies in the laminar region. For laminar flow Cotter (1965) gave the following expression to evaluate the vapour pressure drop ΔP_v

$$\Delta P_v = -\{1-(4/\pi^2)\}\{m_v^2/(8\rho_v R_{eq}^4)\} - \{(8\mu_v m_v L_a)/(\pi\rho_v R_{eq}^4)\} \qquad \text{(A15.7)}$$

where L_a is the length of the adiabatic section in the HSA panel. However, from the total enclosed volume and the volume of working fluid approximate length can be estimated. The total enclosed volume is about 623 cc (Figs. A15.2a,b,c) and the volume of Dowtherm A is about 200 cc. As the total length of the heat pipe is 0.3 m, the approximate evaporator length is 0.1 m and condenser length is about 0.05 m and hence L_a = 0.15 m. ΔP_v may be estimated from Eq. (A15.7) and is listed at various temperatures in Table A15.1.

A15.1.3 To estimate the liquid pressure drop (ΔP_l)

The flow regime in the liquid phase is almost always laminar and assuming the condensate flowing down 25 channels of the panel in a thin layer, Hagen Poiseuilles equation can be used to find the approximate value of ΔP_l

$$\Delta P_l = (\delta \mu_l L_{hp} V_l) / R_{eq}^2 \qquad \text{(A15.8)}$$

where δ is the average film thickness, μ_l is the liquid viscosity and V_l is the average film velocity. δ and V_l are given by (Bird et al., 1960).

$$\delta = \{3 \mu_l m_l\} / \{\rho_l^2 g W_l \cos \phi\} \qquad \text{(A15.9)}$$

$$V_l = \{\rho_l g \delta^2 \cos \phi\} / \{3 \mu_l\} \qquad \text{(A15.10)}$$

where m_l = mass flow rate of the liquid; ρ_l = liquid density; W_l = film width (16 mm from Fig. A15.2a); ϕ = angle of inclination (45°). ΔP_l can be evaluated from Eqs. A15.8 to A15.10 and it is listed in Table A15.1 at various temperatures.

A15.1.4 Observations

The pressure losses and vapour velocity increase with decreasing temperature. It can be seen from the Table A15.1 that

at lower temperatures (about 100°C) the vapour pressure losses are excessively high. In fact at about 100°C the gravitational head is not enough to maintain proper fluid circulation and Eq. A15.1 is violated, thus resulting in hot spots and nonisothermal behaviour of the panel. This is a direct result of the very low vapour density (or vapour pressure) of Dowtherm A at lower temperatures.

However, there is one draw back in estimating these pressure losses. All the expressions used have been derived for tubes with circular cross setion, but in the HSA panel the situation is different. It has been assumed that the panel consisted of 26 separate channels each with an equivalent diameter of 4.8 mm. Actually there are no circular channels, also they are zigzag and interconnected, which would make the flow path very complicated. However, the trend remains the same though the absolute values differ, thus giving an indication of the pressure drop range.

The temperature drop ΔT_v due to the vapour pressure drop ΔP_v may be estimated from Clausius Clapeyron equation as given below.

$$\Delta T_v = \{T_v \Delta P_v\} / \{\lambda \rho_v\} \qquad \text{(A15.11)}$$

where T_v is the vapour temperature. For T_v value of 150°C and substituting for other variables ΔT_v = 7°C. However this temperature drop increases with decreasing T_v because ΔP_v increases. this once again confirms the unsuitability of Dowtherm A at low temperatures.

A15.2 Low Vapour Density

Chisholm (1971) points out that if the initial vapour density is sufficiently high, uniform vapour temperatures can be obtained very fast. On the other hand if the initial vapour density is low, compressible flow effects can be of importance and sonic velocities may occur resulting in large axial temperature variations in the vapour. In case of Dowtherm A the vapour densities at ambient temperature are very low.

A15.3 Limitations to Heat Transport

The output from a heat pipe can be limited by a number of considerations and the important ones are described below.

A15.3.1 Sonic limit

The velocity of vapour can not exceed velocity of sound in vapour. During startup and with high temperature heat pipes the

vapour velocity may reach sonic values. In such cases compressibility effects must be taken into consideration. Also at low vapour pressures the sonic velocity may be the limiting factor as the gas density will be low. This condition is called choking, when the flow is restricted due to the sonic velocity occuring at some point in the heat pipe. It should be noted that under these conditions of sonic limitation considerable axial temperature and pressure changes will exist and the heat pipe operation will be far from isothermal. Expressions are available in the literature to find the maximum heat flux, vapour density and mass flow rate at sonic limit. Chisholm (1971) has given expressions for the vapour sonic velocity V_{vs} and maximum circulation rate m_s and they are

$$V_{vs} = \{(\gamma P_v) / \rho_v\}^{0.5} \qquad \text{(A15.12)}$$

$$m_s = \pi R_{eq}^2 V_{vs} \rho_v \qquad \text{(A15.13)}$$

where γ is the specific heat ratio = 1.039 at 100°C

Substituting the required quantities at 100°C in Eqs. $m_s = 1x10^4$ kg.s^{-1}. But the actual flow rate (Table A15.1) is $2.8x10^4$ kg.s^{-1}, which indicates the possible violation of sonic limit at lower temperatures.

A15.3.2 Viscous limit

At low temperatures viscous forces are dominant in the vapour flow down the pipe. Busse (1967) has shown that the axial heat flux rapidly increases as the pressure in the condenser is reduced, the maximum heat flux occuring when the pressure is reduced to zero. In the present case the vapour pressure is low at lower temperatures indicating a possibility of viscous limit.

A15.3.3 Entrainment limit

In a heat pipe when vapour flows from evaporator to condenser, it exerts a shear force on the liquid flowing in the opposite direction. The magnitude of the shear force will depend on the vapour properties and vapour velocity. The net result will be the tendency to entrain droplets of liquid and transport them back to the condenser end. This tendency is resisted by the surface tension in the liquid. The Weber number We provides a convenient measure of entrainment and it is defined as the ratio between inertial vapour forces and liquid surface tension forces.

$$We = \{\rho_v V_v^2 z\} / \{2 \pi \sigma_l\} \qquad \text{(A15.14)}$$

FIGURE A15.3 Limitations to Heat Transport in a Heat Pipe

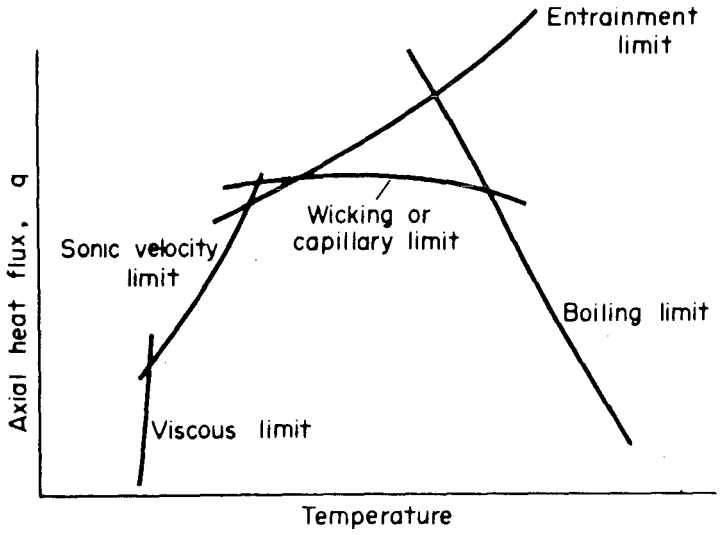

FIGURE A15.4 Merit Number of Selected Working Fluids

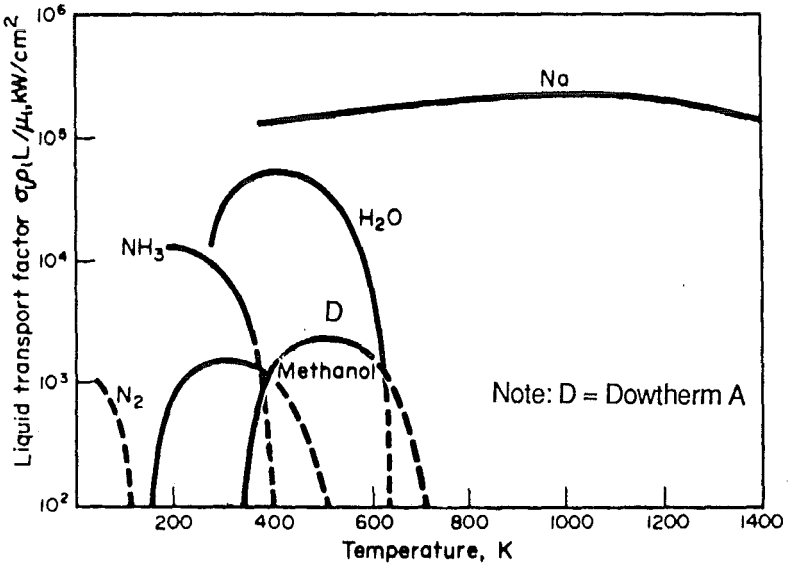

where σ_l is the surface tension of the liquid and z is a dimension characterising the vapour liquid interface, which in the present case may be taken as D_{eq}. Substituting the appropriate values for 100°C in Eq. (A15.14), We = 0.3. Hence entrainment is not a problem with HSA1.

A15.3.4 Circulation limit

For efficient operation of the HSA panel Eq. (A15.1) should be satisfied. This ensures proper circulation of the fluid. Dunn and Reay (1978) have given expressions for finding out the maximum circulation rate and corresponding maximum value for heat transport. This aspect has already been described in section.

A15.3.5 Boiling limit (Burnout)

Film boiling must be avoided due to poor heat transfer coefficients. Burnout will occur at the evaporator at high radial fluxes. Ferrell and Davis (1973) have provided equations for the boiling limit. It is desirable to have a working fluid with a high super heat to reduce the chance of nucleation, which could finally lead to film boiling. Dowtherm A was found to have reasonably good super heat values, thus eliminating the chances for burnout.

A15.3.6 Observations

All these limitations may be plotted against temperature leading to a shape of the curve as shown in Fig. A15.3. It is necessary for the operating point to be chosen in the area lying below these curves. The actual shape of this area depends on the working fluid and the heat pipe type and will vary appreciably for different heat pipes. However the properties of the working fluid which determine maximum heat transport can be combined to form a figure of merit M_n and is given by the following expression.

$$M_n = \{\rho_l \sigma_l \lambda\} / \mu_l \qquad \text{(A15.15)}$$

M_n can be evaluated at various temperatures from Eq. (A15.15) and plotted against temperature as shown in Fig. A15.4. It may be seen from this figure that M_n reaches a maximum value at about 250°C and decreases on both sides. Hence the HSA panel operates better at higher temperatures.

A15.4 Presence of Noncondensible Gases

The presence of noncondensible gases in the vapour will radically influence the performance of the heat pipe. In such cases vapours must diffuse through the gases, to reach the cooled surface and this creates a considerable temperature gradient. The gases are generally swept towards the condenser by the motion of the vapour and hence sharp temperature gradients should result. However, there is no clear indication of this behaviour in HSA1. In order to avoid the presence of any noncondensibles extra care may be taken while degassing, baking and loading the panel.

FIGURE A16.1 Schematic Diagram of the Experimental Setup to Find the Vapour Pressure of the Mixture of Dowtherm A and Toluene

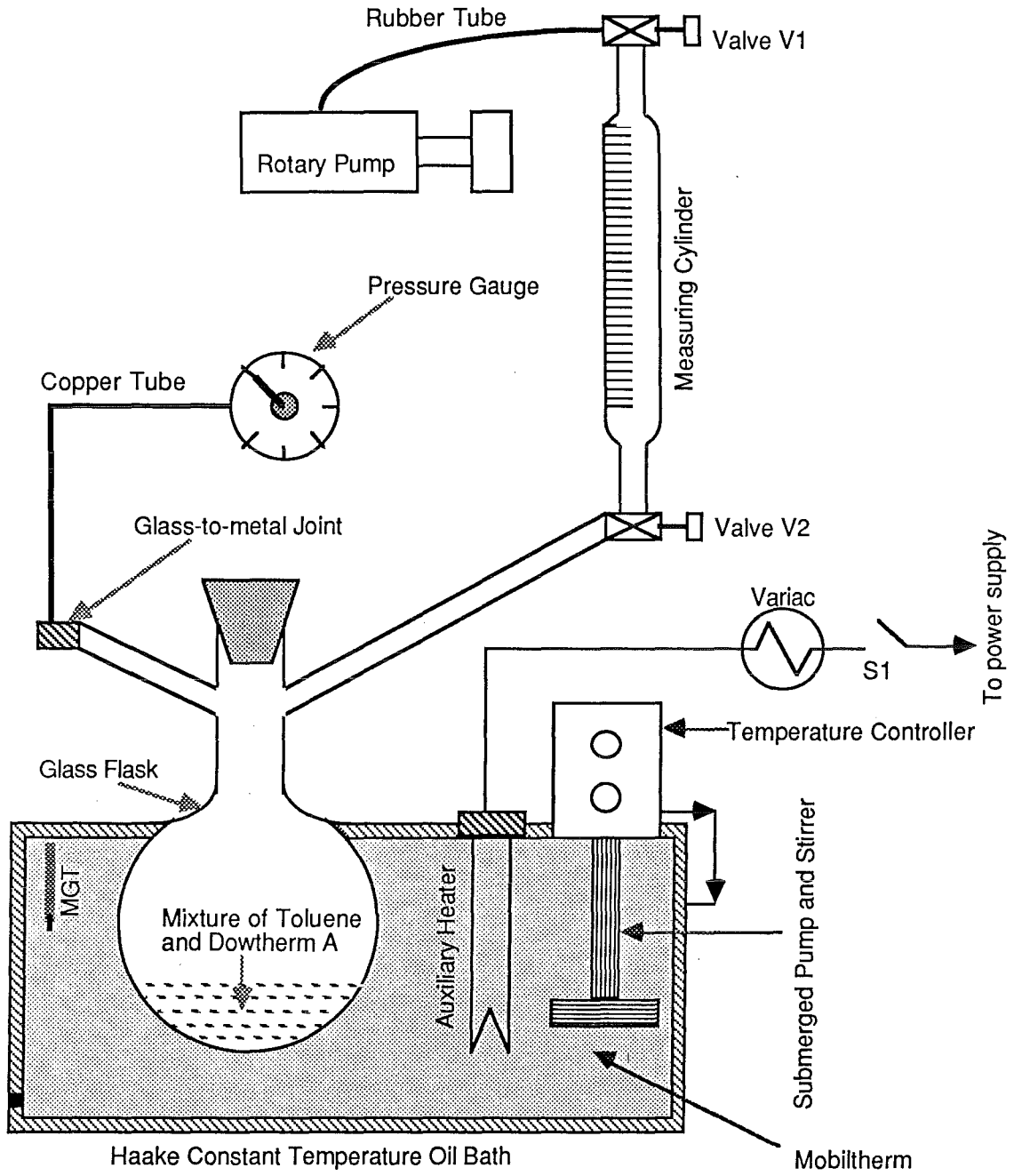

Notes: S1 = Switch

MGT = Mercury-in-glass thermometer

APPENDIX A16

WORKING FLUID FOR HSA2

It was necessary to find a suitable combination of Dowtherm A and toluene so that the vapour pressure of the mixture does not exceed atmospheric pressure at about 220°C. At the same time it was desirable to have sufficient quantities of toluene to increase the vapour pressure of the mixture appreciably in the low temperature range. Hence an experiment was conducted, the setup of which is shown in Fig. A16.1. A one litre capacity measuring flask with two side tubes was immersed partially in the constant temperature oil bath (the details of which are given in Section 4.9) provided with an auxiliary heating element. One side tube was connected to a vacuum guage and the other to a calibrated measuring tube via valves V1 and V2.

The measuring tube was calibrated by introducing measured amounts of acetone into the tube and then the acetone was pumped out. A rotary vacuum pump was used to pump down the whole system for a day with both valves V1 and V2 open. After checking the system for leaks Dowtherm was introduced into the measuring tube and it was degassed for several hours, intermittently heating the tube carefully with a gas flame till the liquid boils. A total of 200 cc of Dowtherm was charged into the flask, each time degassing and introducing about 50 cc. The vacuum gauge was calibrated by heating Dowtherm A to a specified temperature, allowing the system to come to steady state and noting the temperature and the vacuum guage reading. Then toluene was introduced into the measuring tube, degassed and added to Dowtherm A. The temperature of the mixture was increased. The temperatures and corresponding vapour pressures were noted down after attaining steady state conditions.

This experiment was repeated with different amounts of toluene. It was found that 28 cc of toluene added to 190 cc Dowtherm gave high vapour pressures in low temperature range, but at the same time the vapour pressure of the mixture did not exceed 100 kPa, even at 210°C (Table 4.5). Thus a 15% by volume (or 0.2 mole fraction) of toluene was found to be an appropriate mixture for HSA2.

The various properties of these three fluids are listed in the Table A12.1, along with their costs.

On comparing the various desirable properties Mobiltherm was found to be appropriate in the present situation as it has higher operating and film temperatures, higher oxidation stability, lower viscosity, higher thermal conductivity, lower density and higher heat capacity as compared to Thermia oils.

APPENDIX A17

ERRORS IN MEASURING INSTRUMENTS

The errors involved with a few selected measuring instruments are tabulated below.

Instrument	Quantity Measured	Value of Error
Kipp & Zonen Pyranometer and Millivoltmeter	Total insolation	±3%
Digital Microvoltmeter	Temperature	±0.1°C
Graduated Cylinder and Stopwatch	Flow rate	±5 $cc.min^{-1}$
Measuring Tape	Dimensions	±1 mm
Copper-Constantan Thermocouples	Temperature	±0.7oC for <93°C ±0.7% for 93-371°C
Quartz Thermometer (Hewlett Packard)	Temperature (Standard for comparison)	±0.01°C
Ice Bath	Zero Reference Point	±0.1 to ±0.5 °C
Mercury in Glass Thermometer	Temperature	±0.5°C for <100°C ±1.0°C for >100°C